AD/A-005 574

THE AERODYNAMIC CHARACTERISTICS OF WRAP-AROUND FINS, INCLUDING FOLD ANGLE AT MACH NUMBERS FROM 0.5 TO 3.0

C. Wayne Dahlke, et al

Army Missile Research, Development and Engineering Laboratory
Redstone Arsenal, Alabama

15 November 1974

DISTRIBUTED BY:

NTIS

National Technical Information Service
U. S. DEPARTMENT OF COMMERCE

UNCLASSIFIED

SECURITY CLASSIFICATION OF THIS PAGE (When Data Entered)

REPORT DOCUMENTATION PAGE		READ INSTRUCTIONS BEFORE COMPLETING FORM
1. REPORT NUMBER RD-75-15	2. GOVT ACCESSION NO.	3. RECIPIENT'S CATALOG NUMBER AD/A-005574
4. TITLE (and Subtitle) THE AERODYNAMIC CHARACTERISTICS OF WRAP-AROUND FINS, INCLUDING FOLD ANGLE AT MACH NUMBERS FROM 0.5 TO 3.0		5. TYPE OF REPORT & PERIOD COVERED Technical Report 6. PERFORMING ORG. REPORT NUMBER
7. AUTHOR(s) C. Wayne Dahlke Lewis D. Flowers		8. CONTRACT OR GRANT NUMBER(s)
9. PERFORMING ORGANIZATION NAME AND ADDRESS US Army Missile Research, Development and Engineering Laboratory US Army Missile Command Redstone Arsenal, Ala. 35809		10. PROGRAM ELEMENT, PROJECT, TASK AREA & WORK UNIT NUMBERS (DA) 1M262303A214 AMCMSC 632303.11.21405
11. CONTROLLING OFFICE NAME AND ADDRESS		12. REPORT DATE 15 November 1974 13. NUMBER OF PAGES 368
14. MONITORING AGENCY NAME & ADDRESS(if different from Controlling Office)		15. SECURITY CLASS. (of this report) Unclassified 15a. DECLASSIFICATION/DOWNGRADING SCHEDULE

16. DISTRIBUTION STATEMENT (of this Report)

Approved for public rele se; distribution unlimited.

17. DISTRIBUTION STATEMENT (of the abstract entered in Block 20, if different from Report)

18. SUPPLEMENTARY NOTES

None

Reproduced by
NATIONAL TECHNICAL
INFORMATION SERVICE

19. KEY WORDS (Continue on reverse side if necessary and identify by block number)

Wind tunnel test
Wrap-around fins
Transonic testing
Trisonic wind tunnel

20. ABSTRACT (Continue on reverse side if necessary and identify by block number)

An experimental investigation was conducted in the McDonnell Douglas Aerophysics Laboratory 4-foot trisonic wind tunnel to study the aerodynamic characteristics of wrap around fins. Wrap around fins with leading edge sweep angle and exposed semi-span variations were tested. One unswept fin was tested simulating various opening angles from 10 degrees beyond fully open to a folding angle of 112.5 degrees. Force and moment data were obtained at Mach Numbers from 0.5 to 3.0 at angles of attack up to 14 degrees and roll angles from

DD FORM 1 JAN 73 1473 EDITION OF 1 NOV 65 IS OBSOLETE

PRICES SUBJECT TO CHANGE

SECURITY CLASSIFICATION OF THIS PAGE (When Data Entered)

Block 20 (Concluded)

0 to 45 degrees. The complete results of this test are presented in plotted form for the main balance and all four fin balances.

CONTENTS

		Page
1.	Introduction.	3
2.	Apparatus	3
3.	Data Accuracy	6
4.	Reduction of Data	7
5.	The Data.	7

SYMBOLS

Main Balance

ALFA'	Angle of attack
CAF' CORR, CAF	Axial force coefficient
CN_α	Normal force coefficient derivative with respect to angle of attack, $\alpha = 0$ deg
CNF'	Normal force coefficient
CM_α	Pitching moment coefficient with respect to angle of attack, $\alpha = 0$ deg
CPM'	Pitching moment coefficient
CRM', C_ℓ	Rolling moment coefficient
CSF'	Side force coefficient
CYM'	Yawing moment coefficient
XCP	Center of pressure, body diameters from nose apex
$\Delta CN_{\alpha F}$	Incremental normal force coefficient derivative with respect to angle of attack, $\alpha = 0$ deg
$\Delta CM_{\alpha F}$	Incremental pitching moment coefficient derivative with respect to angle of attack, $\alpha = 0$ deg

Fin Balance

CMH1 (2,3,4)	Fin hinge moment coefficient
CMR1 (2,3,4)	Fin root bending moment coefficient
CN1 (2,3,4)	Fin normal force coefficient
CN_α	Normal force coefficient derivative with respect to angle of attack, $\alpha = 0$ deg
XCP	Chordwise center of pressure, positive forward of 50% chord line, reference to root chord
YCP	Spanwise center of pressure, reference to exposed semi-span

Other Symbols

CR	Fin root chord
D	Model diameter, 4 inches
M	Mach number
P_t	Total pressure, psi
q	Dynamic pressure, psi
RN	Reynolds number/foot
T_t	Total temperature, °F
α	Angle of attack
θ	Fin opening angle, degrees
Λ	Leading edge sweep angle, degrees
ϕ	Model roll angle, degrees

1. Introduction

Aerodynamic stability studies of missile designs that have tube-launched applications have been conducted during the last 3 years. The major emphasis has been placed on the definition of the aerodynamic characteristics of missiles with wrap around fins (WAF). Wind tunnel tests have been planned and conducted to study the effects of many geometric and flow parameters for the WAF[1].

This report contains the last of a series of planned wind tunnel test conducted to study the WAF. The geometric variables covered during this test were opening angle, exposed semi-span, leading edge sweep angle, step-down body, and aspect ratio. Previously, all WAF's tested have had a theoretical maximum semi-span defined by one-fourth the body circumference. Two additional spans were tested during this phase of approximately 80 and 50 percent of the theoretical maximum fin. The opening angle variation was a continuation of the previous transonic testing[2] where opening angles, from 10 degrees beyond fully open to 112.5 degrees closed, are considered. The remaining configurations were tested to extend the data for these into the supersonic regime and to fill voids and make checks on the transonic range.

2. Apparatus

a. Test Facility and Operation

The test was conducted in the McDonnell Douglas Aerophysics Laboratory 4-Foot Trisonic Wind Tunnel[3], which is an intermittent blow-down-to-atmosphere facility that operates in a Mach number range from 0.2 to 5.0. During the transonic operation, the 24 to 30 inch pass duct was installed, and for supersonic operation the diffuser ejectors were connected.

---

[1]Dahlke, C. W., Craft, J. C., The Effect of Wrap-Around Fins on Aerodynamic Stability and Rolling Moment Variations, U.S. Army Missile Command, Redstone Arsenal, Alabama, July, 1973, Technical Report RD-73-17.

[2]Dahlke, C. W., Flowers, L. D., The Aerodynamic Characteristics of Wrap-Around Fins, Including Fold Angle at Mach Numbers From 0.5 to 1.3, U.S. Army Missile Command, Redstone Arsenal, Alabama, December 1974, Technical Report RD-75-19.

[3]Raddatz, L. A., The Douglas Aerophysics Laboratory Four-Foot Trisonic Wind Tunnel, Douglas Report DAC-59809, October 1967.

Multiple modes of operation were conducted during each blow.. Most blows consisted of a pitch sweep at each of two or three roll angles (0, 22.5, and 45.0 degrees). Other modes used were multiple Mach numbers and roll angles, multiple total pressures, Reynolds Numbers, and roll sweeps (0 to 90 degrees) at three pitch angles. For all the pitch modes of operation the pitch rate was about 4 deg/sec and for the roll sweep mode the roll rate reached maximums of about 17 deg/sec.

The tunnel total pressure was varied for each Mach number to maintain the Reynolds number of approximately 7×10^6 per foot which is near the minimum operating conditions for most Mach numbers. Reynolds number was varied at Mach numbers of 1.6 and 2.5 for the following configurations:

Blow No.	Configuration	M_∞	RN $\times 10^{-6}$ 1/ft	P_t (psi)
33	B2F1	1.6	12	40.08
			7	22.125
45	B3F2	2.5	4	17.93
			11	49.7
46	B2F1	2.5	4	17.9
			7	31.8
			11	49.66
47	B1F2	2.5	4	17.93
			7	32.19
			11	49.63

The nominal tunnel conditions were:

Mach No.	P_t (psia)	T_t (°F)	q(psi)
0.5	32.35	61.3	4.51
0.8	23.94	58	6.935
0.95	22.3	65	7.8
1.0	22.0	65.12	8.03
1.1	21.35	65.35	8.31
1.2	21.94	44	9.16
1.3	24	50.2	10.25
1.6	22.7	67.75	9.41
2.0	26.135	69.3	9.235
2.5	32.35	61.9	8.375
3.0	41.5	57	7.15

b. Instrumentation

Aerodynamic loads of the complete model were measured by the McDonnell Douglas Aerophysics Laboratory No. 17 6-component strain-gage balance. Aerodynamic loads for each of the four fins was measured by a MICOM 3-component fin balance. The fin balances are identified by MICOM drawing, RDK-12500 series.

The maximum rated capacities for the McDonnell Douglas Aerophysics Laboratory No. 17 balance are:

Normal force	1000 lb
Side force	1000 lb
Pitching moment	3000 in.-lb
Yawing moment	2500 in.-lb
Rolling moment	400 in.-lb
Axial force	150 lb

The maximum rated capacities for each of the fin balances are:

Normal force	60 lb
Hinge moment	100 in.-lb
Root-bending moment	100 in.-lb

Because of the 3-component limitation of the fin balances, the normal force and the hinge moment data are inadequate for the folding fin configurations. This is discussed in detail in Section 3. Other tunnel instrumentation consisted of tunnel pressure and temperature transducers, two base pressure transducers, and a model grounding circuit indicating continuity between fins and body, and between body and sting.

c. Model

The models consisted of a 2-caliber secant ogive nose with an eight caliber cylindrical afterbody and six fin configurations. The basic body configuration (B1) had a straight cylindrical afterbody, 4 inches in diameter. Alternate afterbody shapes (B2) and (B3) stepped down to a diameter of 3.6 inches over lengths of 7 and 4 inches from the base respectively (Figure 1).

The six WAF configurations tested are shown in Table 1 and Figure 2. The basic fin F1 was tested at six fold angles of -10, 0, 10, 22.5, 45, and 112.5 degrees. The other fin variables were one additional chord variation F2, two additional leading sweep angles F16 and F17, and two additional exposed semi-spans F20 and F21. A gap of 0.020 inch was maintained (Figure 2) between body and each fin root chord to allow for fin balance deflections under load. Photographs of model installed in the McDonnell 4-foot tunnel are shown in Figure 3.

The complete model, balance and sting, was rolled by the McDonnell Douglas Aerophysics Laboratory remote roll mechanism when roll attitudes other than zero were called for. Model changes consisted of exchange of fins or fin components. When fins of different root chord lengths were exchanged, body spacers were also exchanged such that the fin trailing edge was flush with the body base. Each fin attachment plate was at 50 percent root chord.

3. Data Accuracy

The quoted precision of the McDonnell Douglas Aerophysics Laboratory No. 17 strain gage balance is one-half of one percent of the capacity of the balance or better.

The results of the fin balance calibrations performed by Arnold Engineering Development Center were used while testing. During pretest procedures each fin was check loaded to 30 pounds in 10-pound increments, at each of three locations on the calibration fin. The check loads proved to be unsatisfactory, and McDonnell Douglas Aerophysics Laboratory performed a post-test calibration. The results of this calibration show the standard deviation for 15 loads of 30 pounds each distributed over different locations of the four fins to be as follows:

	Percent of applied load
Normal Force	0.68
Hinge Moment	0.72
Bending Moment	0.48

The proper hinge moments and normal forces are not adequately defined for the fin opening angles other than the fully open case, $\theta = 0$ degree. The fin balance orientation with respect to the body remained fixed for all fin opening angles, while the technique used to vary opening angle was in the fin design concept. This technique would require 5-component fin balances with additional measurements of span force or side force and moment. Flat fin normal force may be approximated for $\theta = \pm 10.0$, 22.5, and 45 degrees by Fin normal force = Balance normal force/cosθ. This type of approximation should not be used for $\theta = 112.5$ degree (fin nearly closed) because of fin forces induced by the body fin flow field interaction. The accuracy of using the component method is made more questionable because force loadings on the WAF and flat fin are different.

4. Reduction of Data

All main balance force coefficients are referenced to the cross sectional area of the body (12.566 $in.^2$). The moments are all about the nose apex (Figure 1), and are based on the body cross sectional area times the body diameter (4 in.).

All fin force coefficients are referenced to their respective fin panel geometry listed below:

Fin Reference Data

Fin	b/2(in.)	C_R(in.)	S_f($in.^2$)
F1	2.64	7.0	18.48
F2	2.64	4.0	10.40
F16	2.70	4.0	9.45
F17	2.63	7.0	12.52
F20	2.14	7.0	14.98
F21	1.39	7.0	9.73

The fin hinge moment coefficients are about the fin 50 percent root chord line and the root bending moment coefficients are about a line parallel to the fin root chord on the body surface.

The standard sign convention used for the main balance is a climbing right turn.

The sign convention for the fin balances is shown in Figure 4.

5. The Data

The data are presented in four groups of plots showing the basic main balance 6-component data and all twelve components of the fin data; fin effectiveness with various opening angles derived from the main balance; main balance summary data; and summary data of fin panel loads.

The basic main balance and fin balance data are presented in Figures 5 through 17. Each figure number represents one complete set of data taken from the 6-component main balance and from four-(three component) fin balances, which was obtained during one blow, usually consisting of 2 or 3 angle-of-attack sweeps. Figure 18 presents the main balance data at Mach 1.0 and 2.0 for roll sweeps through 90 degrees at fixed angle-of-attacks. The run log and data summary are shown in Table 2.

Figures 19 through 31 summarize the main balance data by presenting the static stability derivatives, the zero angle-of-attack forebody axial force coefficients, and the self induced rolling moment of the WAF at zero angle-of-attack. Figures 22, 23, 25, and 31 include data from previous transonic test.[4,5]

Fin effectiveness for the various opening angles was computed from the main balance data by subtracting out the body alone component obtained from the previous test.[6] These data are presented in Figures 32 through 43 for zero roll attitude. Figure 44 shows the small effect of roll at Mach 0.5. All data shown at $\theta = 90$ degrees and other opening angles were included from previous tests.[2]

Figures 45 through 46 show the horizontal fin panel normal force derivative and the spanwise and chordwise center of pressure for serveral configurations.

---

[4] Dahlke and Craft, loc. cit.

[5] Dahlke and Flowers, loc. cit.

[6] Dahlke and Craft, loc. cit.

[7] Dahlke and Flowers, loc. cit.

TABLE 1. FIN CONFIGURATION SUMMARY

Configuration	*A (in.)	C_R (in.)	C_T/C_R	Λ (deg)	t (in.)	R_1 (in.)	R_2 (in.)	R_3 (in.)	δ** (deg)	r (in.)	AR	b/2 (in.)
F_1	1.900	7.0	1.00	0	0.200	1.900	2.000	1.800	45	0.008	0.75	2.64
F_2	↓	4.0	↓	↓	0.114	↓	1.957	1.843	↓	↓	1.30	2.60
F_{16}	↓	4.0	0.75	20.6	0.114	↓	↓	↓	↓	↓	1.54	2.70
F_{17}	↓	7.0	0.36	60.0	0.200	↓	2.000	1.800	↓	↓	1.11	2.63
F_{20}	↓	↓	1.00	0	0.200	↓	↓	↓	↓	↓	0.61	2.14
F_{21}	↓	↓	↓	↓	↓	↓	↓	↓	↓	↓	0.40	1.39

**Leading edge angle. All trailing edges δ = 45 deg.

*For definition of variables see Figure 2.

TABLE 2. RUN LOG AND DATA SUMMARY

θ	Mach No.	Configuration	Run No.	Figure No.	ϕ
-10	0.5	B1F1	53	5a	0, 22.5, 45
-10	0.8	B1F1	57	b	0, 22.5, 45
-10	1.0	B1F1	59	c	0
-10	1.0	B1F1	61	d	0, 22.5
-10	1.1	B1F1	62	e	0, 22.5, -45
-10	1.2	B1F1	66	f	0, 22.5
-10	1.3	B1F1	67	g	0, 22.5, 45
-10	1.6	B1F1	35	h	↓
-10	2.0	B1F1	22	i	↓
-10	2.5	B1F1	7	j	↓
-10	3.0	B1F1	14	k	↓
0	0.8, 1.0	B1F1	80	6a	0, 22.5;0
0	1.2	B1F1	68	b	0, 22.5, 45
0	1.6	B1F1	36	c	↓
0	2.5	B1F1	6	d	↓
0	3.0	B1F1	15	e	↓
10	0.5	B1F1	70	7a	↓
10	0.8	B1F1	71	b	↓
10	1.0	B1F1	72	c	↓
10	1.1	B1F1	73	d	↓
10	1.2	B1F1	74	e	↓
10	1.3	B1F1	75	f	↓
10	1.6	B1F1	37	g	↓
10	2.0	B1F1	27	h	↓
10	2.5	B1F1	8	i	↓
10	3.0	B1F1	16	j	↓
22.5	1.6	B1F1	40	8a	↓
22.5	2.0	B1F1	25	b	↓
22.5	2.5	B1F1	11	c	↓
22.5	3.0	B1F1	19	d	↓
45	1.6	B1F1	41	9a	↓
45	2.0	B1F1	23	b	↓
45	2.5	B1F1	12	c	↓
45	3.0	B1F1	13	d	↓
112.5	0.5	B1F1	83	10a	↓
112.5	0.8	B1F1	84	b	↓
112.5	0.95, 1.0	B1F1	85	c	0, 22.5; 0
0	0.8	B1F2	92	11a,	0, 22.5, 45
0	1.2	B1F2	88	b	0, 22.5, 45
0	2.5	B1F2	47	c	0

TABLE 2. (Concluded)

θ	Mach No.	Configuration	Run No.	Figure No.	φ
0	0.5, 0.8	B1F17	86	12a	0, 22.5; 0
	1.0	B1F17	91	b	0, 22.5, 45
	1.2	B1F17	87	c	↓
	1.6	B1F17	42	d	
	3.0	B1F17	20	e	
	0.5, 0.72	B1F20	78	13a	0, 22.5; 0
	0.95, 1.0	B1F20	79	b	↓
	1.1, 1.3	B1F20	77	c	
	1.2	B1F20	76	d	0, 22.5
	1.6	B1F20	38	e	0, 22.5, 45
	2.0	B1F20	26	f	↓
	2.5	B1F20	9	g	
	3.0	B1F20	17	h	
	0.5, 0.8	B1F21	81	14a	0, 22.5; 0
	0.95, 1.0	B1F21	82	b	↓
	1.1, 1.3	B1F21	90	c	
	1.2	B1F21	89	d	0, 22.5, 45
	1.6	B1F21	39	e	↓
	2.0	B1F21	24	f	
	2.5	B1F21	10	g	
	3.0	B1F21	18	h	
	0.8, 1.0	B2F1	93	15a	0, 22.5; 0
	1.2	B2F1	97	b	0, 22.5, 45
	1.6	B2F1	33	c	0
	2.5	B2F1	46	d	0
	0.8, 1.0	B3F2	94	16a	0, 22.5; 0
	1.2, 1.3	B3F2	95	b	0, 22.5; 0
	1.6	B3F2	43	c	0, 22.5, 45
	2.0	B3F2	49	d	0, 22.5, 45
	2.5	B3F2	45	e	0
	1.2, 1.3	B3F16	96	17a	0, 22.5; 0
	1.6	B3F16	44	b	0, 22.5, 45
	2.0	B3F16	48	c	↓
	3.0	B3F16	50	d	
	1.0	B1F1	69	18a	Varying
↓	2.0	B1F1	28.29	b	Varying

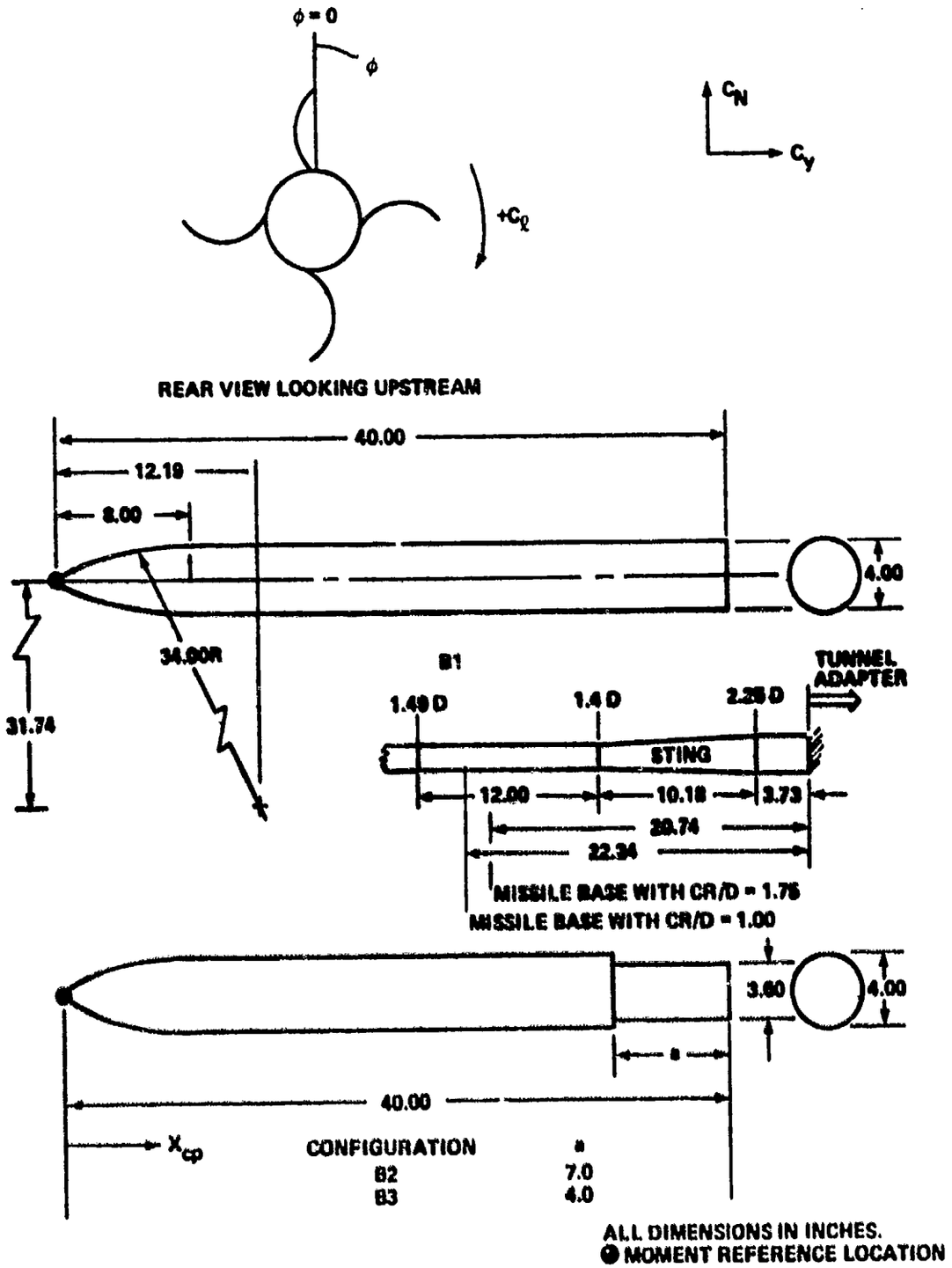
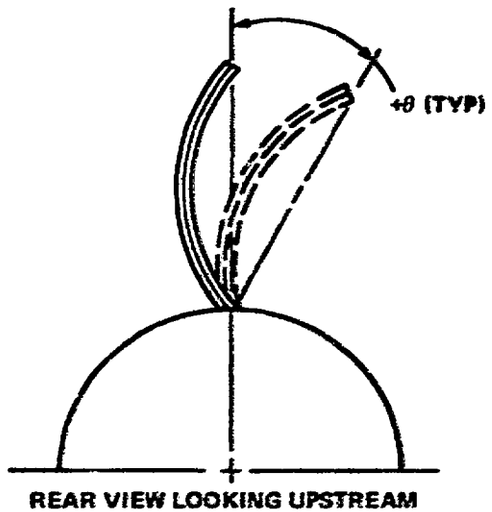
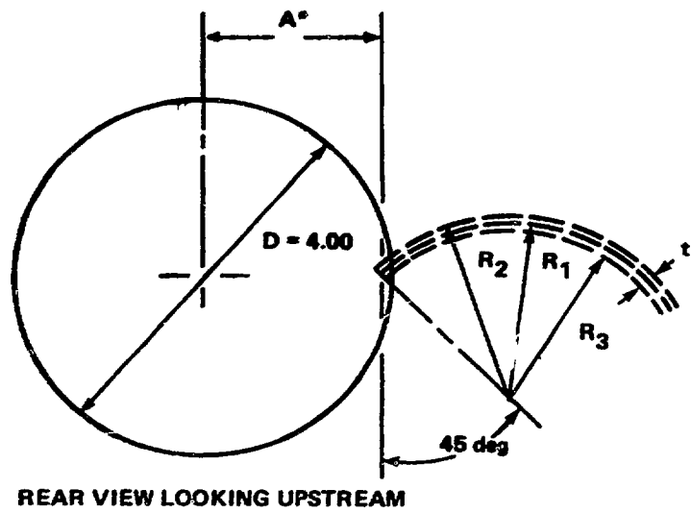
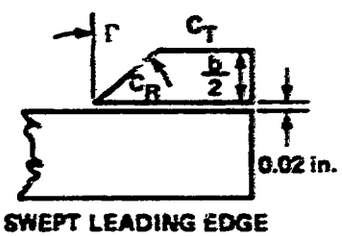
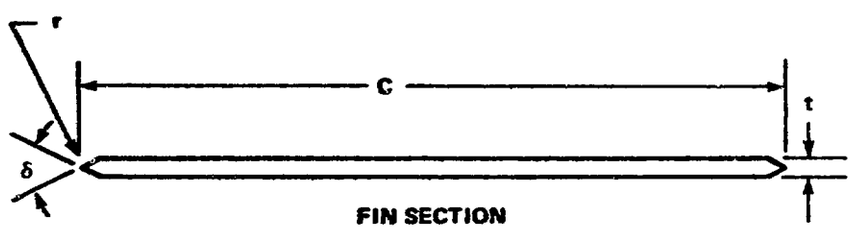


Figure 1. External body geometry.



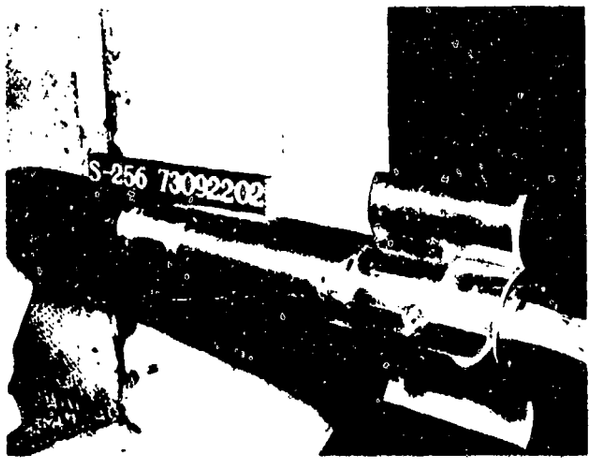




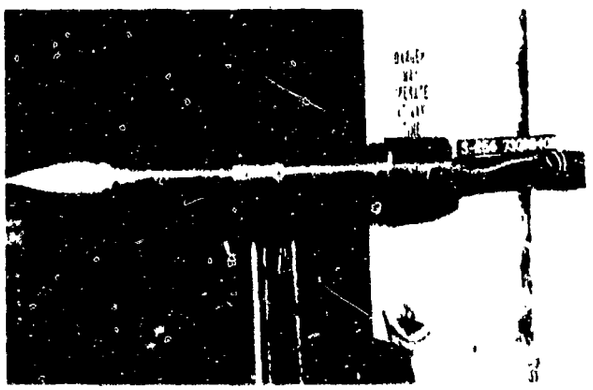


NOTE: * – FOR DIMENSIONS SEE TABLE 1

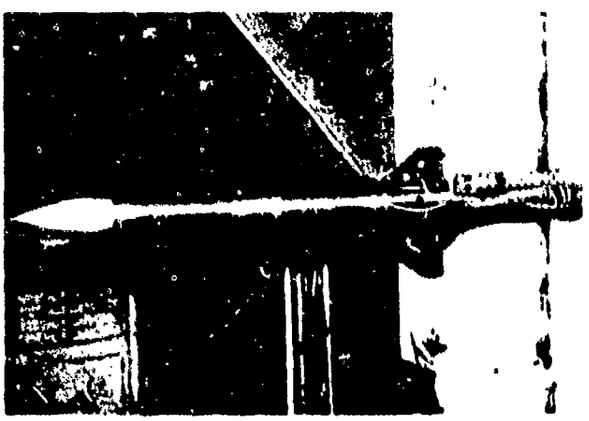
Figure 2. WAF geometry.



MODEL INSTALLATION, BIFI, θ = 0 deg



MODEL INSTALLATION, BIFI, θ = 112.5 deg



MODEL INSTALLATION, BIFI7, Λ = 60 deg, θ = 0

Figure 3. WAF model photos.

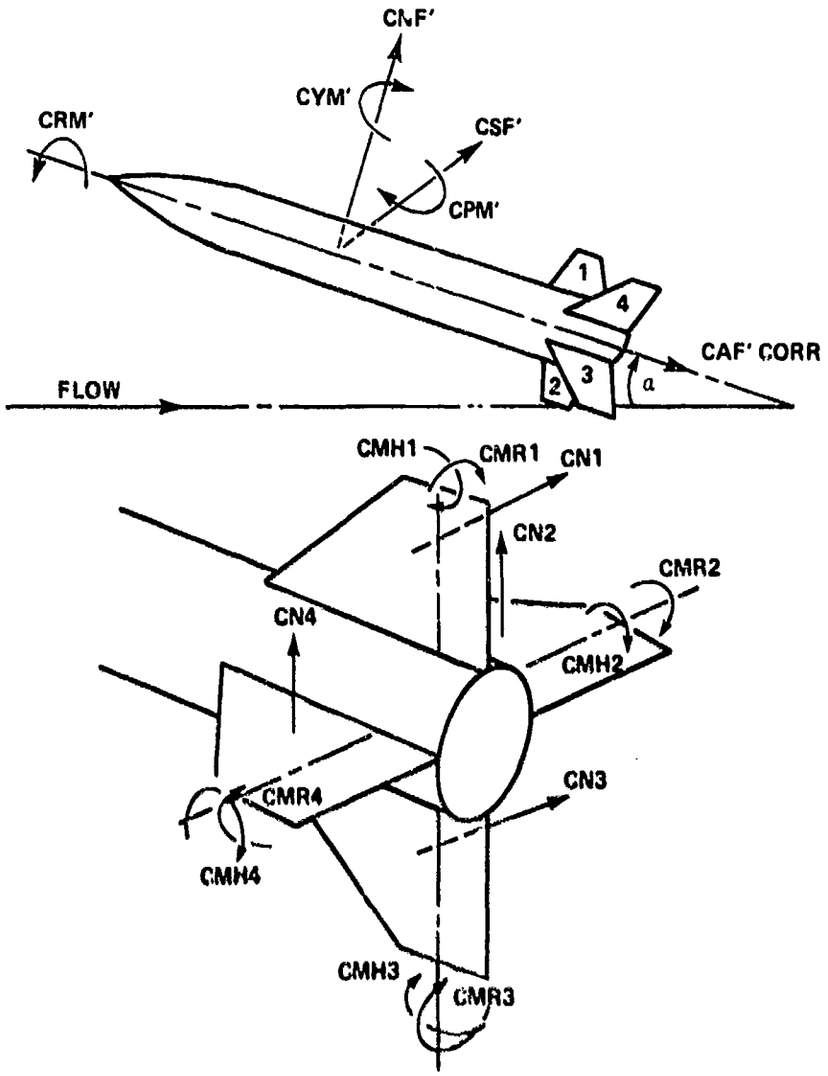


Figure 4. Sign convention.

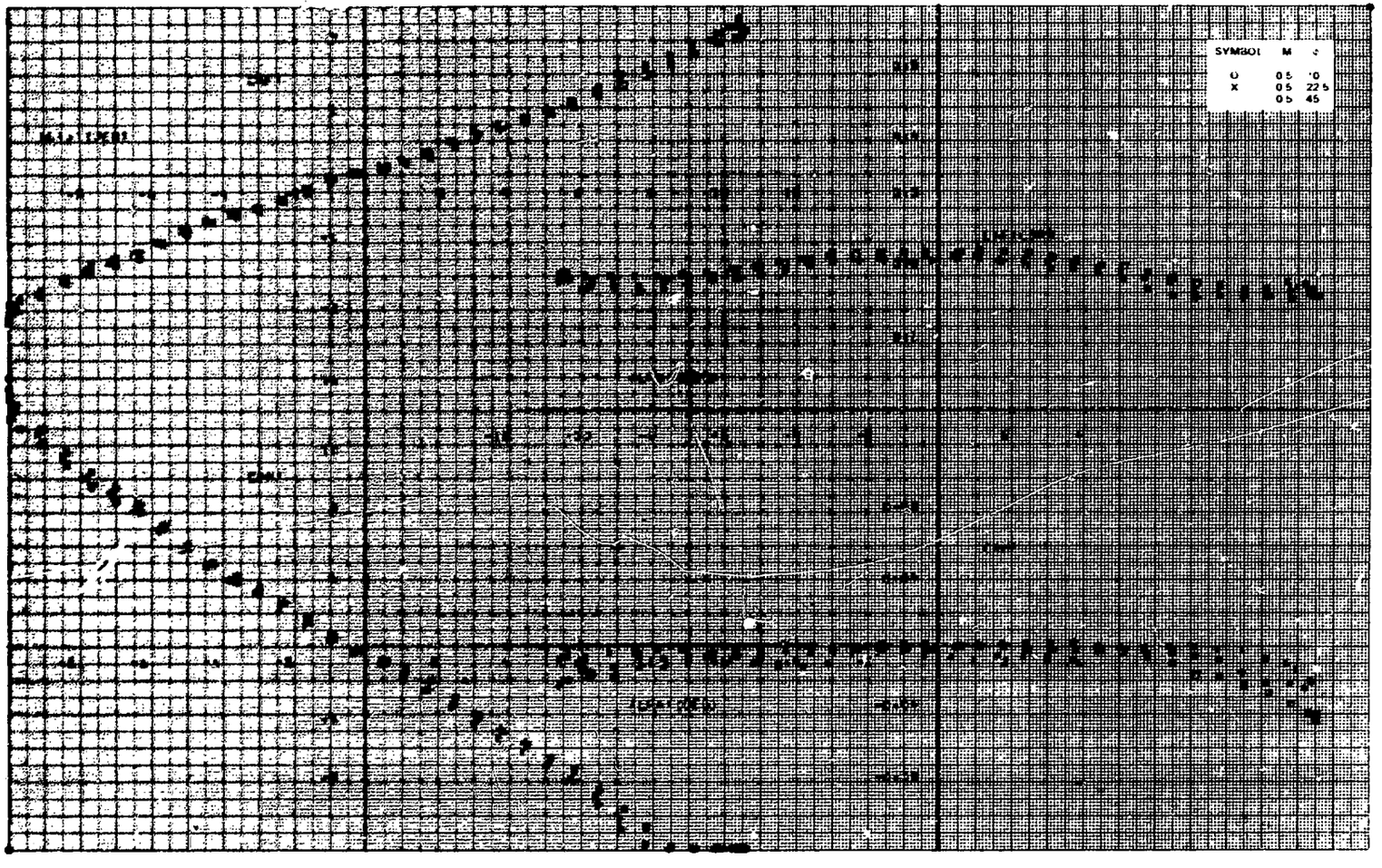


Figure 5a. Aerodynamic stability coefficients, CR/D = 1.75, γ = 0 deg, θ = -10 deg, M_∞ = 0.5.

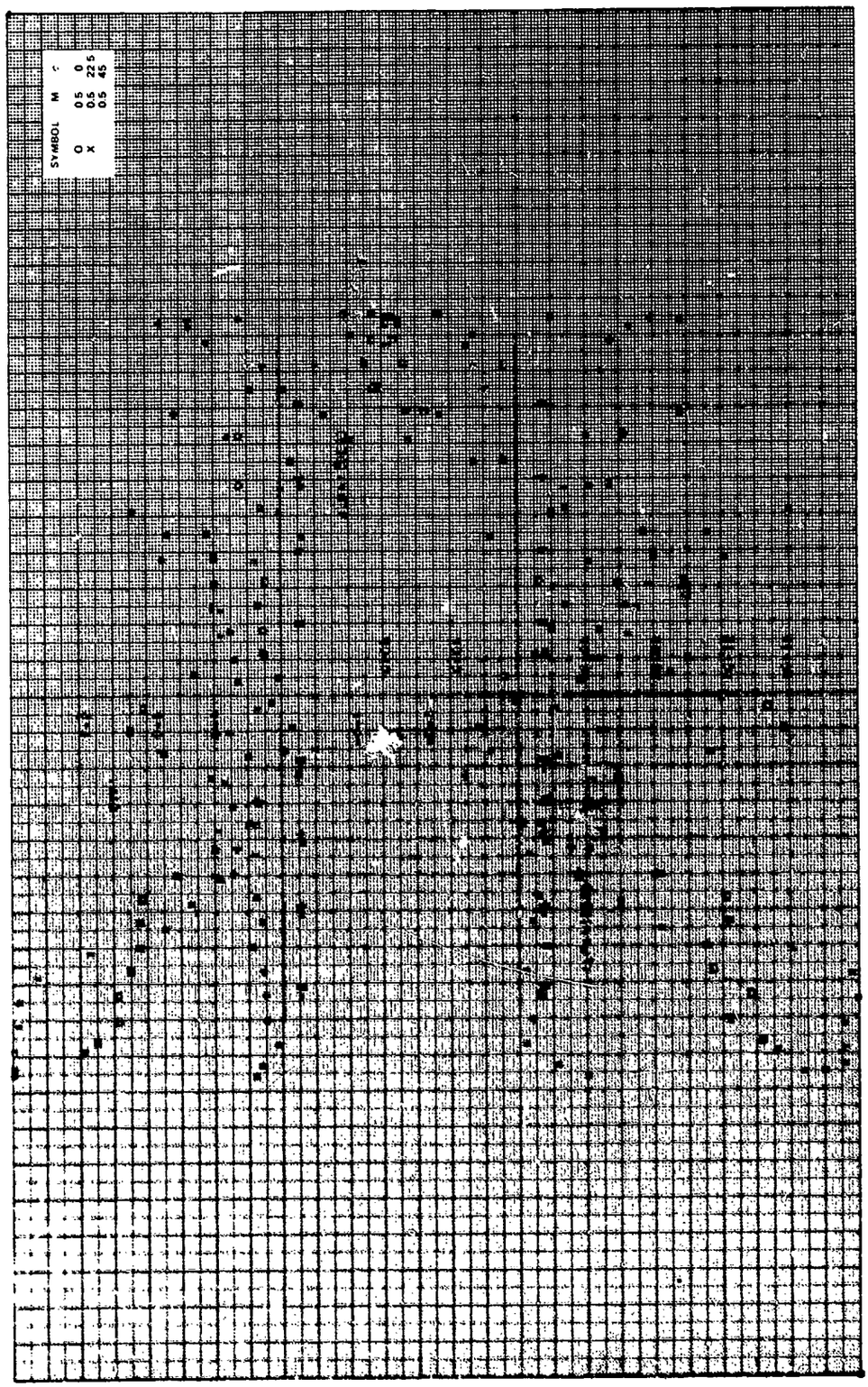


Figure 5a. Continued.

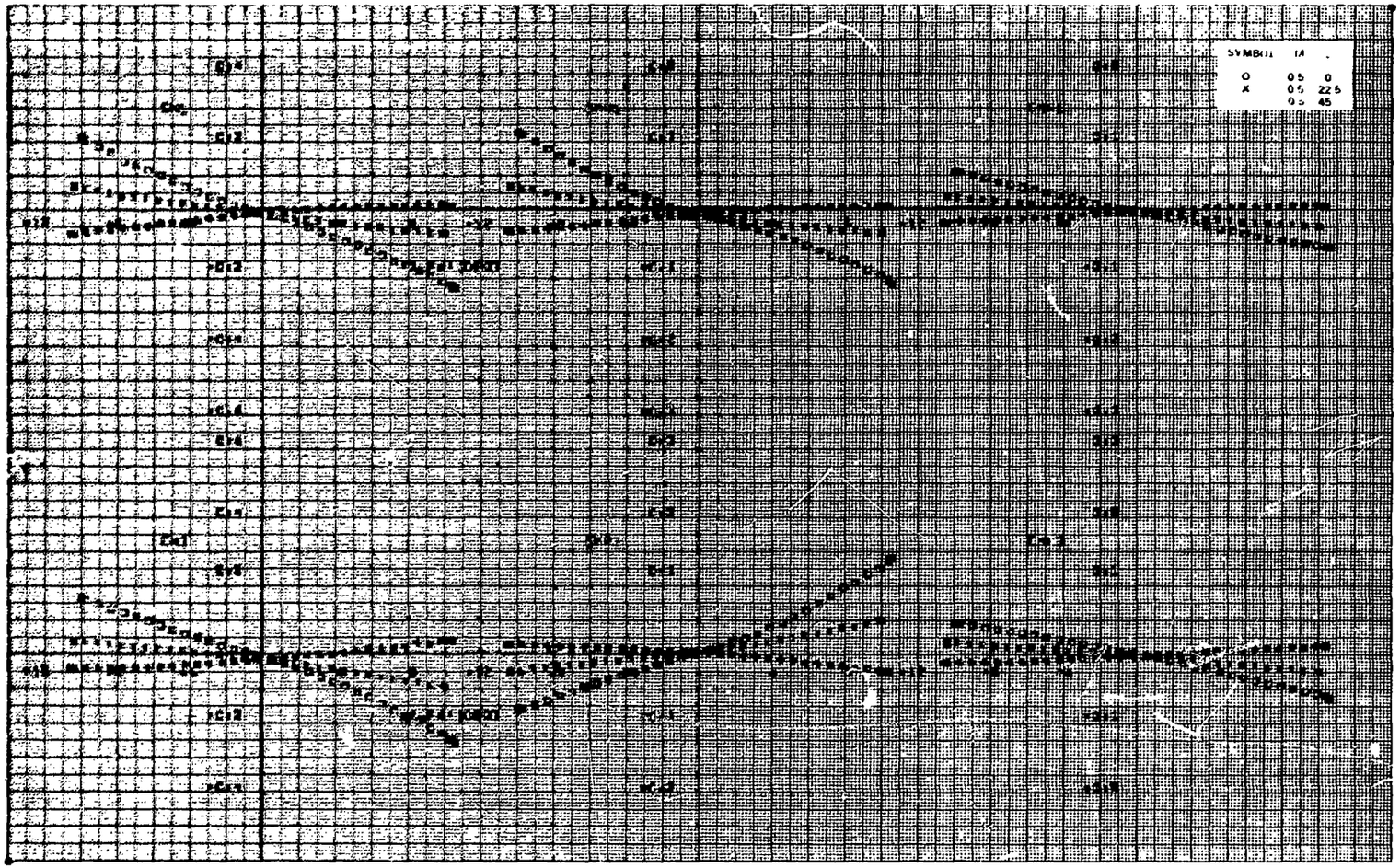


Figure 5a. Continued.

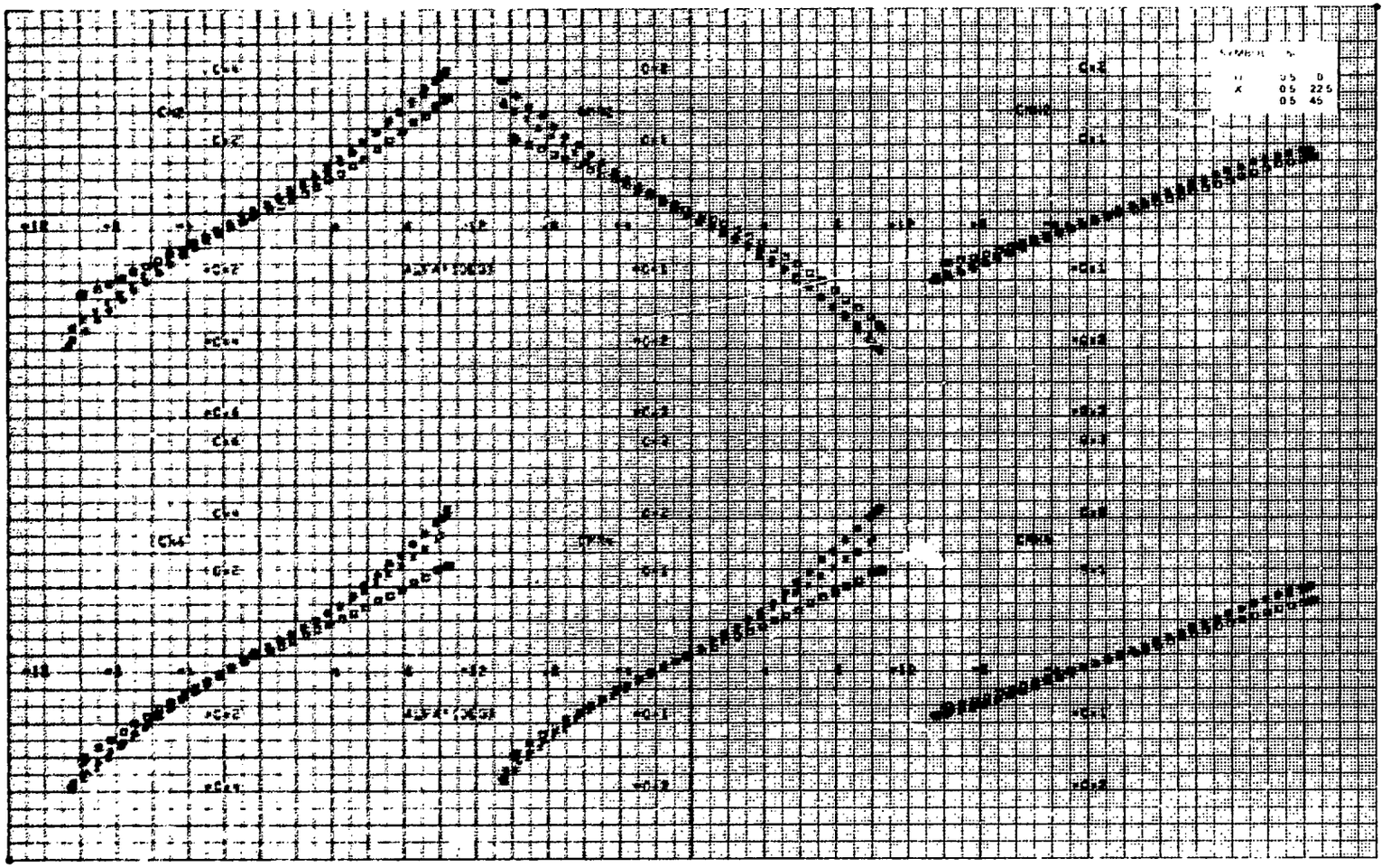


Figure 5i. Concluded.

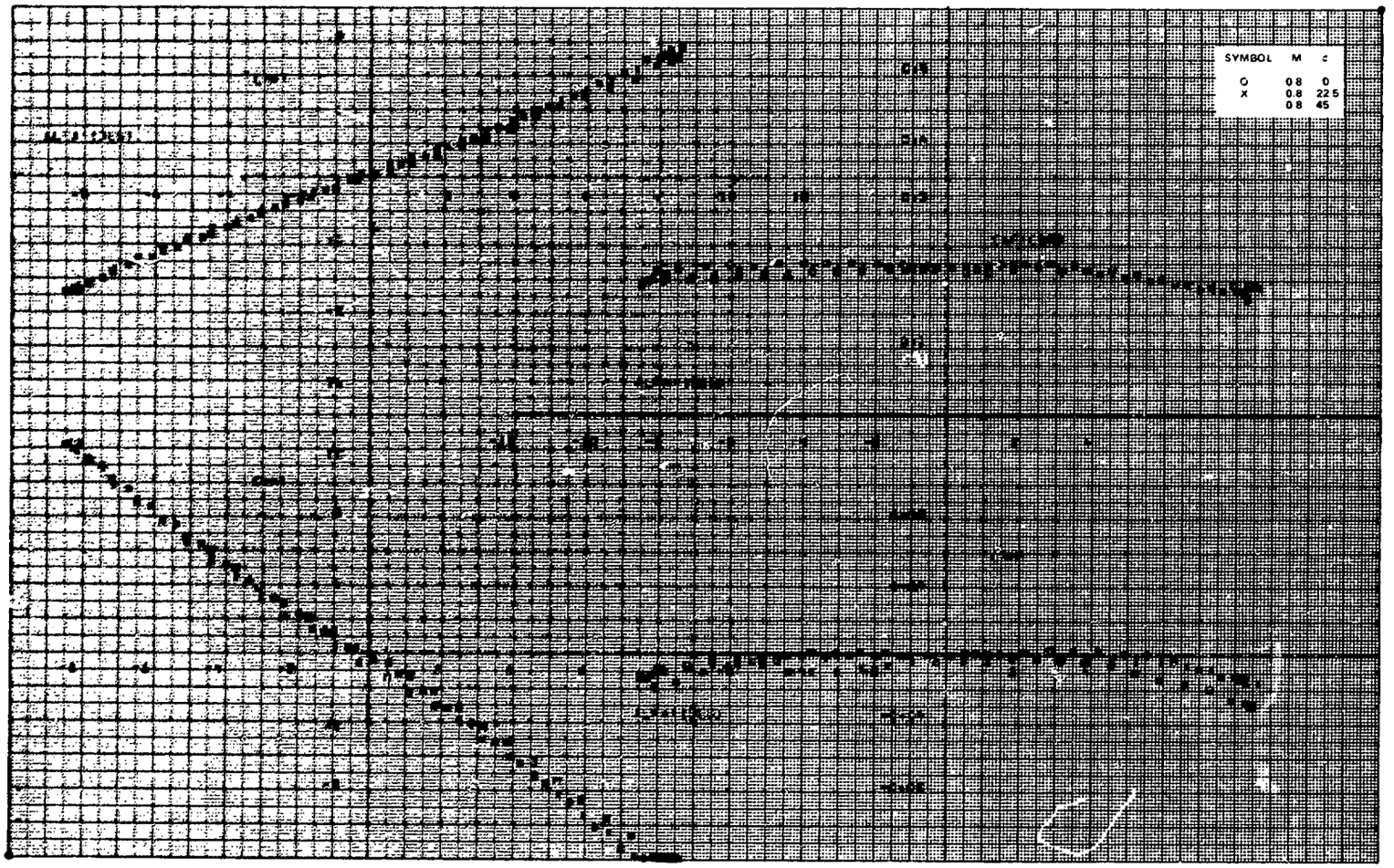


Figure 5b. Aerodynamic stability coefficients, CR/D = 1.75, ϕ = 0 deg, ϵ = -10 deg, M_∞ = 0.8.

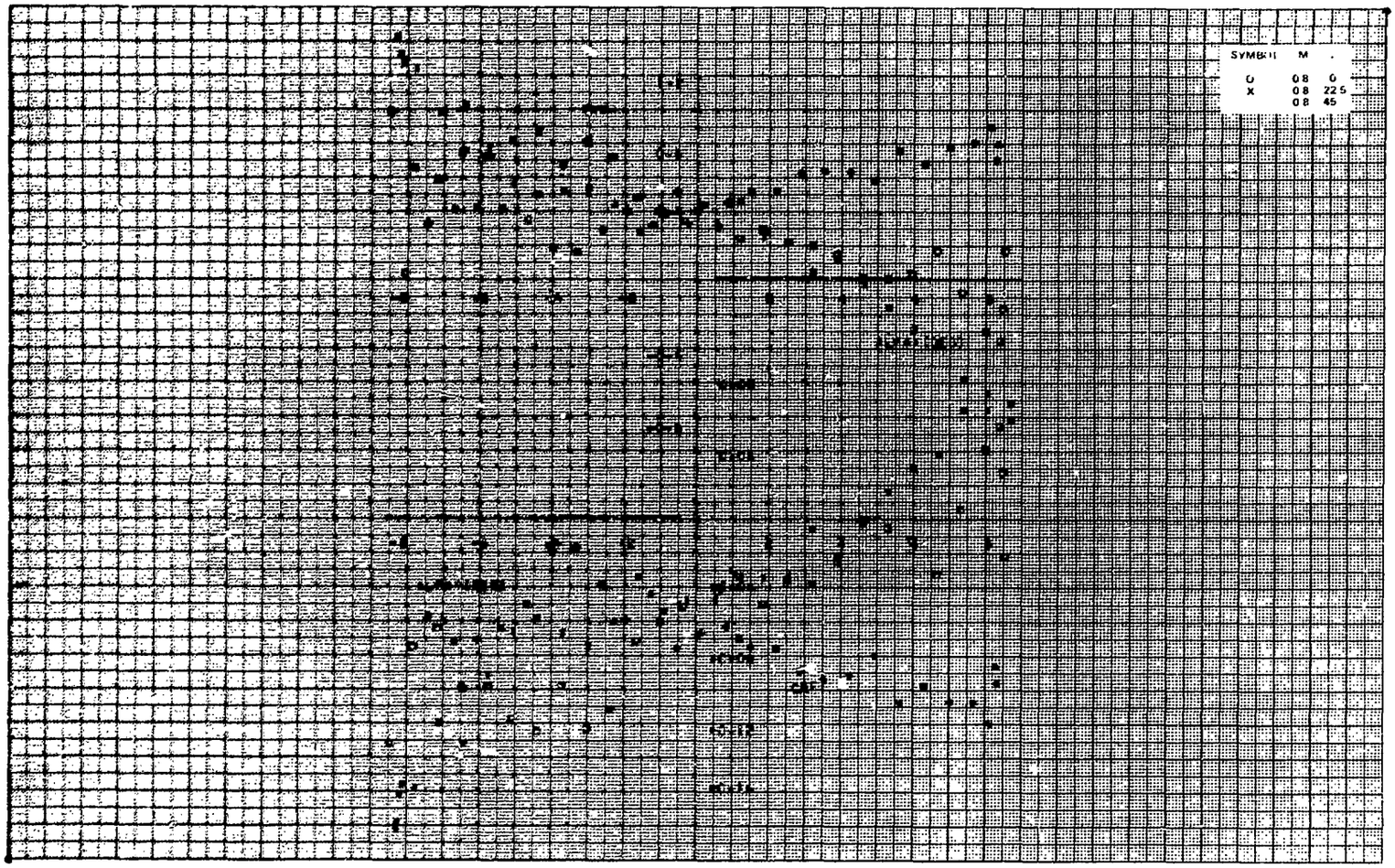


Figure 5b. Continued.

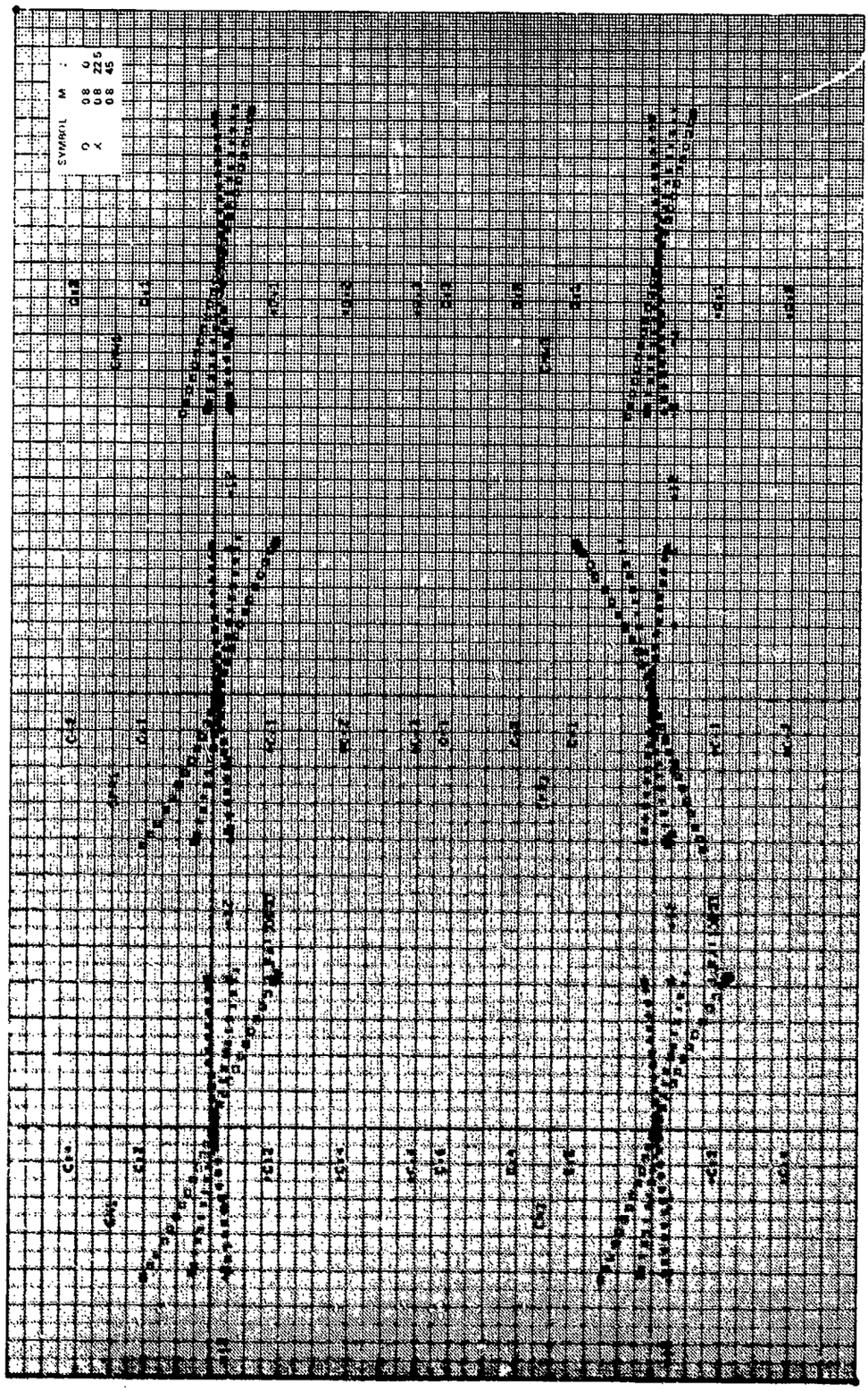
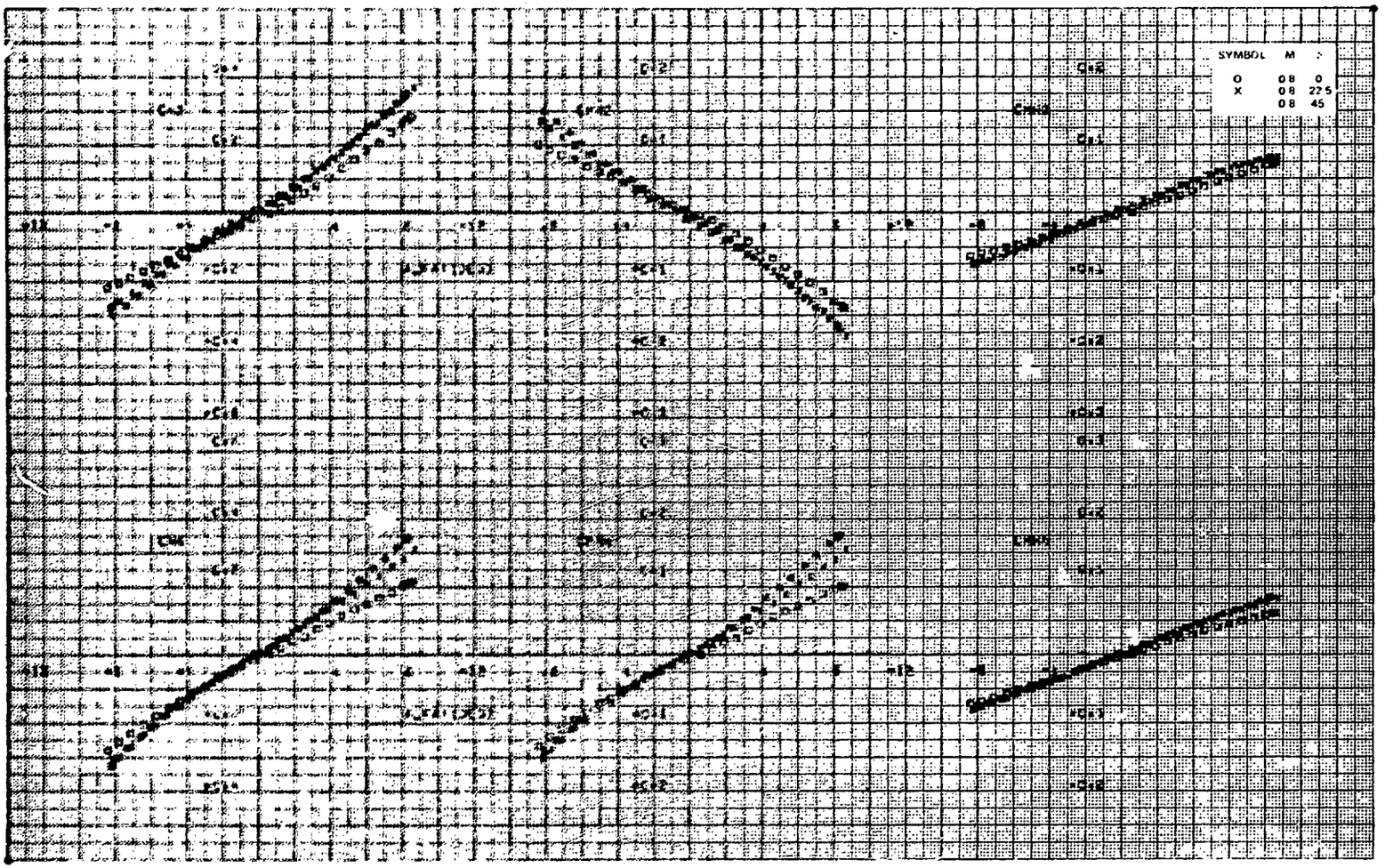


Figure 5b. Continued.


SYMBOL M
O 08 0
X 08 22 5
08 45

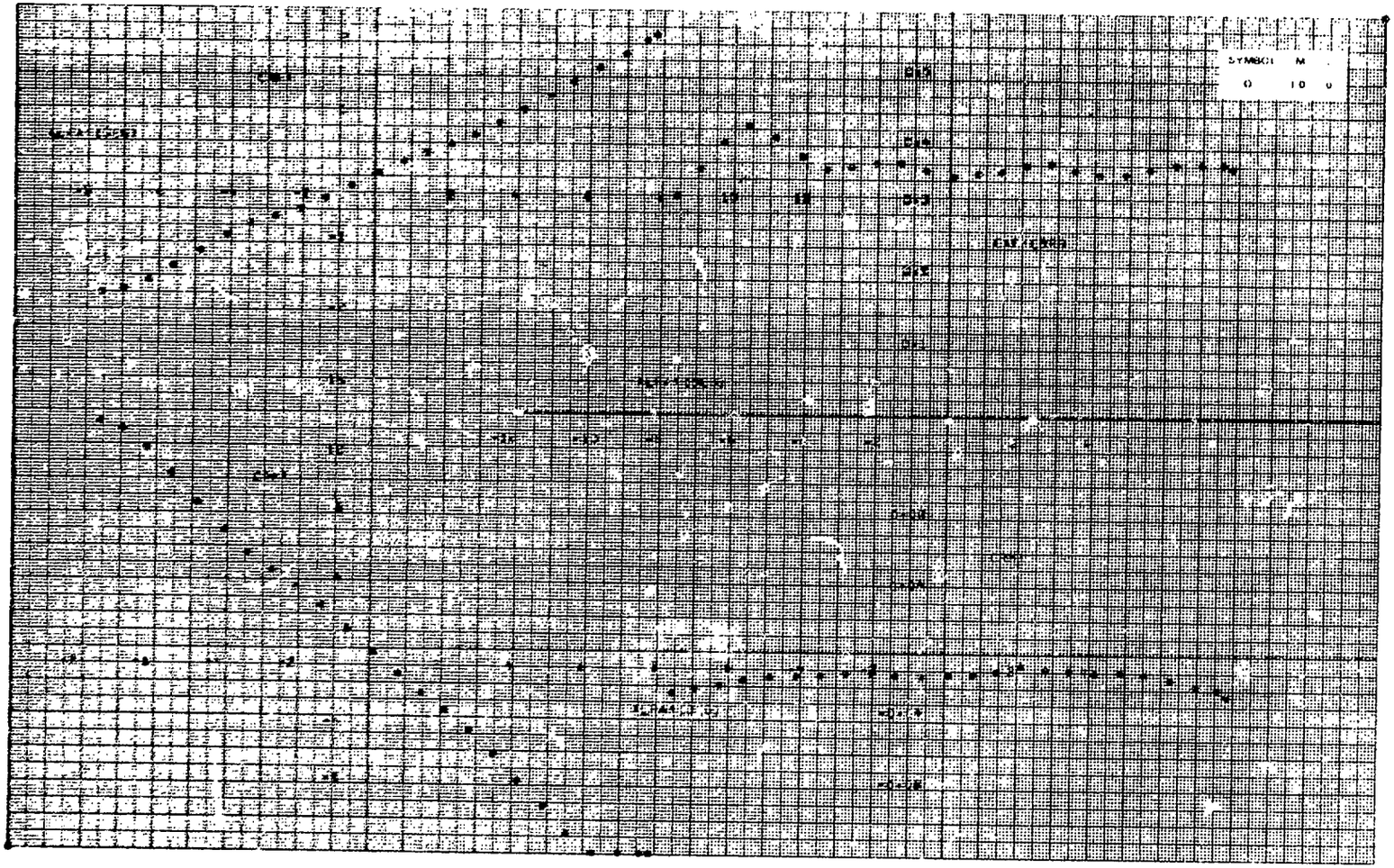


Figure 5a. Aerodynamic stability coefficients, CR/D = 1.75, γ = 0 deg, θ = -10 deg, M_∞ = 1.0.

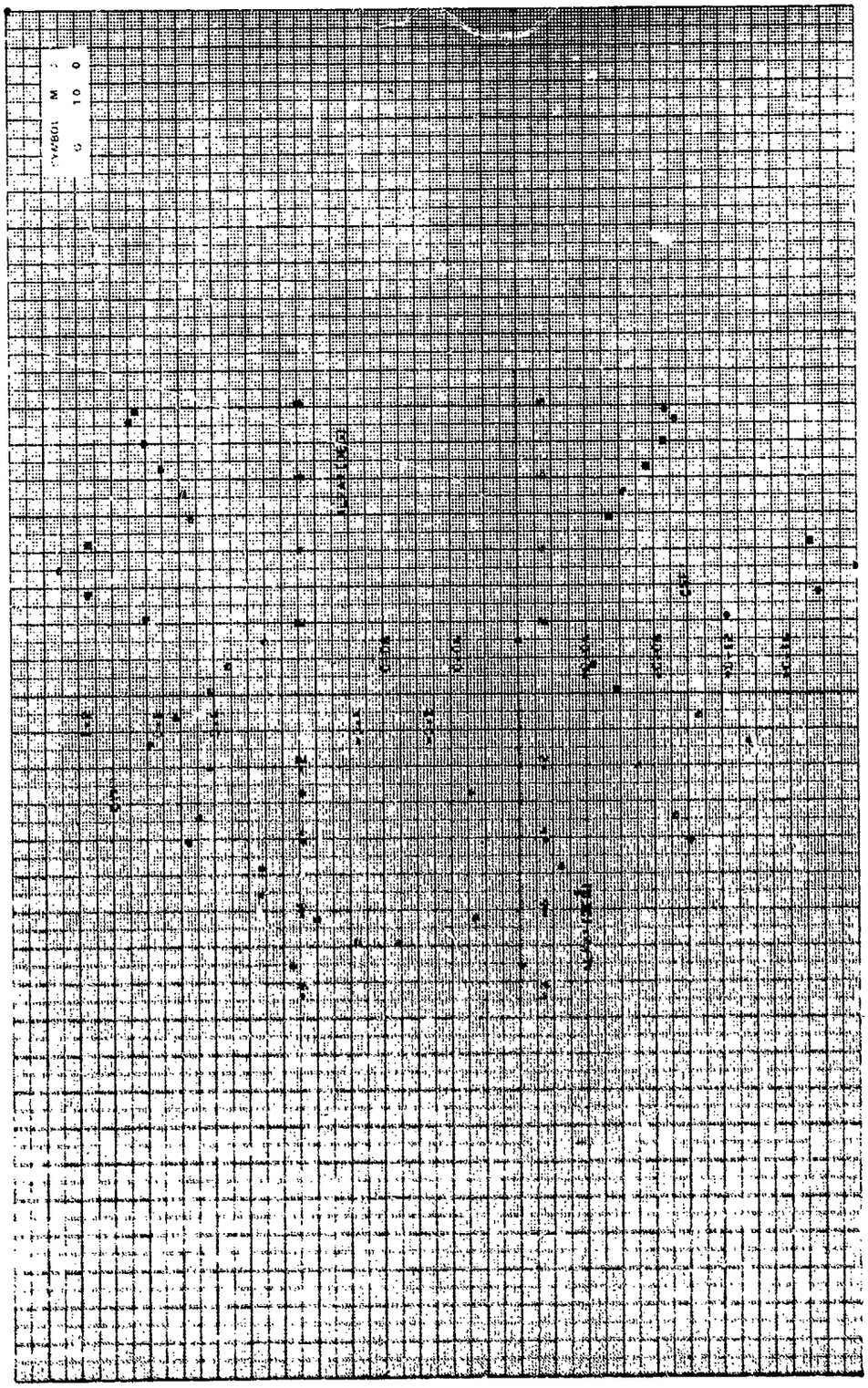


Figure 5c. Continued.

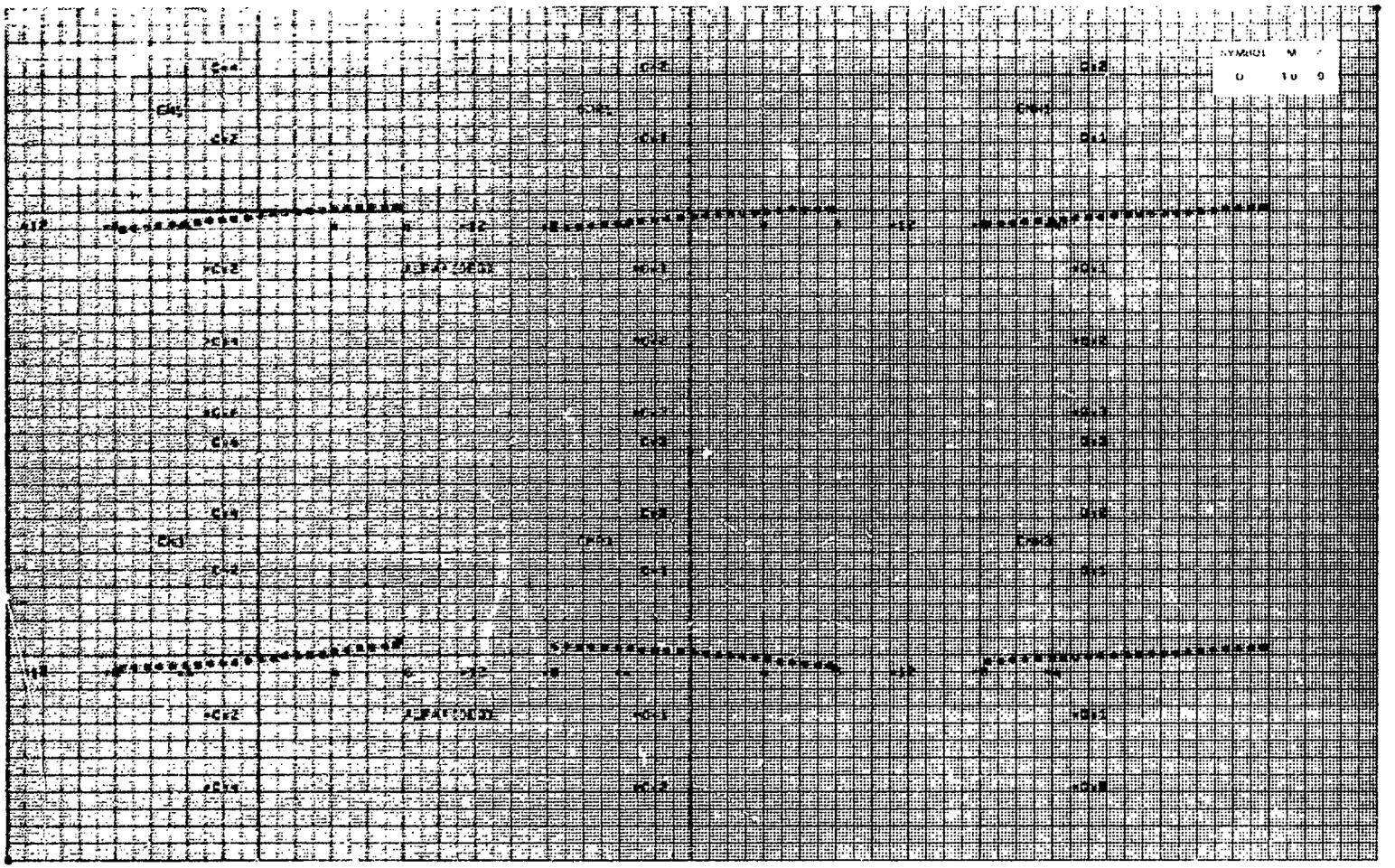


Figure 3c. Continued

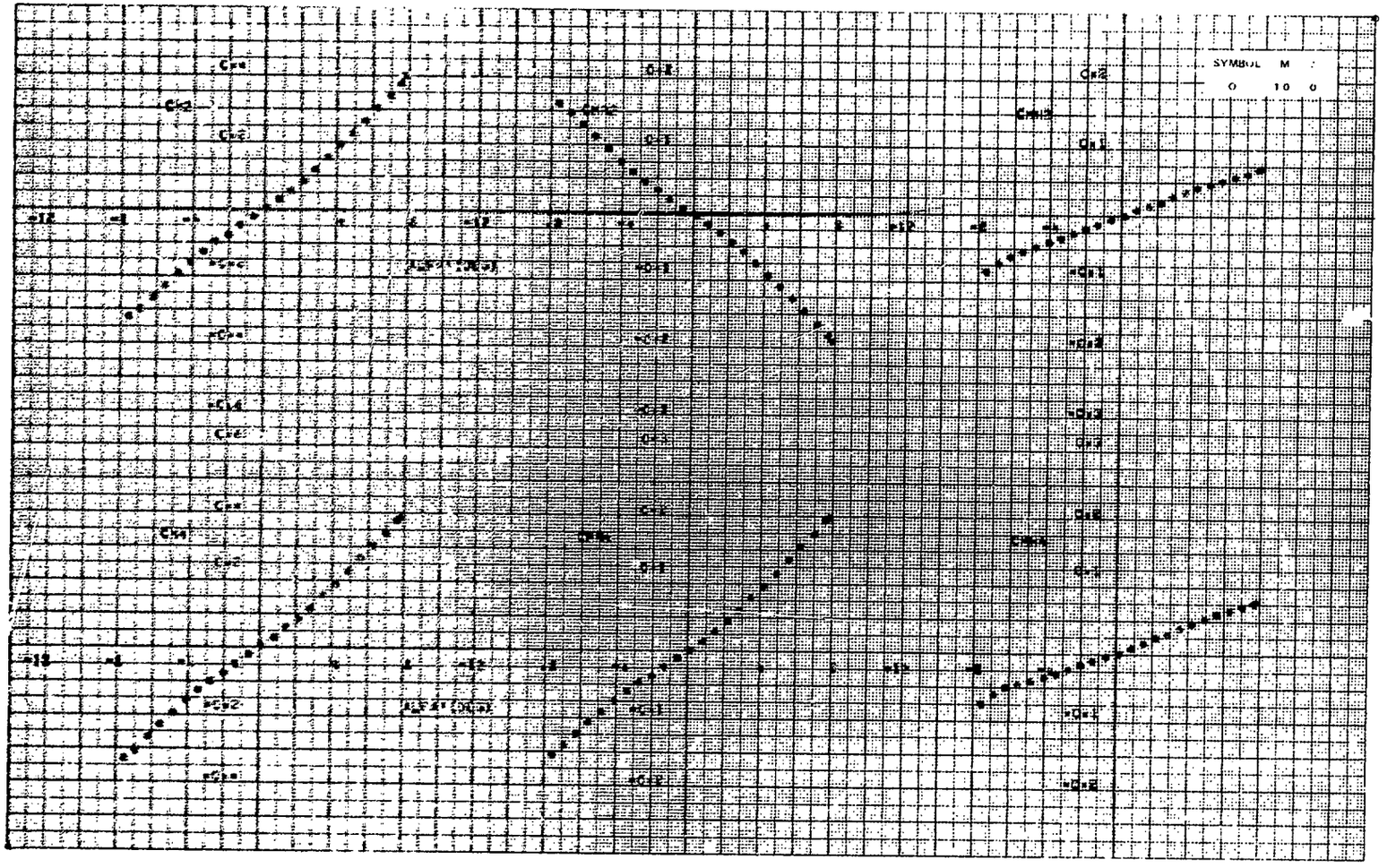
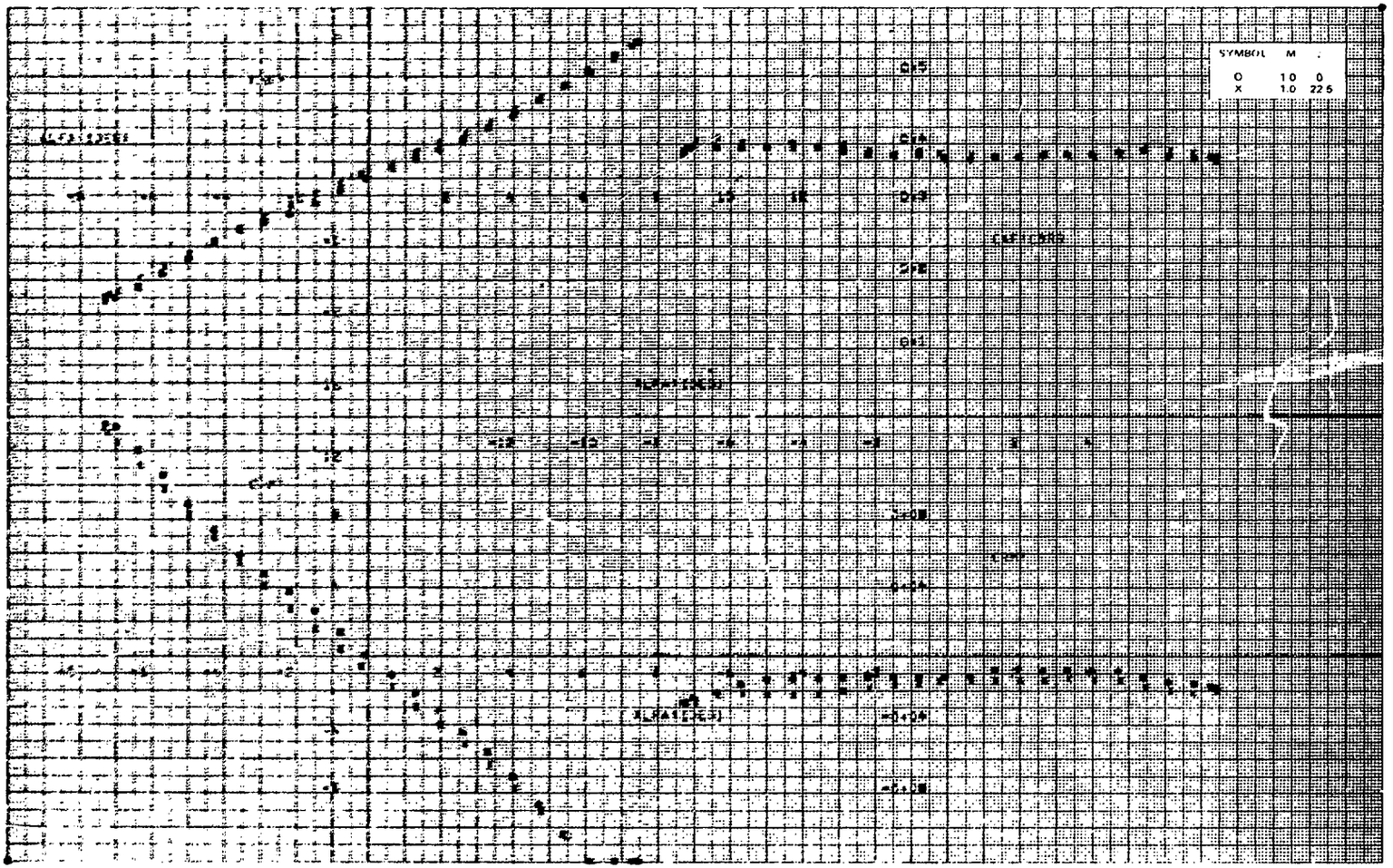
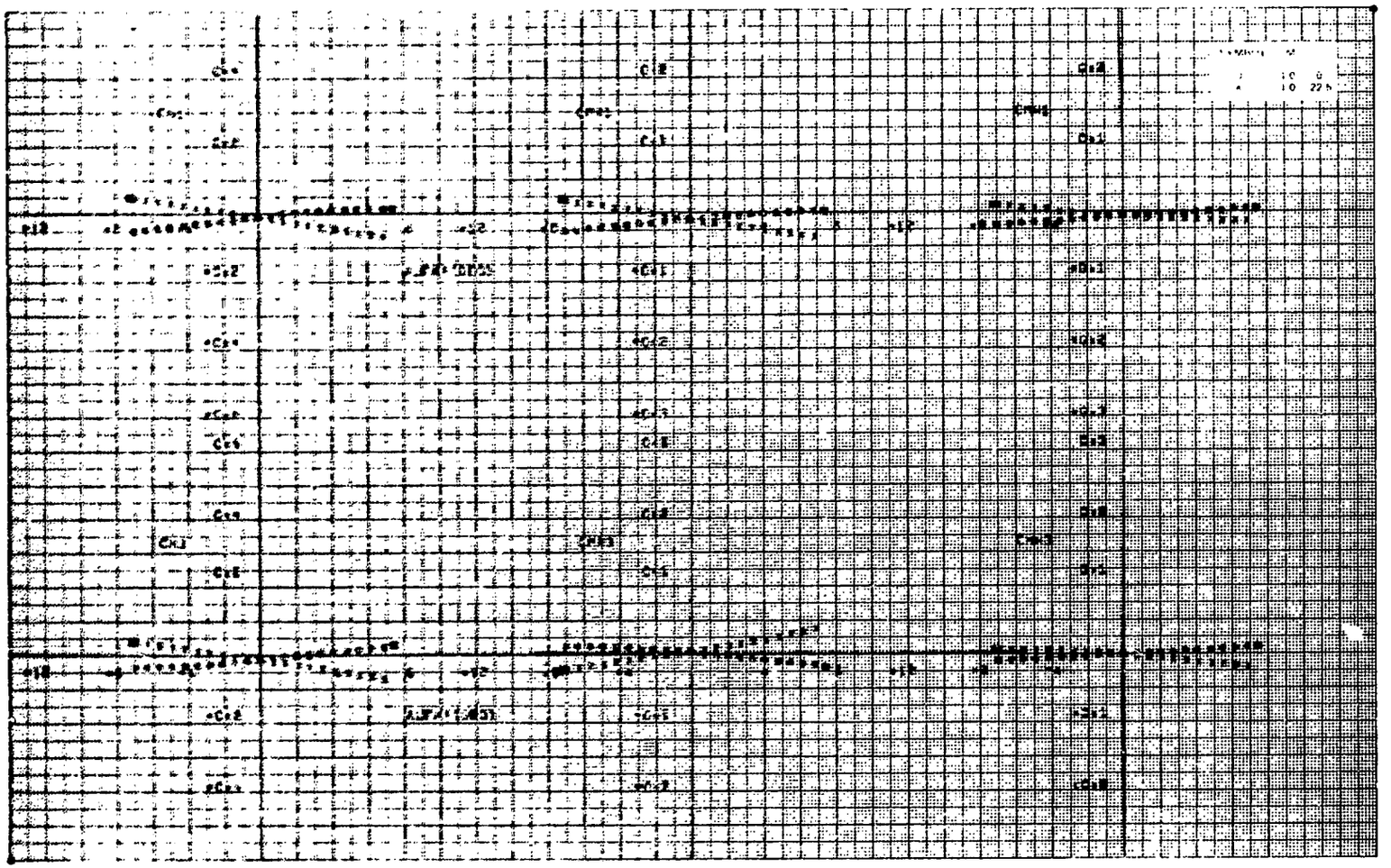


Figure 5c. Concluded.



.0.



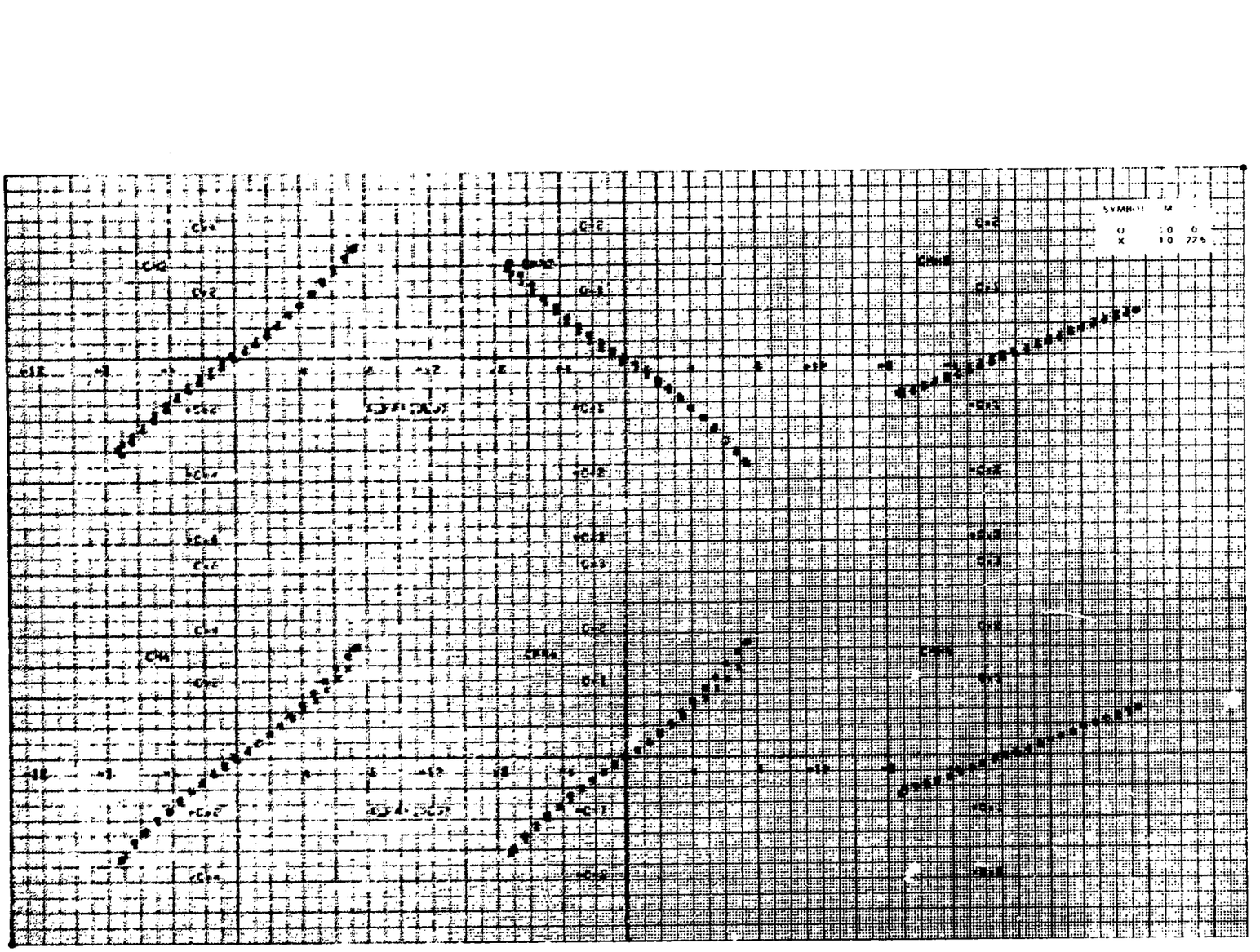
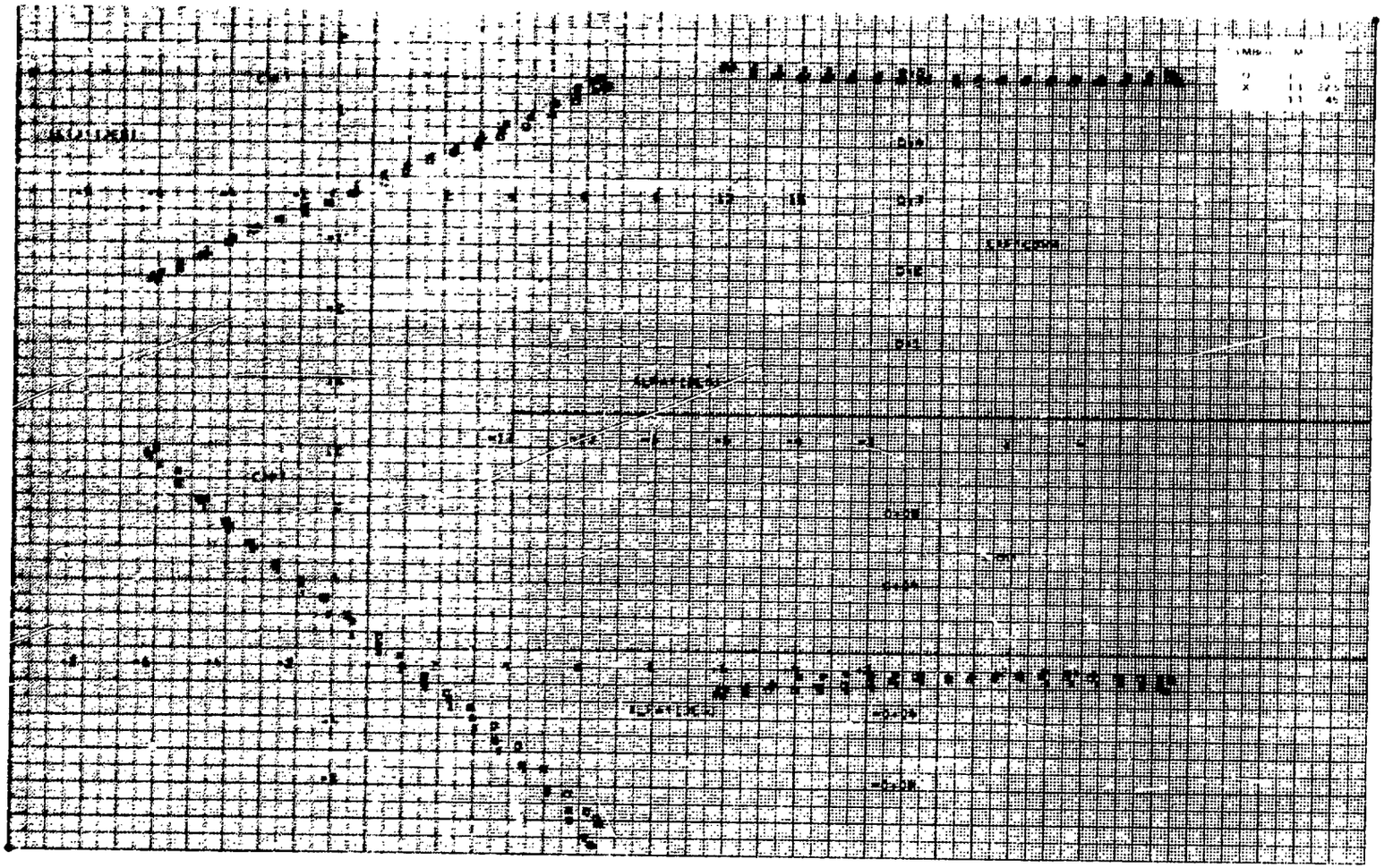
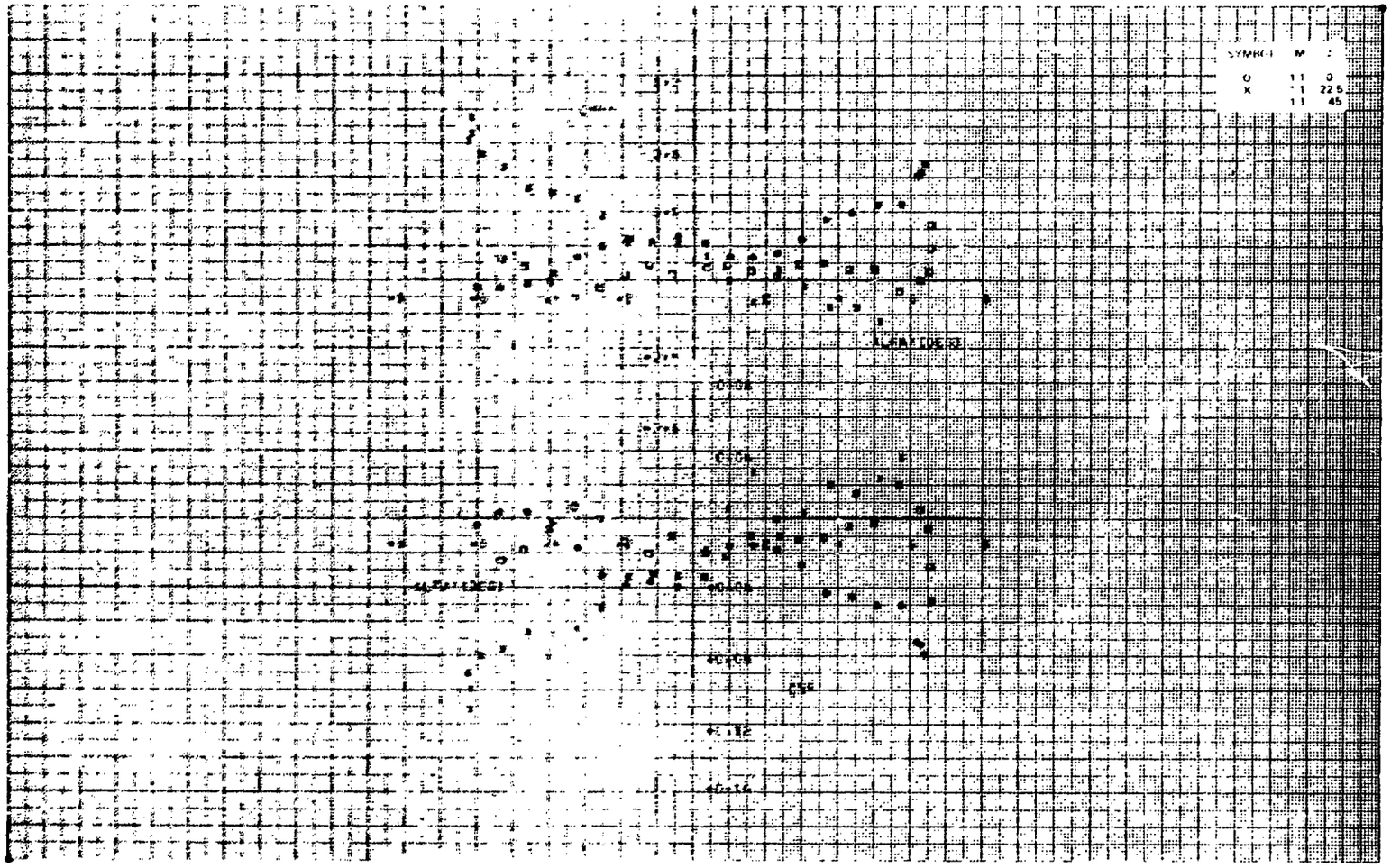


Figure 10. Concluded.




SYMBOL M
O 11 0
X 11 22.5
11 45

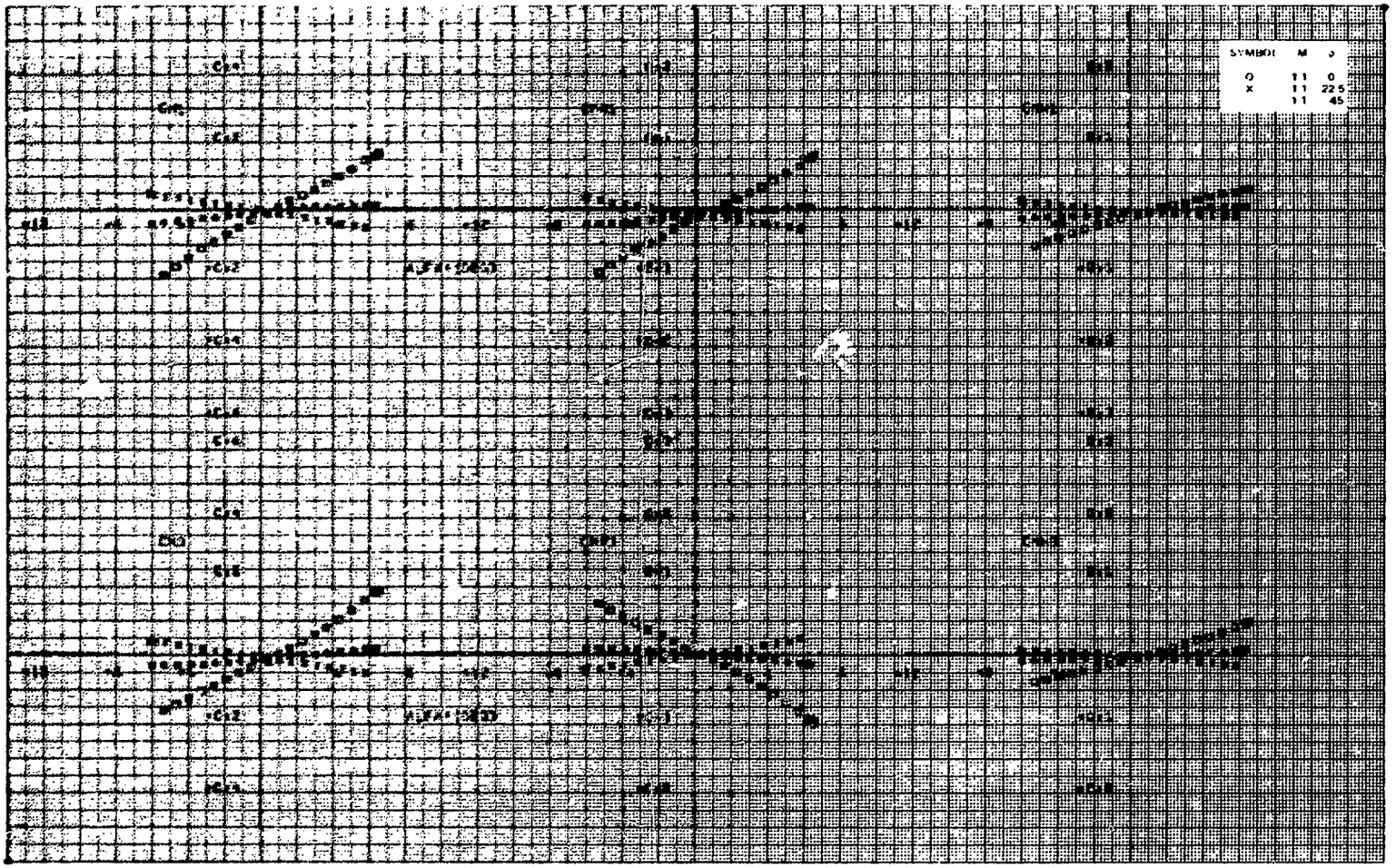


Figure 5e. Continued.

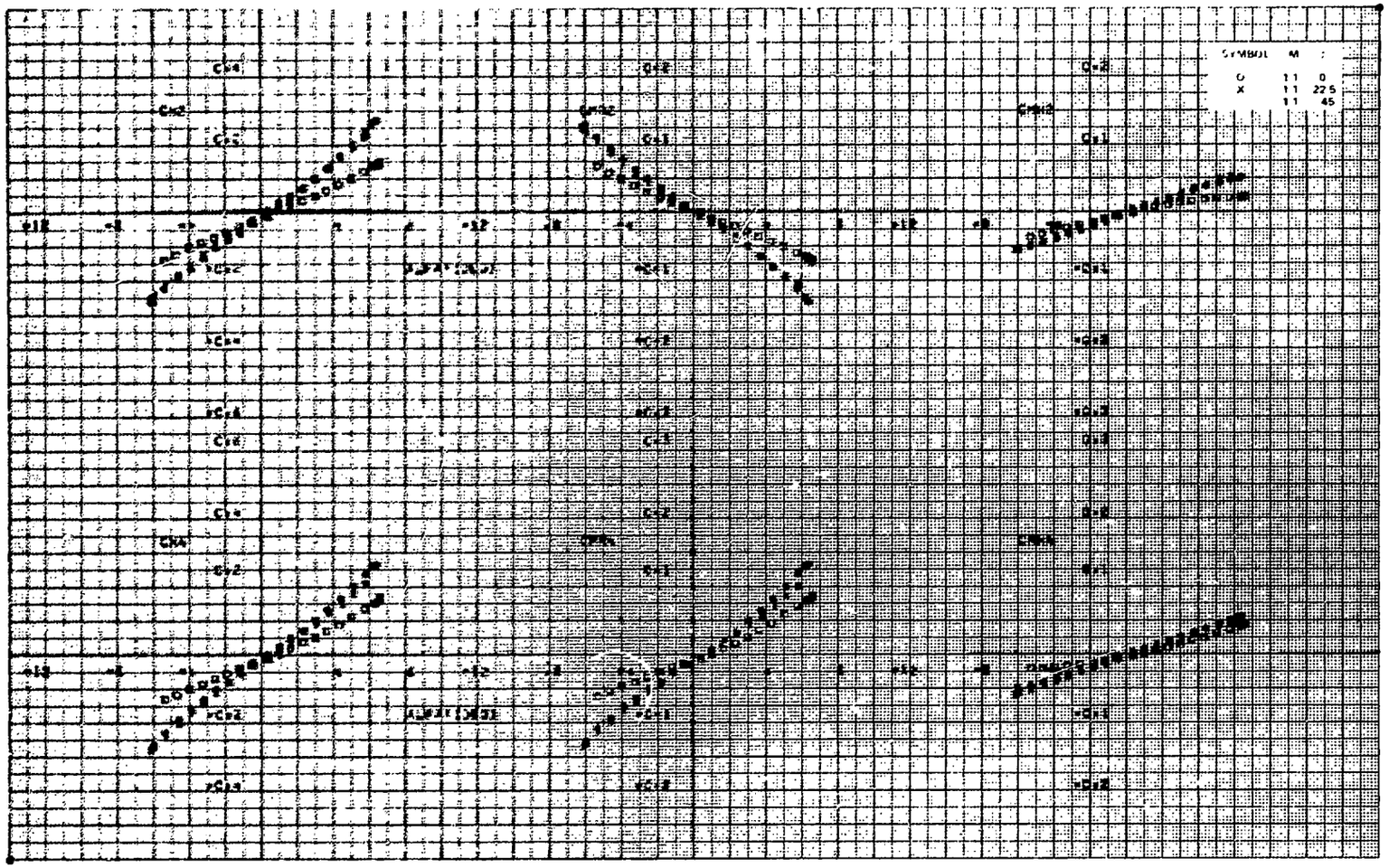
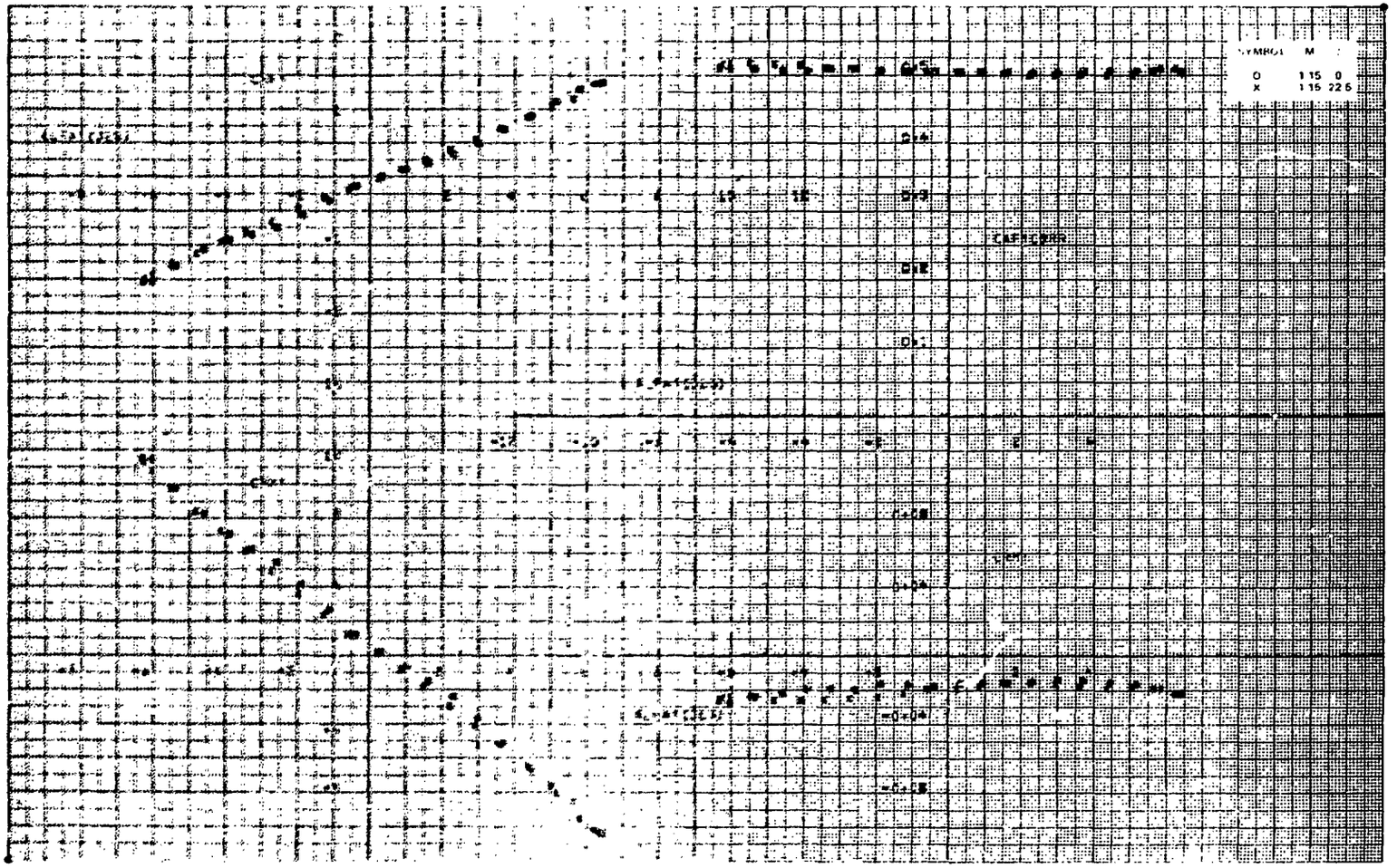
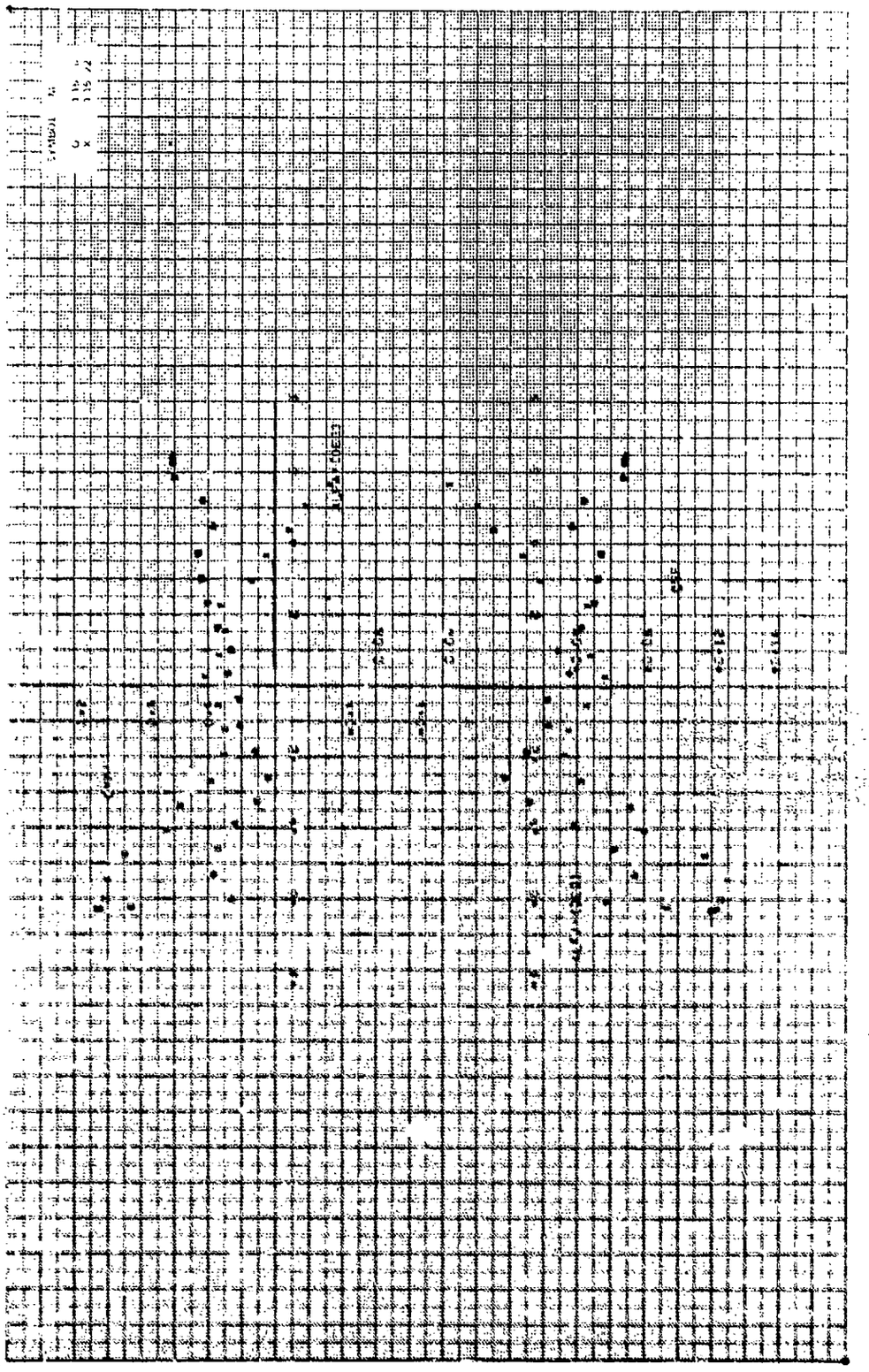


Figure [illegible] Continued.



$M_\infty = 1.2$.



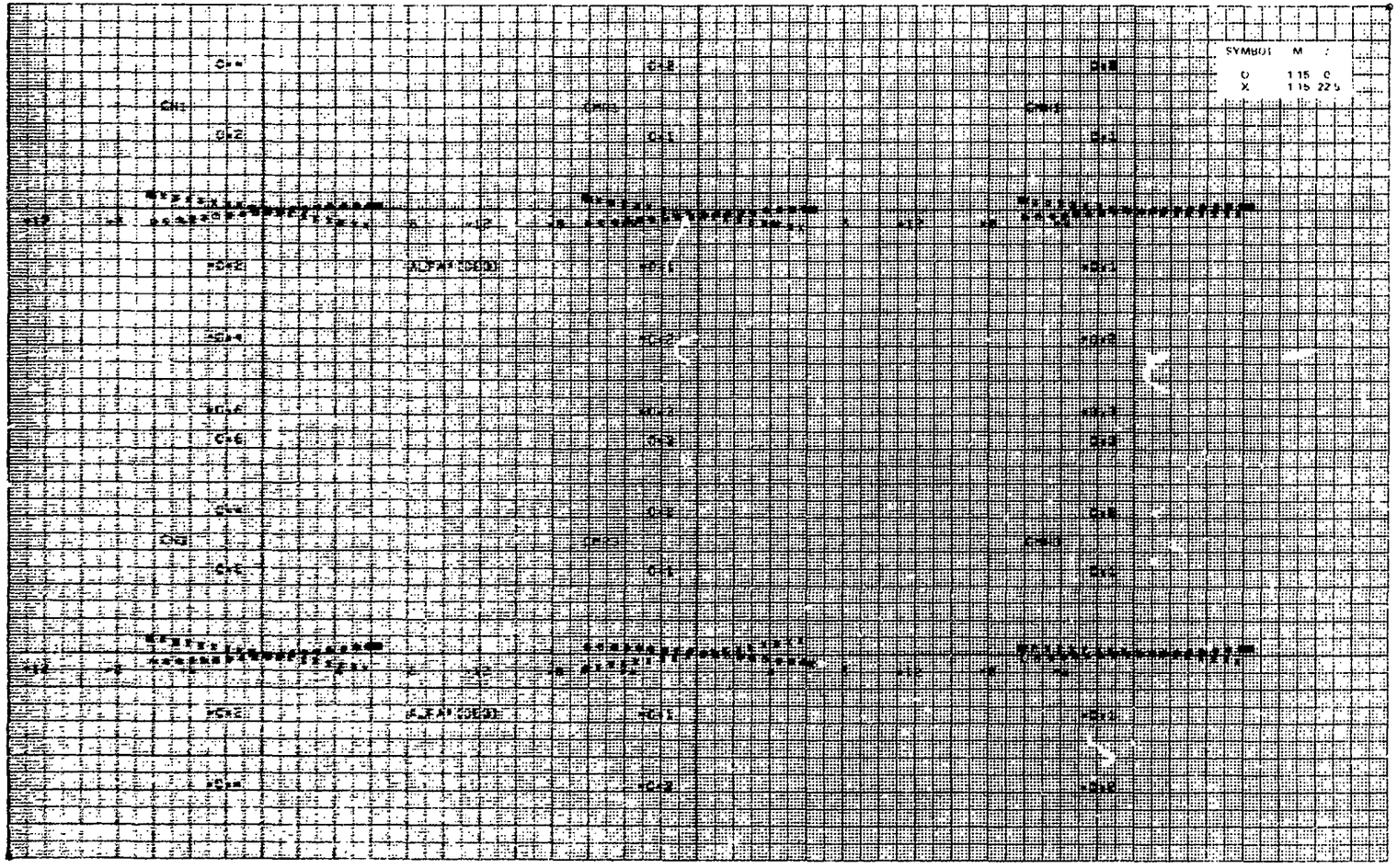
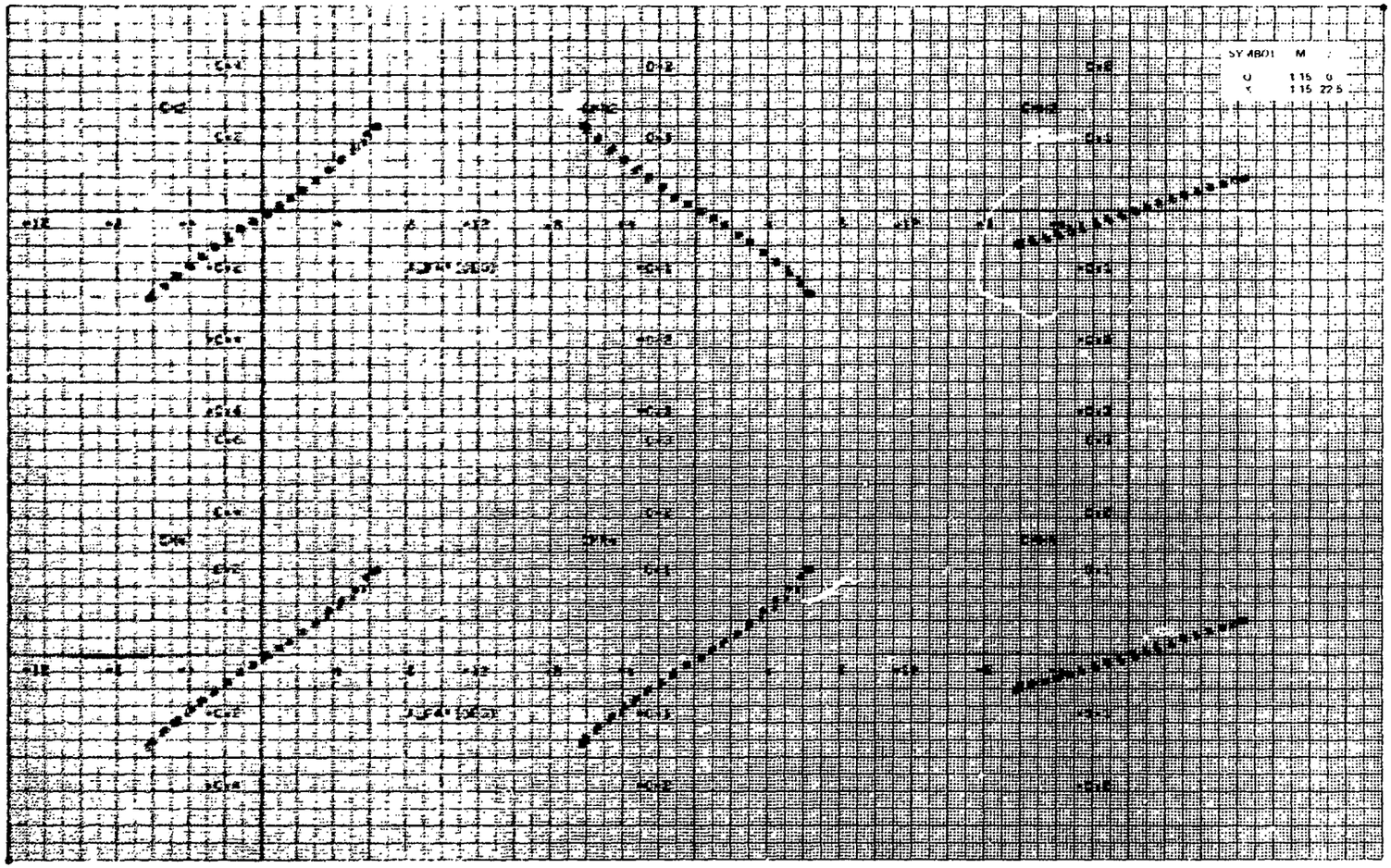


Figure 31. Continued.



Concluded.

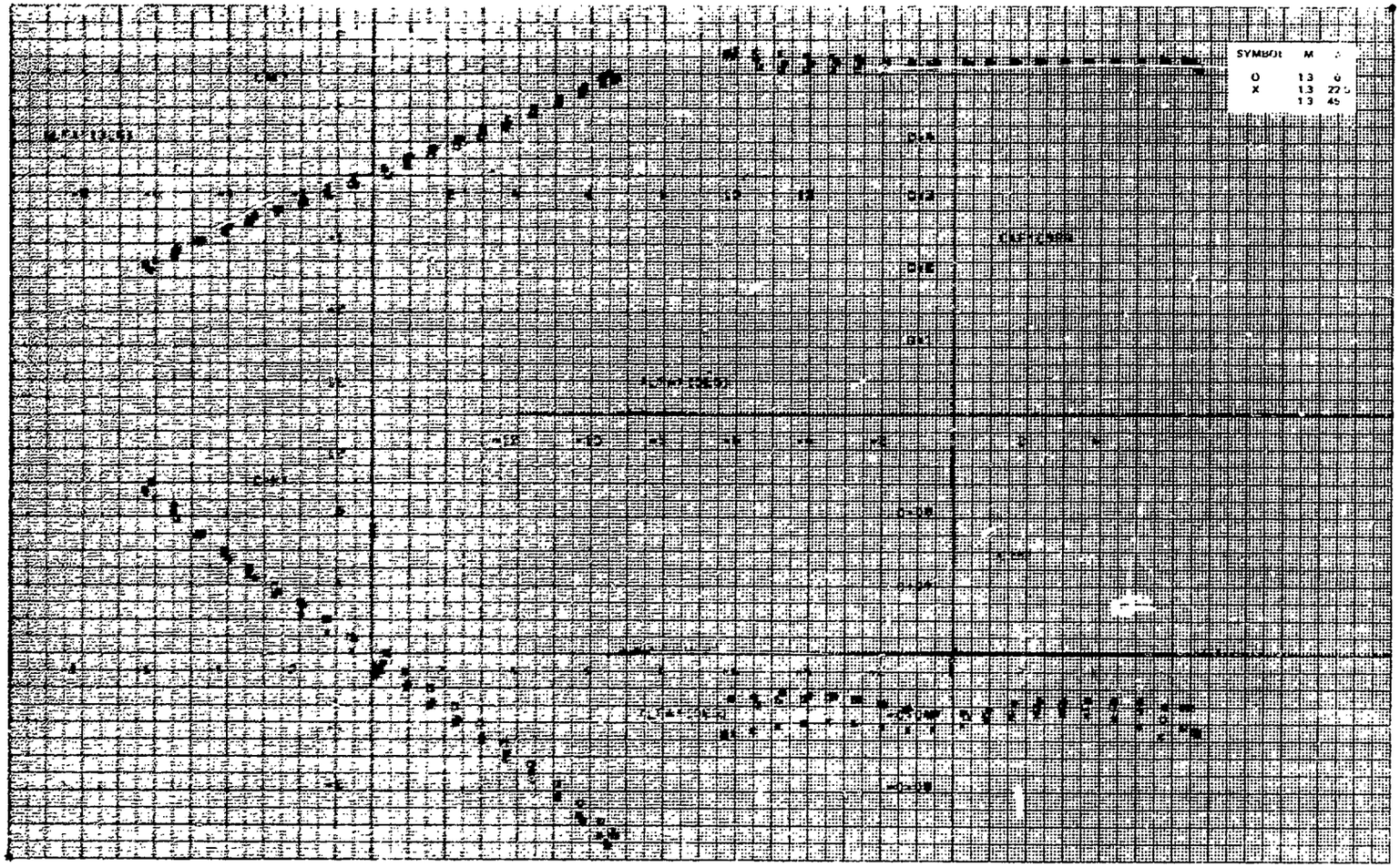


Figure 34. Longitudinal aerodynamic coefficients, $\ell_R/D = 1.75$, $\beta = 0$ deg, $\delta = -10$ deg, $M_\infty = 1.3$.

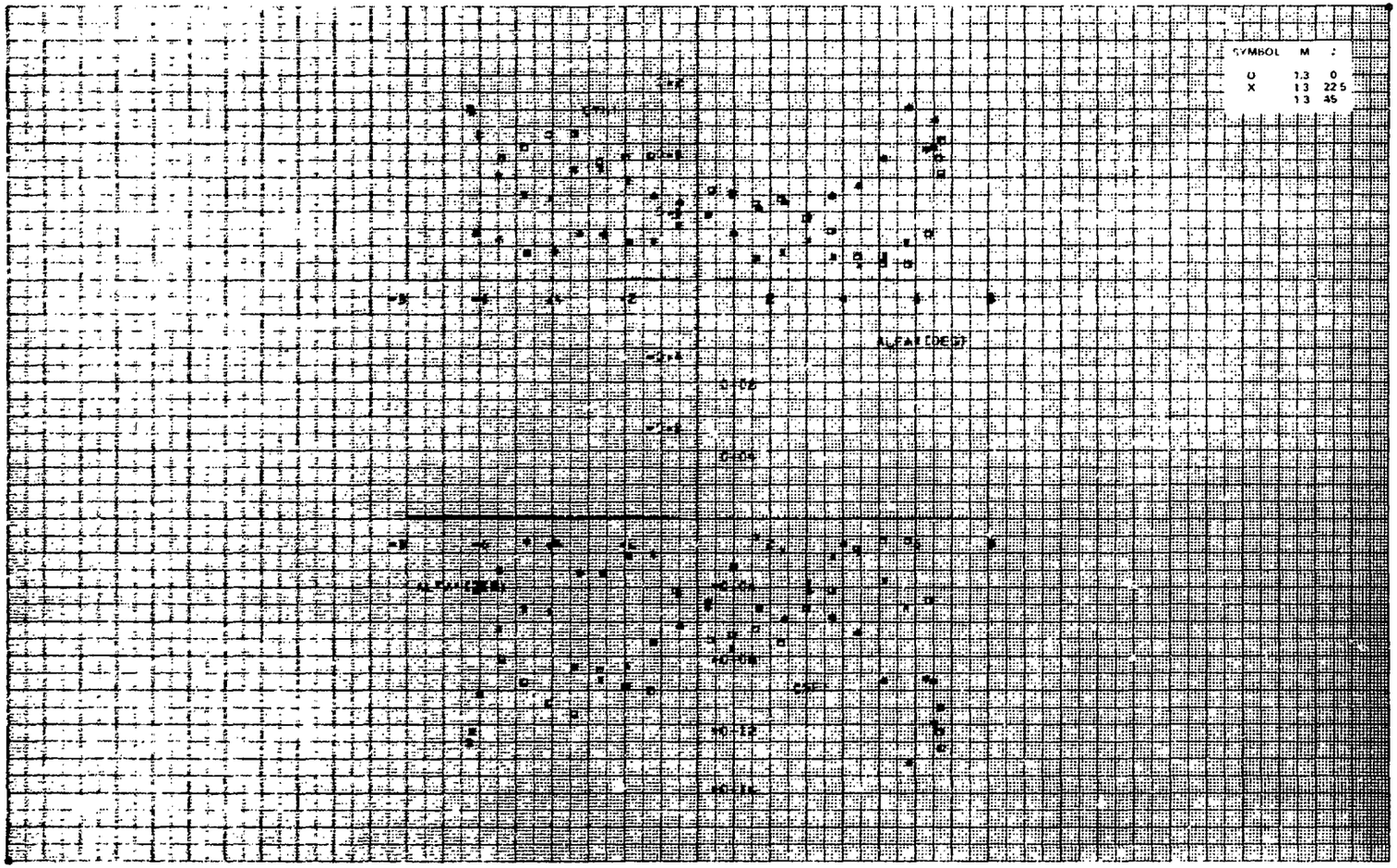


Figure 5g. Continued.

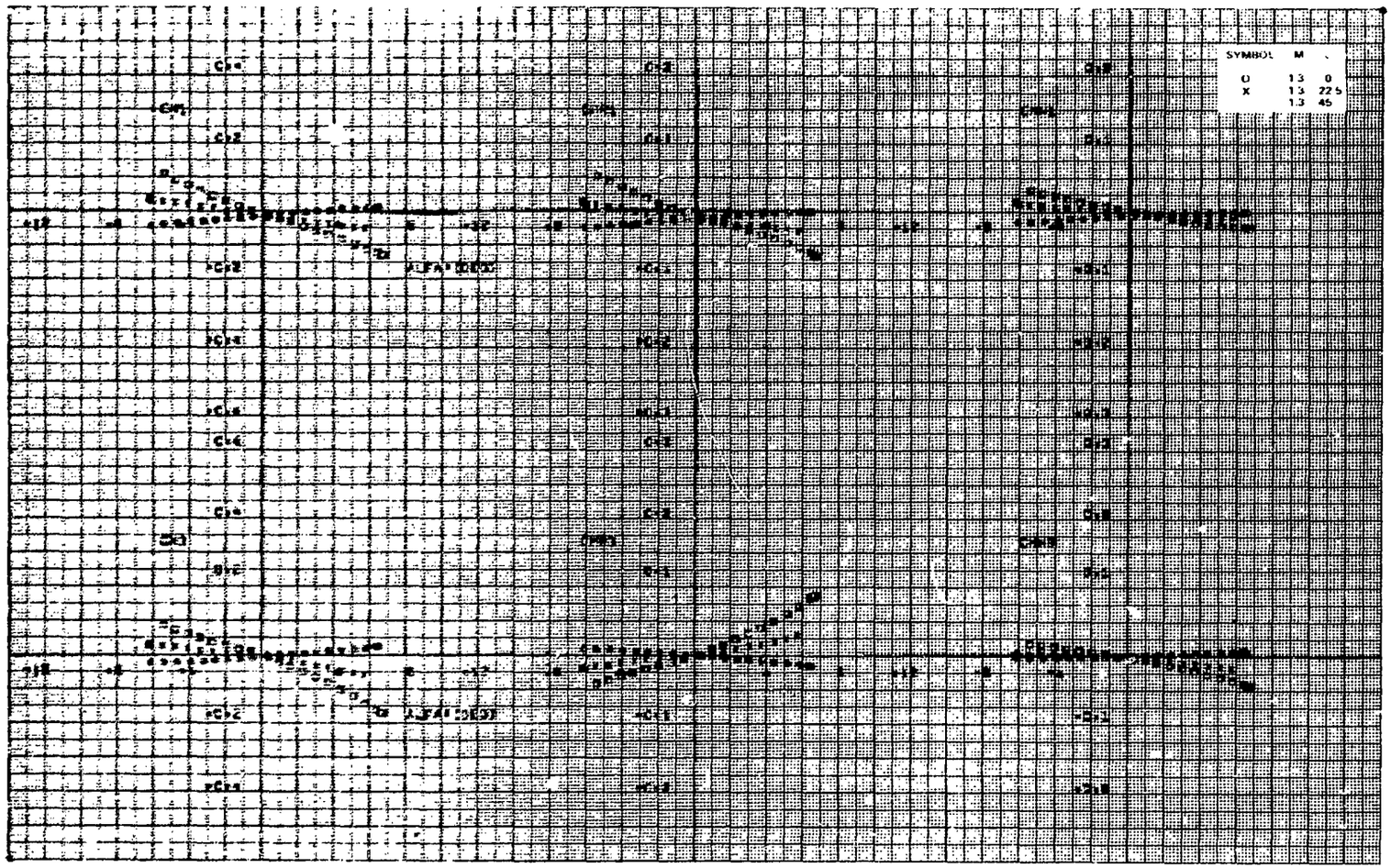


Figure 39. Continued.

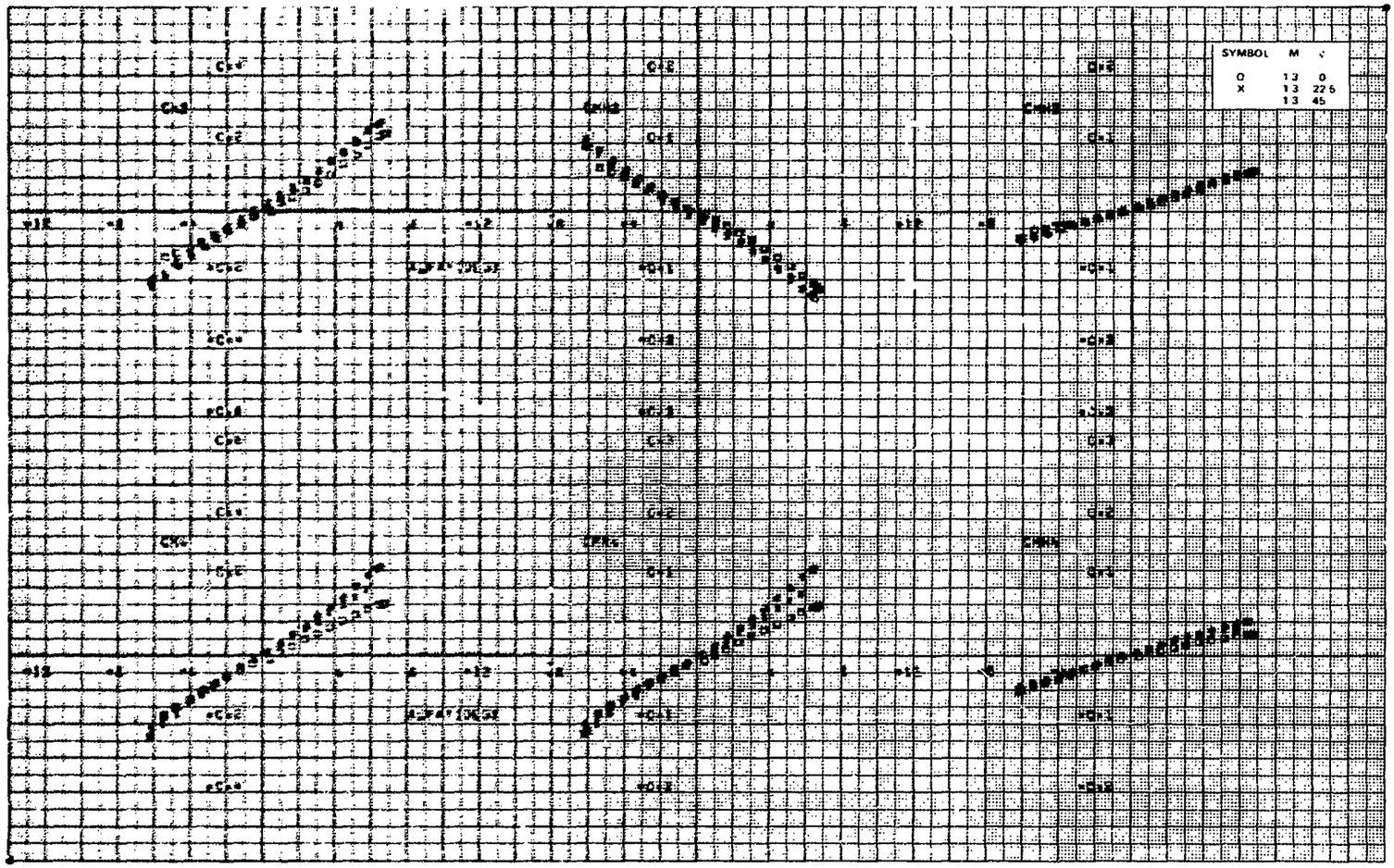
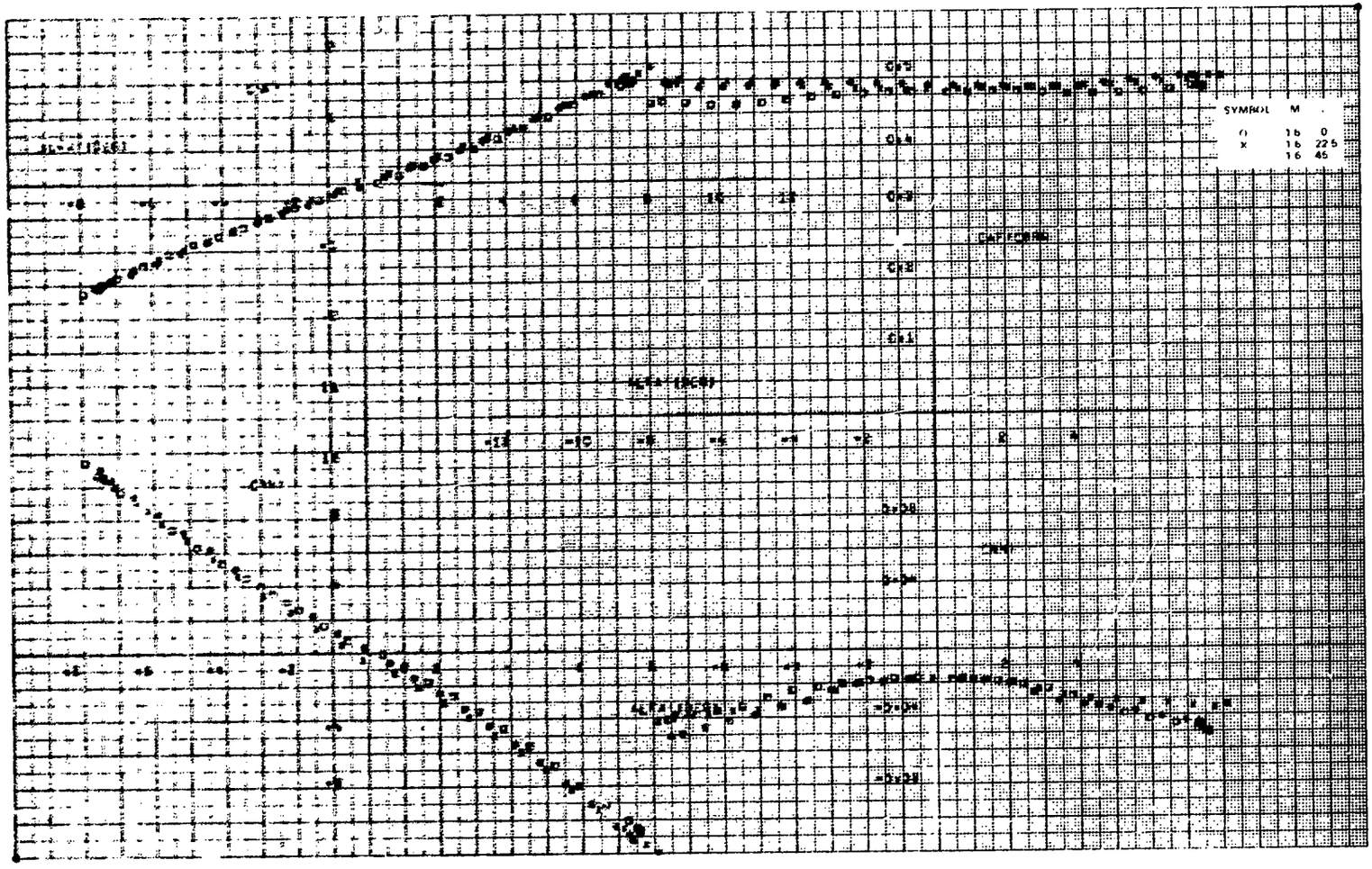


Figure 5g. Concluded.



[illegible] coefficients, CR/D = .75, [illegible] = 0 deg, [illegible] = -11 deg, [illegible] = 1.6.

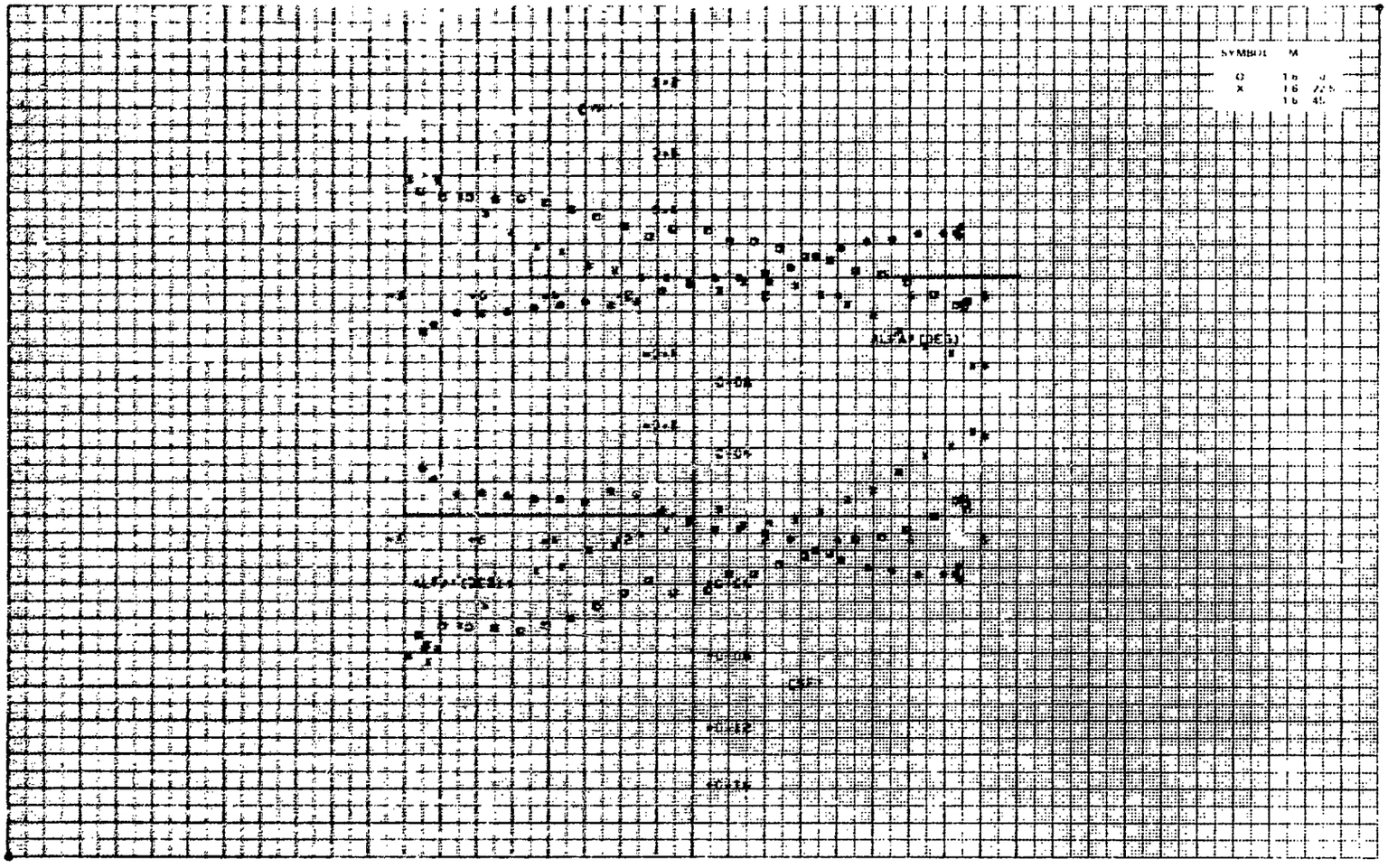


Figure 30. Continued.

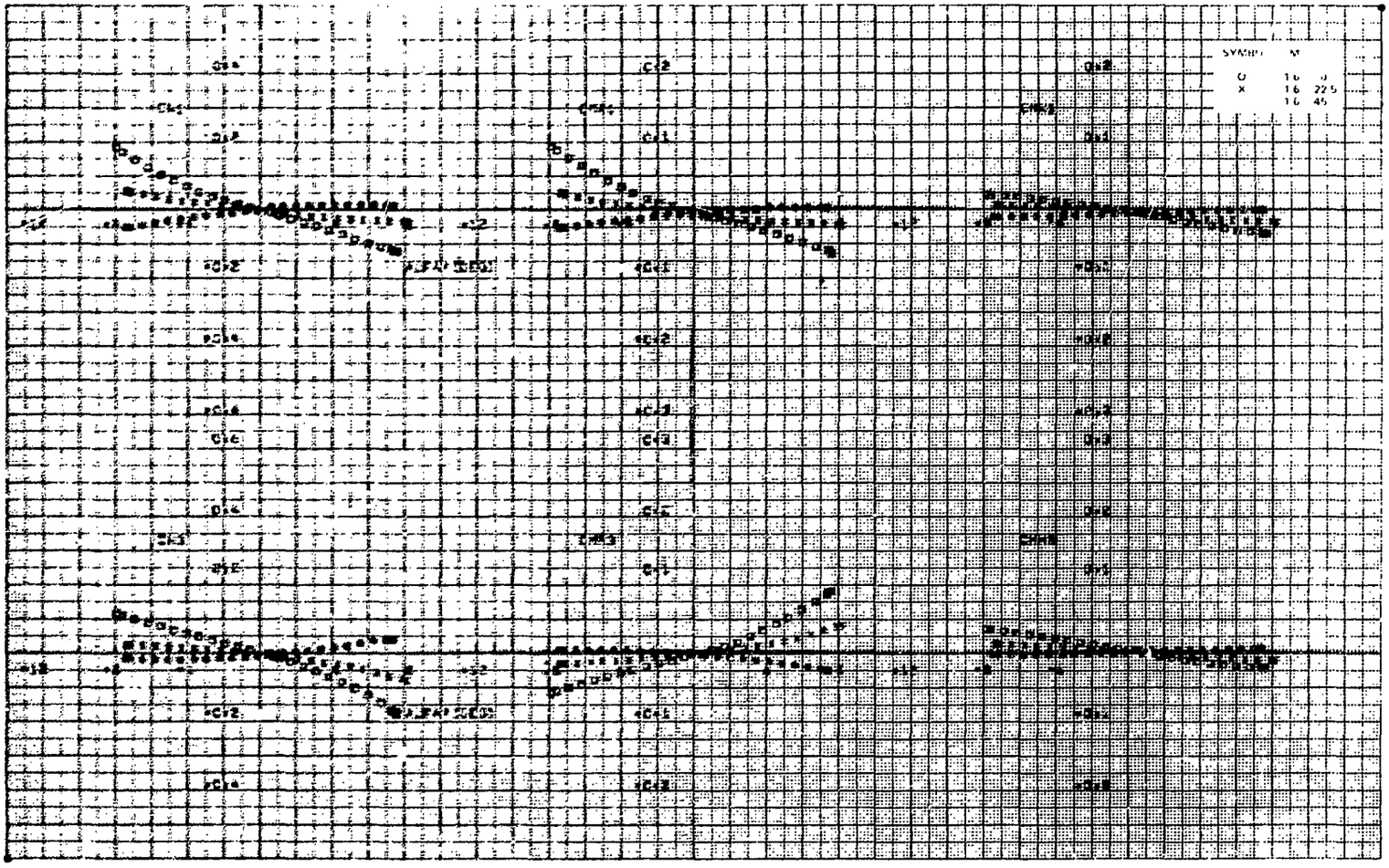


Figure 5h. Continued.

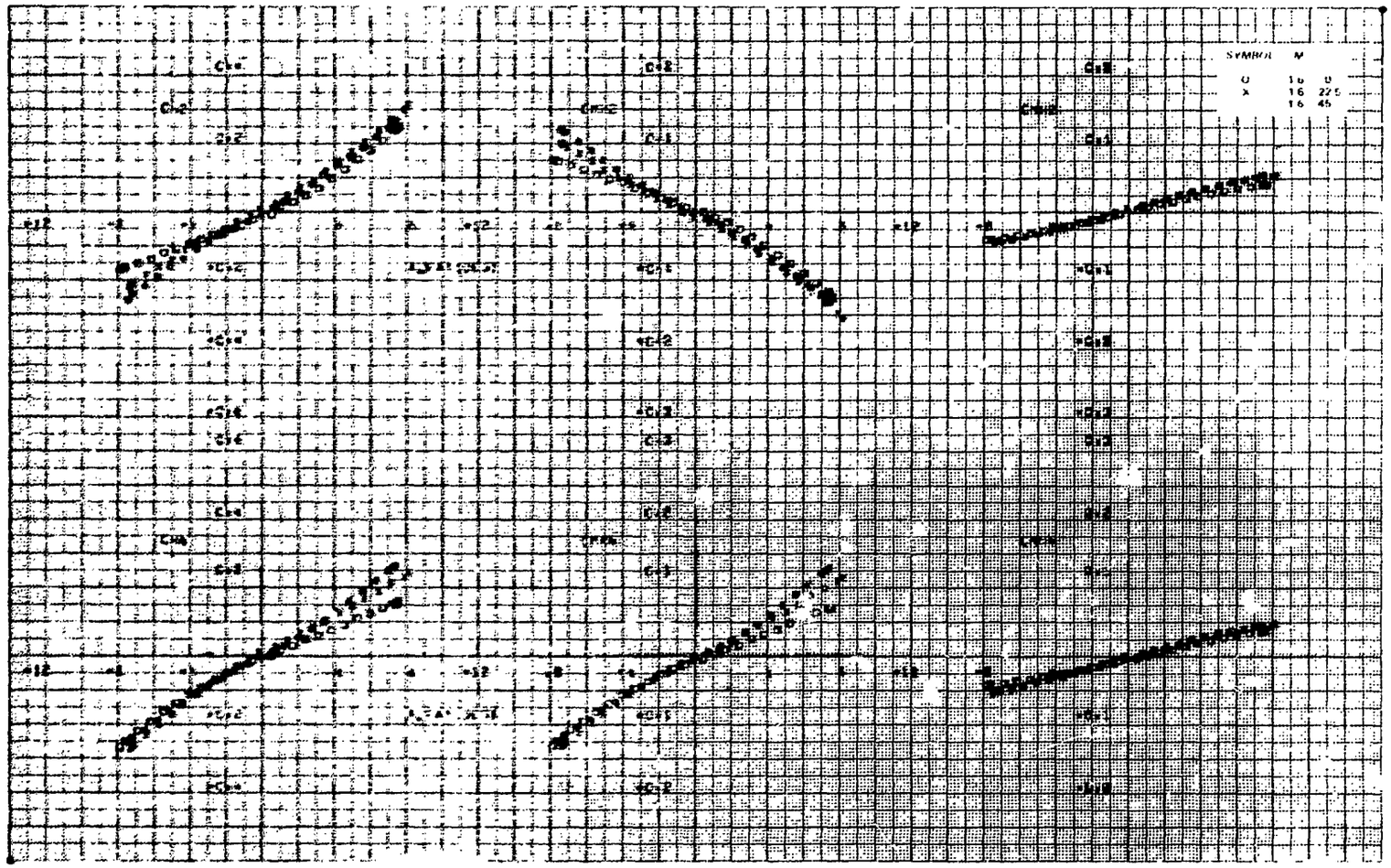


Figure 3b. Concluded.

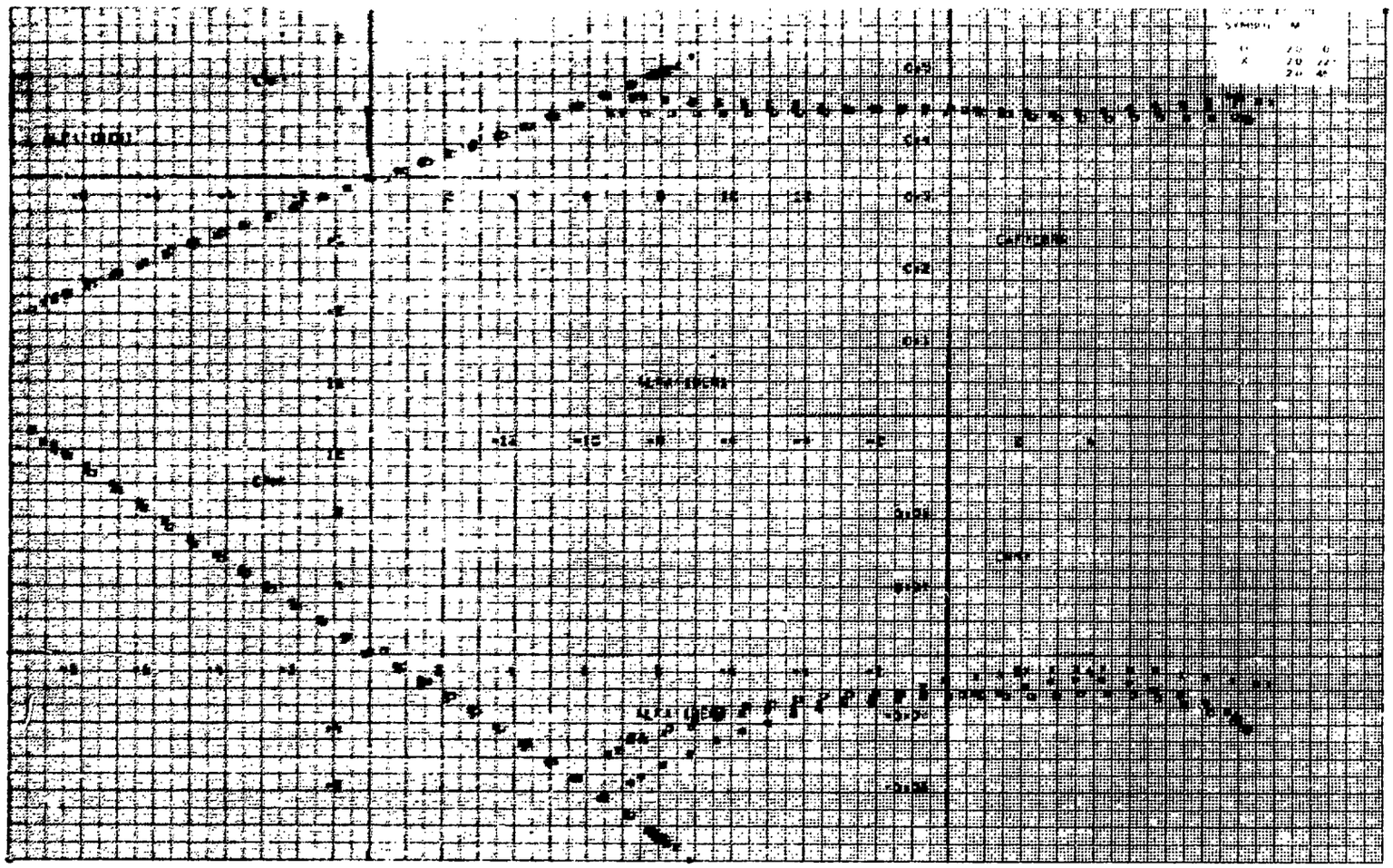


Figure 51. Aerodynamic [illegible] coefficients, R/D = 1.75, ϕ = 0 deg, α = -10 deg, M_∞ = 2.0.

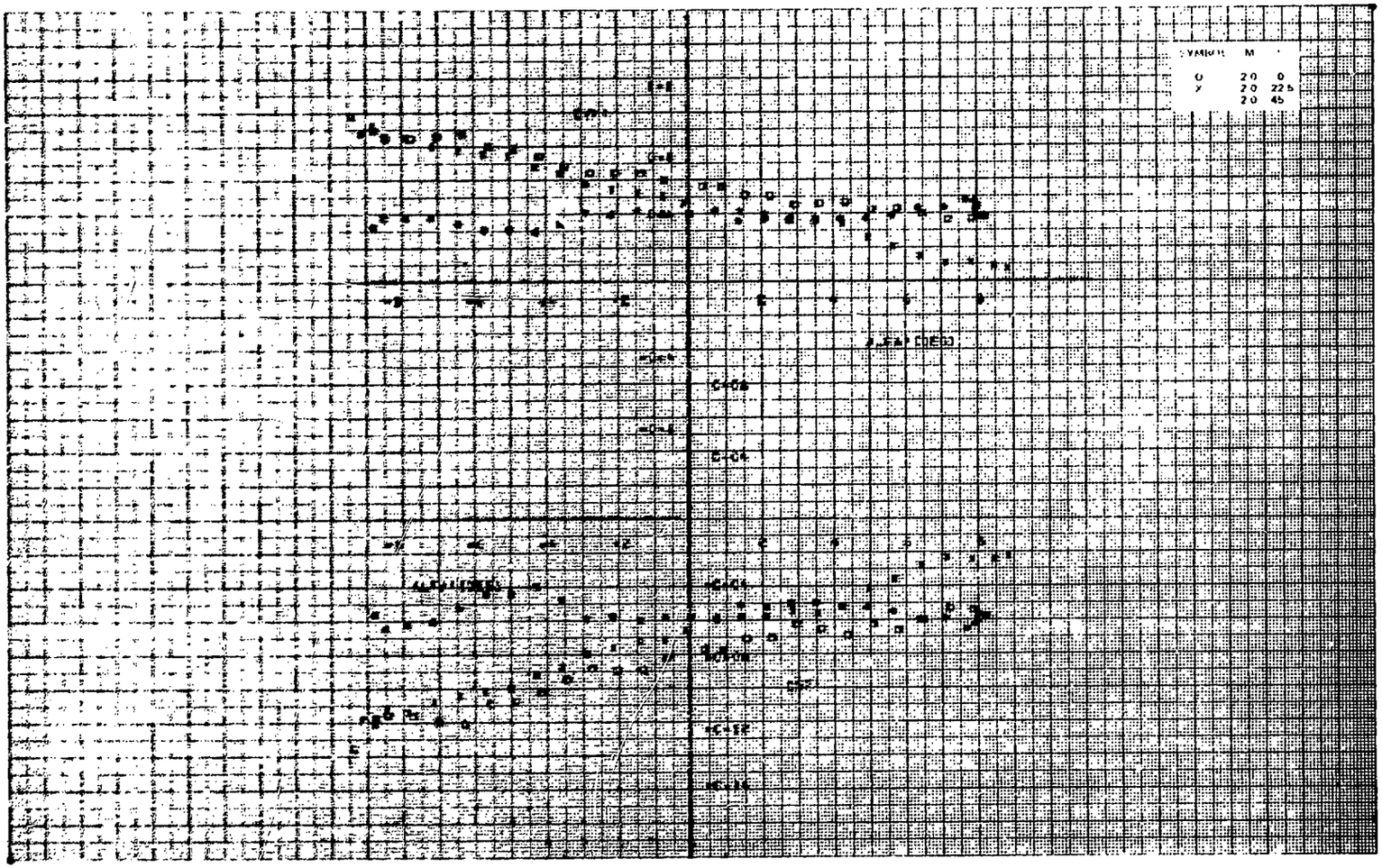


Figure 5i. Continued.

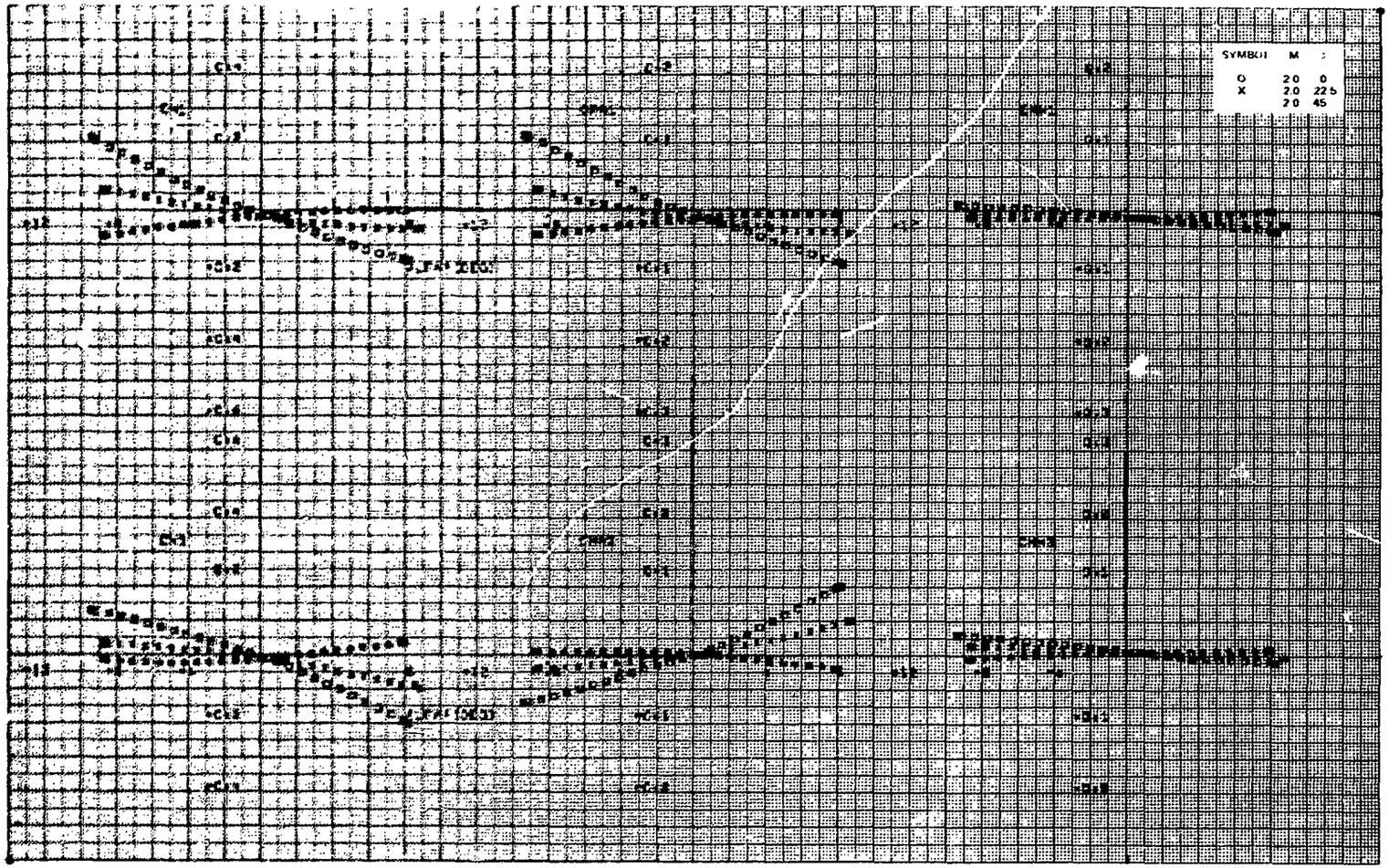


Figure 51. Continued.

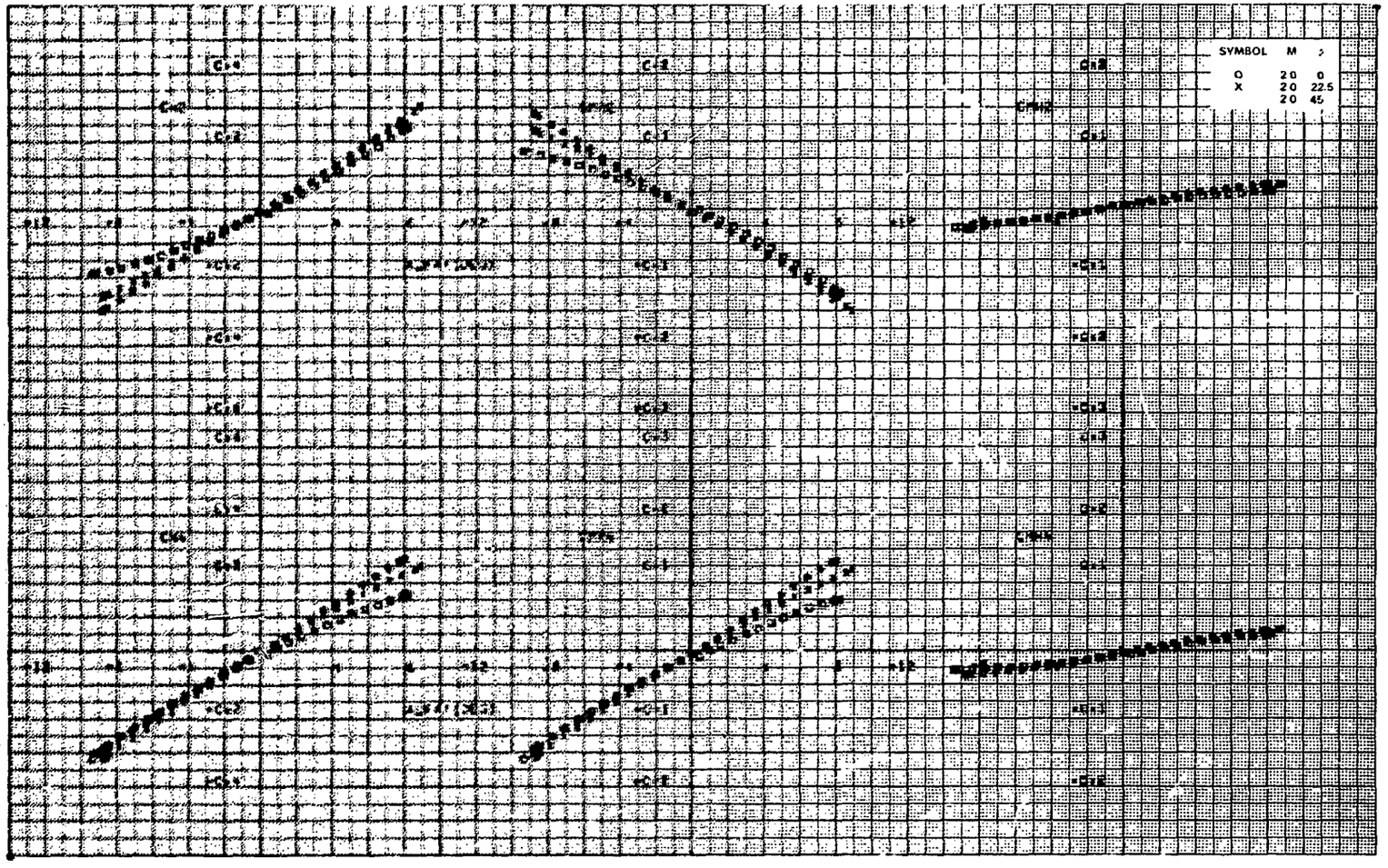
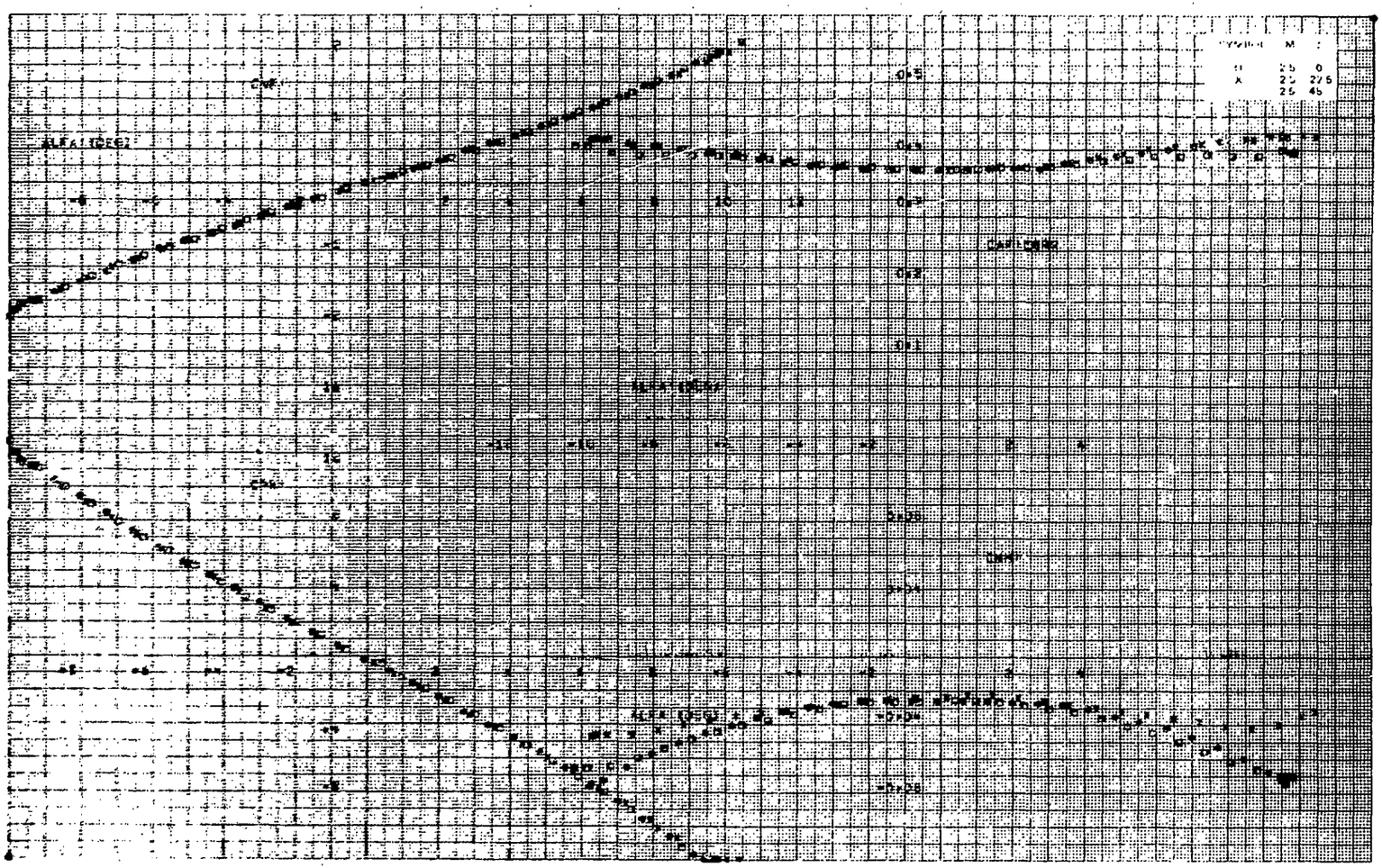
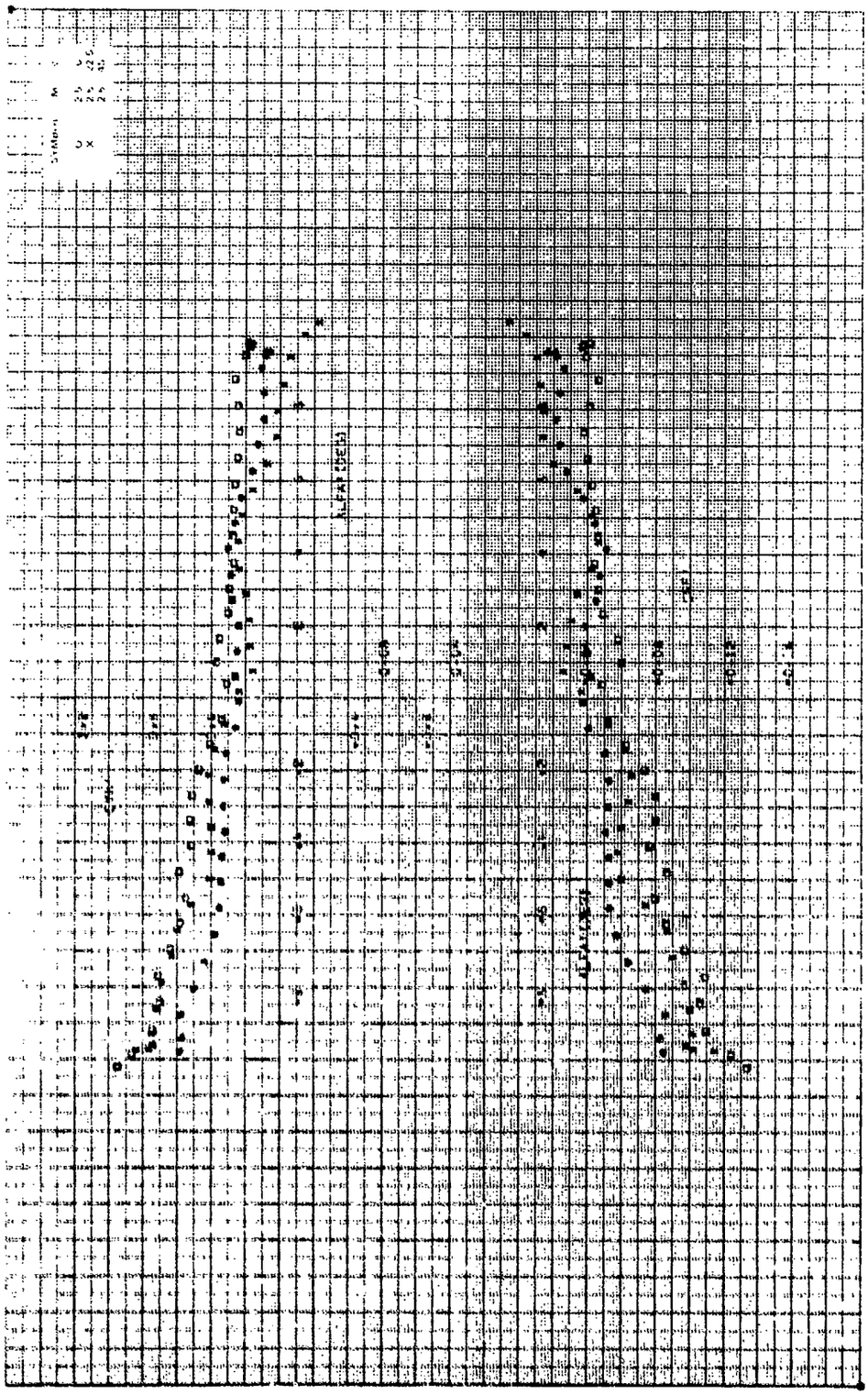


Figure 51. Concluded.



...coefficients, CR/B = 1.75, ... deg, δ = -10 deg, N = 2.5.



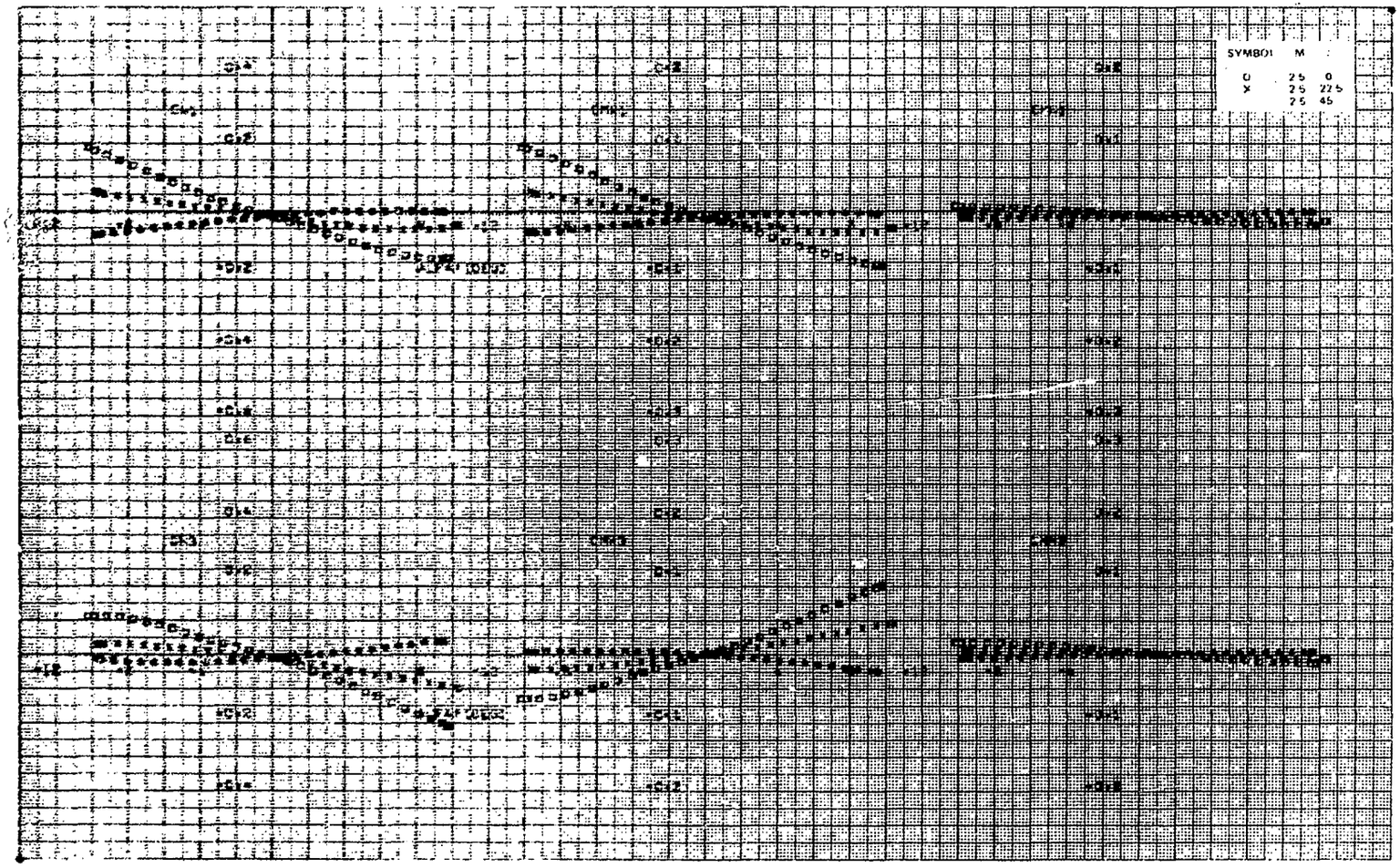


Figure 34. Continued.

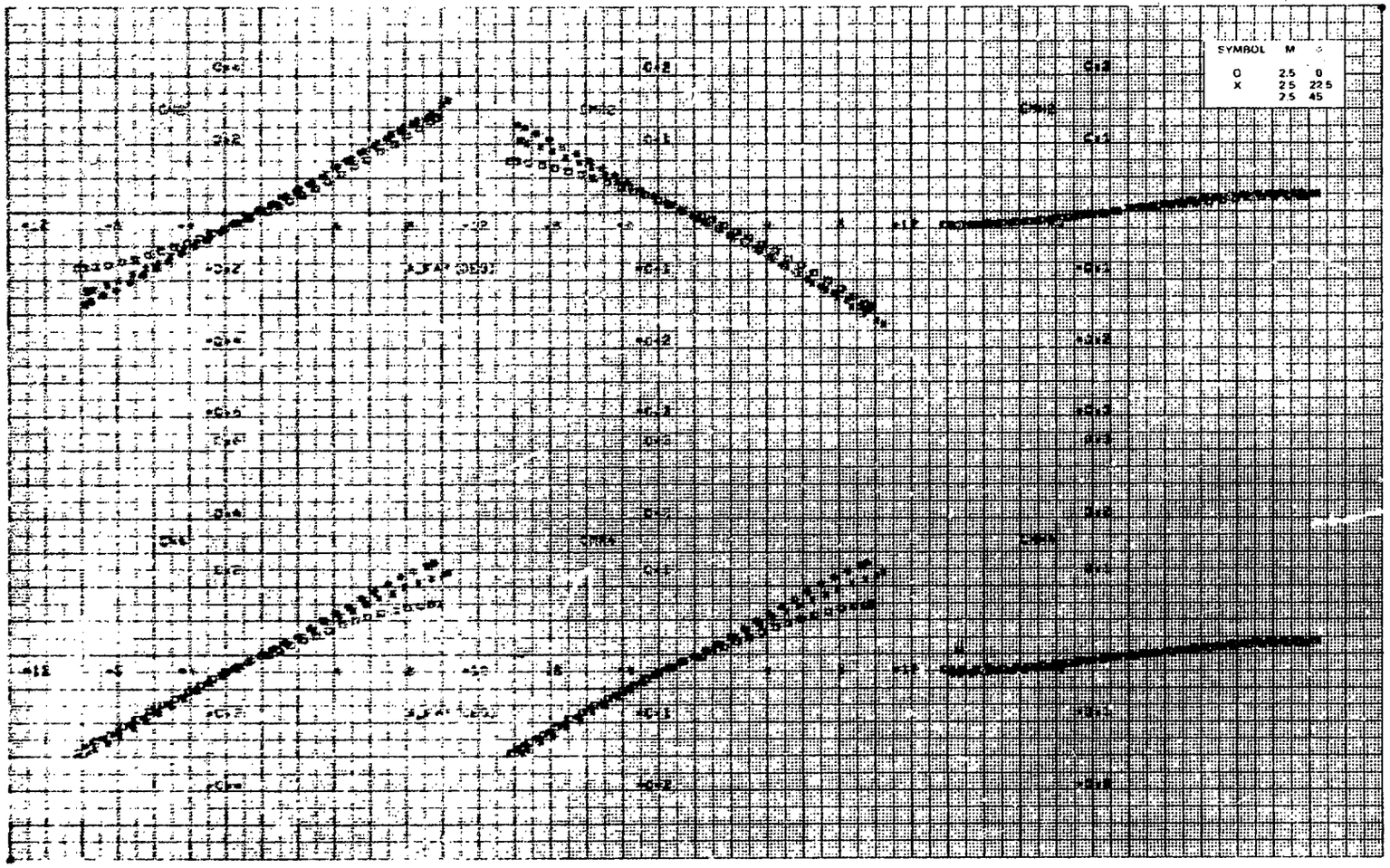


Figure 31. Concluded.

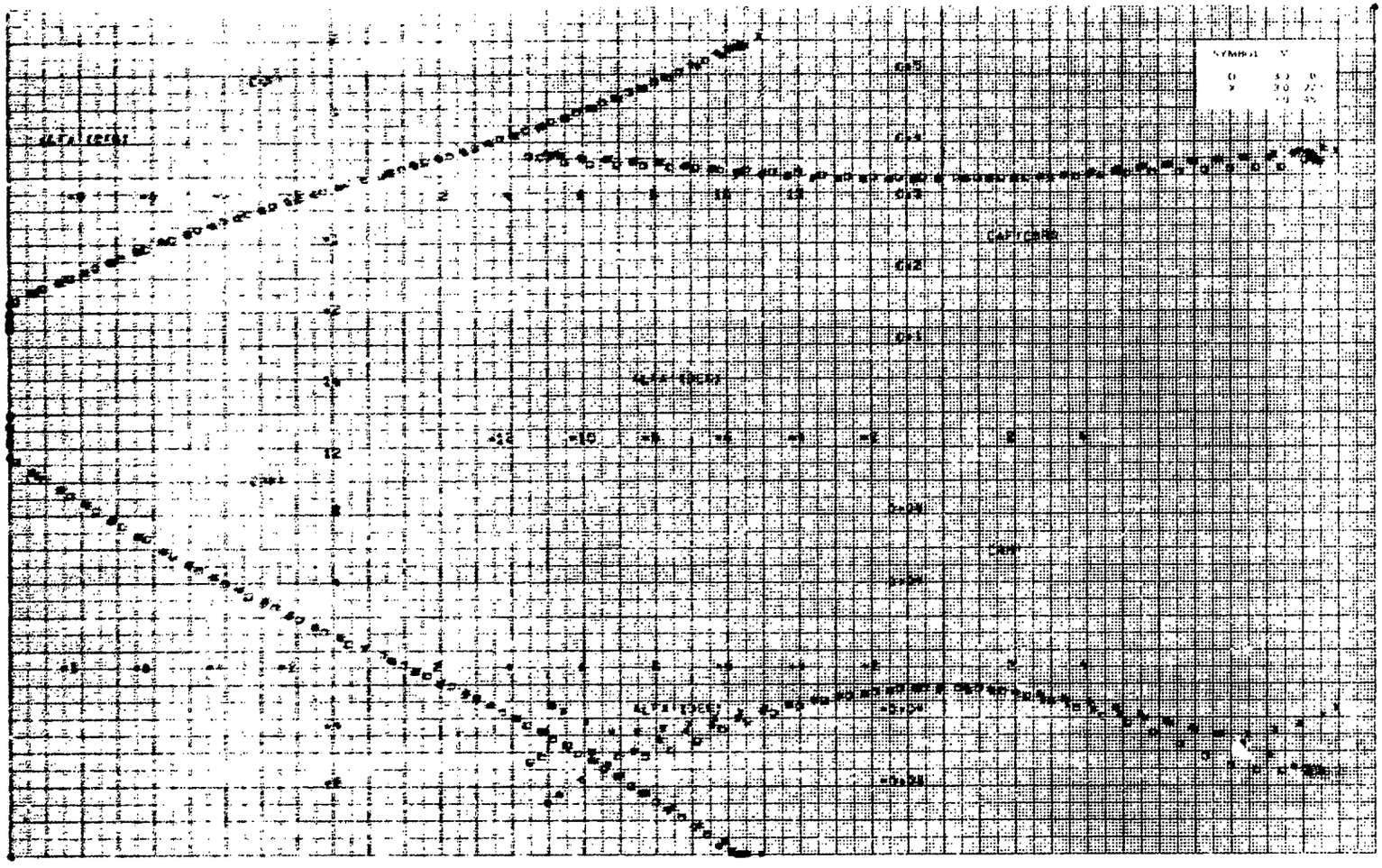
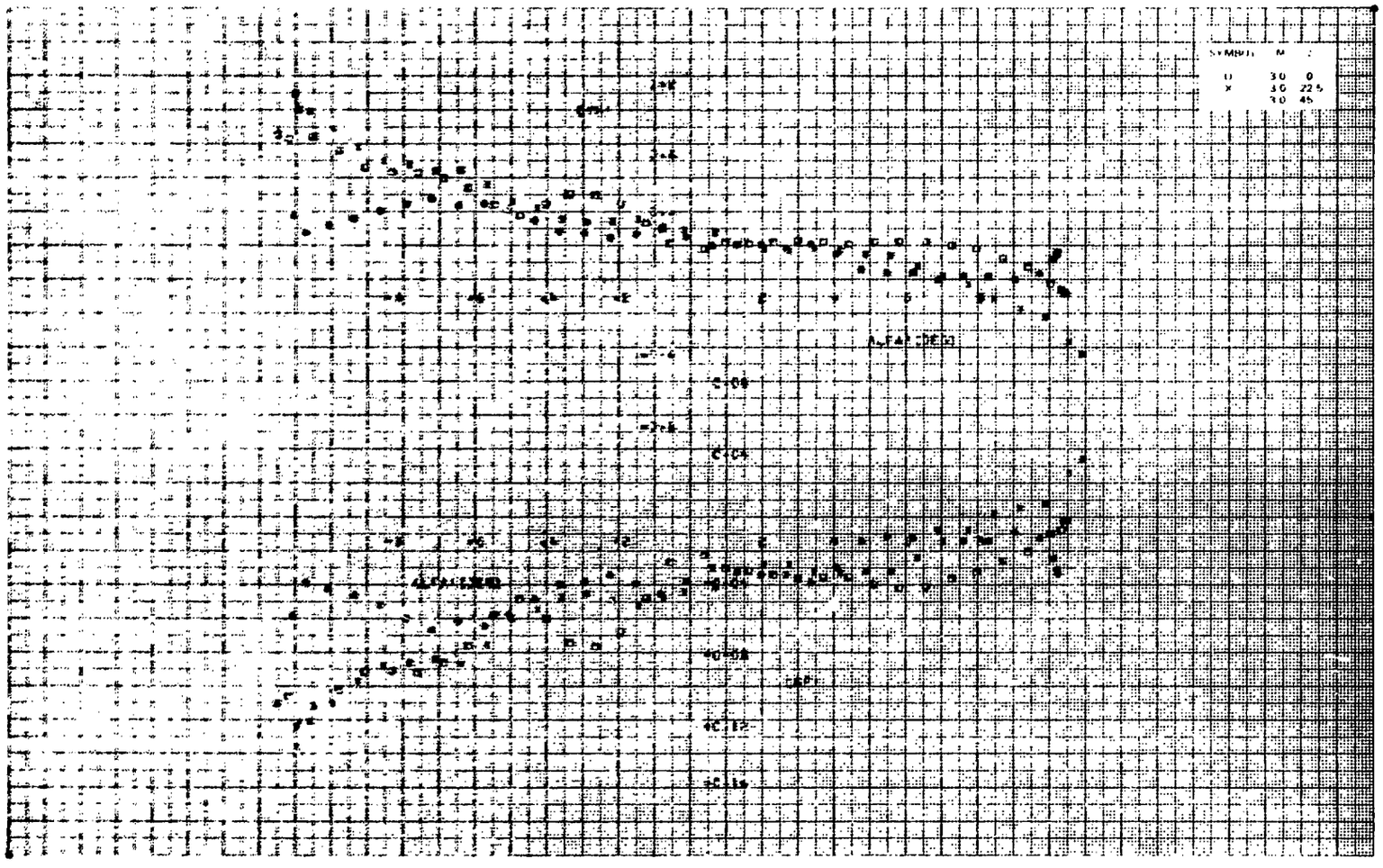


Figure [illegible] $x_{cg}/D = 1.75$, $\alpha = 0$ deg, $\delta = -10$ deg, $M_\infty = 3.0$.


SYMBOL M
O 30 0
X 30 22.5
90 45

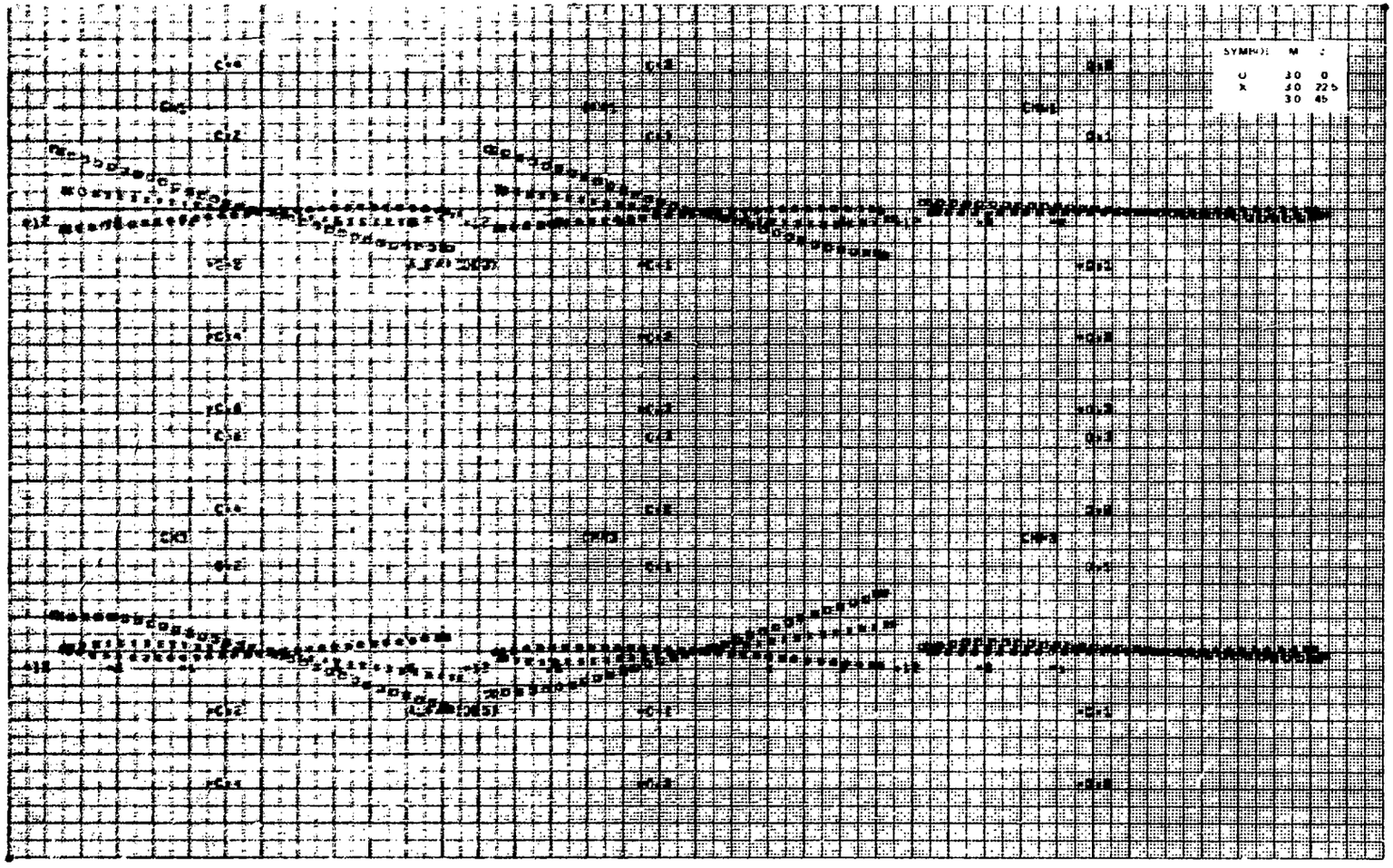


Figure 5c. Continued.

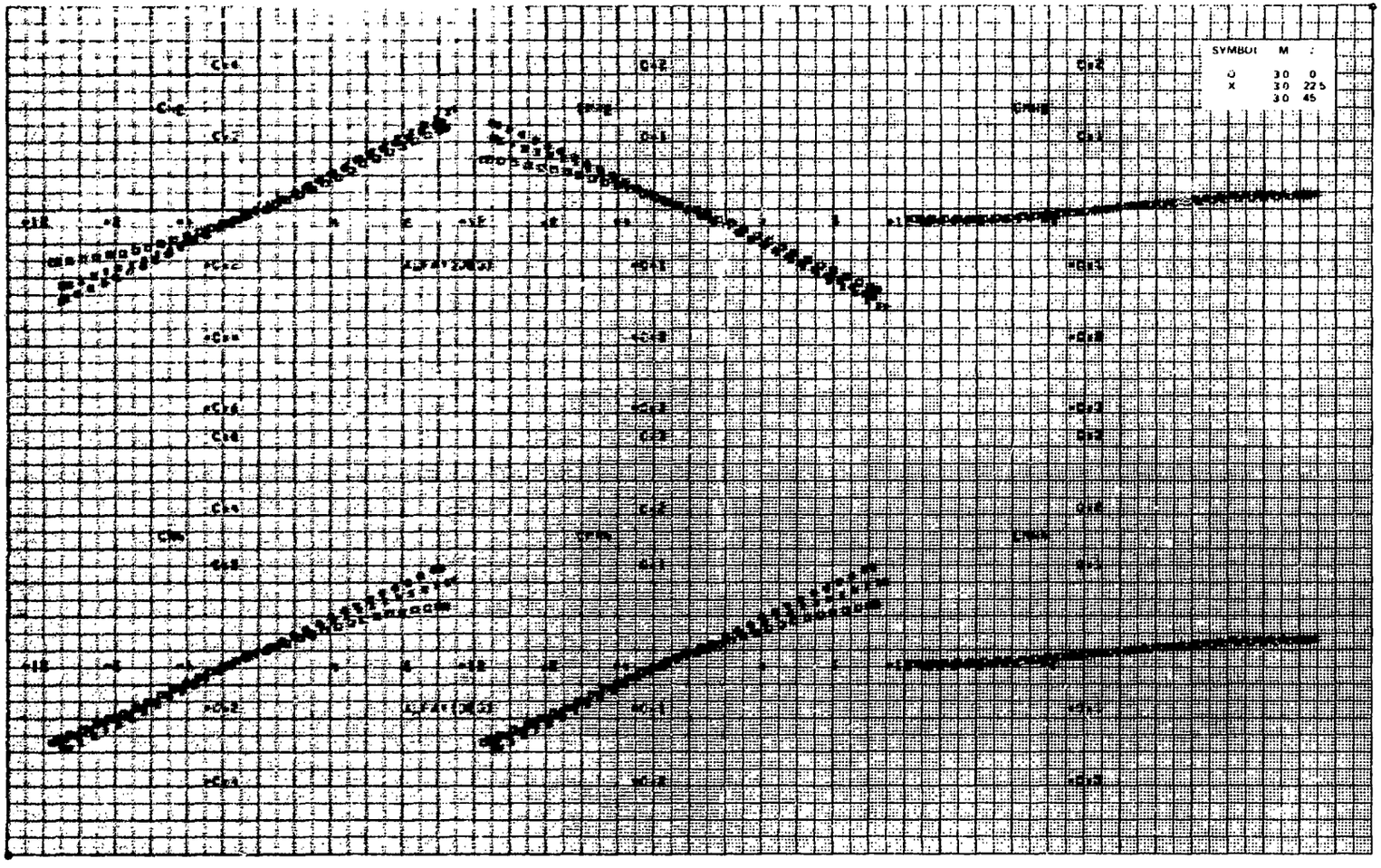
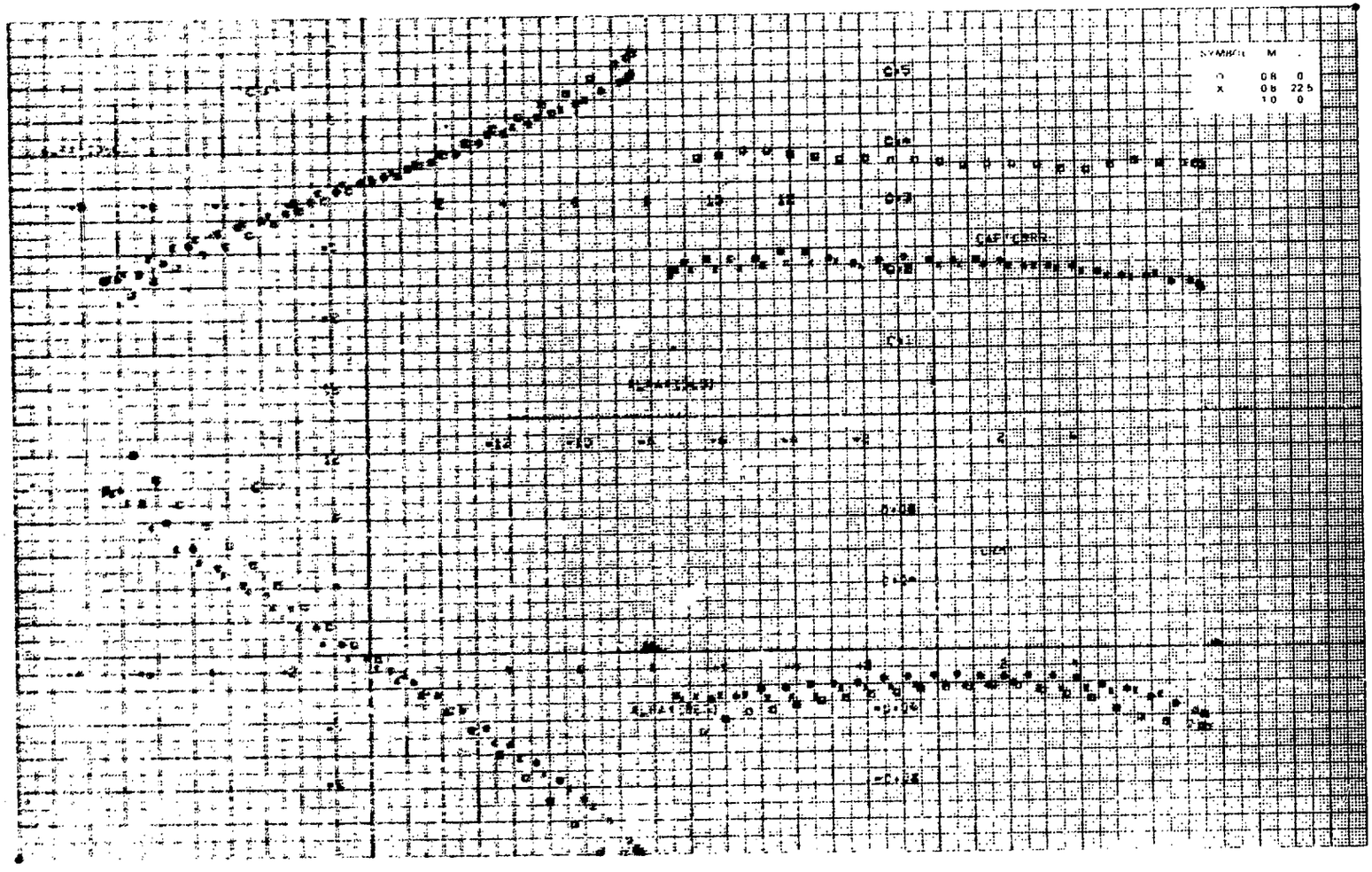
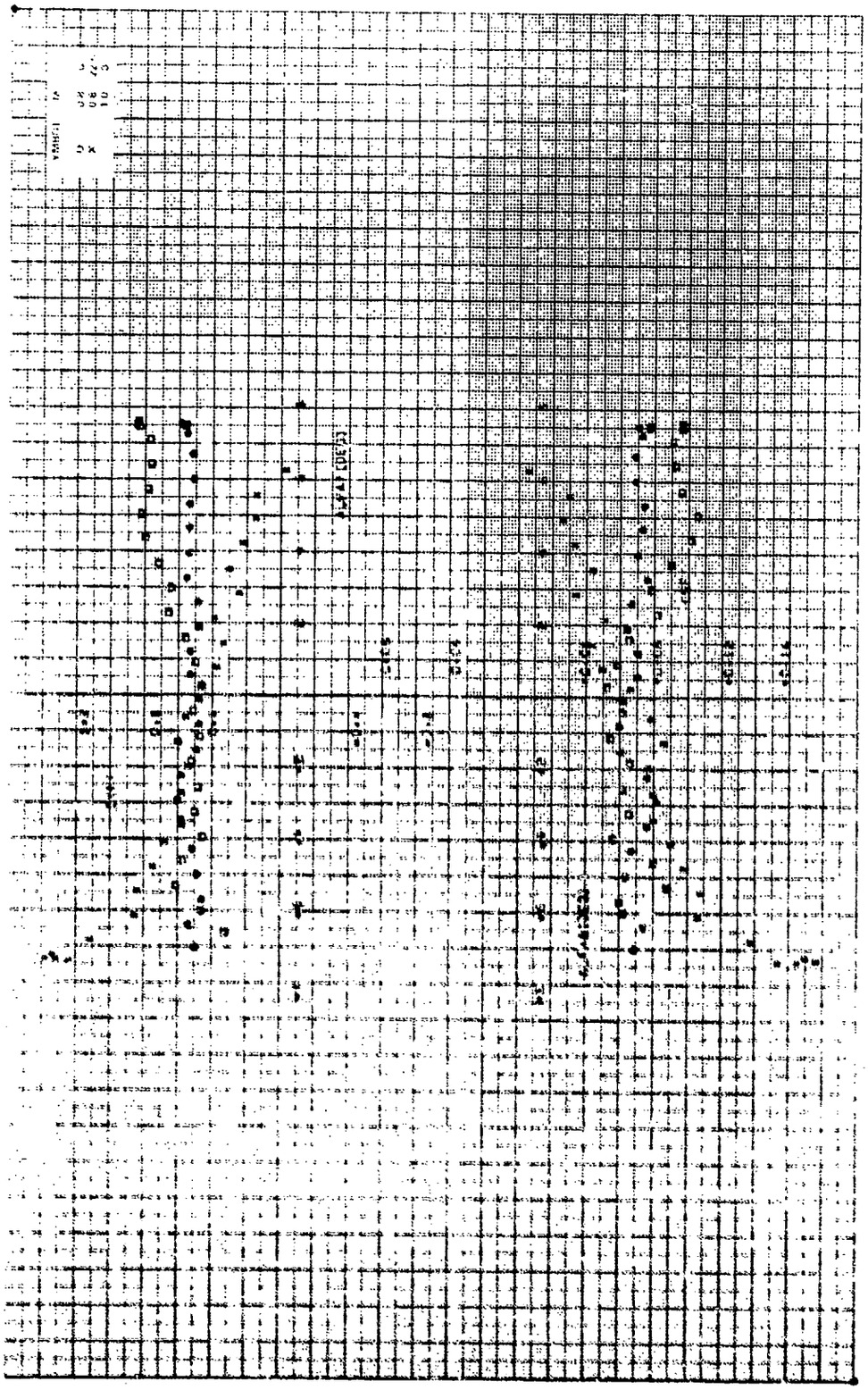


Figure 5k. Concluded.



60

1.0.



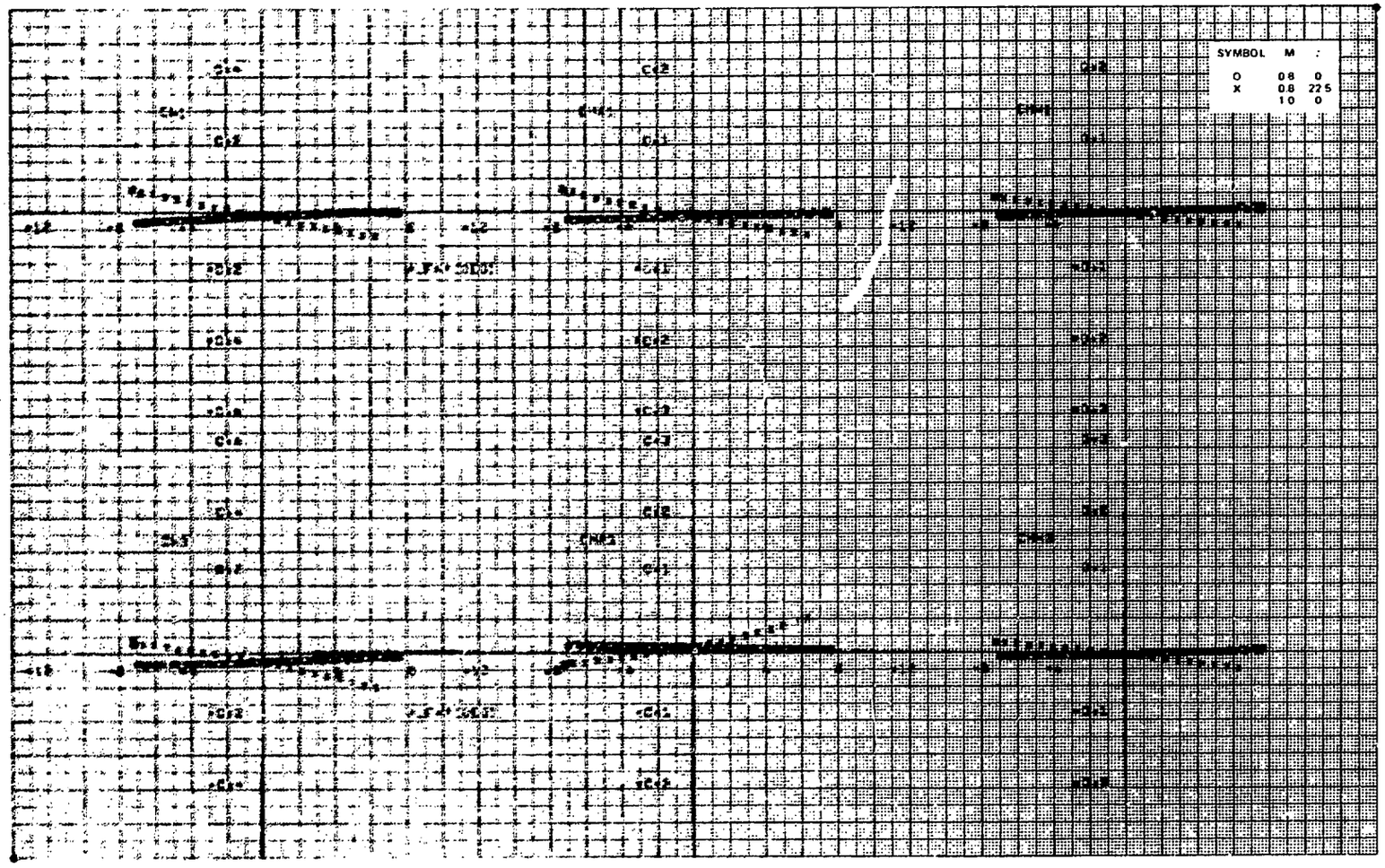


Fig. [illegible] (continued).

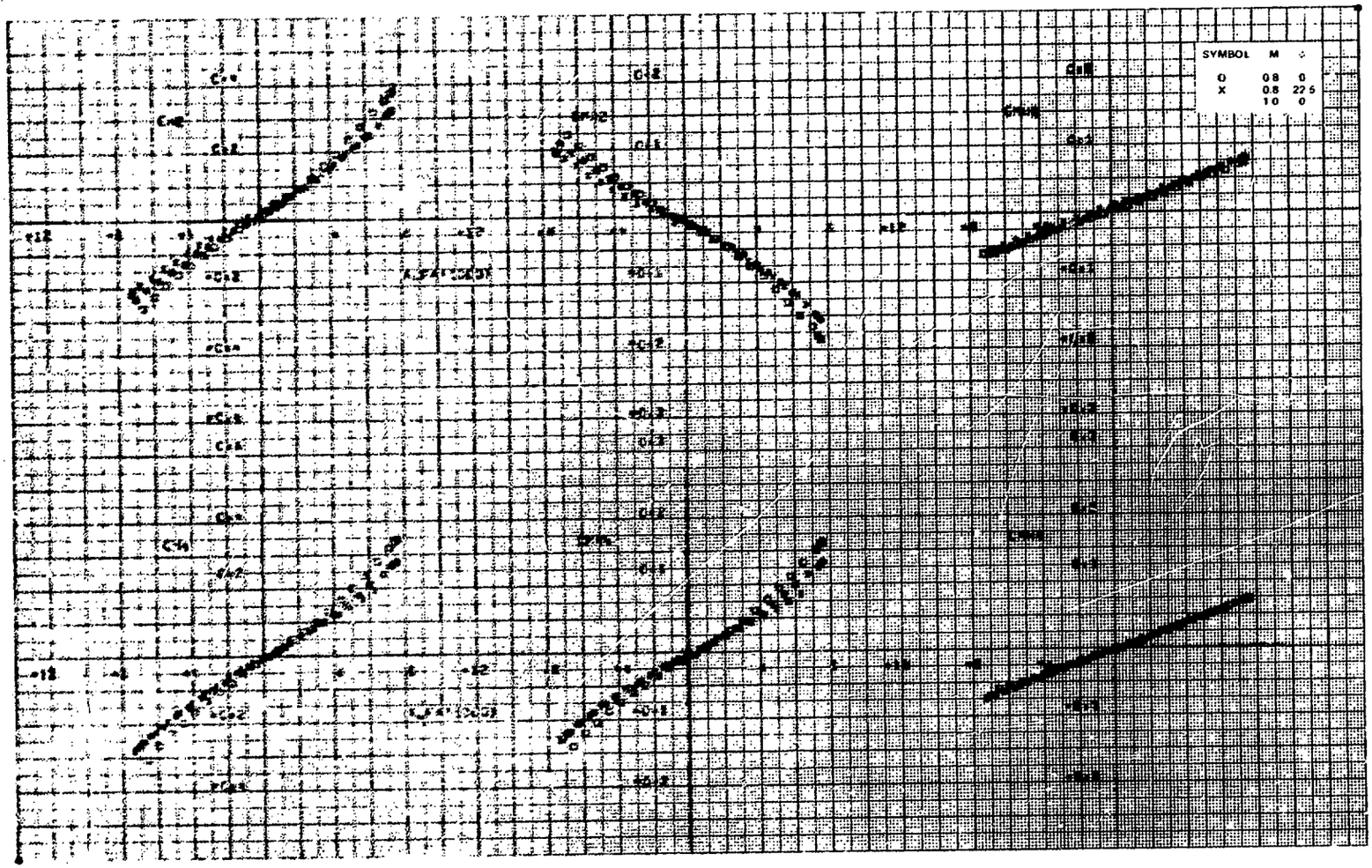


Figure 6a. Concluded.

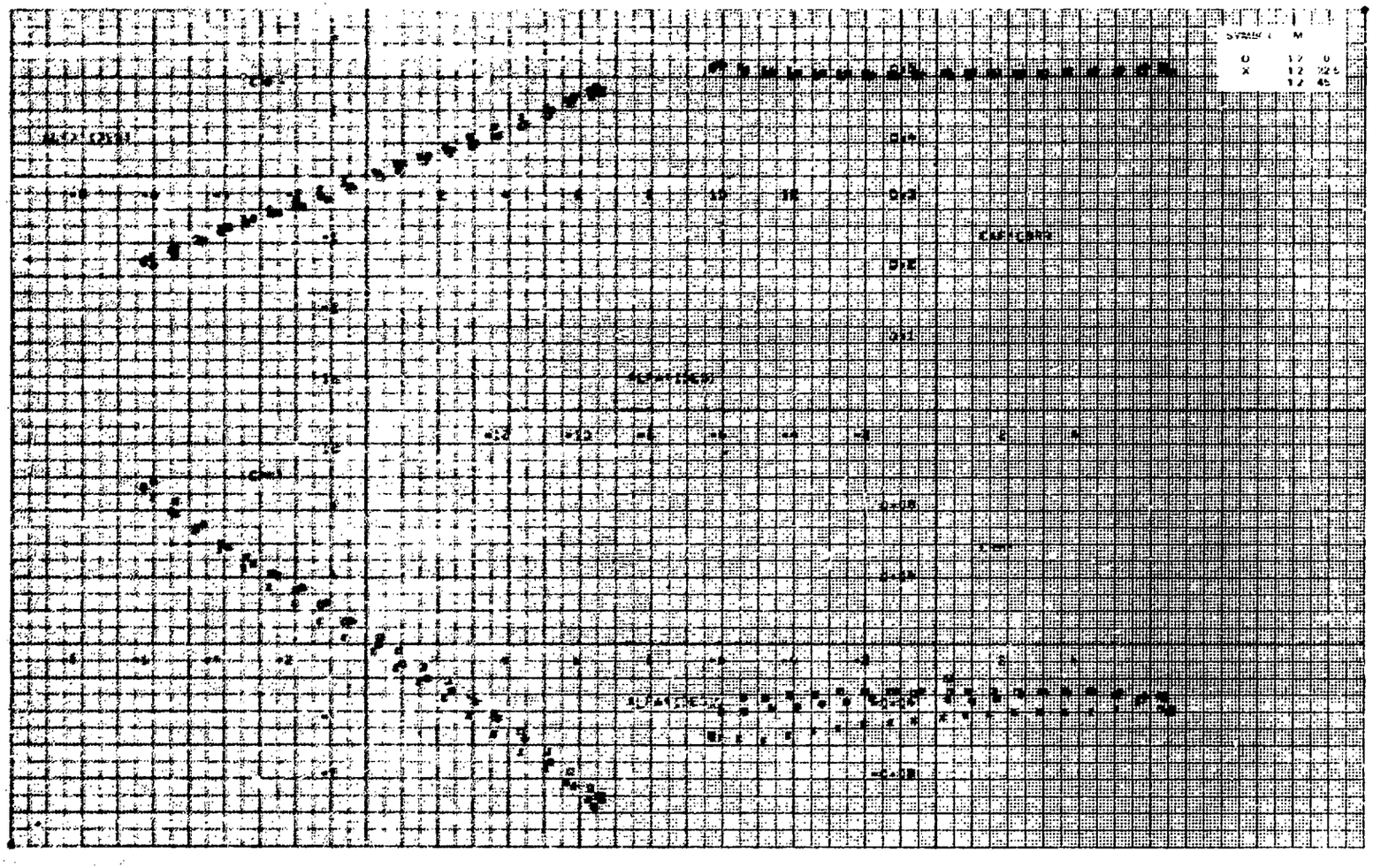


Figure 65. Aerodynamic stability coefficients, CR/D = 1.75, γ = 0 deg, ϕ = 0 deg, M_∞ = 1.2.

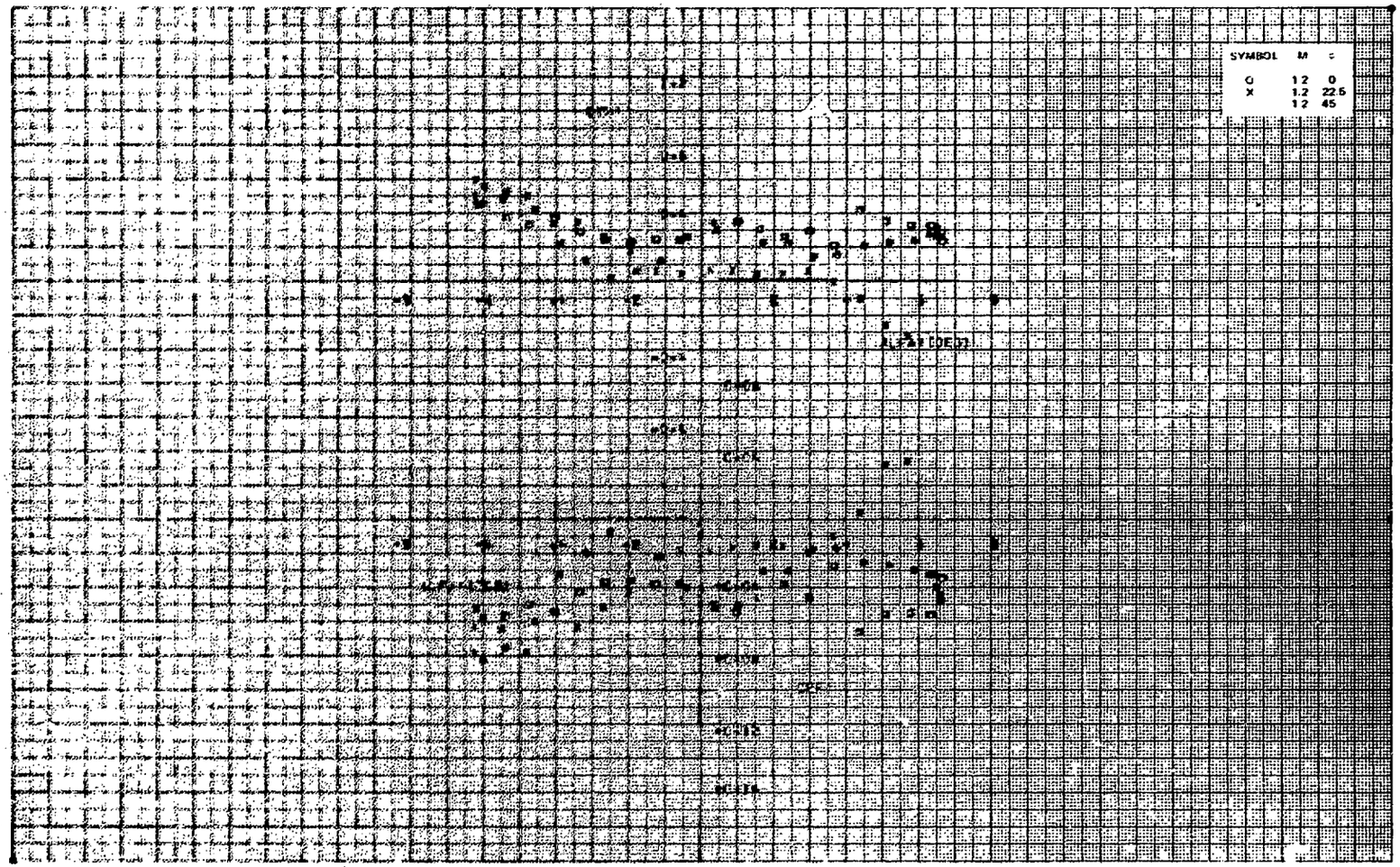


Figure 6b. Continued.

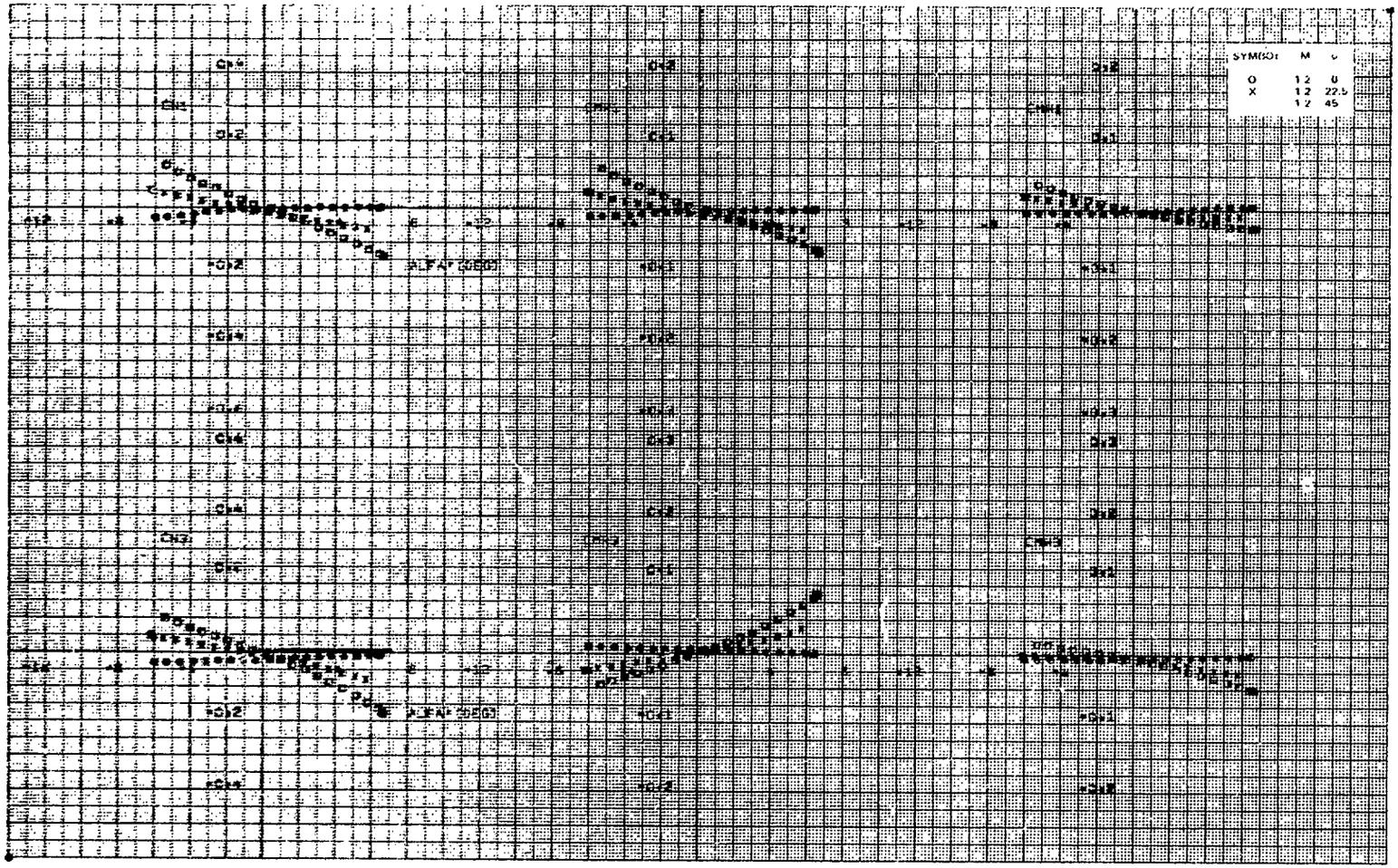


Figure 6b. Continued.

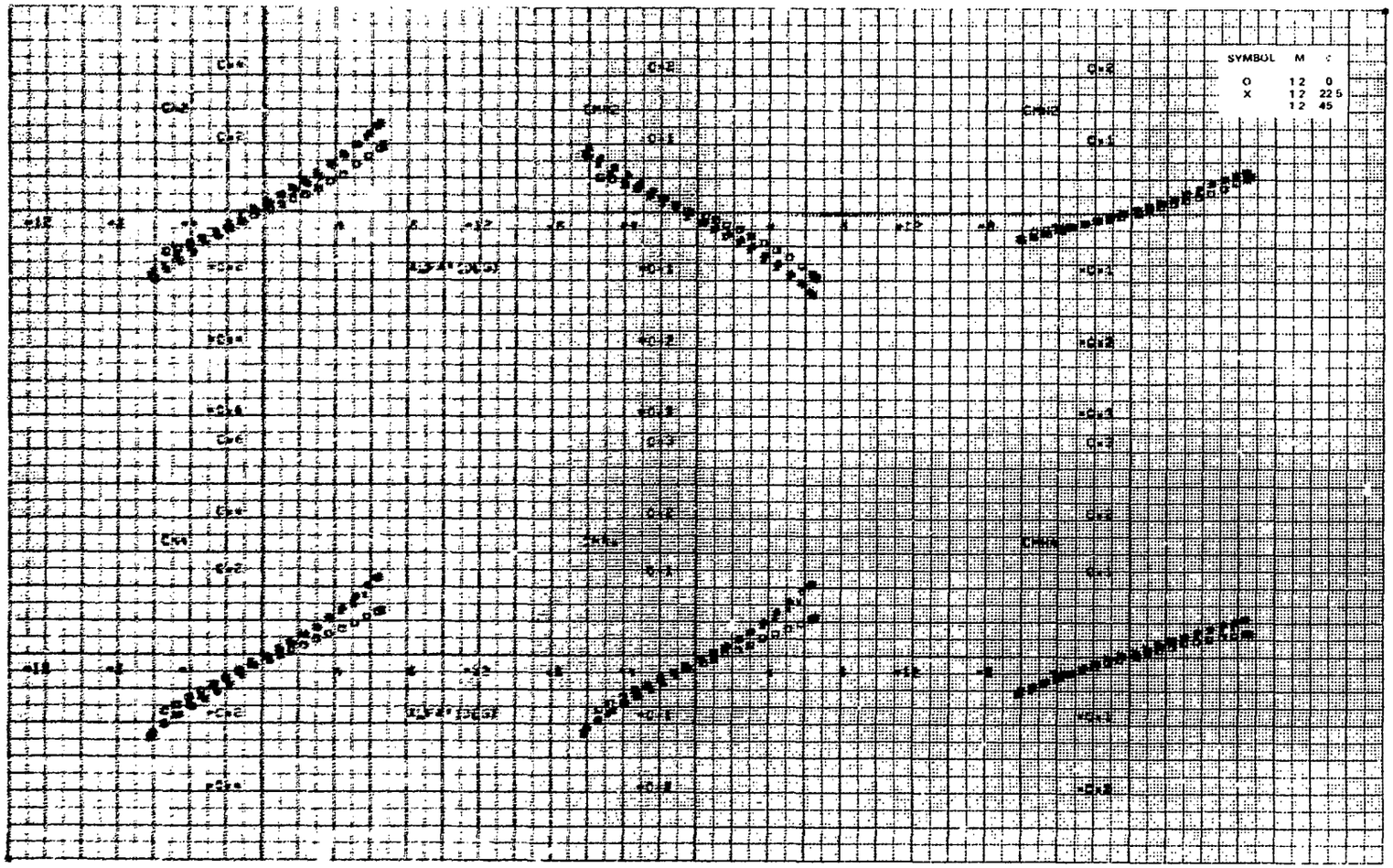
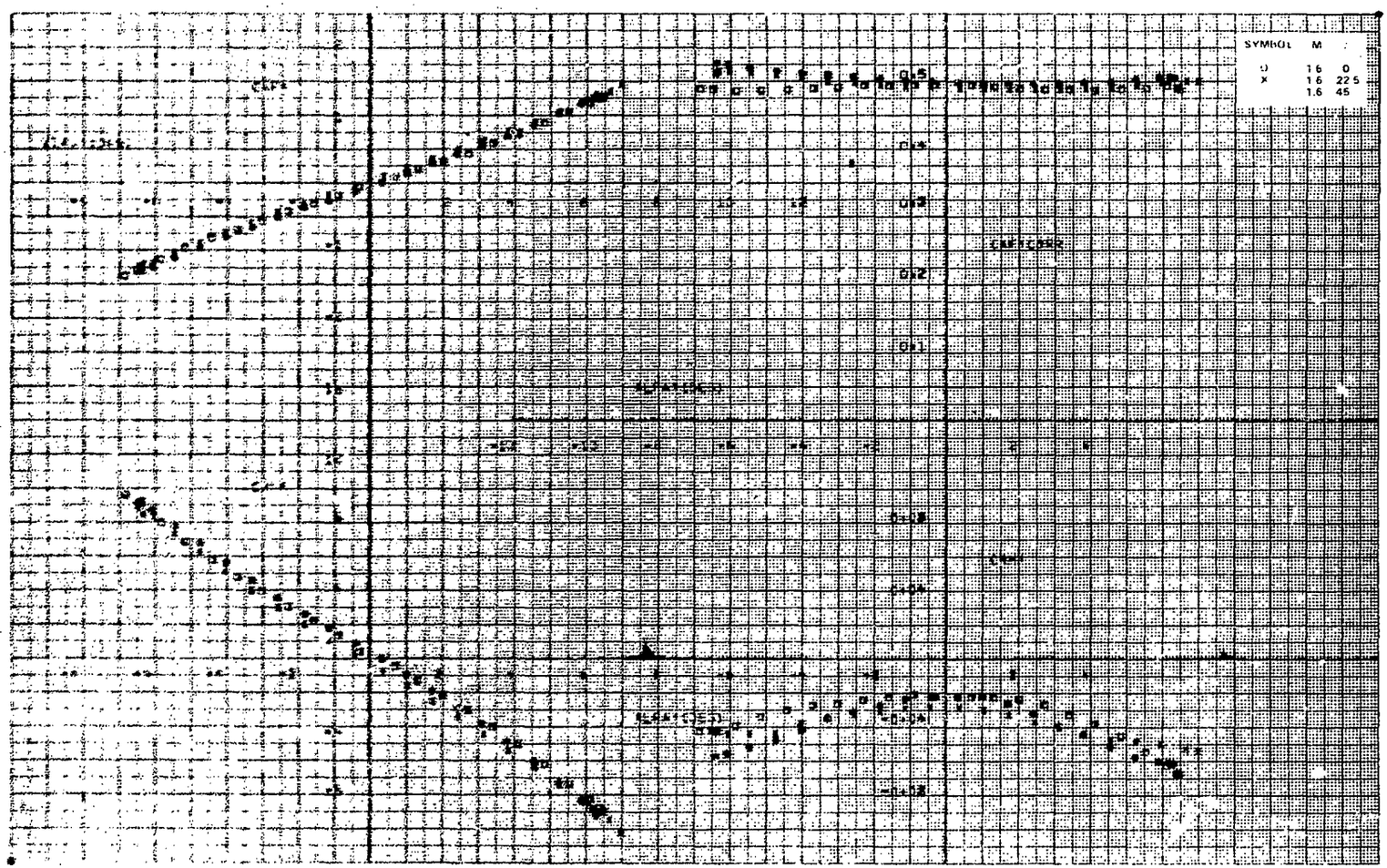


Figure 6b. Concluded.



[illegible] stability coefficients, $CR/\bar{q}$ = 1.75, [illegible] = 0 deg, ϕ = 0 deg, M_∞ = 1.6.

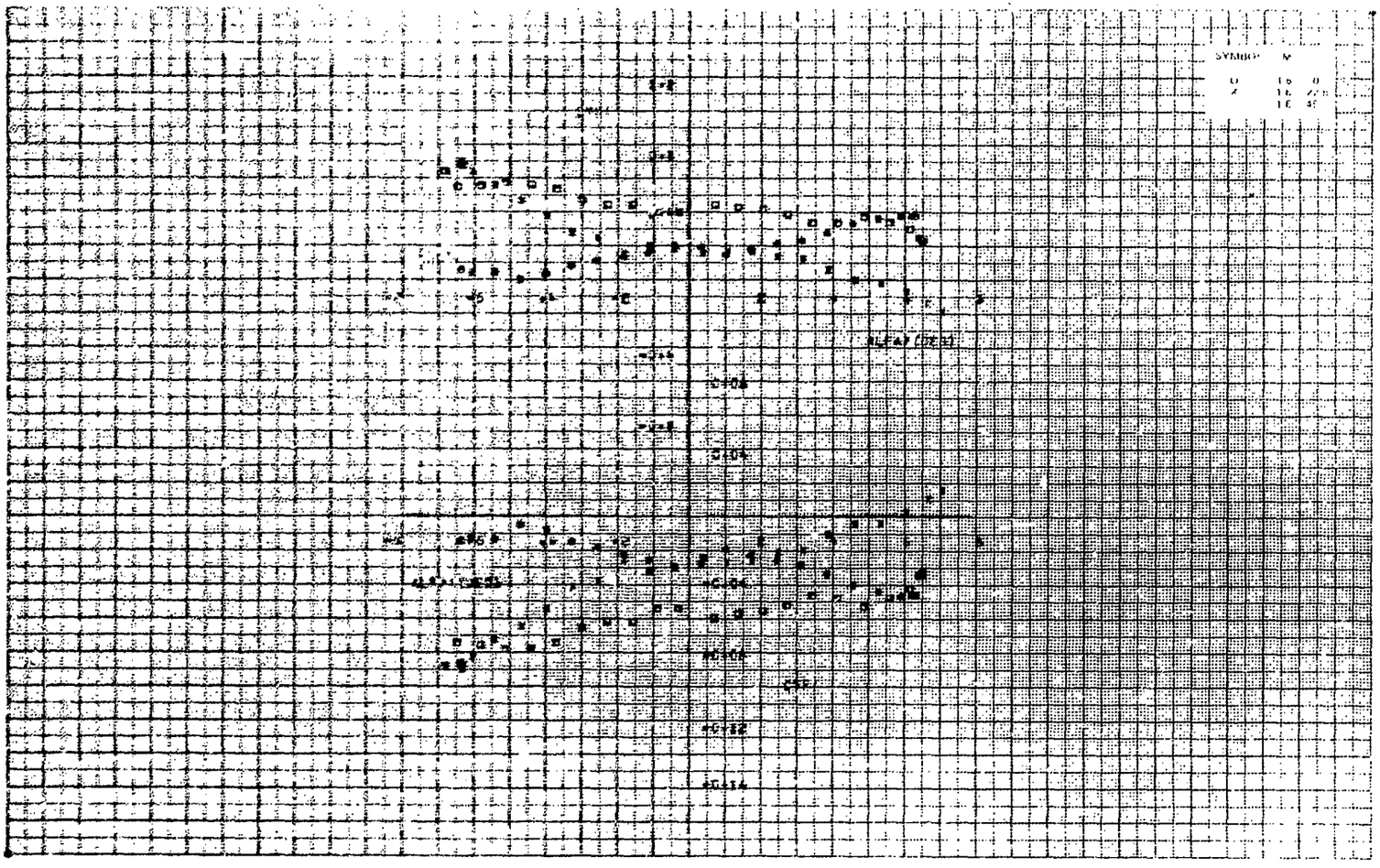
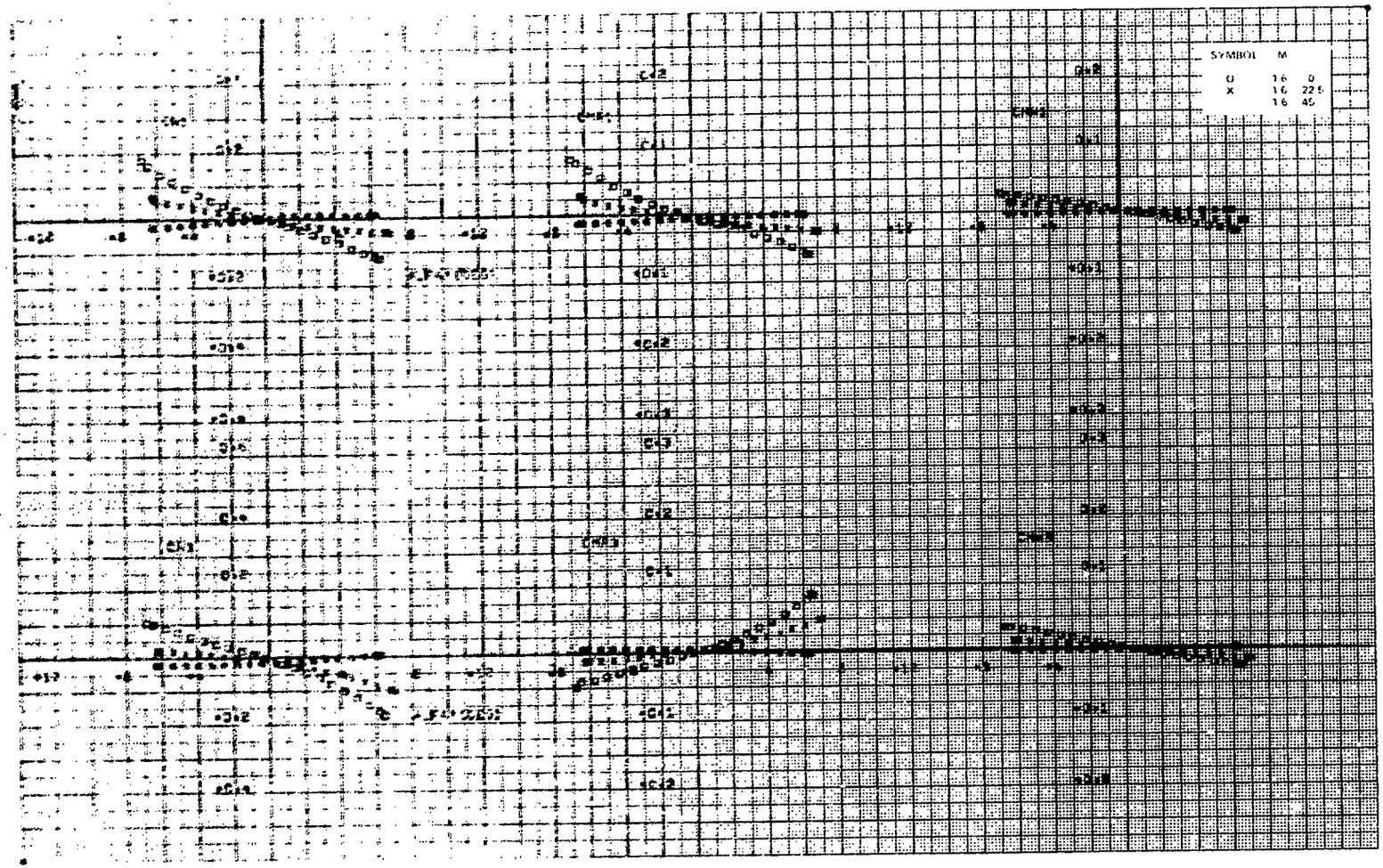


Figure 36. Continued.



Continued.

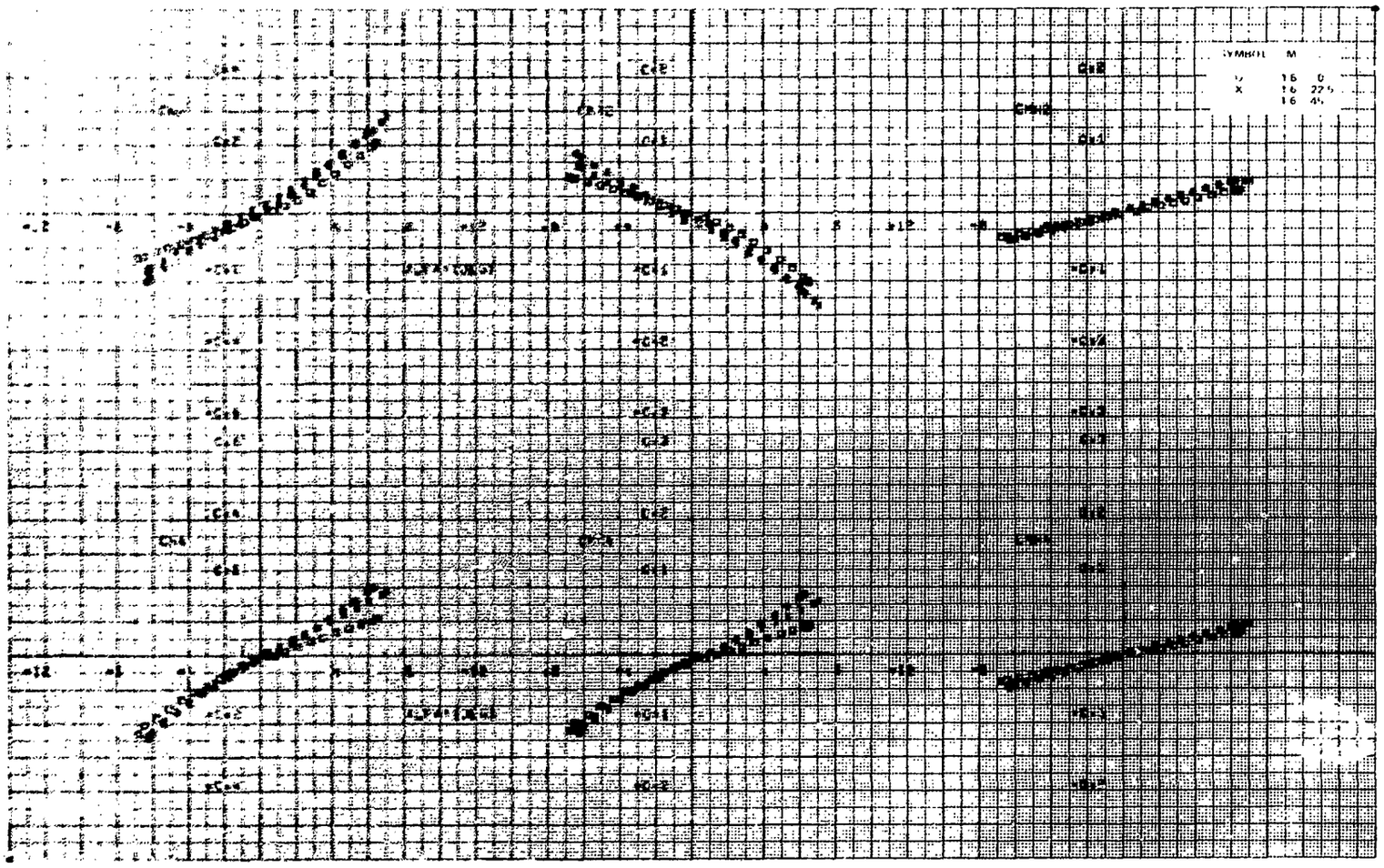


Figure 6c. Concluded.

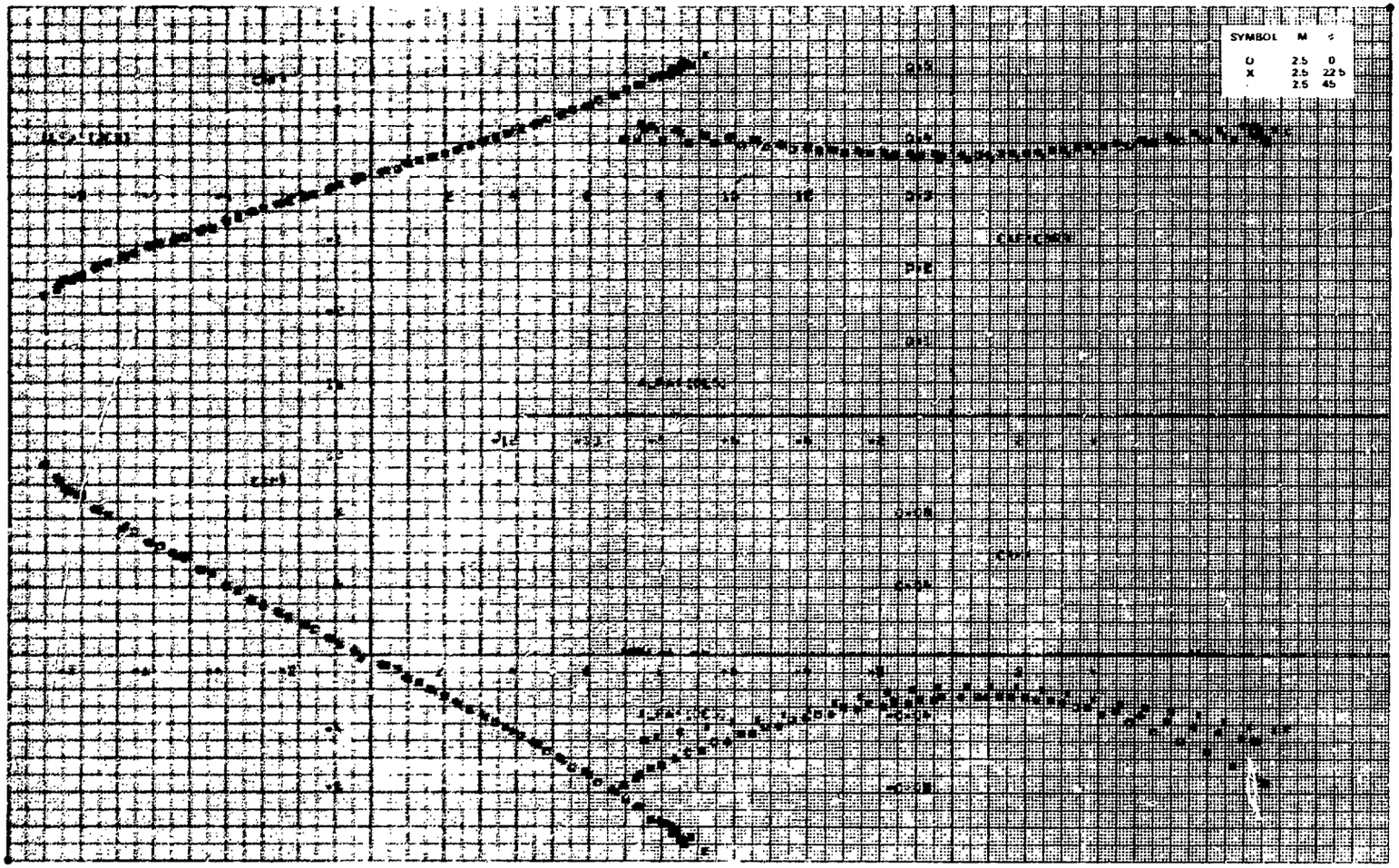


Figure 6d. [illegible], $\delta R/D = 1.75$, $\Gamma = 0$ deg, $\delta = 0$ deg, $M_\infty = 2.5$.

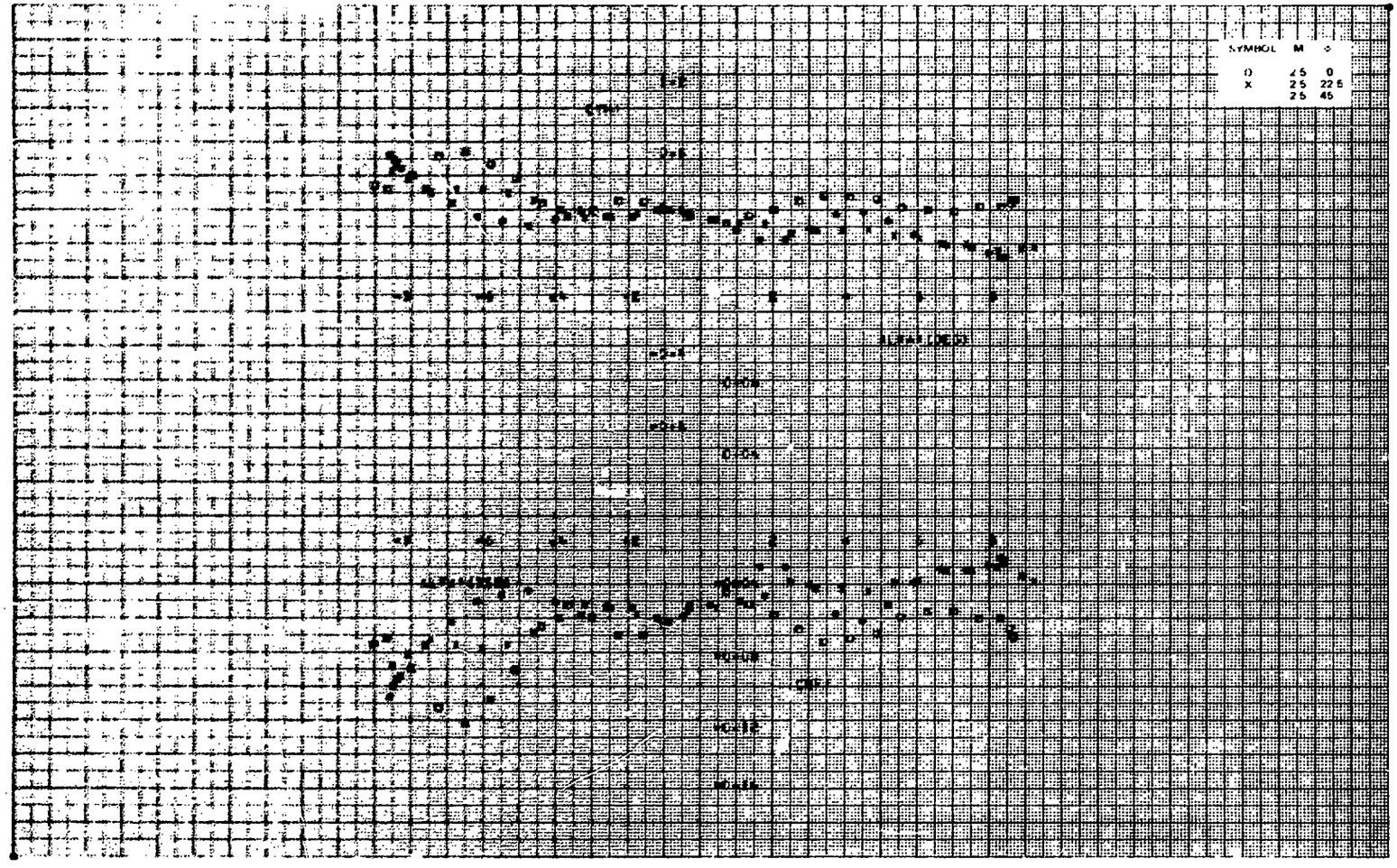


Figure 6d. Continued.

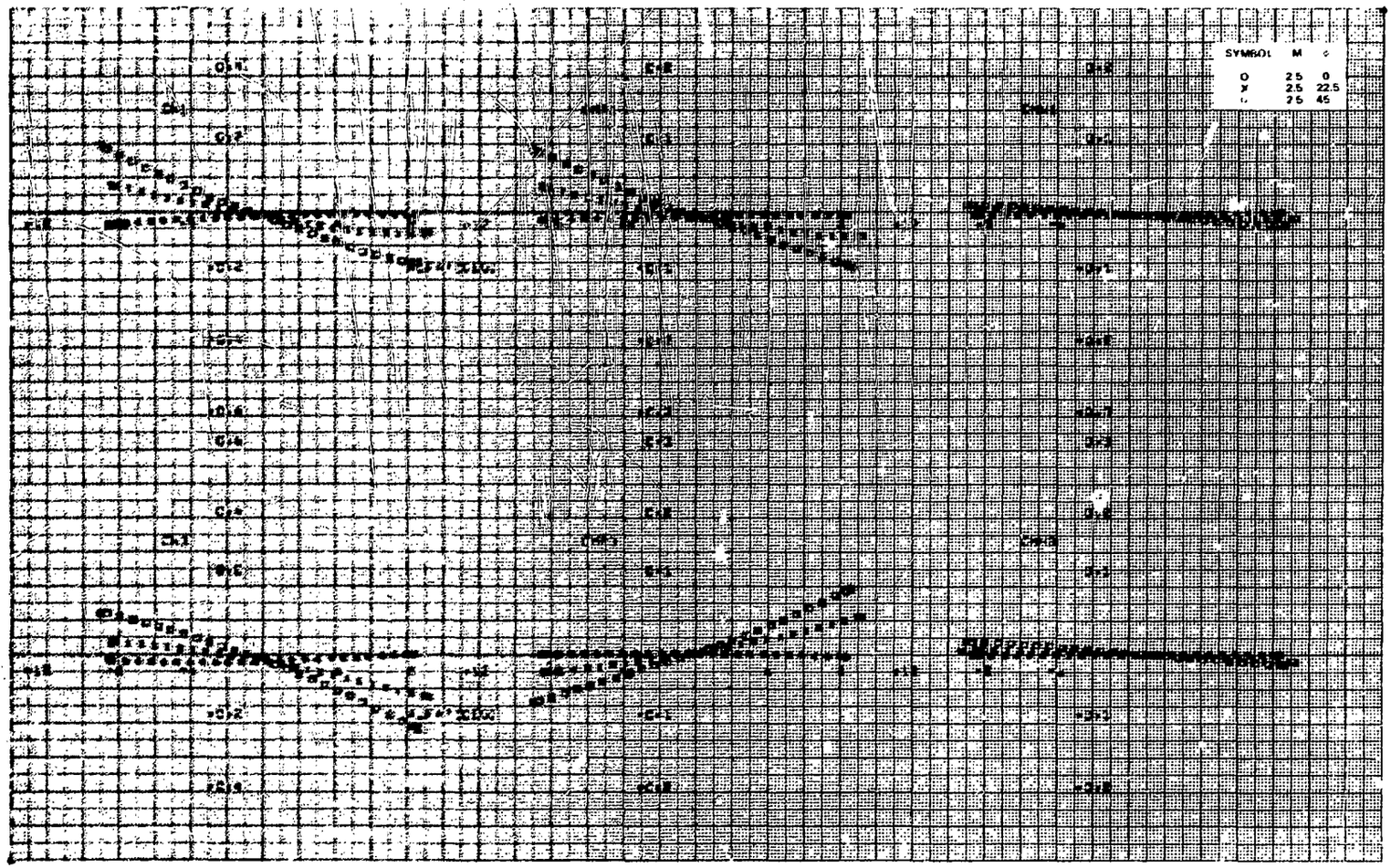


Figure 6d. Continued.

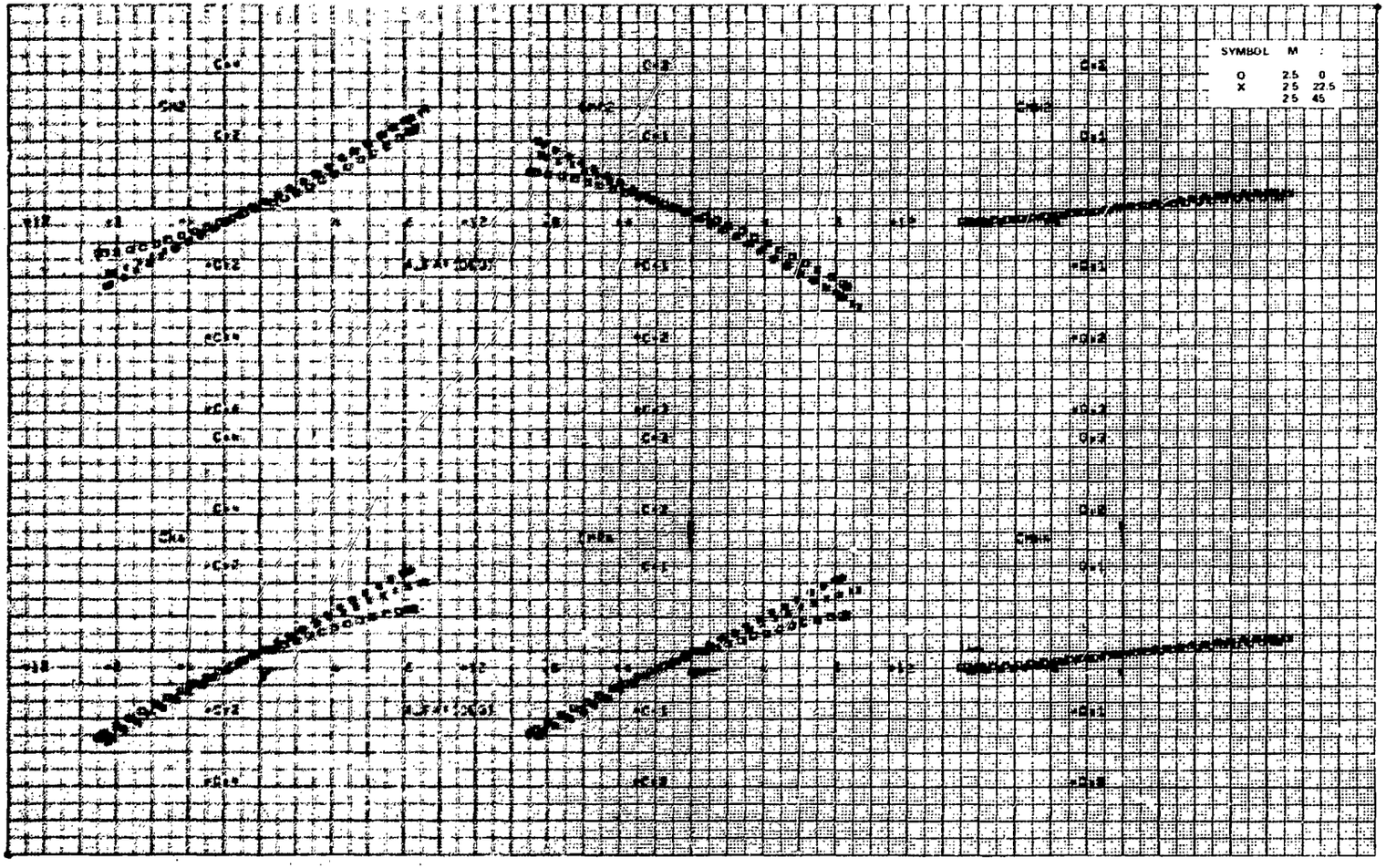


Figure 6d. Concluded.

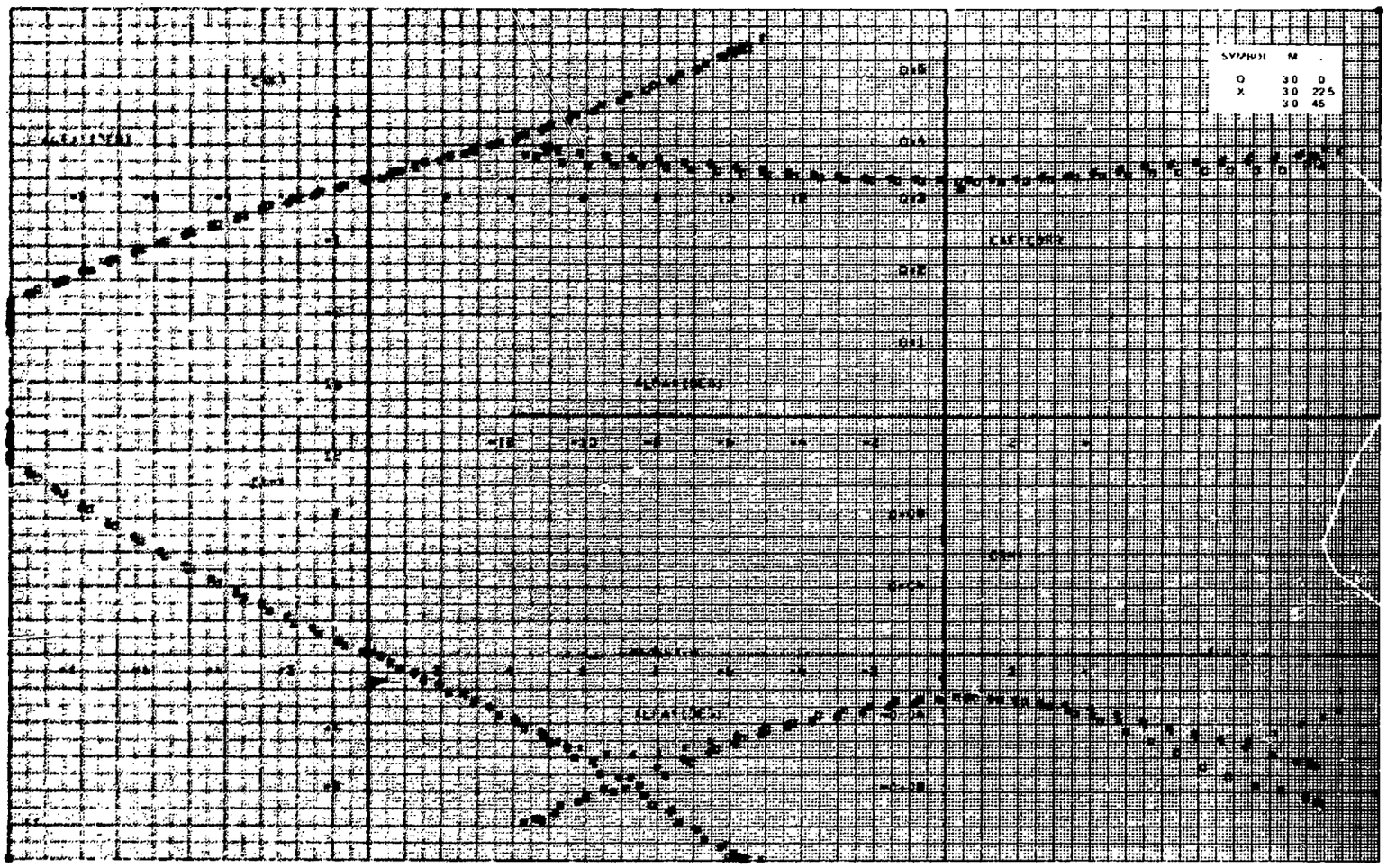


Figure 60. Experimental stability coefficients, CR/D = 1.75, = 0 deg, = 0 deg, M_∞ = 3.0.

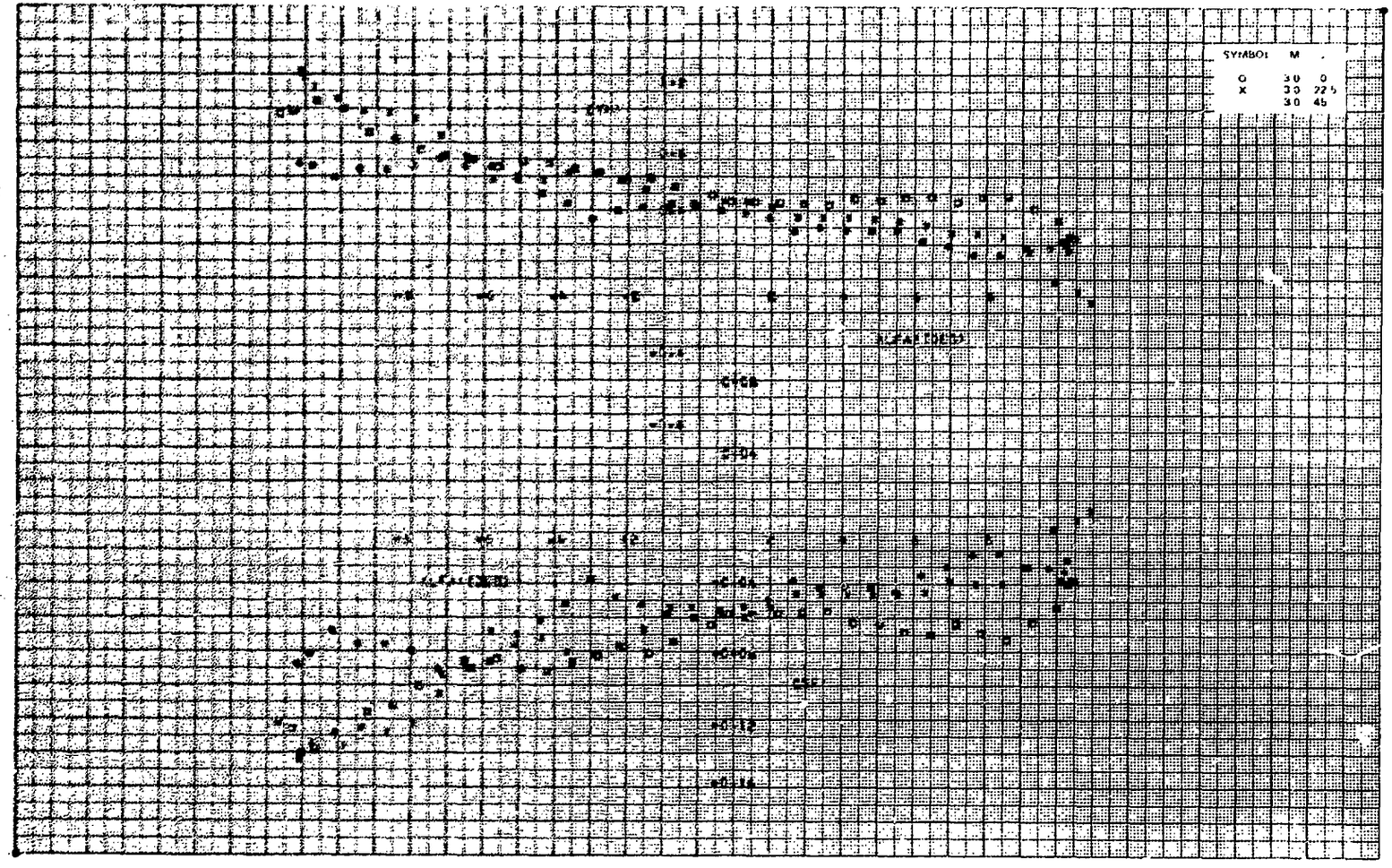


Figure 6c. Continued.

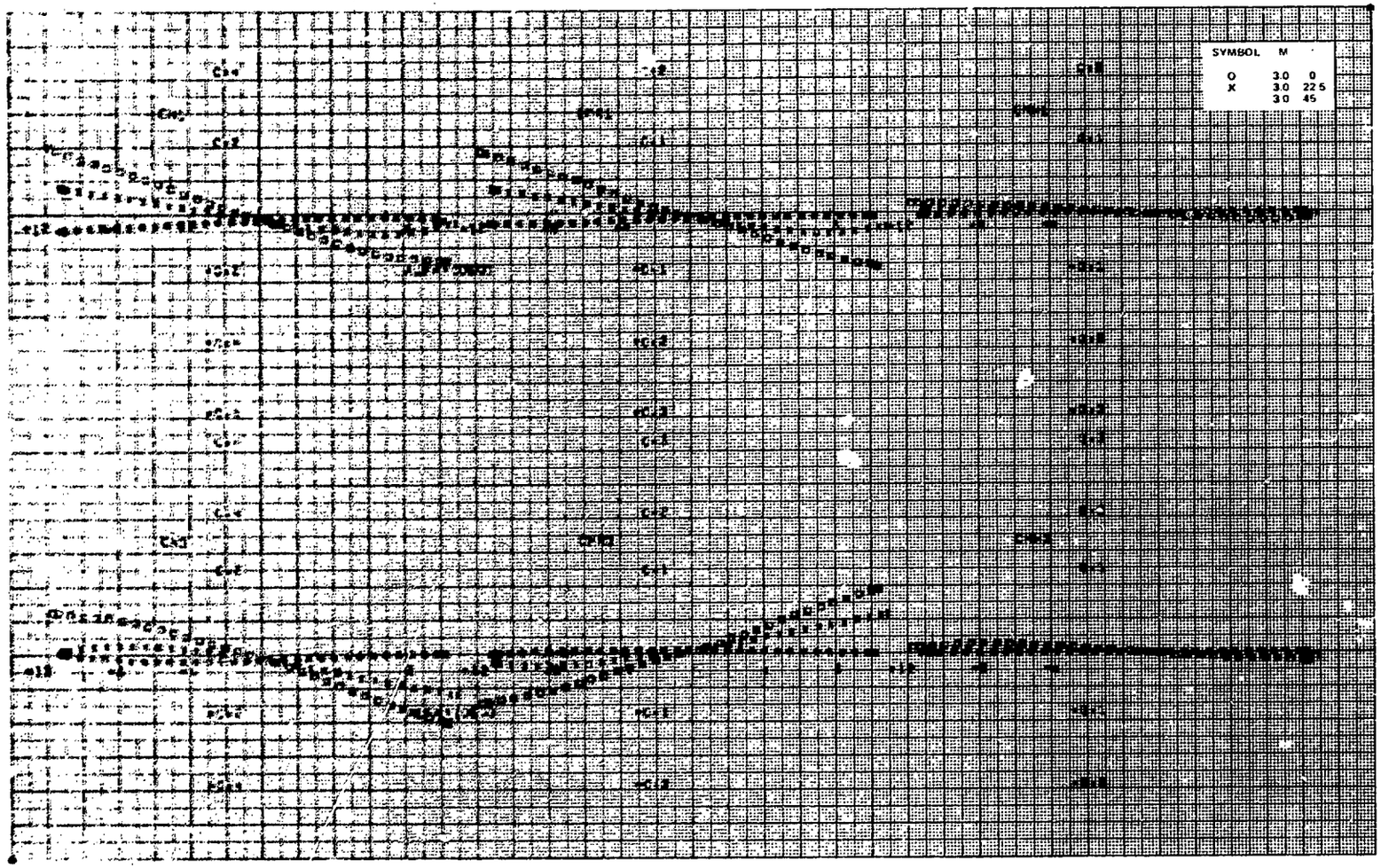


Figure 6e. Continued.

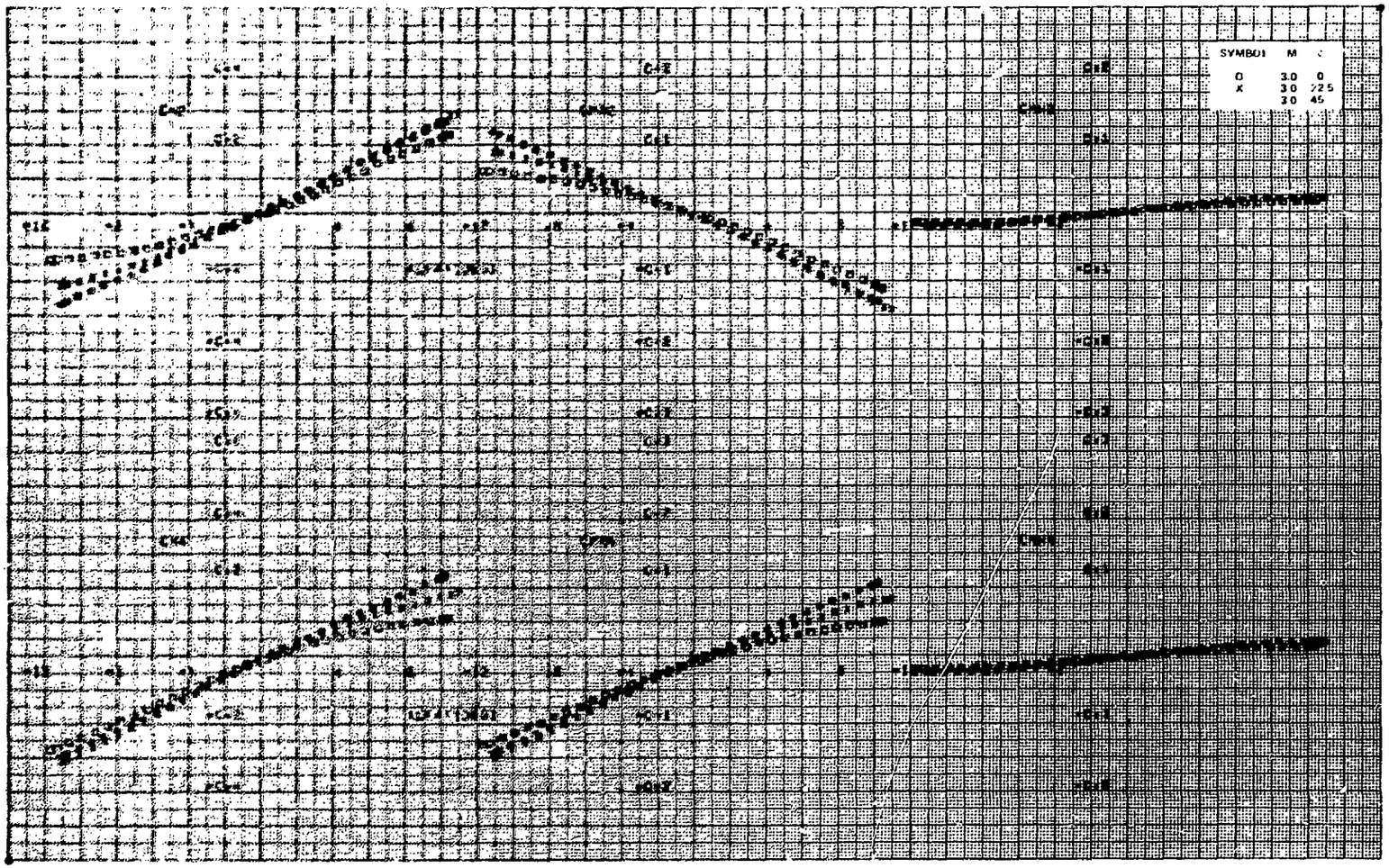


Figure 6c. Concluded.

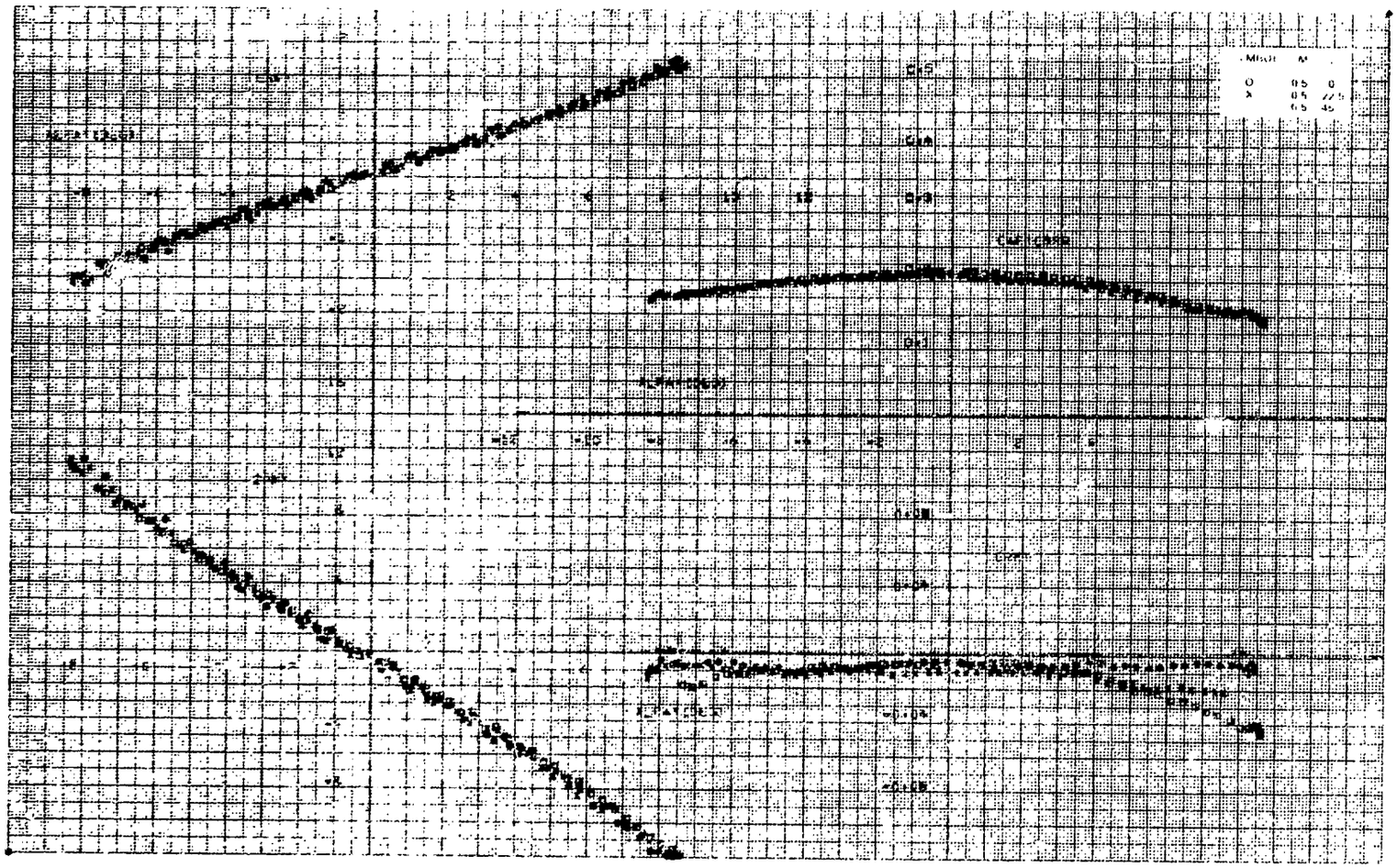


Figure 7.

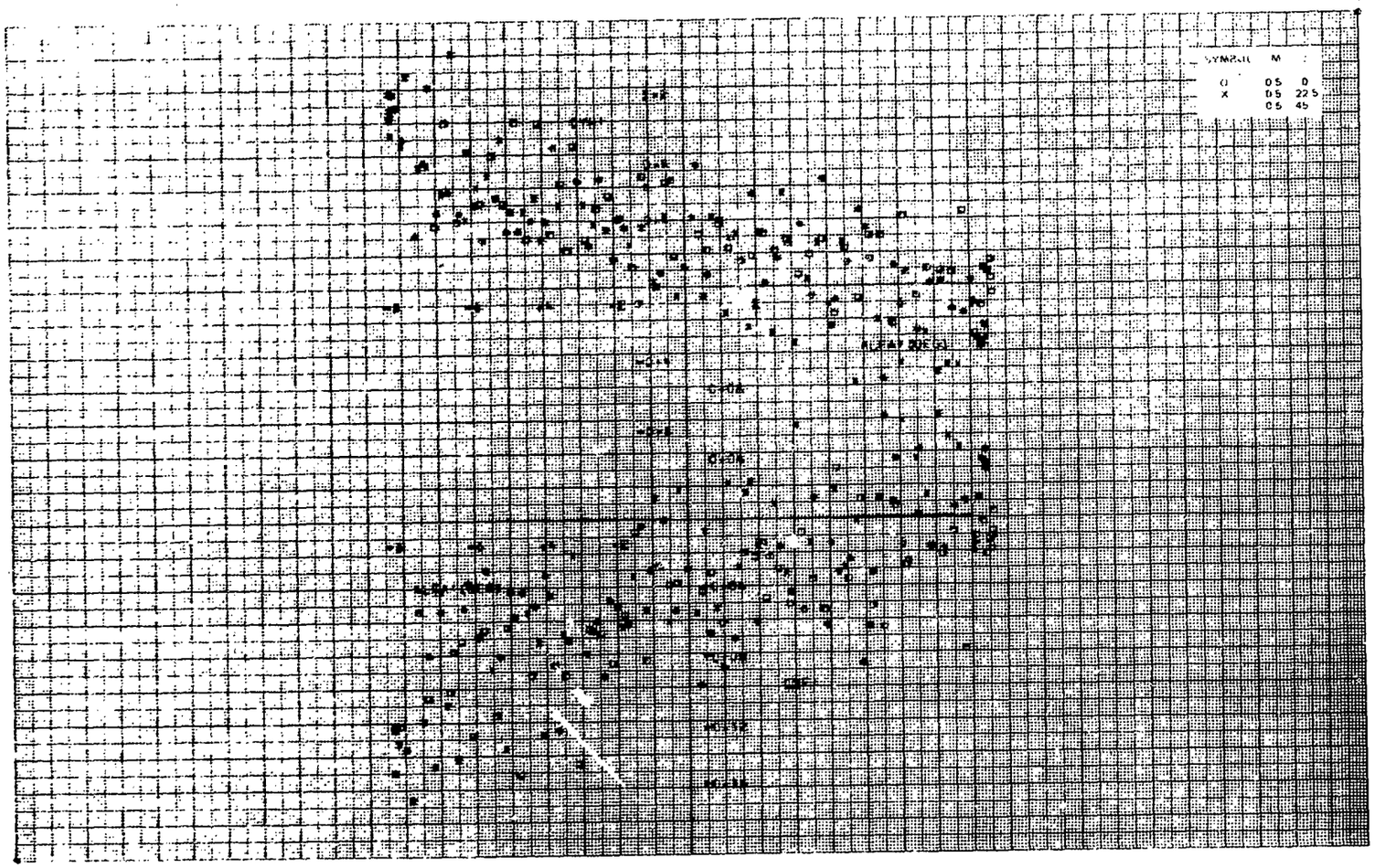


Figure 7a. Continued.

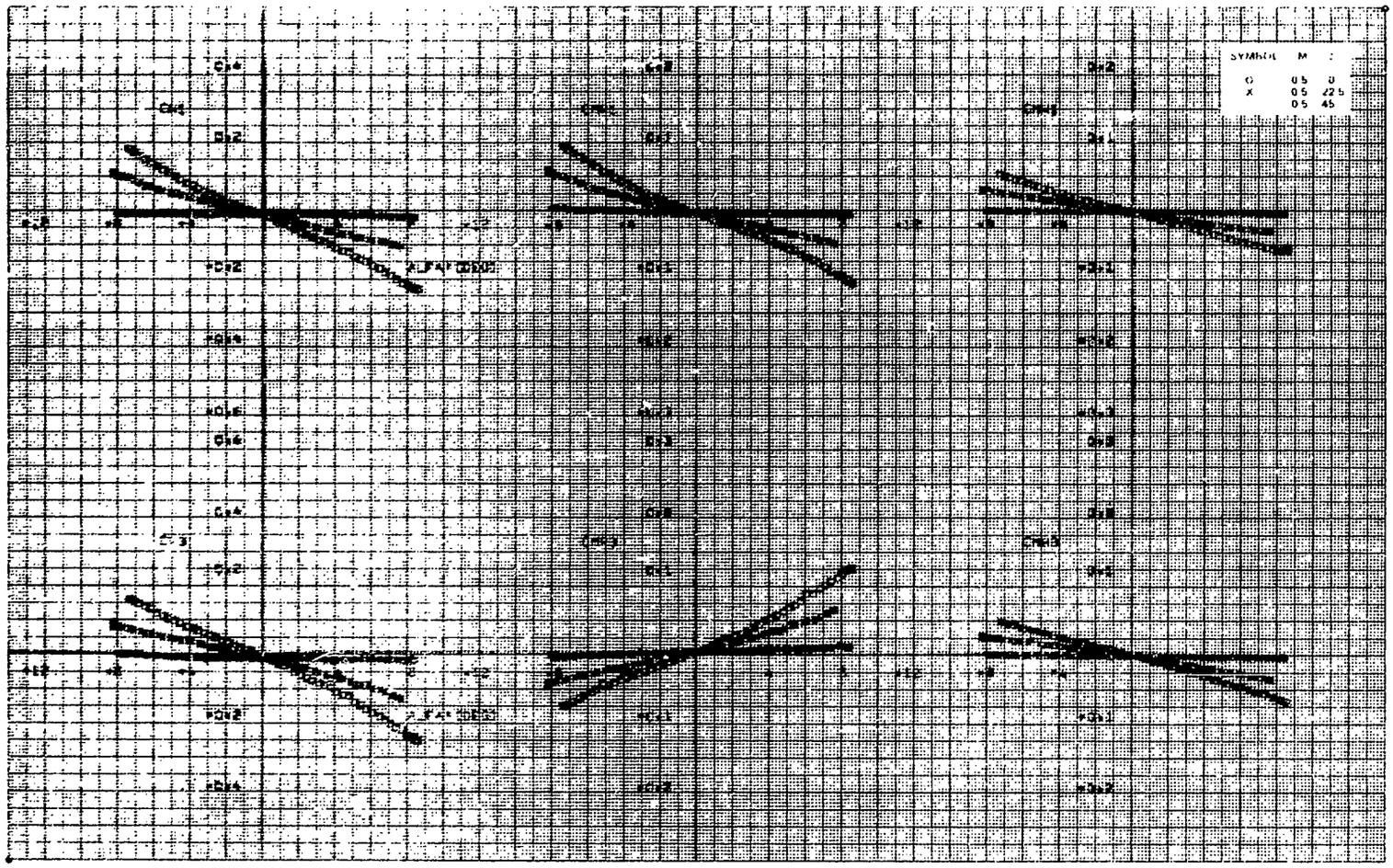


Figure 22. Continued.

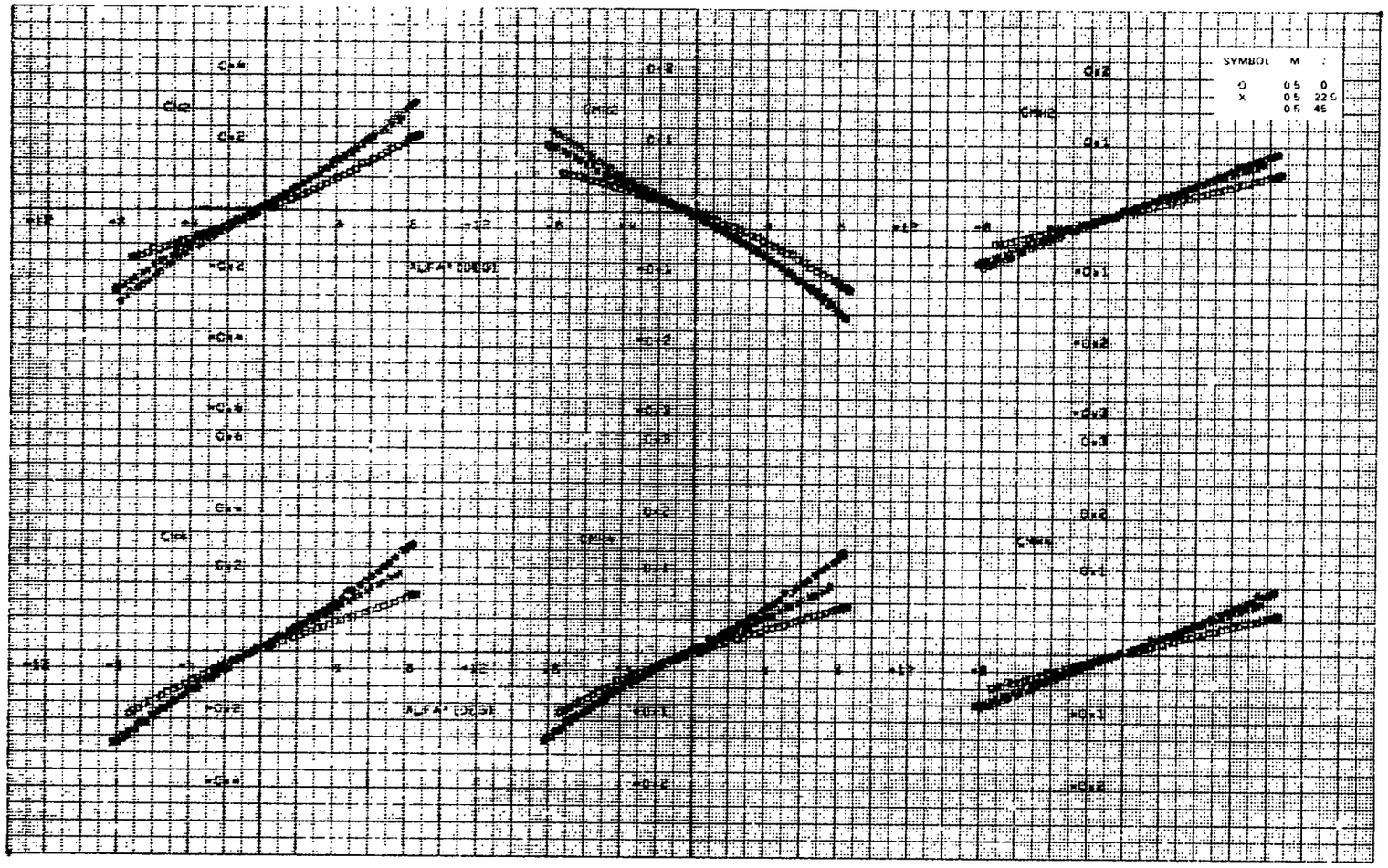
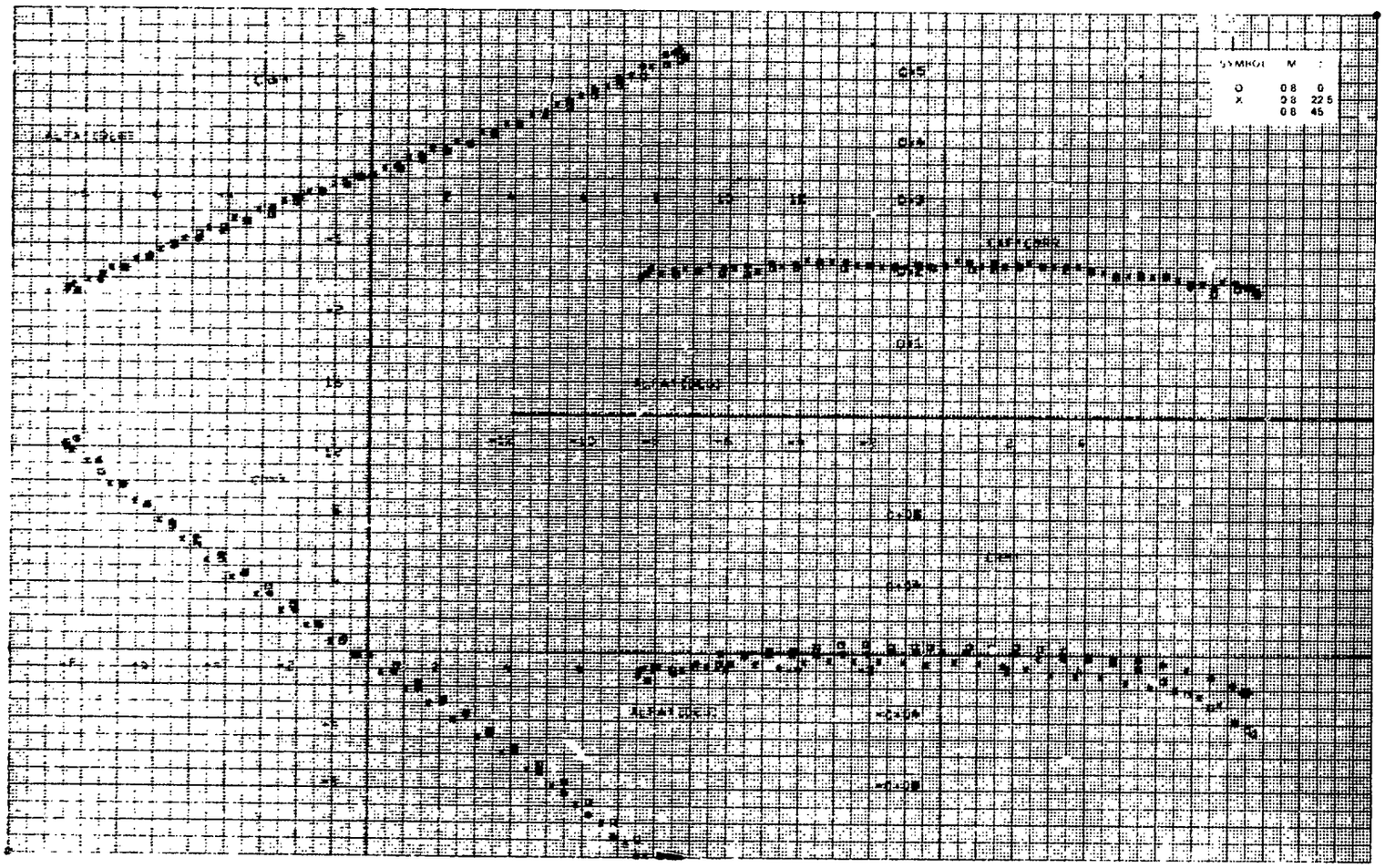


Figure 7a. Concluded.



Aerodynamic stability coefficients, CR/D = 1.75, β = 0 deg, δ_e = 10 deg, M_∞ = 0.8.

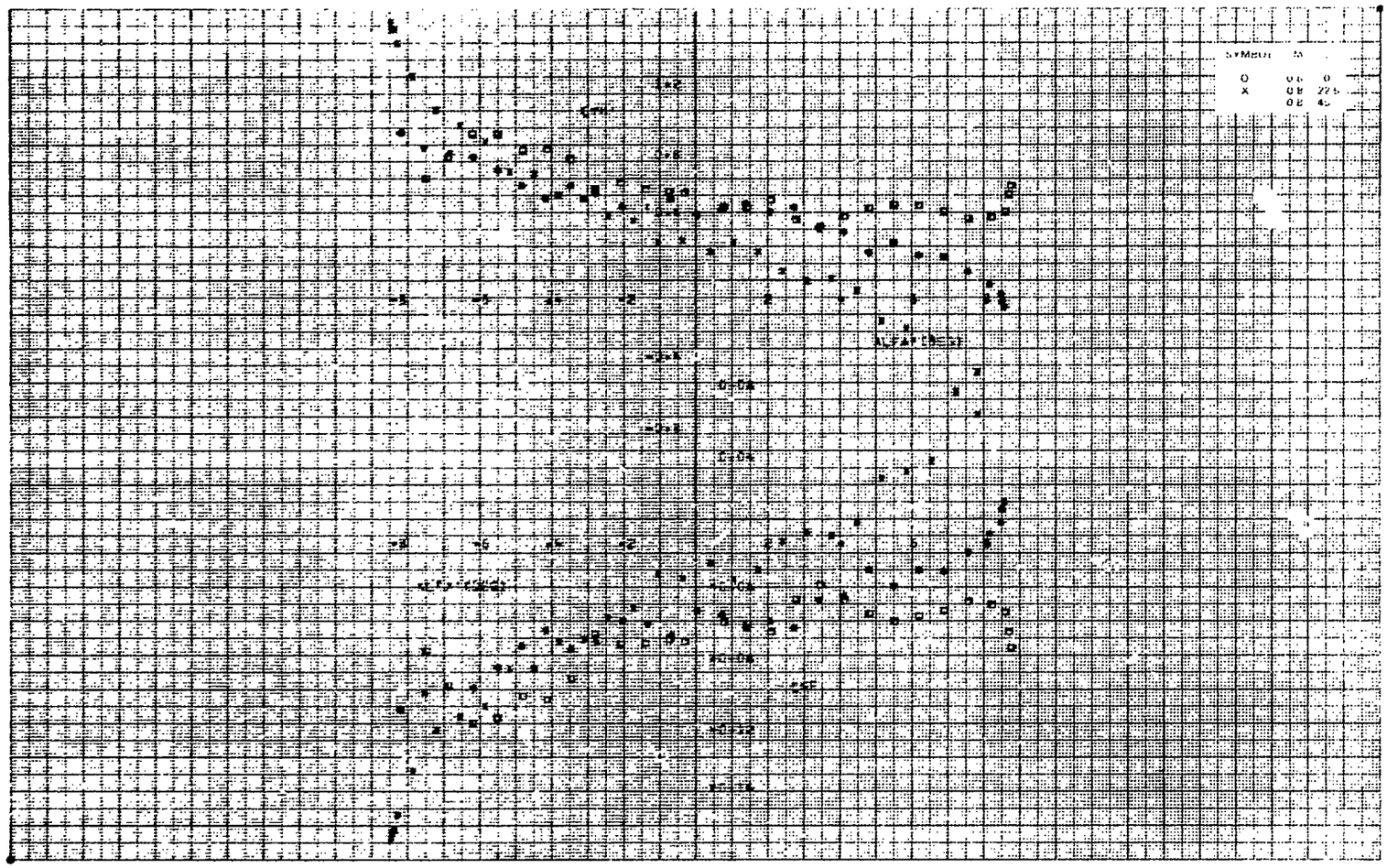


Figure 7b. Continued.

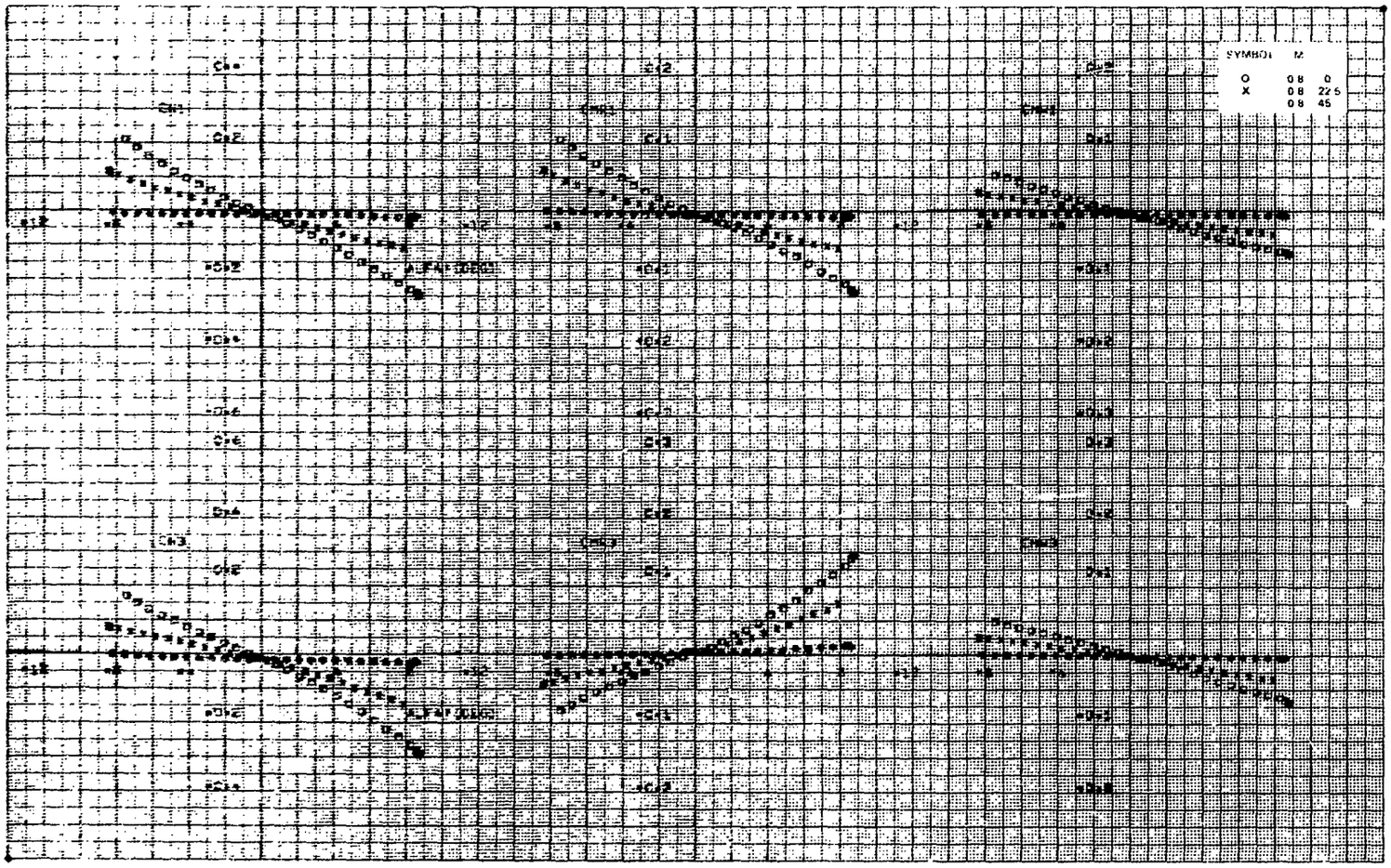


Figure 7b. Continued.

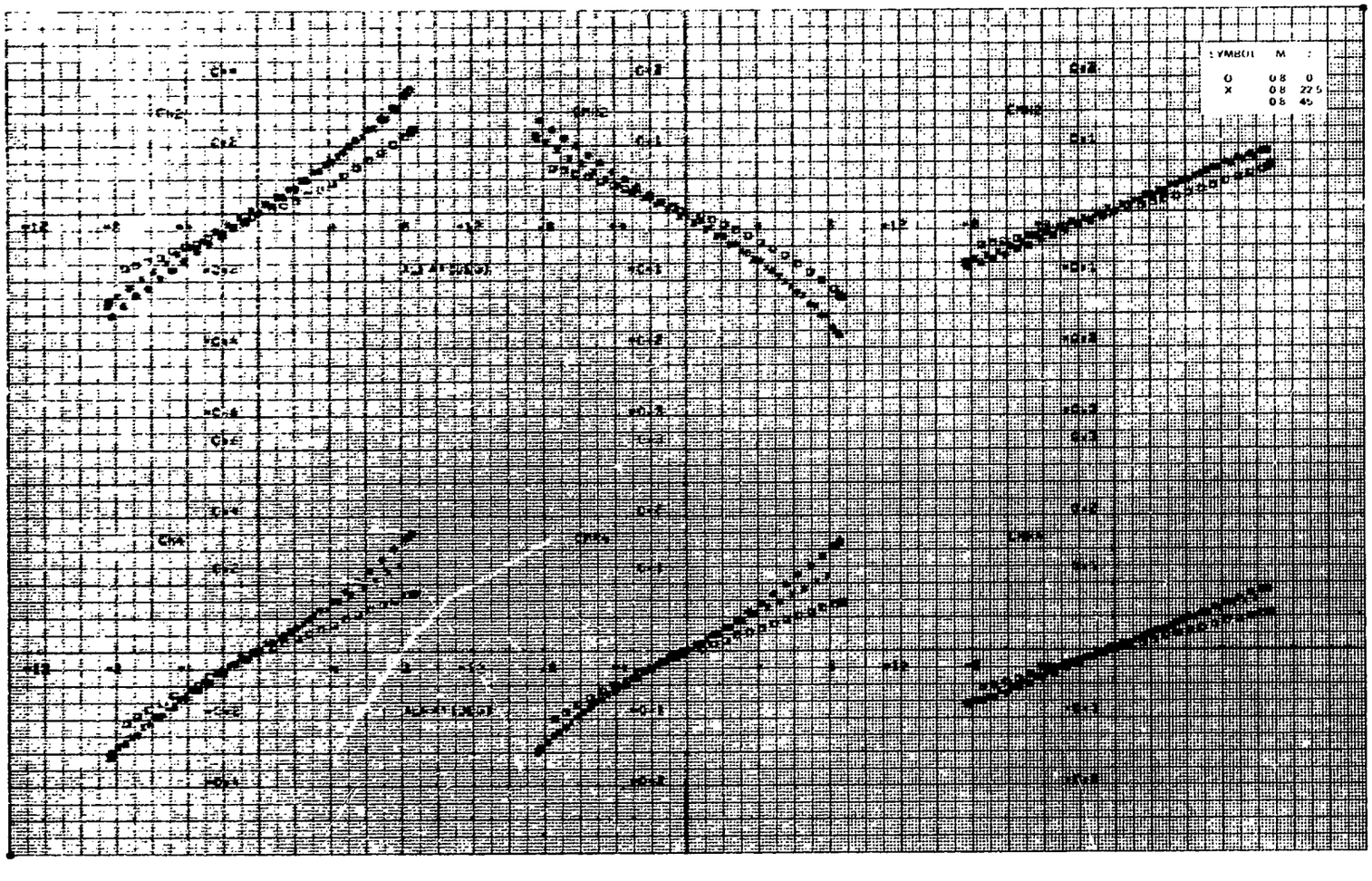


Figure 7b. Concluded.

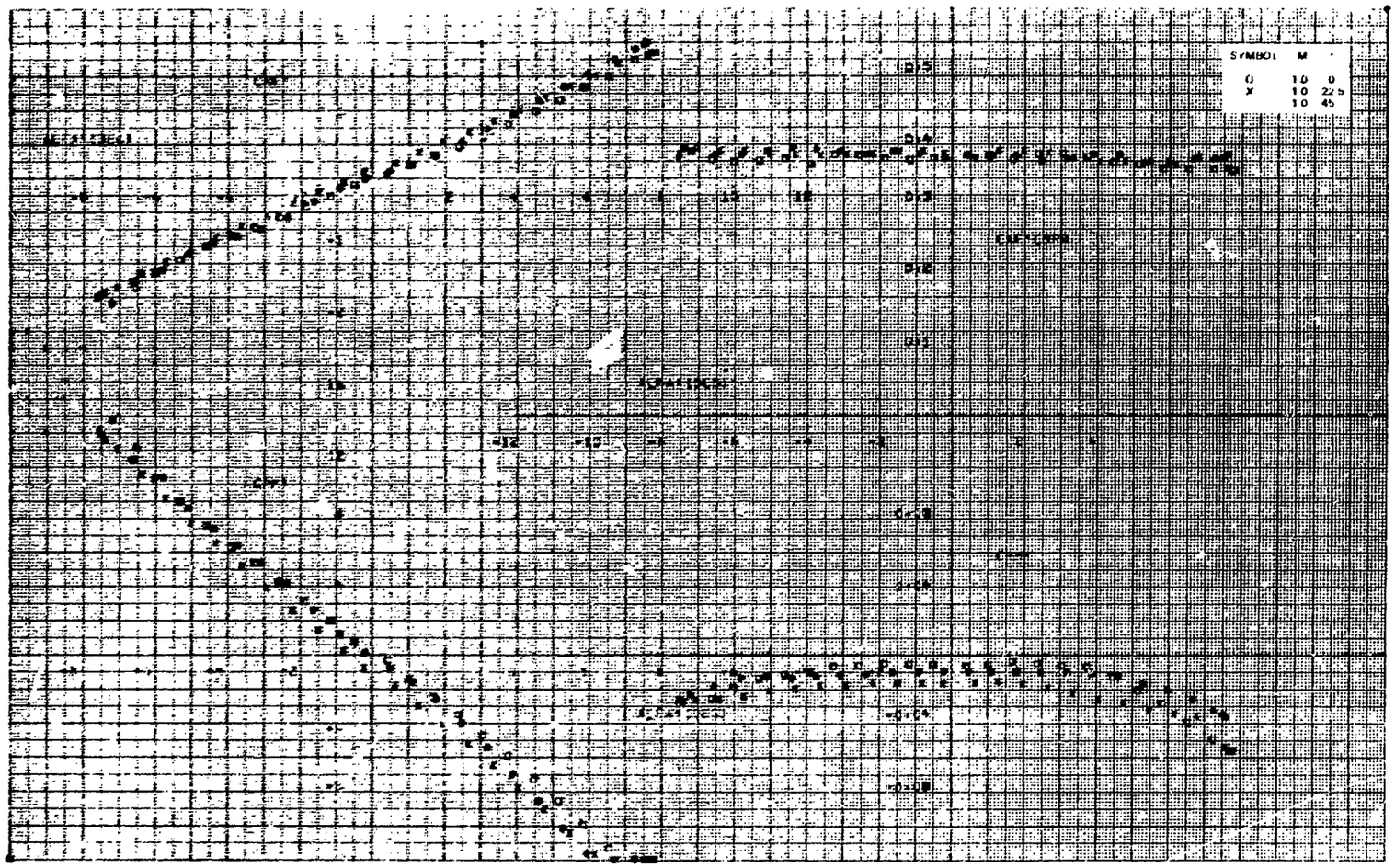


Figure 7c. Aerodynamic stability coefficients, CR/B = 1.5, ϕ = 0 deg, ζ = 10 deg, M_∞ = 1.0.

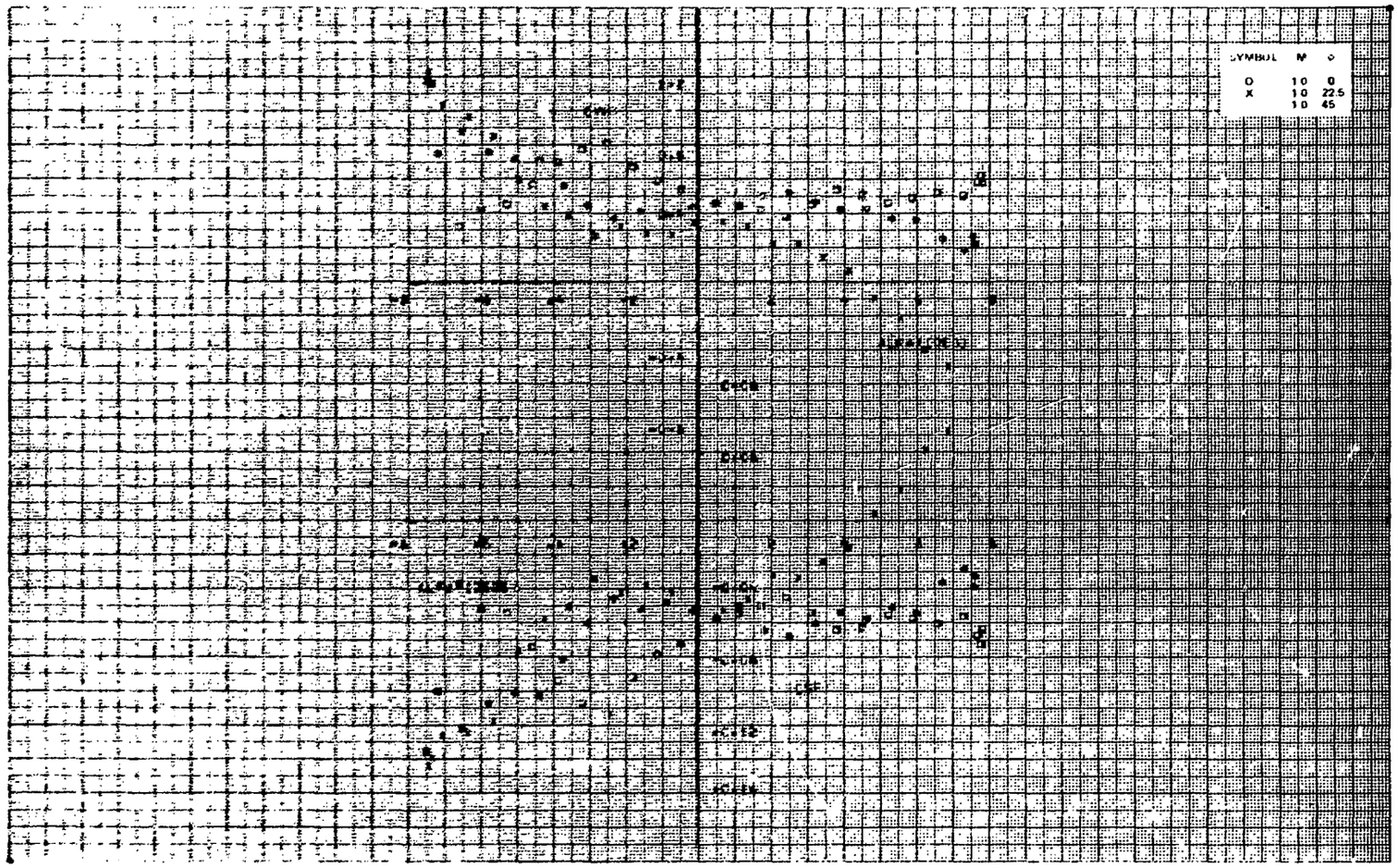


Figure 7c. Continued.

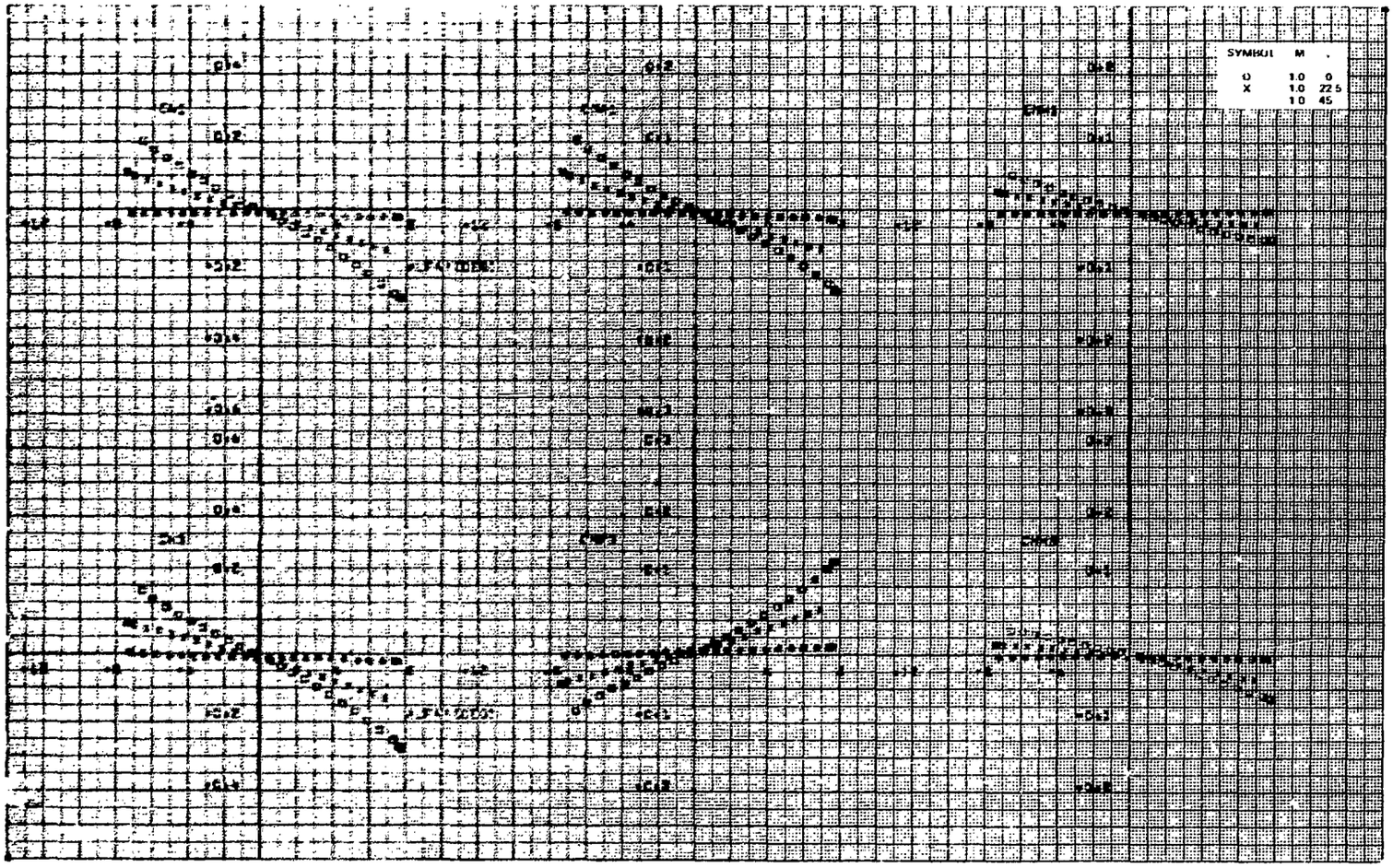


Figure 7c. Continued.

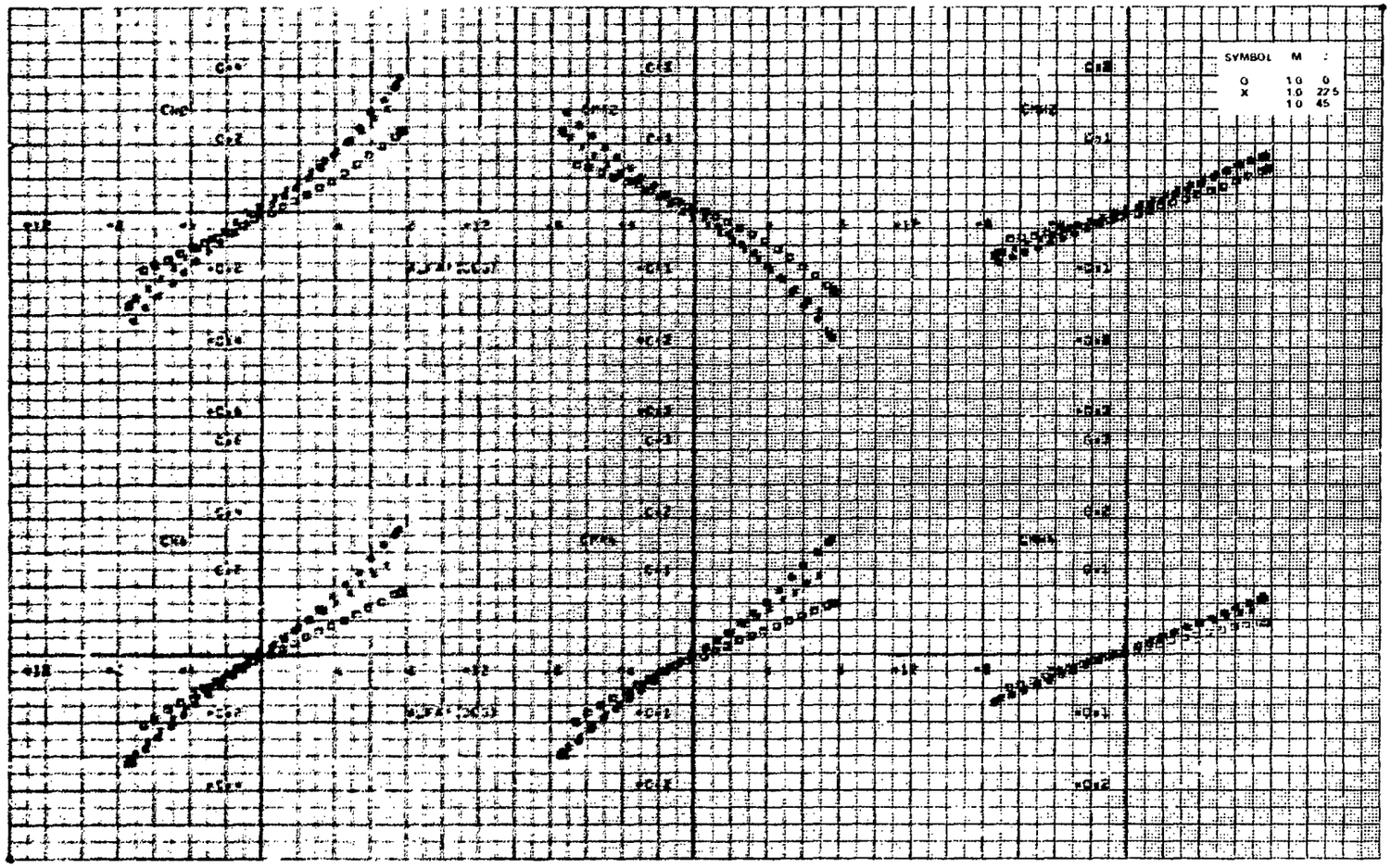
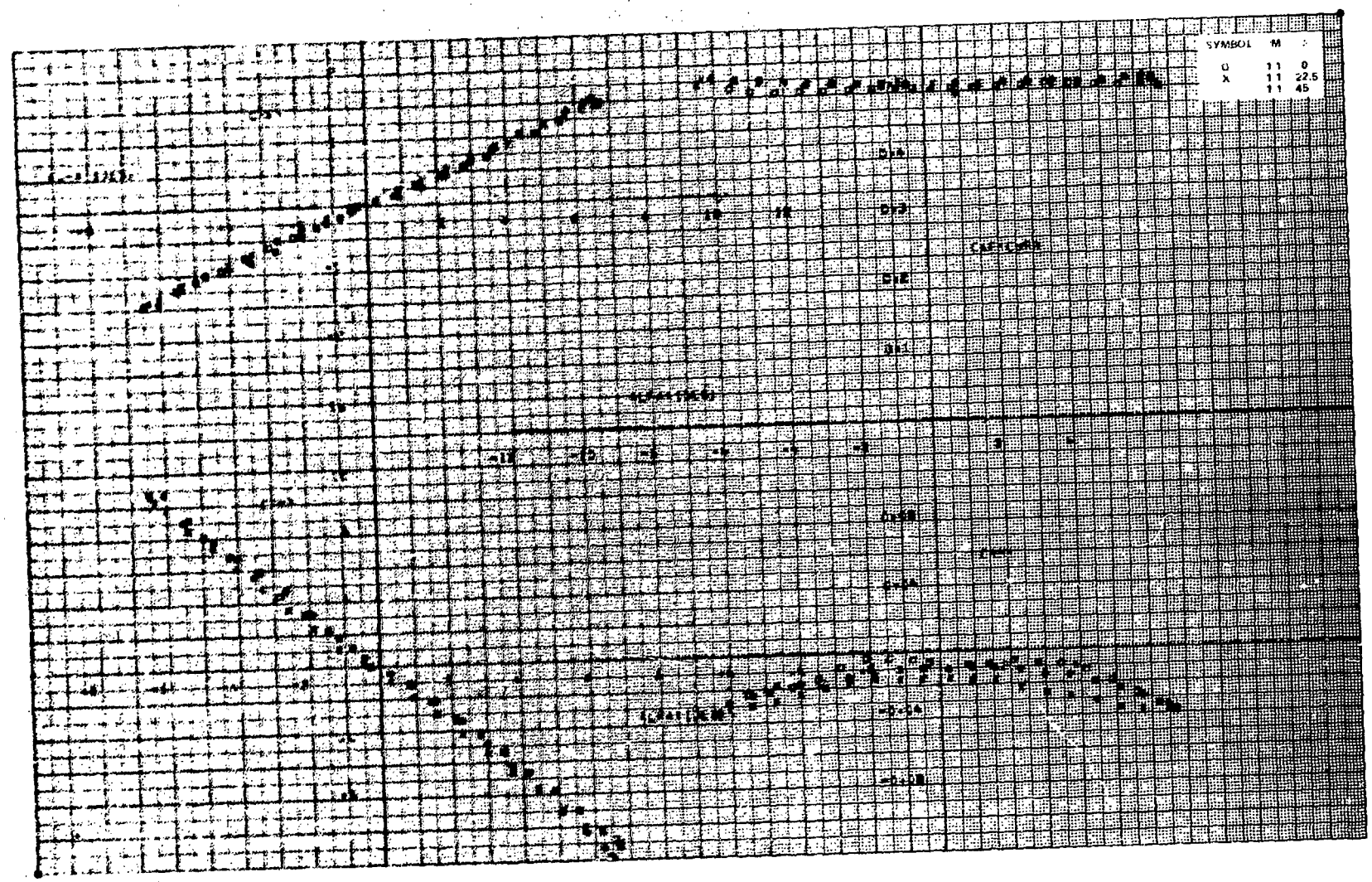
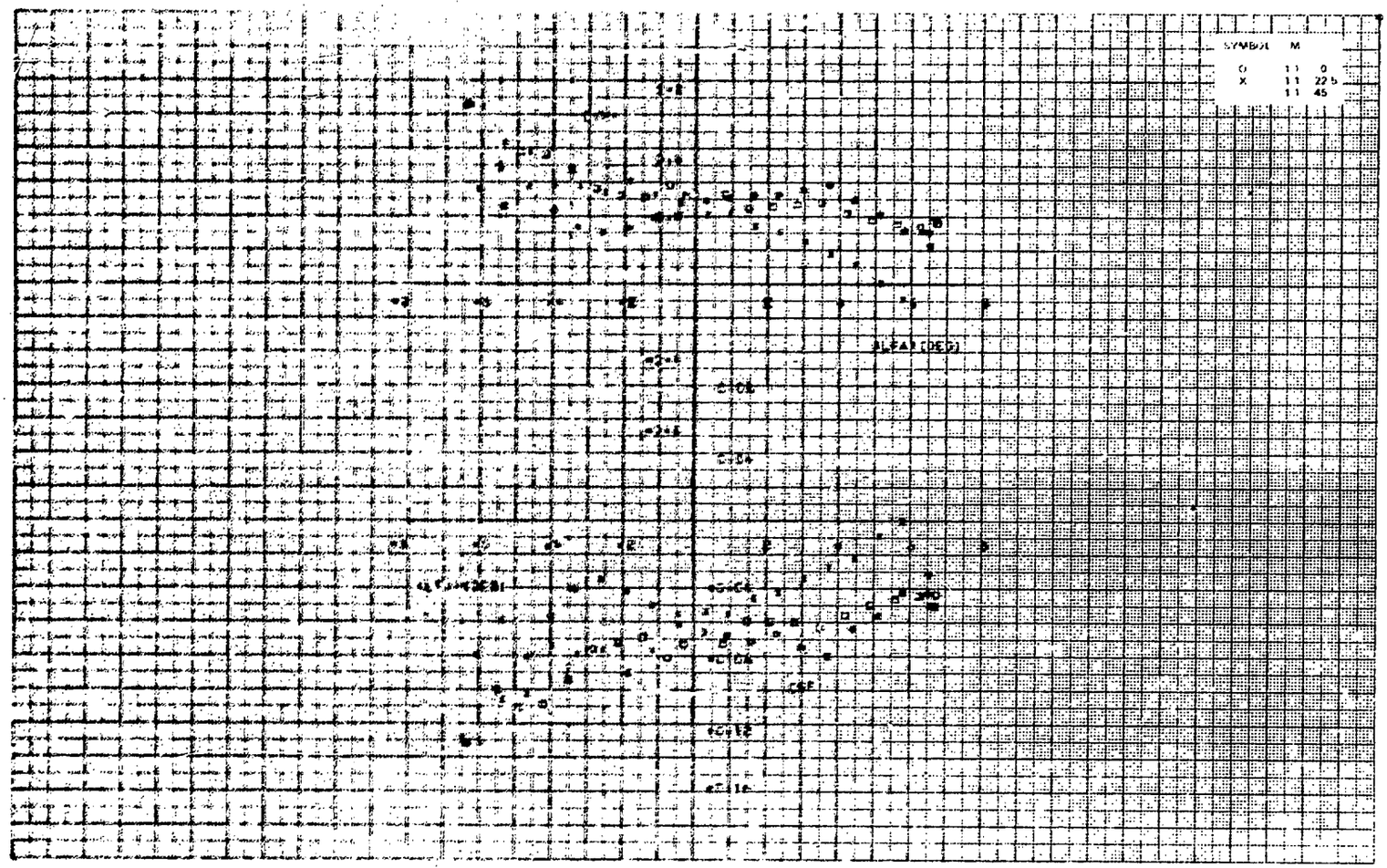


Figure 7c. Concluded.



...stability coefficients, CR/D = 1.75, ' = 0 deg, δ_e = 10 deg, M_∞ = 1.1.


SYMBOL M
O 11 0
X 11 22.5
11 45
ALPHA (DEG)

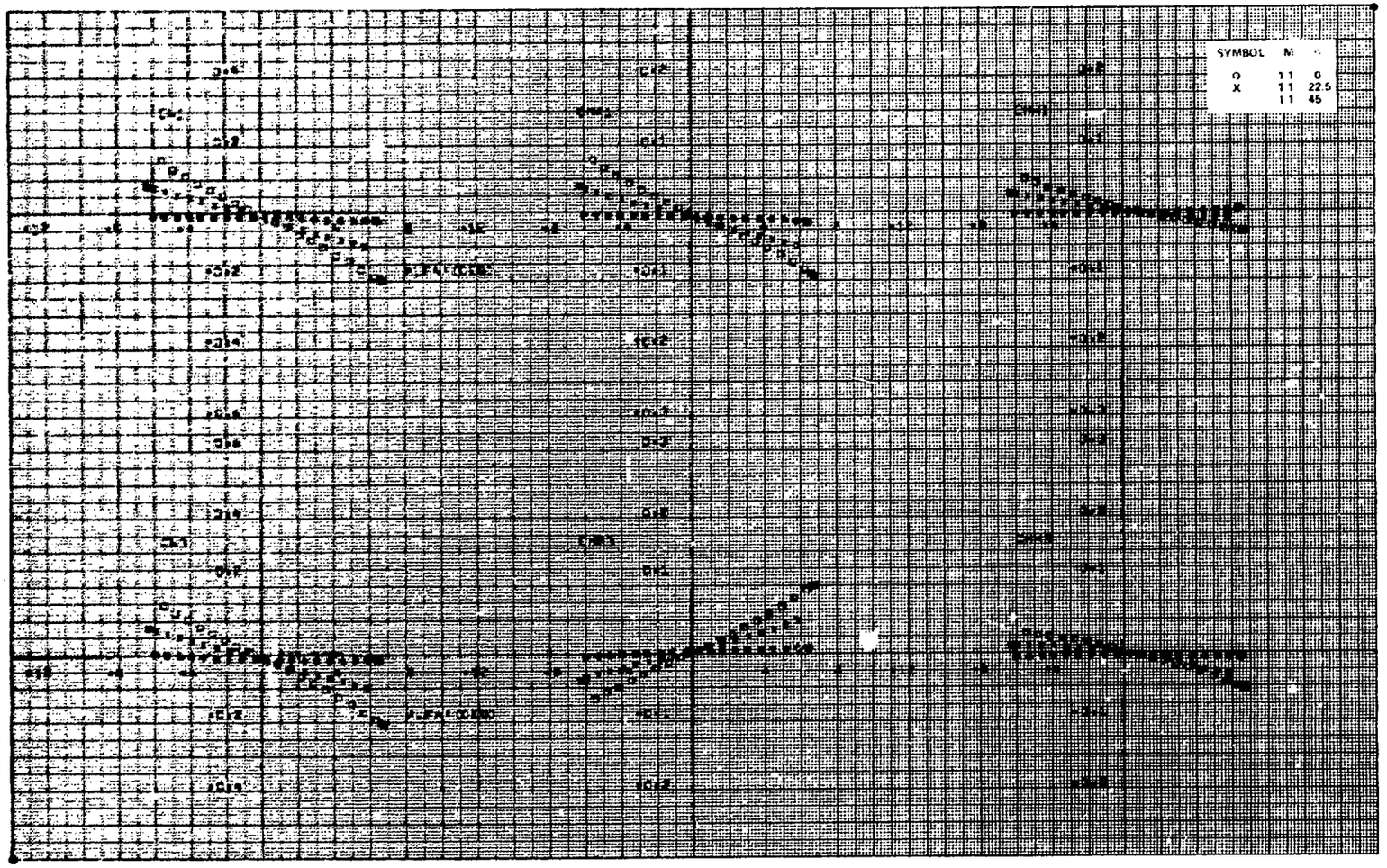


Figure 7d. Continued.

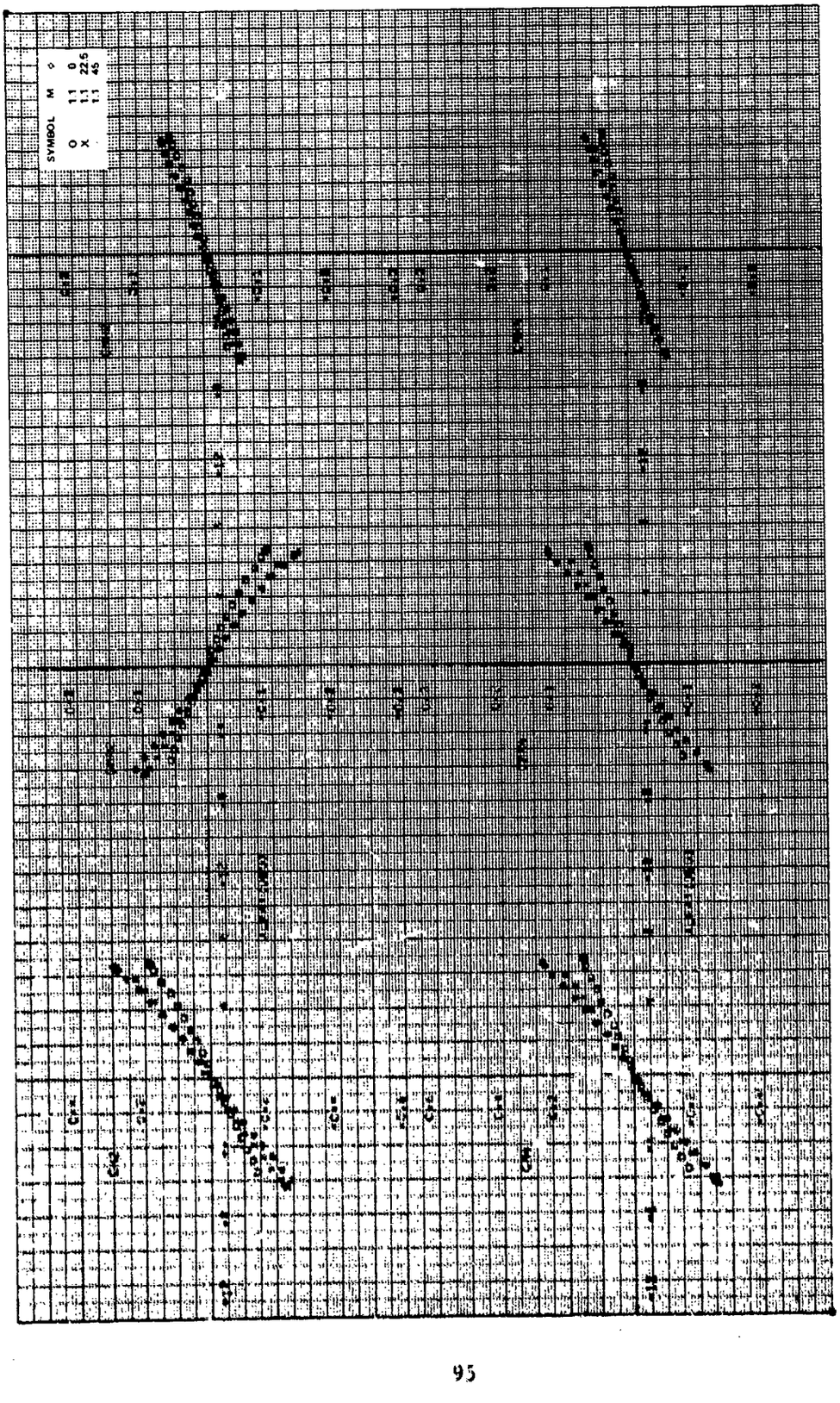


Figure 7d. Concluded.

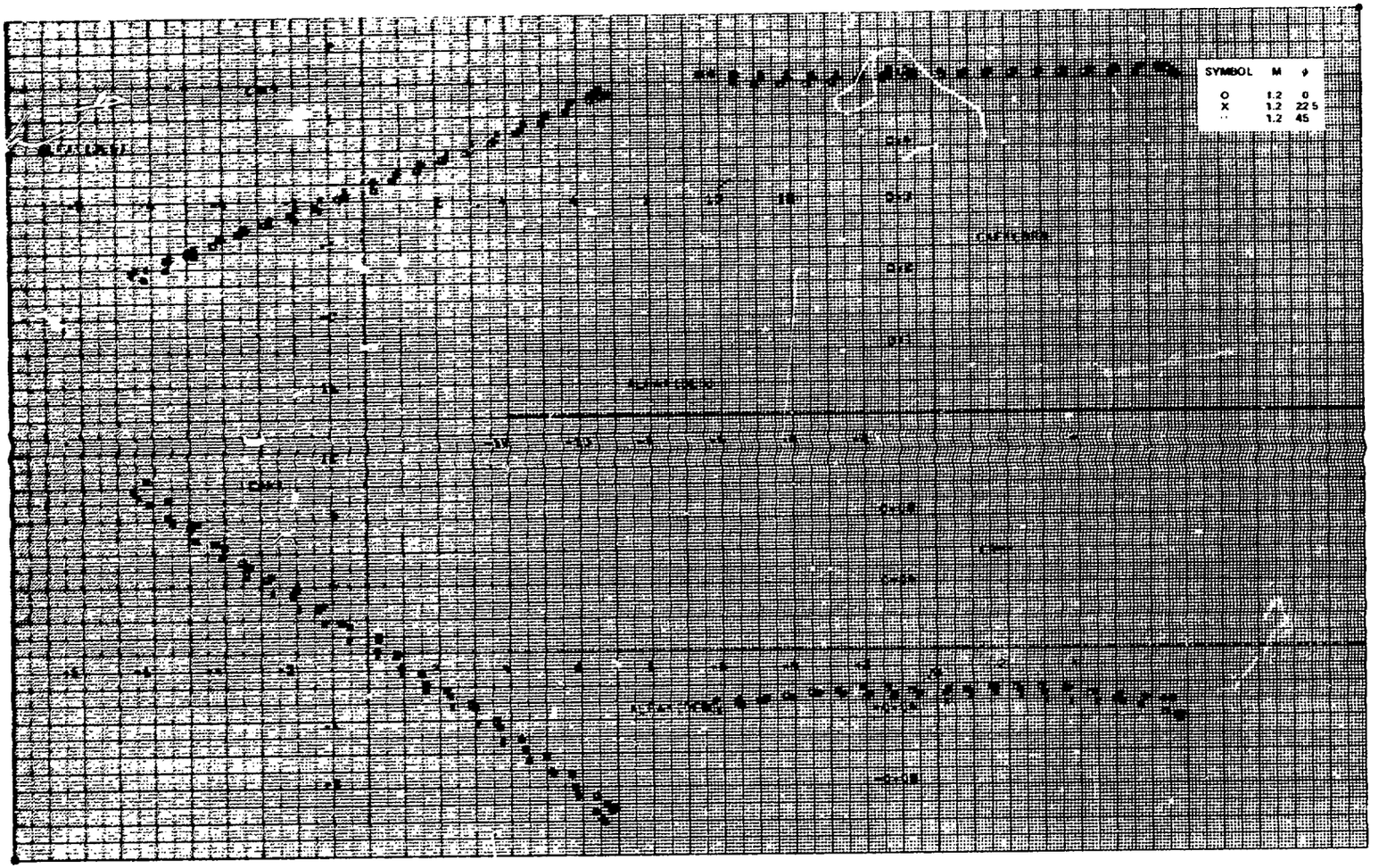


Figure 7e. Aerodynamic stability coefficients, CR/D = 1.75, ϕ = 0 deg, θ = 10 deg, M_∞ = 1.2.

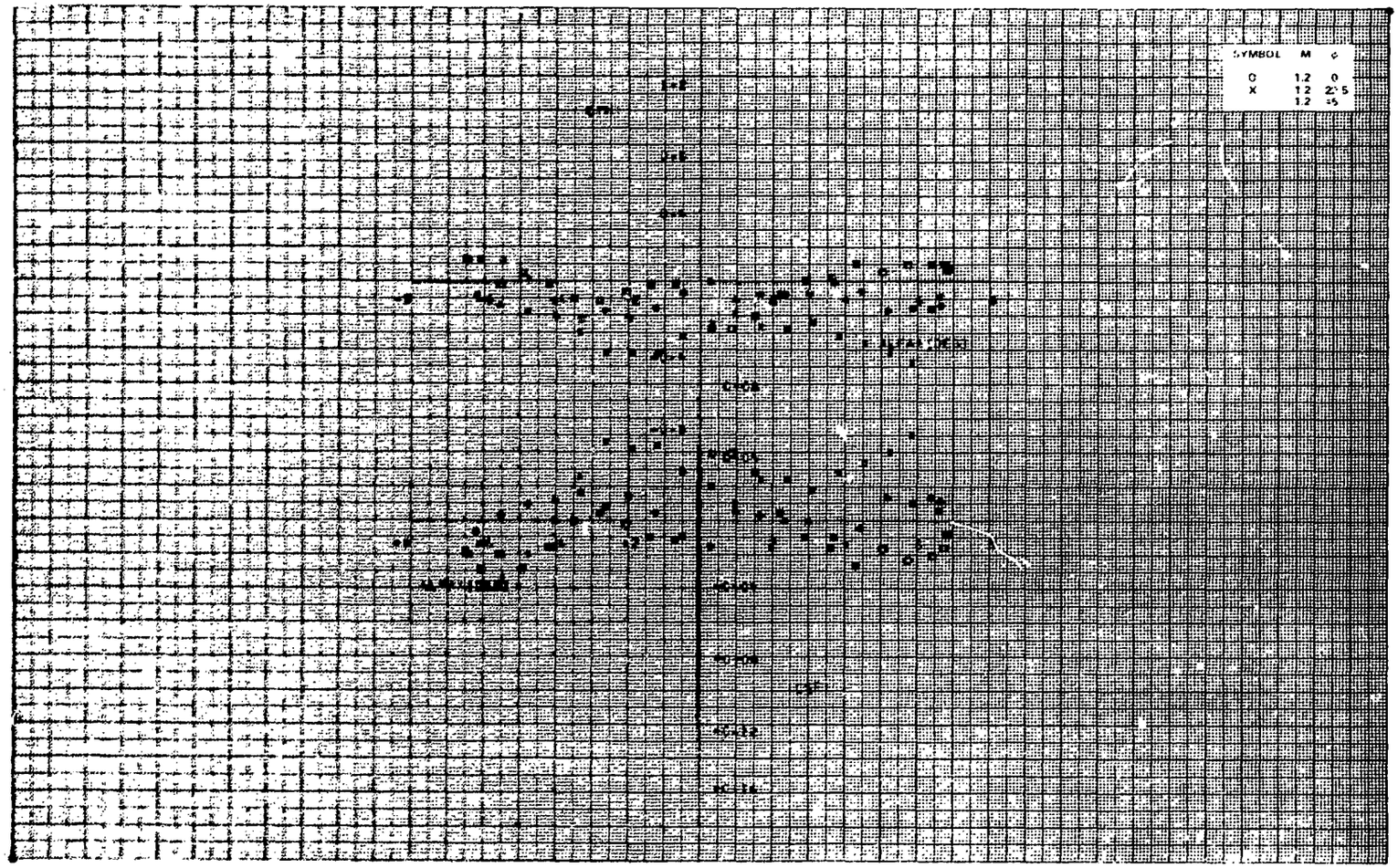


Figure 7e. Continued.

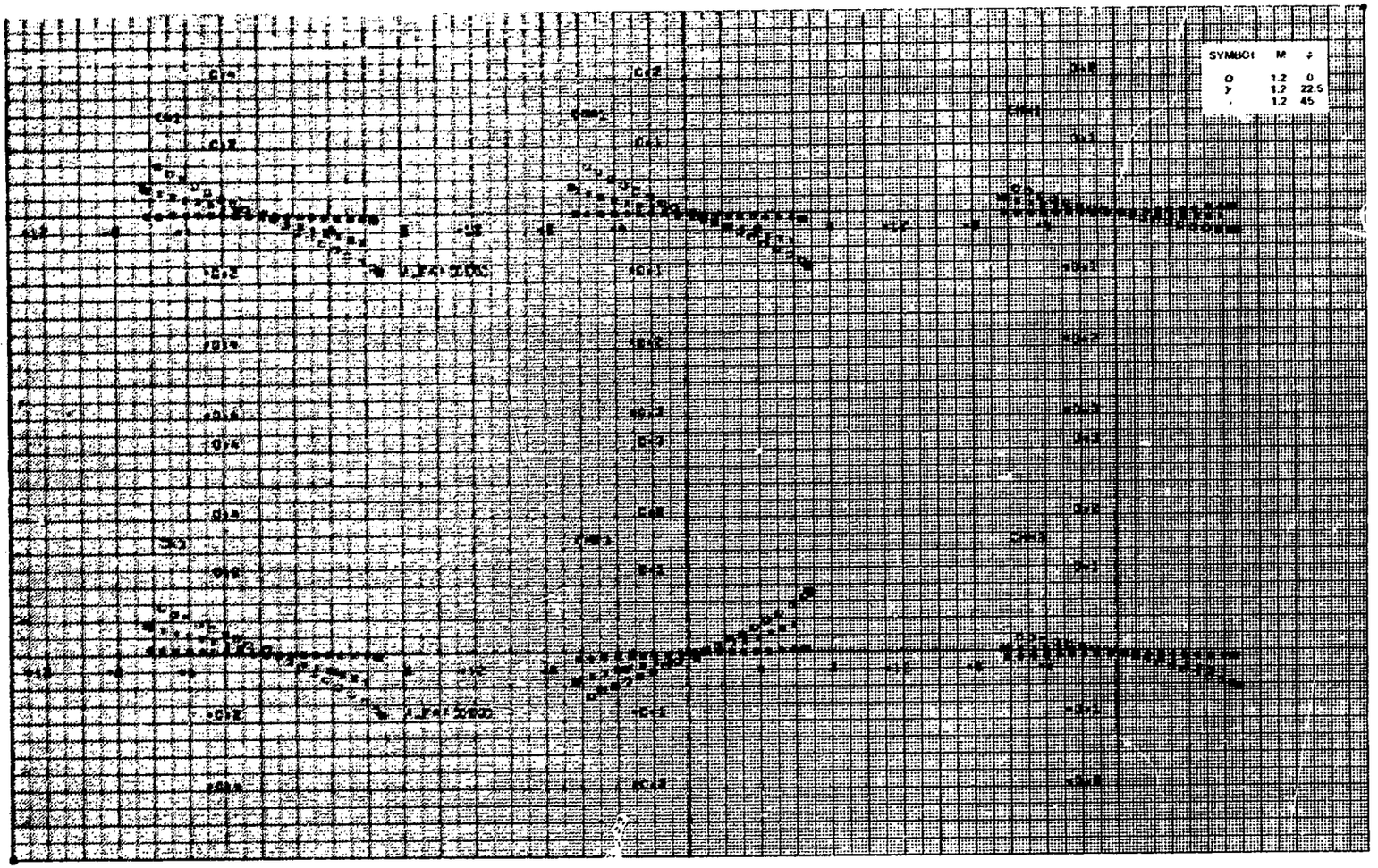


Figure 7e. Continued.

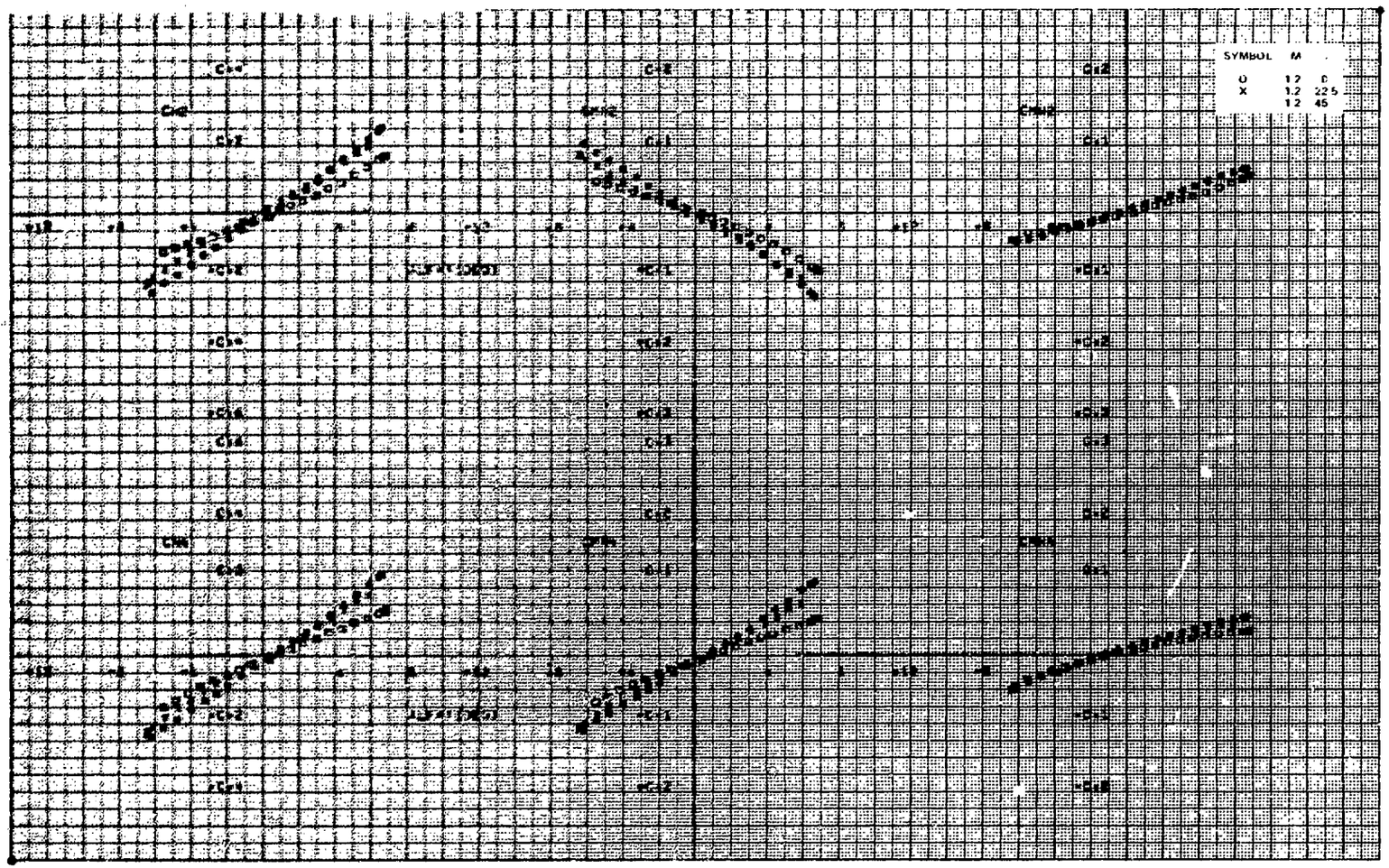


Figure 7e. Concluded.

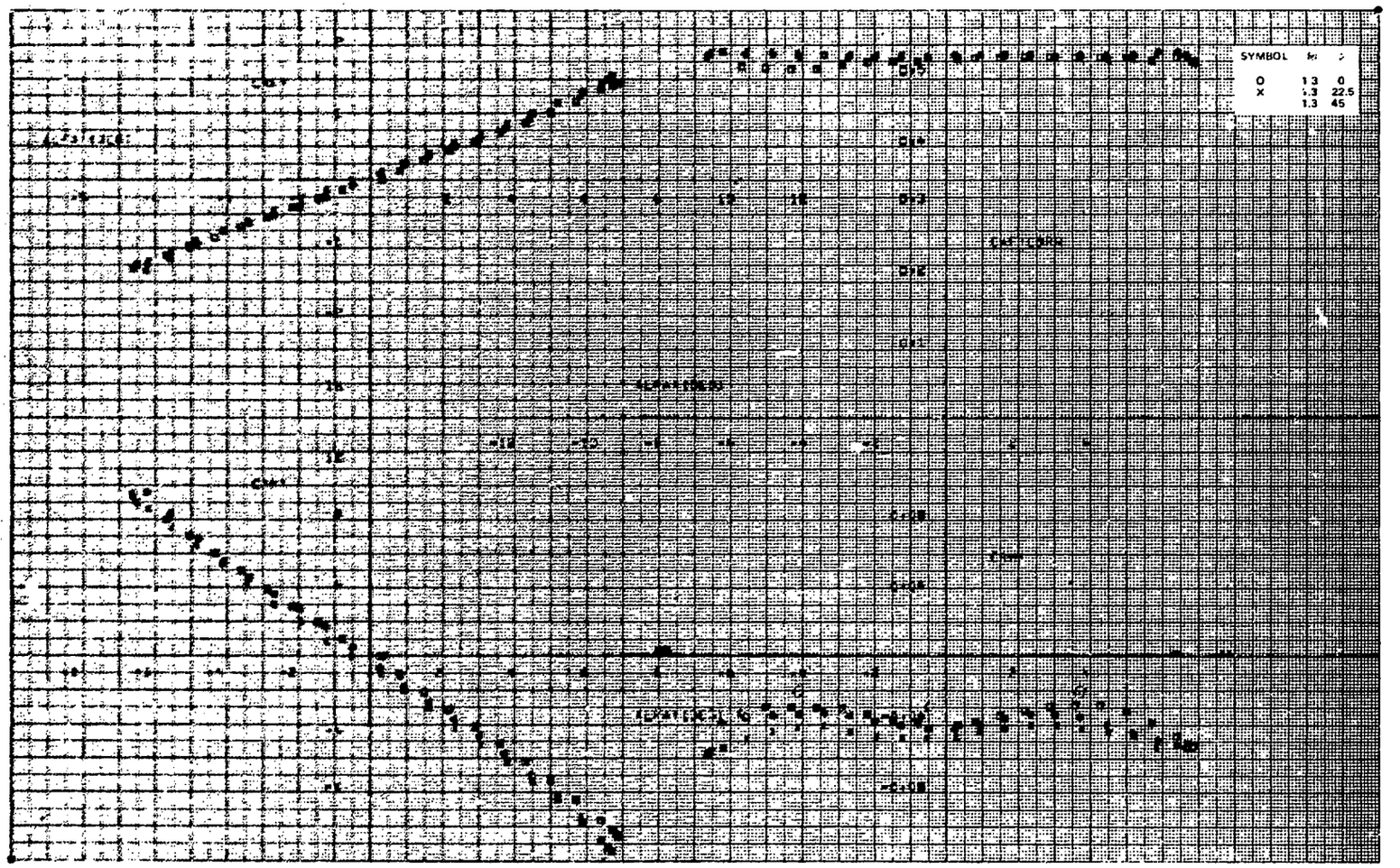


Figure [illegible]. Aerodynamic stability coefficients, CR/D = 1.75, ϕ = 0 deg, θ = 10 deg, M_∞ = 1.3.

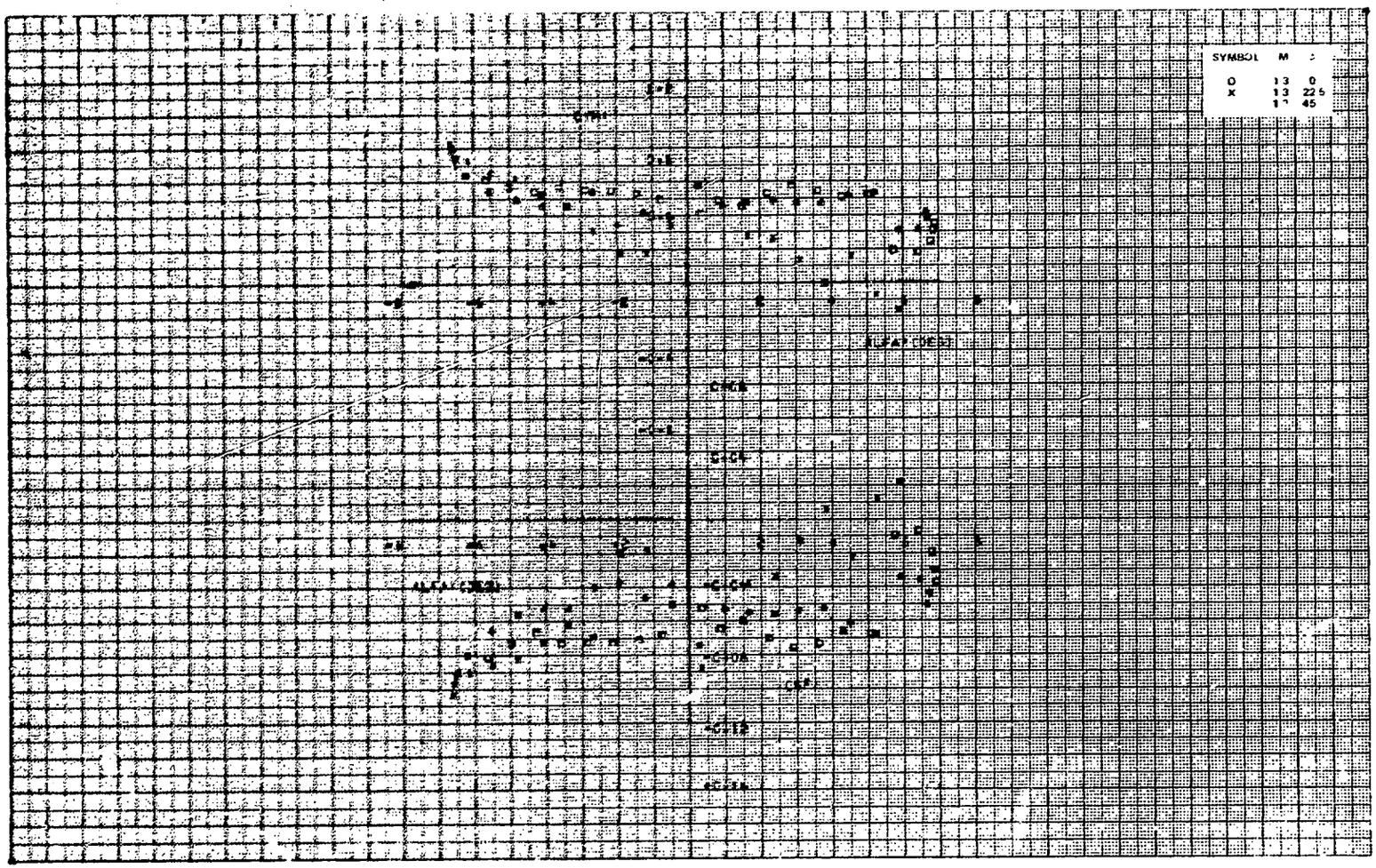


Figure 7f. Continued.

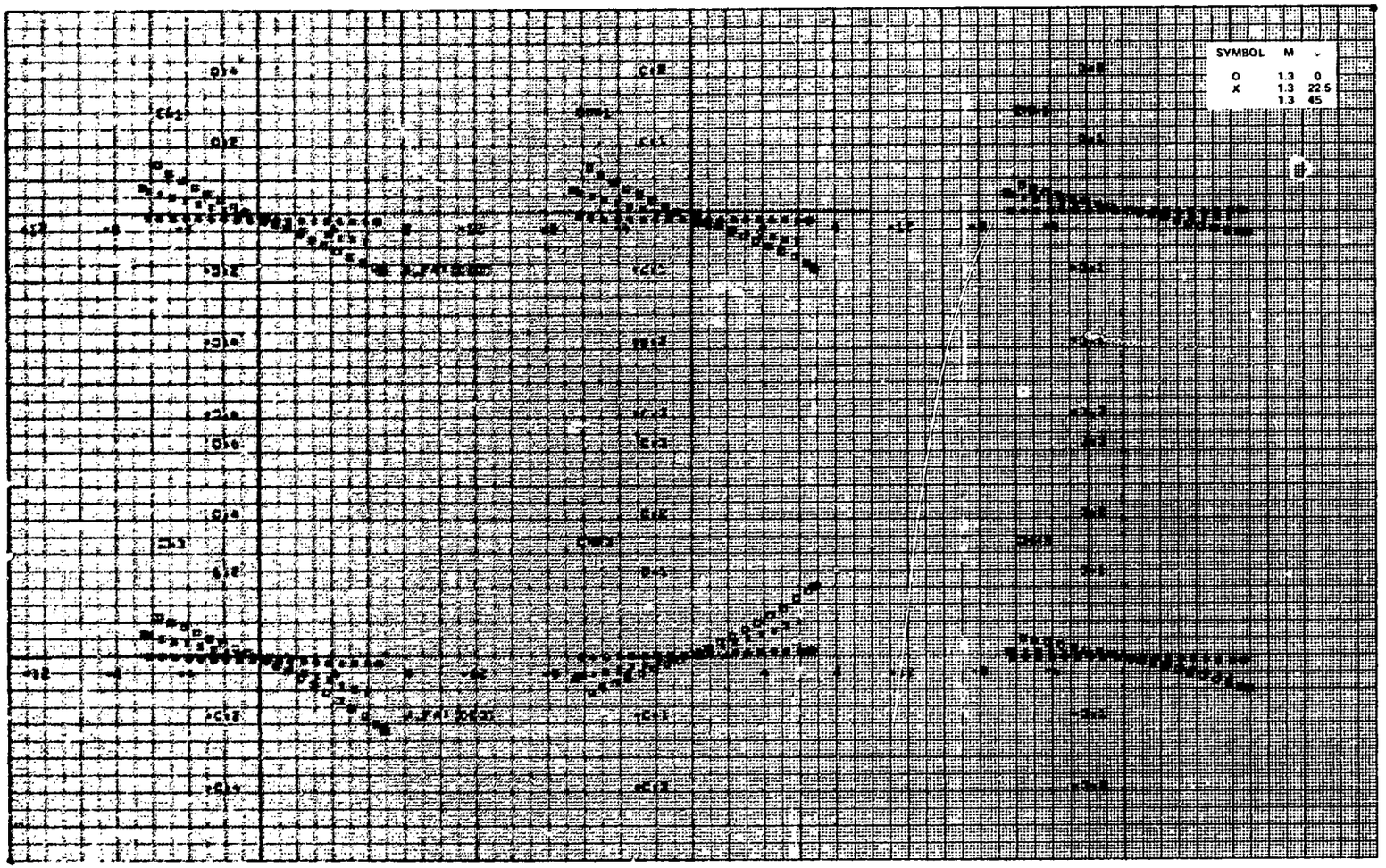


Figure 7f. Continued.

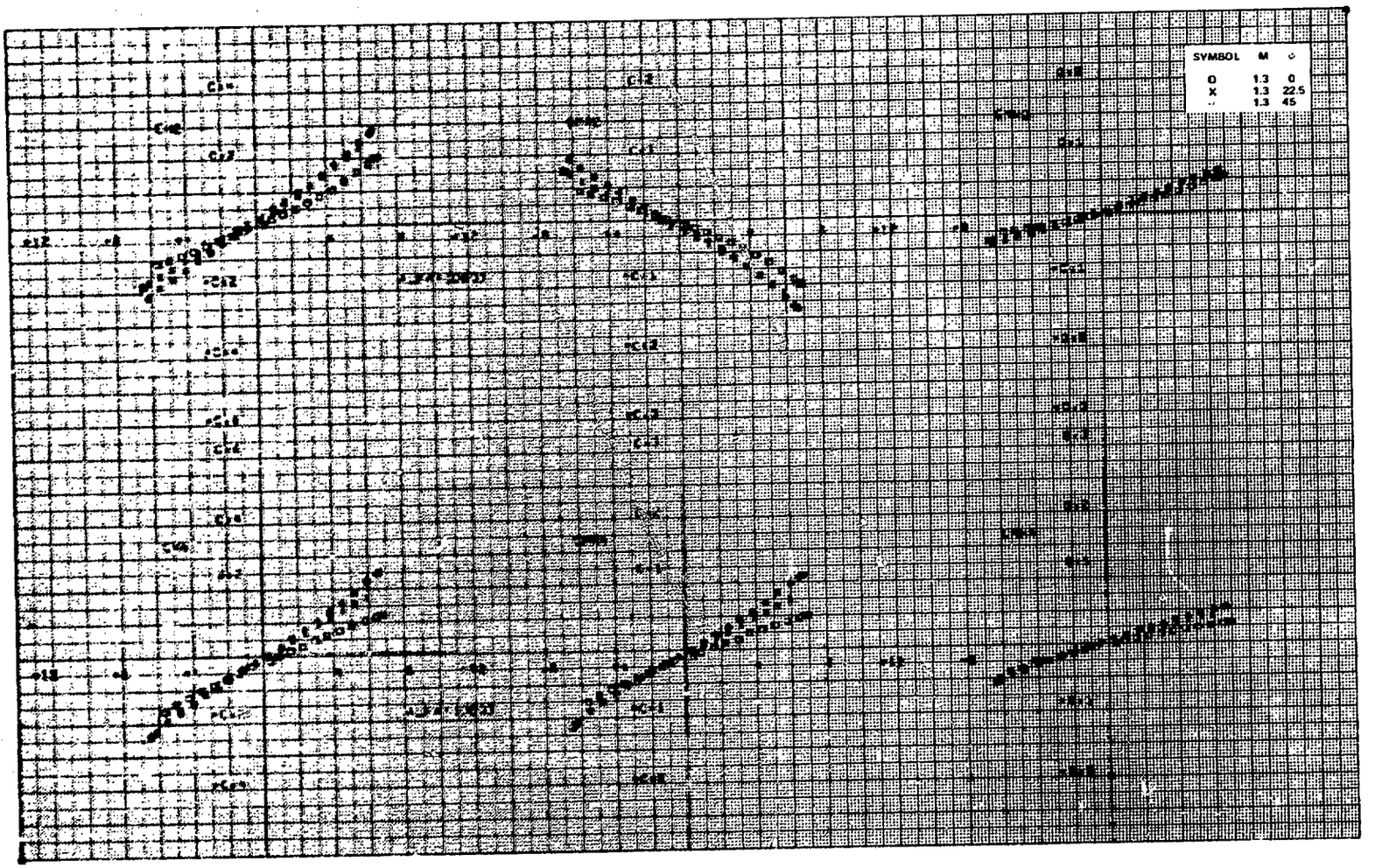


Figure 7f. Concluded.

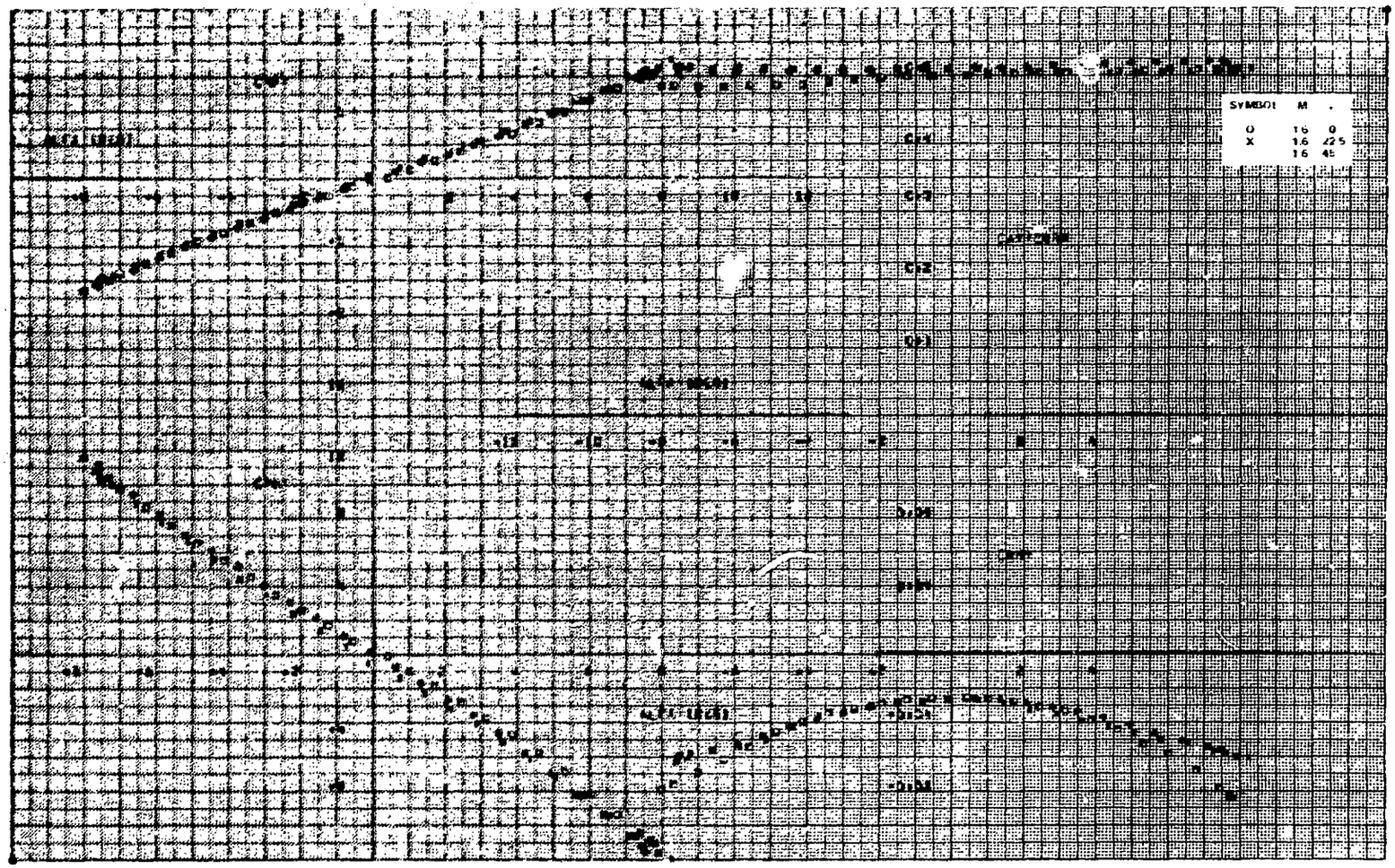


Figure 7g. Aerodynamic stability coefficients, CR/b = 1.75, ϕ = 0 deg, θ = 10 deg, M_∞ = 1.6.

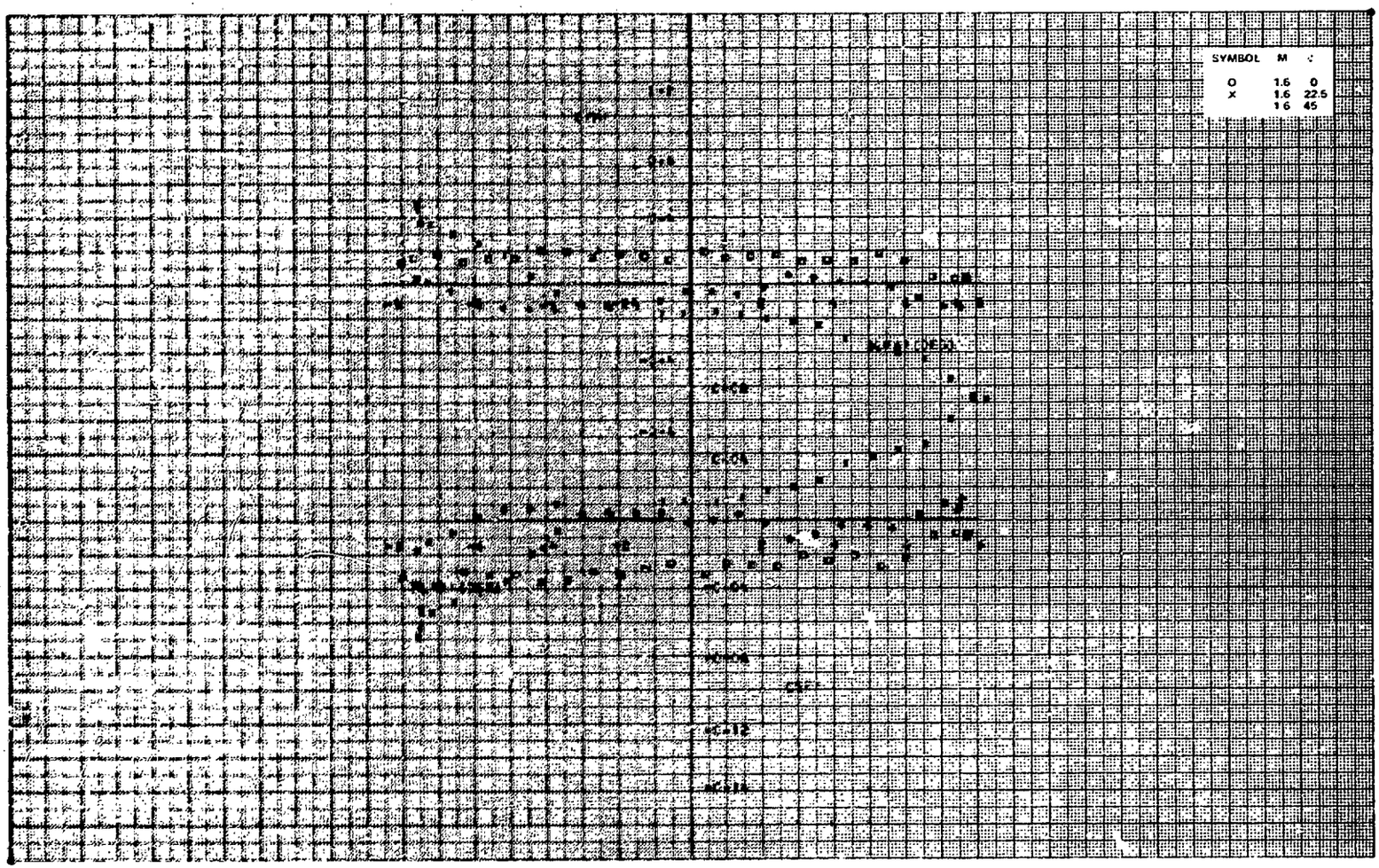


Figure 7g. Continued.

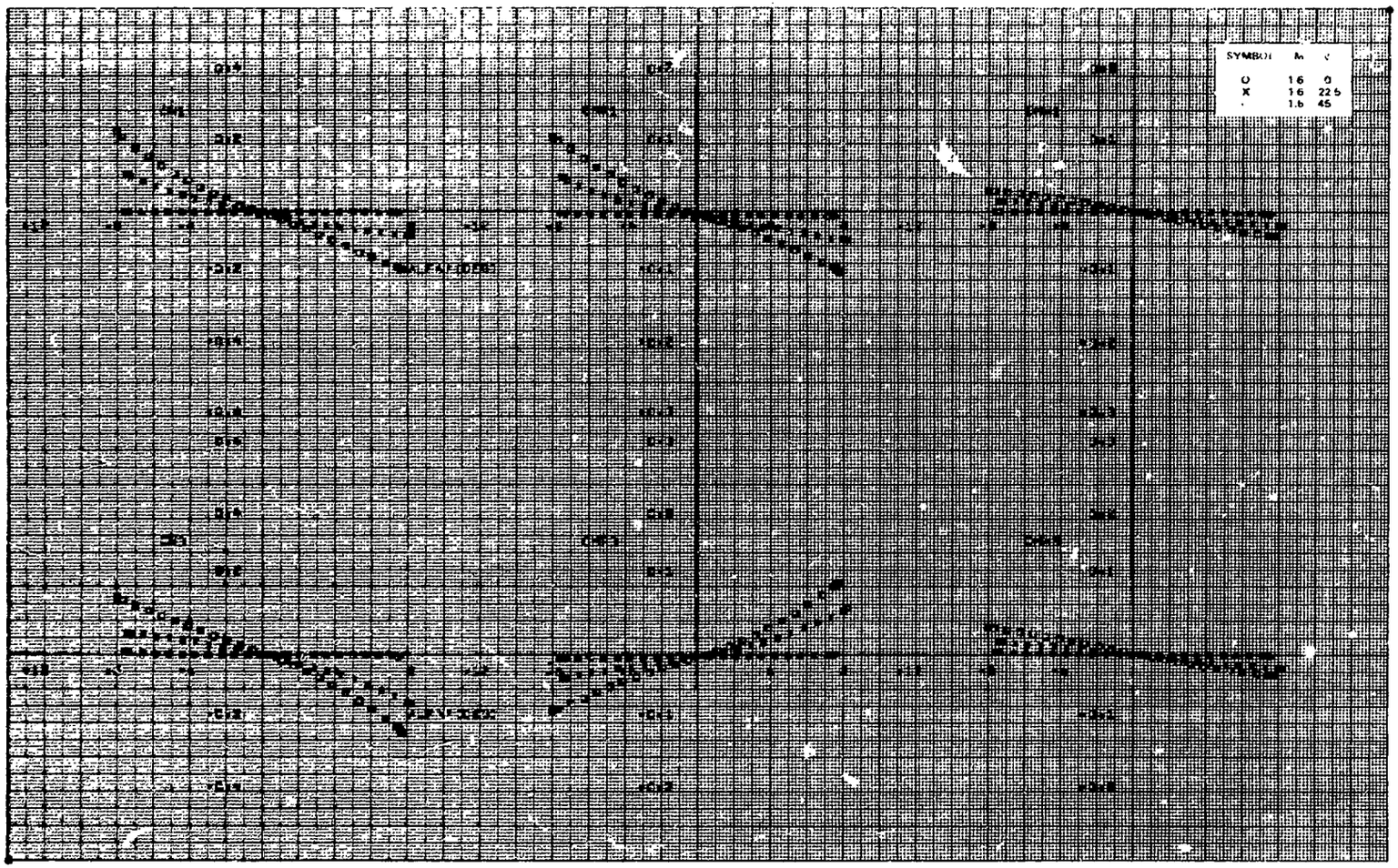


Figure 7g. Continued.

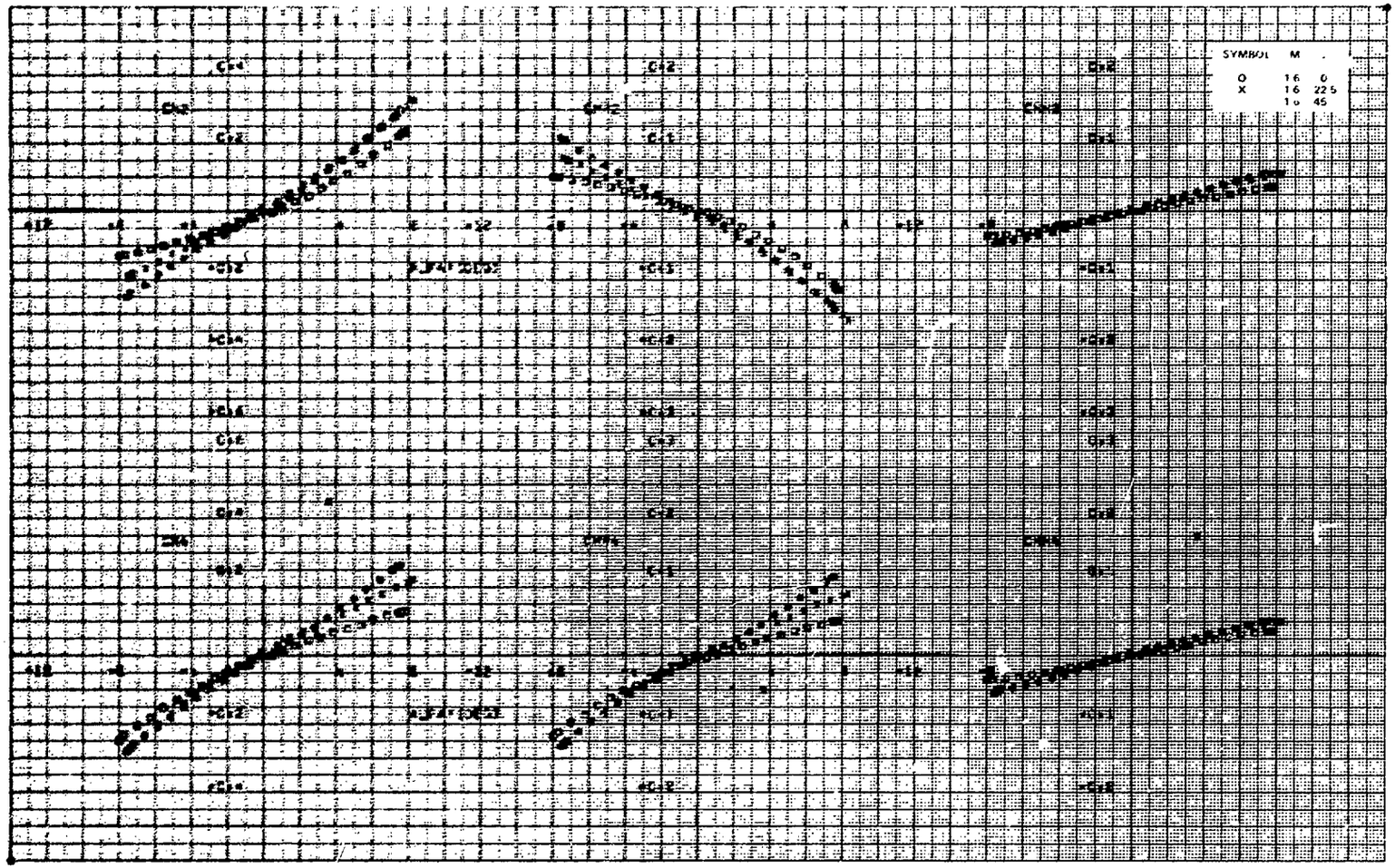


Figure 7g. Concluded.

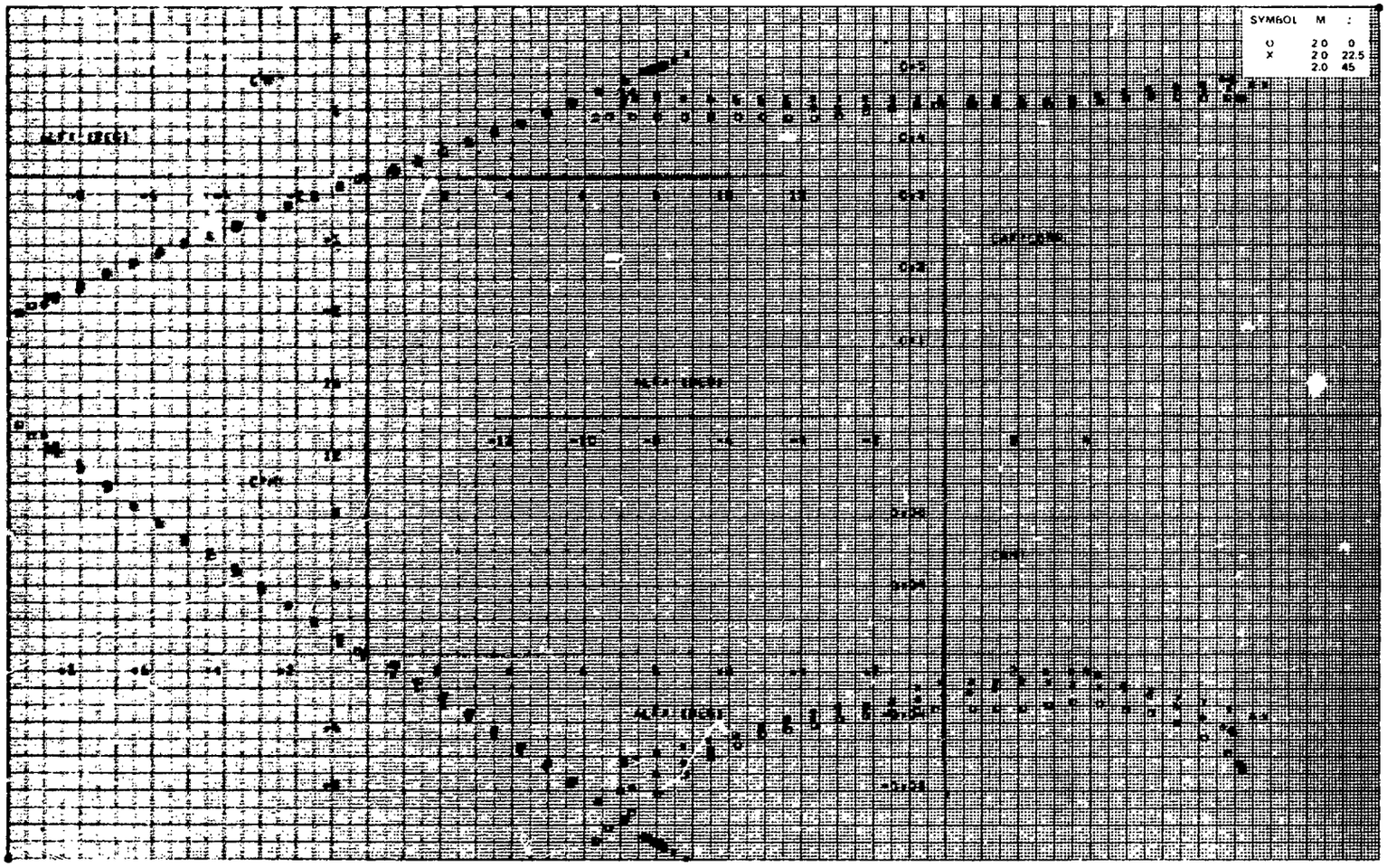


Figure 54. Aerodynamic stability coefficients, CR/D = 1.75, ϕ = 0 deg, θ = 10 deg, M_∞ = 2.0.

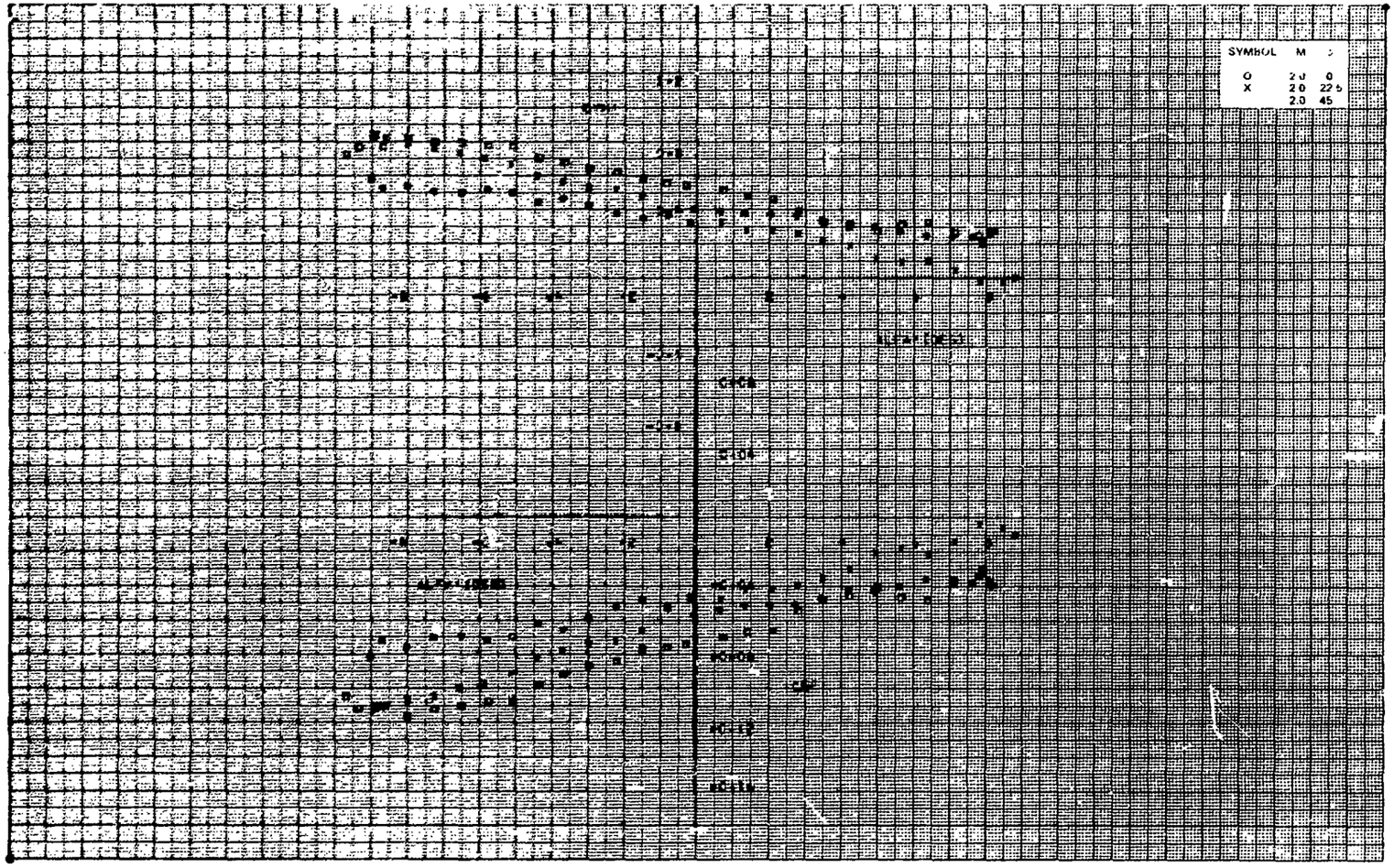


Figure 7h. Continued.

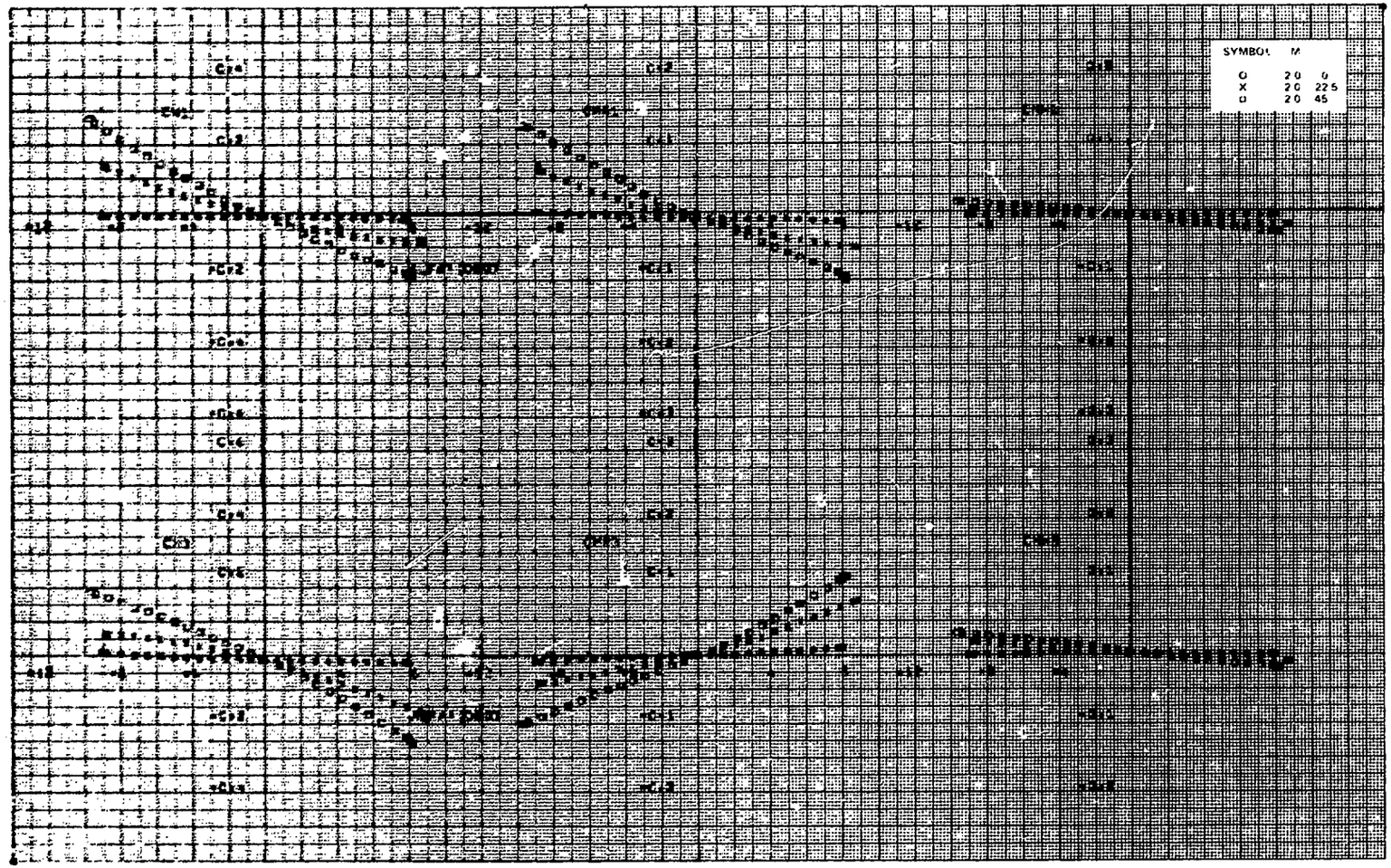


Figure 7h. Continued.

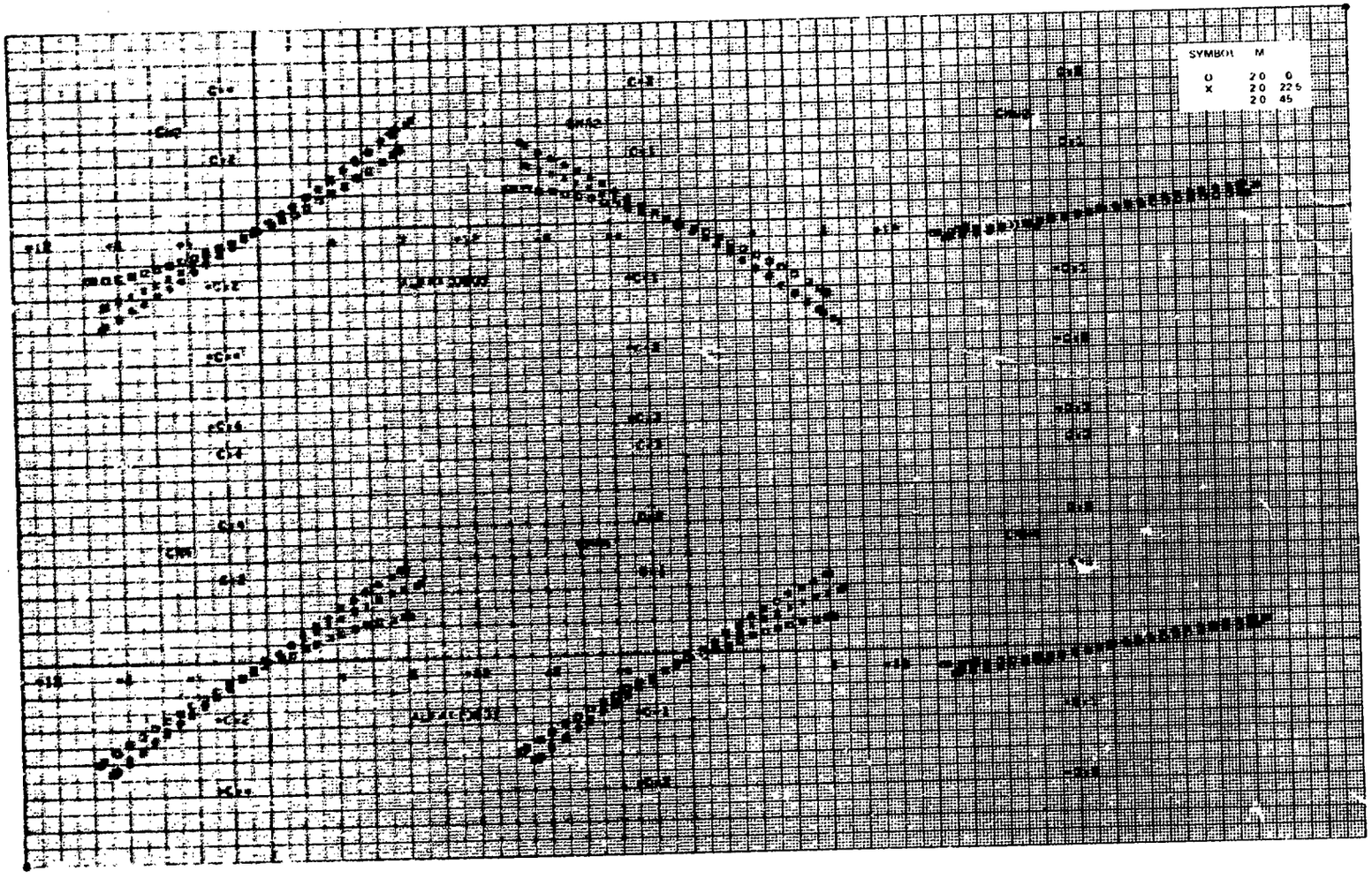


Figure 7h. Concluded.

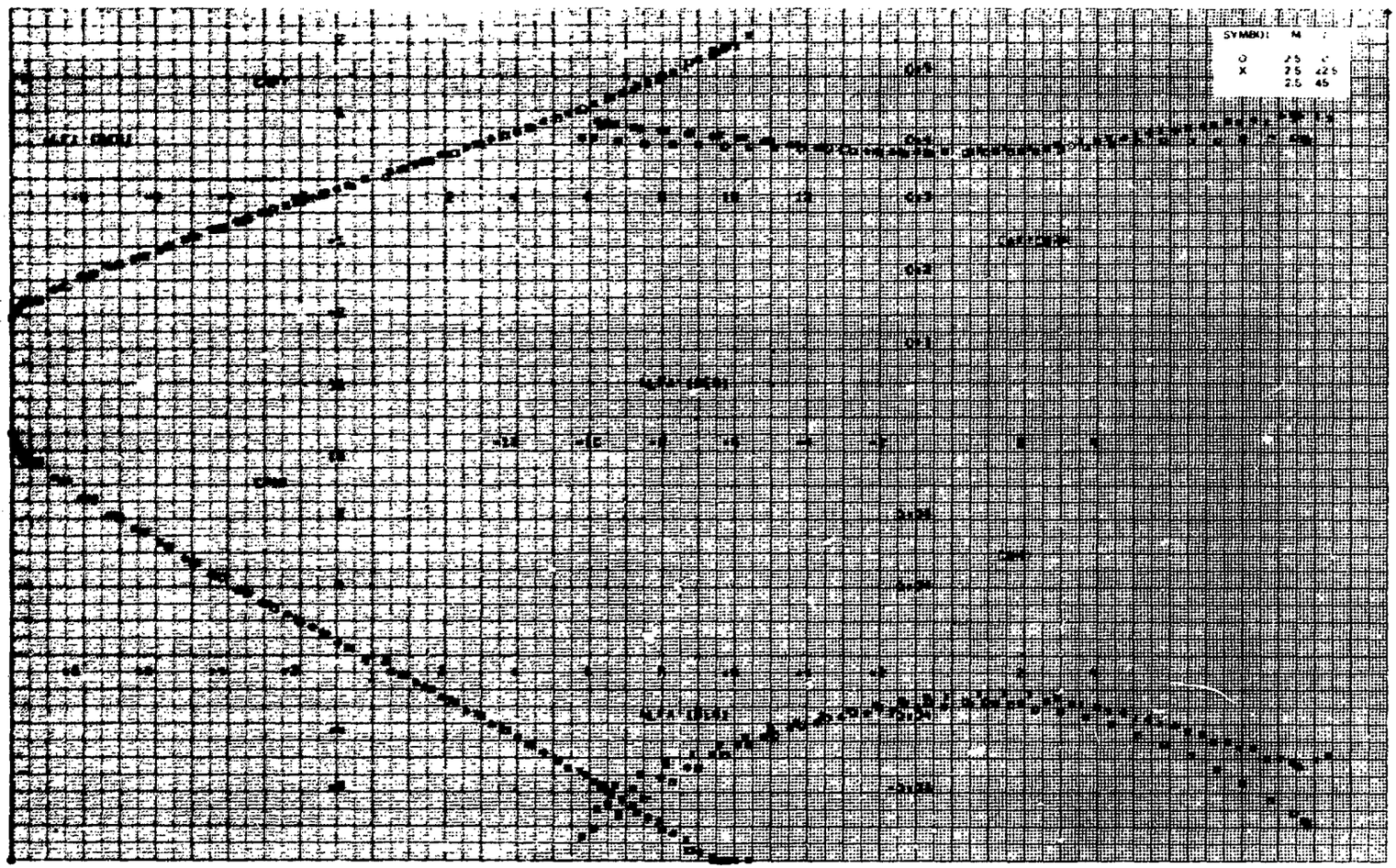


Figure 7i. Aerodynamic lift coefficients, CR/D = 1.75, ϕ = 0 deg, α = 10 deg, M_∞ = 2.5.

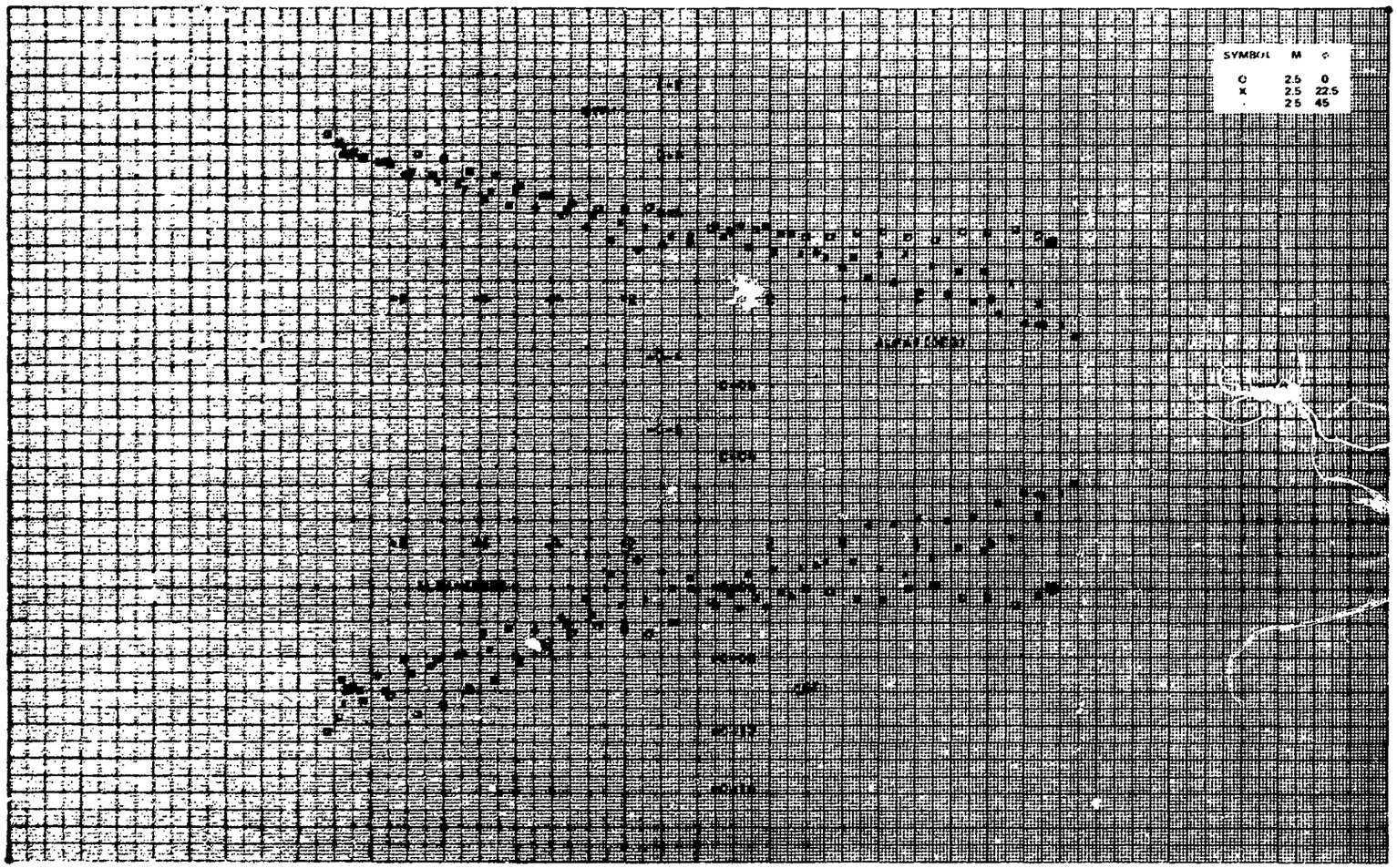


Figure 7i. Continued.

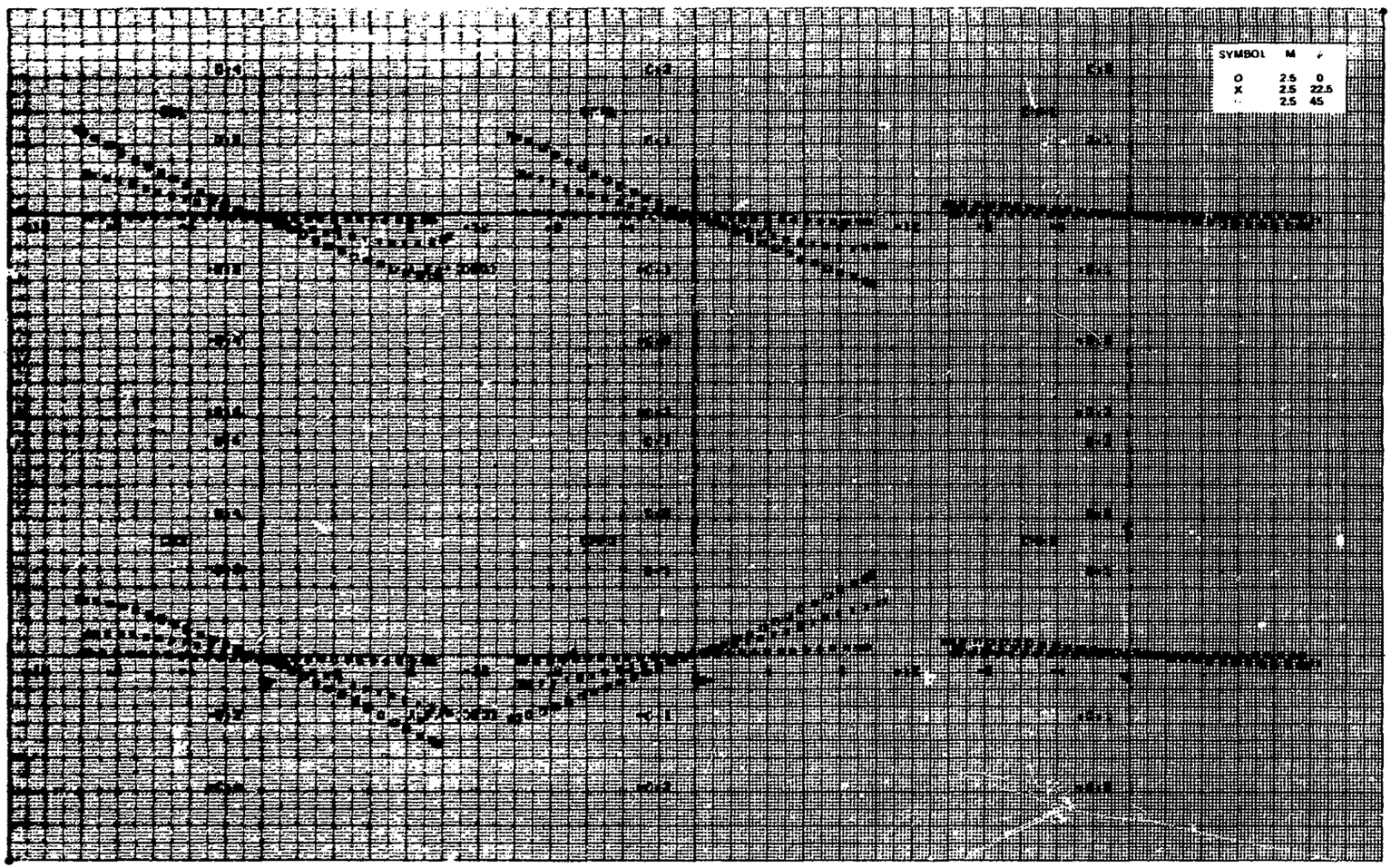


Figure 7i. Continued.

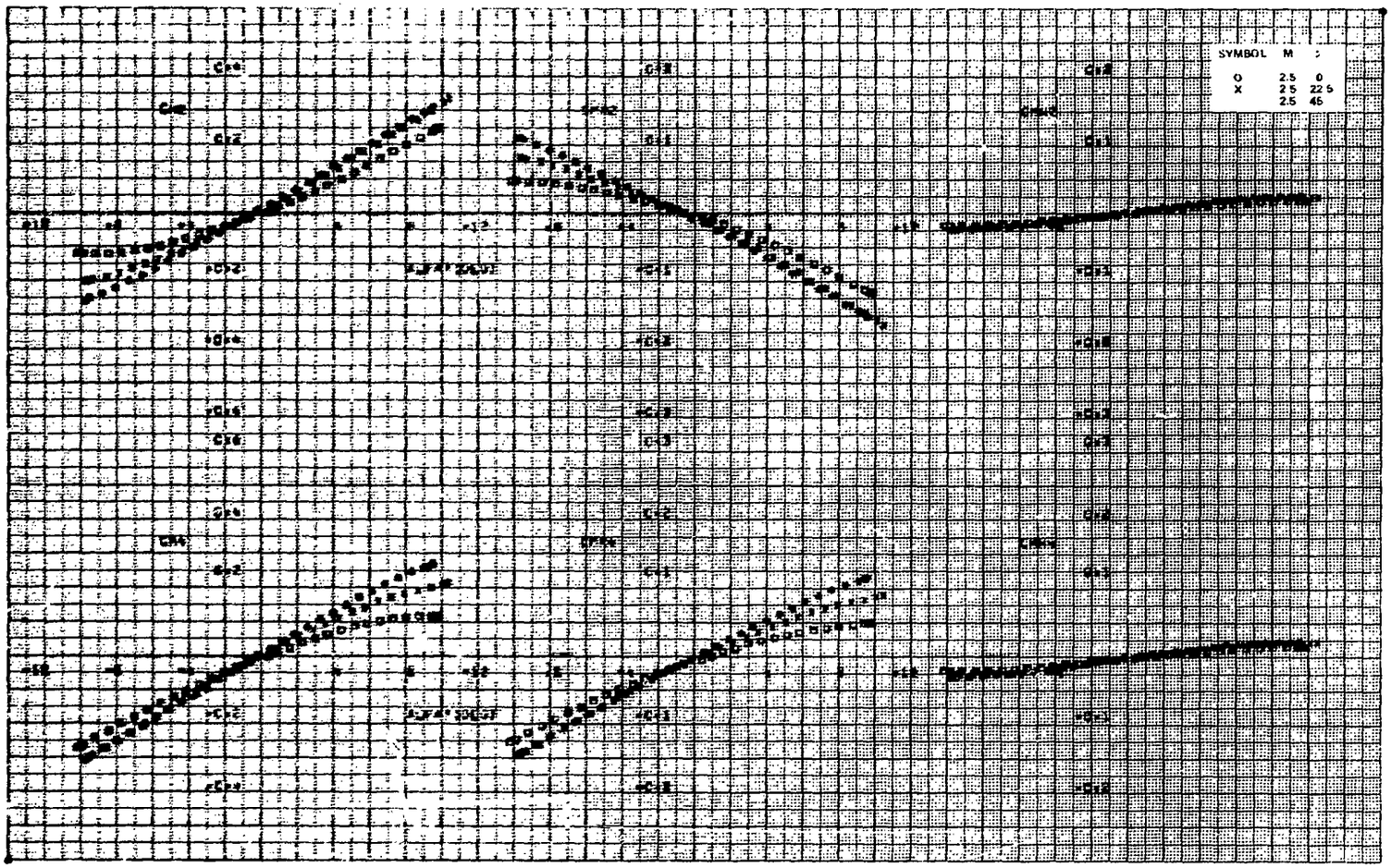
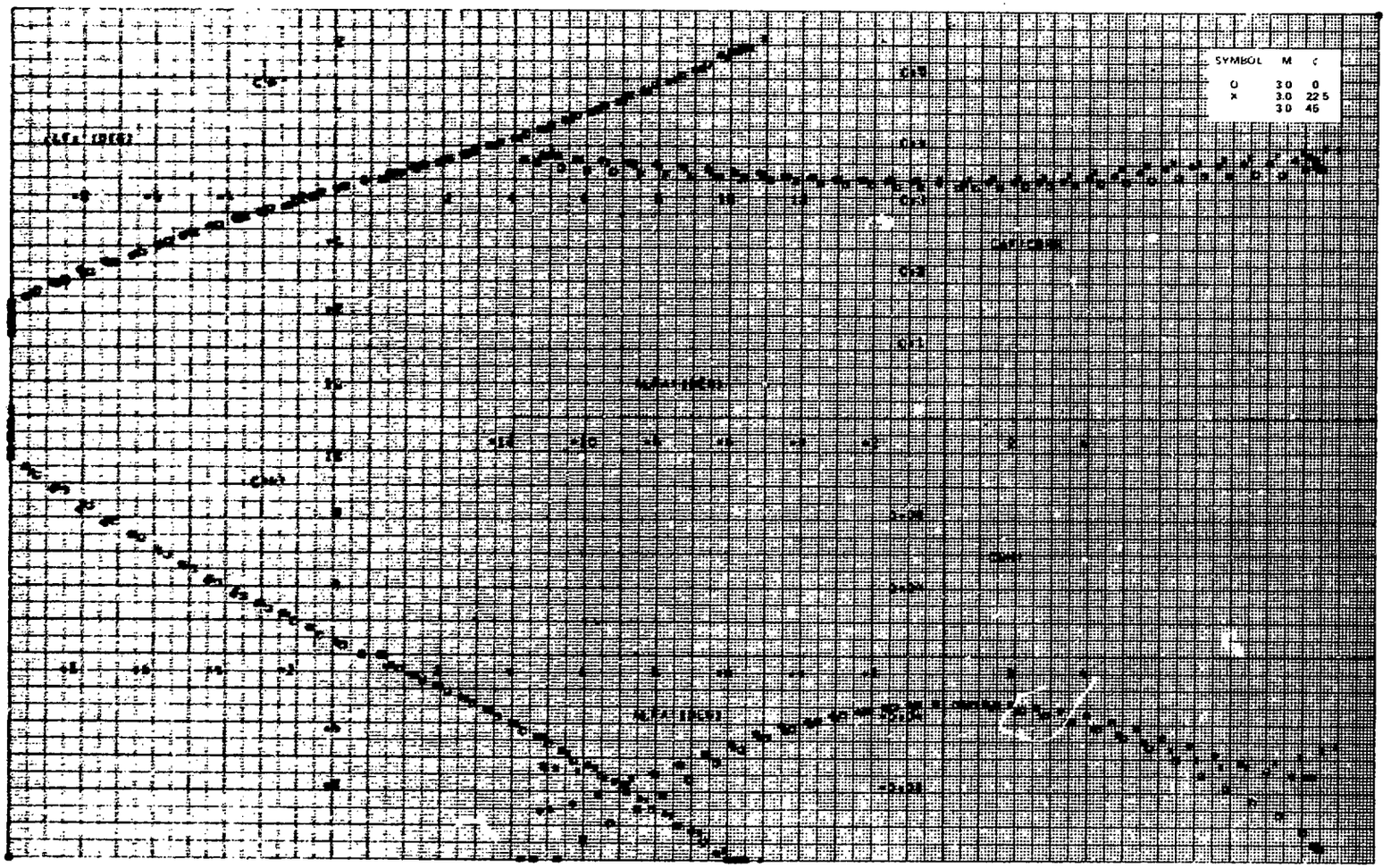


Figure 71. Concluded.



Longitudinal dynamic stability coefficients, CR/D = 1.75, ϕ = 0 deg, θ = 10 deg, M_∞ = 3.0.

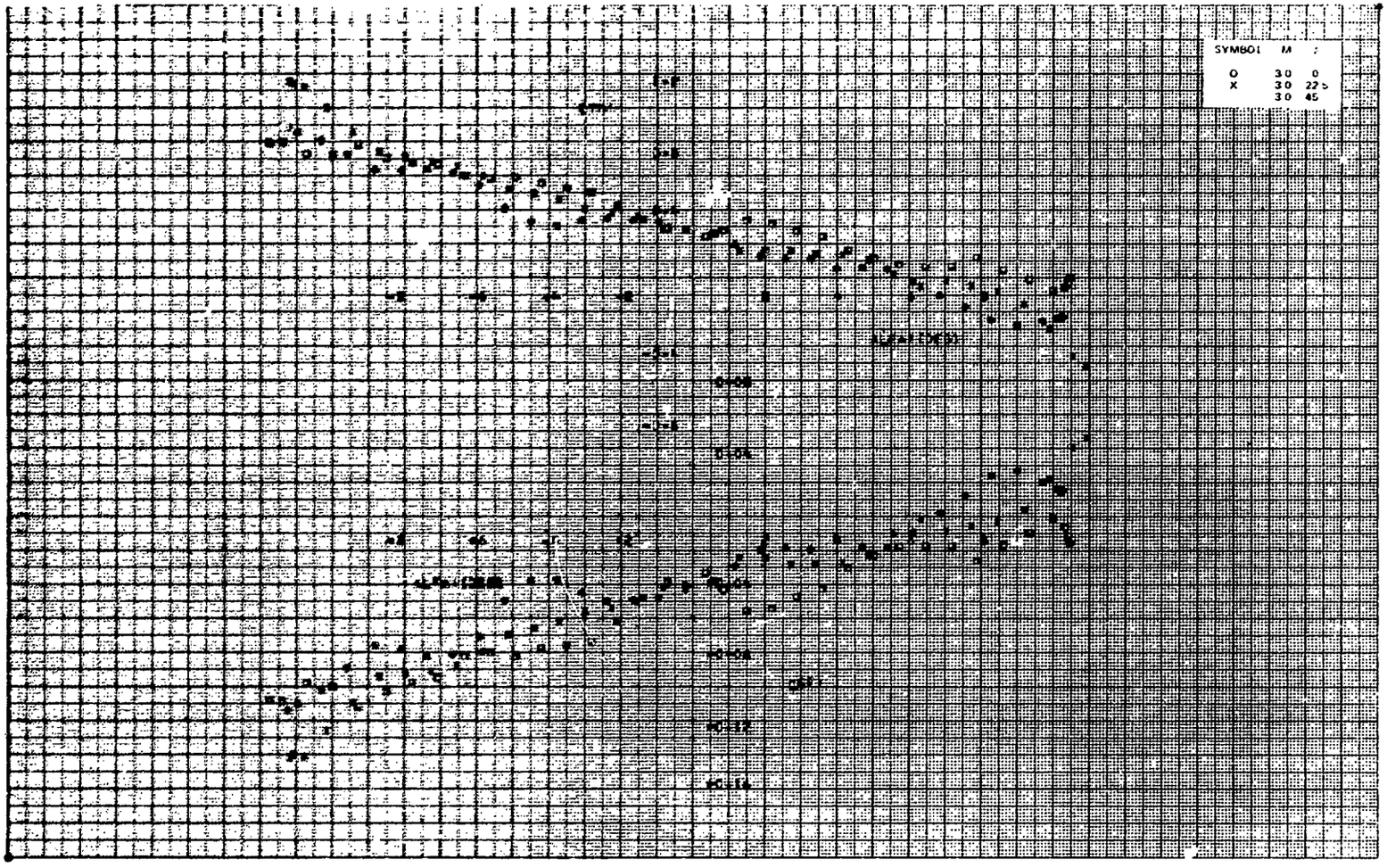


Figure 7j. Continued.

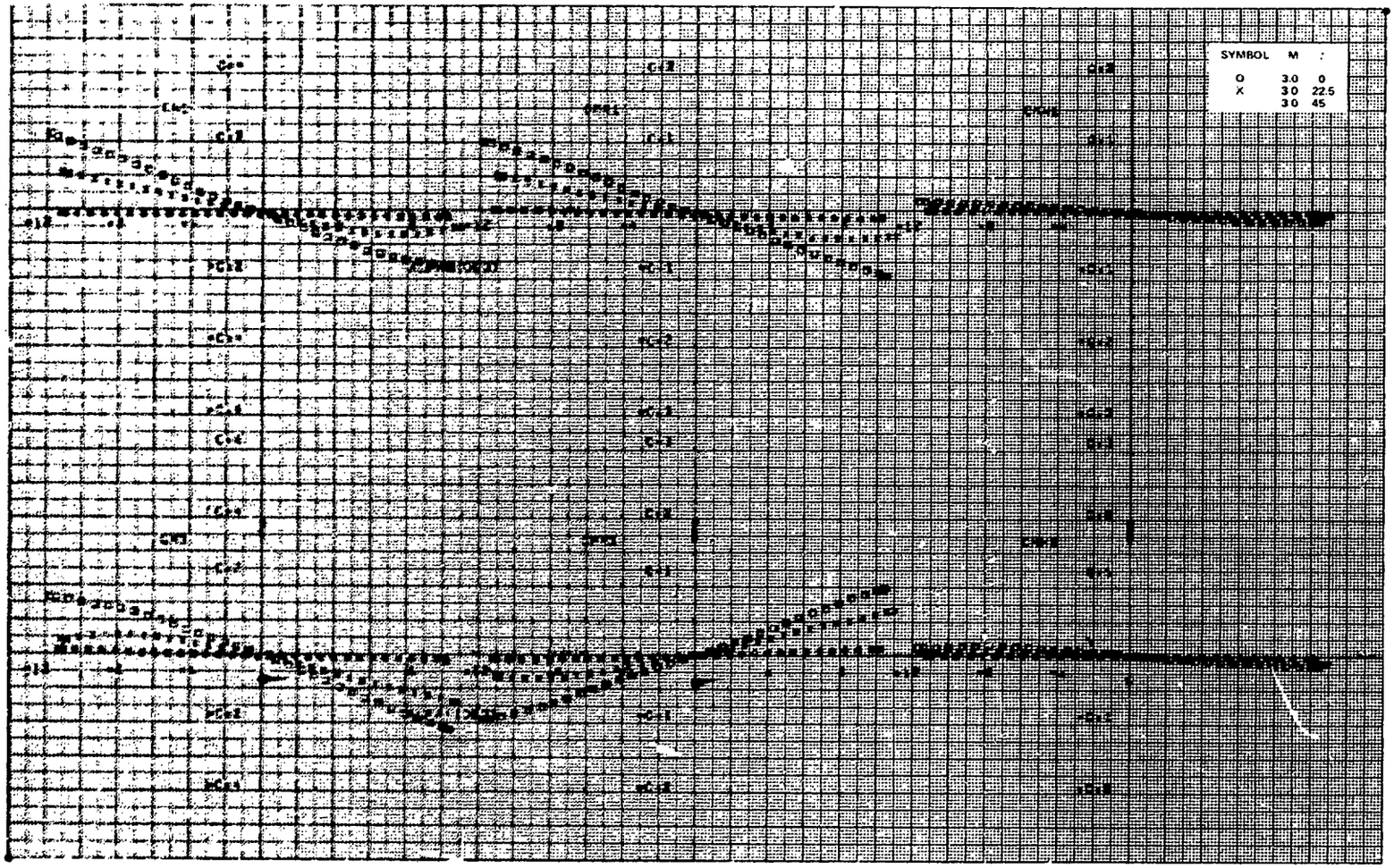


Figure 7j. Continued.

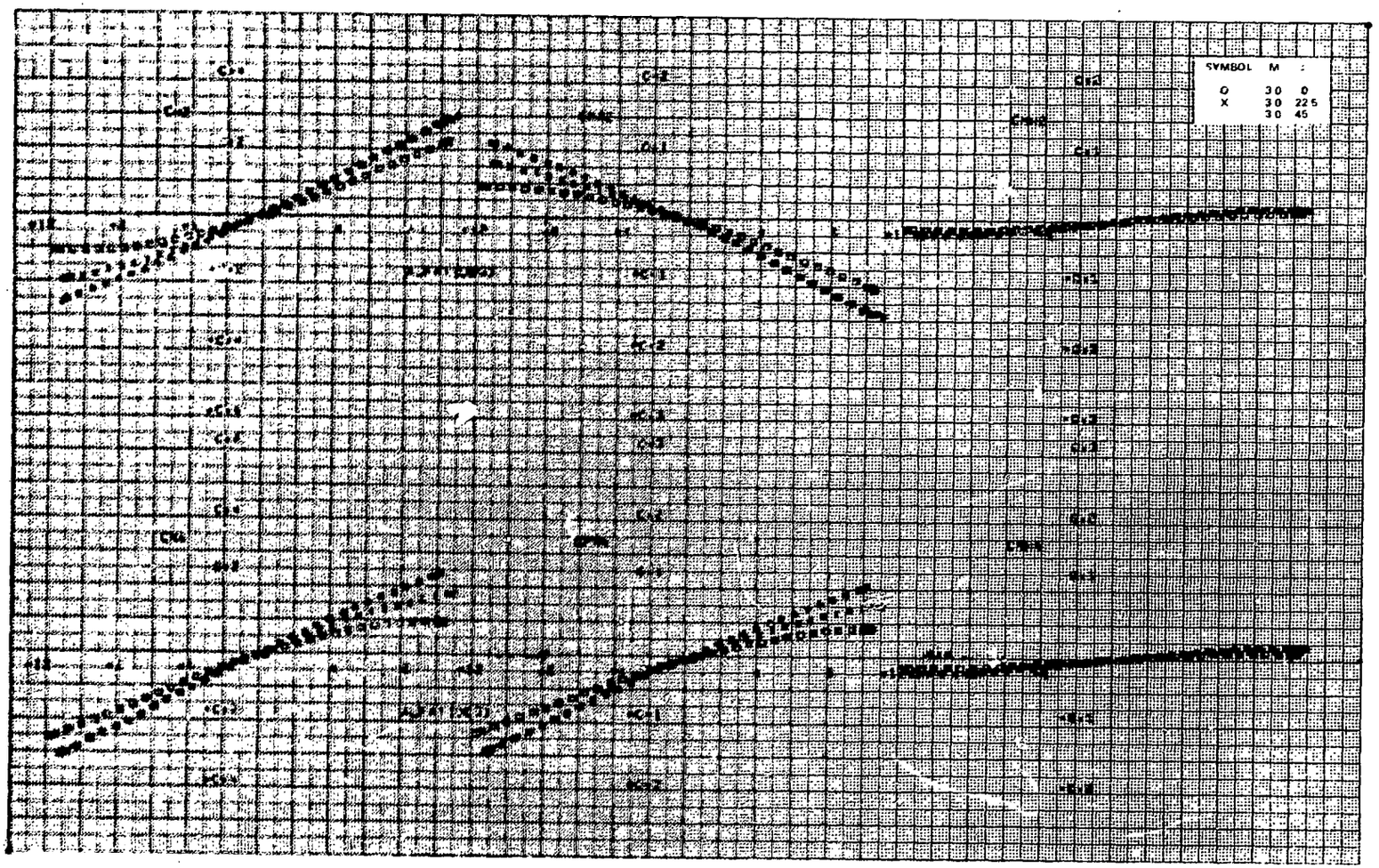


Figure 7j. Concluded.

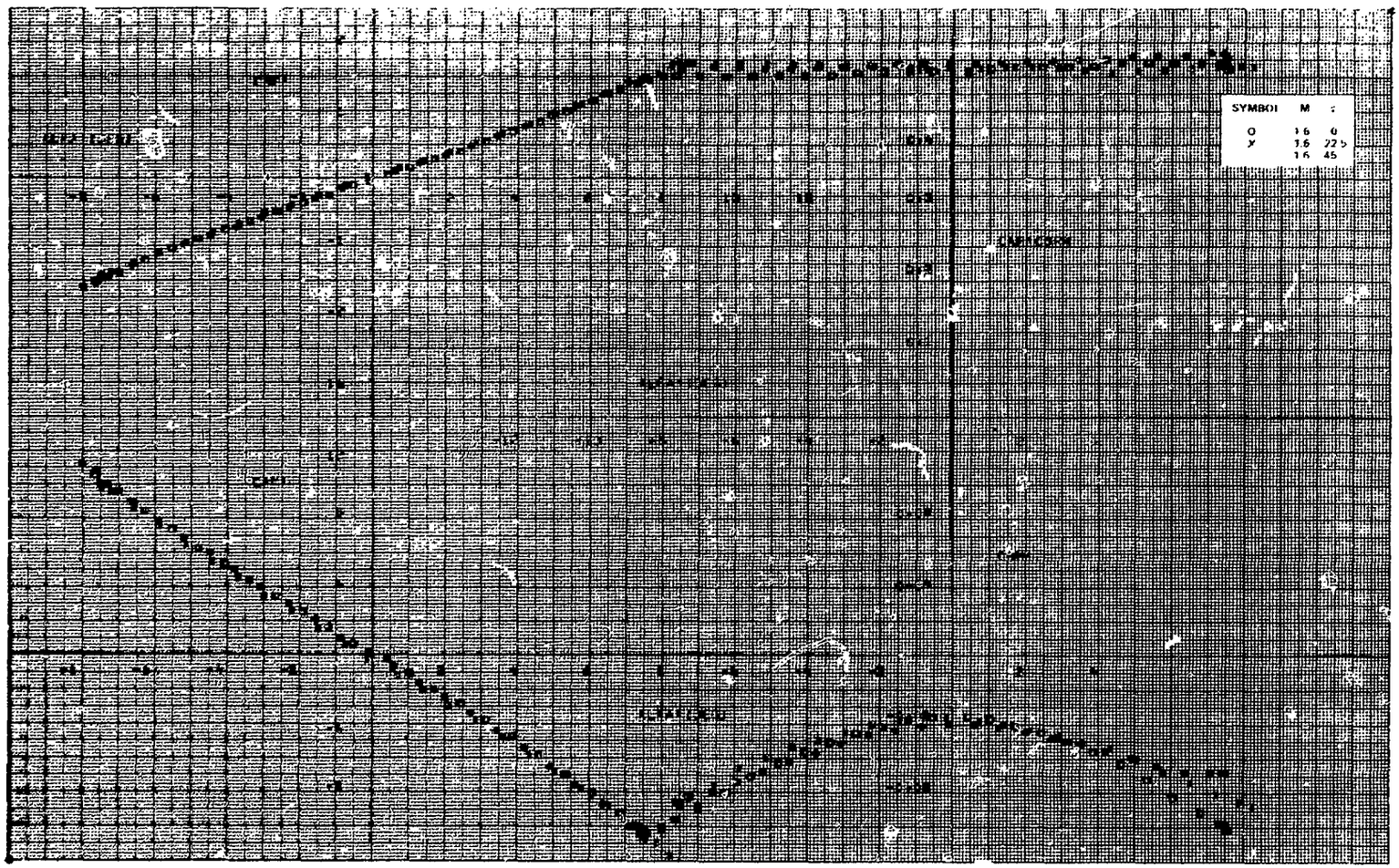


Figure 8a. Aerodynamic stability coefficients, CR/D = 1.75, Λ = 0 deg, θ = 22.5 deg, M_∞ = 1.6.

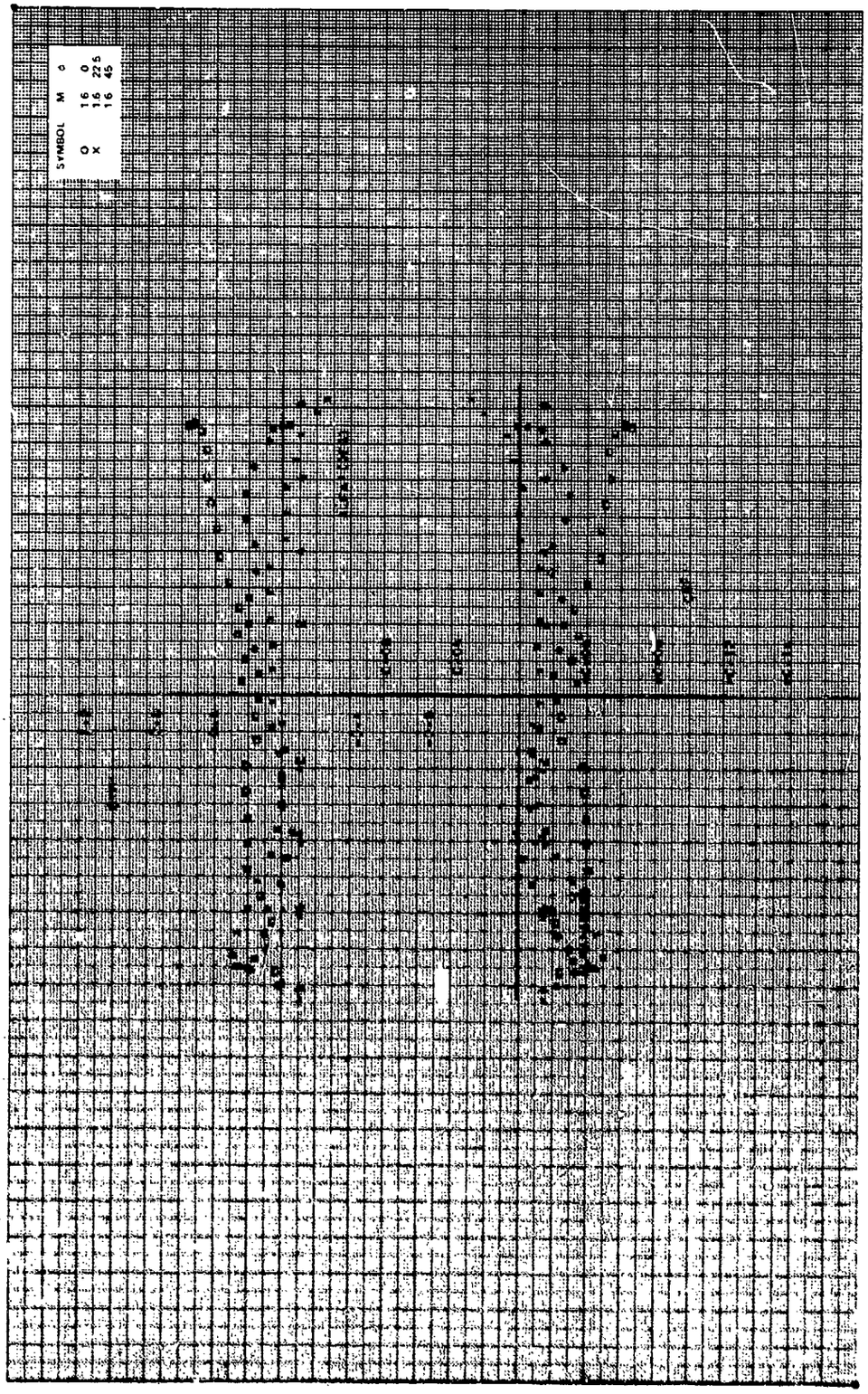


Figure 84. Continued.

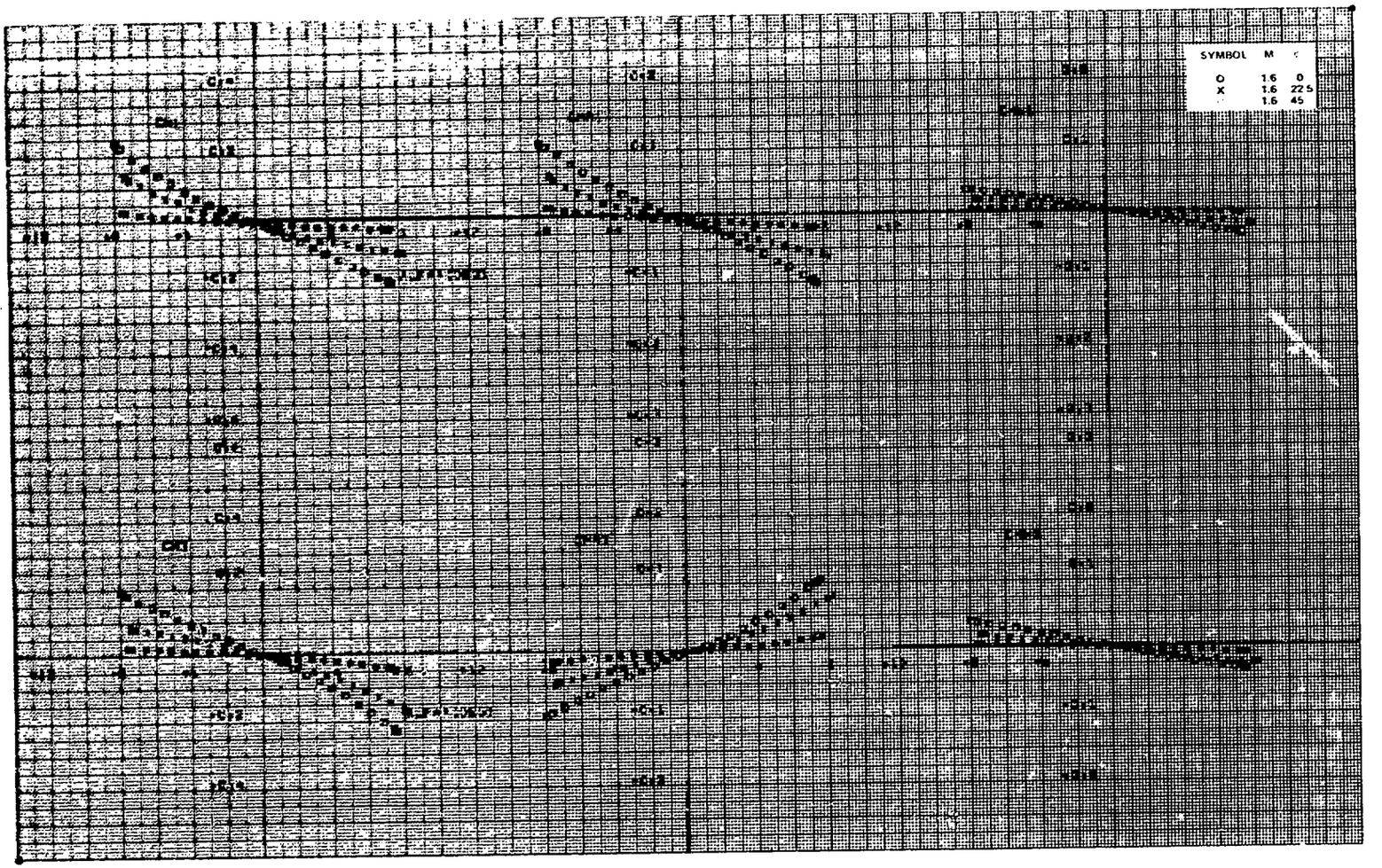


Figure 8a. Continued.

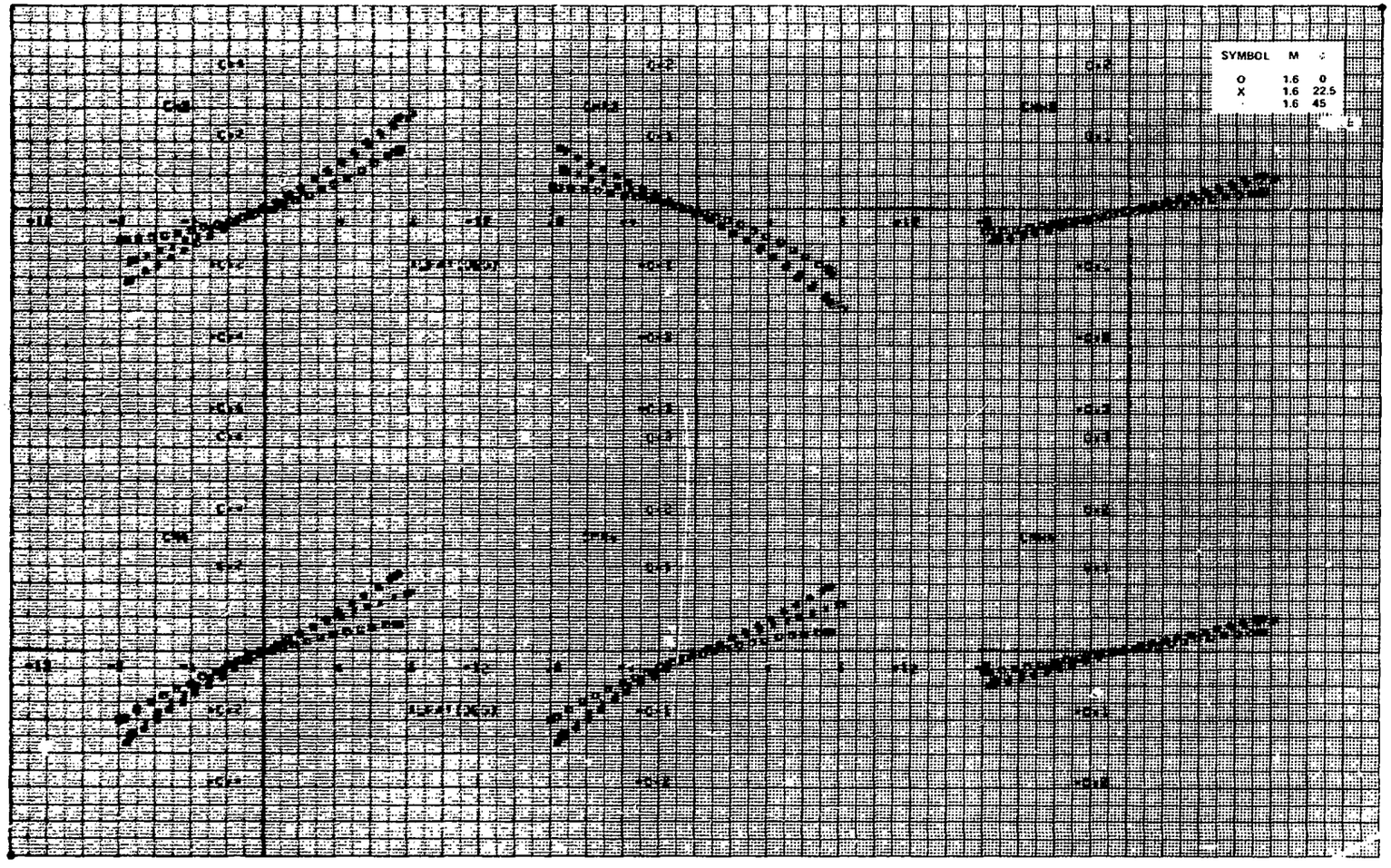


Figure 8a. Concluded.

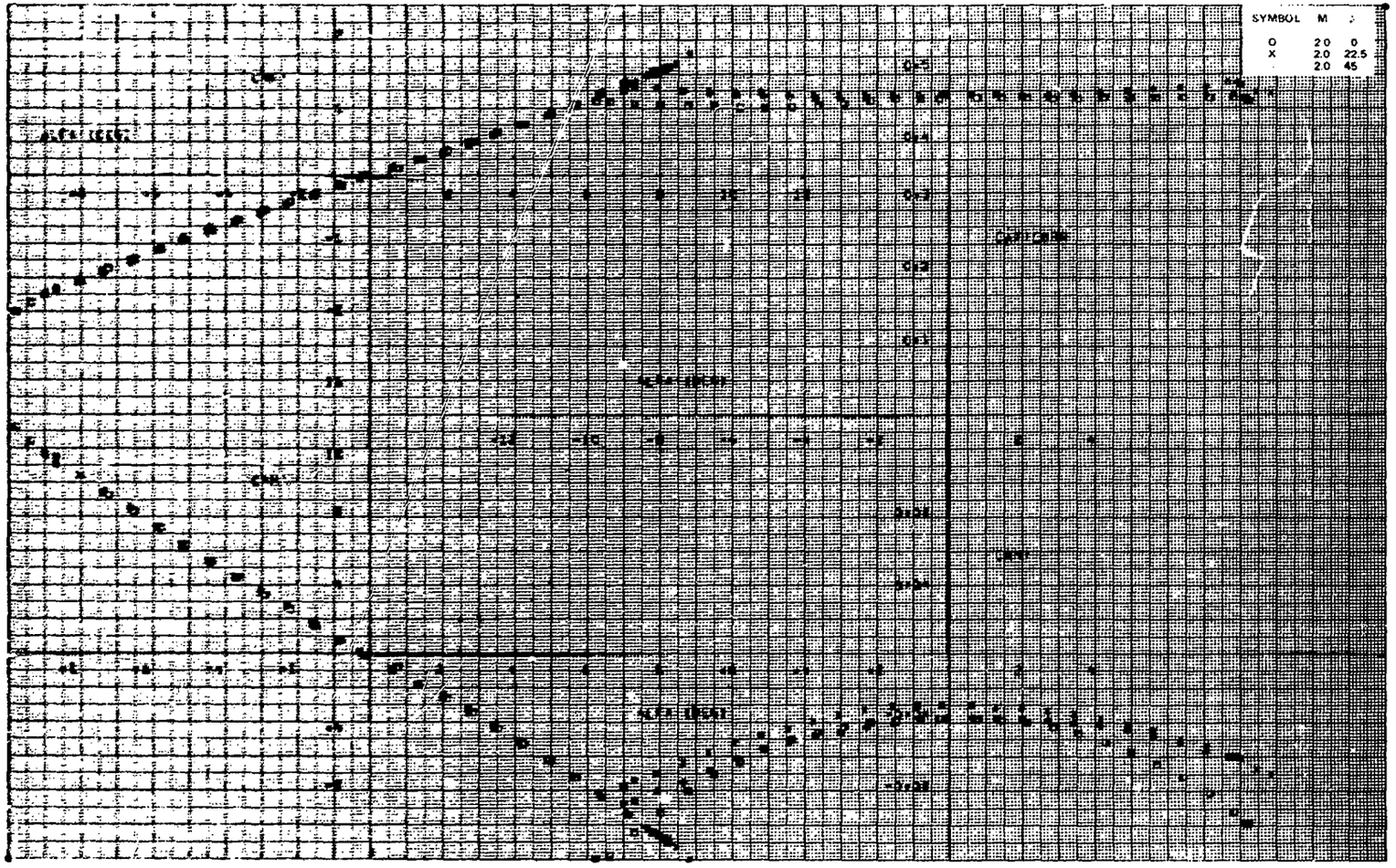


Figure 66. [illegible] stability coefficients, CR/D = 1.75, γ = 0 deg, θ = 22.5 deg, M_∞ = 2.0.

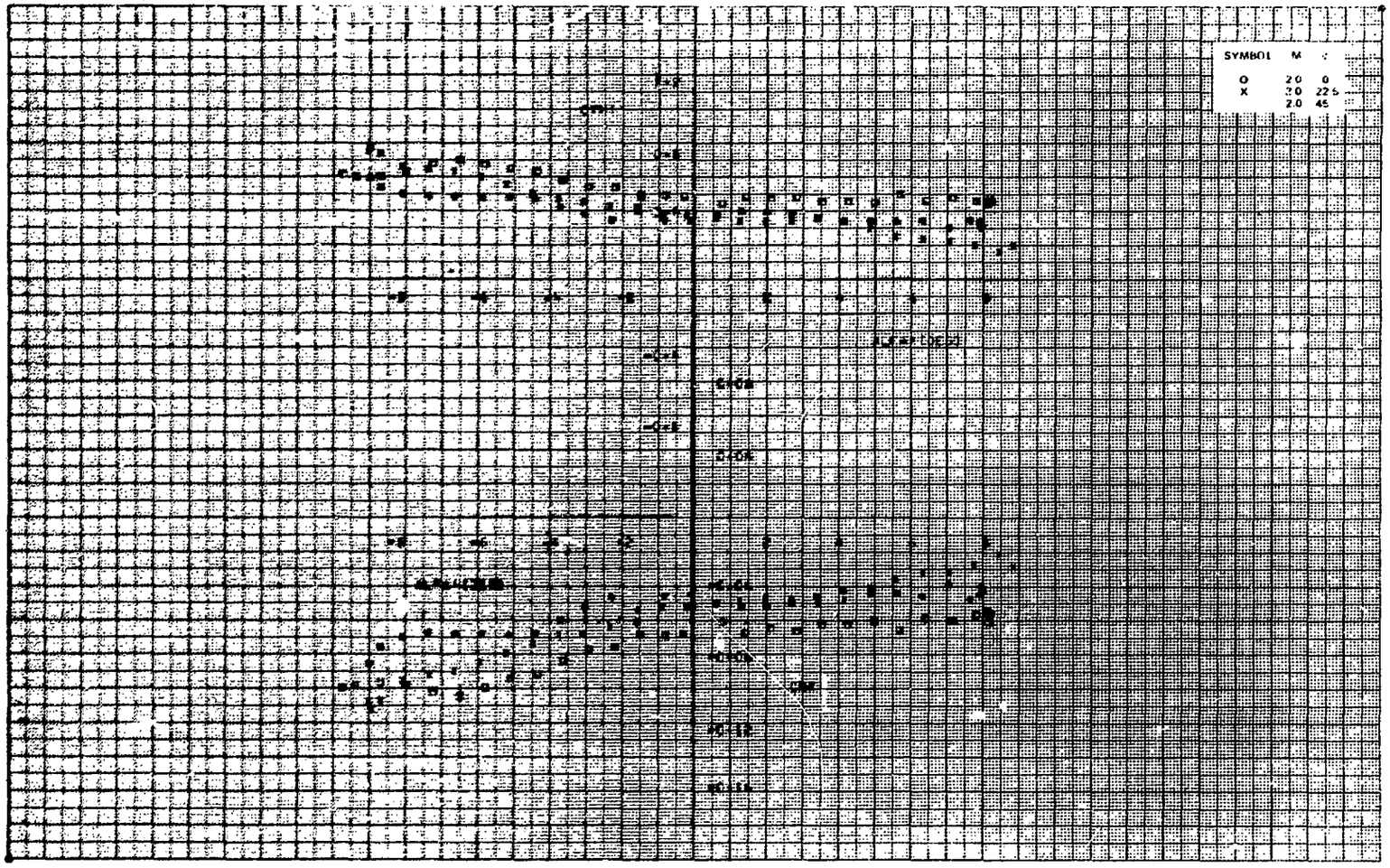


Figure 8b. Continued.

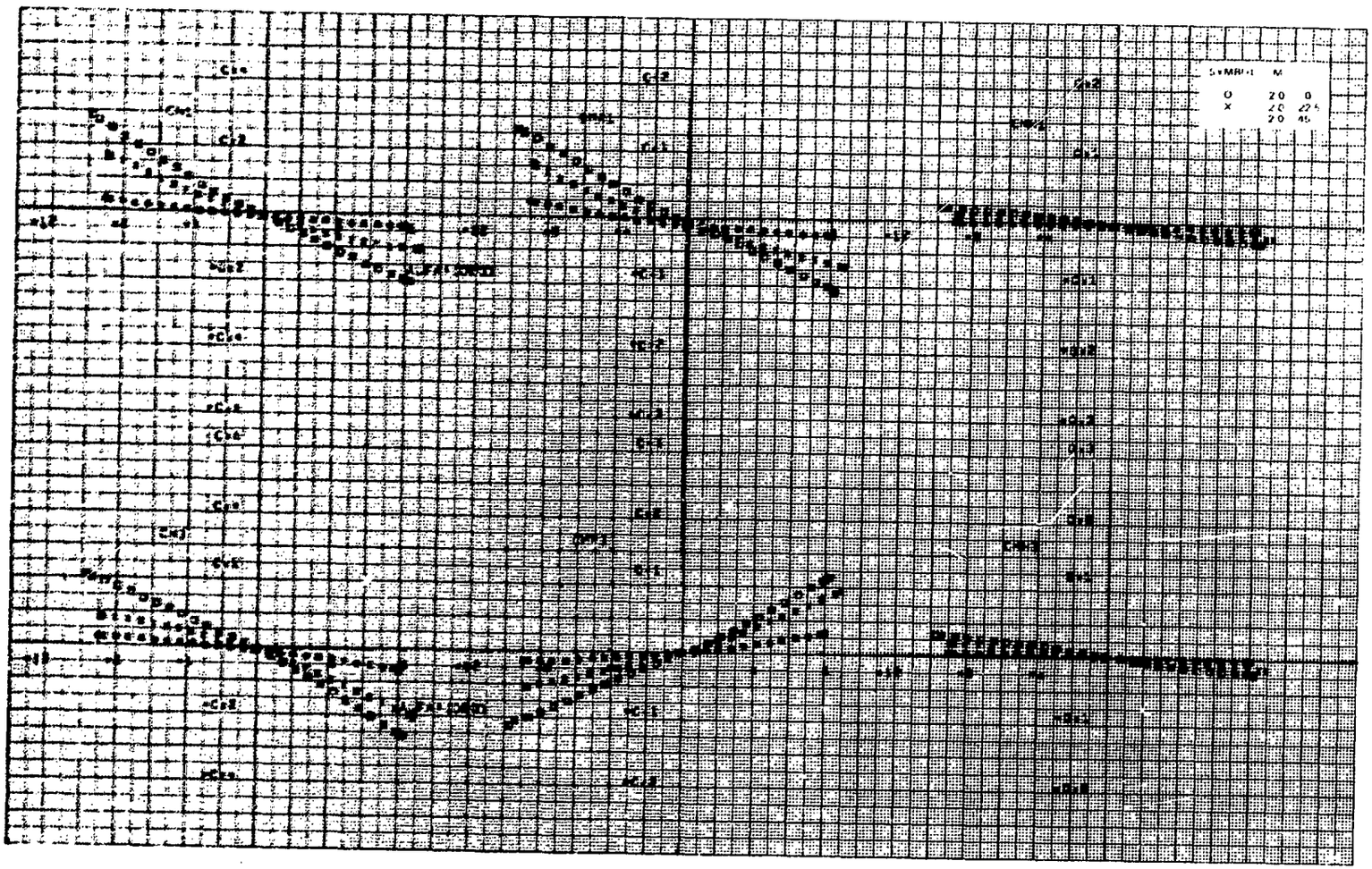


Figure 8b. Continued.

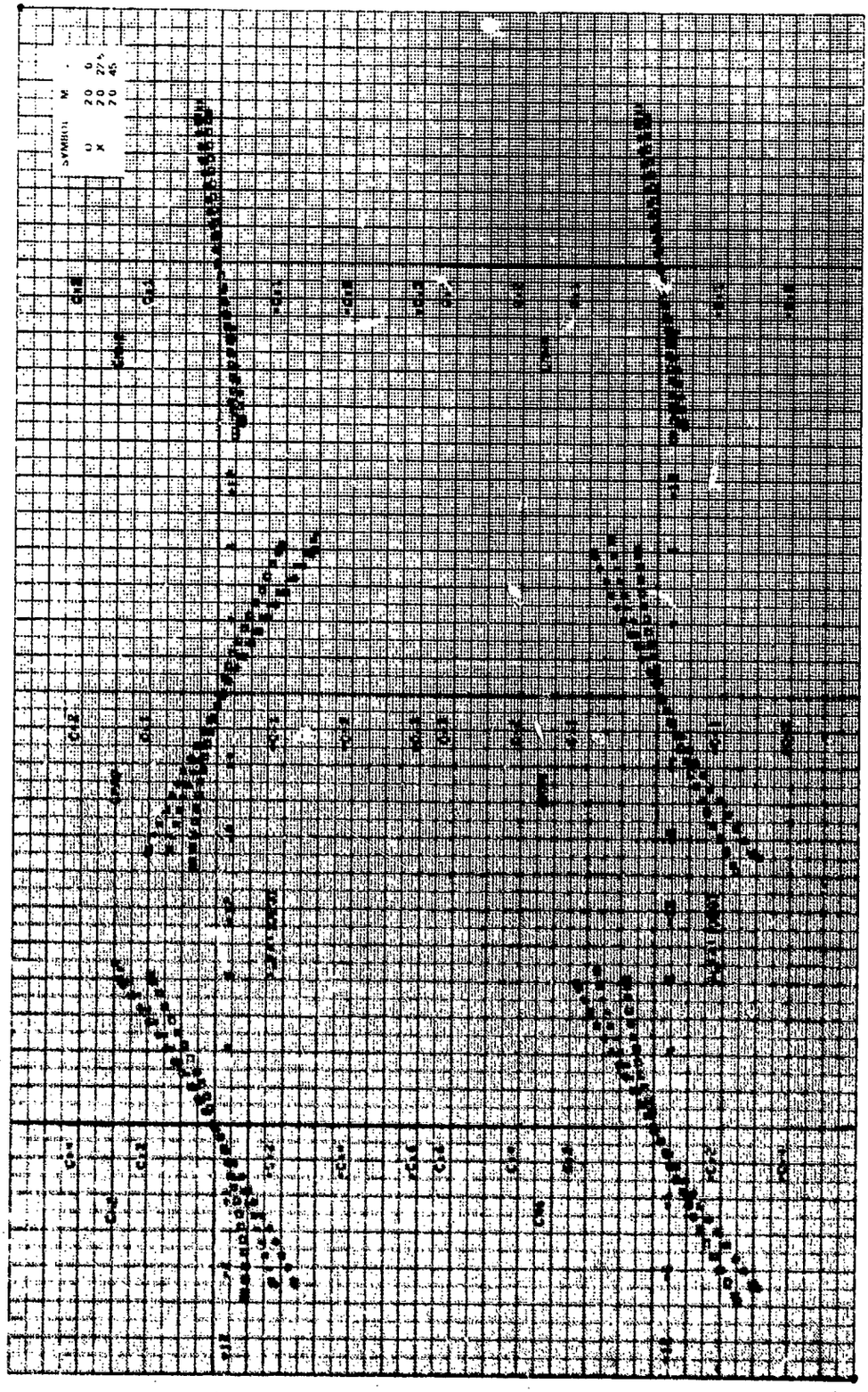


Figure 8b. Concluded.

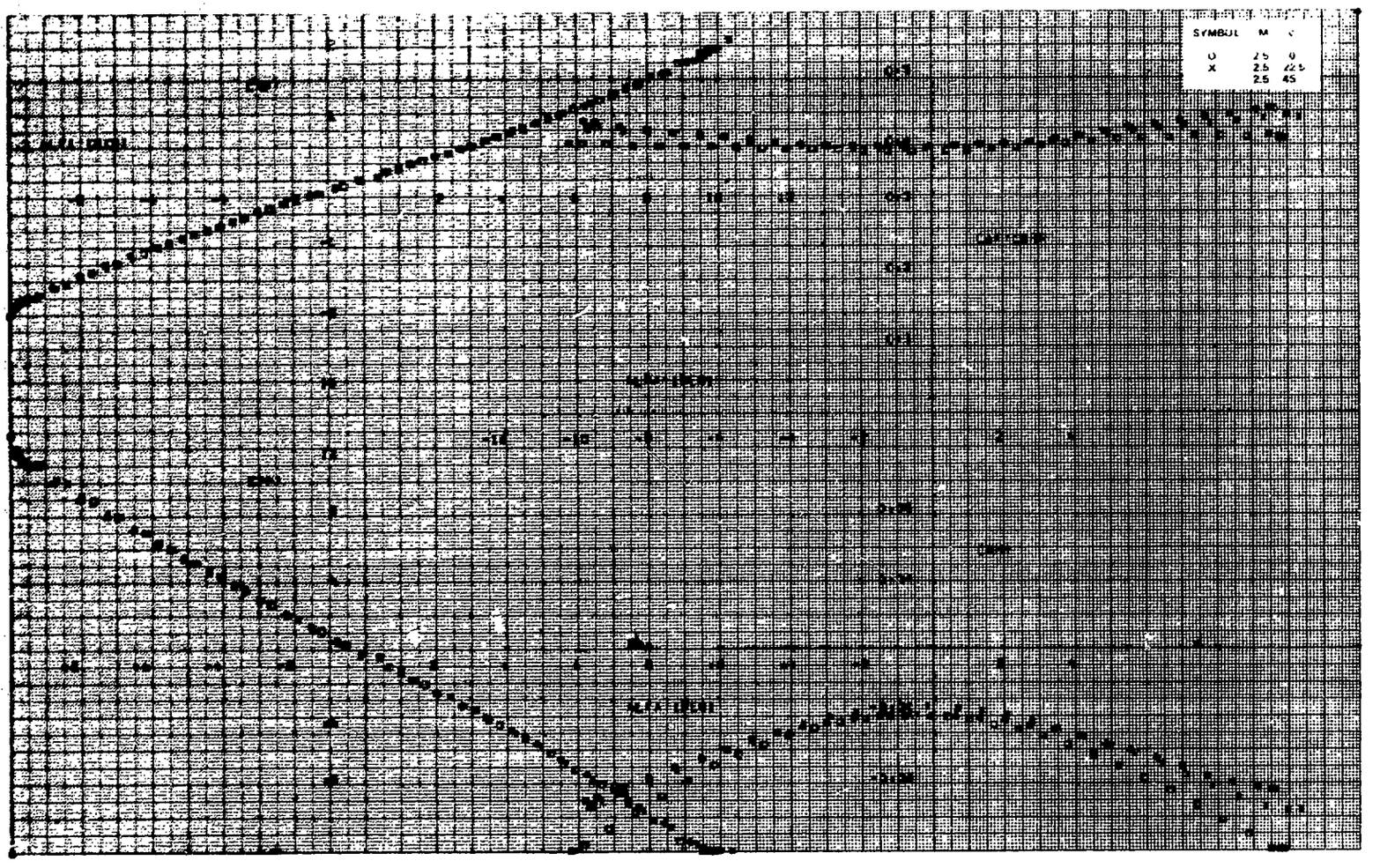


Figure 8c. Aerodynamic stability coefficients, CR/D = 1.75, γ = 0 deg, θ = 22.5 deg, M_∞ = 2.5.

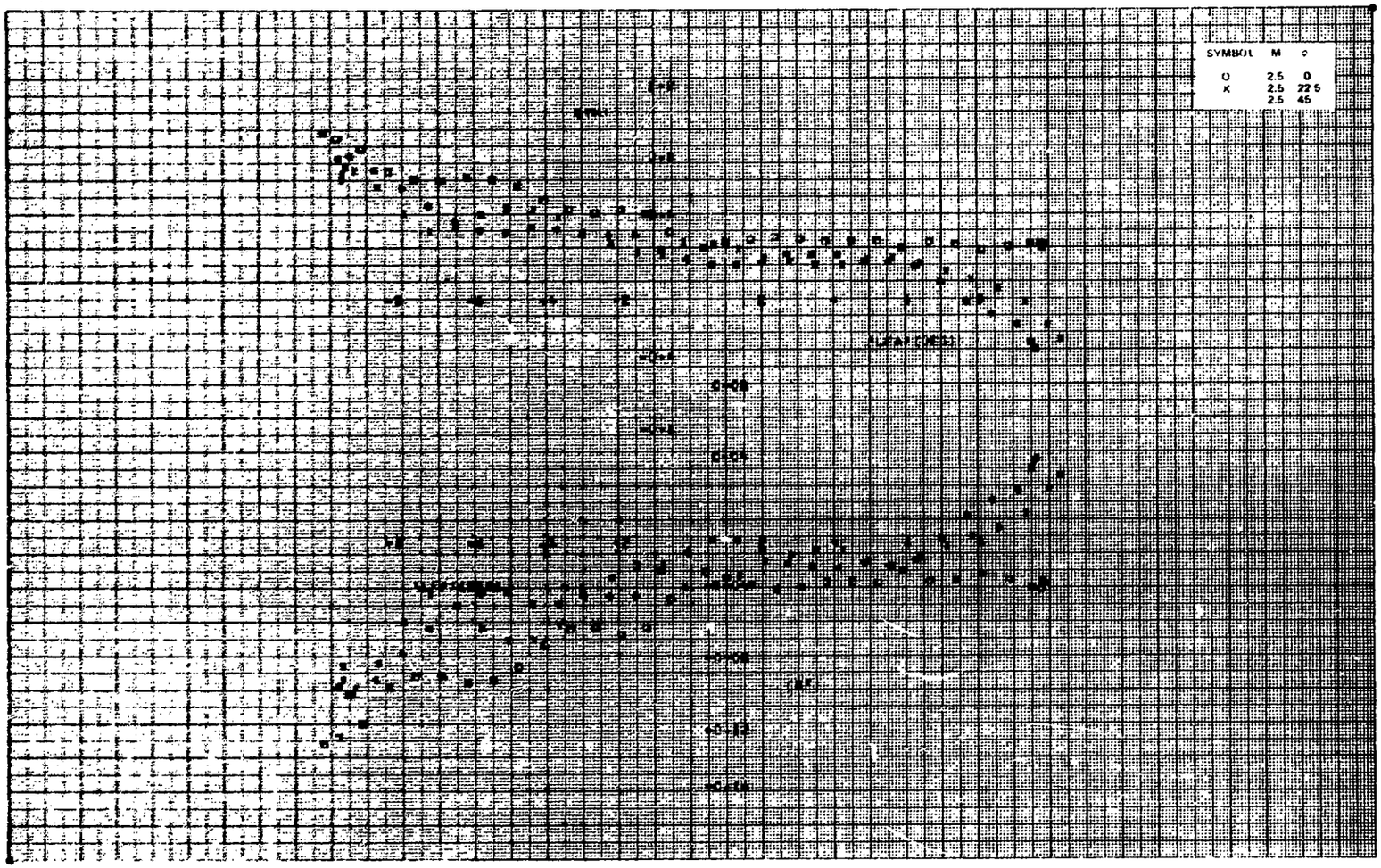


Figure 8c. Continued.

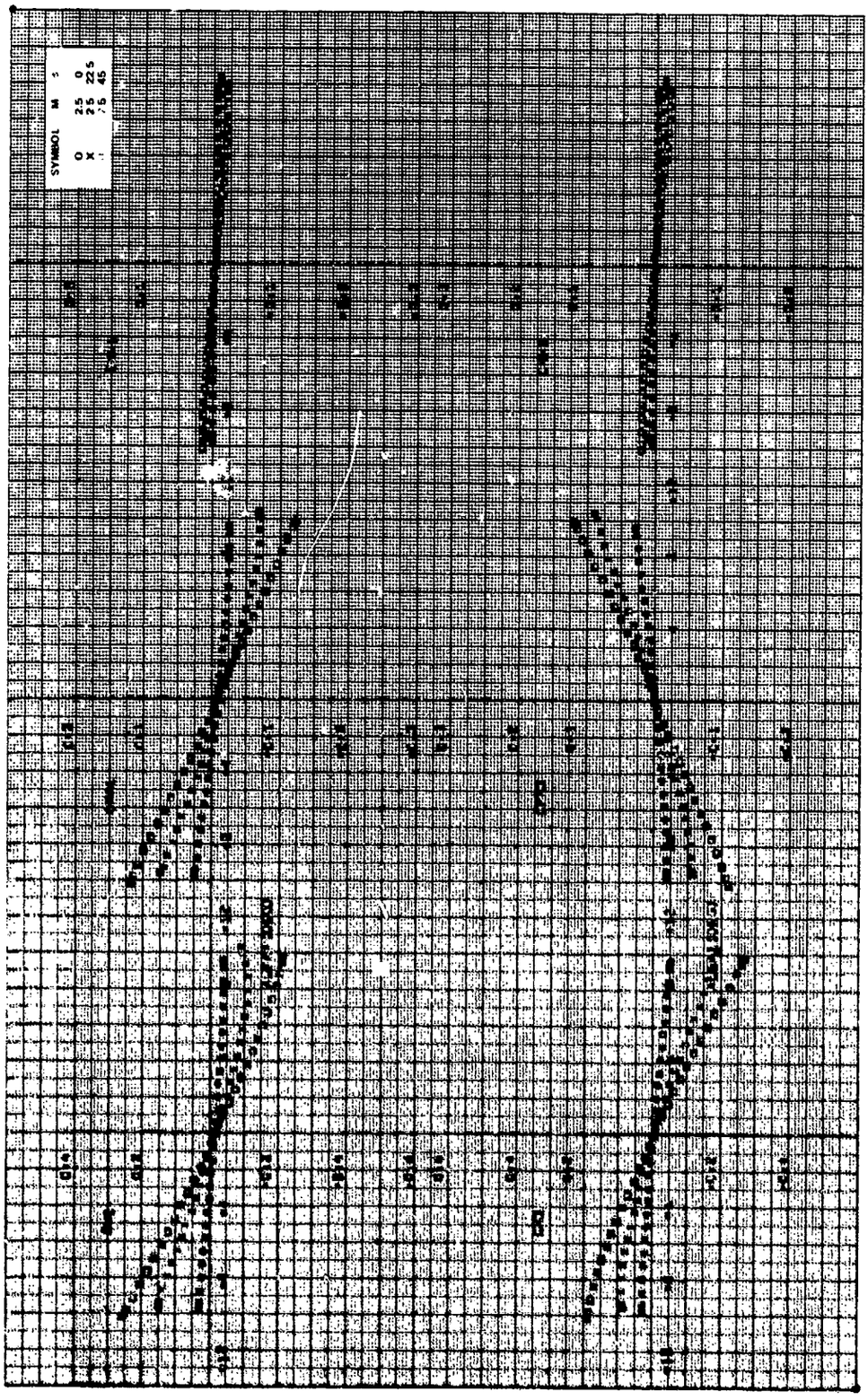


Figure 8c. Continued.

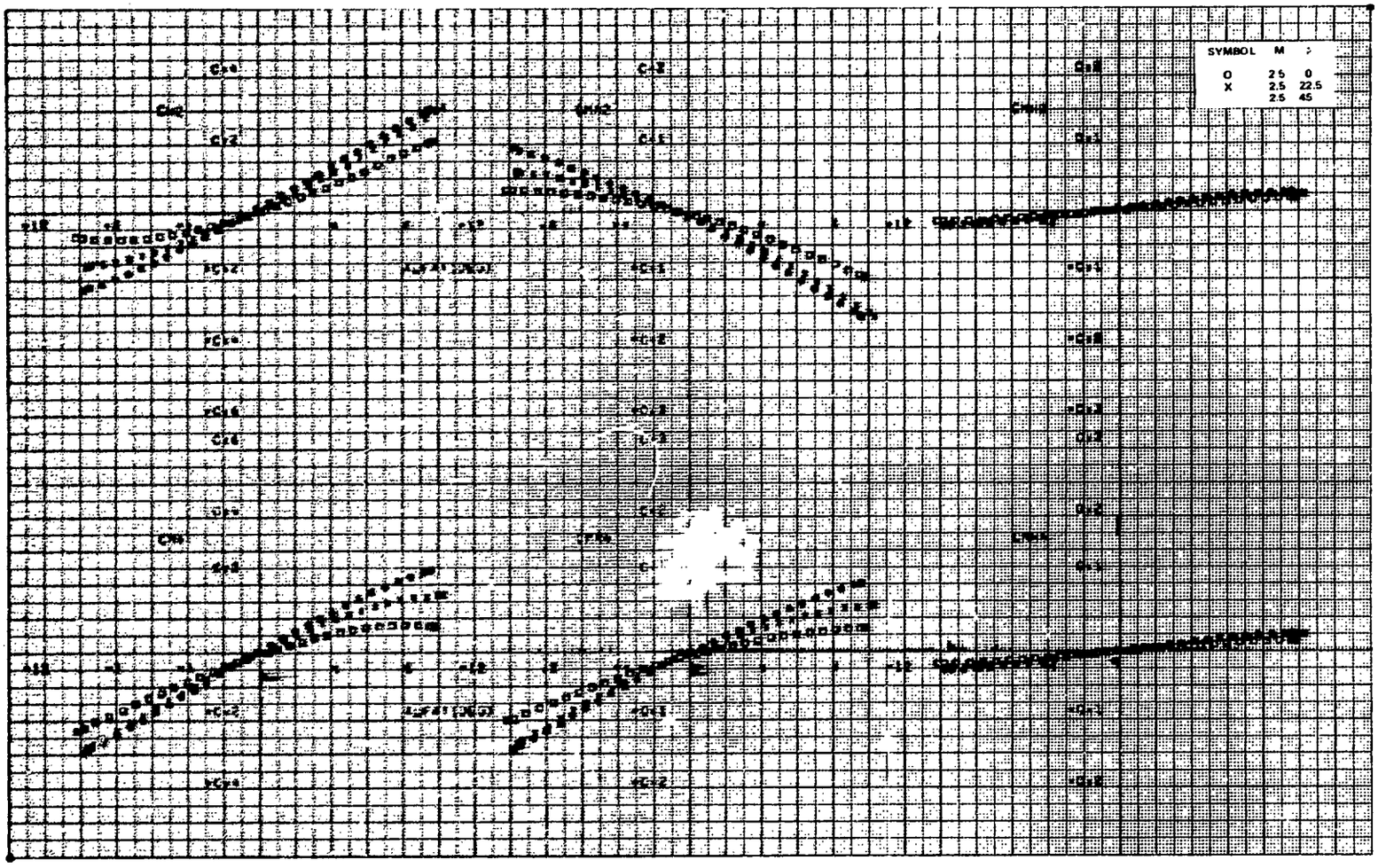


Figure 8c. Concluded.

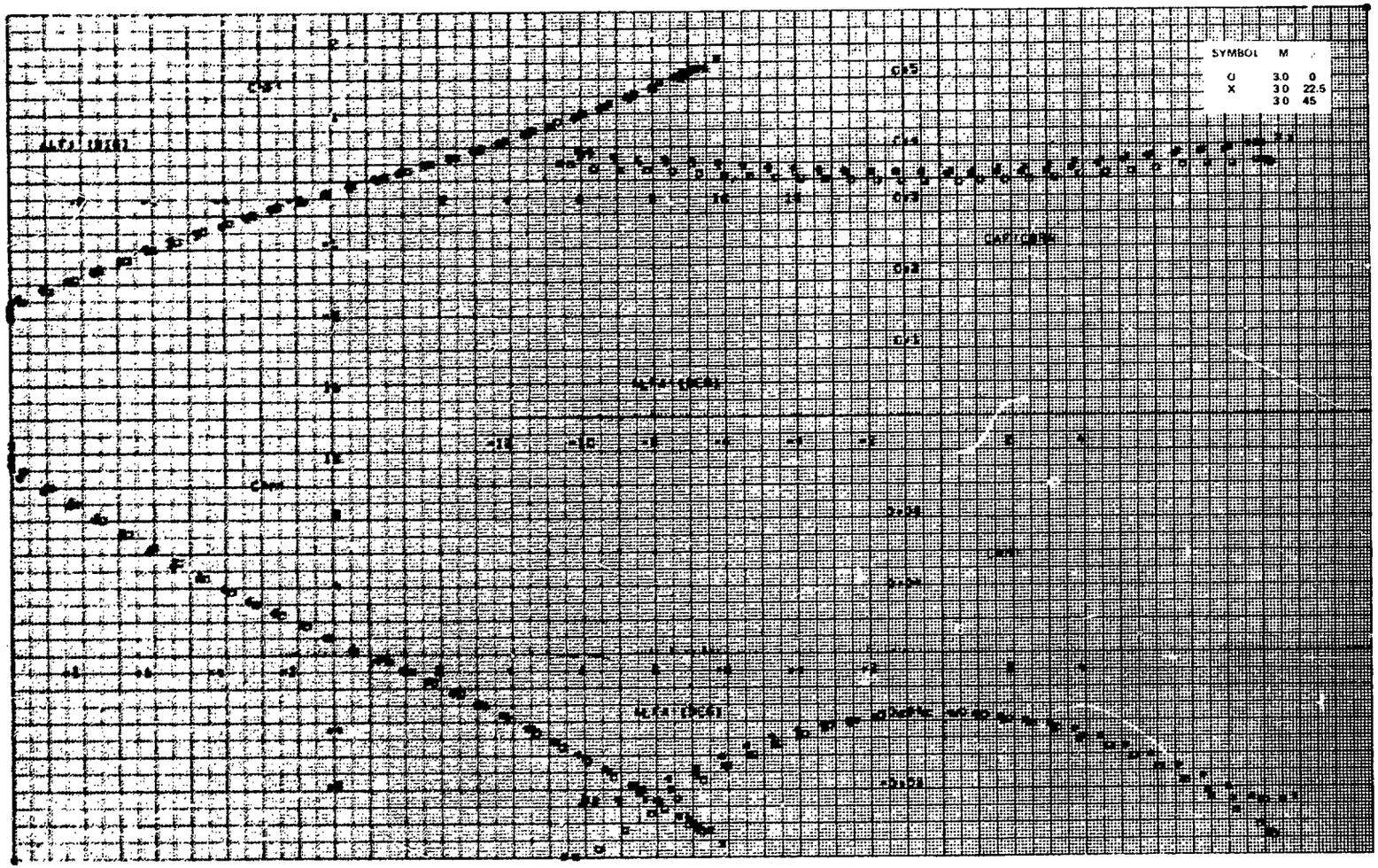
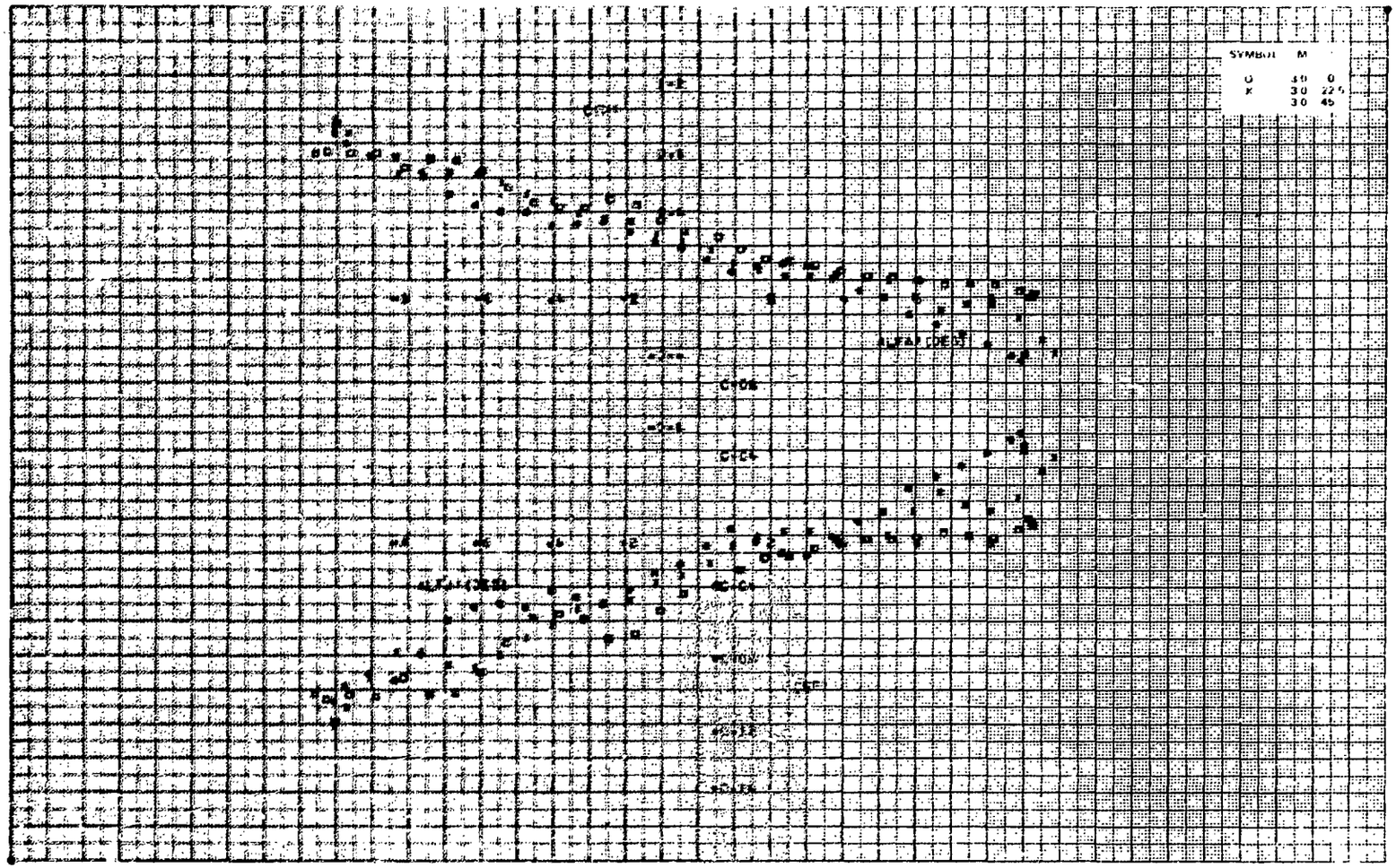


Figure 58. Aerodynamic stability coefficients, CR/D = 1.75, ϕ = 0 deg, ϵ = 22.5 deg, M_∞ = 3.0.


SYMBOL M
O 10 0
X 30 22.5
30 45

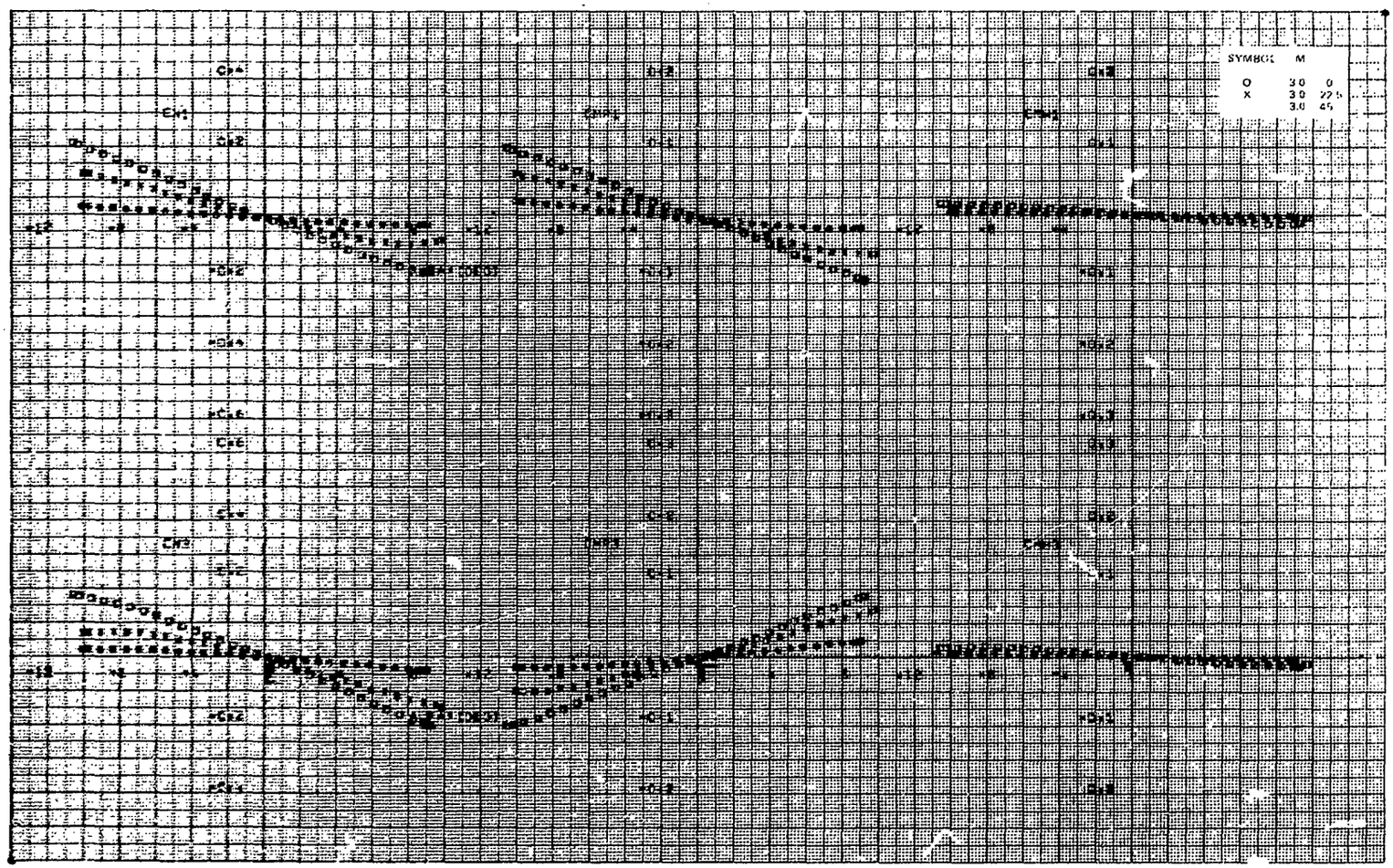


Figure 8d. Continued.

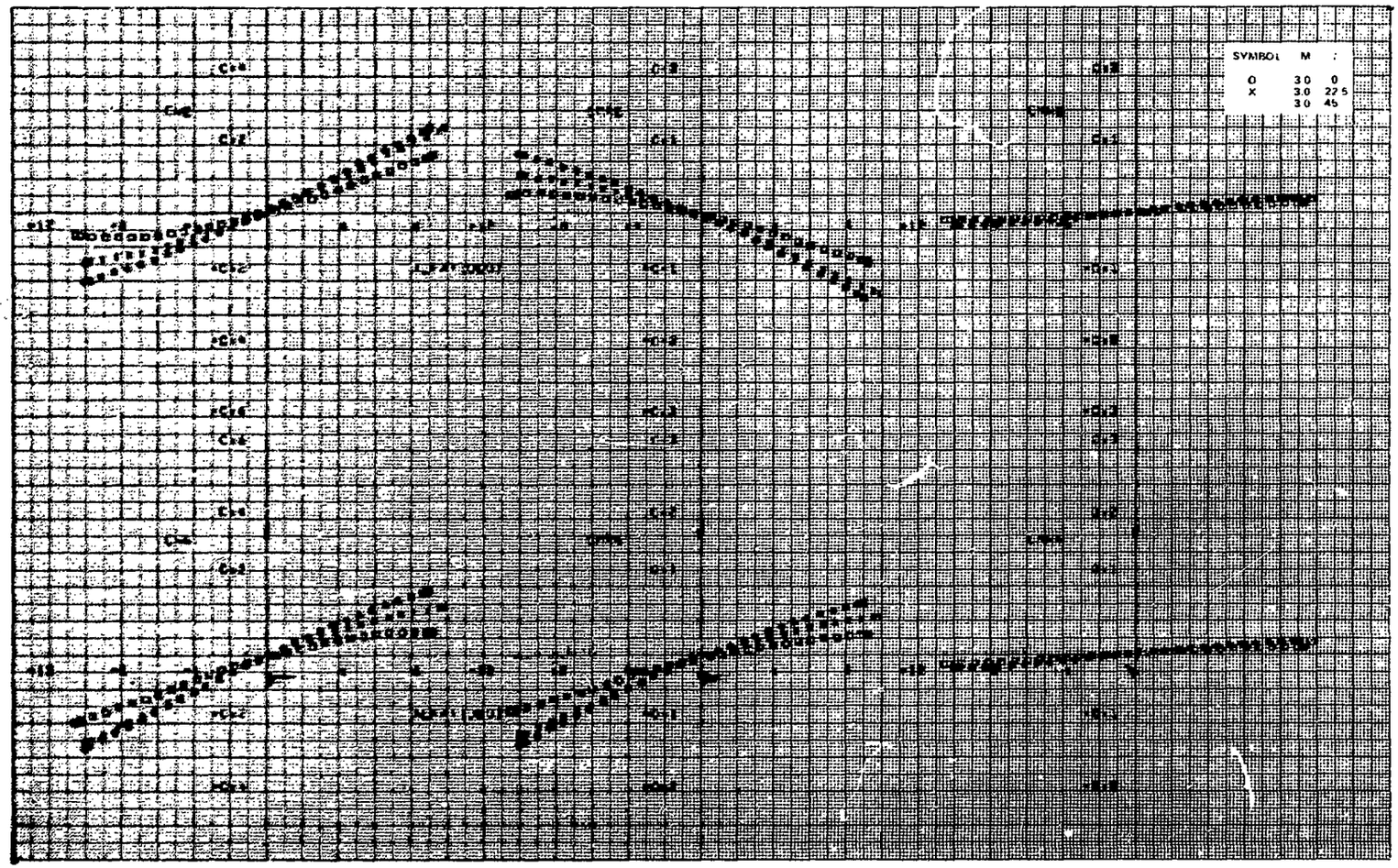


Figure 8d. Concluded.

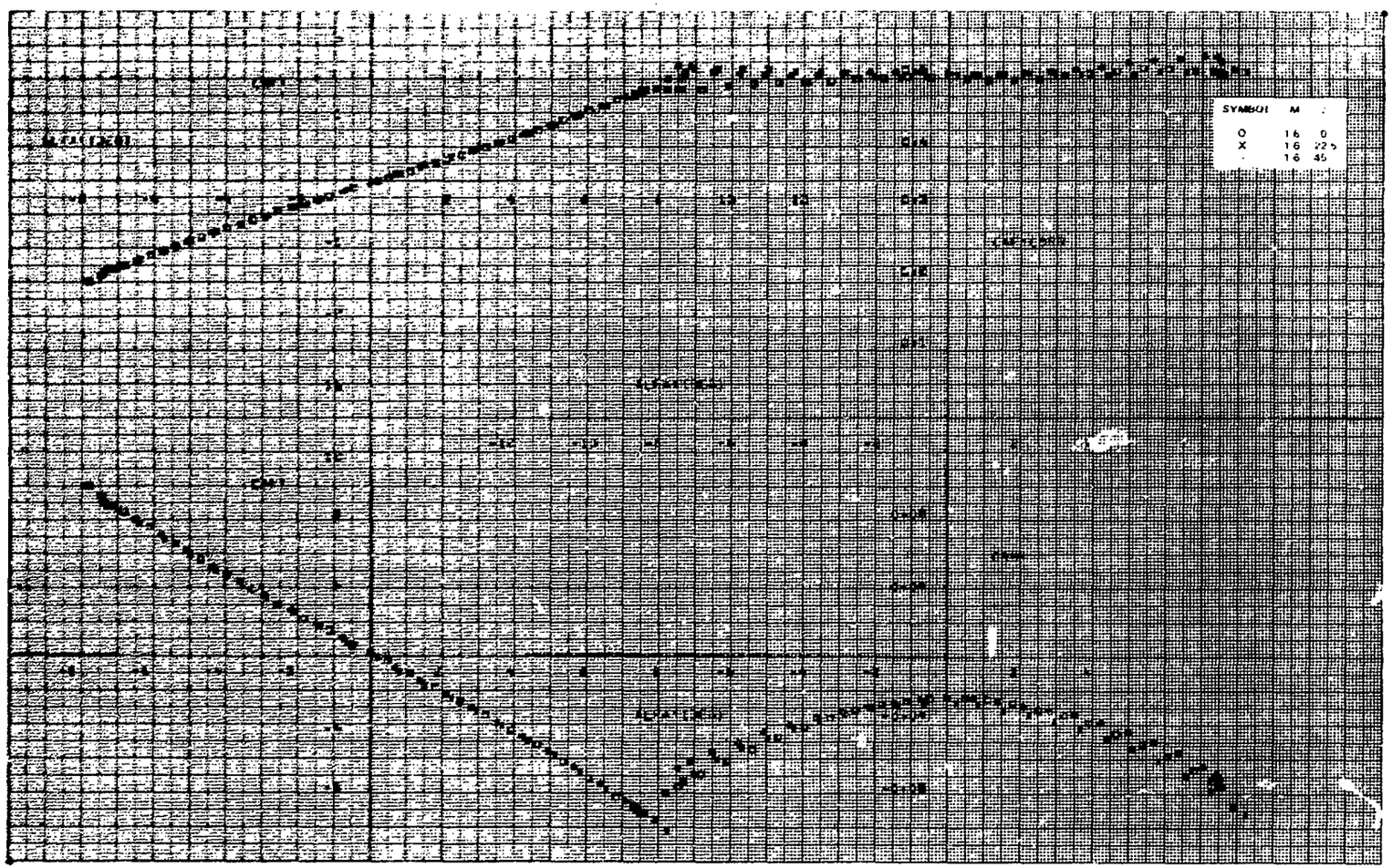


Figure 9a. Aerodynamic stability coefficients, CR/D = 1.75, Λ = 0 deg, θ = 45 deg, M_{∞} = 1.6.

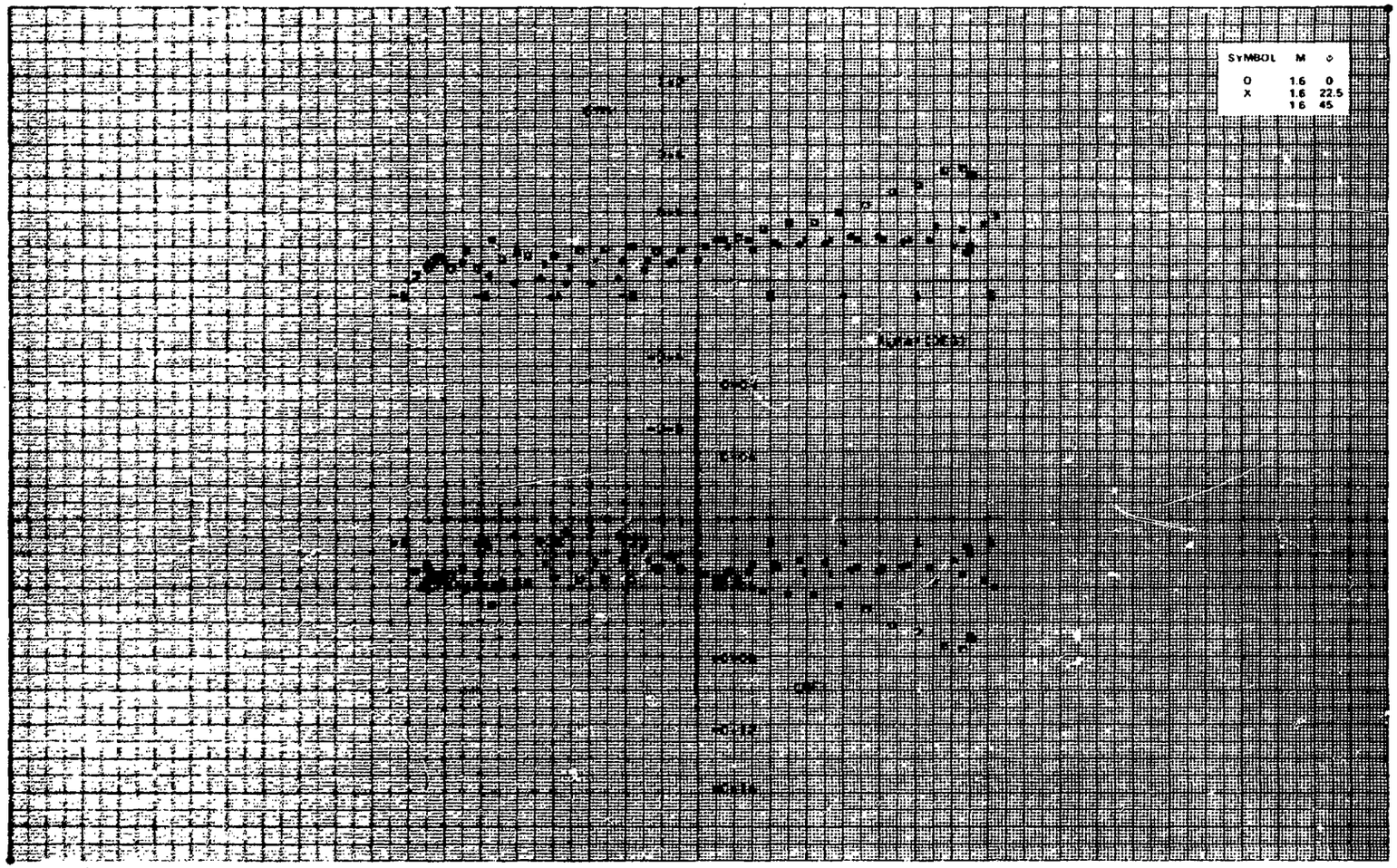


Figure 9a. Continued.

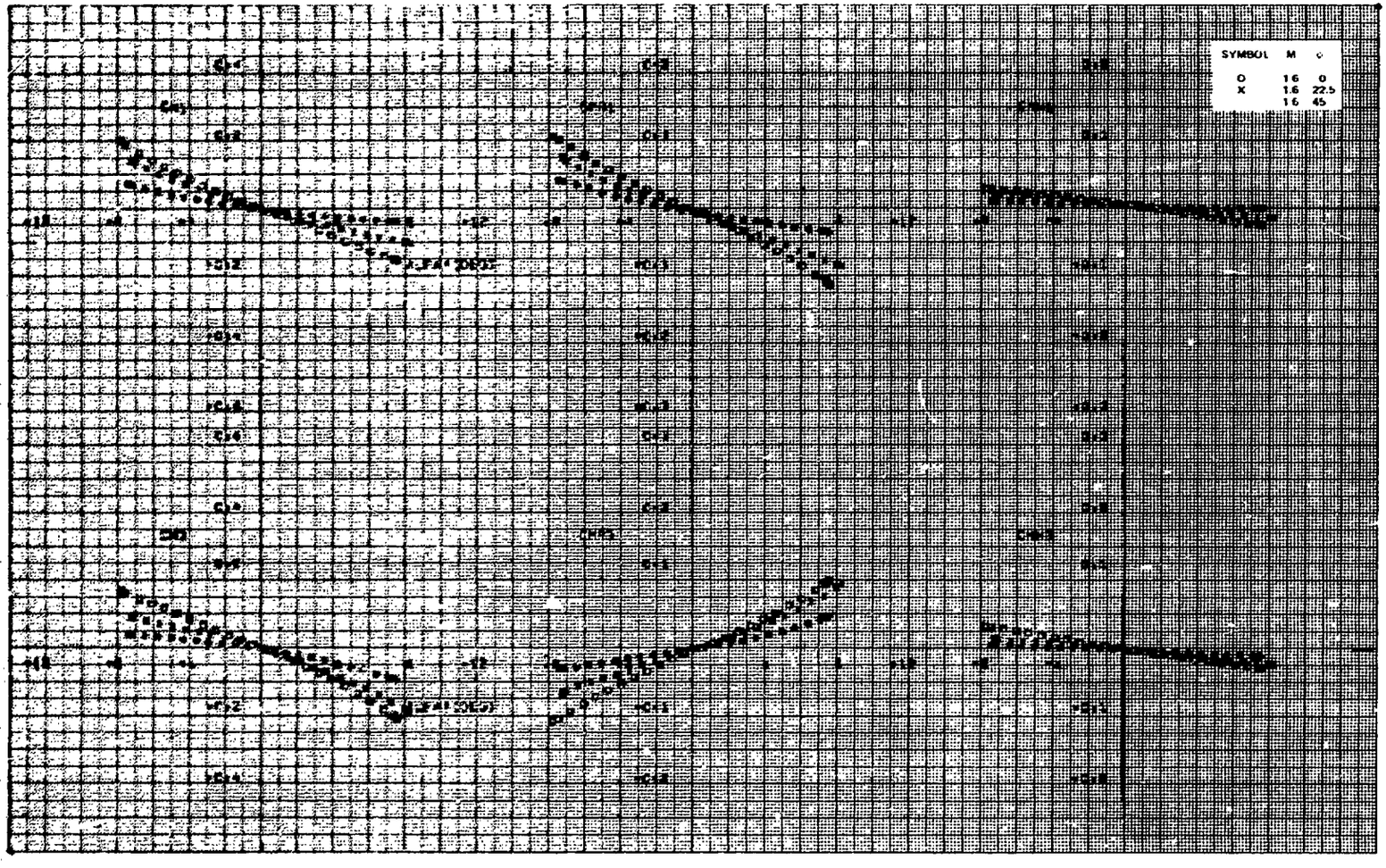


Figure 41. Continued.

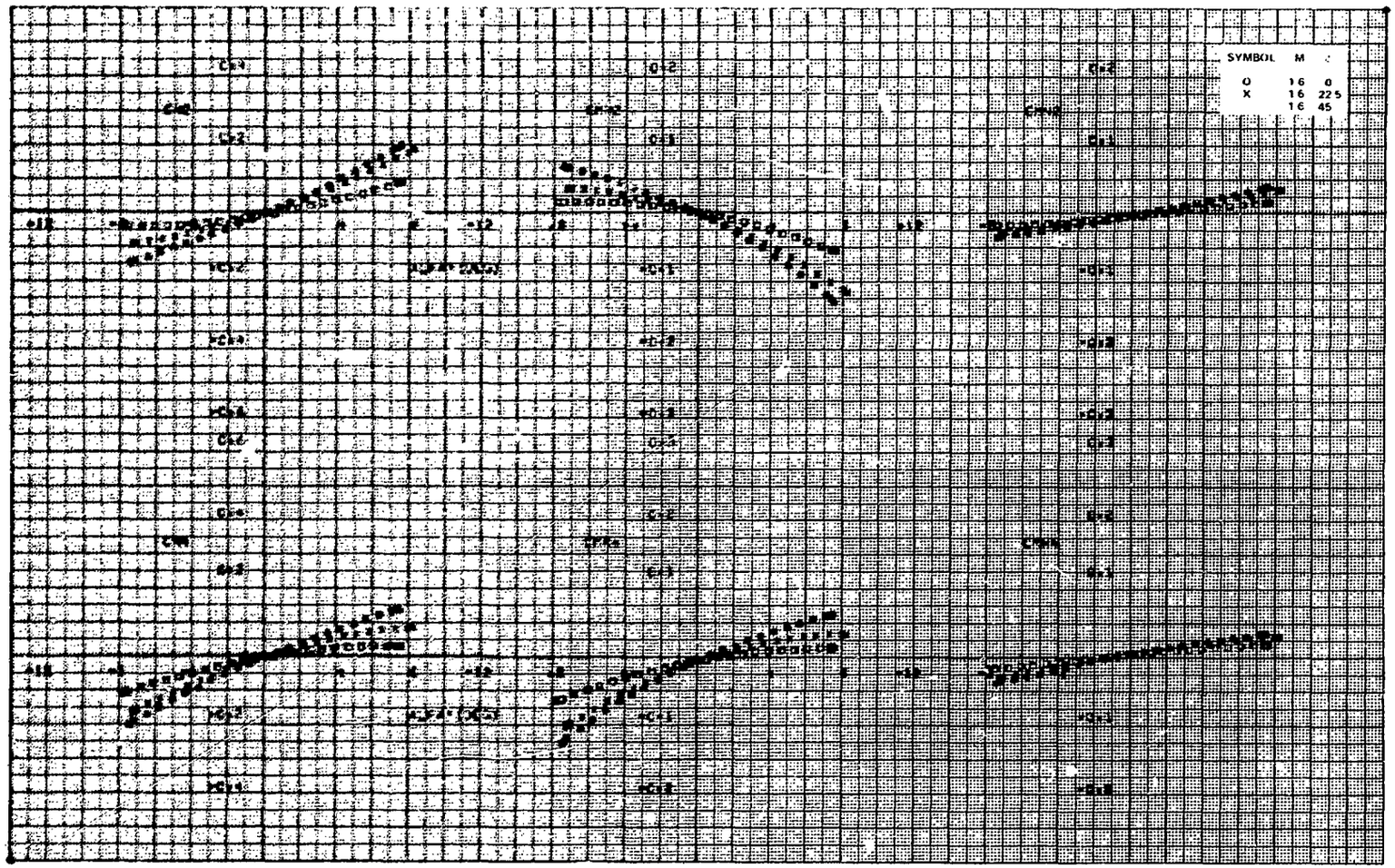
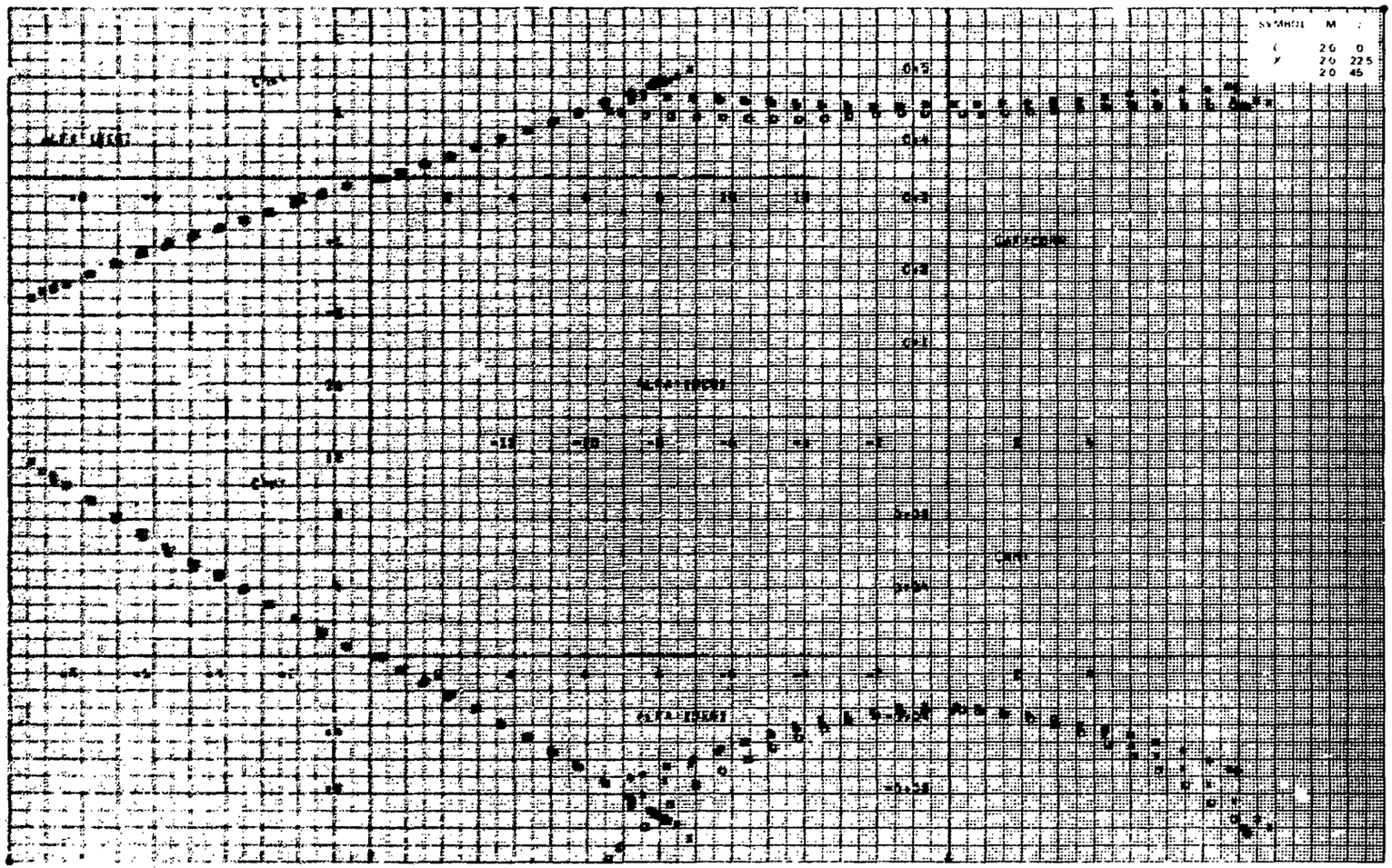


Figure 9a. Concluded.



...ic coefficients, $M_\infty = 1.5$, $\alpha = 0$ deg, $\alpha = 45$ deg, $\gamma = 2.0$.

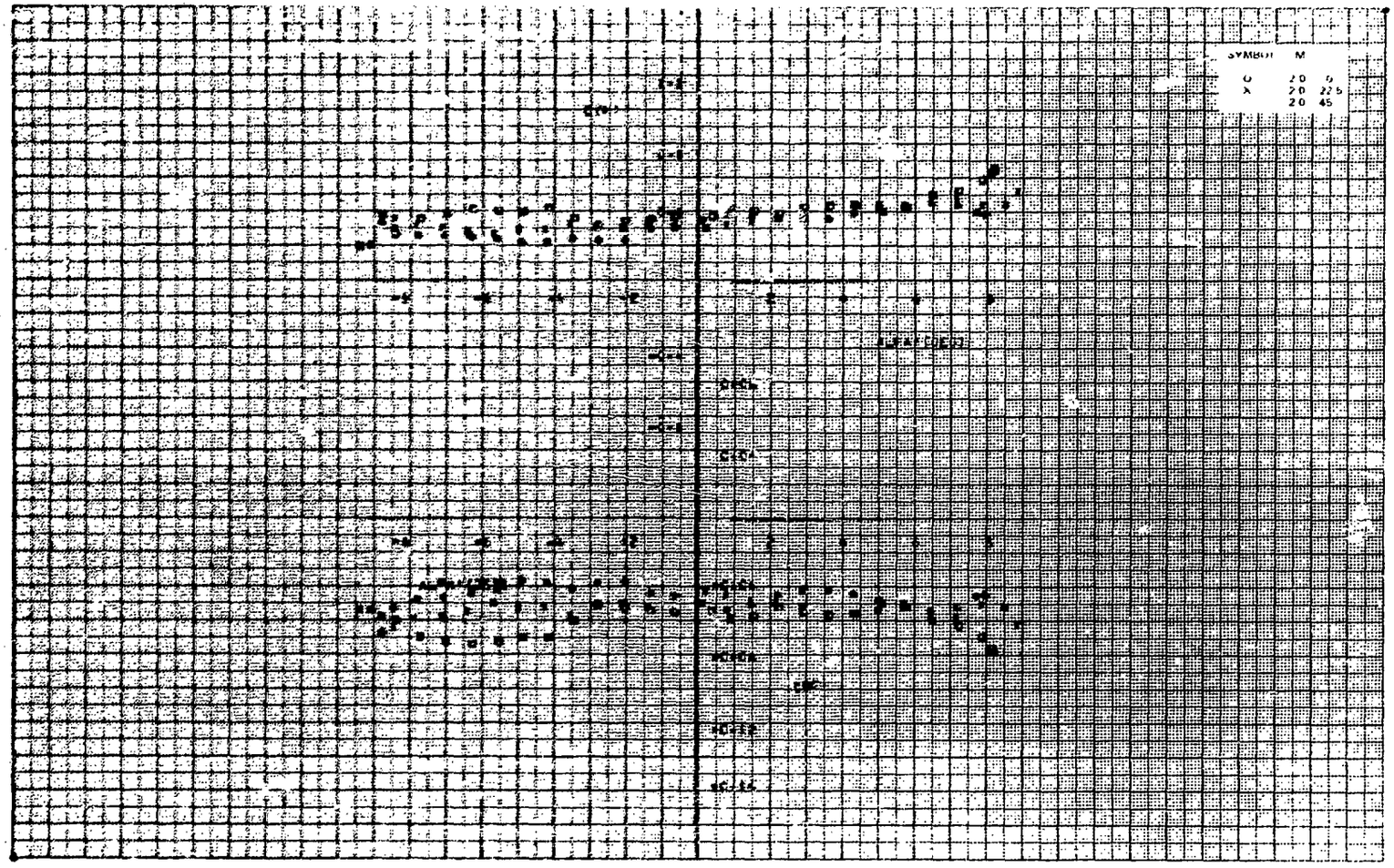


Figure 9b. Continued.

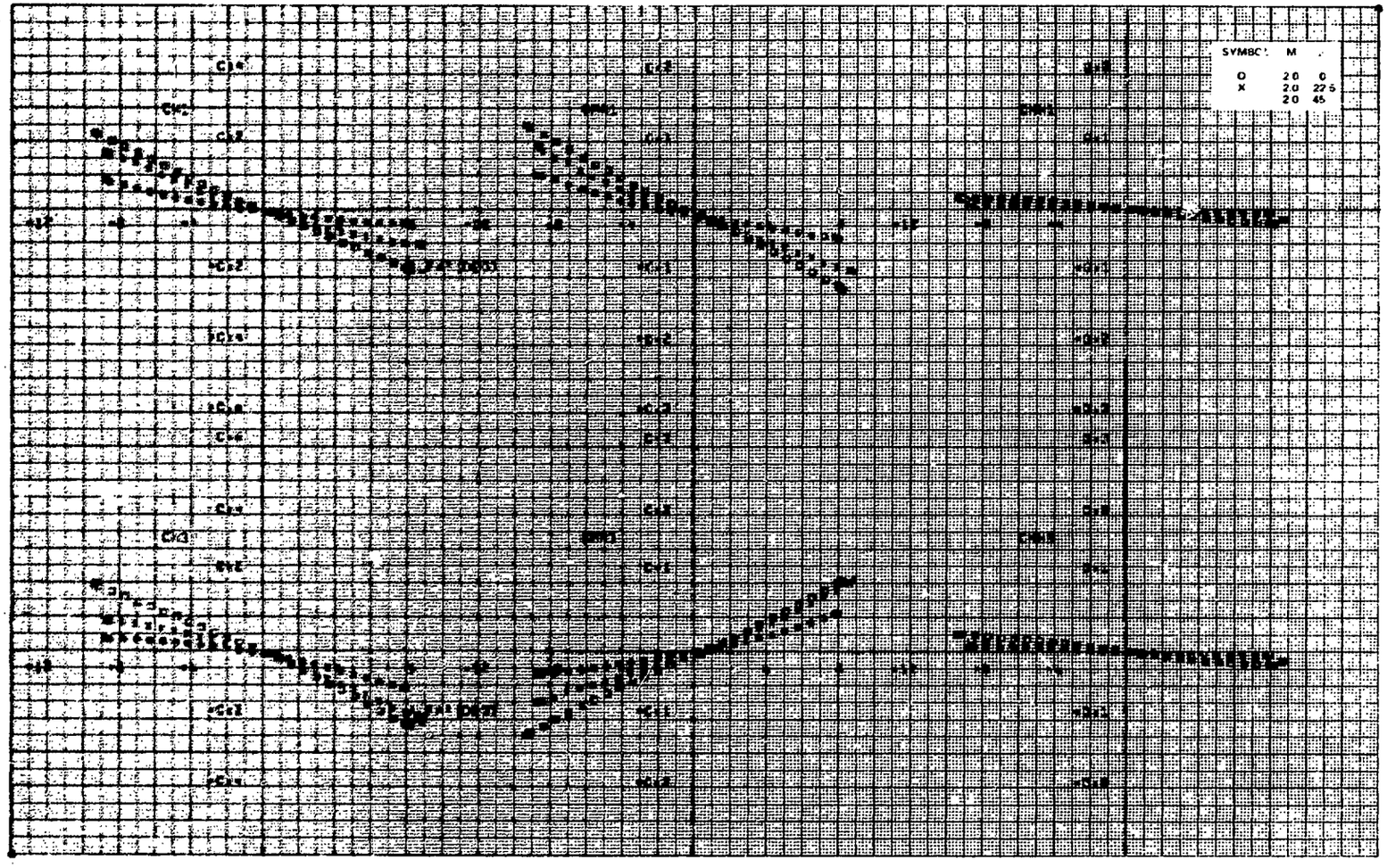


Figure 9b. Continued.

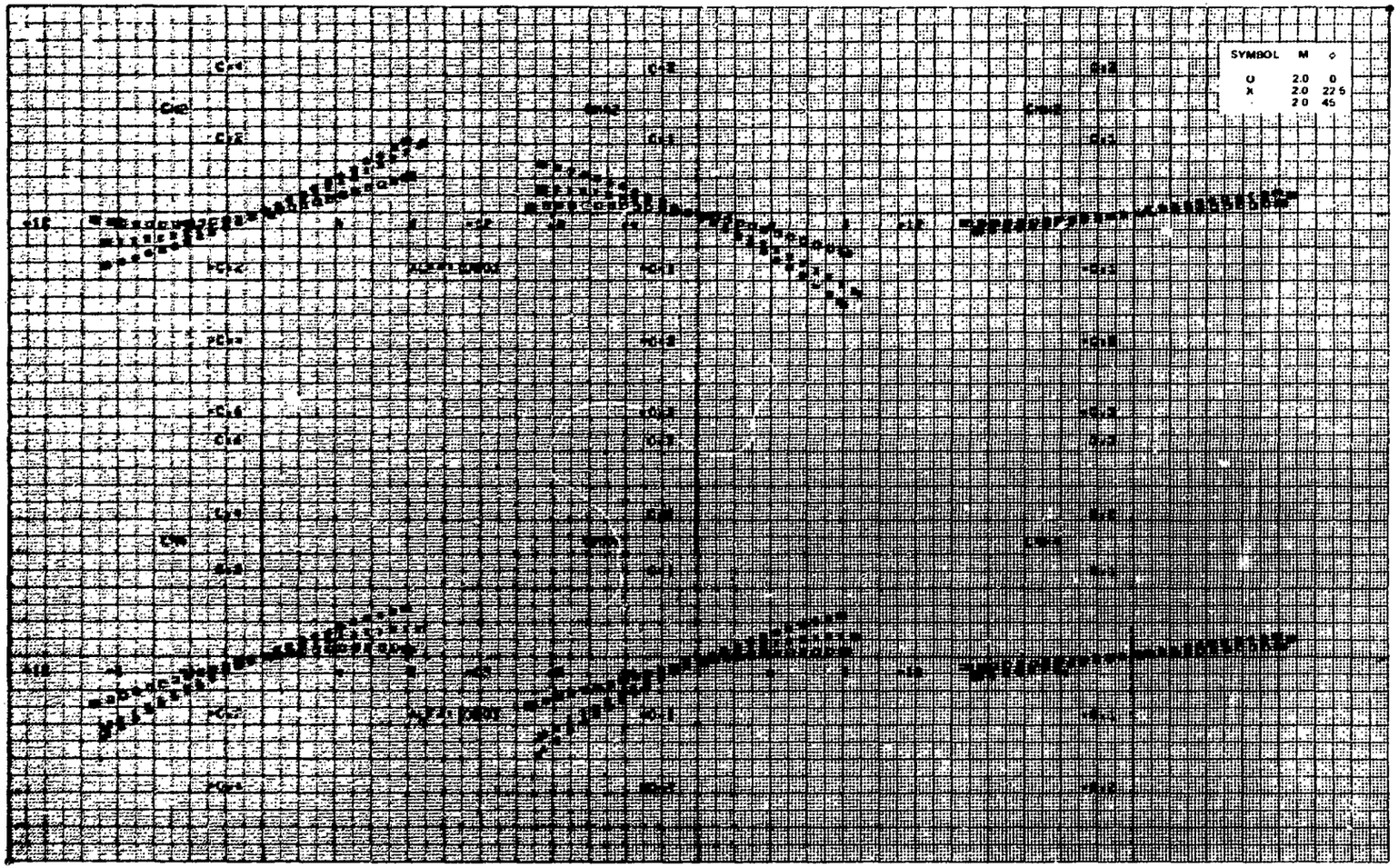


Figure 9b. Concluded.

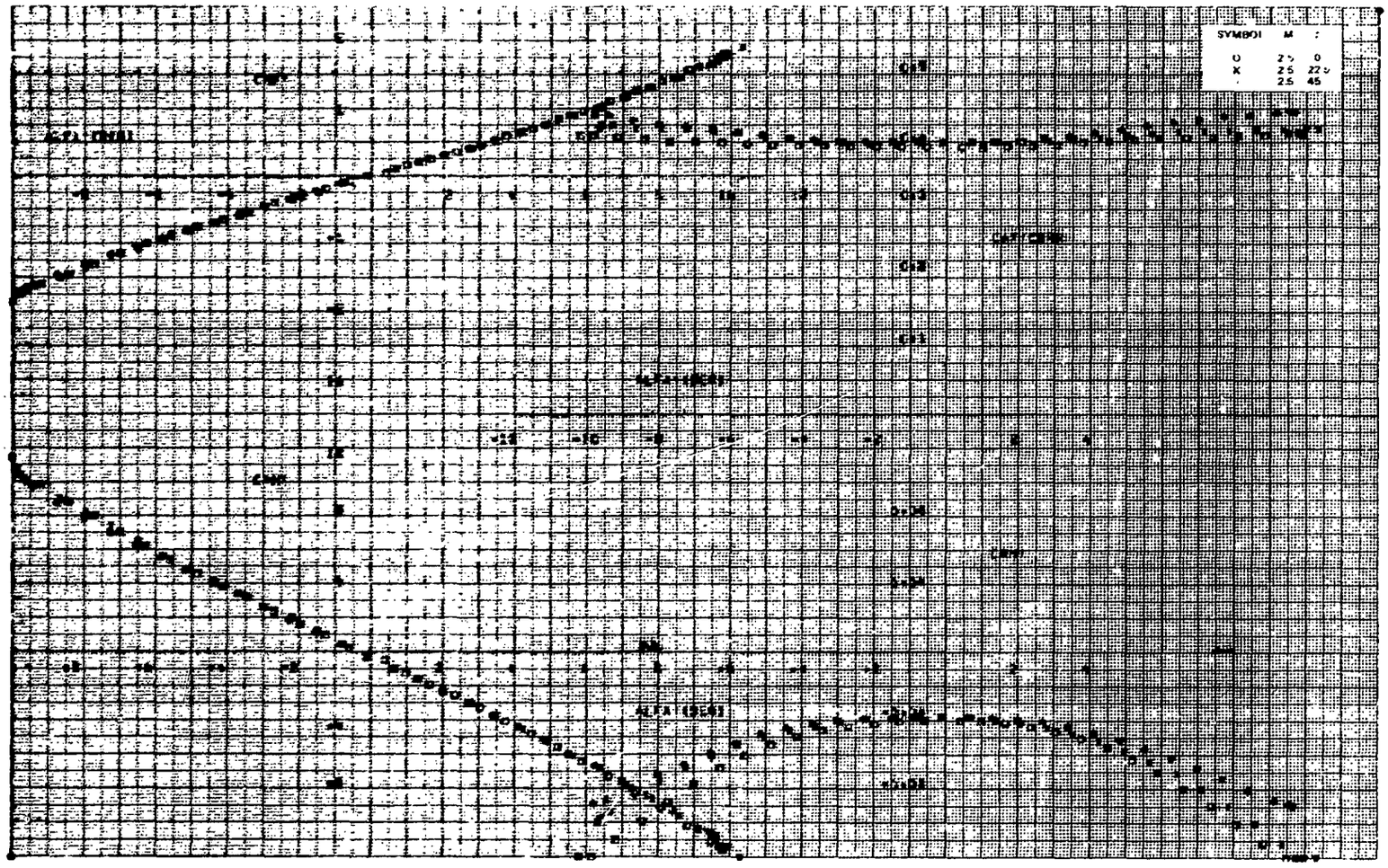


Figure 9c. Aerodynamic stability coefficients, CR/D = 1.75, γ = 0 deg, ϕ = 45 deg, M_∞ = 2.5.

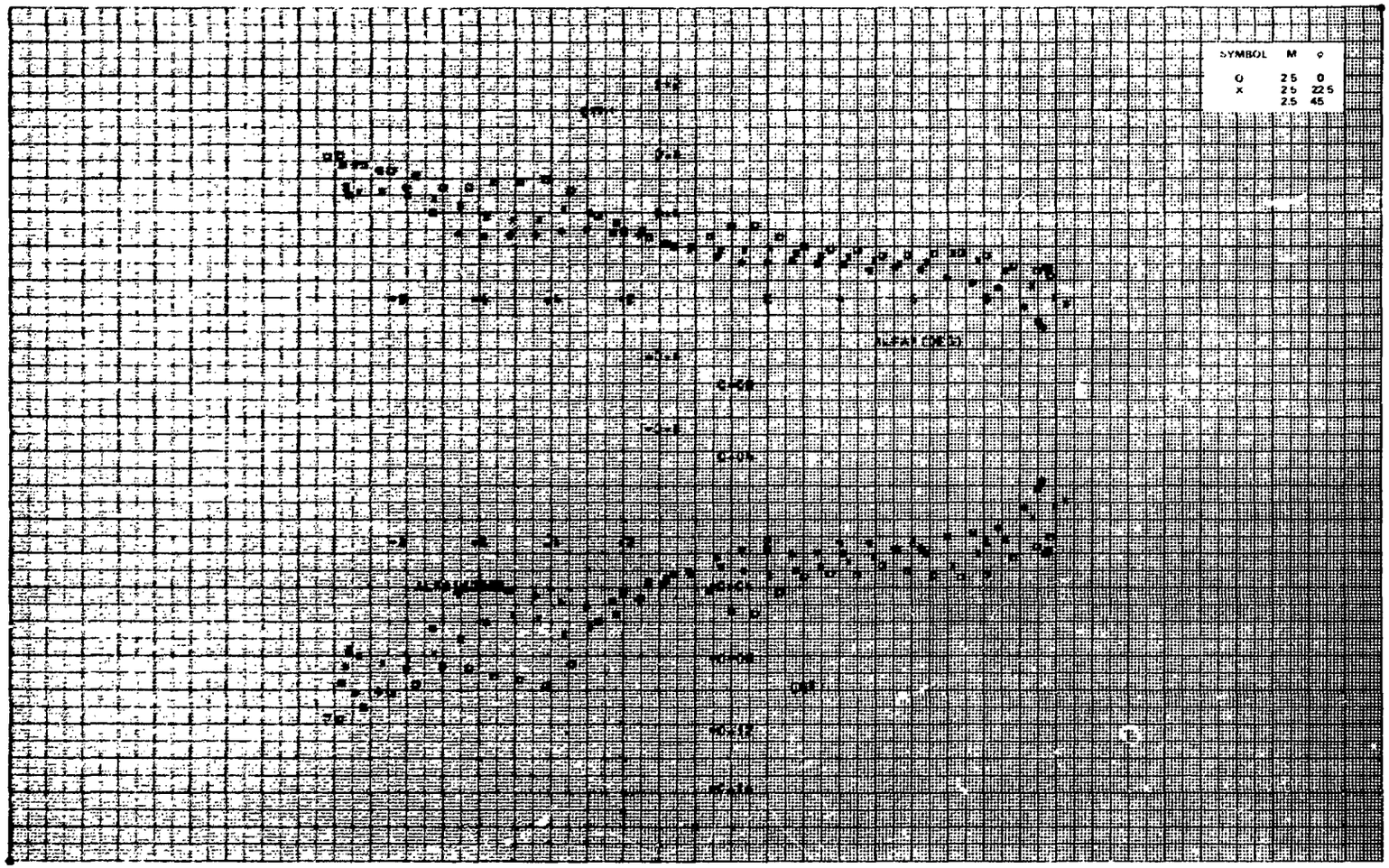


Figure 9c. Continued.

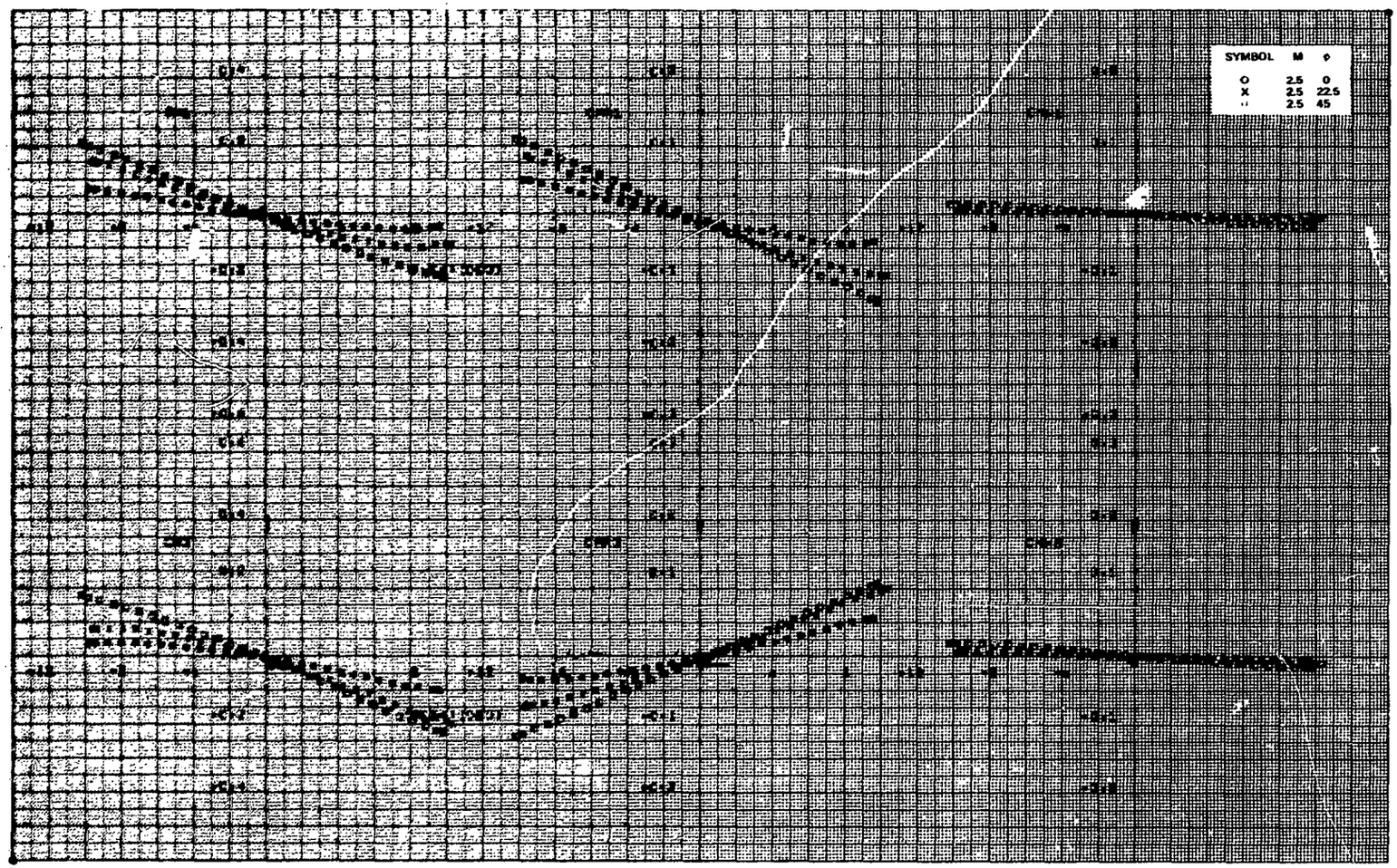


Figure 9c. Continued.

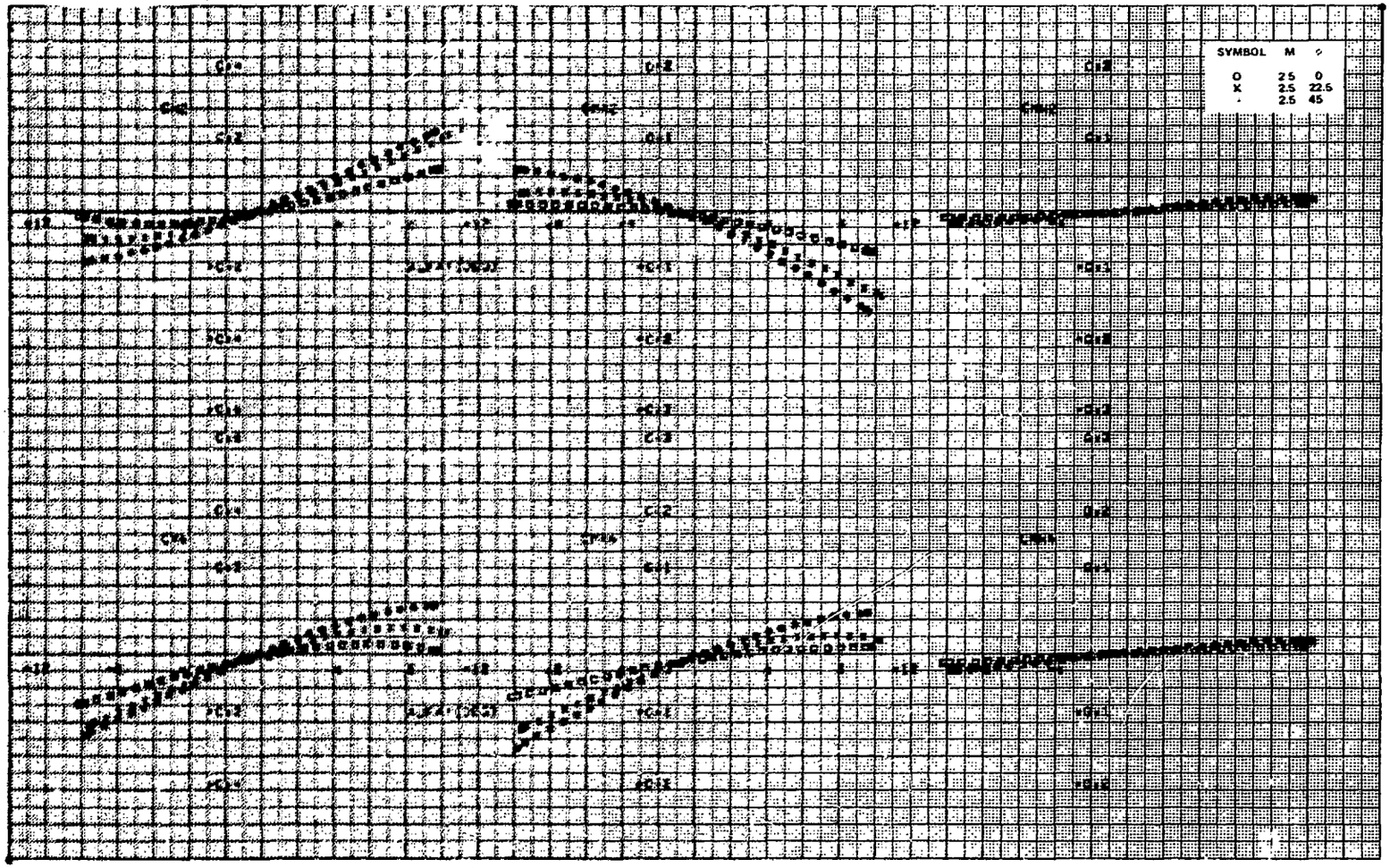


Figure 9c. Concluded.

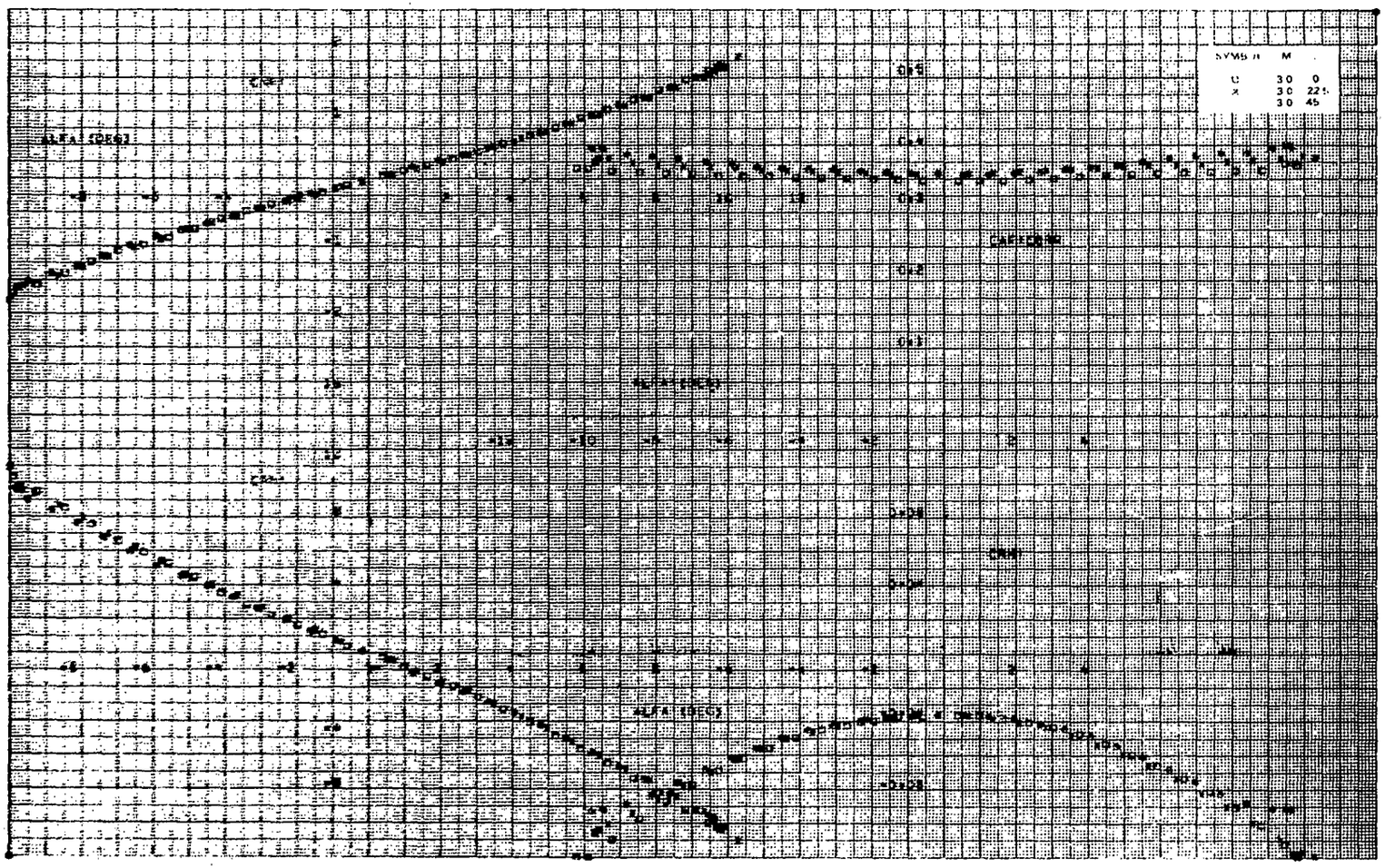


Figure [illegible]. Aerodynamic stability coefficients, CR/D = 1.75, ϕ = 0 deg, θ = 45 deg, M_∞ = 3.0.

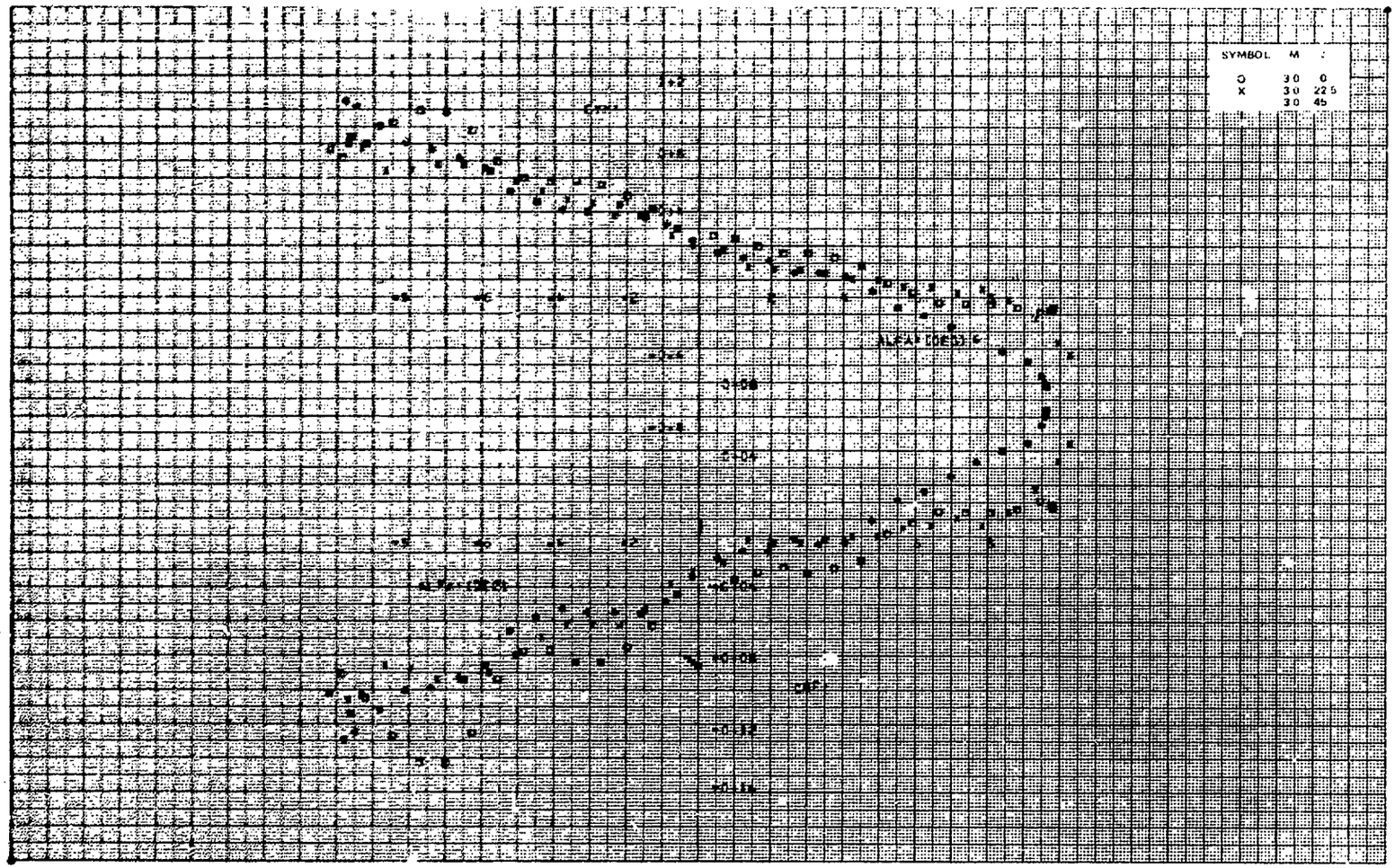


Figure 9d. Continued.

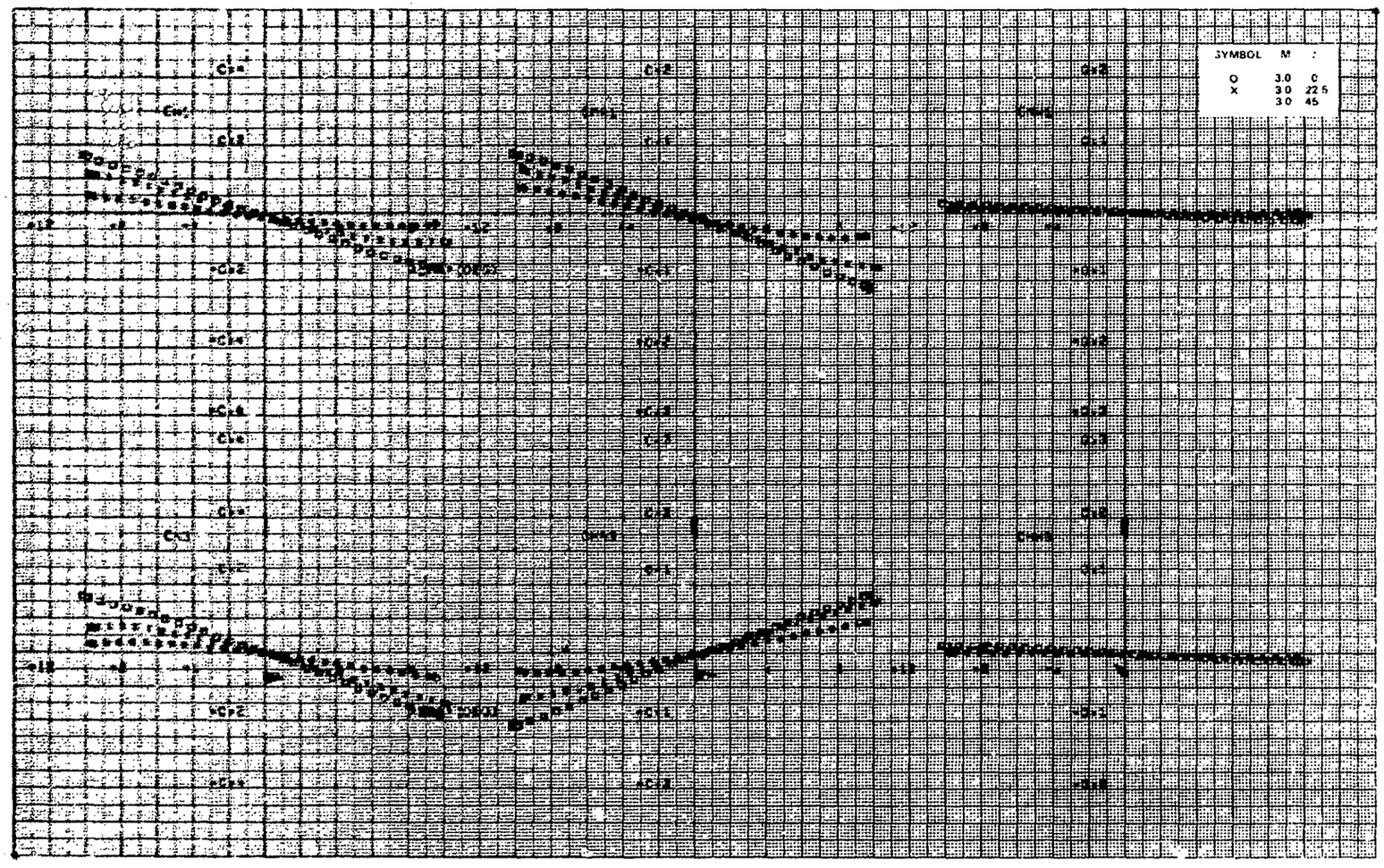


Figure 9d. Continued.

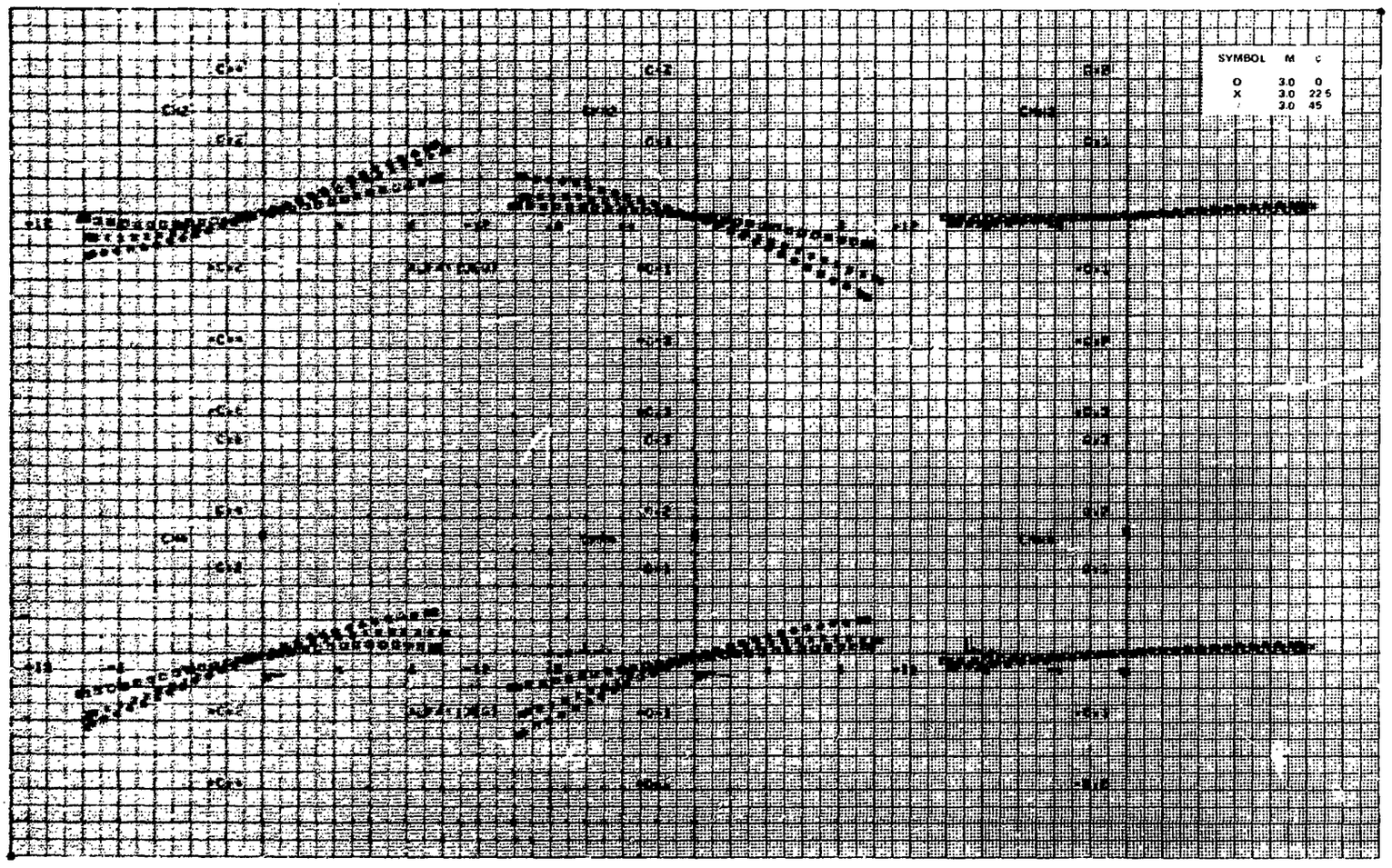


Figure 9d. Concluded.

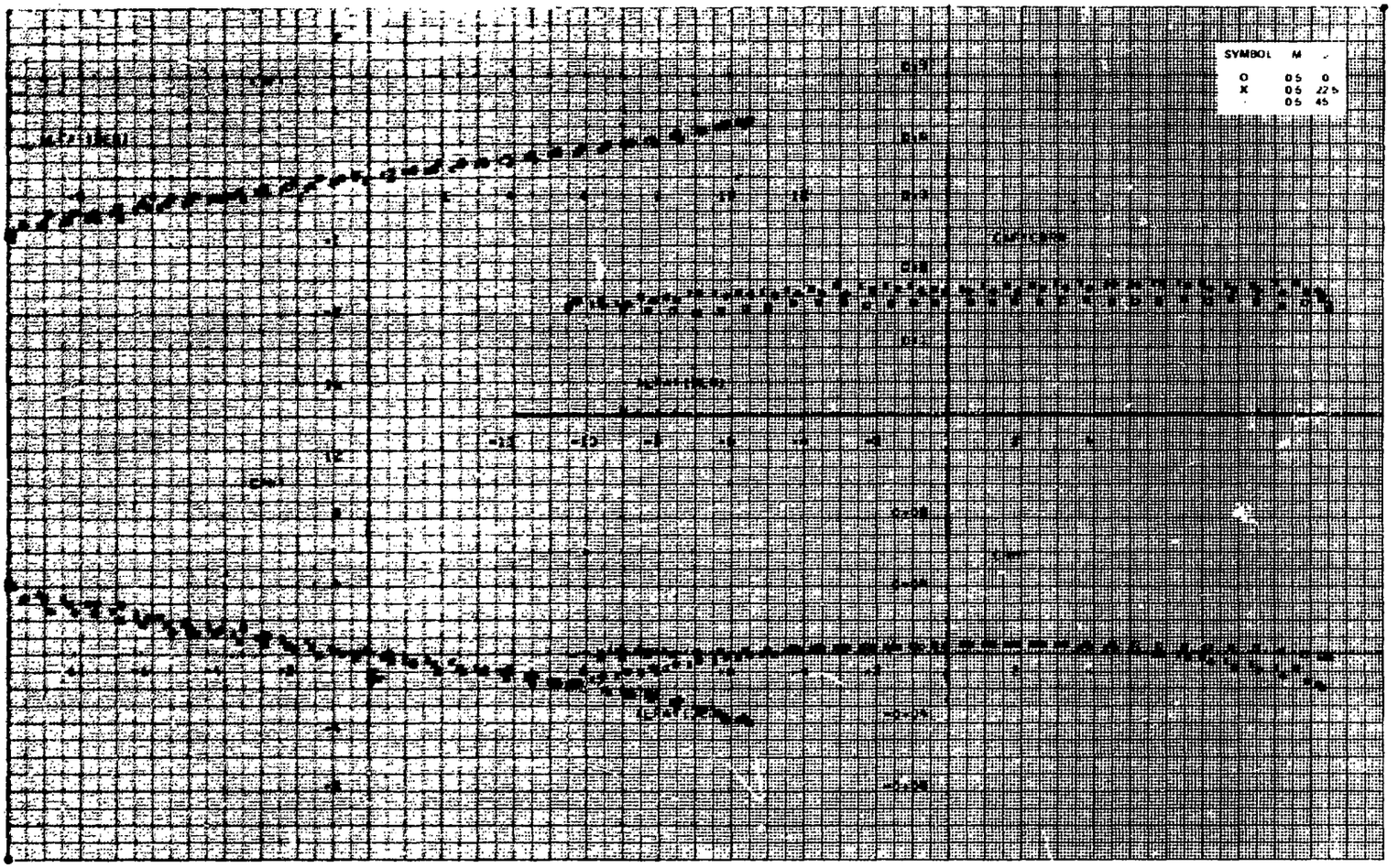


Figure 10a. Aerodynamic stability coefficients, CR/D = 1.75, λ = 0 deg, ϵ = 112.5 deg, M_∞ = 0.5.

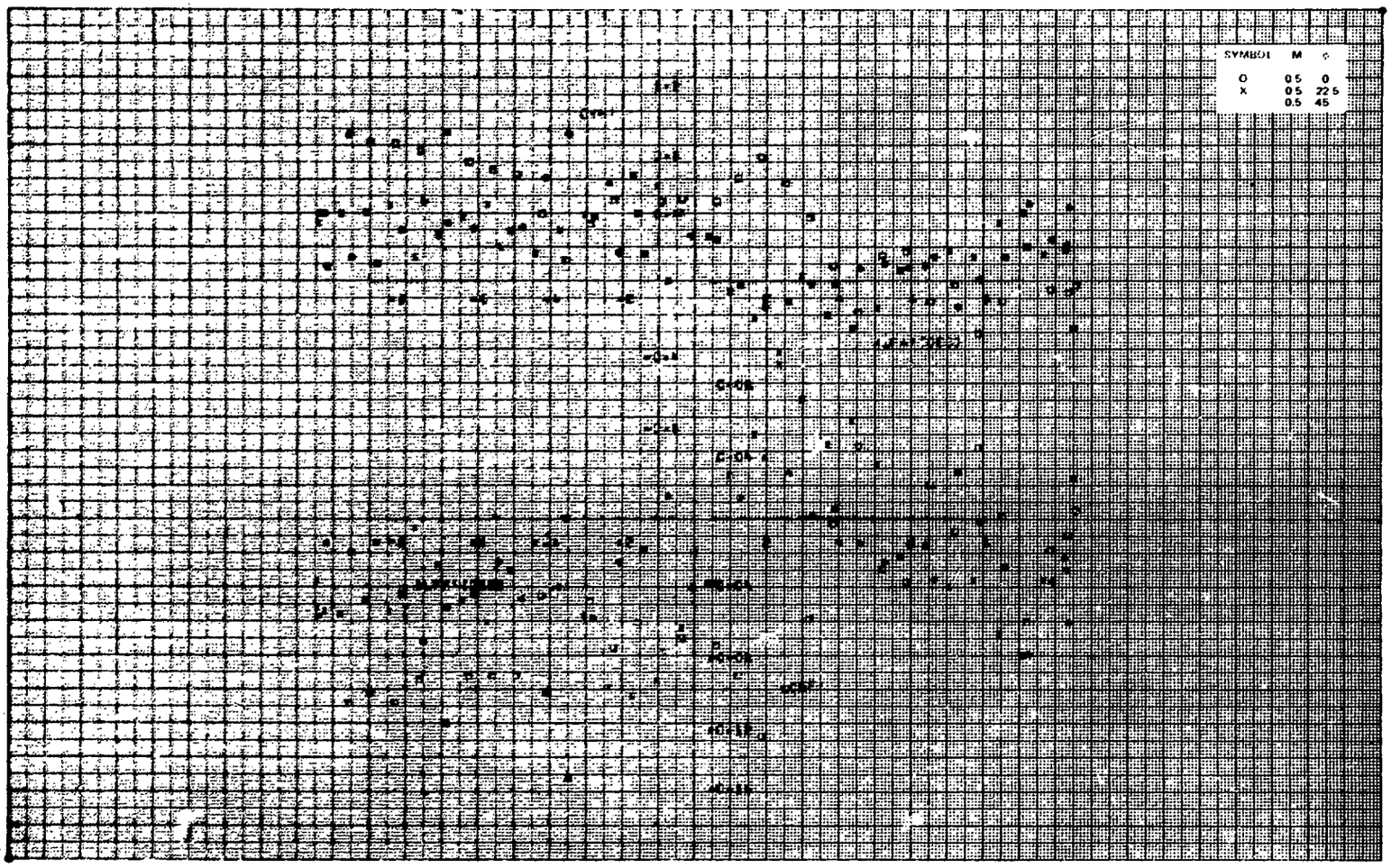


Figure 10a. Continued.

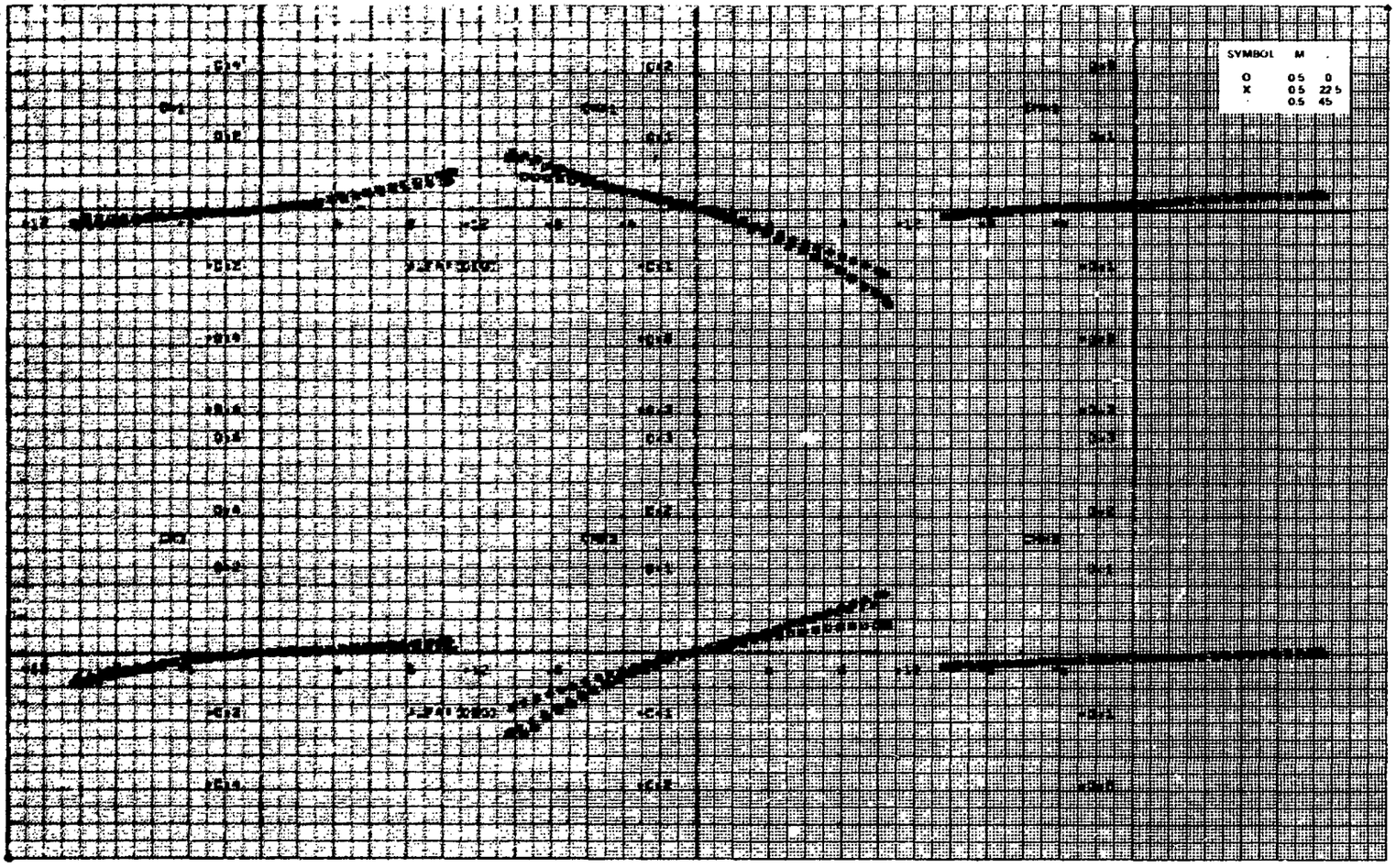


Figure 10a. Continued.

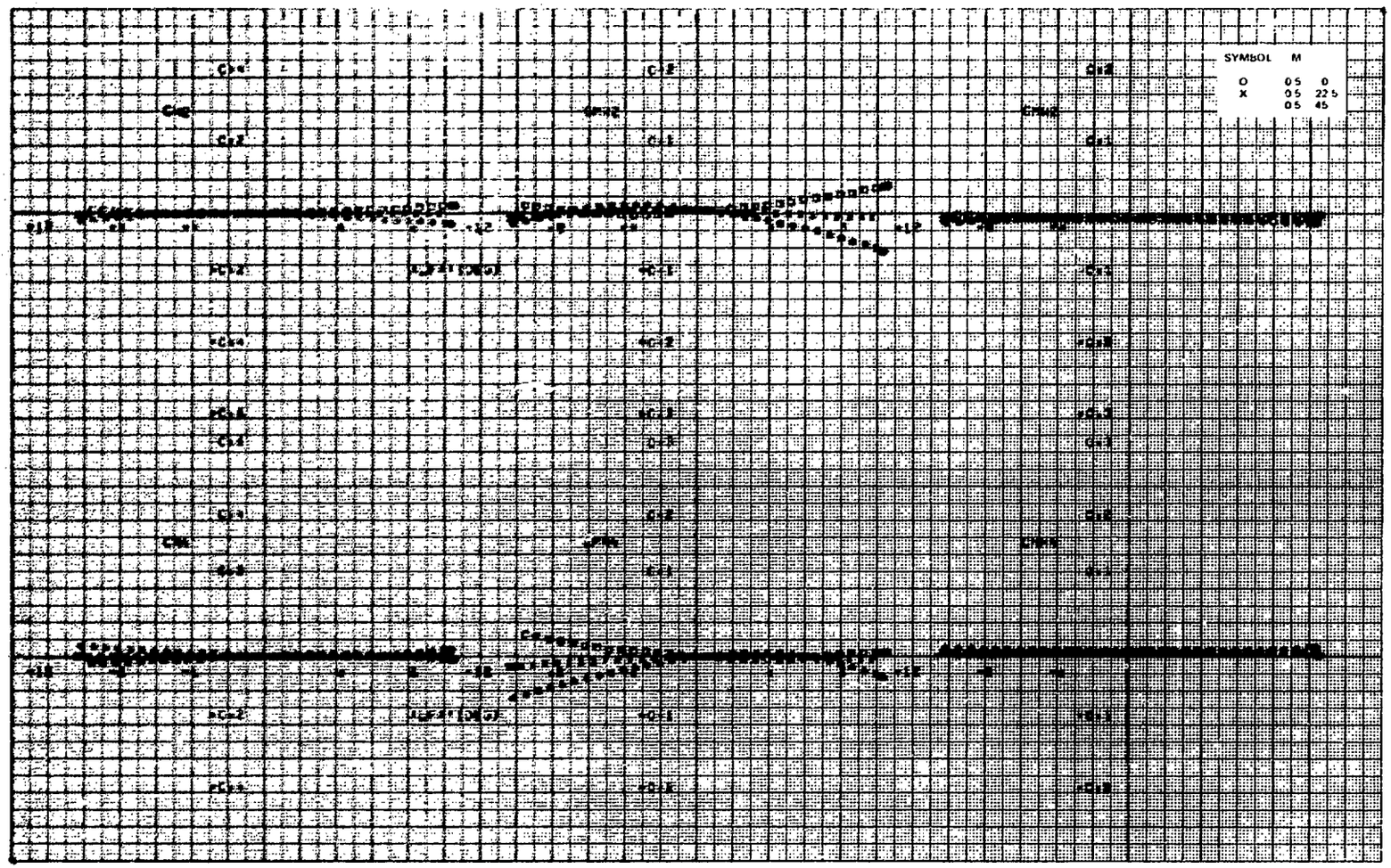


Figure 10a. Concluded.

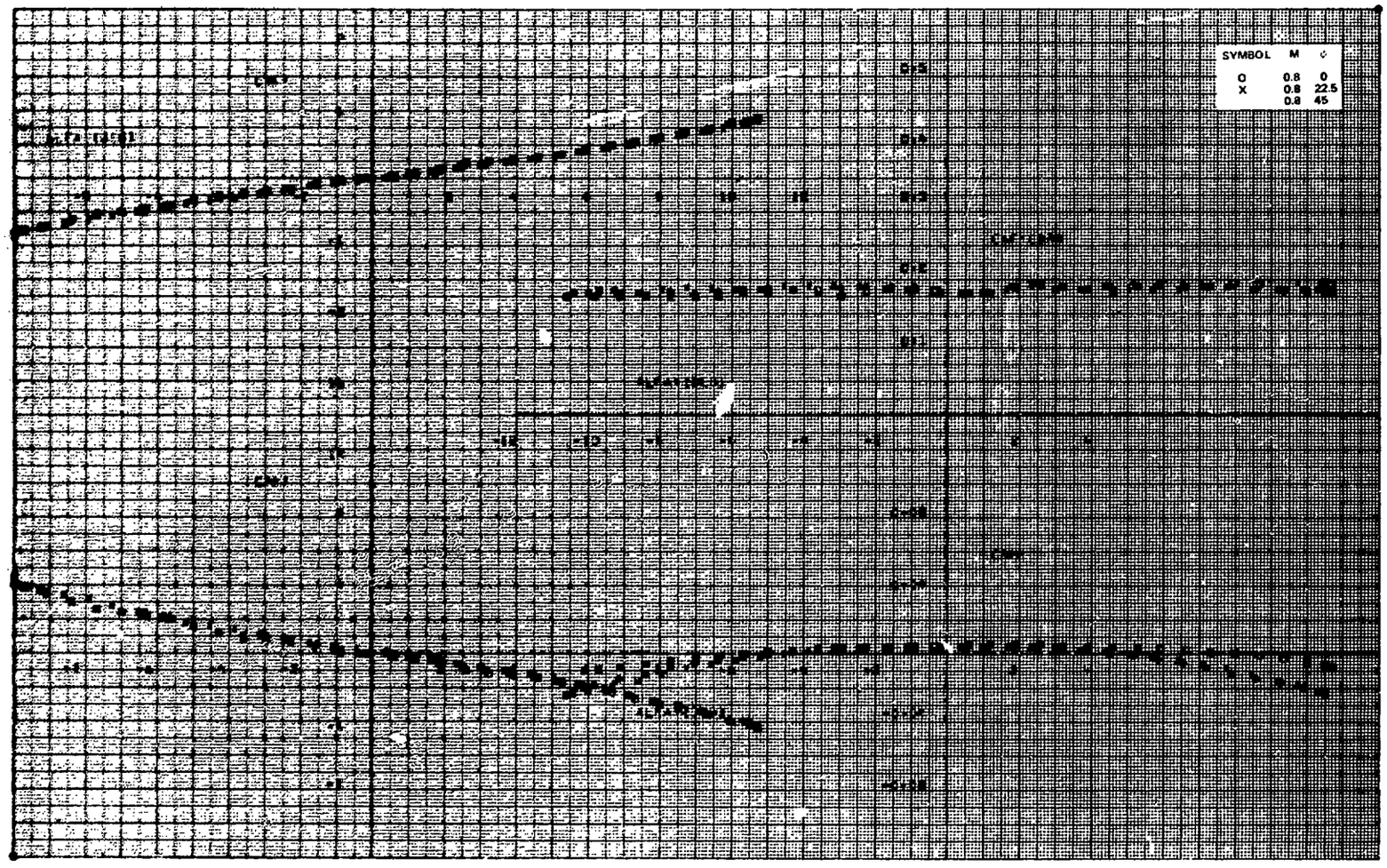


Figure 10b. Aerodynamic stability coefficients, CR/D = 1.75, ϕ = 0 deg, θ = 112.5 deg, M_∞ = 0.8.

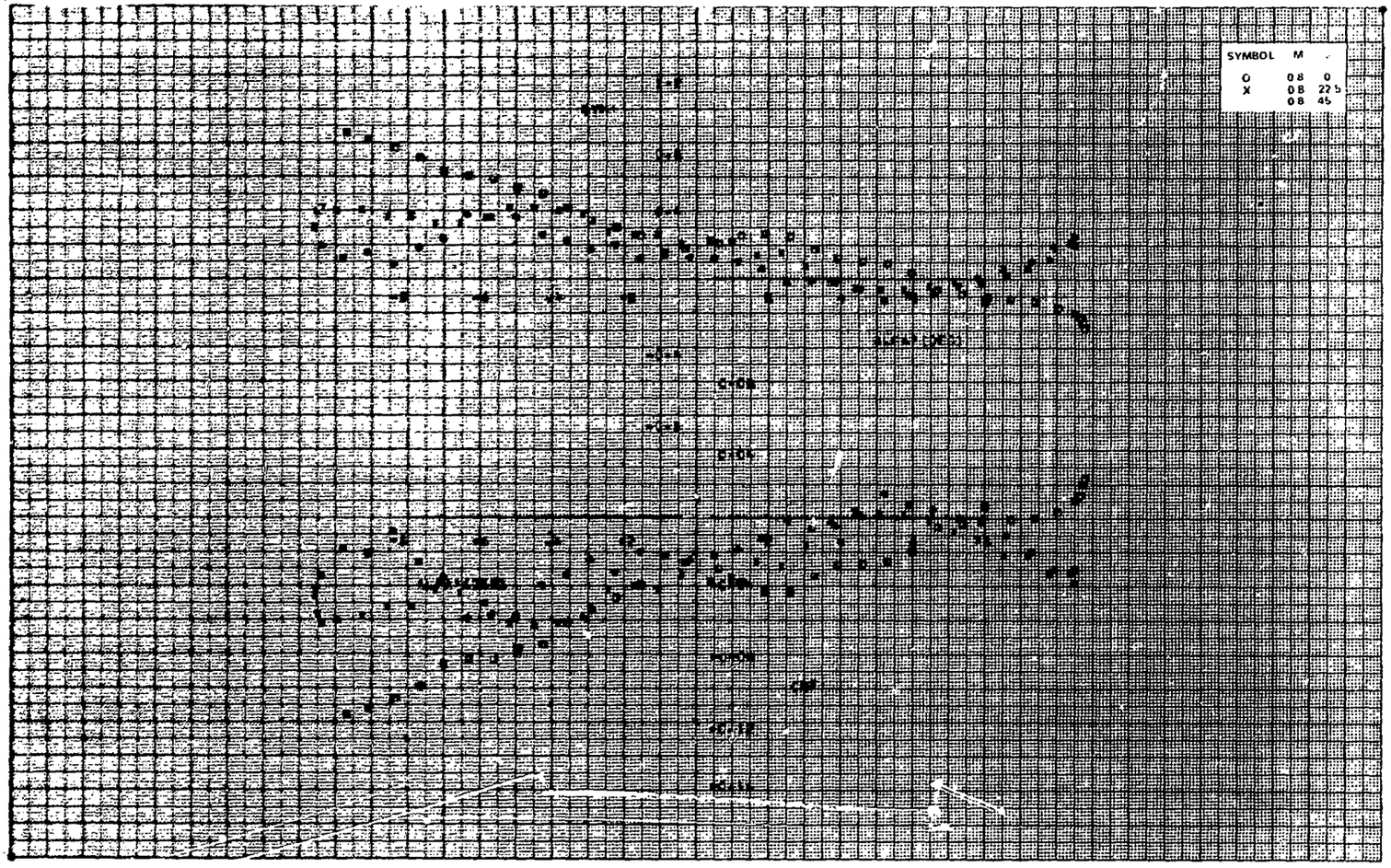


Figure 10b Continued.

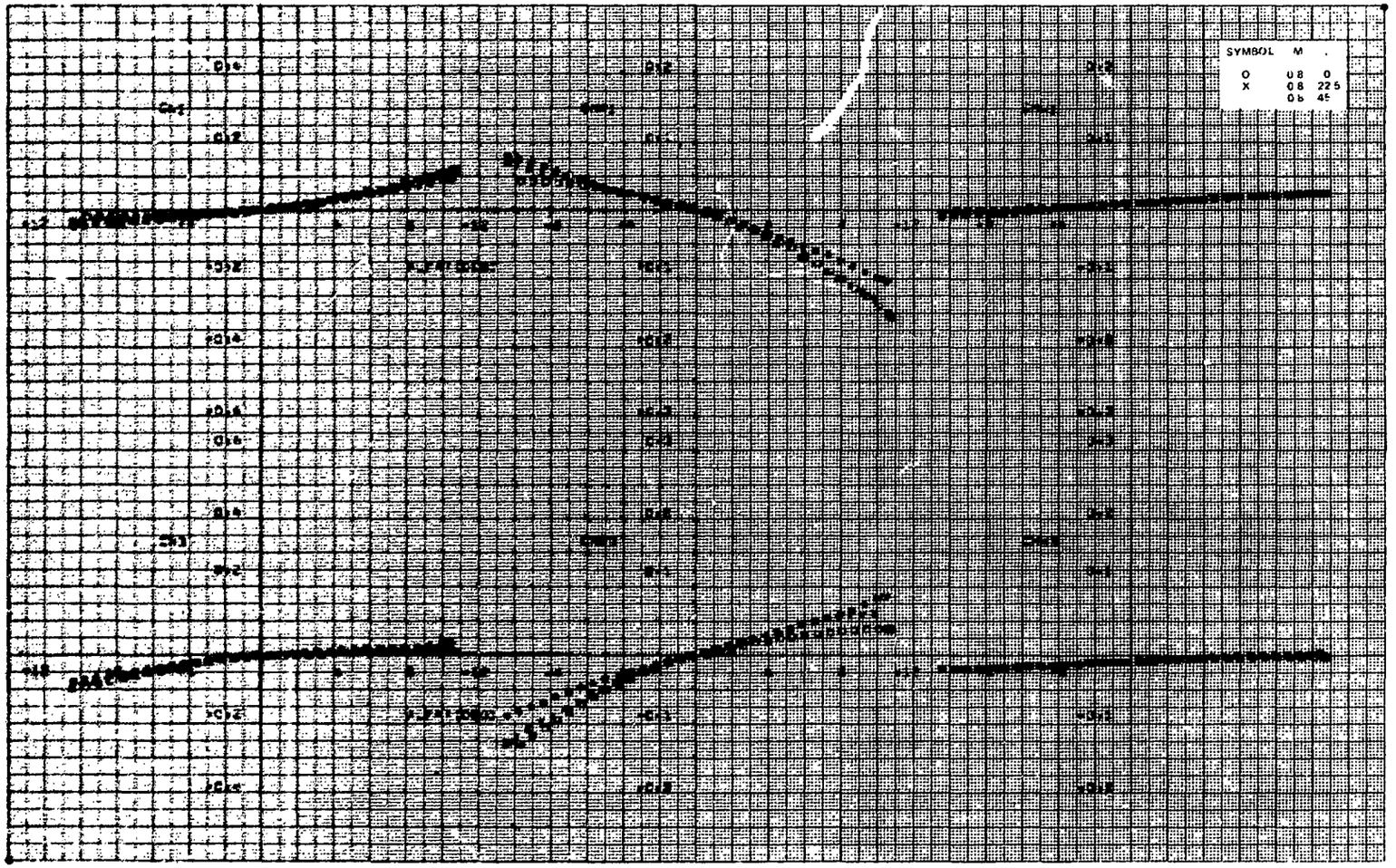


Figure 10b. Continued.

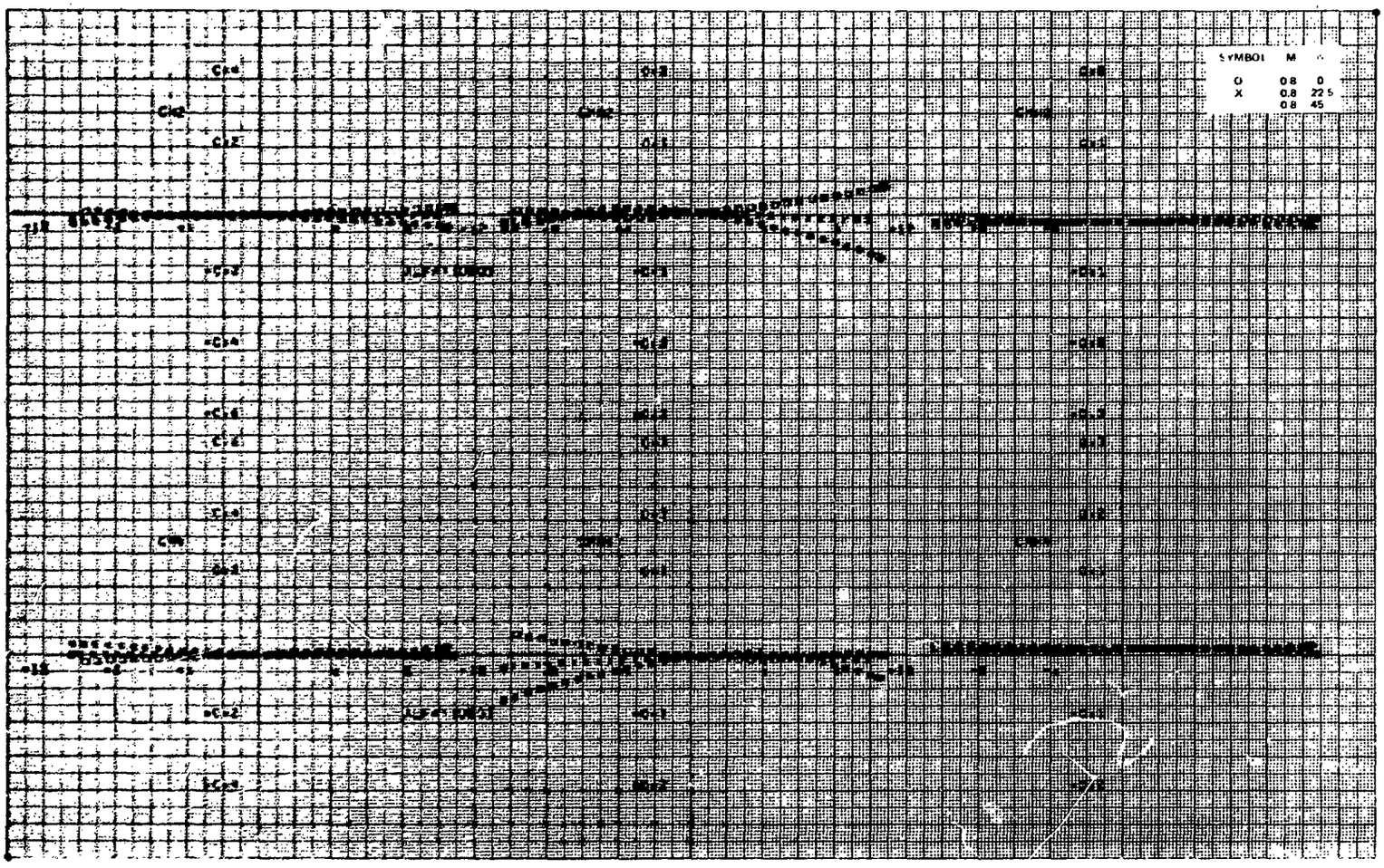


Figure 10b. Concluded.

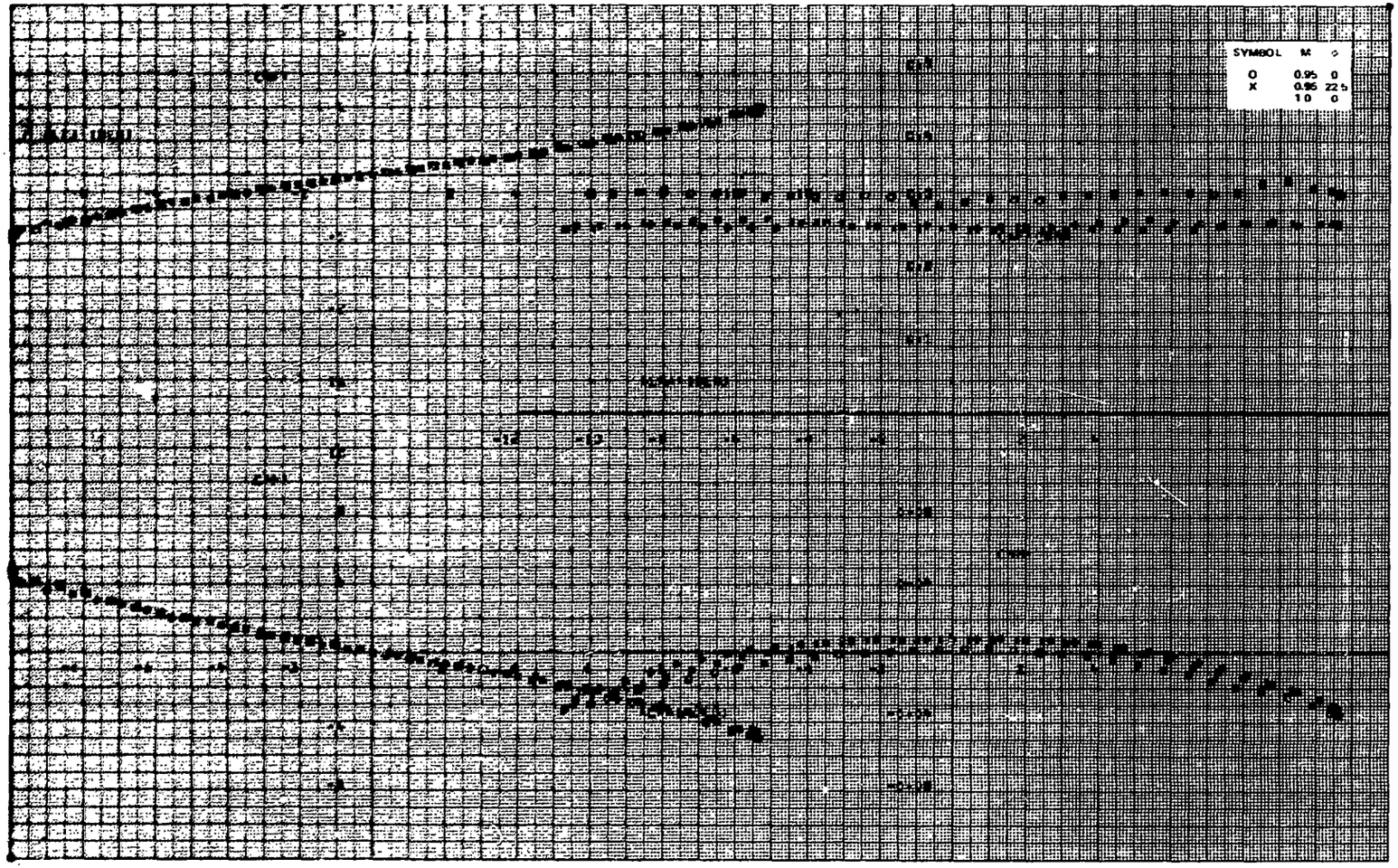


Figure 10c. Aerodynamic stability coefficients, CR/D = 1.75, Λ = 0 deg, θ = 112.5 deg, M_∞ = 0.95, 1.0.

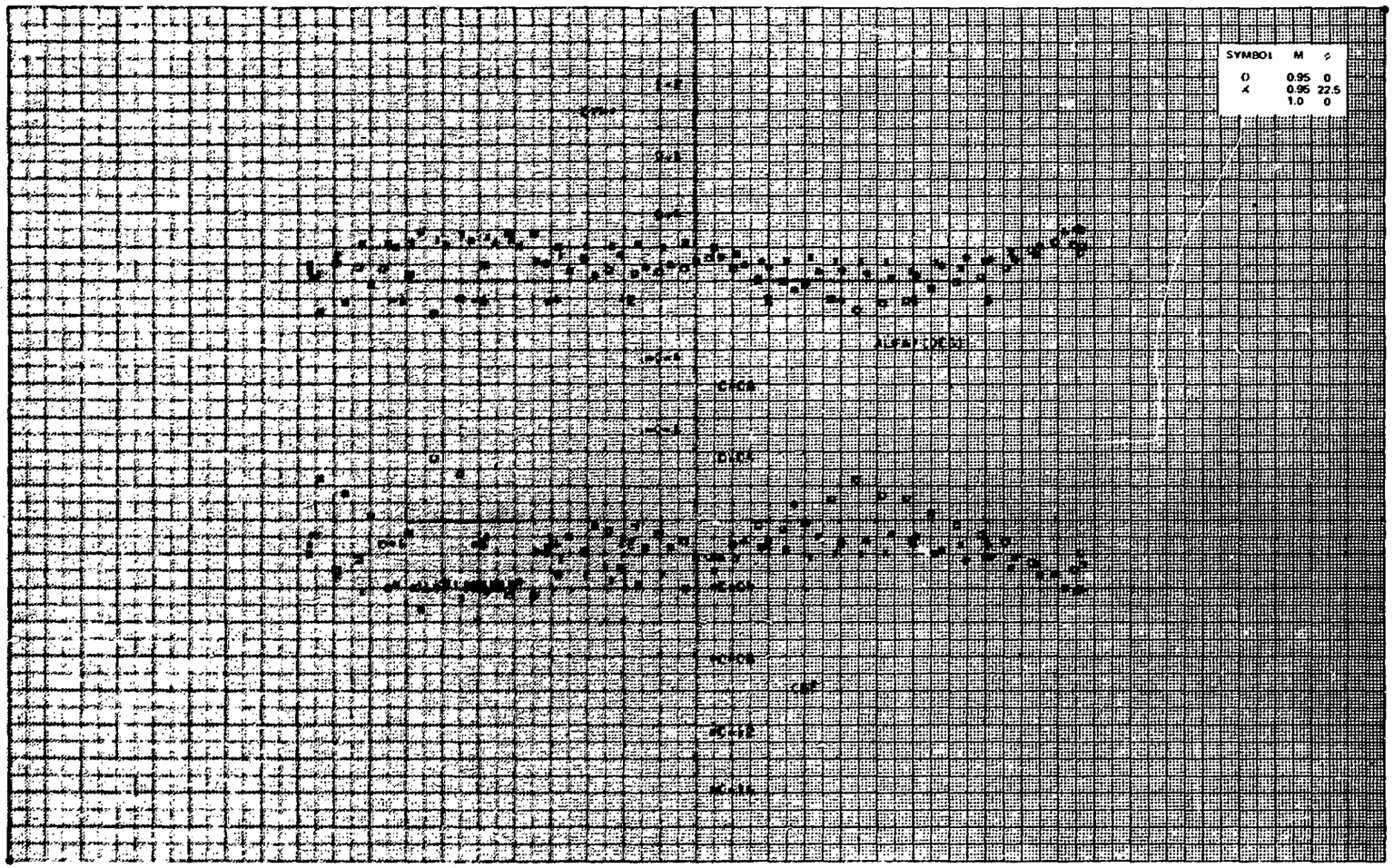


Figure 10c. Continued.

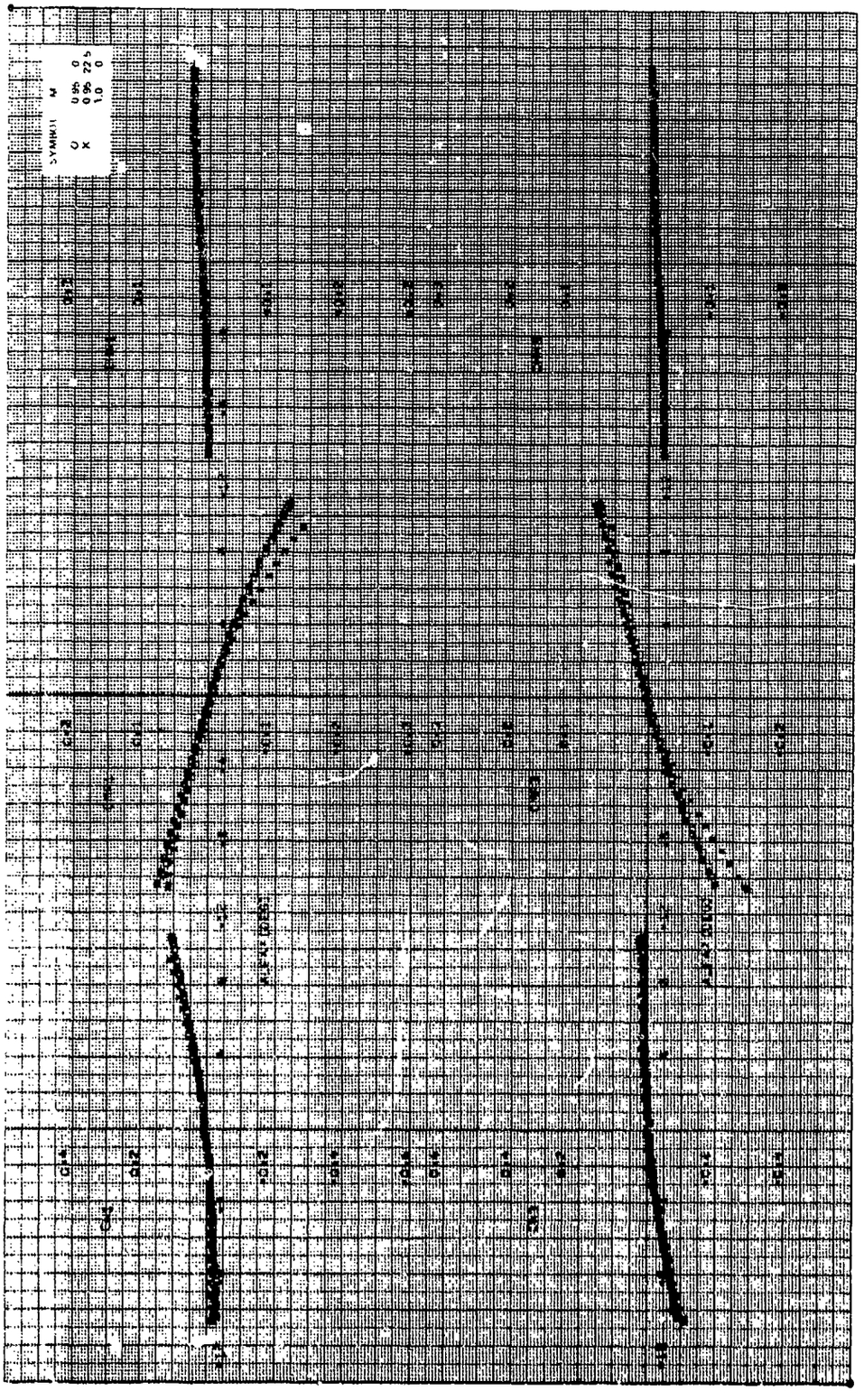


Figure 10c. Continued.

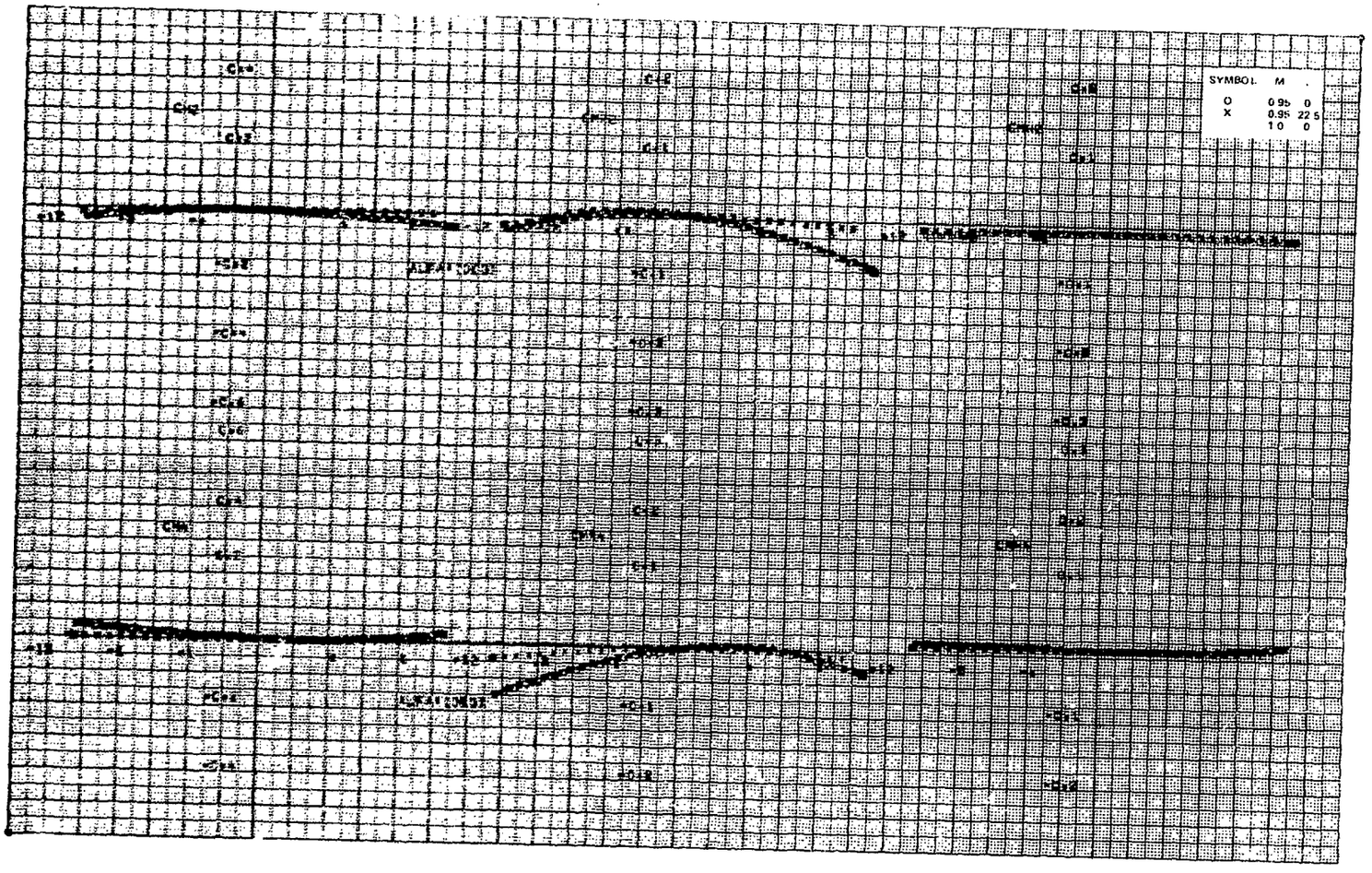


Figure 10c. Concluded.

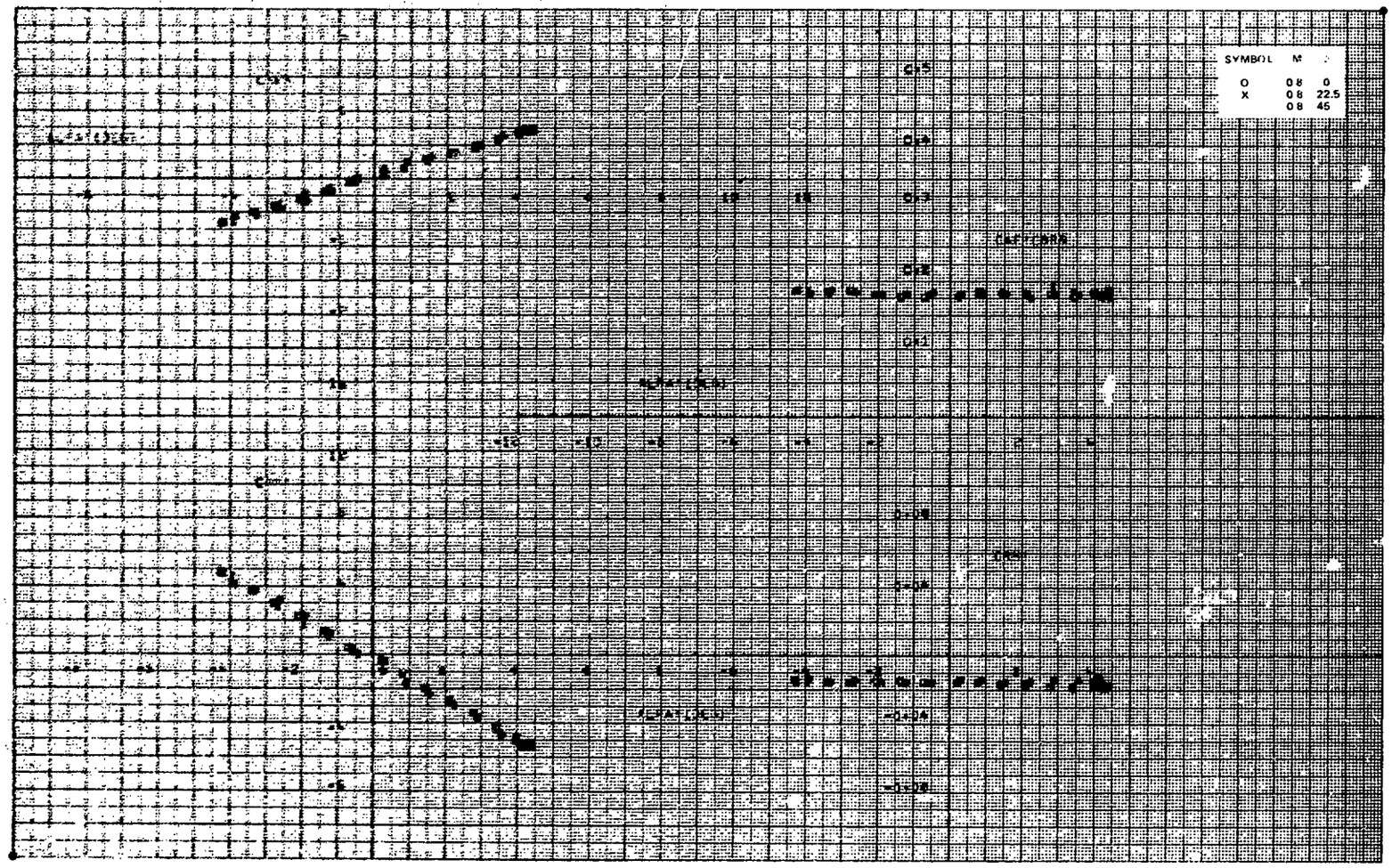


Figure 11a. Aerodynamic stability coefficients, CR/D = 1.0, Λ = 0 deg, M_∞ = 0.8.

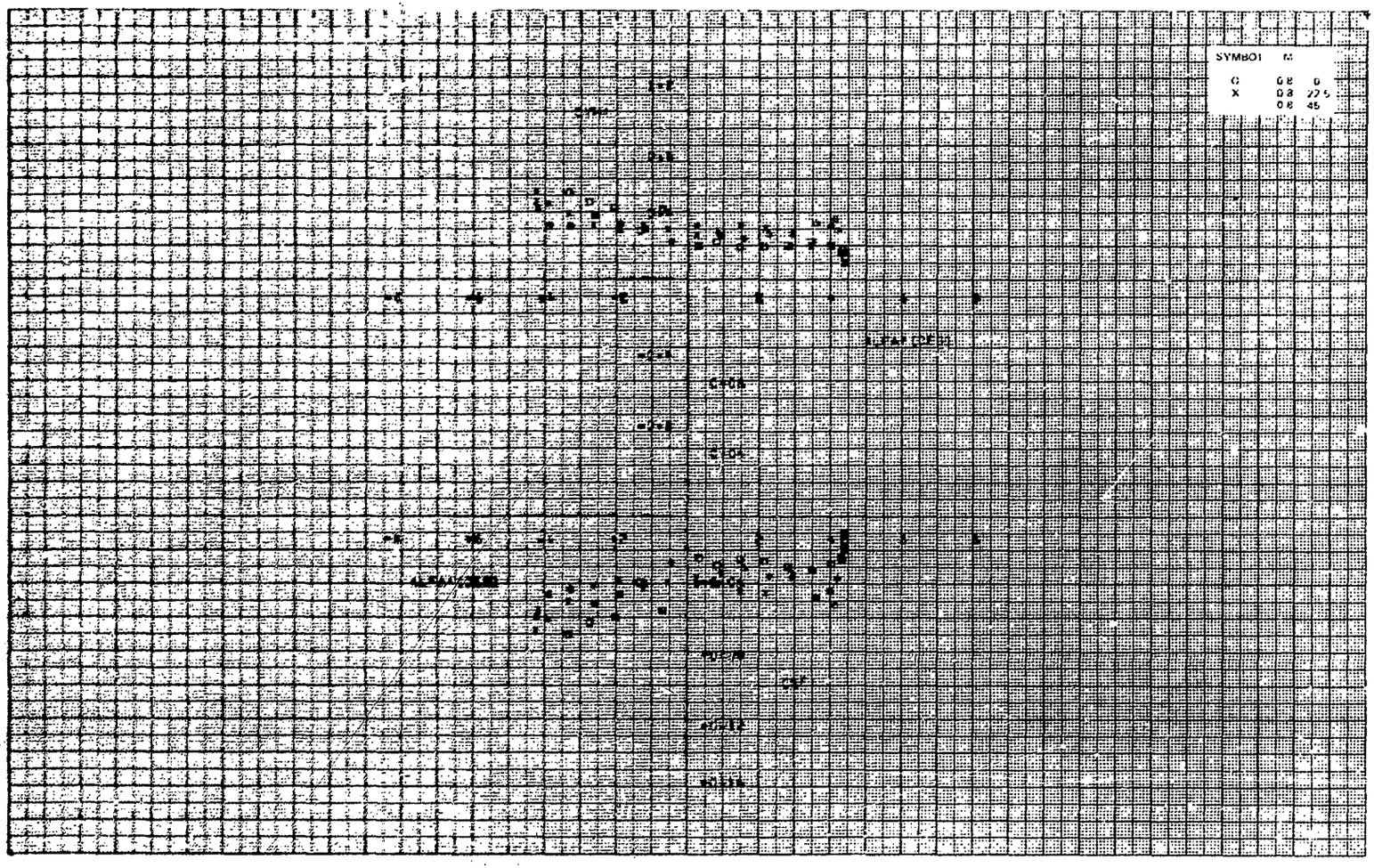


Figure 11a. Continued.

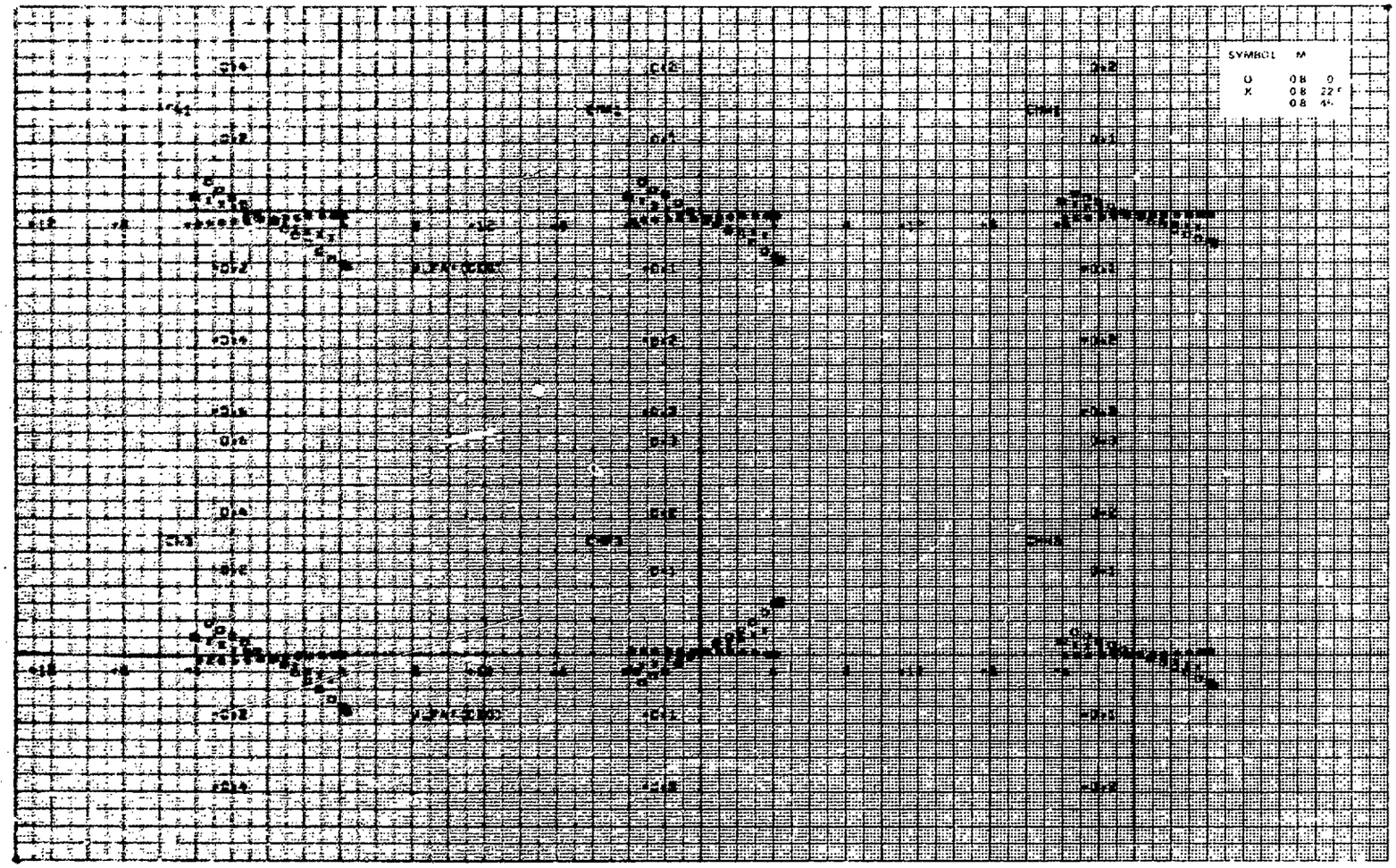


Figure 11a. Continued.

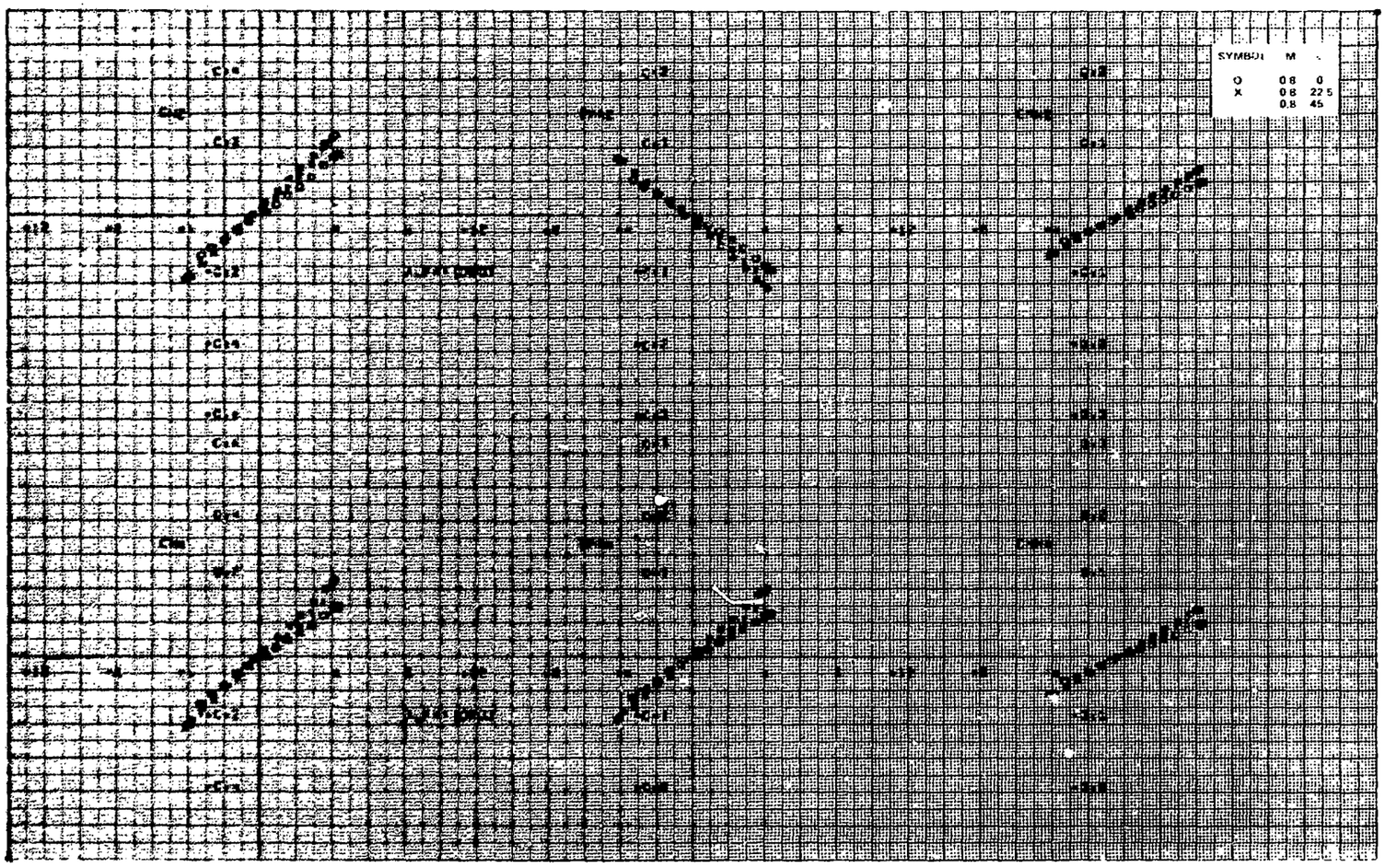


Figure 11a. Concluded.

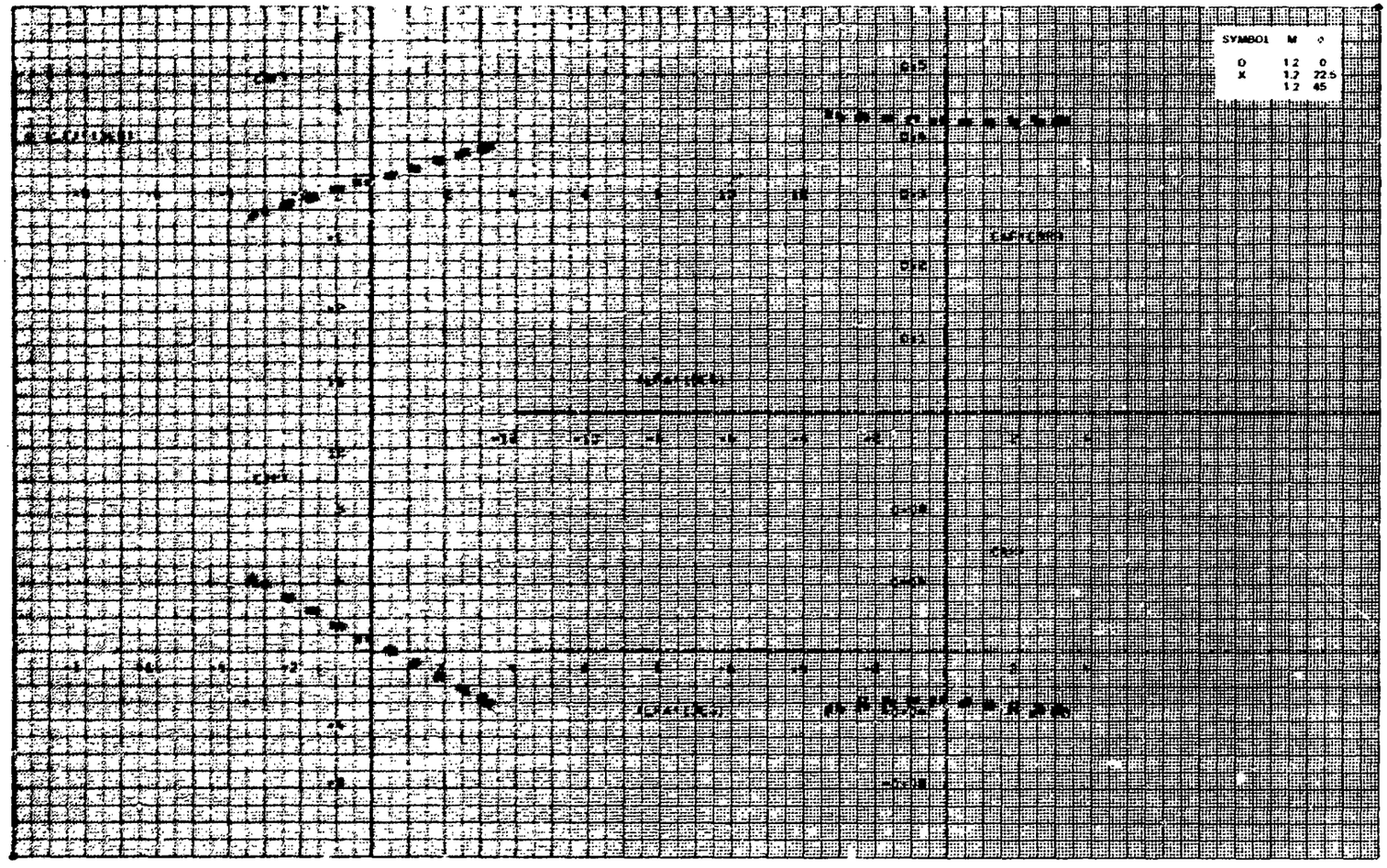


Figure 115. Aerodynamic stability coefficients, CR/D = 1.0, α = 0 deg, M_∞ = 1.2.

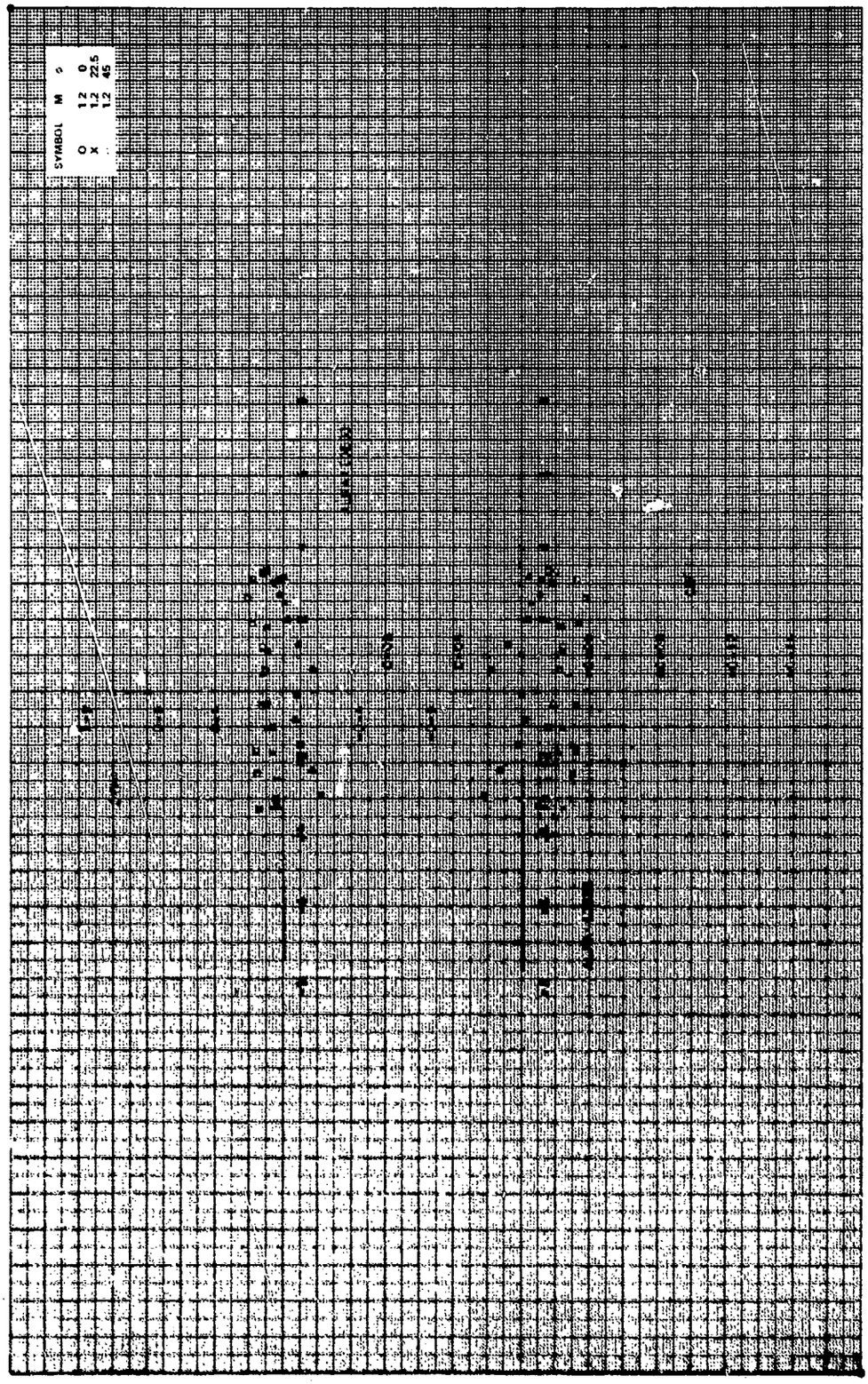


Figure 11b. Continued.

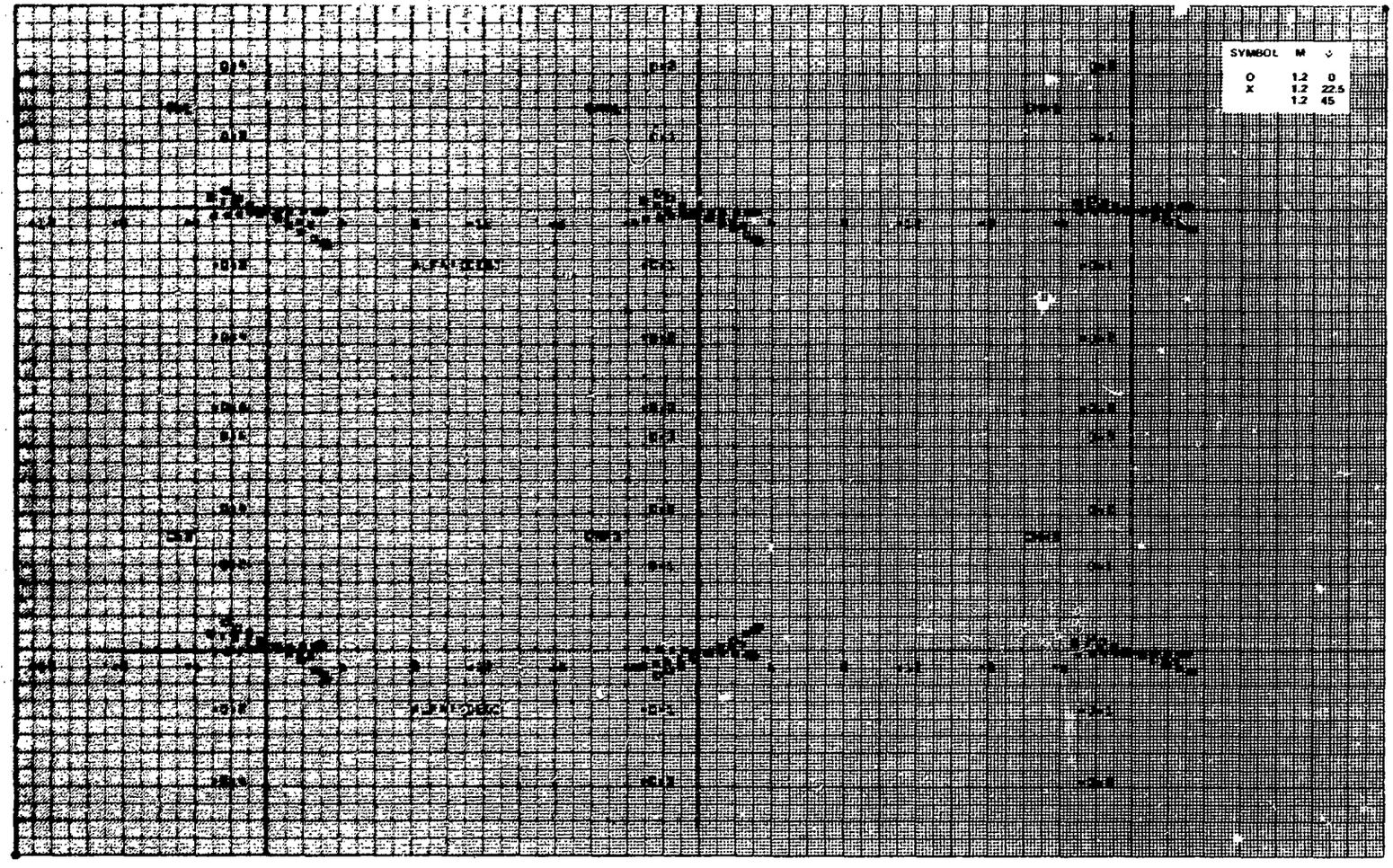


Figure 11b. Continued.

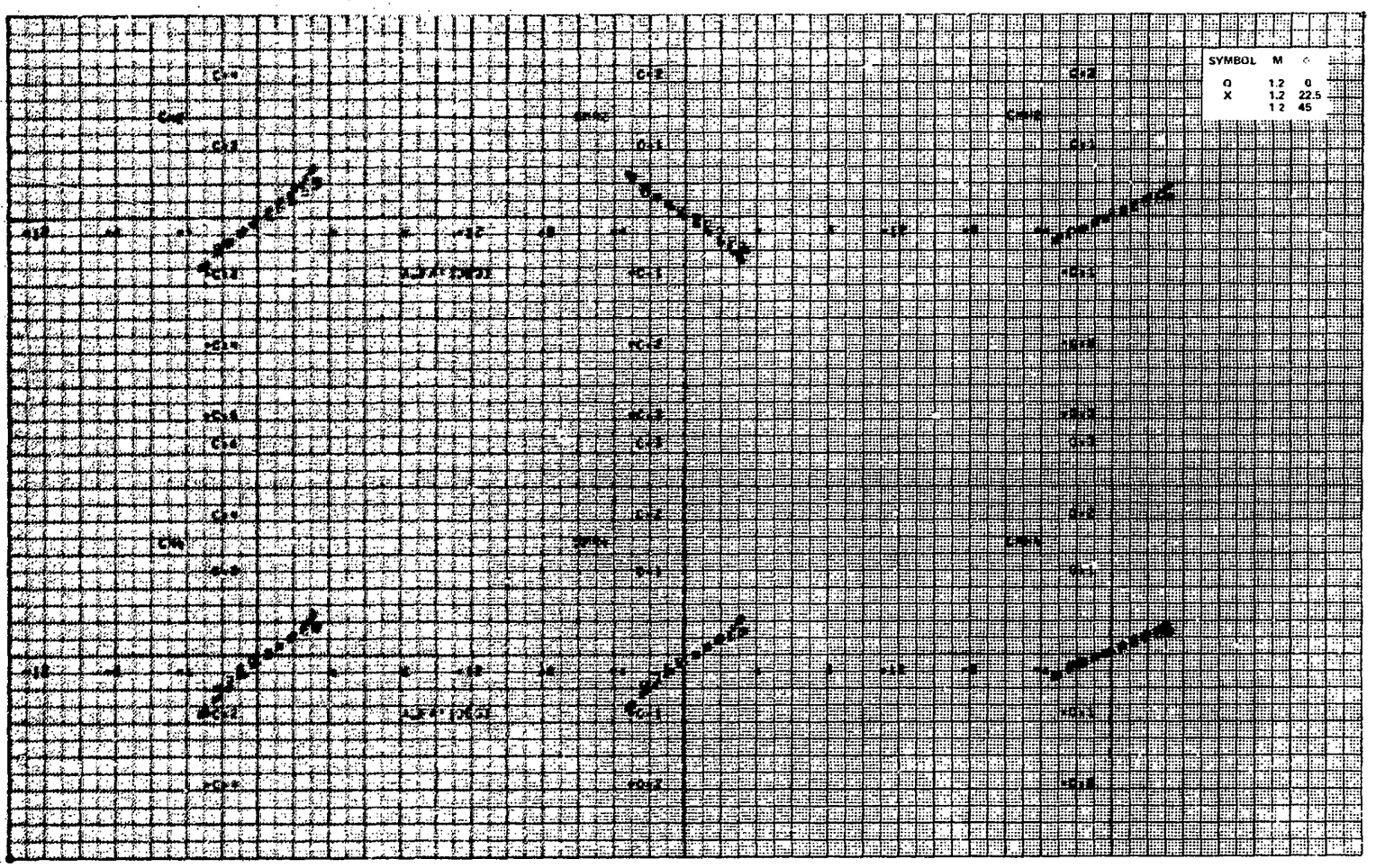


Figure 11b. Concluded.

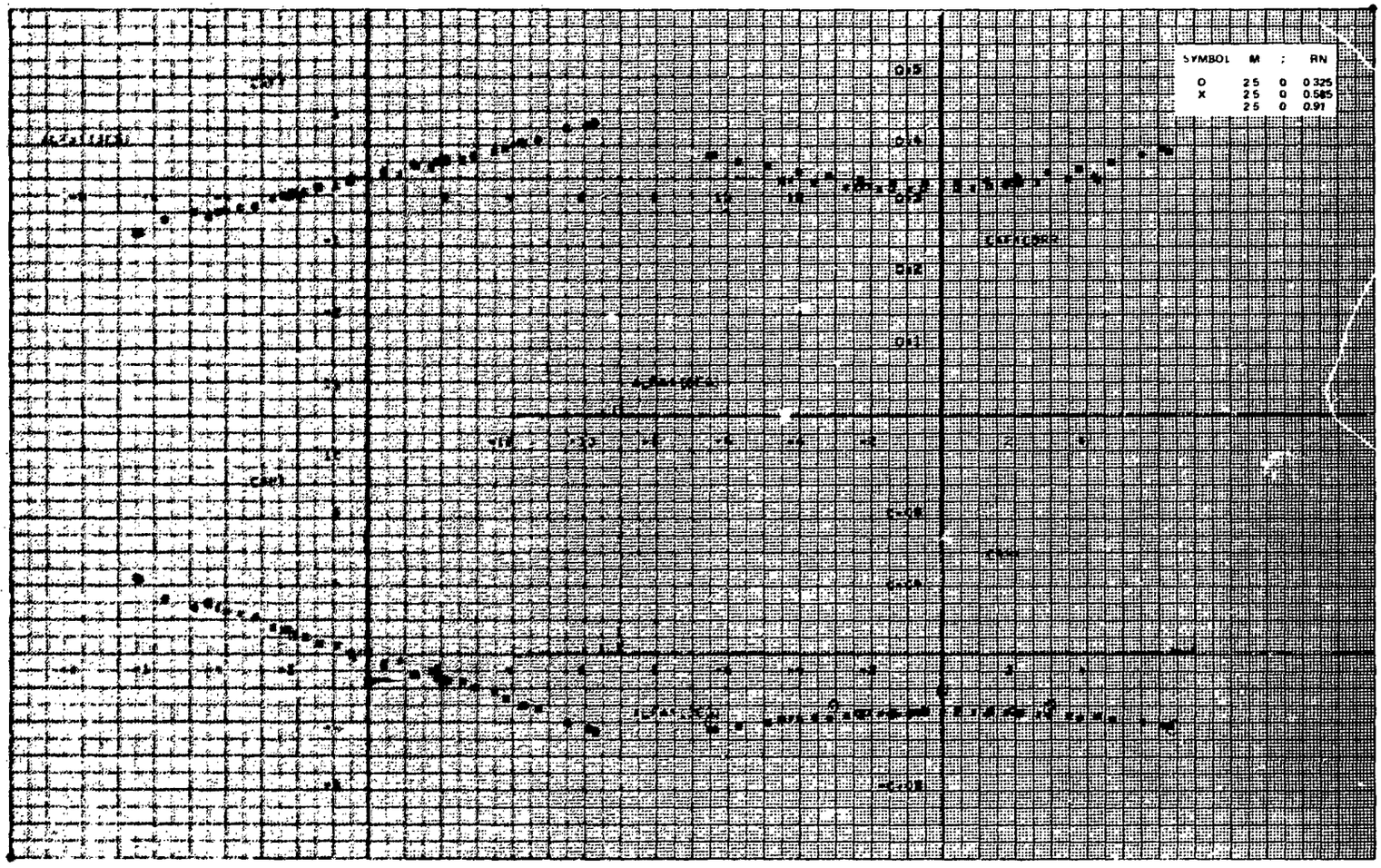


Figure IIc. Aerodynamic stability coefficients, CR/D = 1.0, Λ = 0 deg, M_∞ = 2.5.

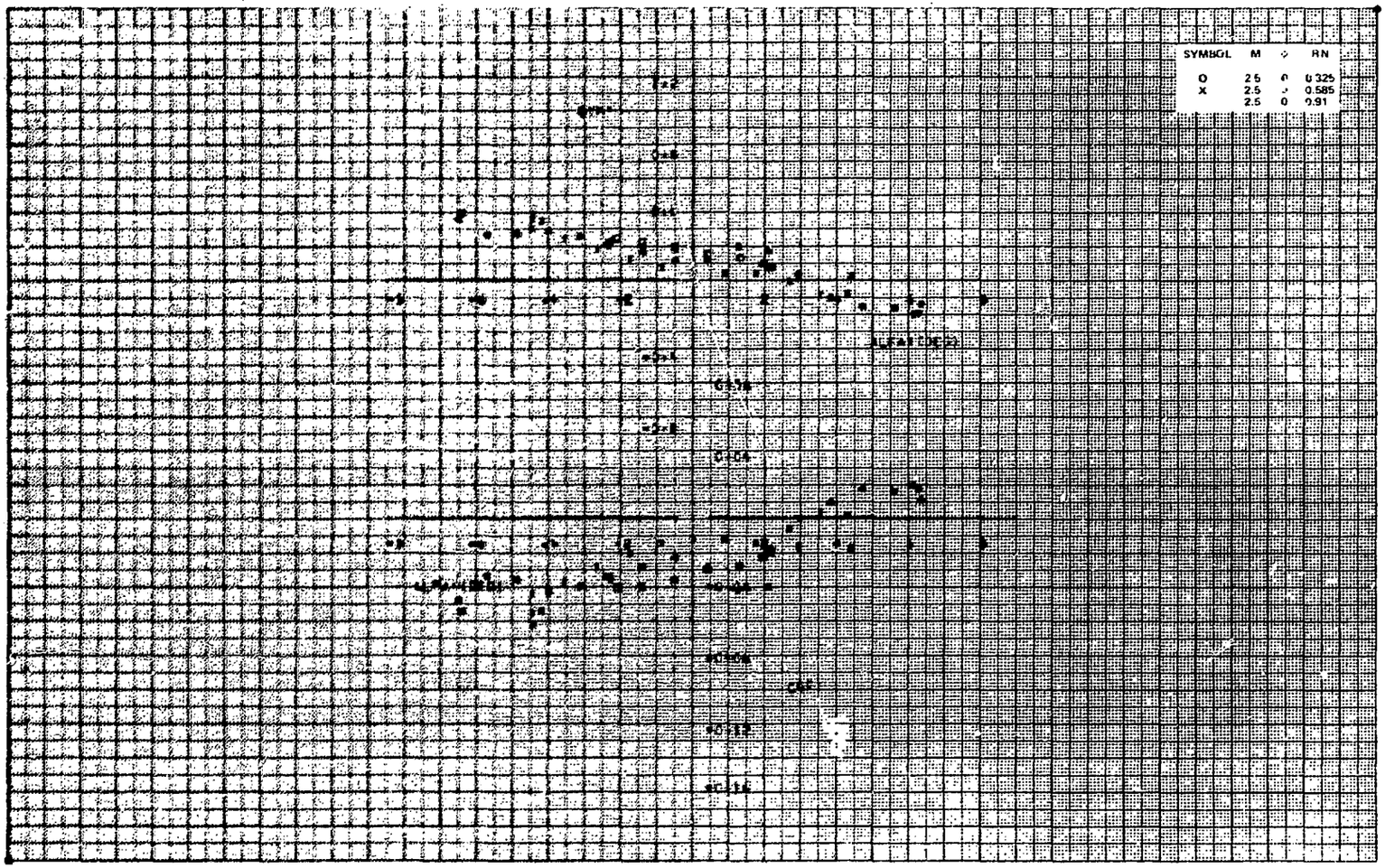


Figure 11c. Continued.

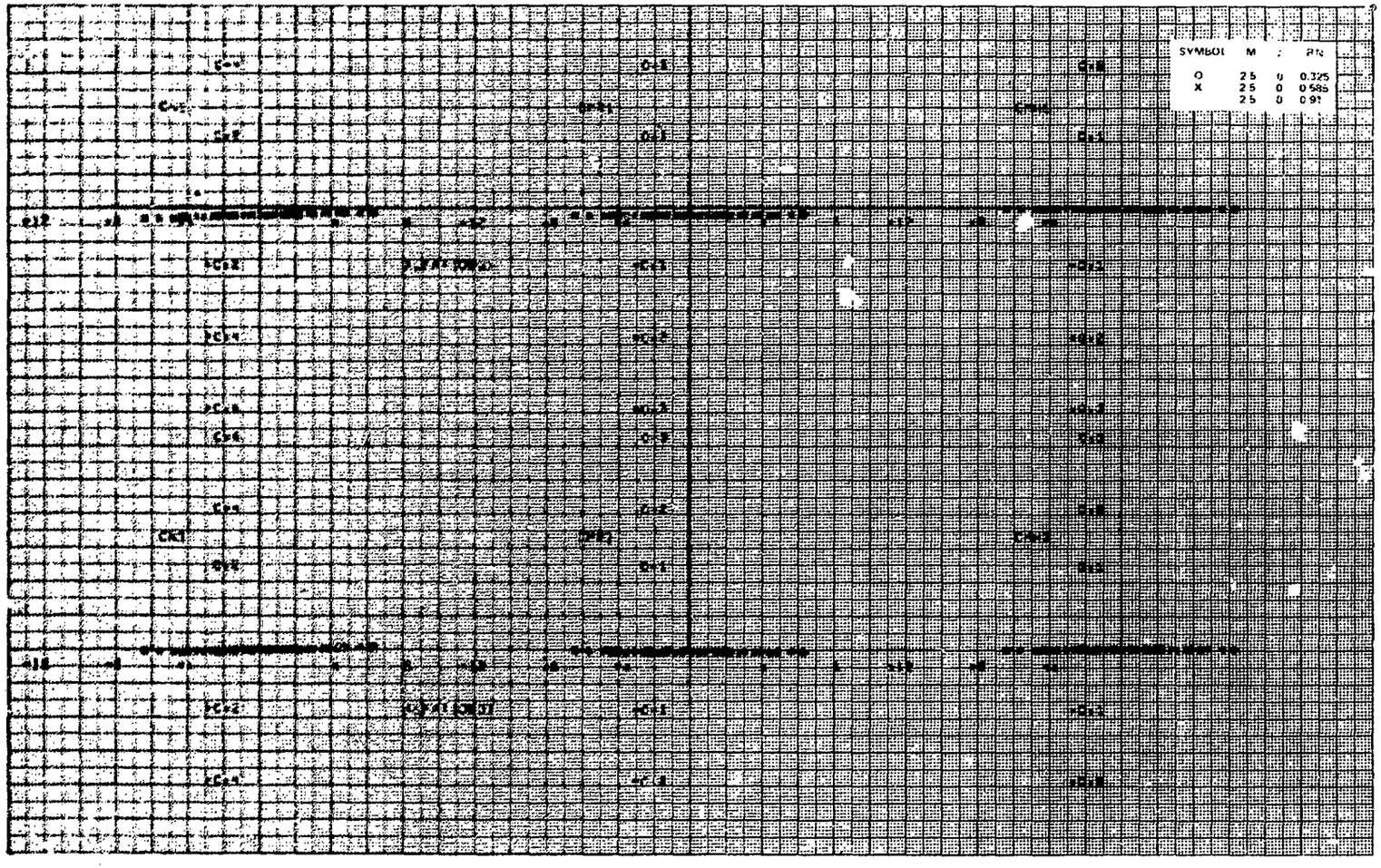


Figure 11c. Continued.

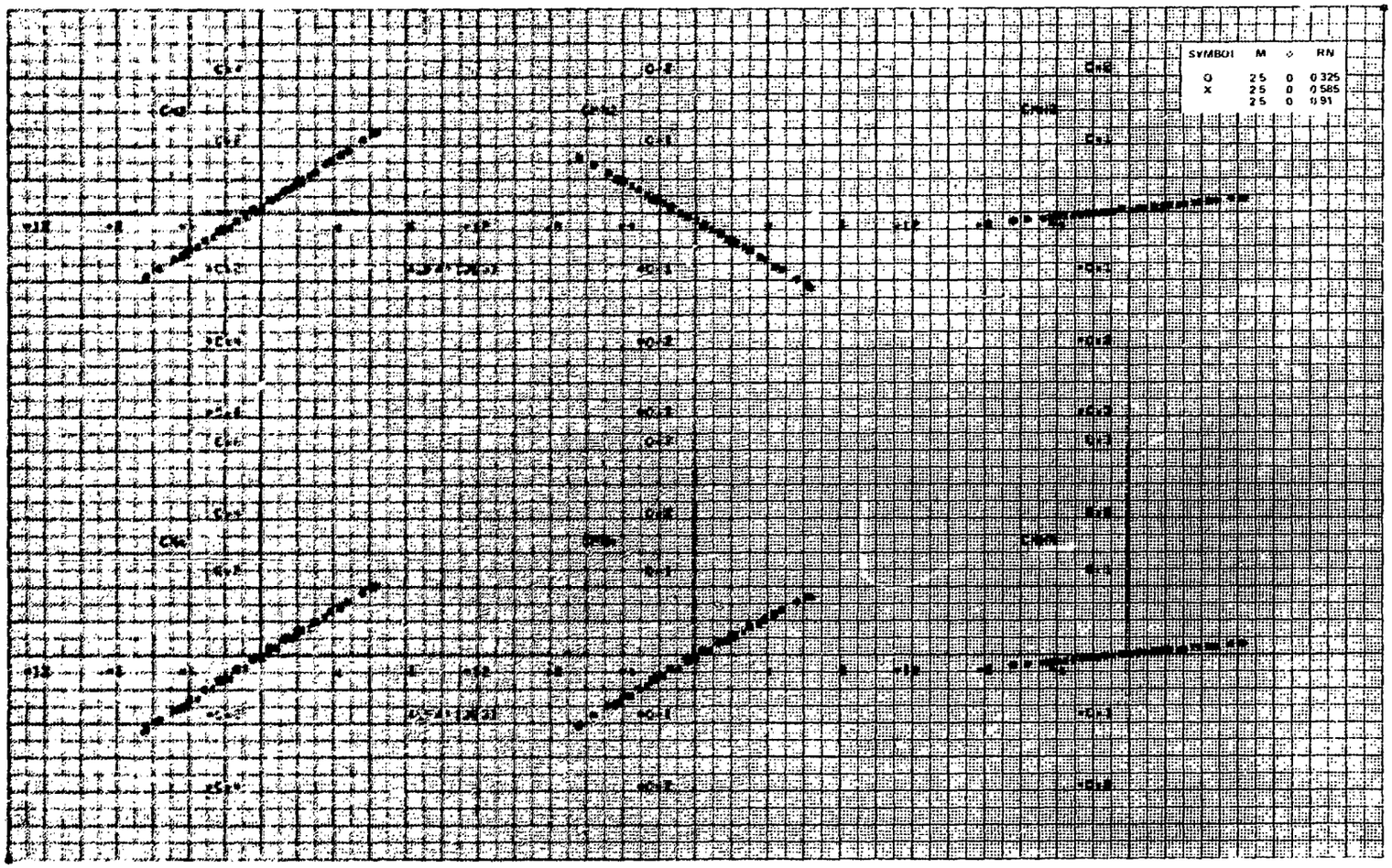


Figure 11c. Concluded.

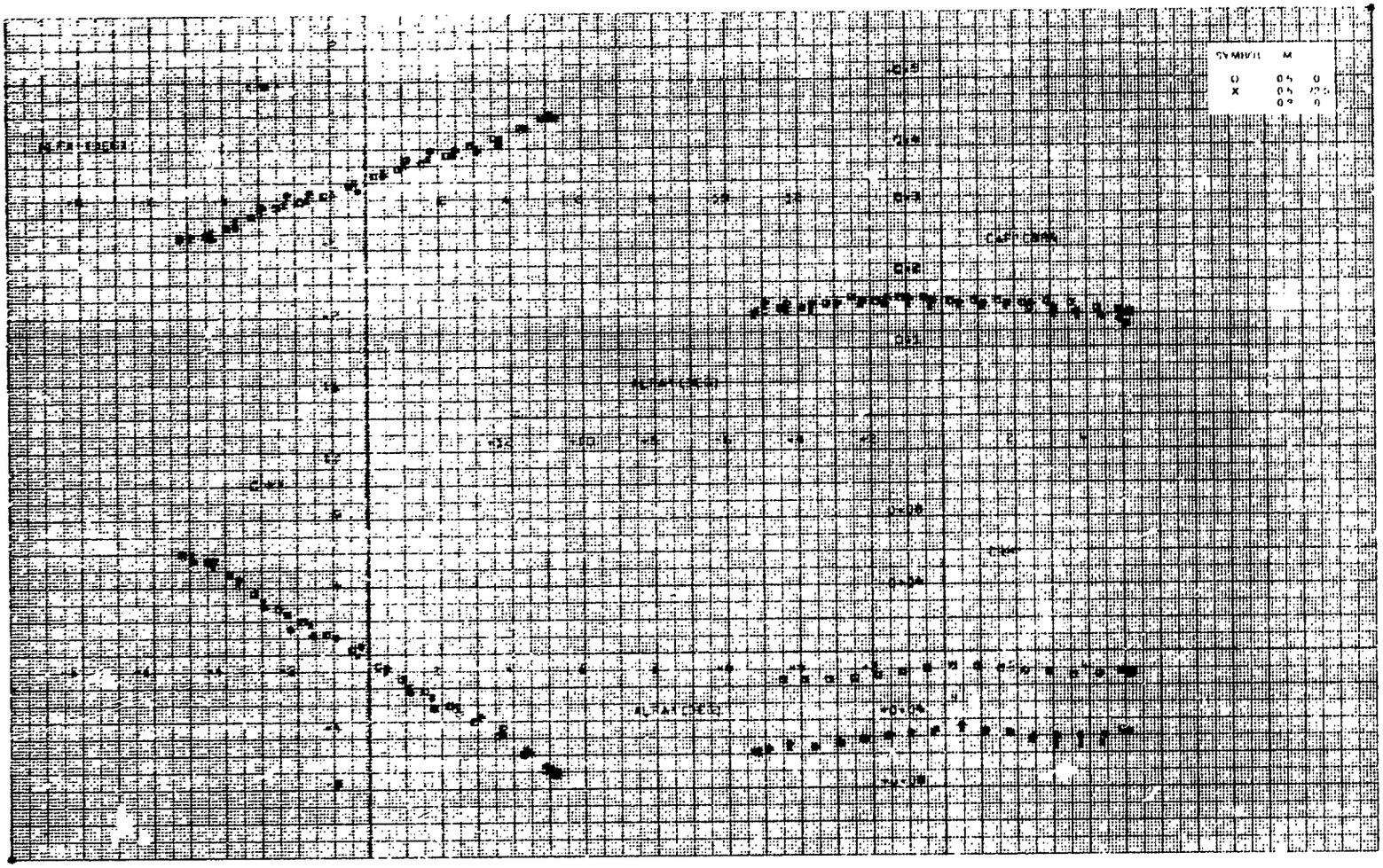


Figure 12a. Aerodynamic stability coefficients, CR/D = 1.75, Λ = 60 deg, M_∞ = 0.5, 0.8.

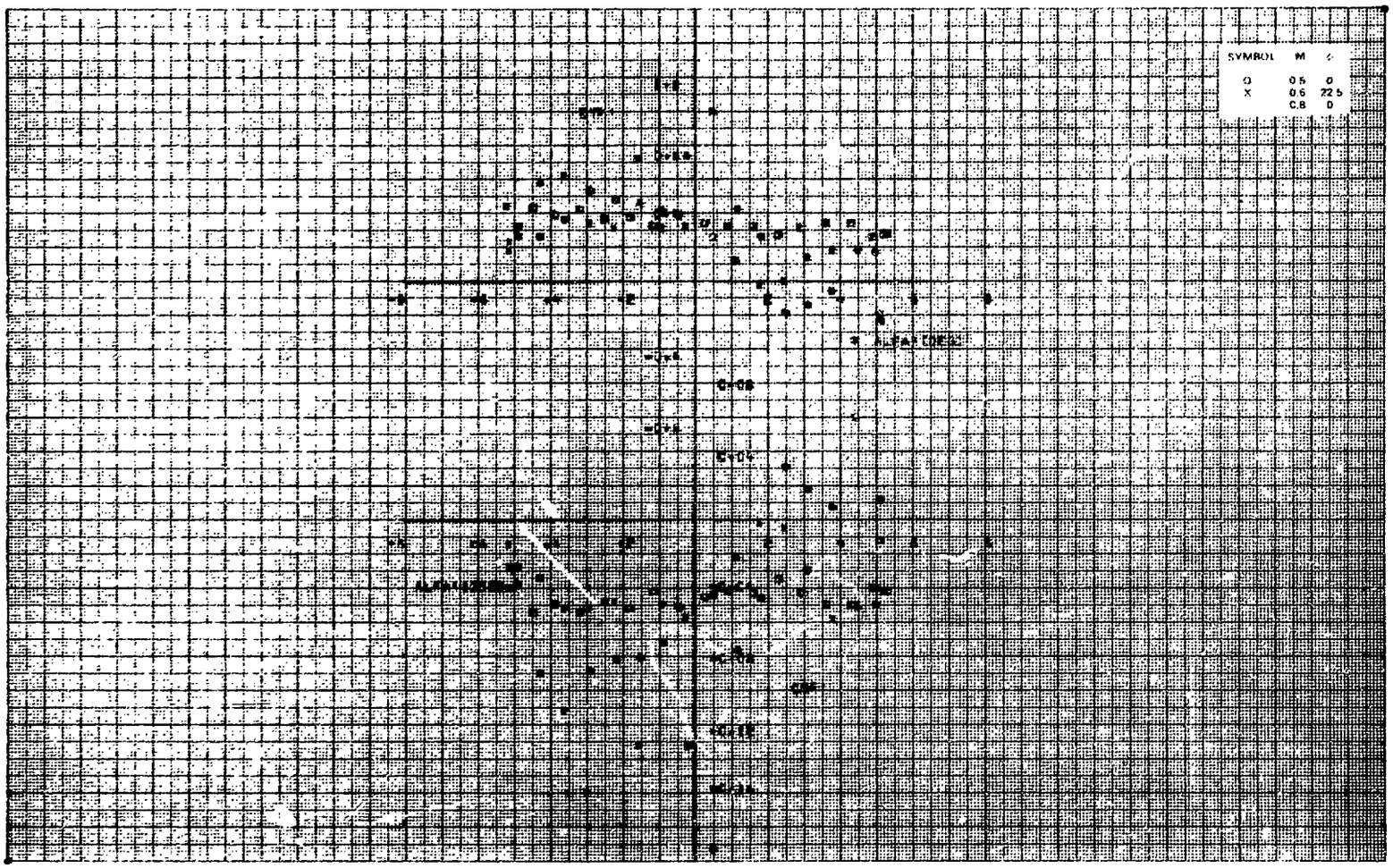


Figure 12a. Continued.

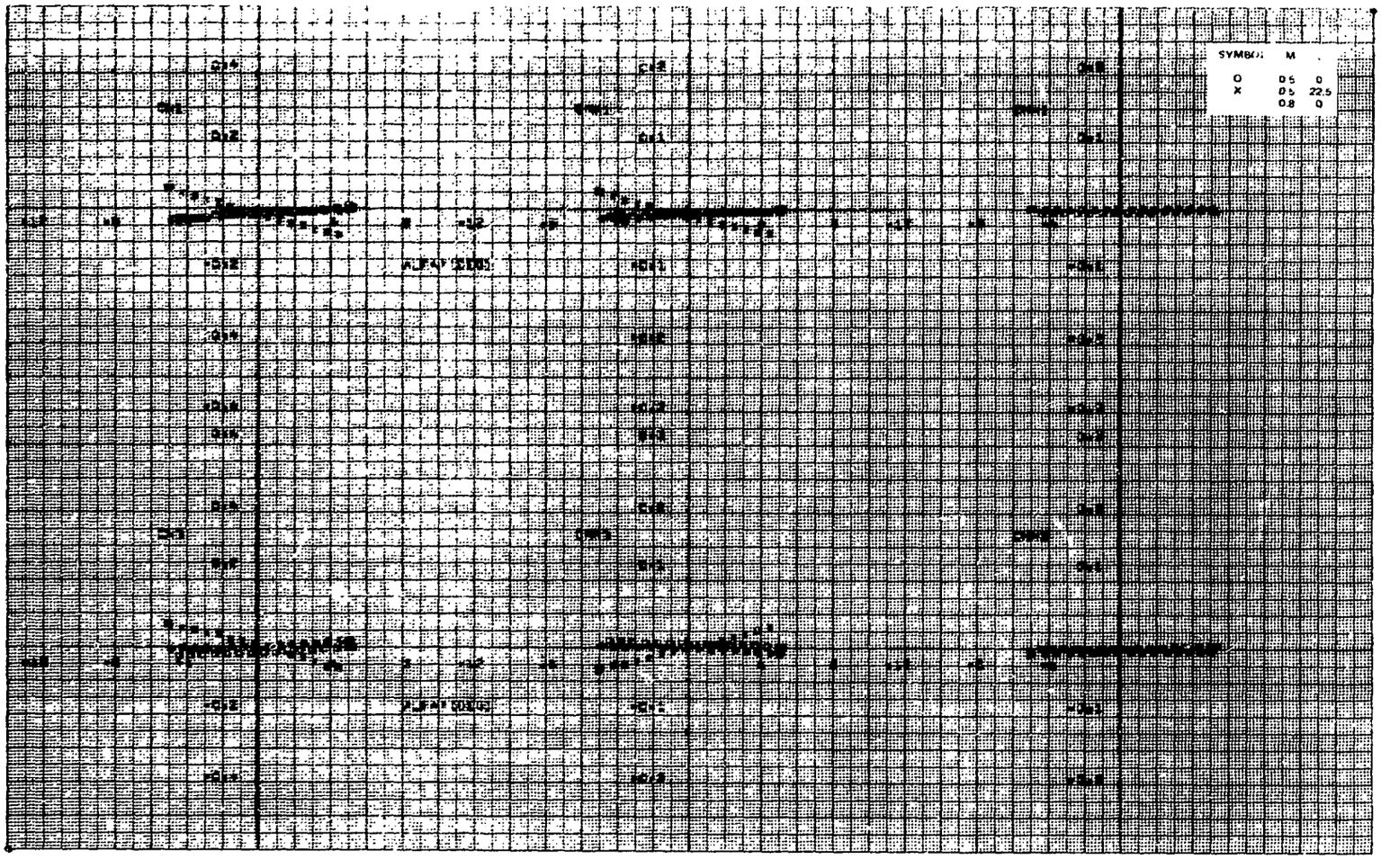


Figure 12a. Continued.

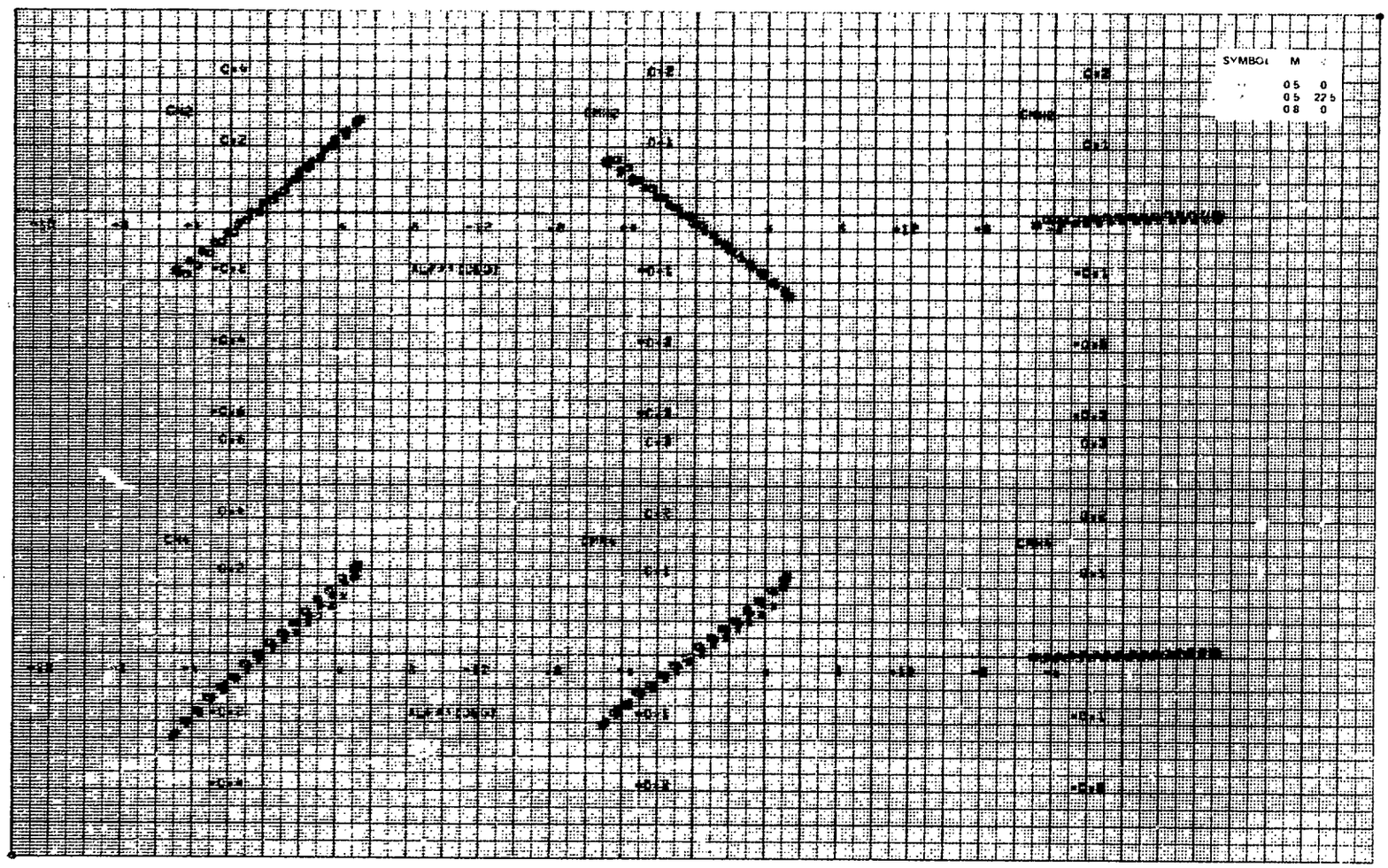


Figure 12a. Concluded.

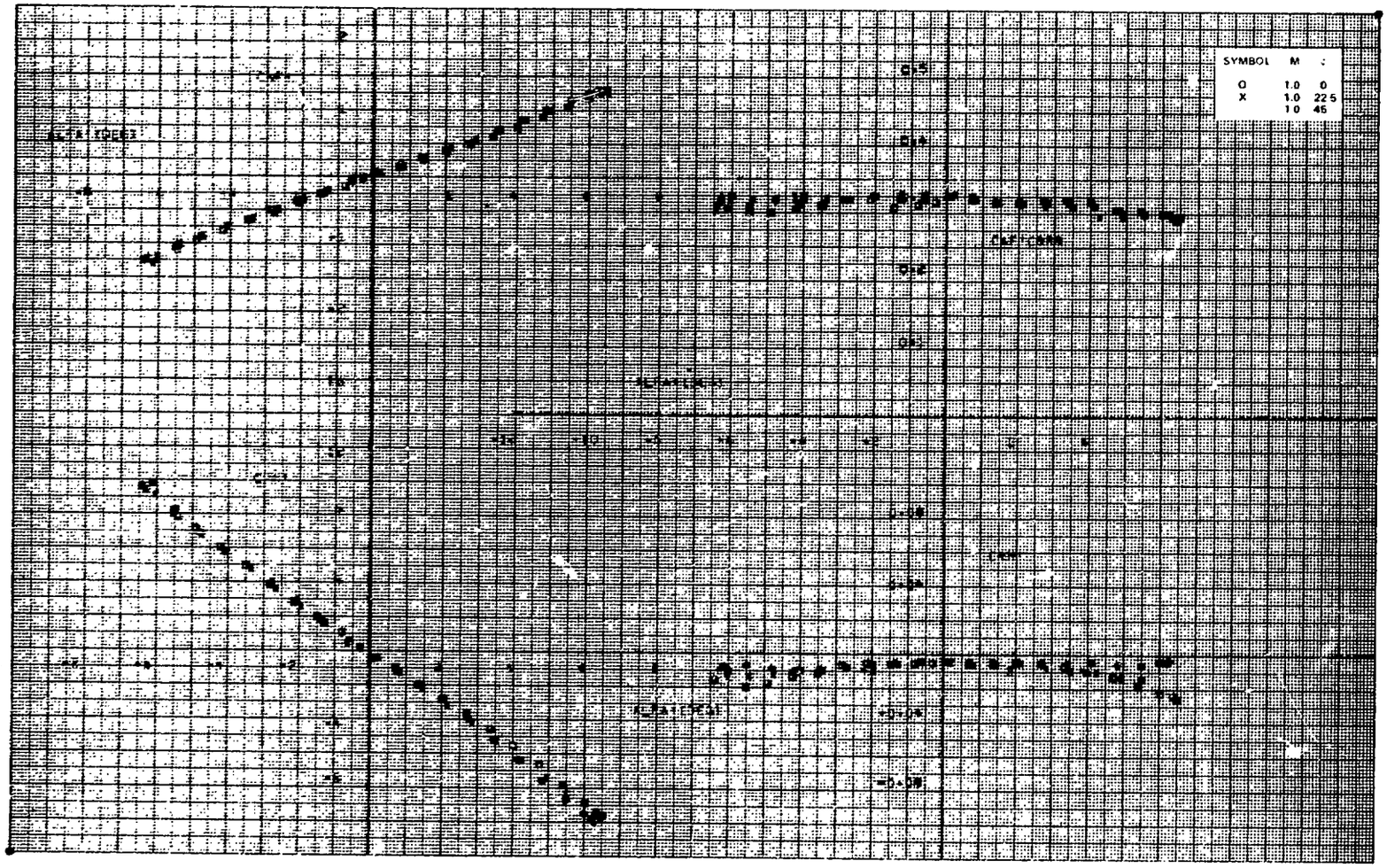


Figure 125. Aerodynamic stability coefficients, CR/D = 1.75, γ = 60 deg, M_∞ = 1.0.

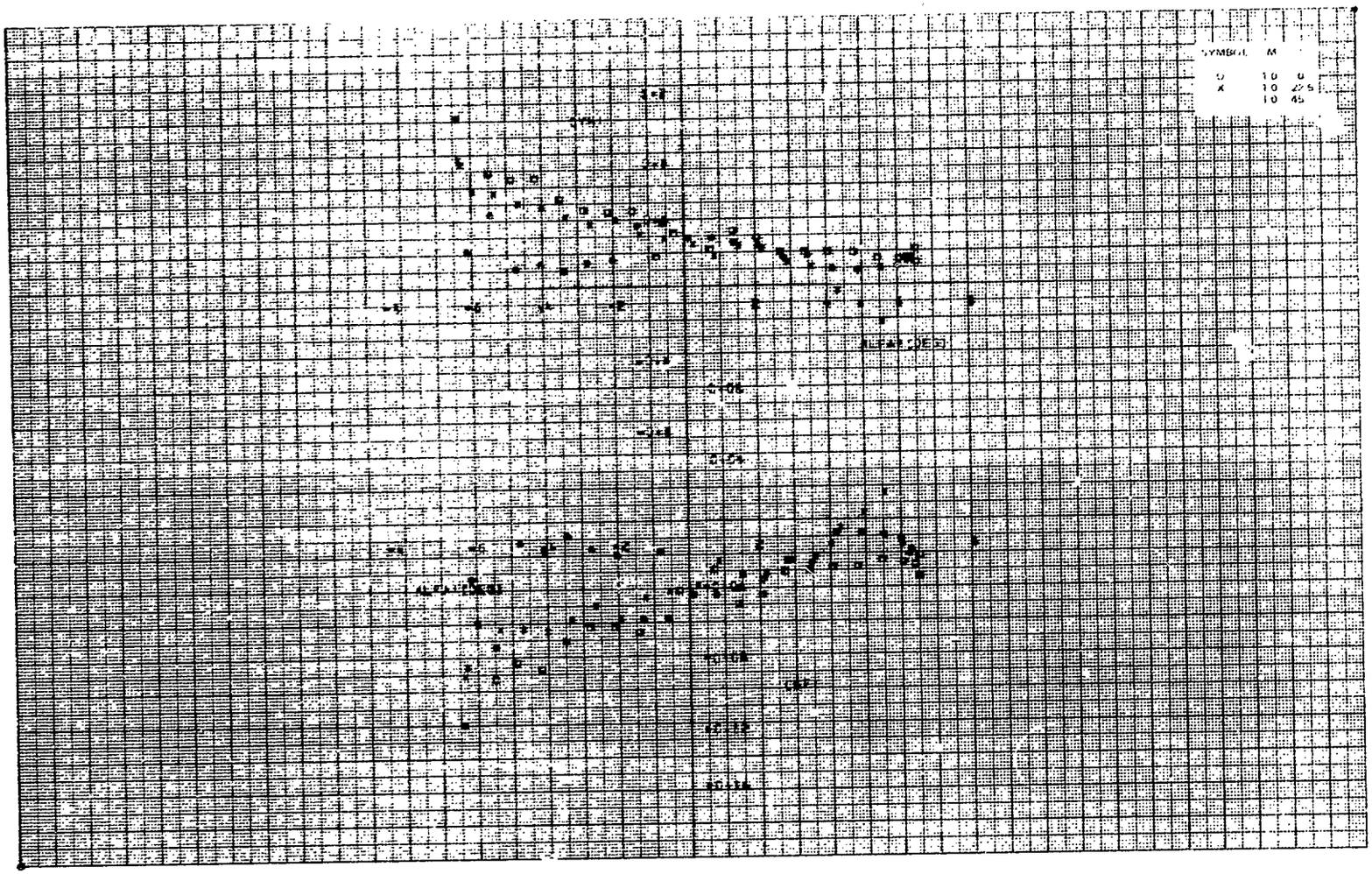


Figure 12b. Continued.

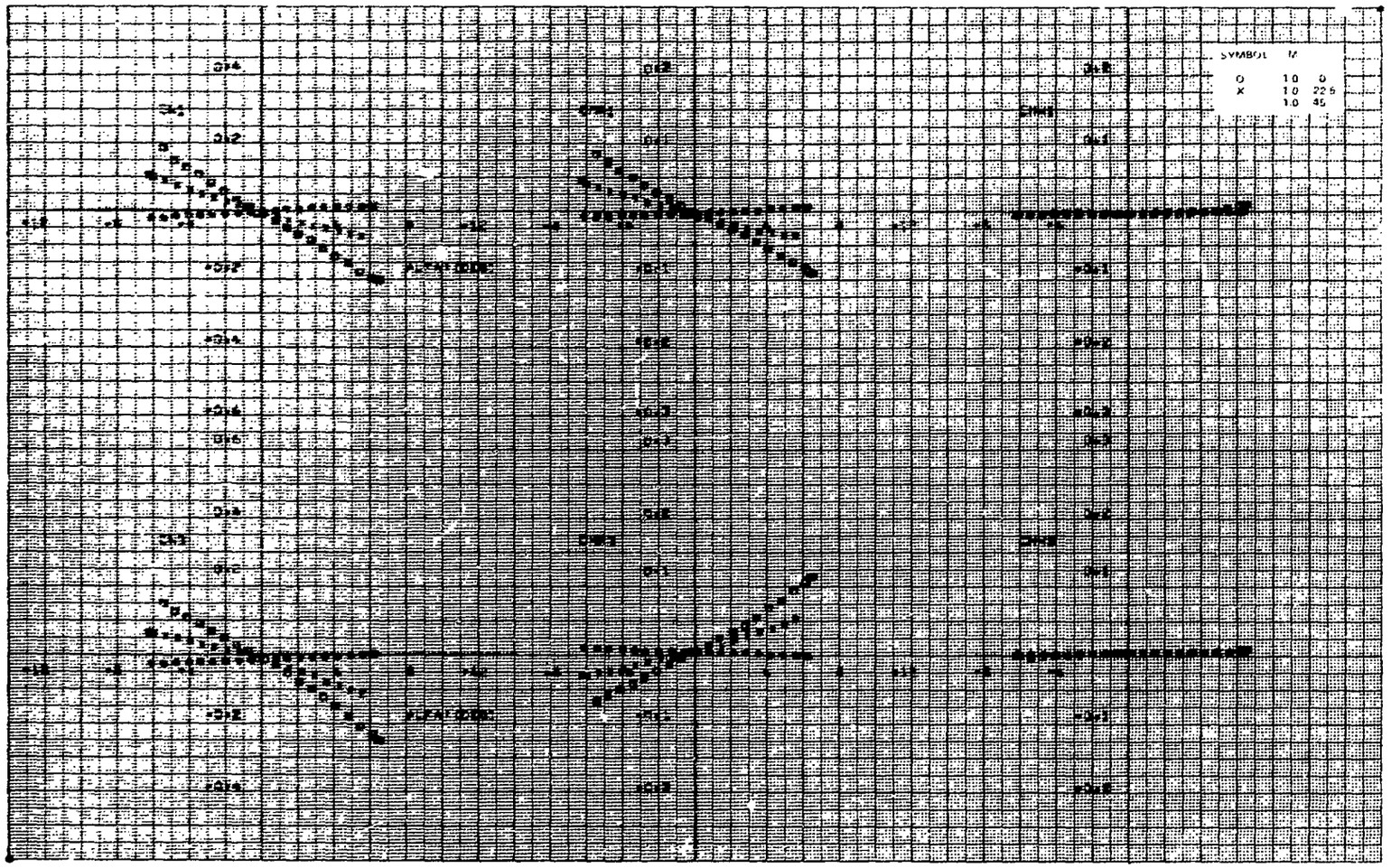


Figure 12b. Continued.

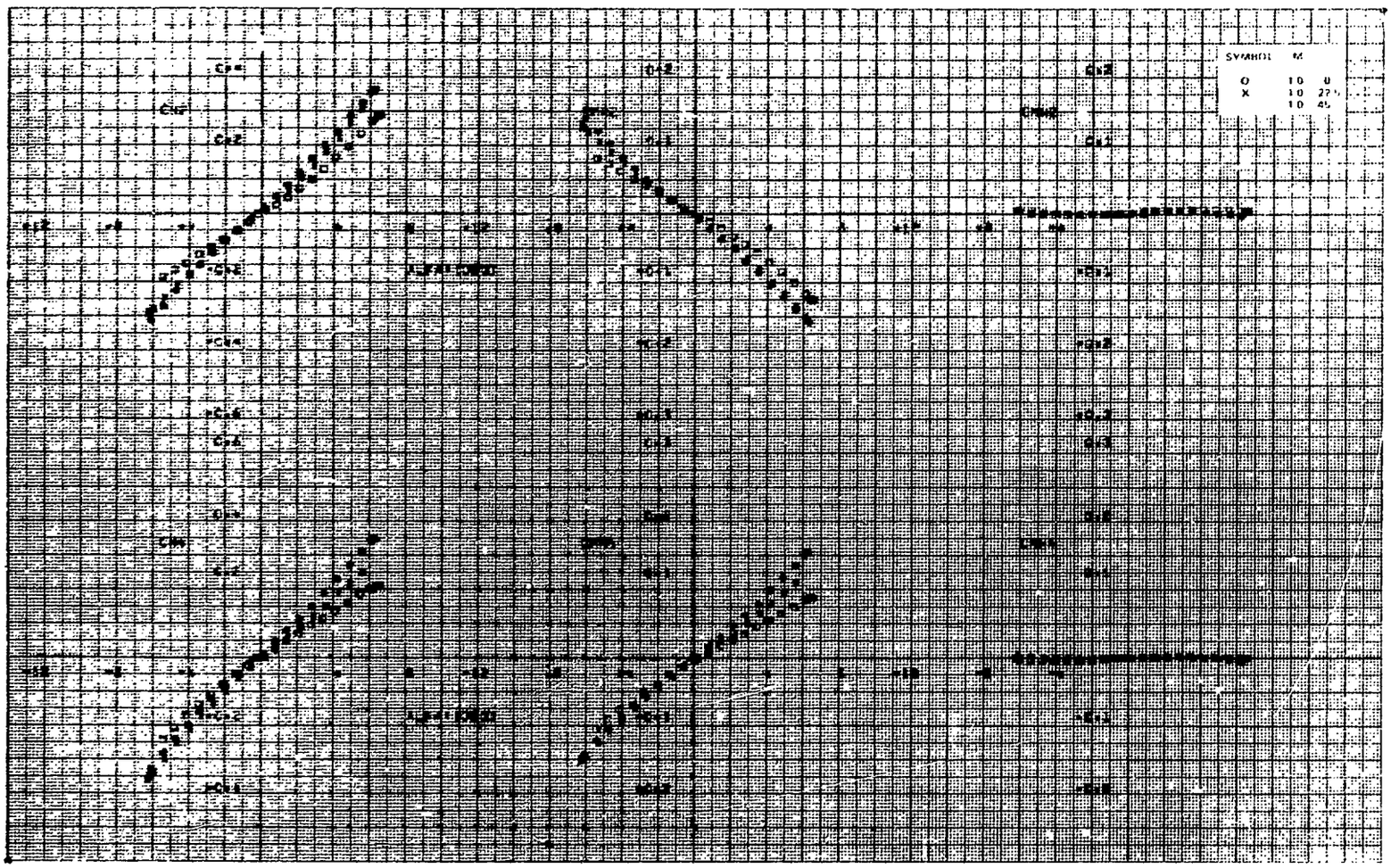


Figure 12b. Concluded.

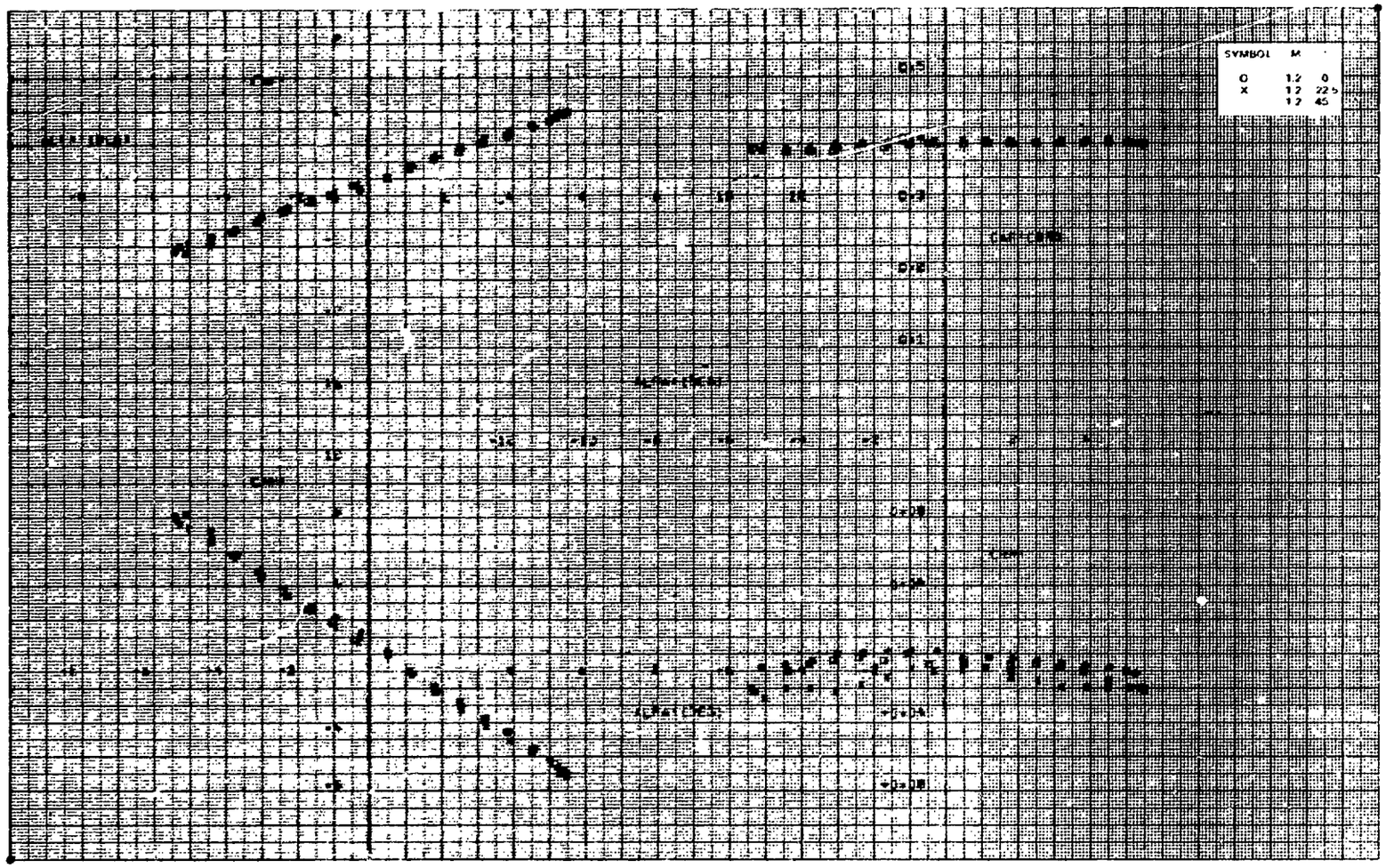


Figure 12c. Aerodynamic stability coefficients, CR/D = 1.75, = 60 deg, M_∞ = 1.2.

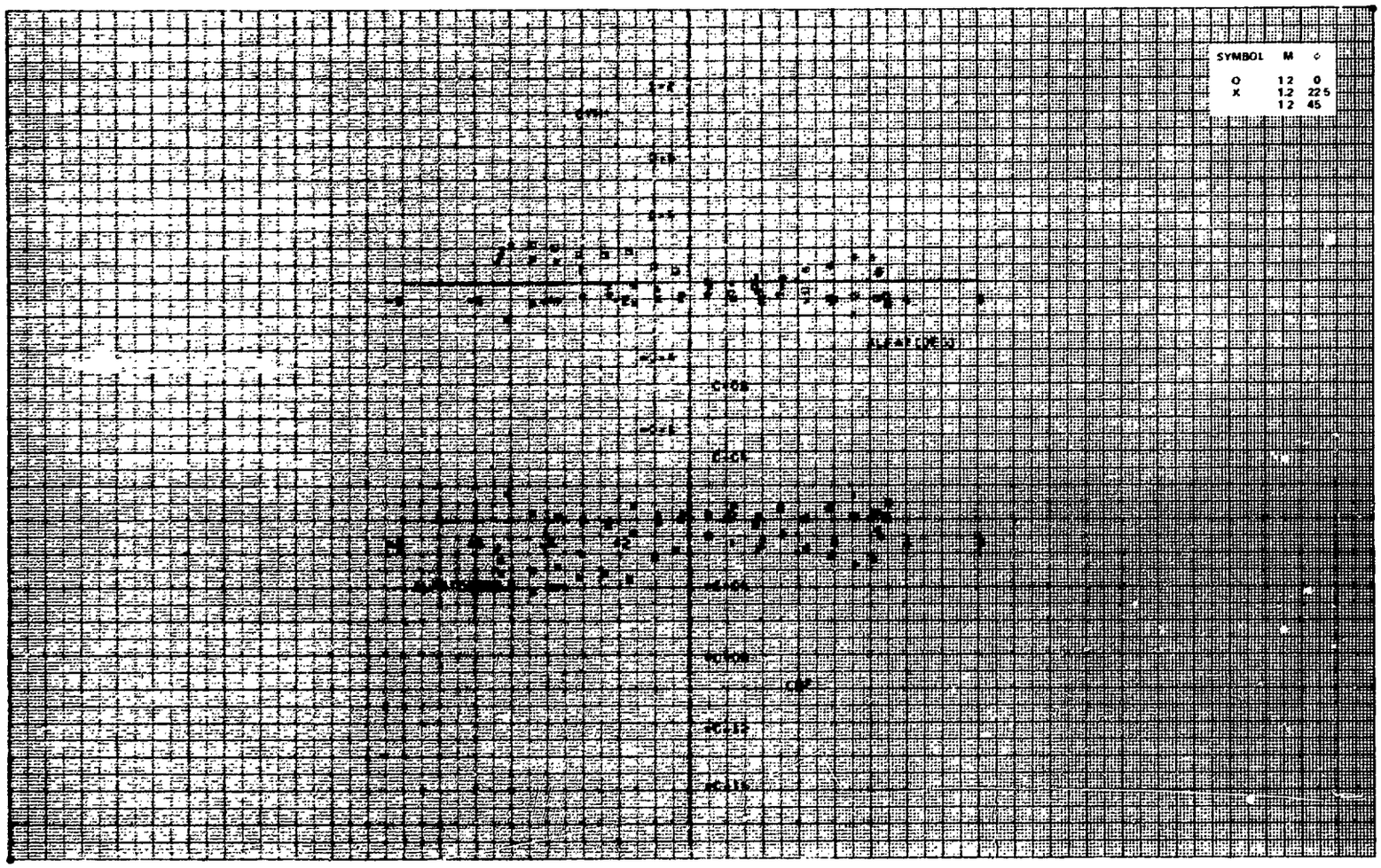


Figure 12c. Continued.

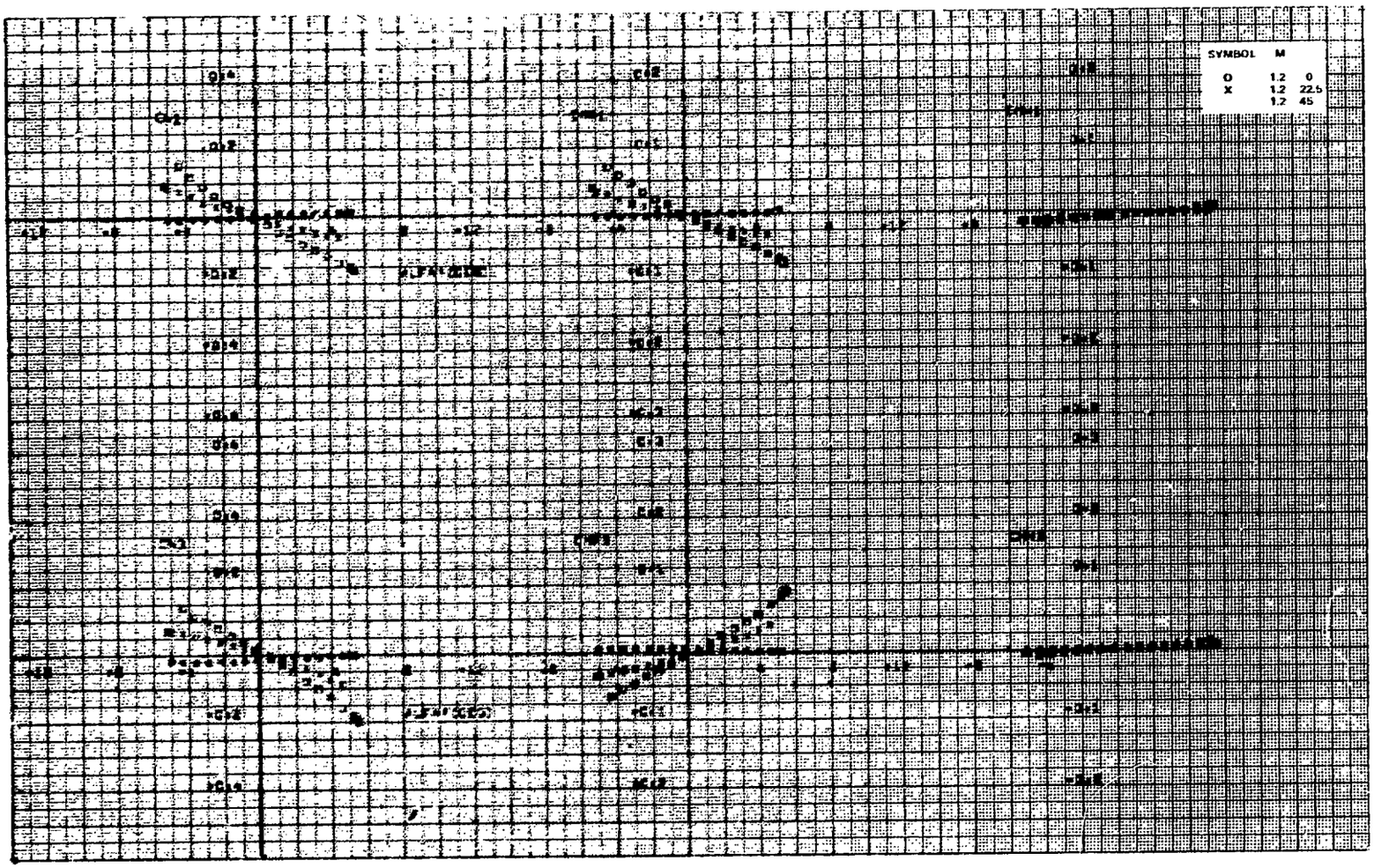


Figure 12c. Continued.

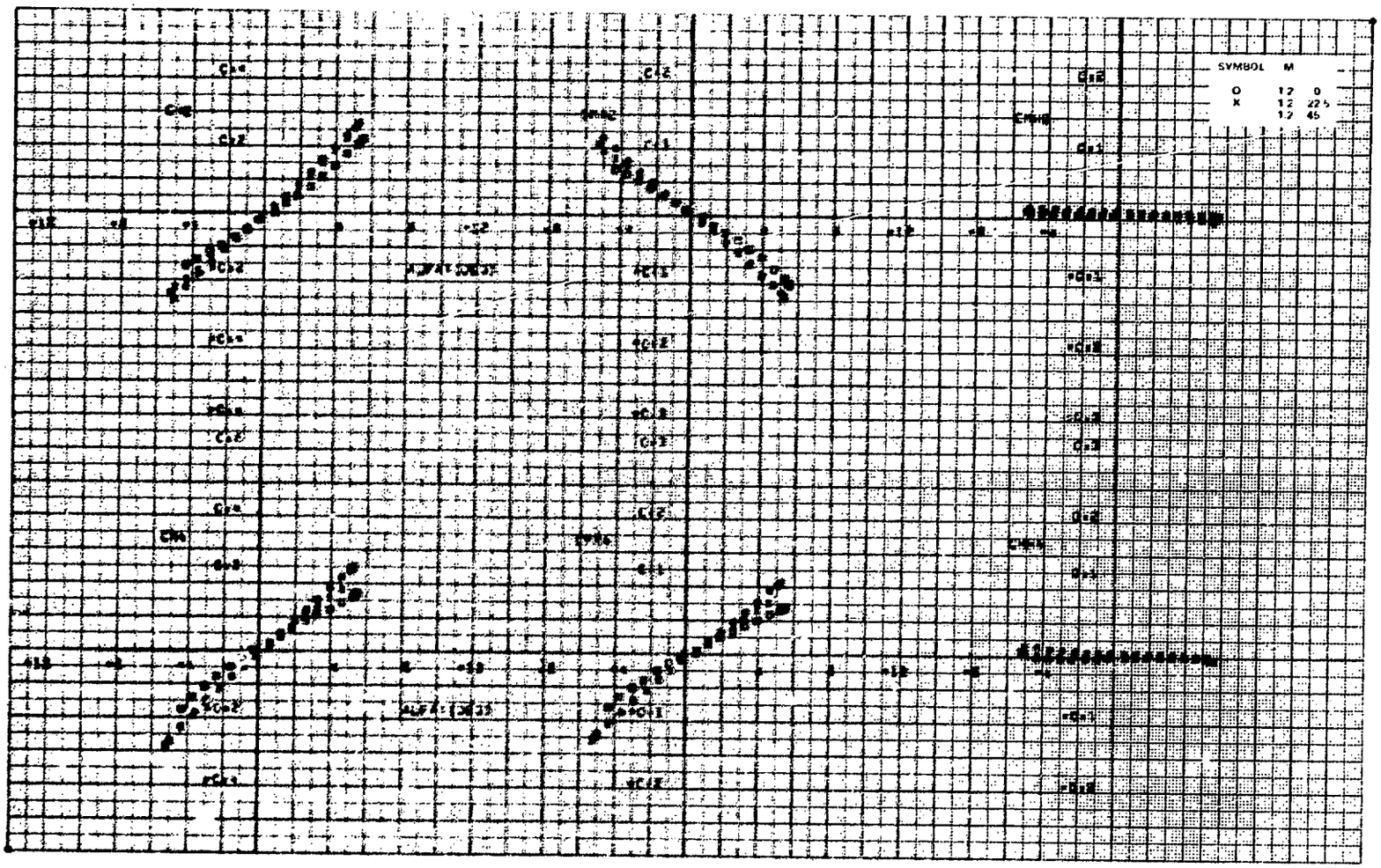


Figure 12c. Concluded.

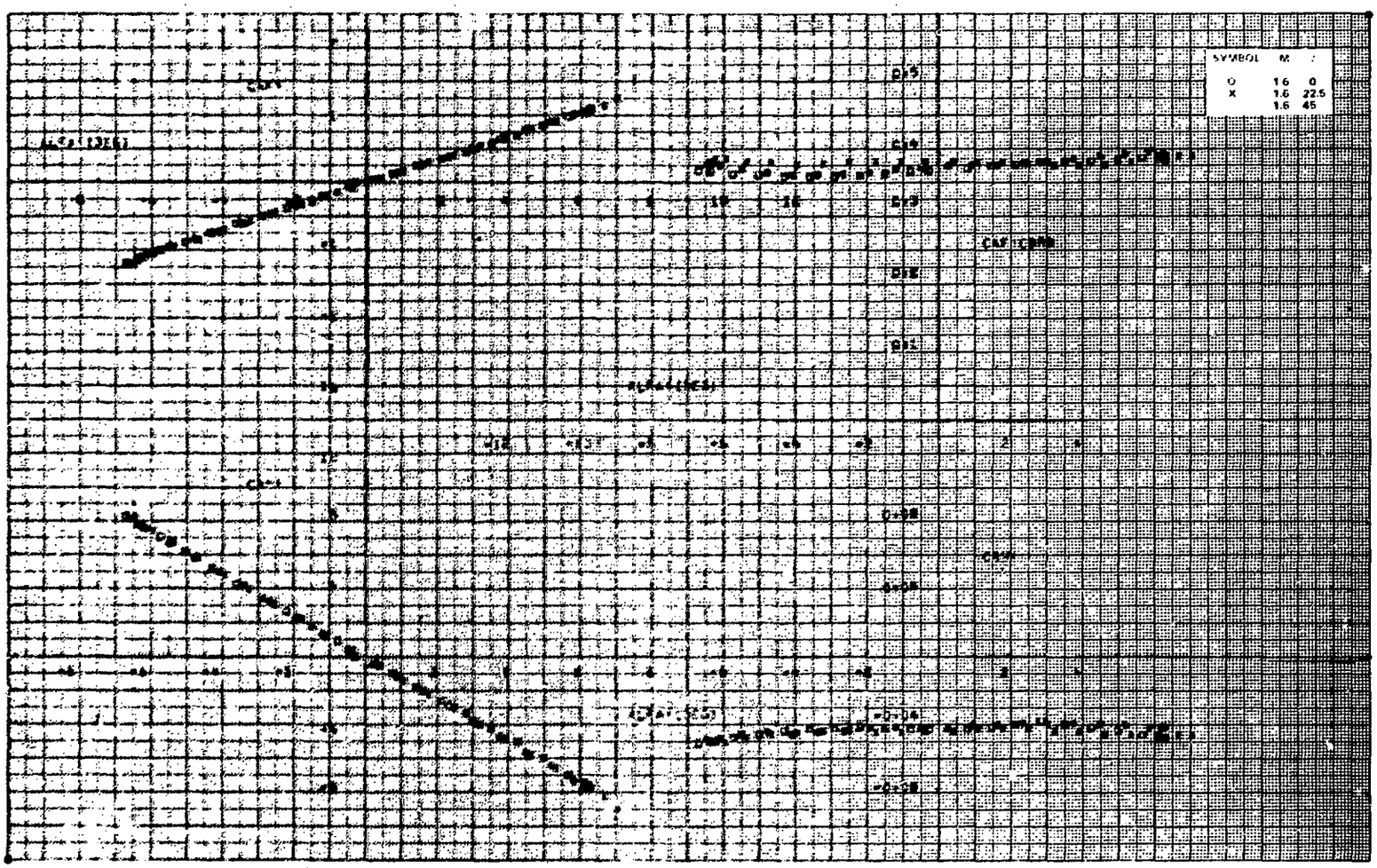


Figure 7.5. Aerodynamic stability coefficients, $x_{cg}/\ell = 1.75$, $\Lambda = 60$ deg, $M_\infty = 1.6$.

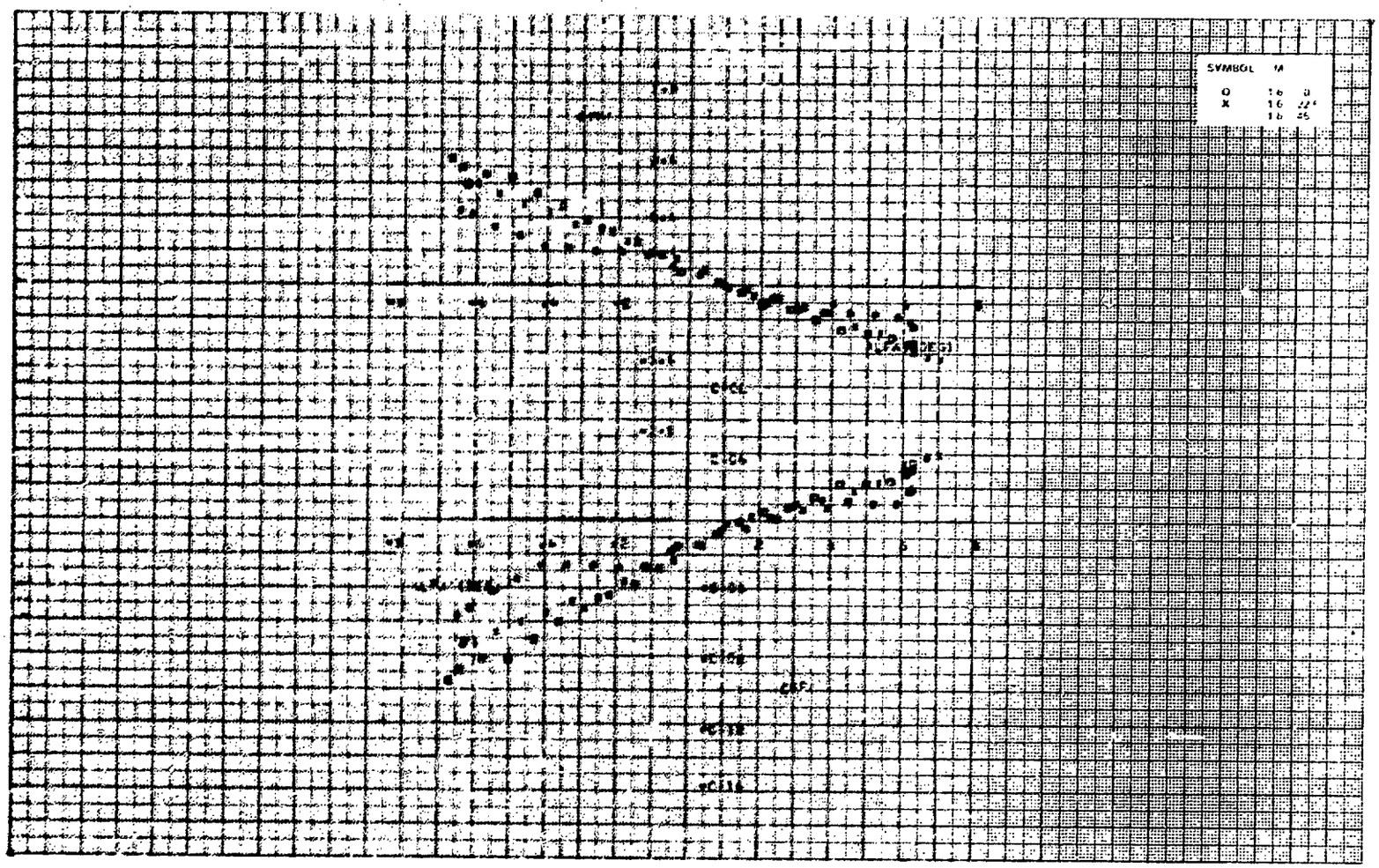


Figure 12.5. Continued.

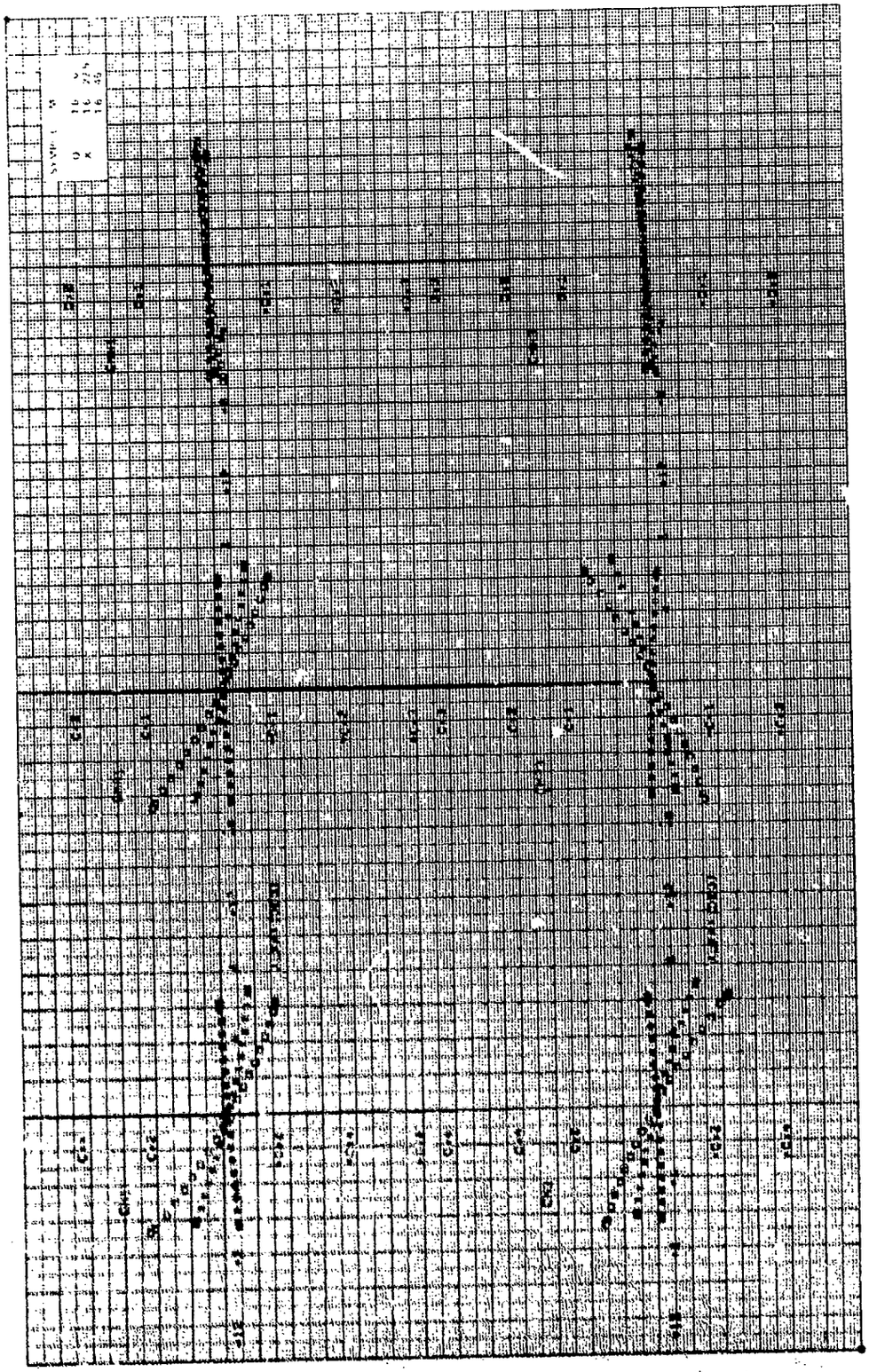


Figure 12d. Continued.

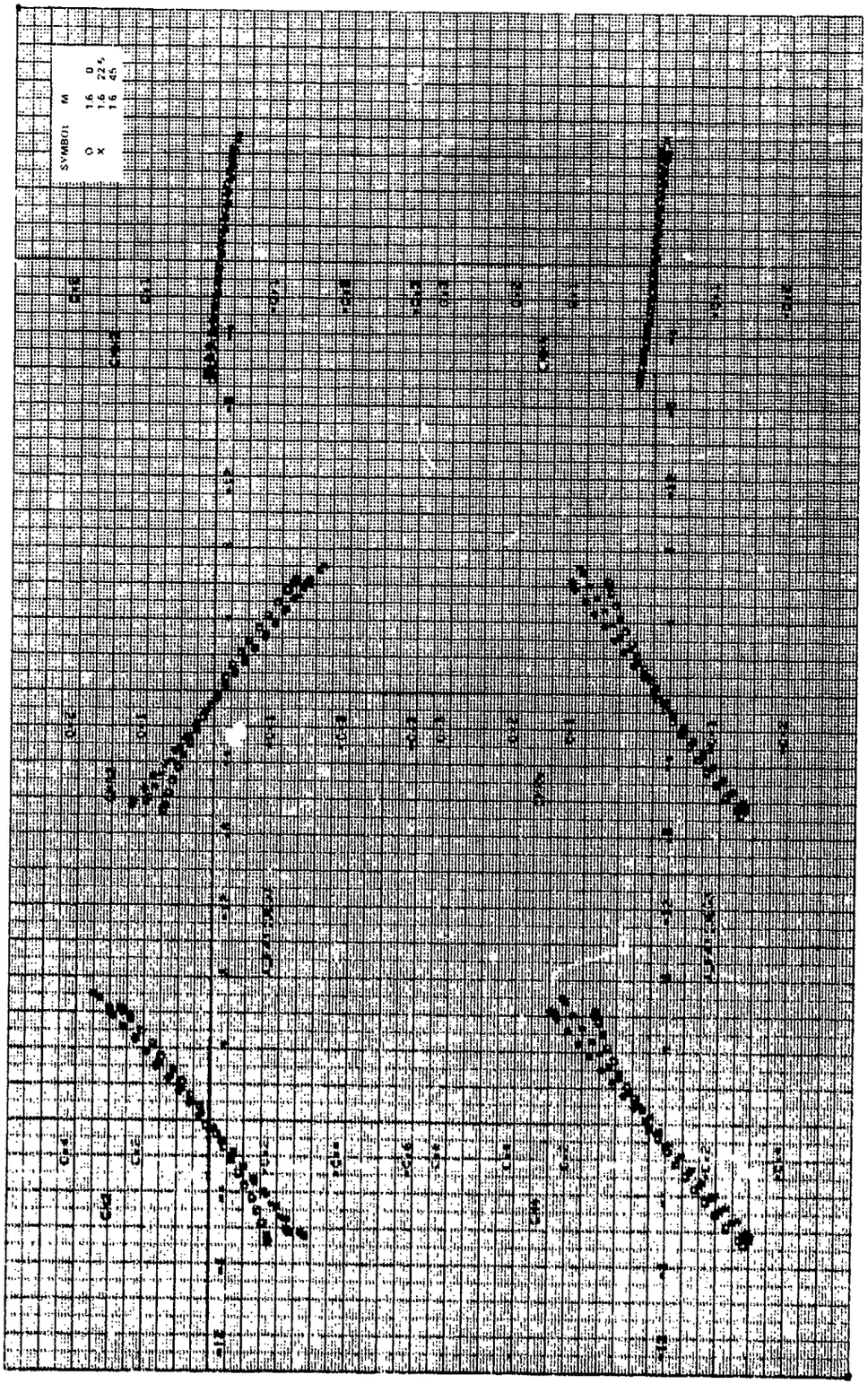


Figure 12d. Concluded.

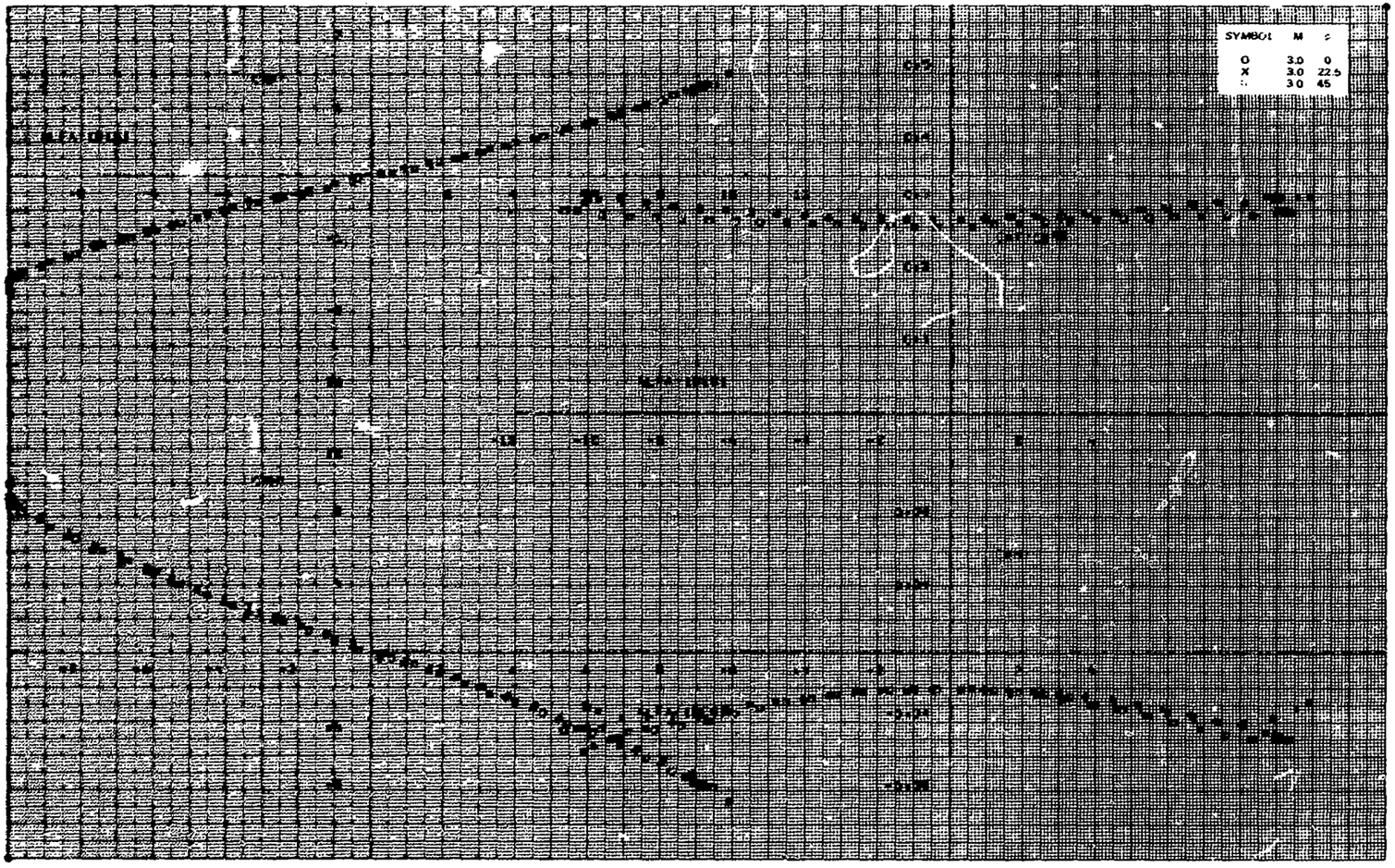


Figure 12e. Aerodynamic stability coefficients, CR/D = 1.75, Λ = 60 deg, M_∞ = 3.0

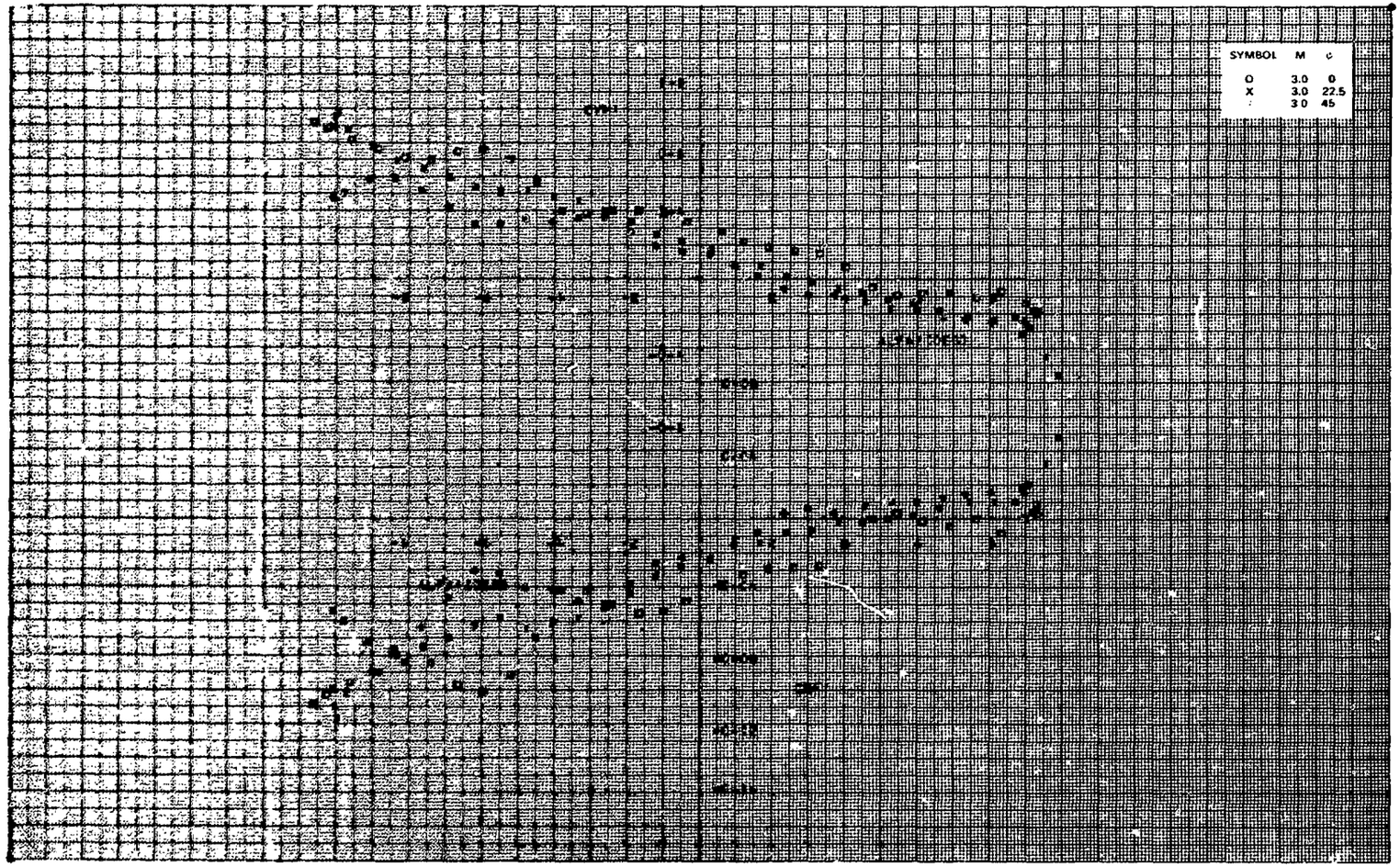


Figure 12e. Continued.

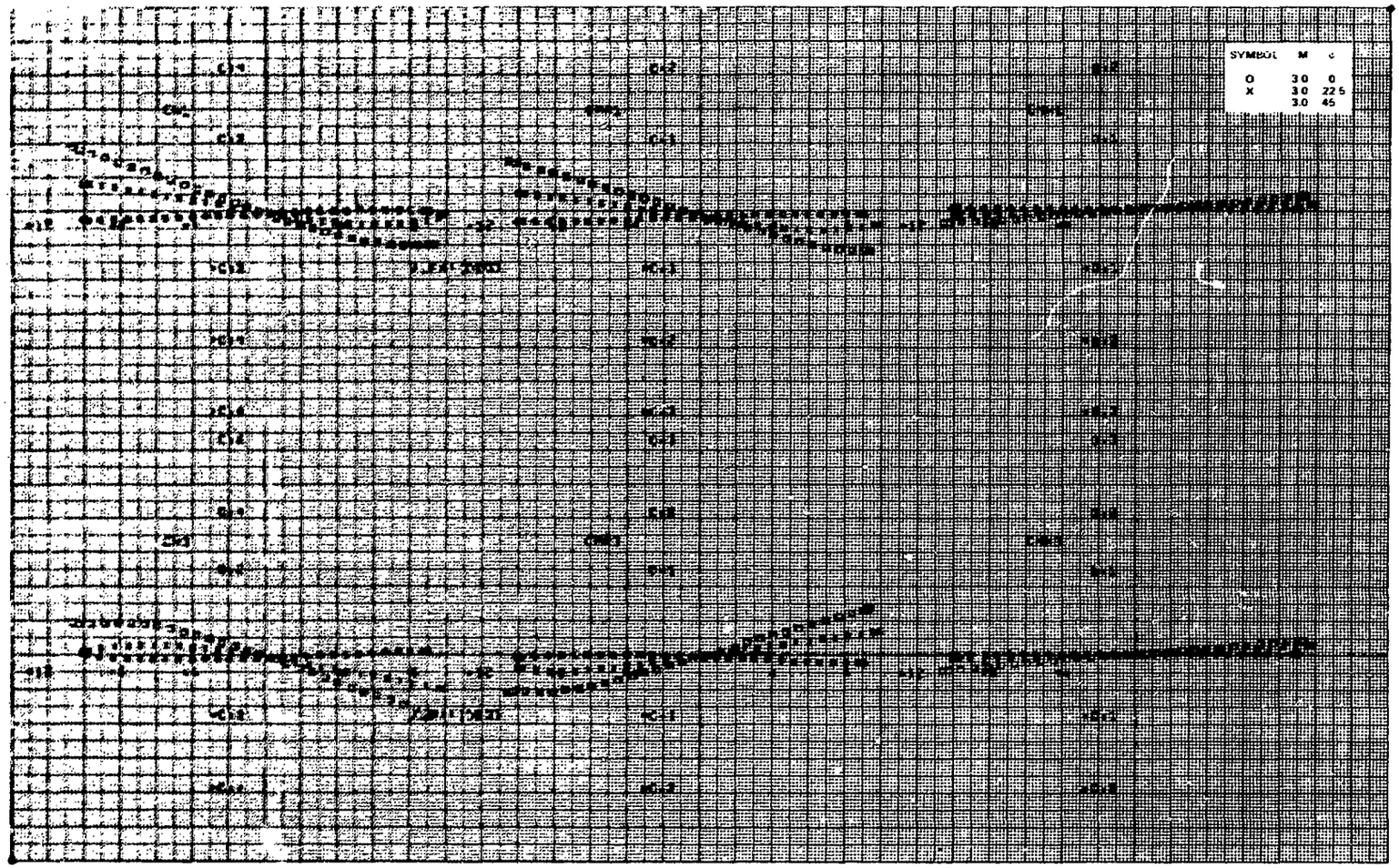


Figure 12e. Continued.

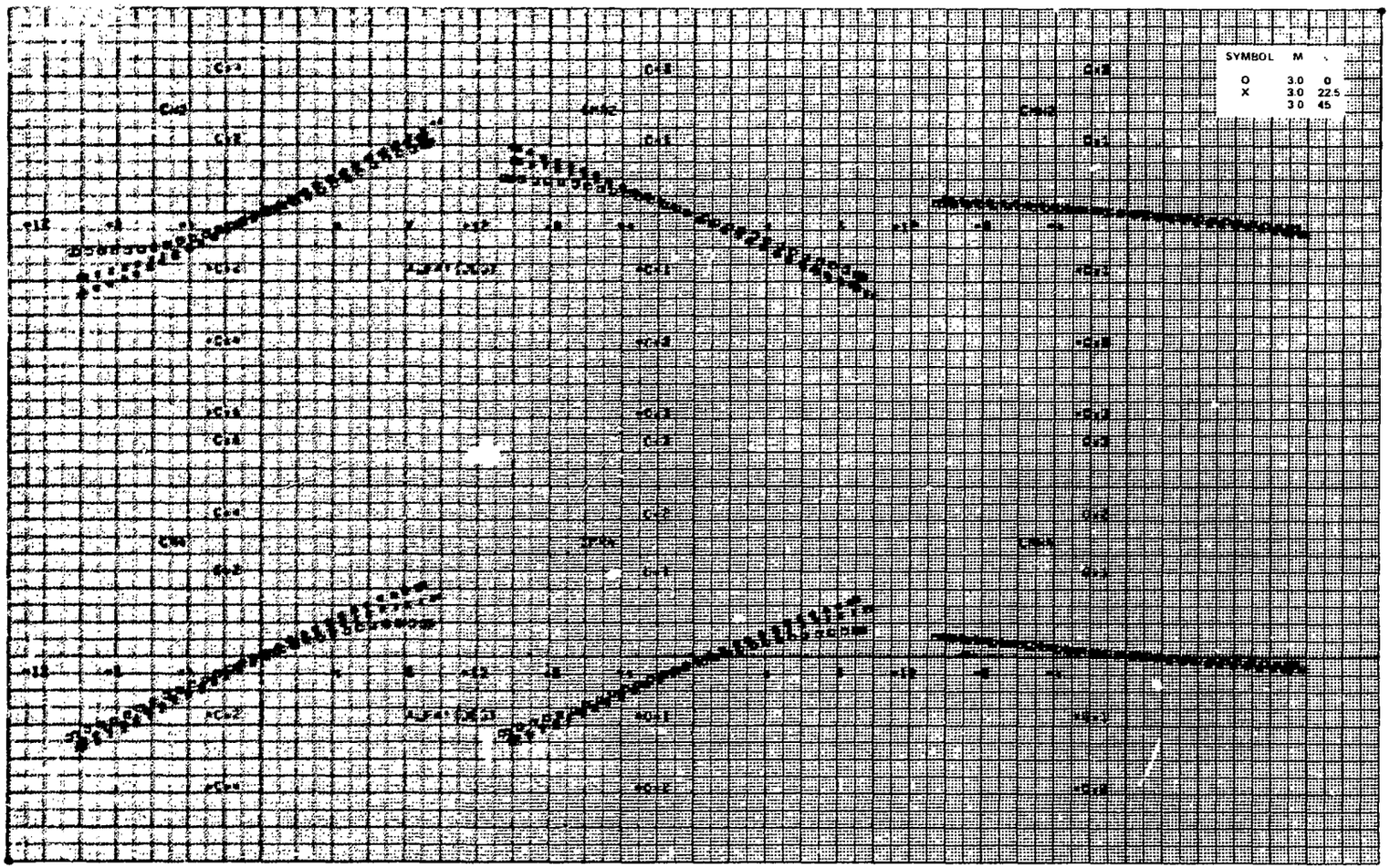


Figure 12e. Concluded.

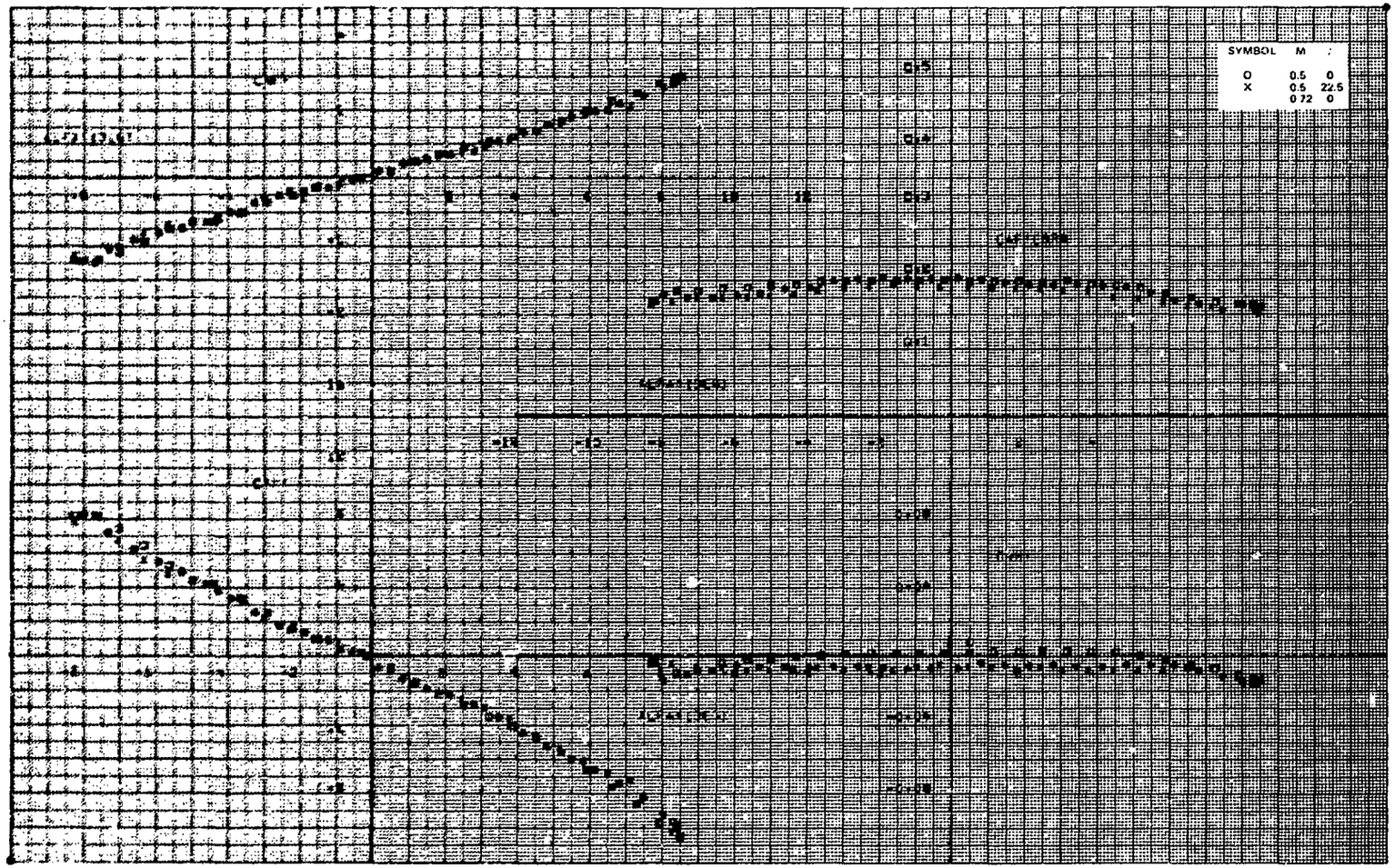


Figure 131. Aerodynamic stability coefficients, CR/D = 1.75, Λ = 0 deg, B/2D = 0.535, M_∞ = 0.5, 0.72.

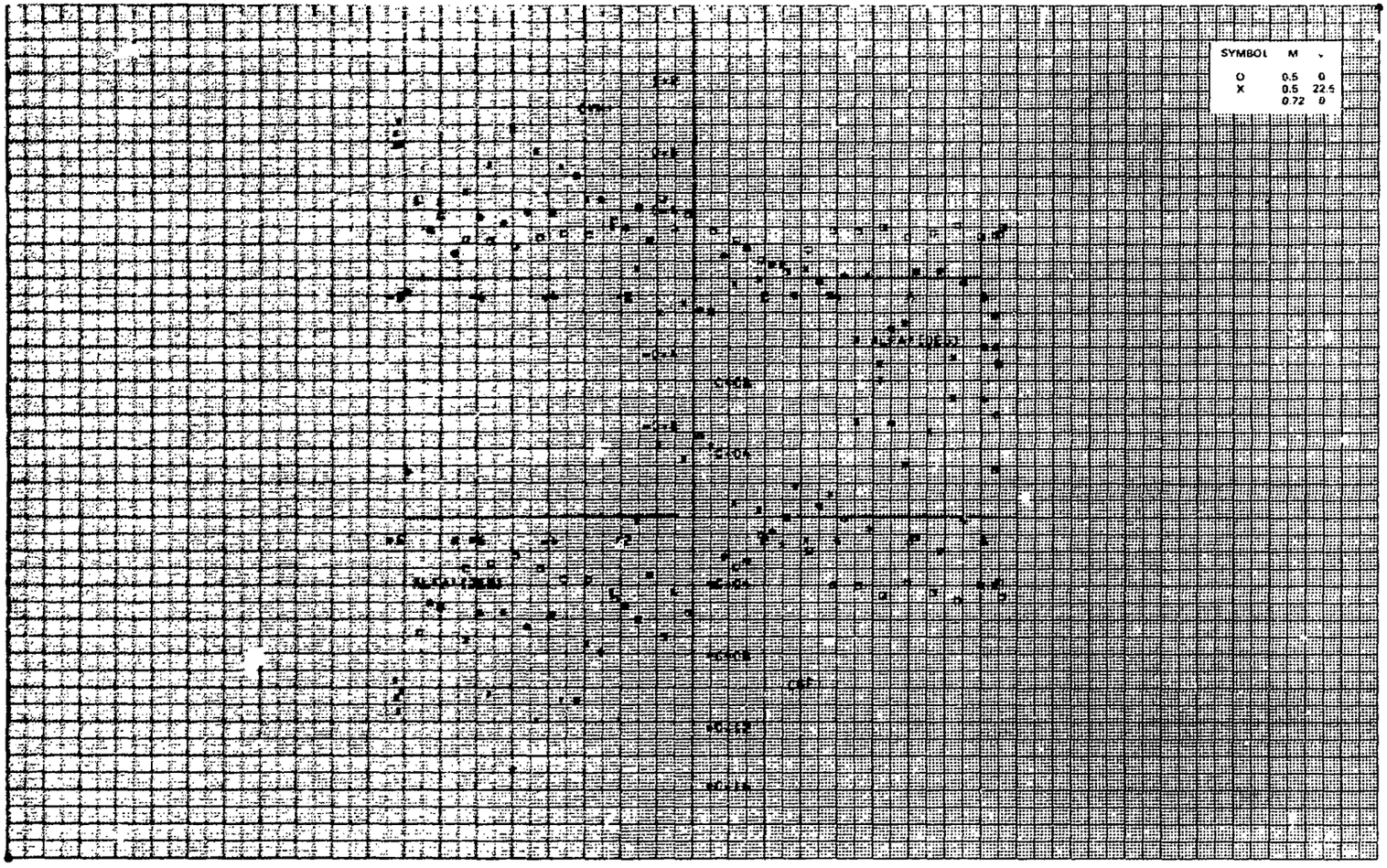


Figure 13a. Continued.

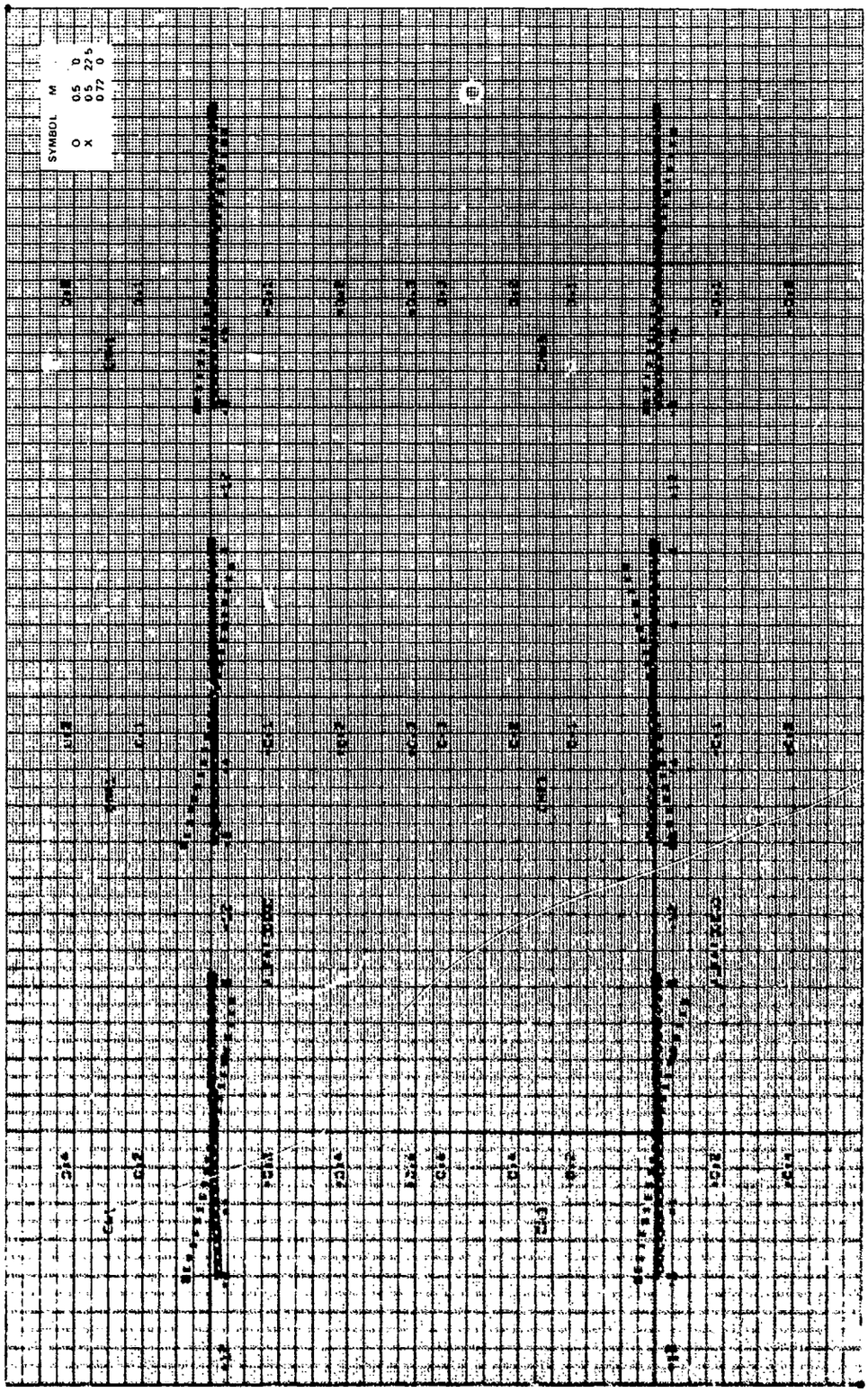


Figure 13a. Continued.

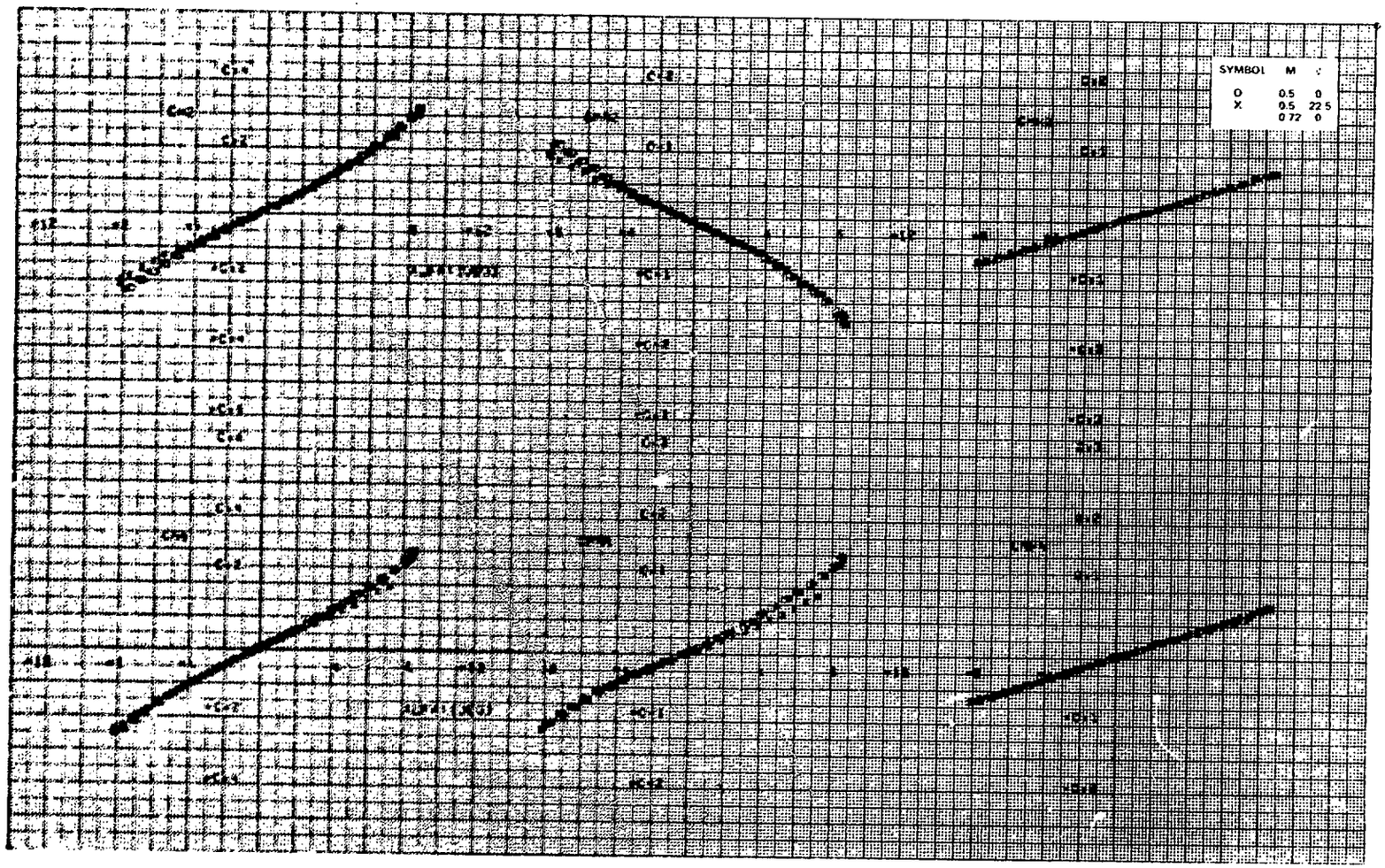


Figure 13a. Concluded.

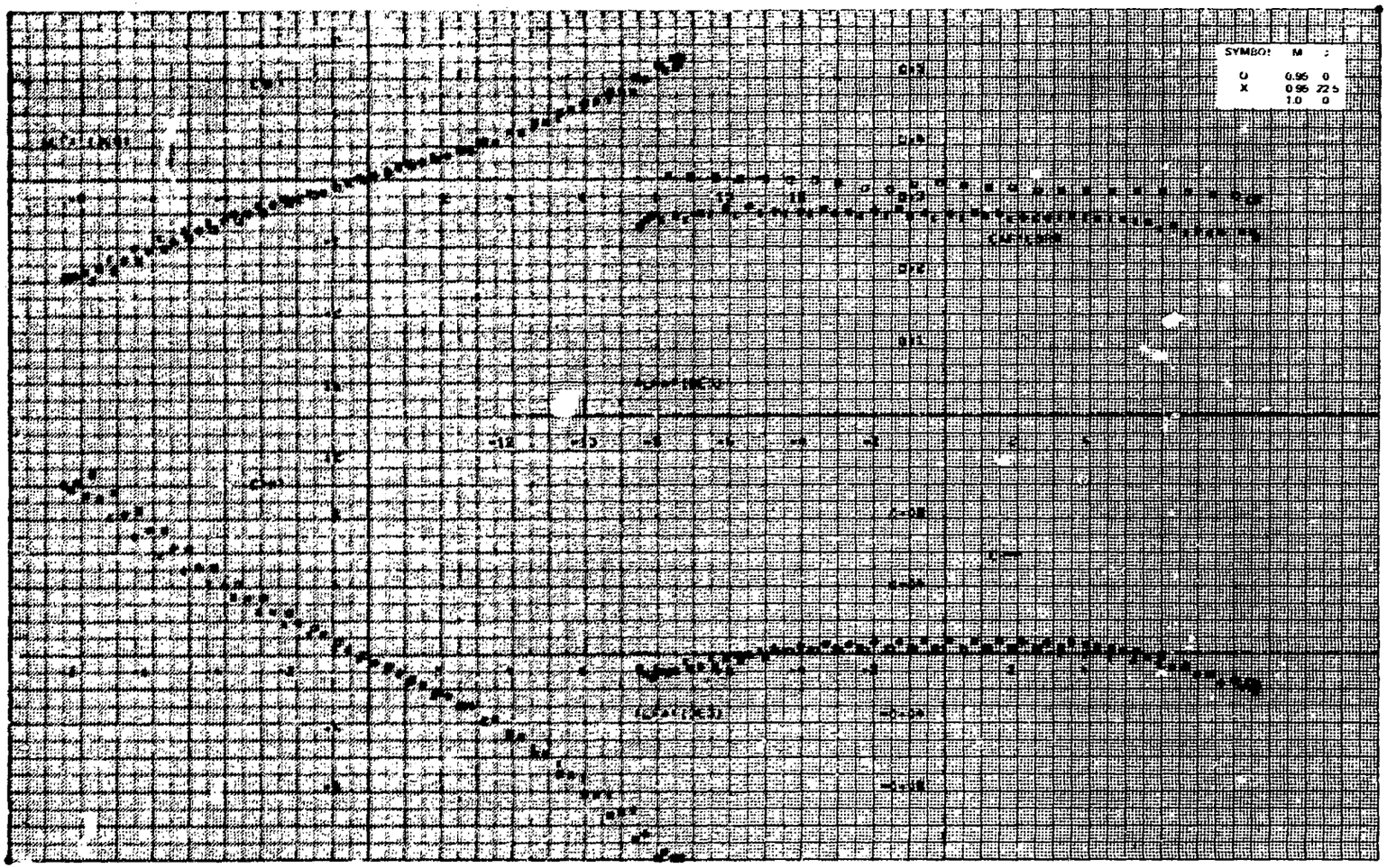


Figure 13b. Aerodynamic stability coefficients, CR/D = 1.75, λ = 0 deg, B/2D = 0.535, M_∞ = 0.95, 1.0.

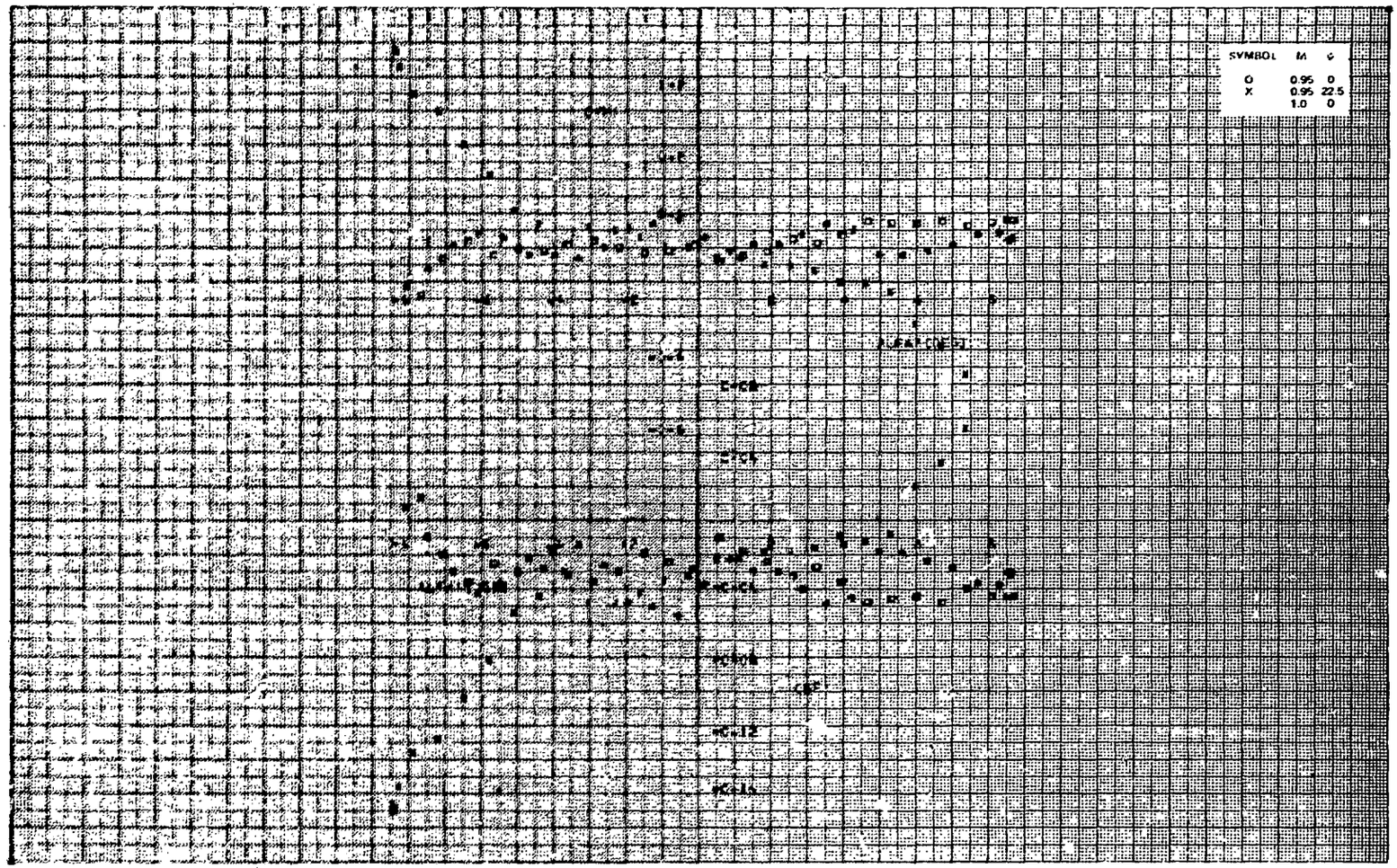


Figure 13b. Continued.

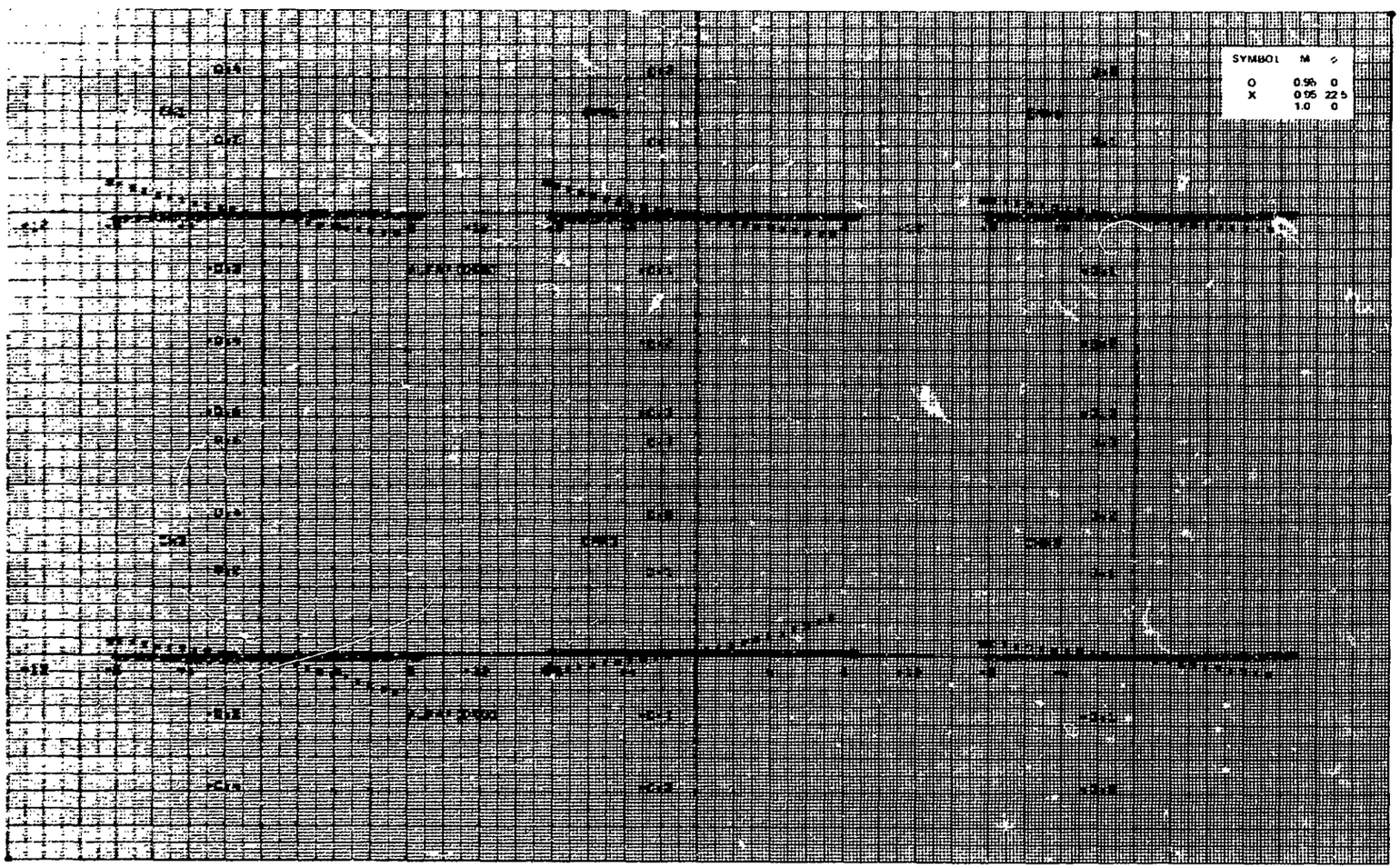


Figure 13b. Continued.

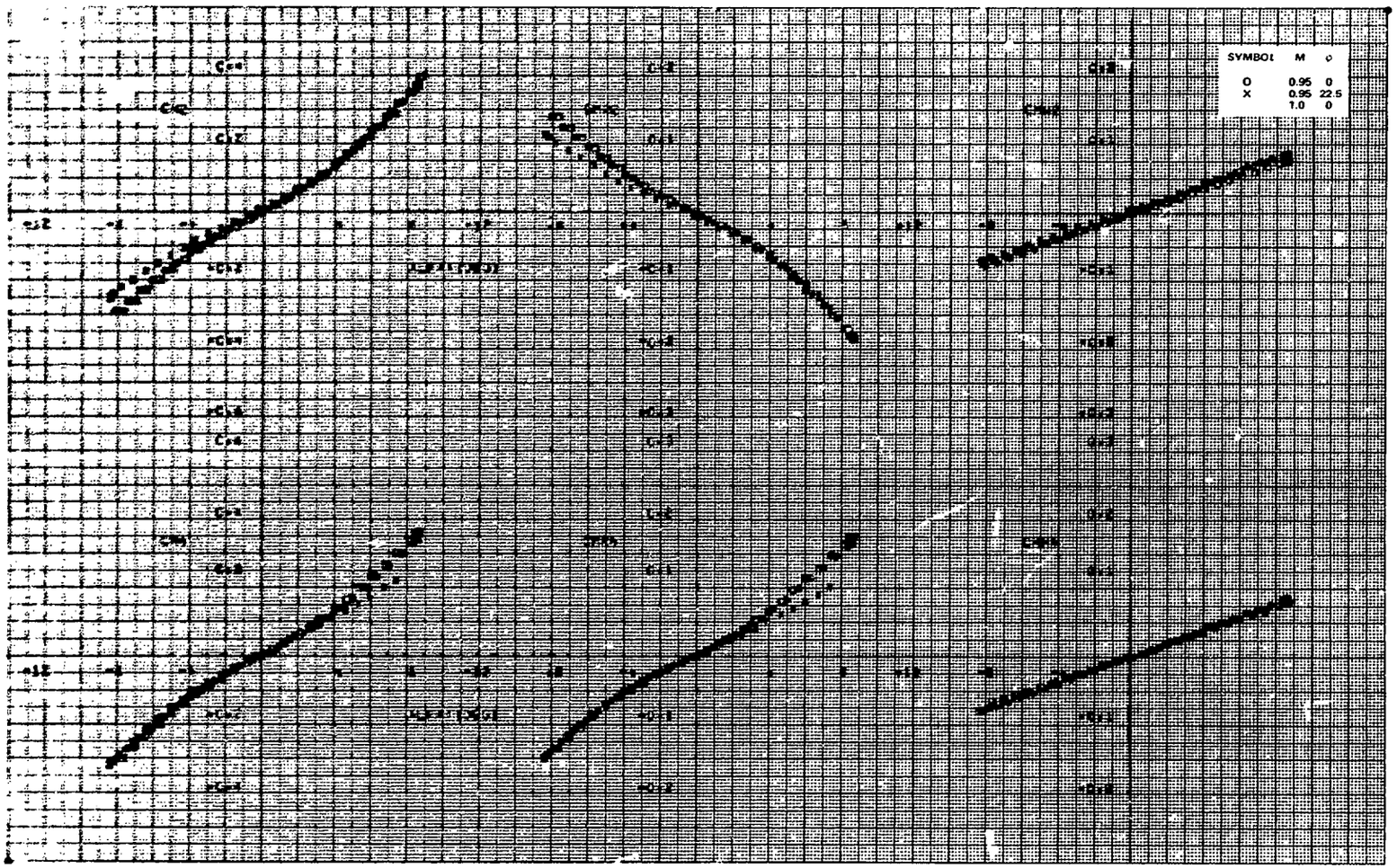


Figure 13b. Concluded.

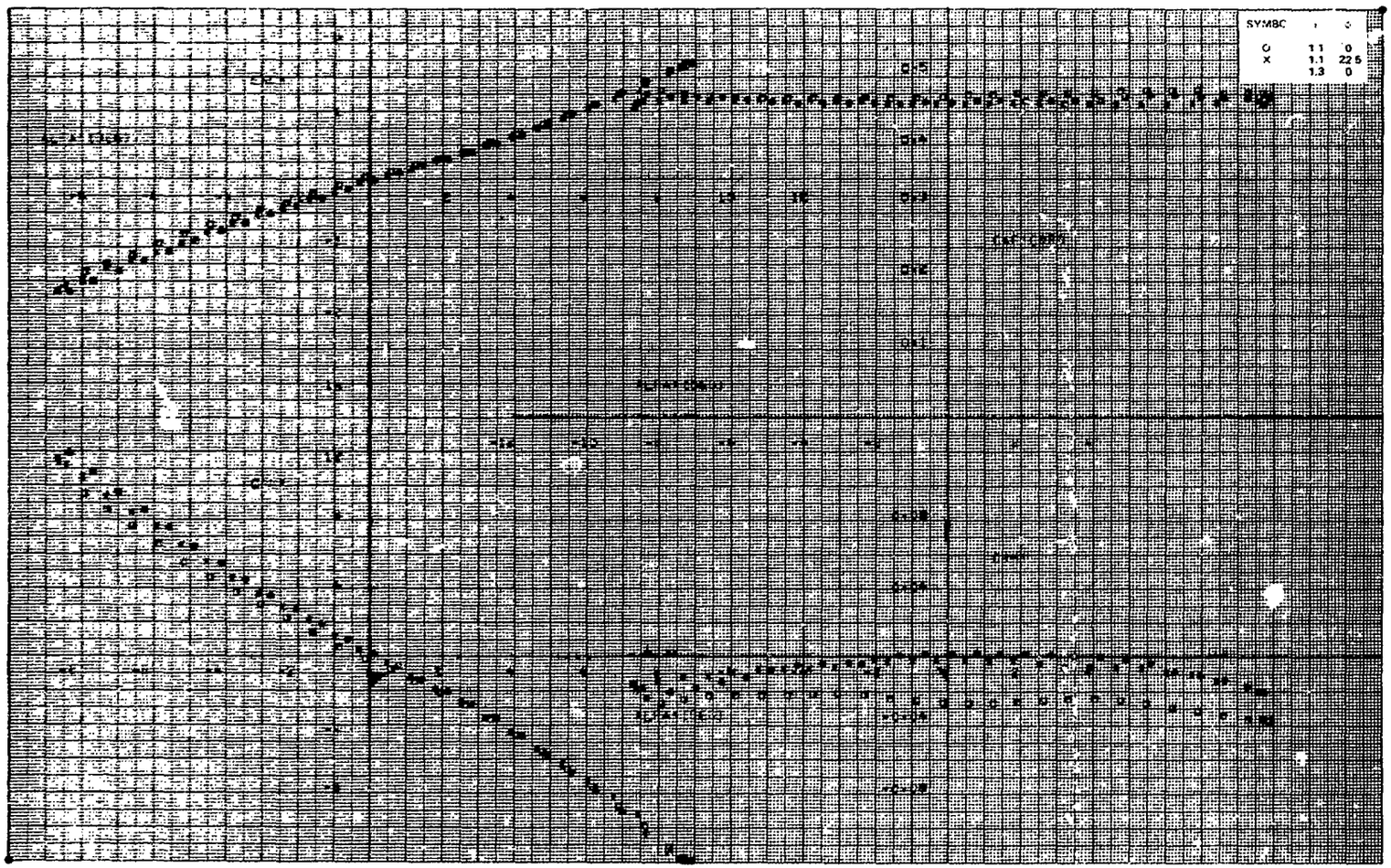


Figure 13c. Aerodynamic stability coefficients, CR/D = 1.75, Λ = 0 deg, B/2D = 0.535, M_∞ = 1.1, 1.3.

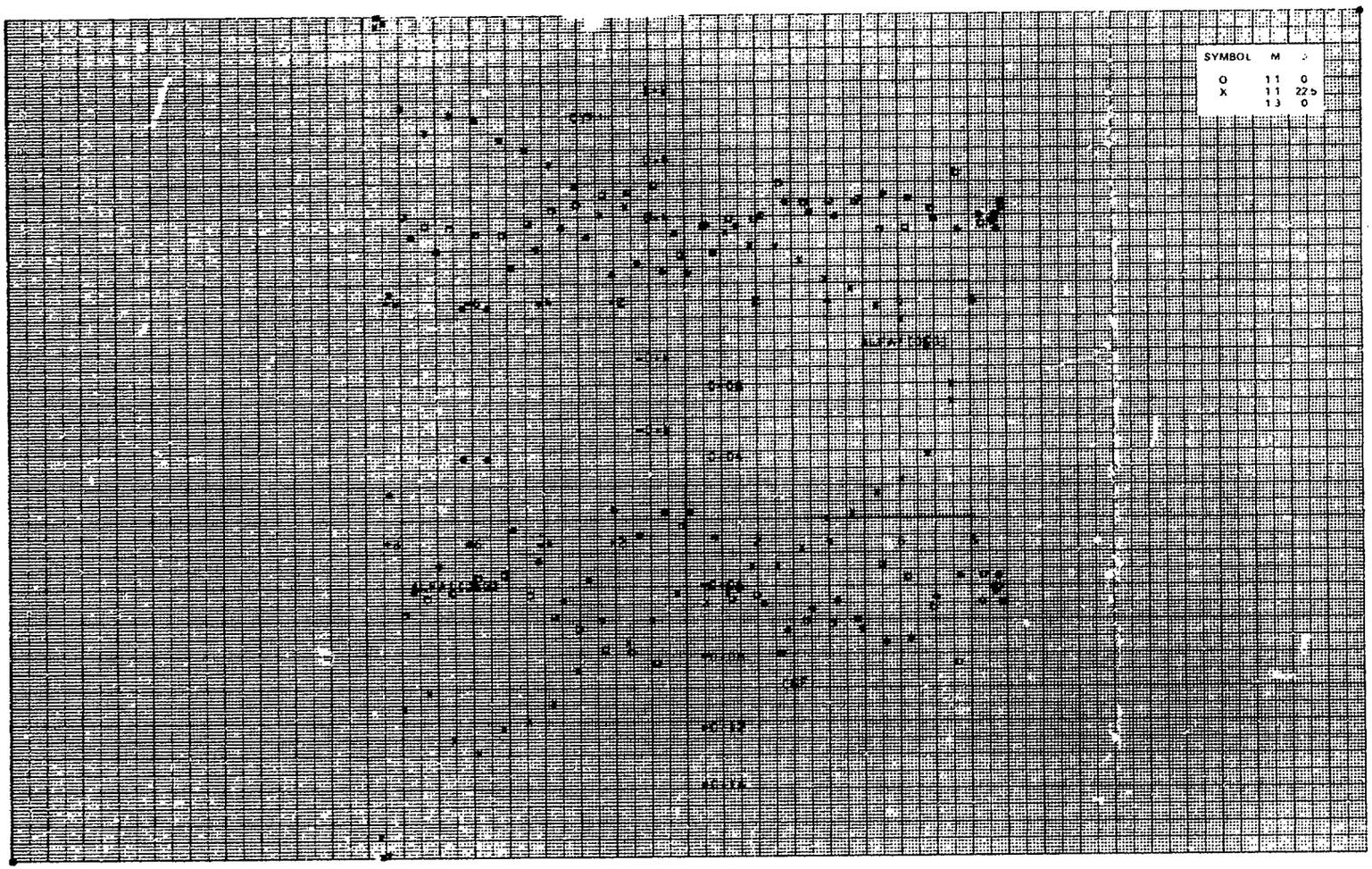


Figure 13c. Continued.

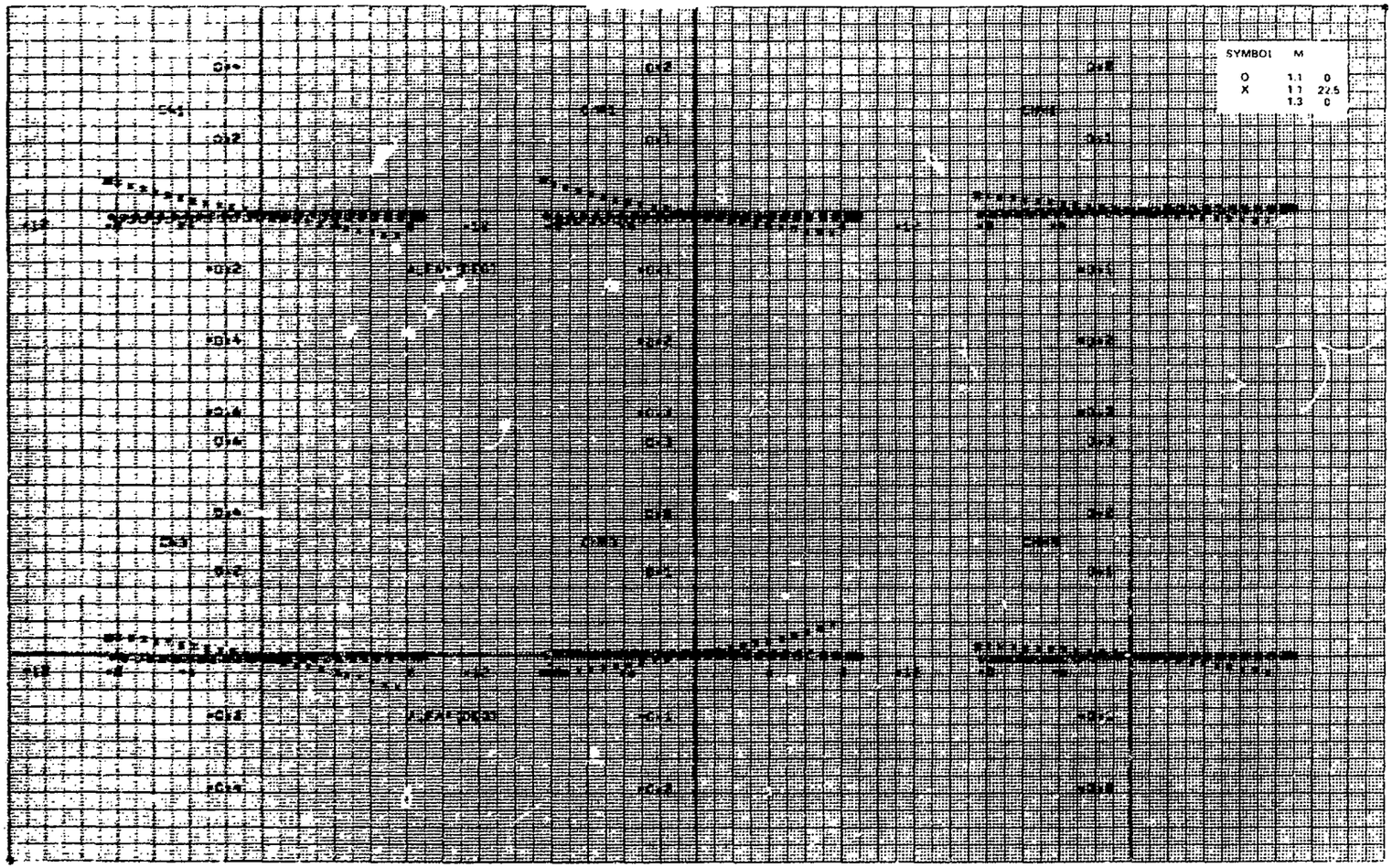


Figure 13c. Continued.

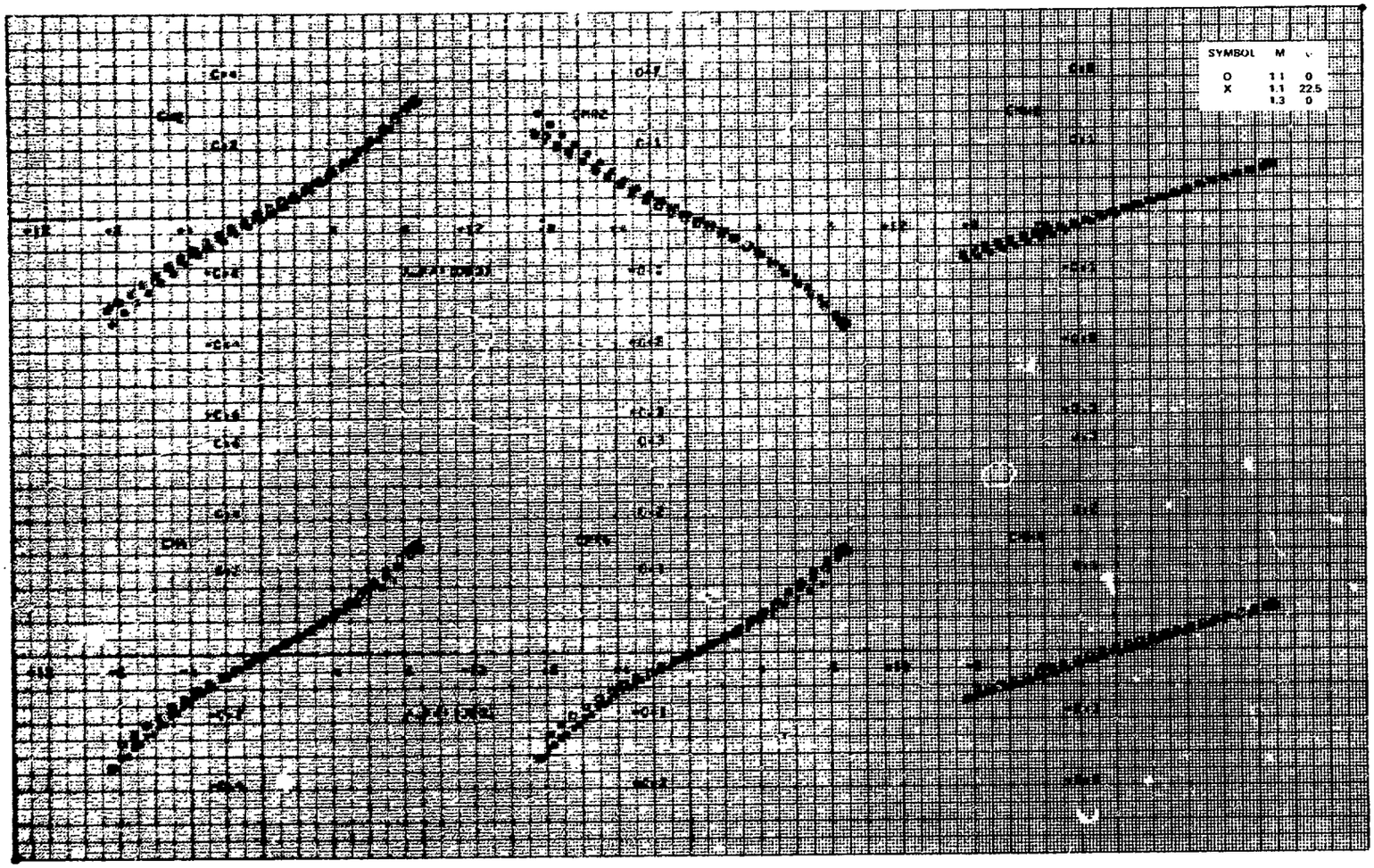


Figure 13c. Concluded.

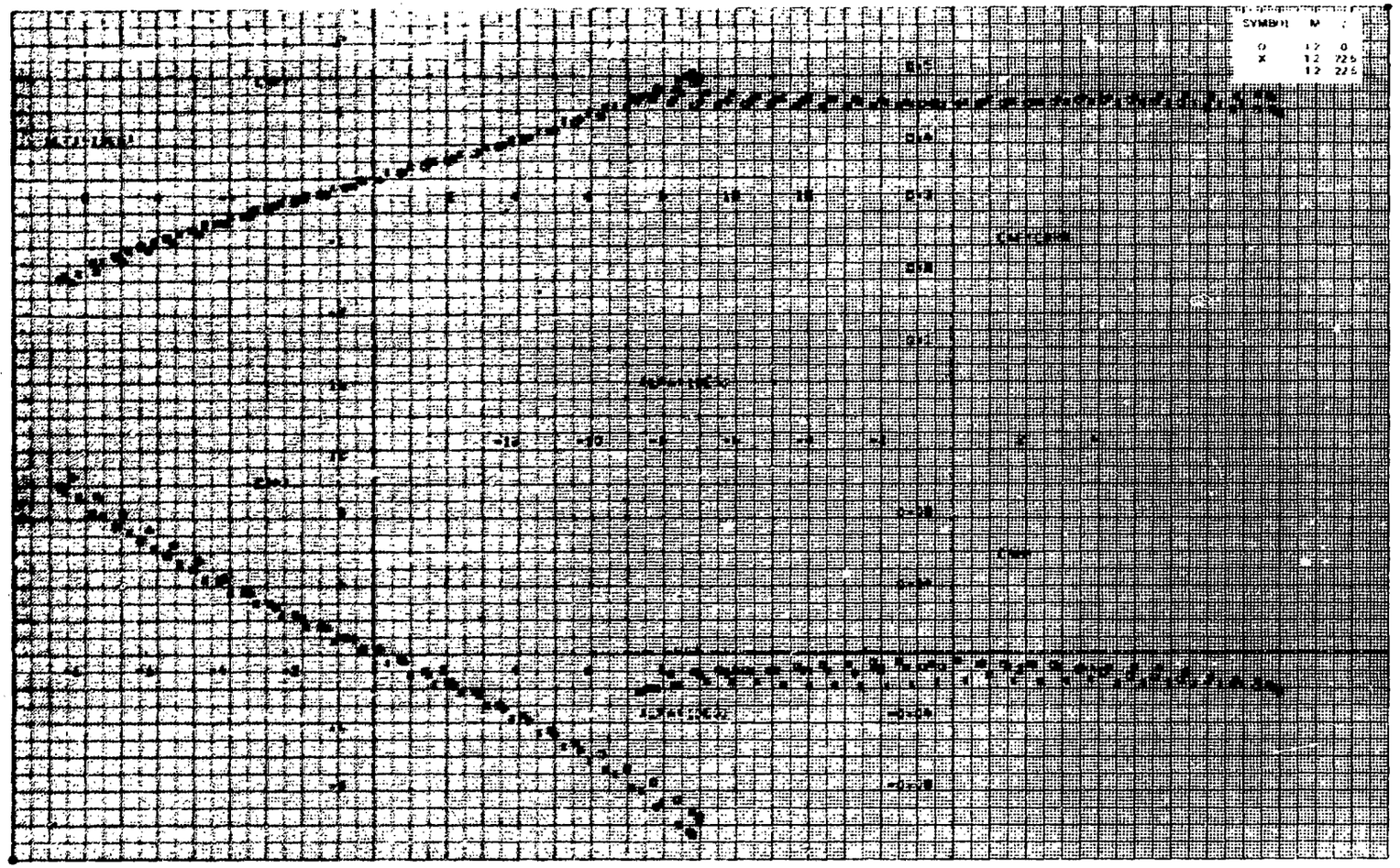


Figure 134. Aerodynamic stability coefficients. OR/D = 1.75, Γ = 0 deg., B/2D = 0.535, M_∞ = 1.7.

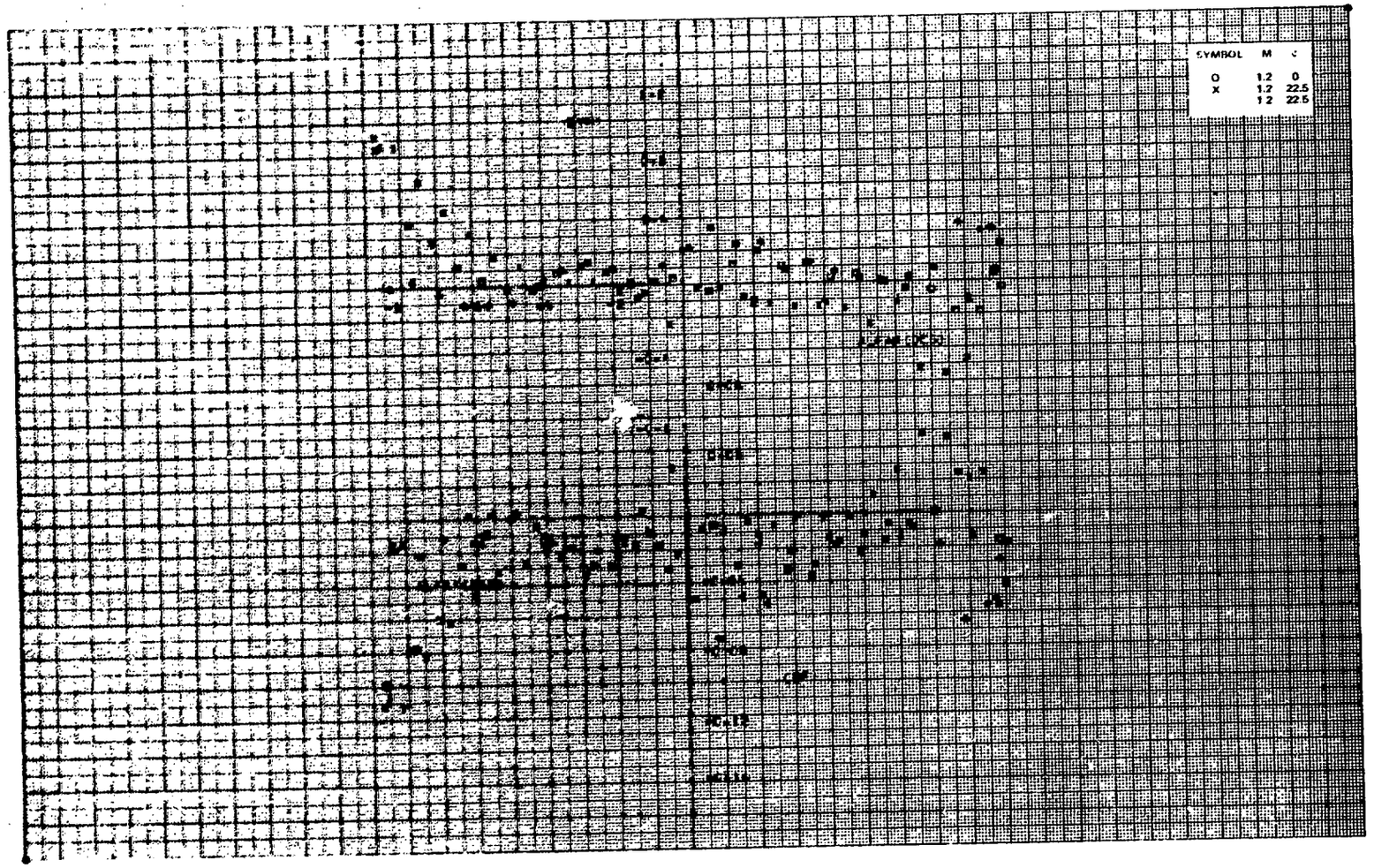
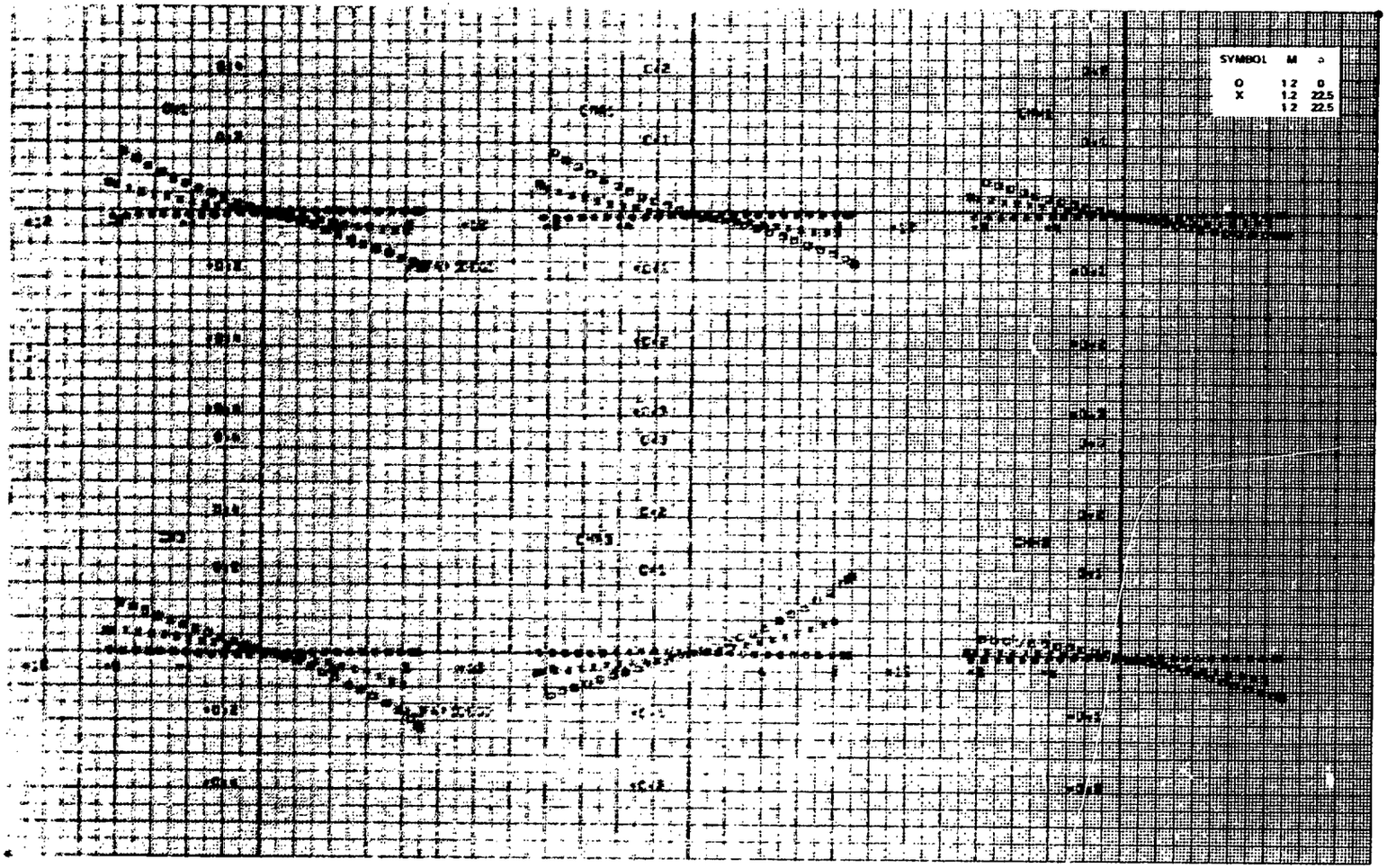
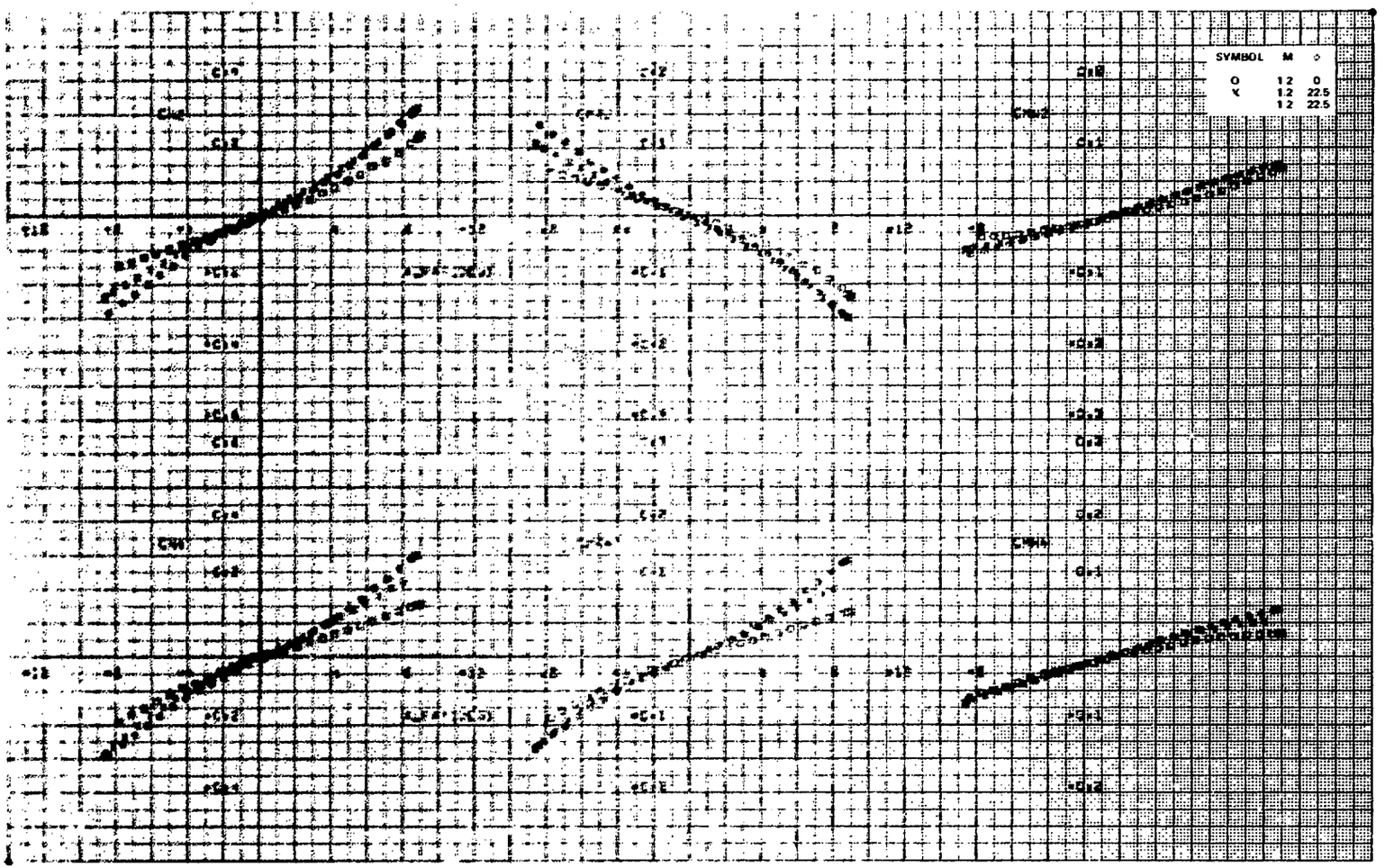
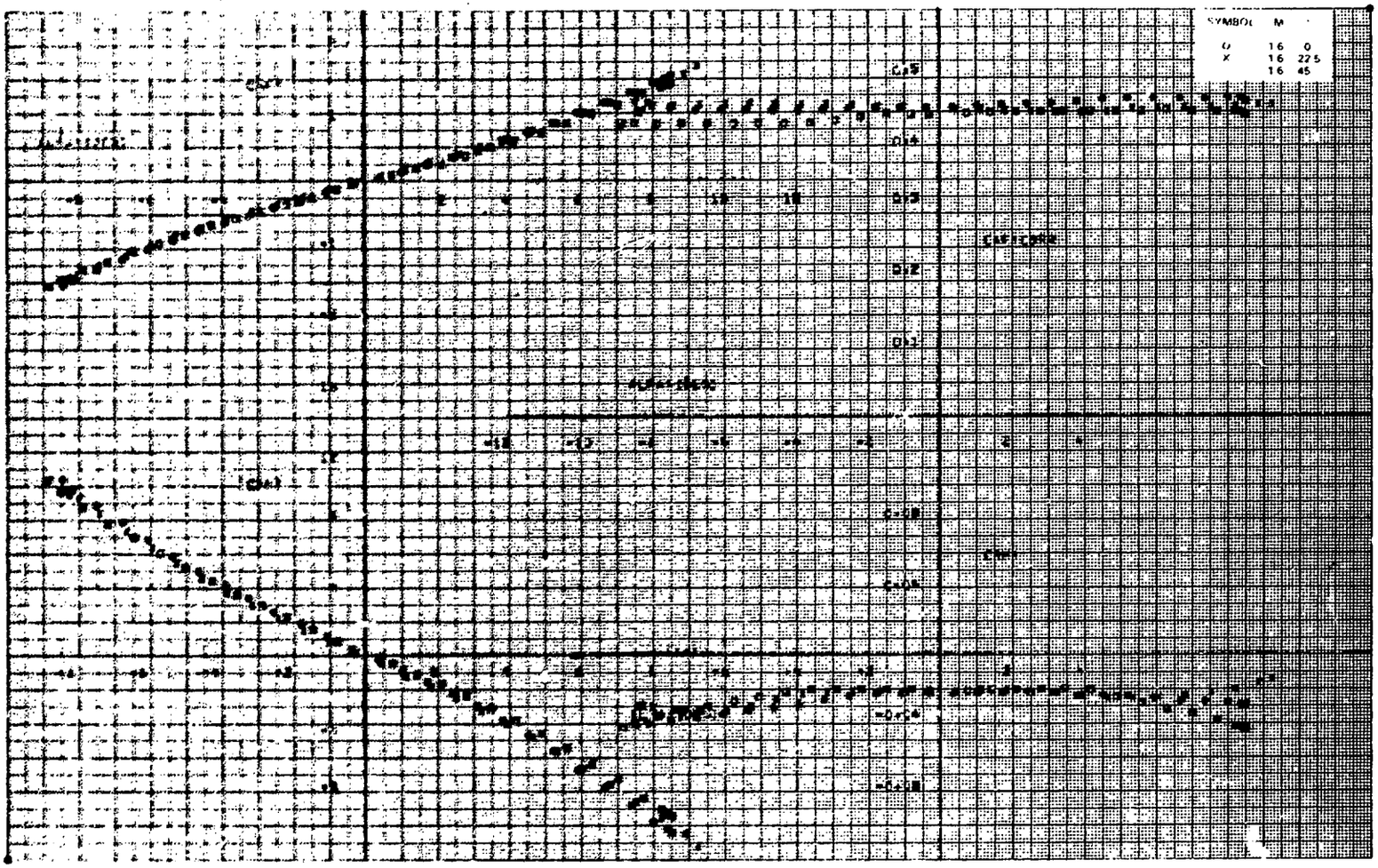


Figure 13d. Continued.


SYMBOL M δ
O 12 0
X 12 22.5
12 22.5


SYMBOL M ◇
O 12 0
▽ 12 22.5
12 22.5



[illegible] coefficients, CR/B = 1.7[illegible], [illegible] = 0 deg., B/2D = 0.535, M = 1.6.

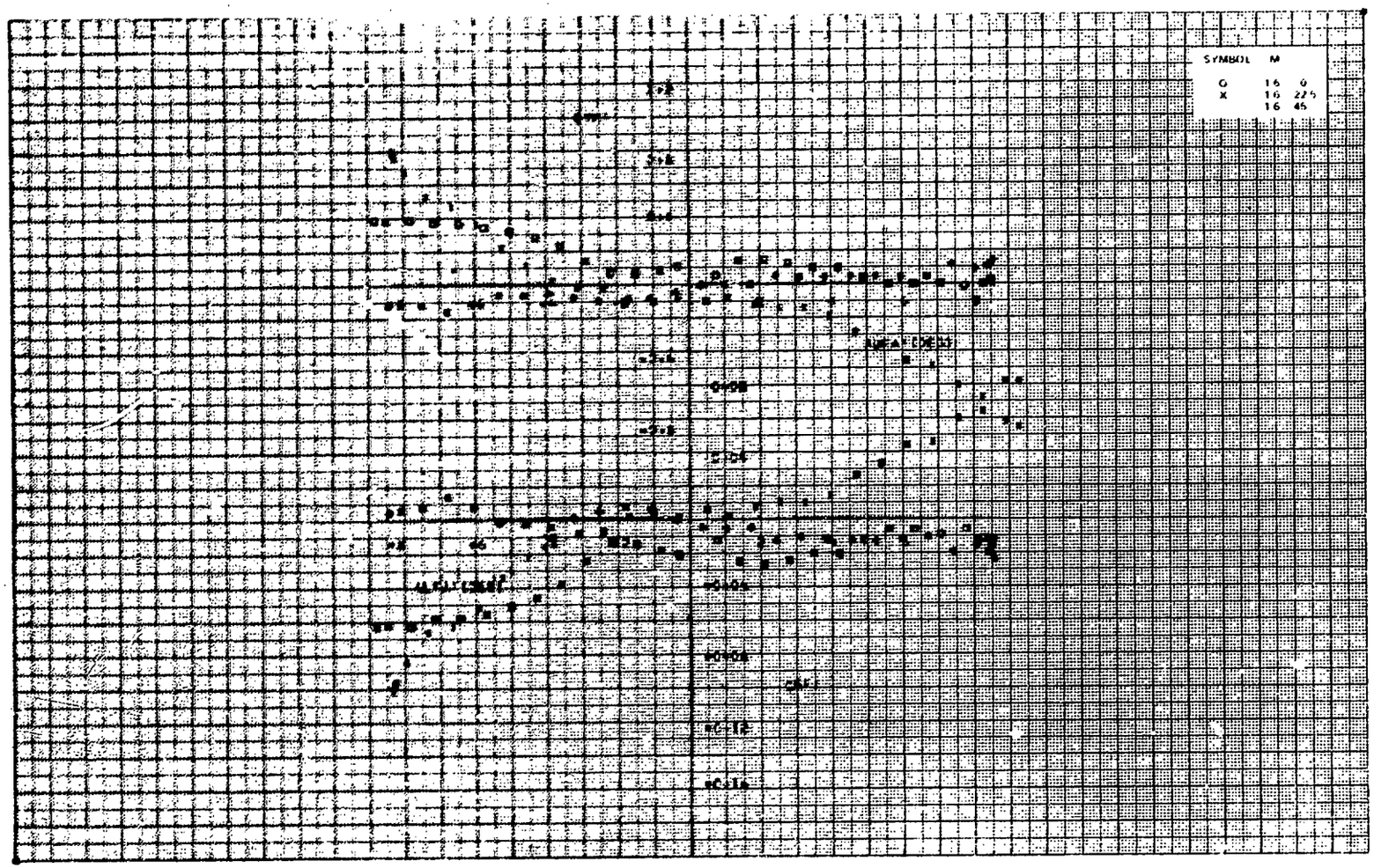


Figure 13e. Continued.

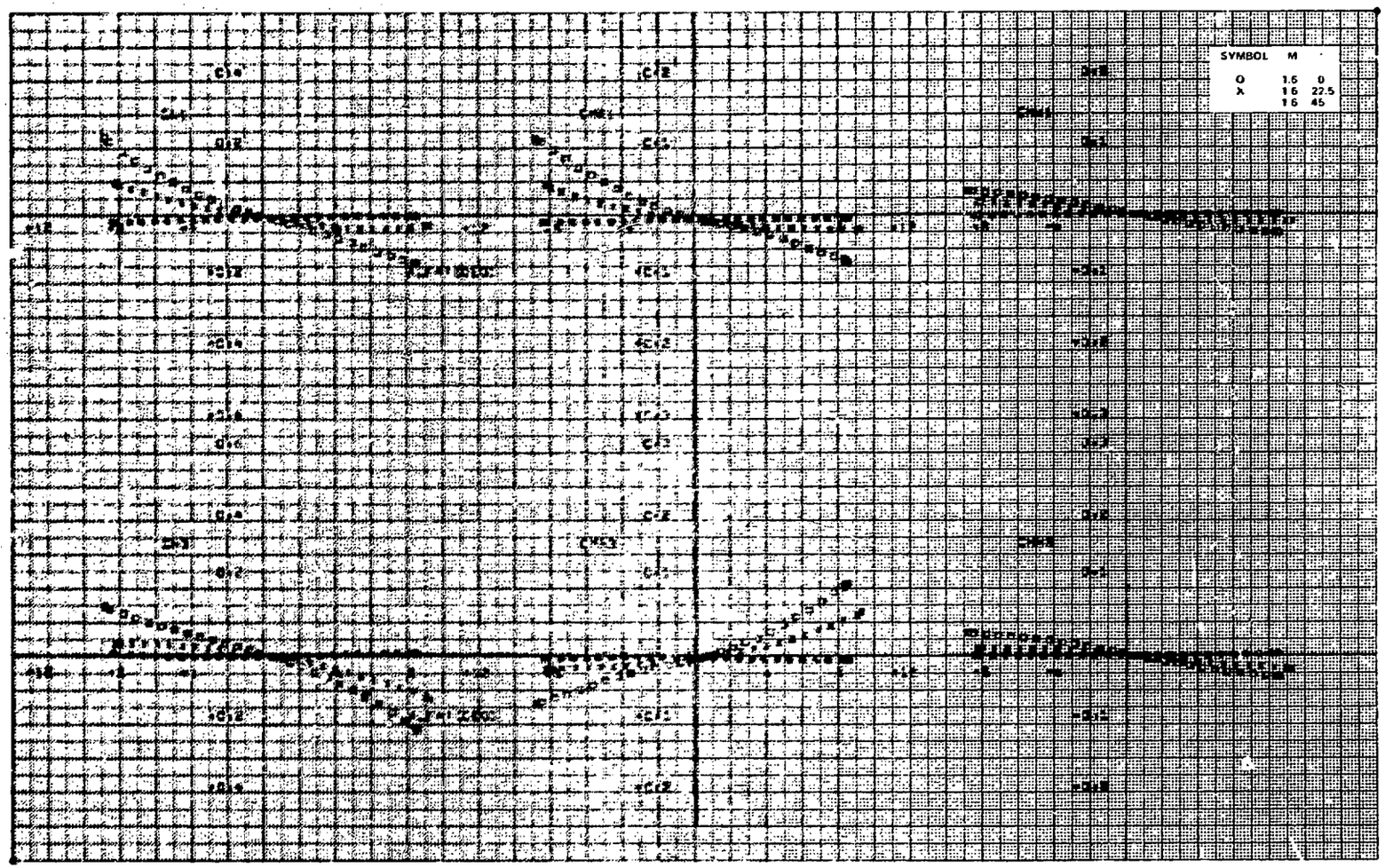


Figure 13. (Concluded)

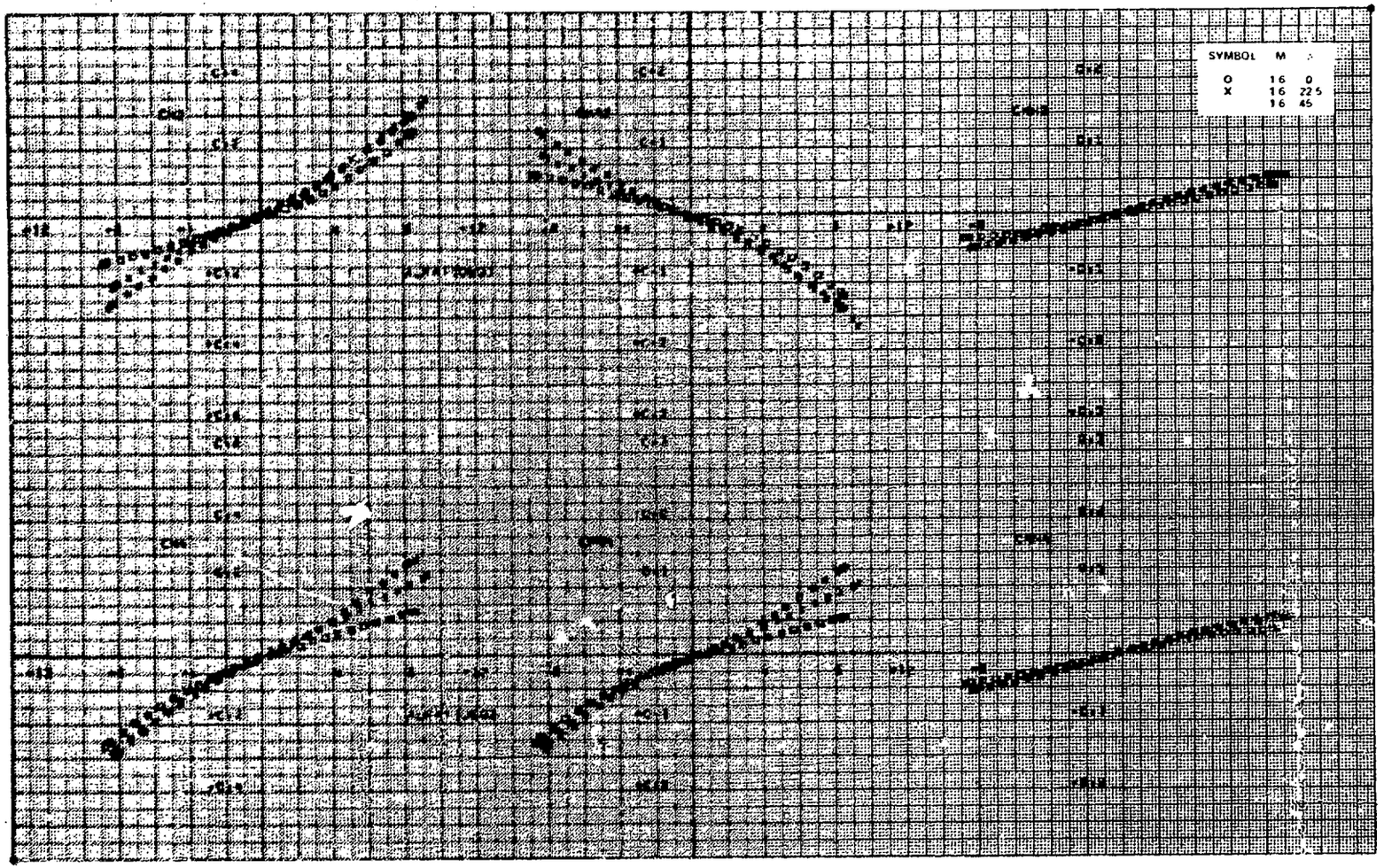


Figure 13e. Concluded.

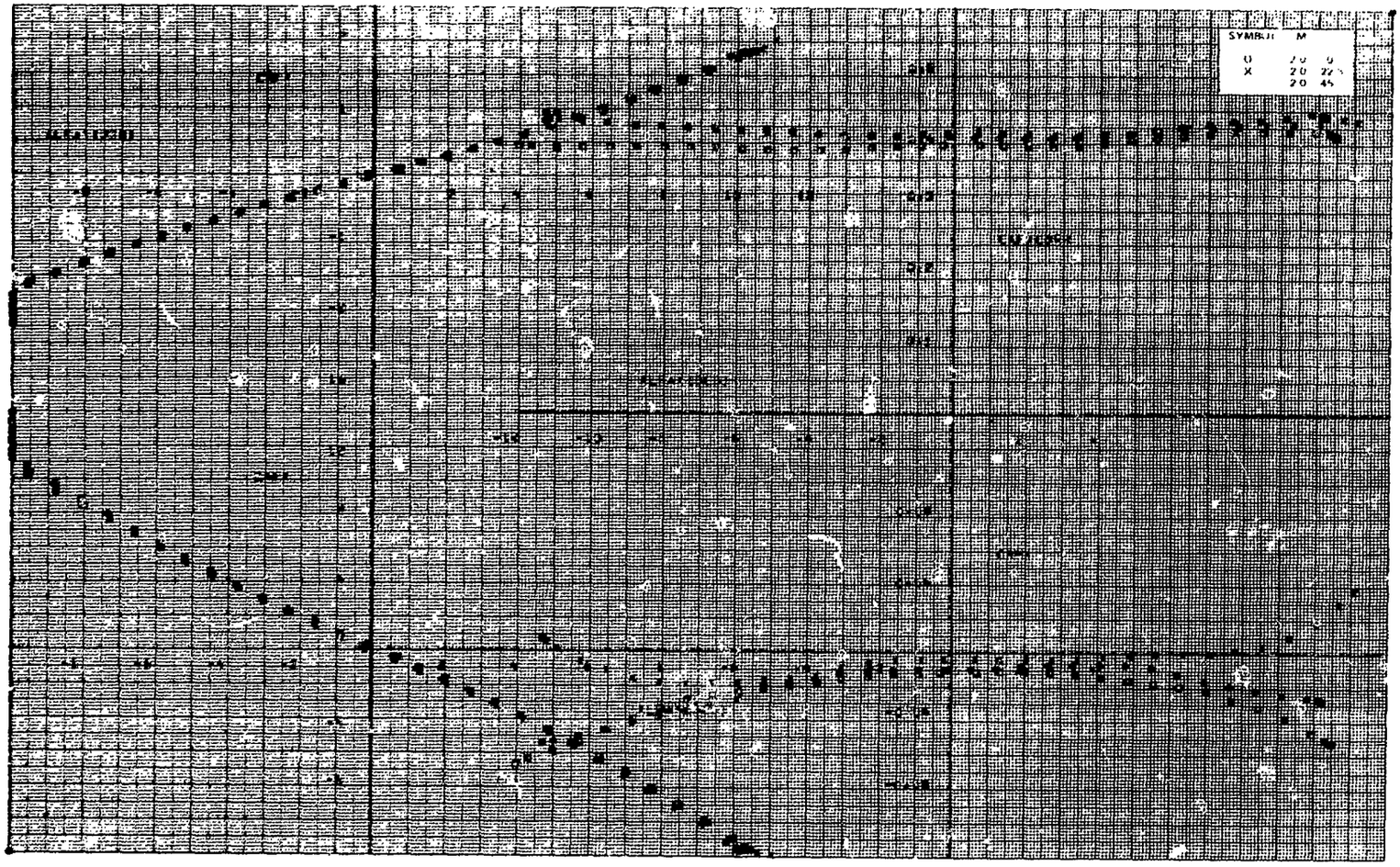


Figure 13f. Aerodynamic stability coefficients, CR/D = 1.75, Λ = 0 deg, B/2D = 0.535, M_∞ = 2.0.

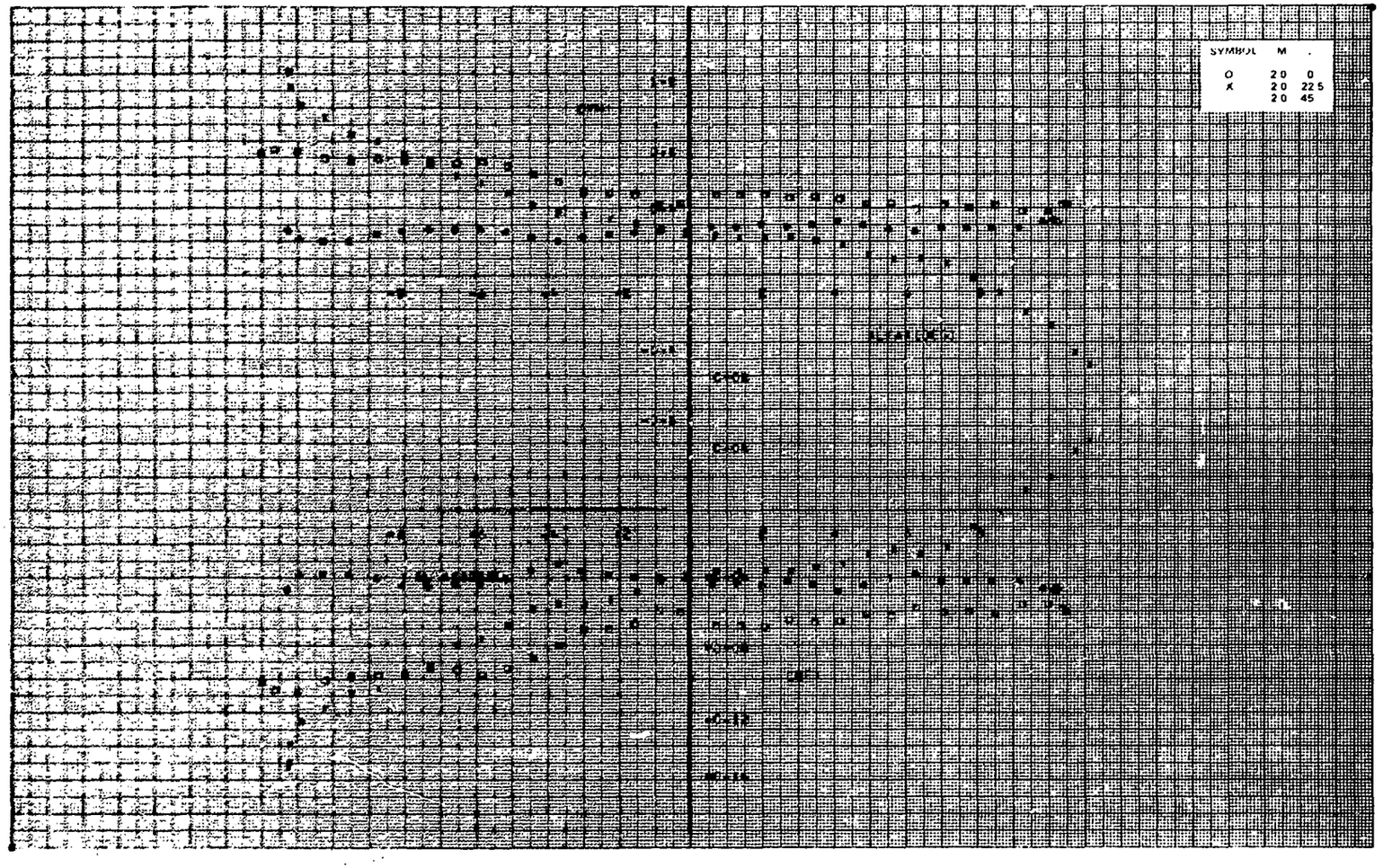


Figure 13f. Continued.

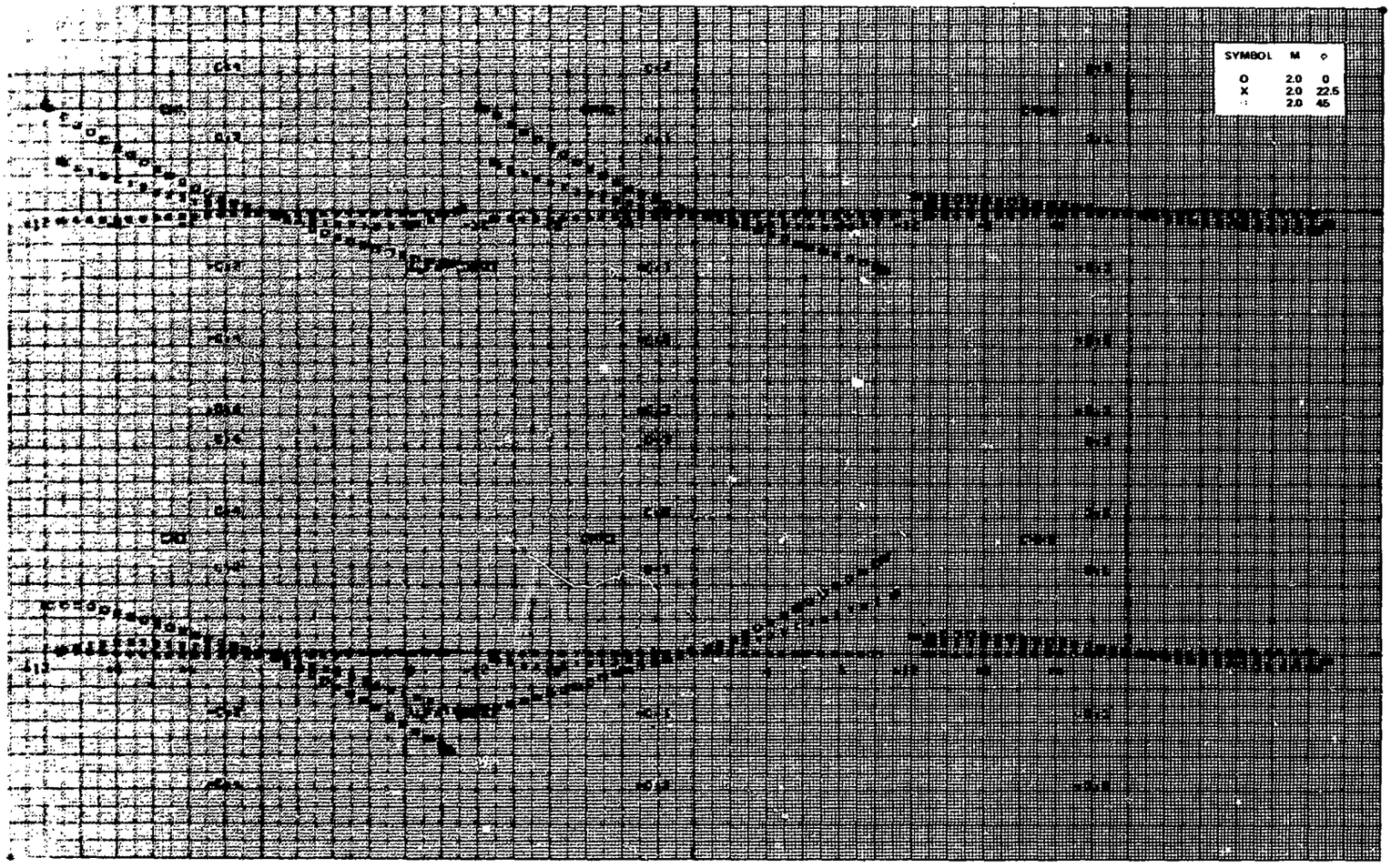


Figure 13f. Continued.

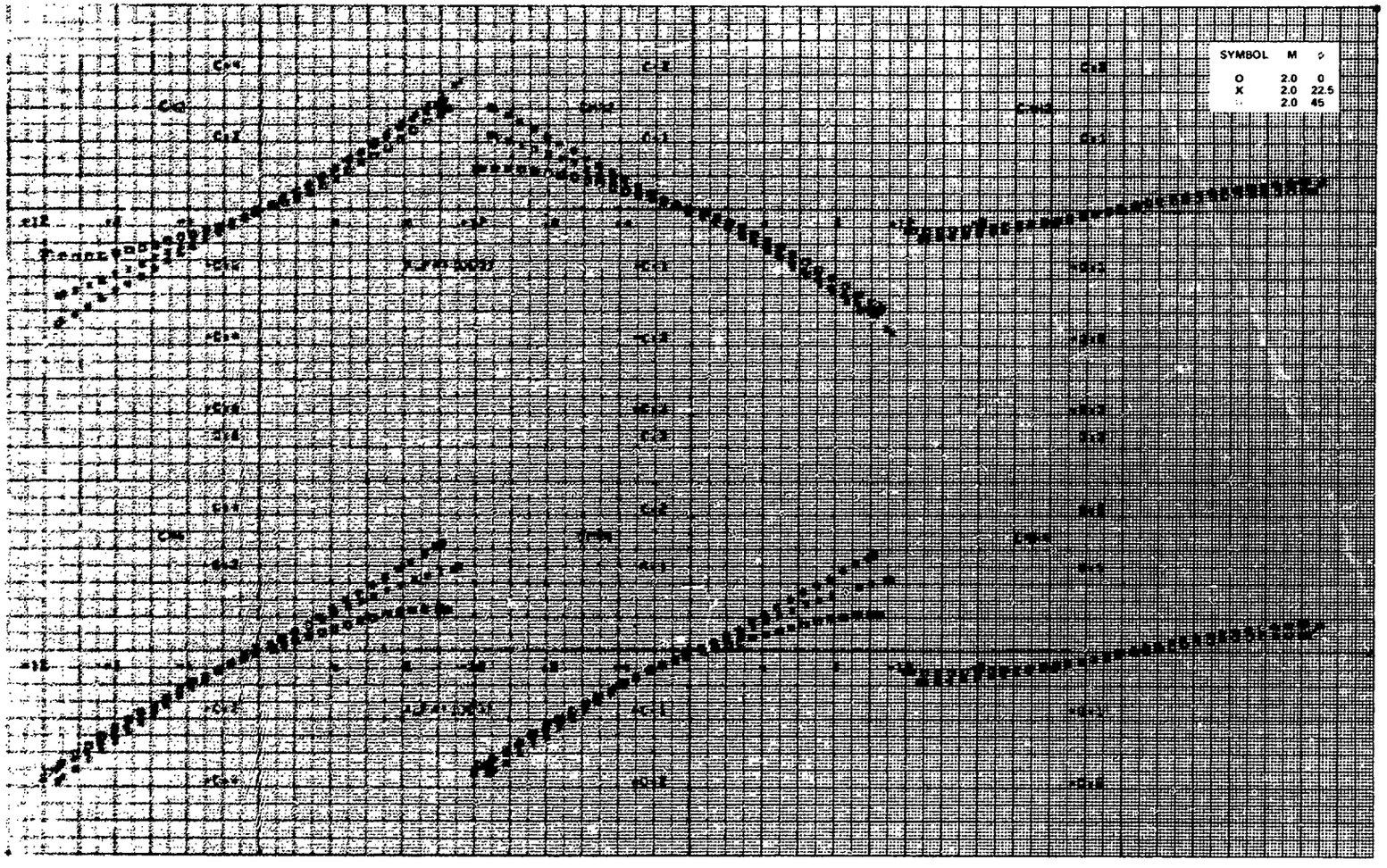


Figure 13f. Concluded.

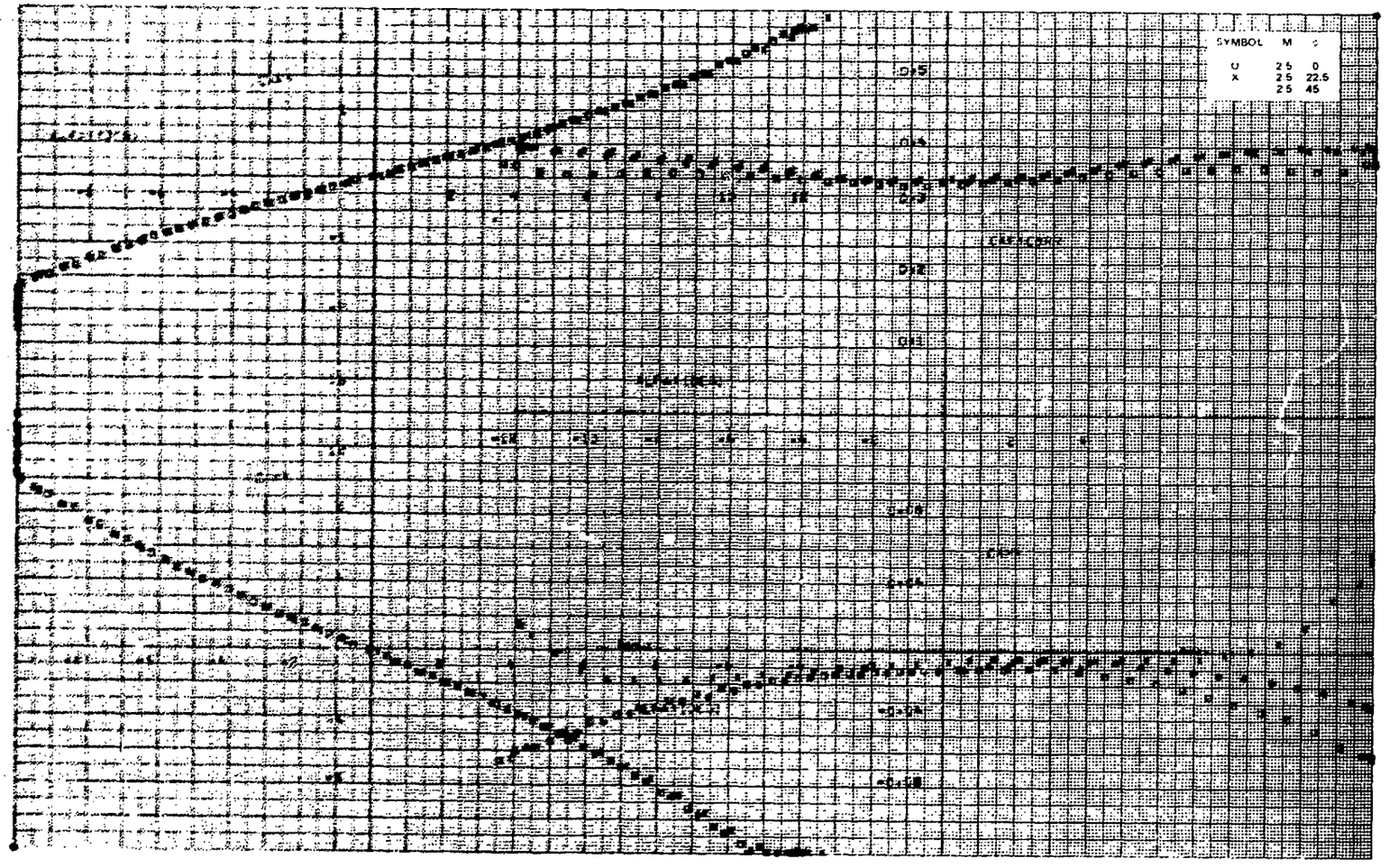


Figure 100. Longitudinal dynamic stability coefficients, CR/D = 1.75, Γ = 0 deg, B/2D = 0.535, M_∞ = 2.5.

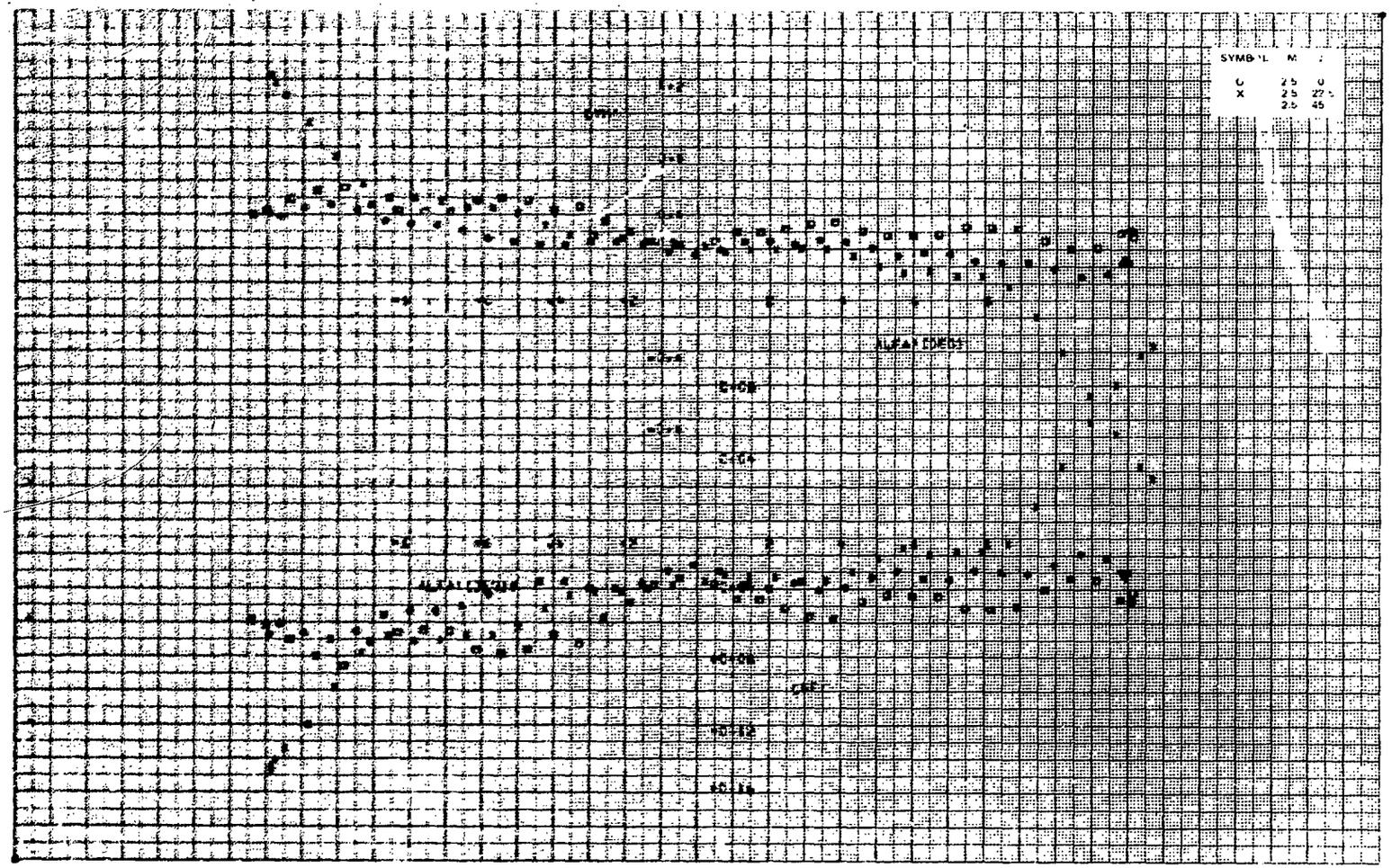


Figure 13g. Continued.

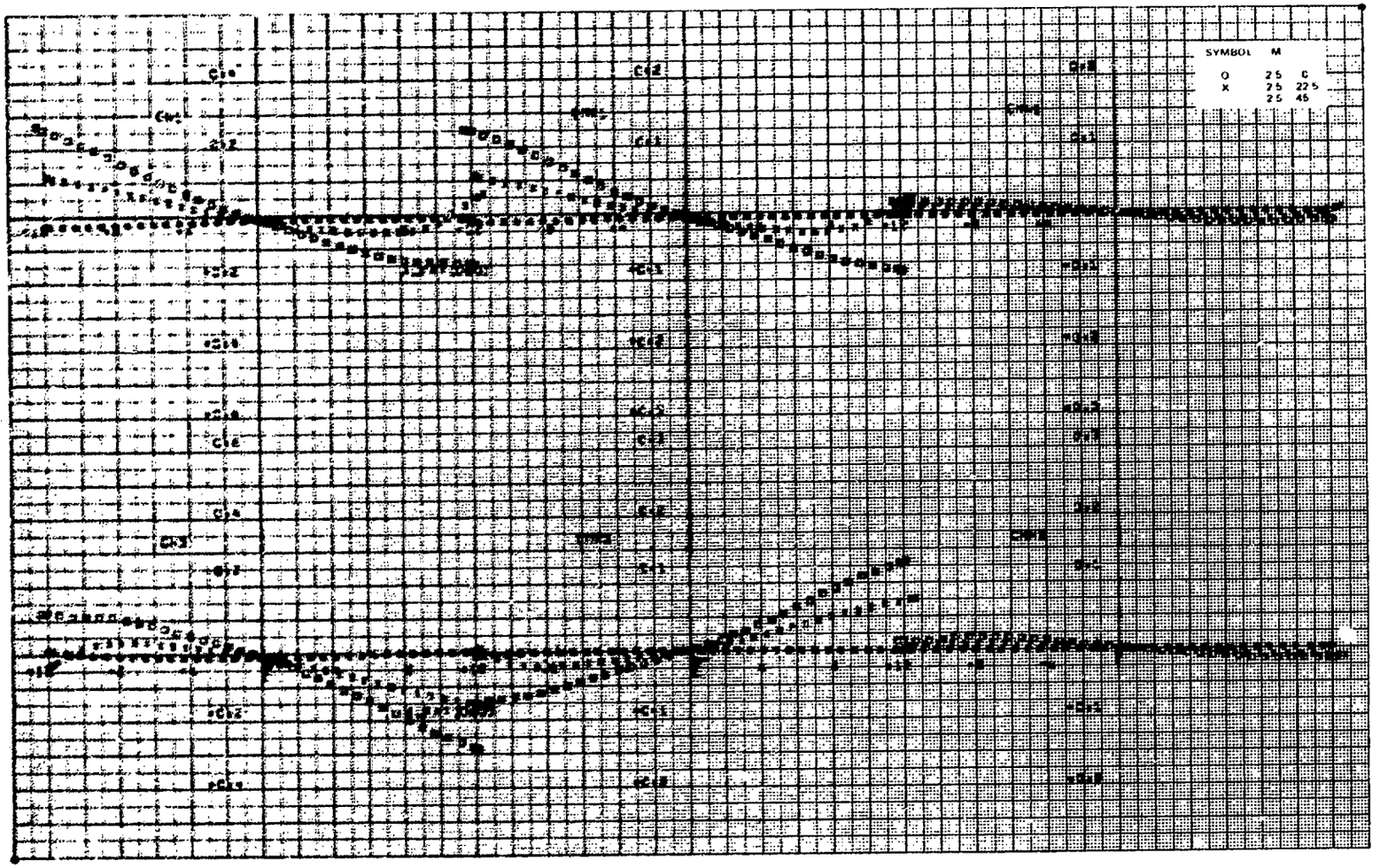


Figure 13g. Continued.

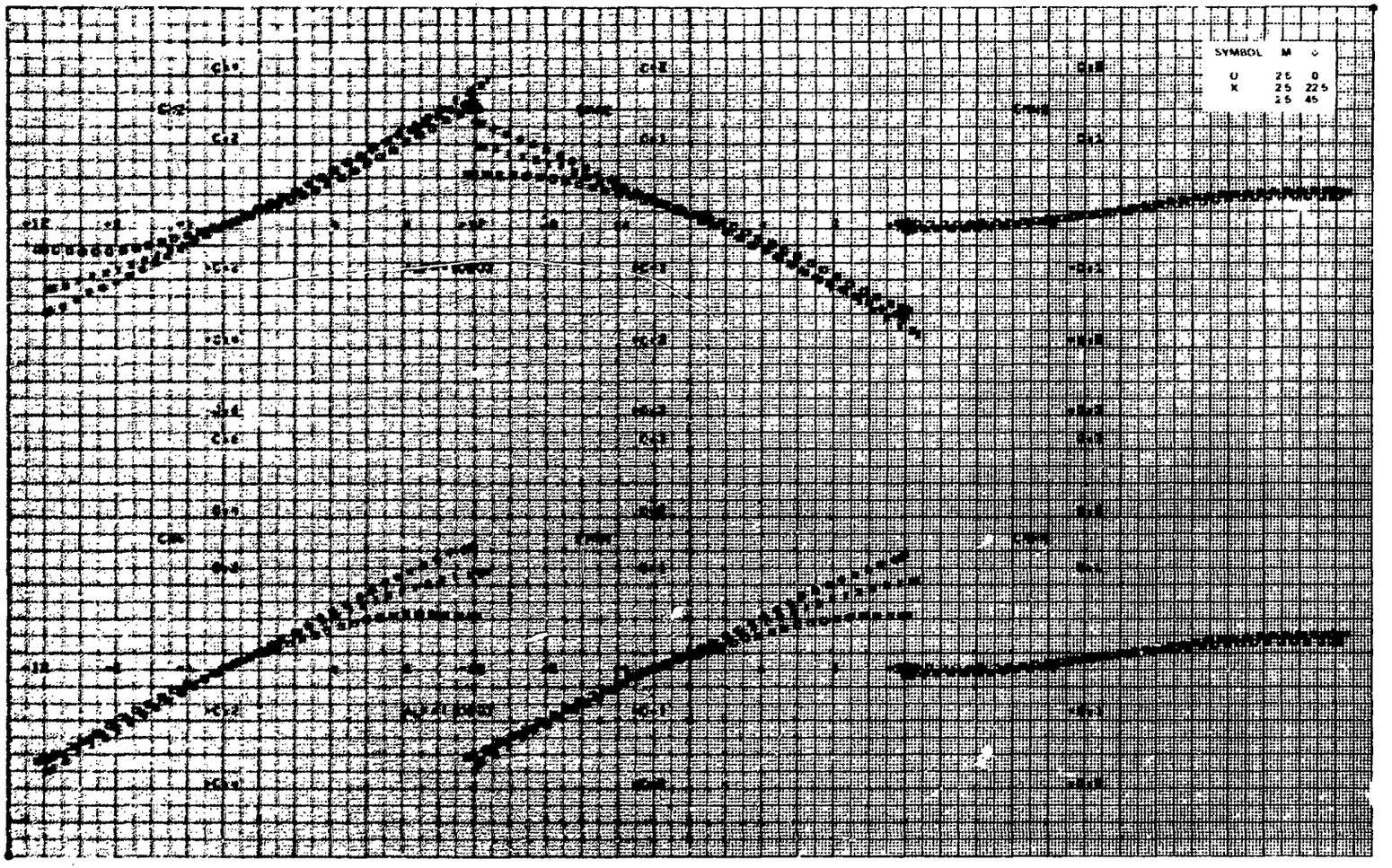


Figure 13g. Concluded.

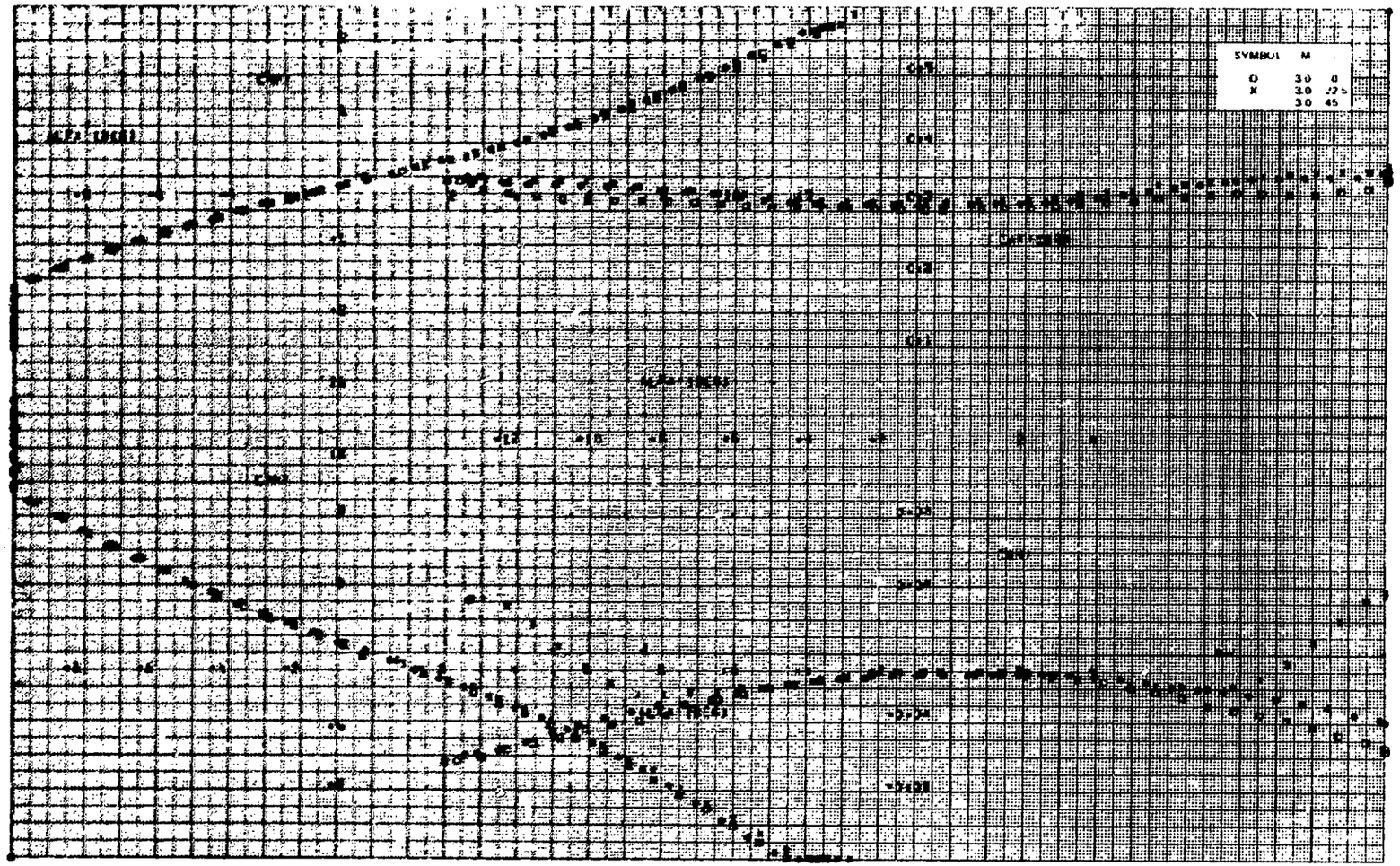


Figure 13h. Aerodynamic stability coefficients, CR/D = 1.75, Λ = 0 deg, B/2D = 0.535, M_∞ = 3.0.

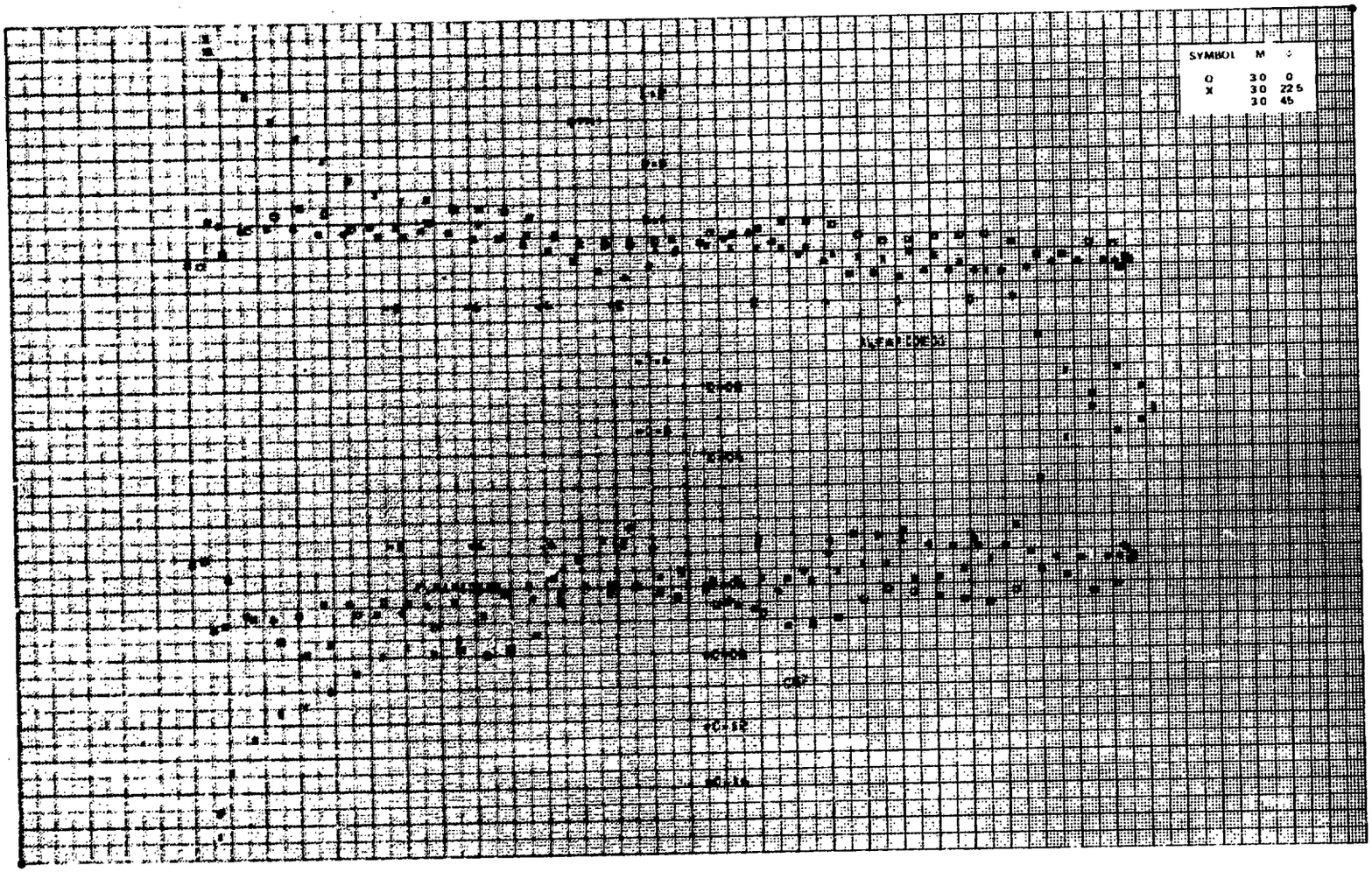


Figure 13h. Continued.

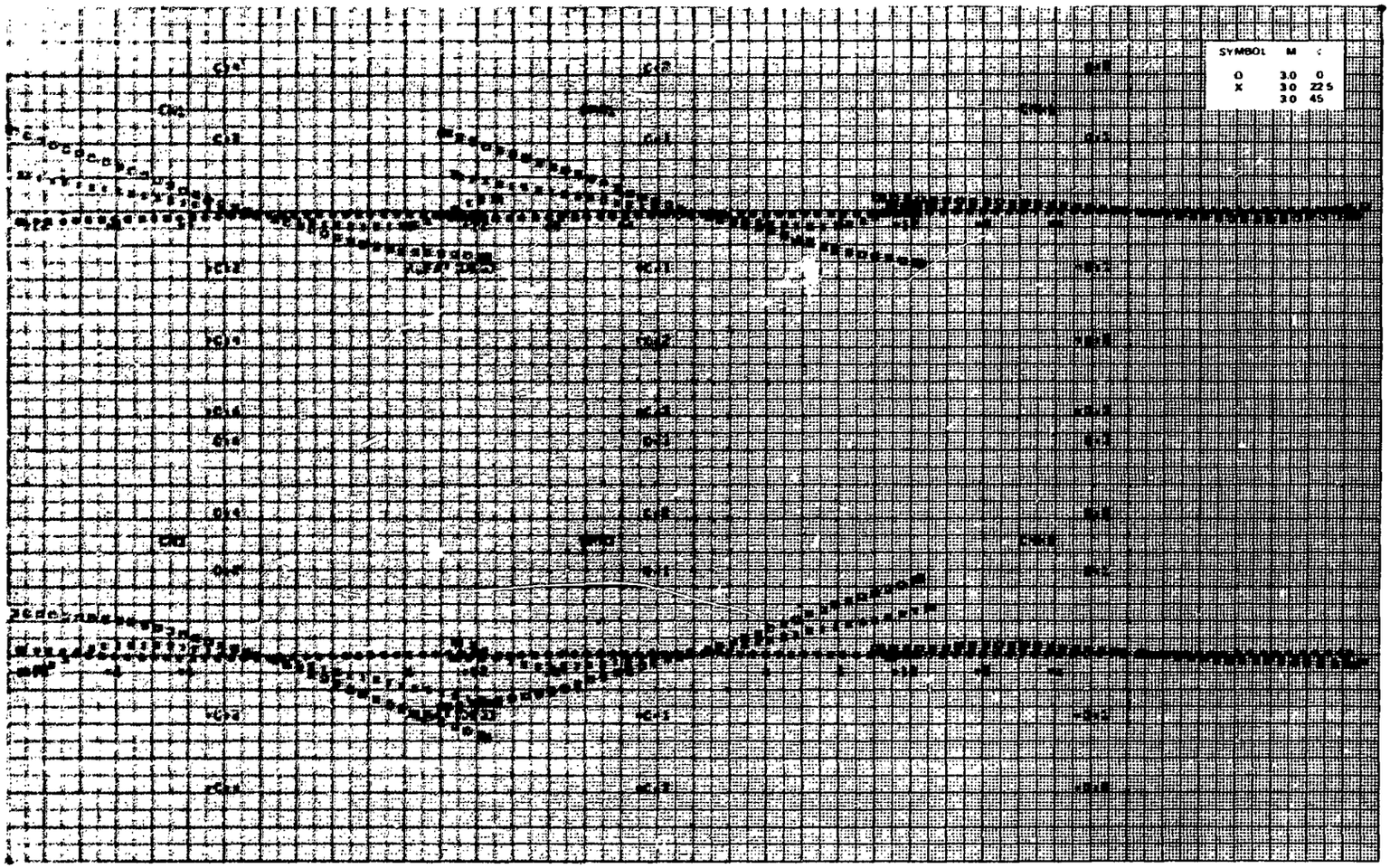


Figure 13h. Continued.

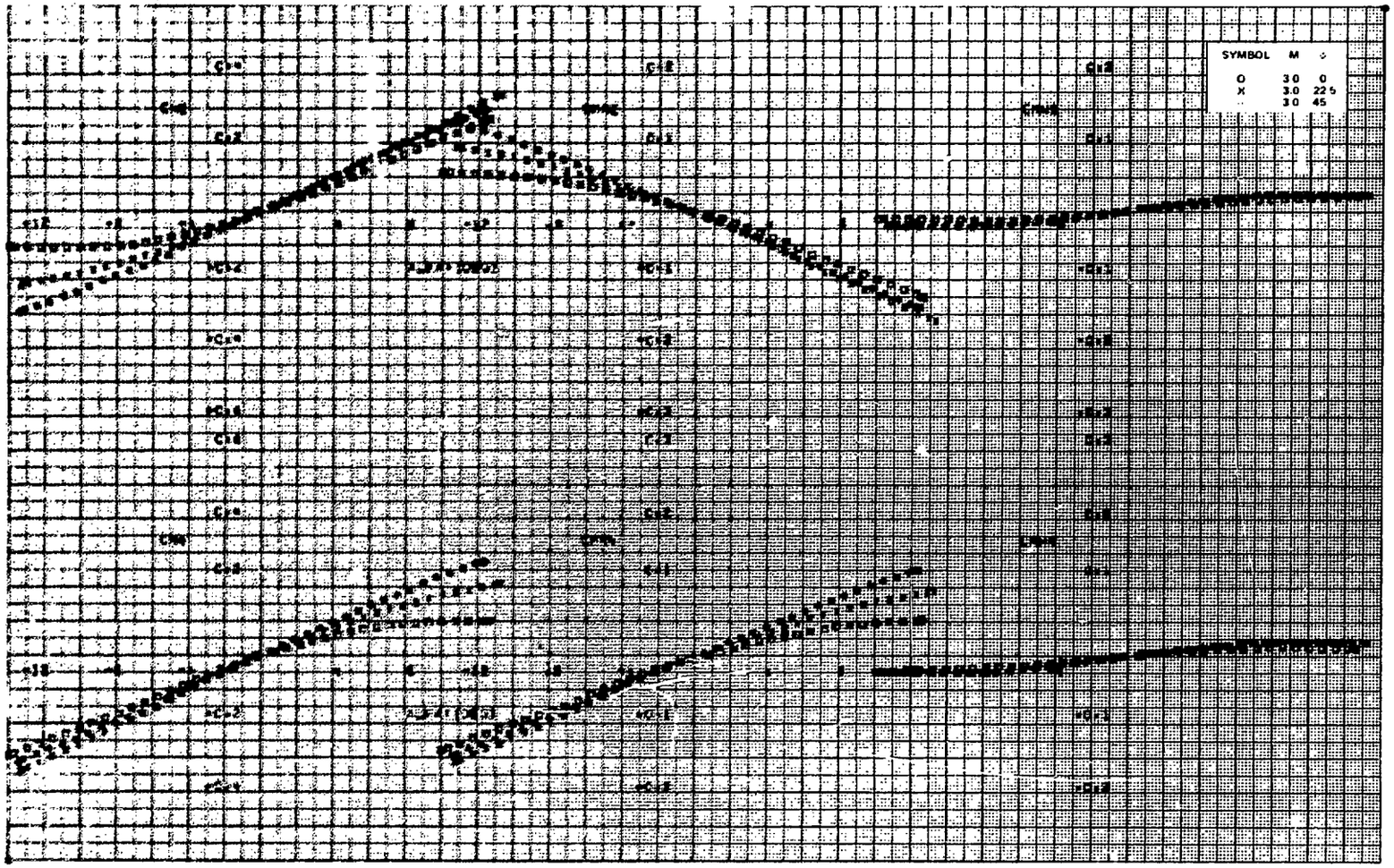


Figure 13h. Concluded.

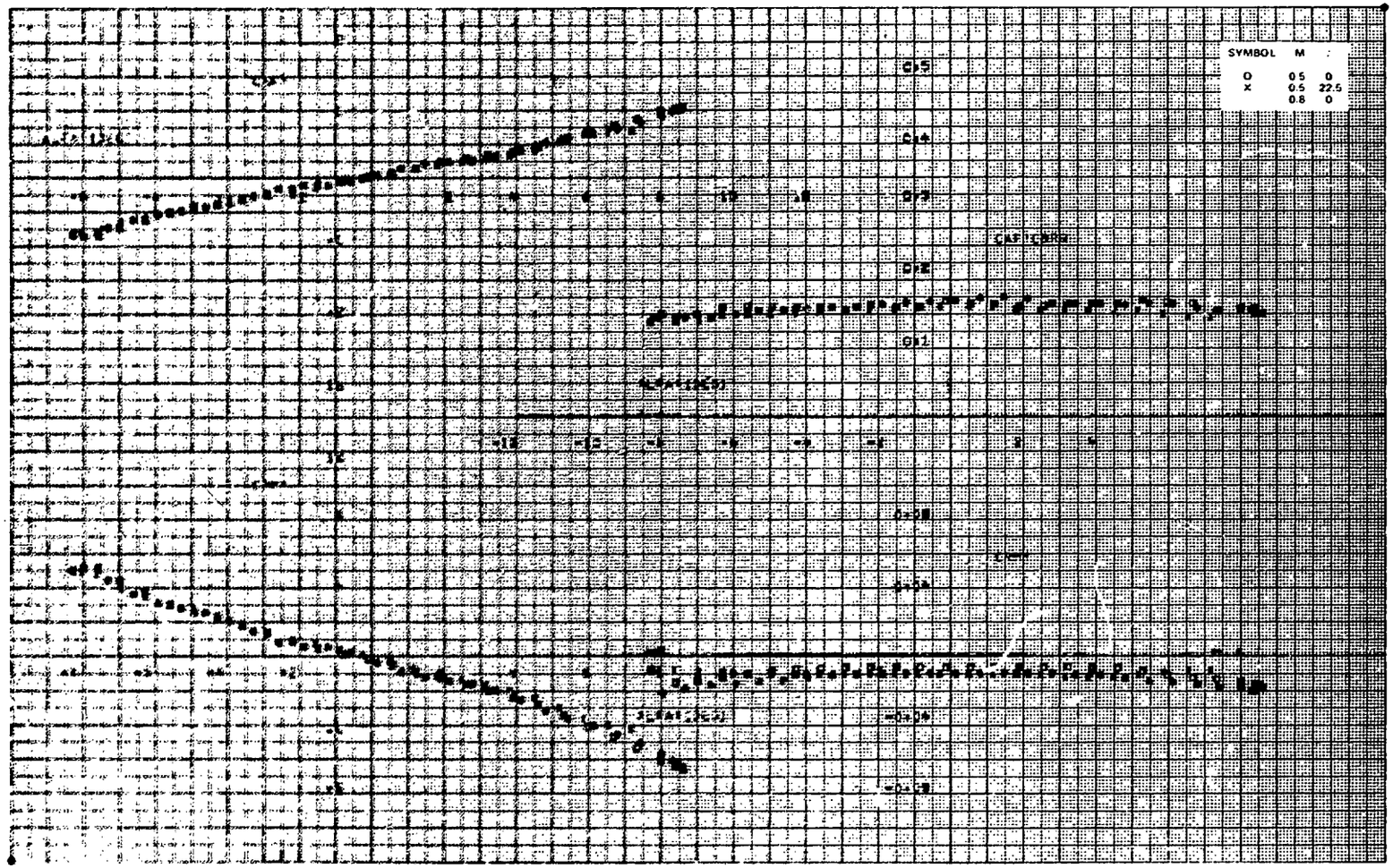


Figure [illegible] Aerodynamic stability coefficients, CR/D = 1.75, γ = 0 deg, B/2D = 0.3475, M_∞ = 0.5, 0.8.

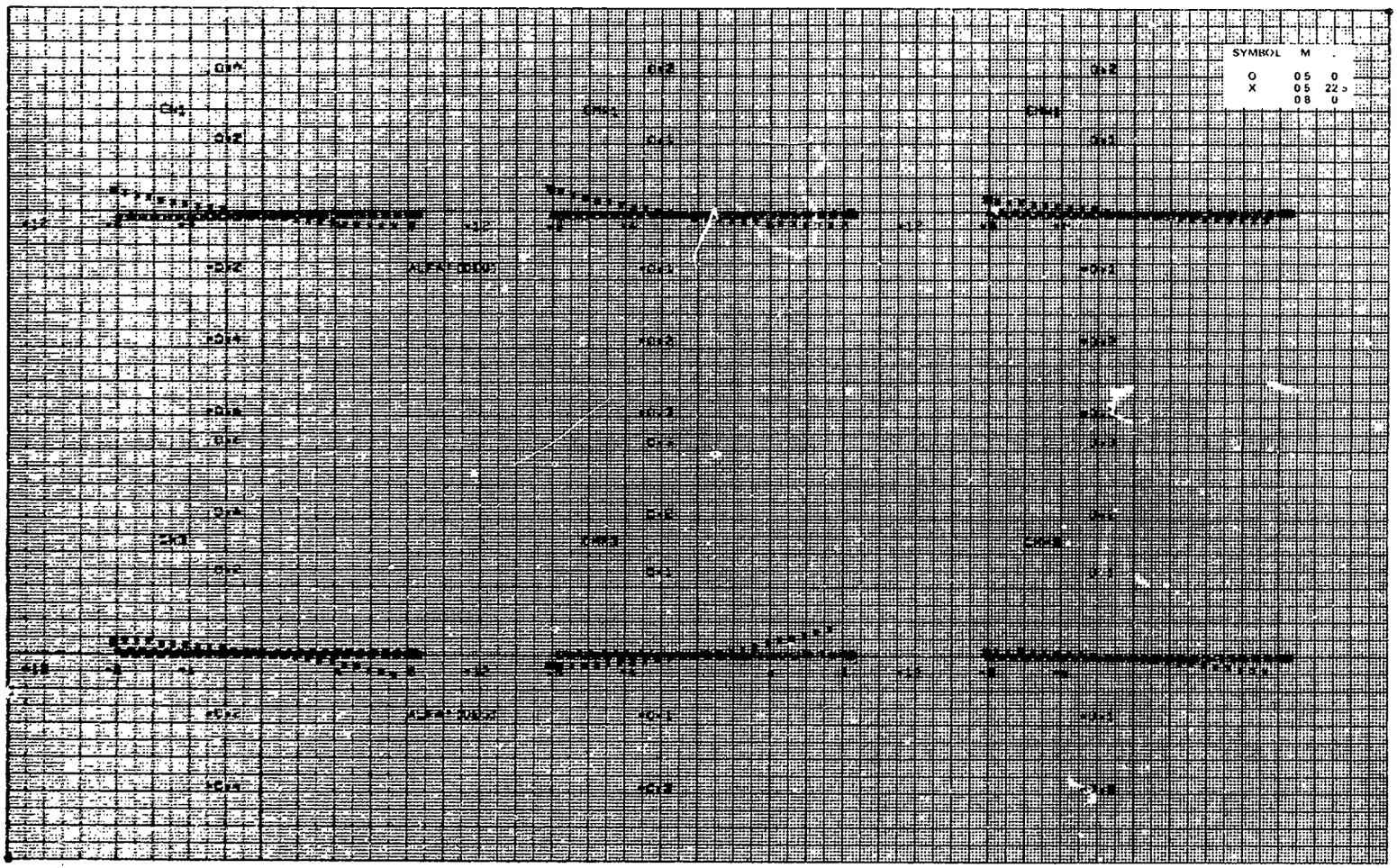


Figure 14a. Continued.

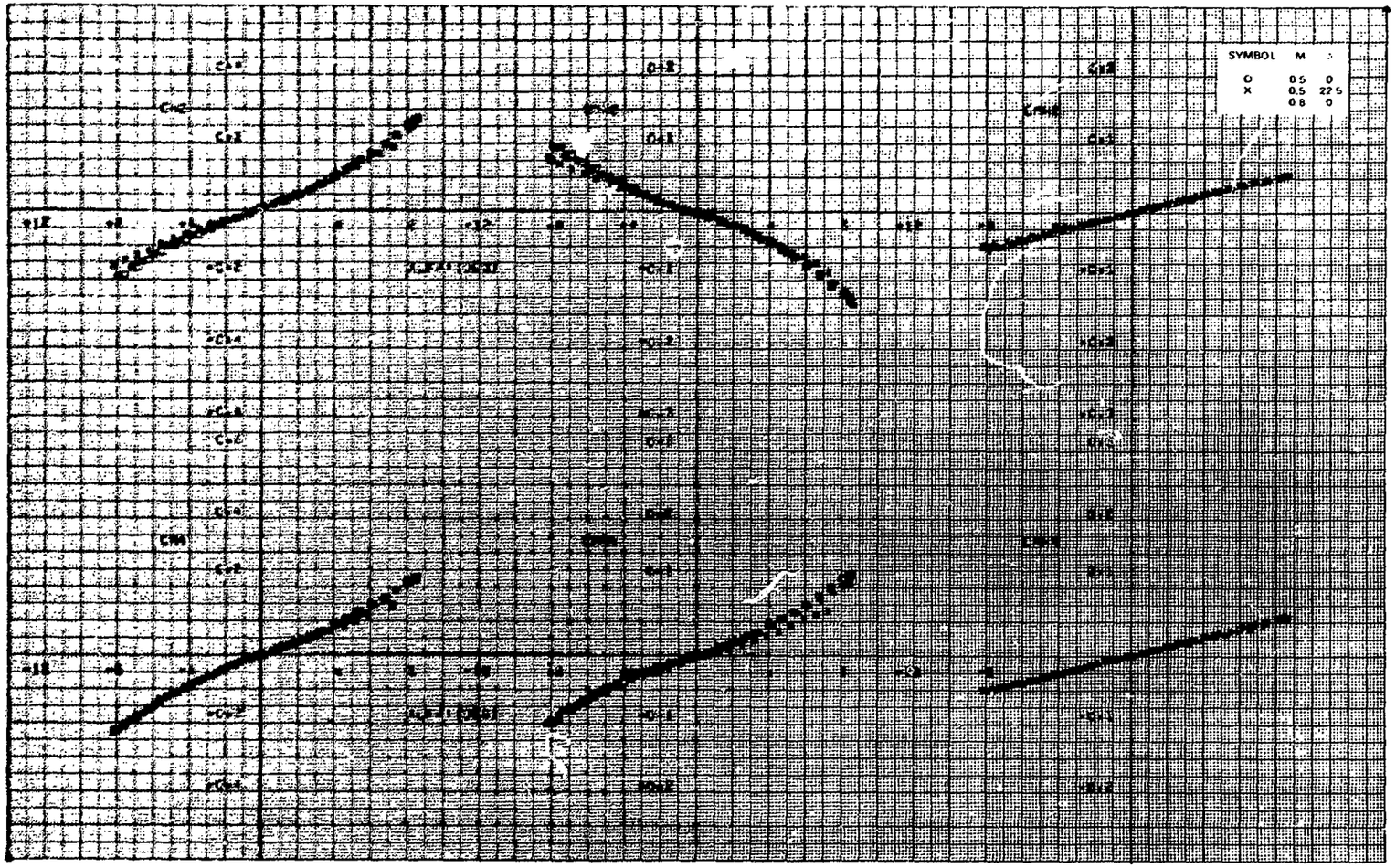


Figure 14a. Concluded.

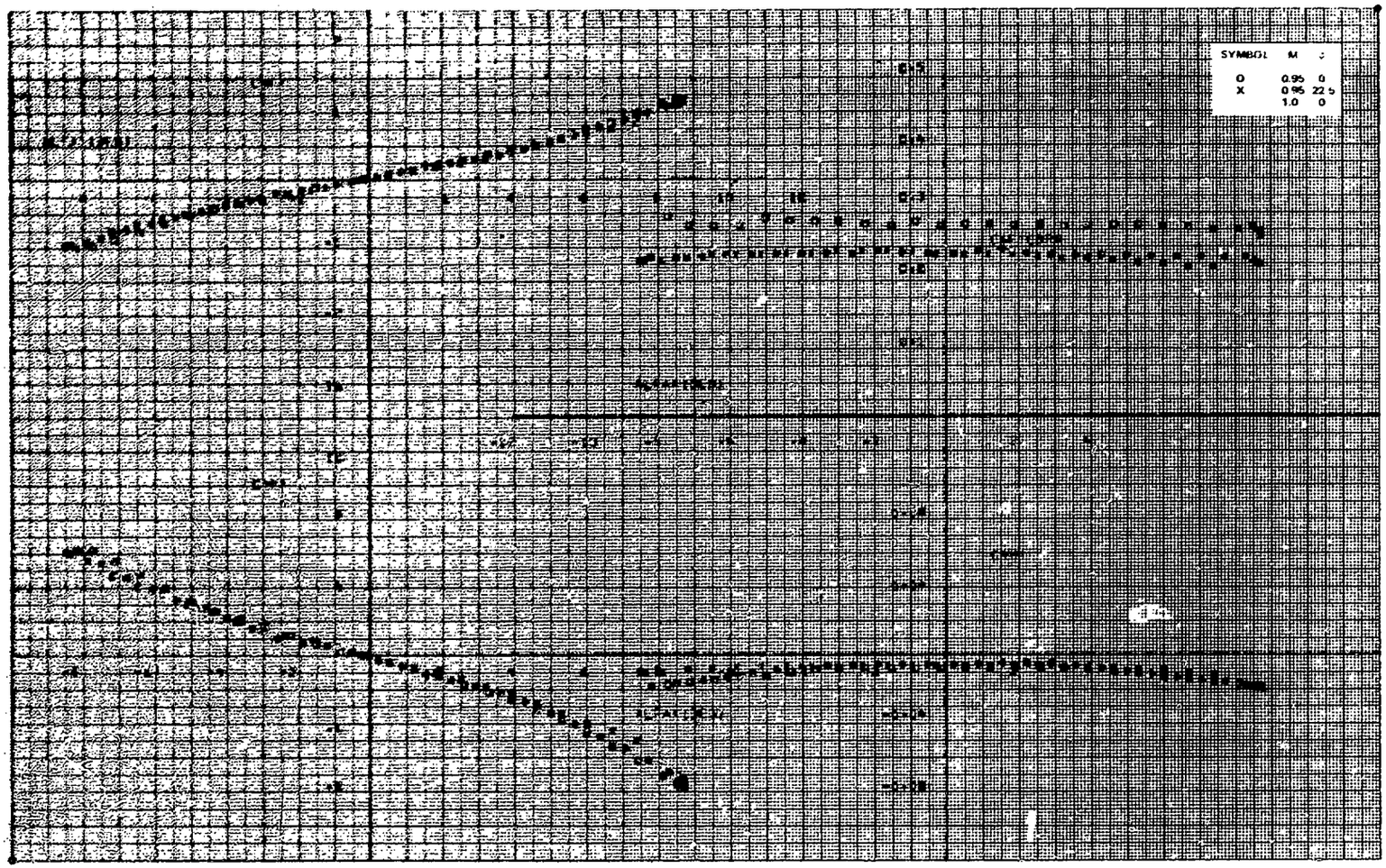


Figure 14b. Aerodynamic stability coefficients, CR/D = 1.75, ' = 0 deg, B/2D = 0.3475, M_∞ = 0.95, 1.0.

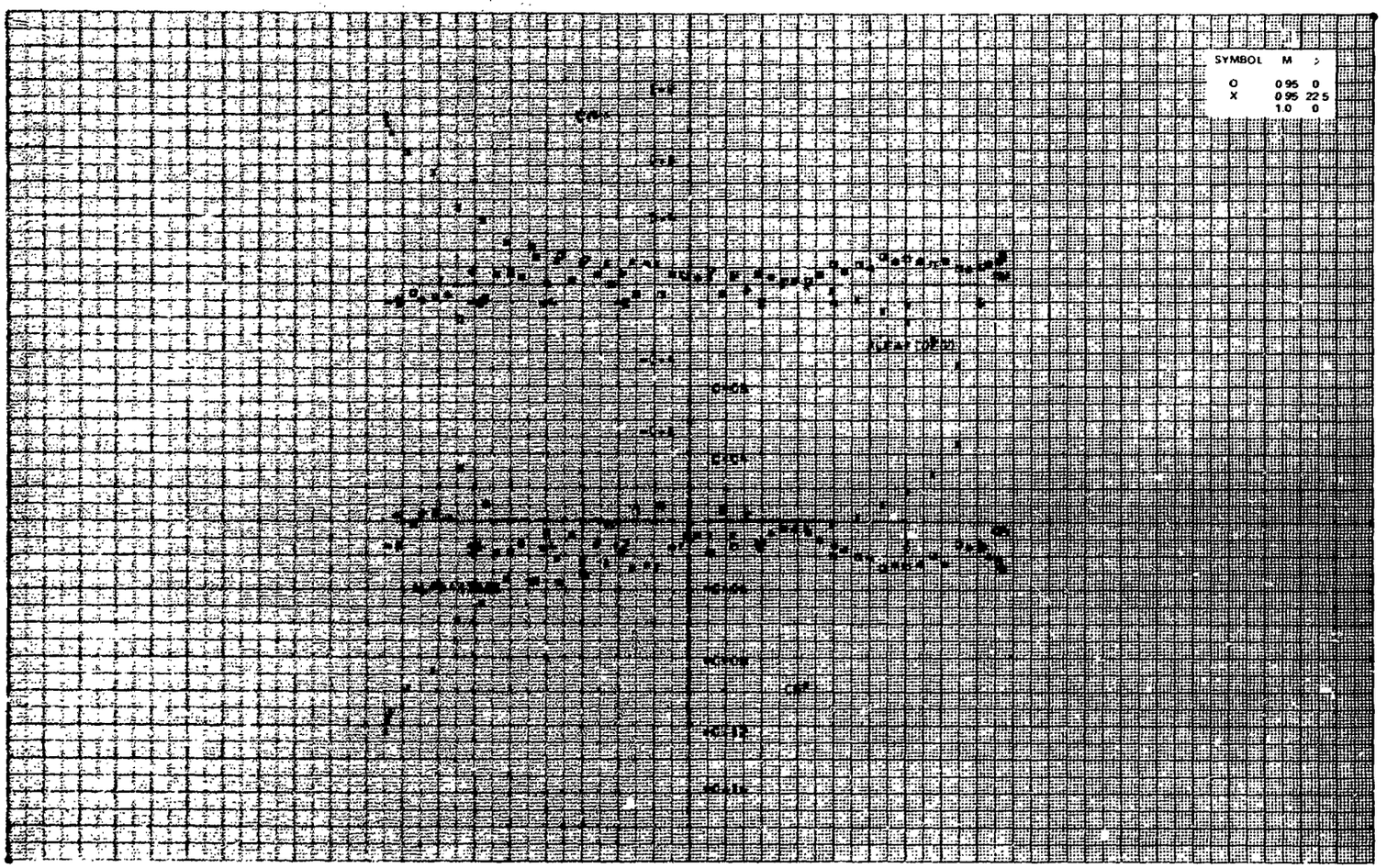


Figure 14b. Continued.

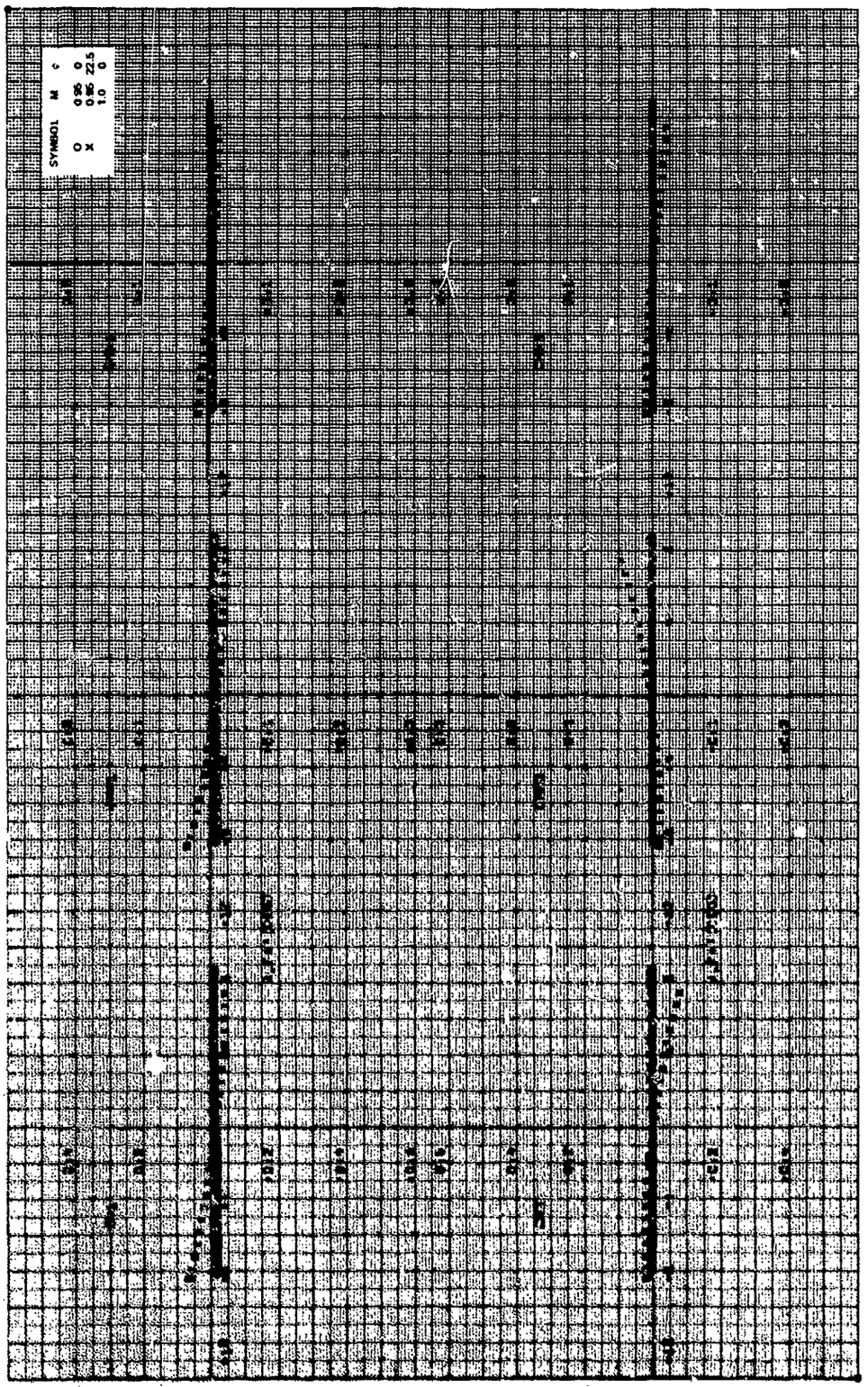


Figure 14b. Continued.

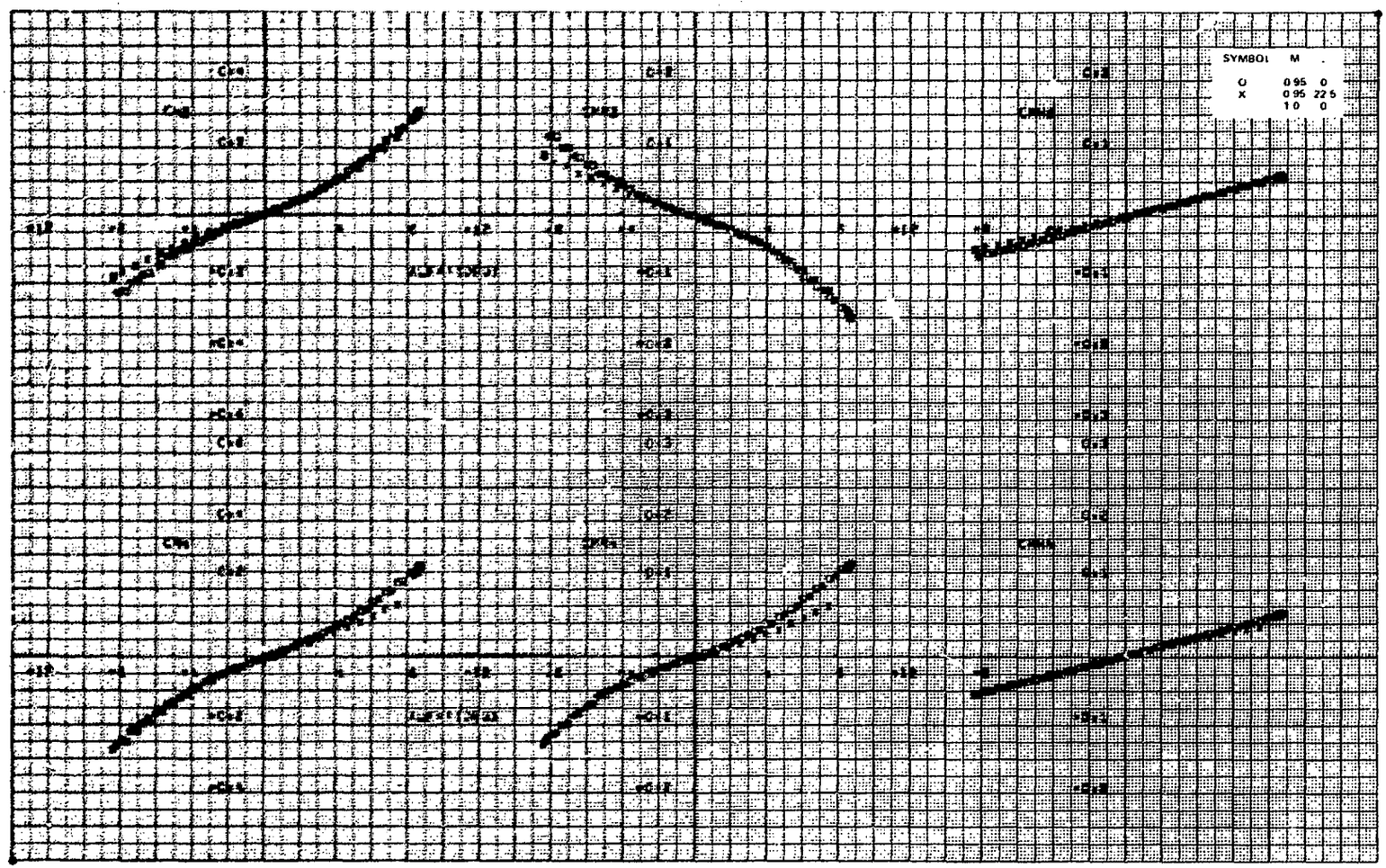


Figure 14b. Concluded.

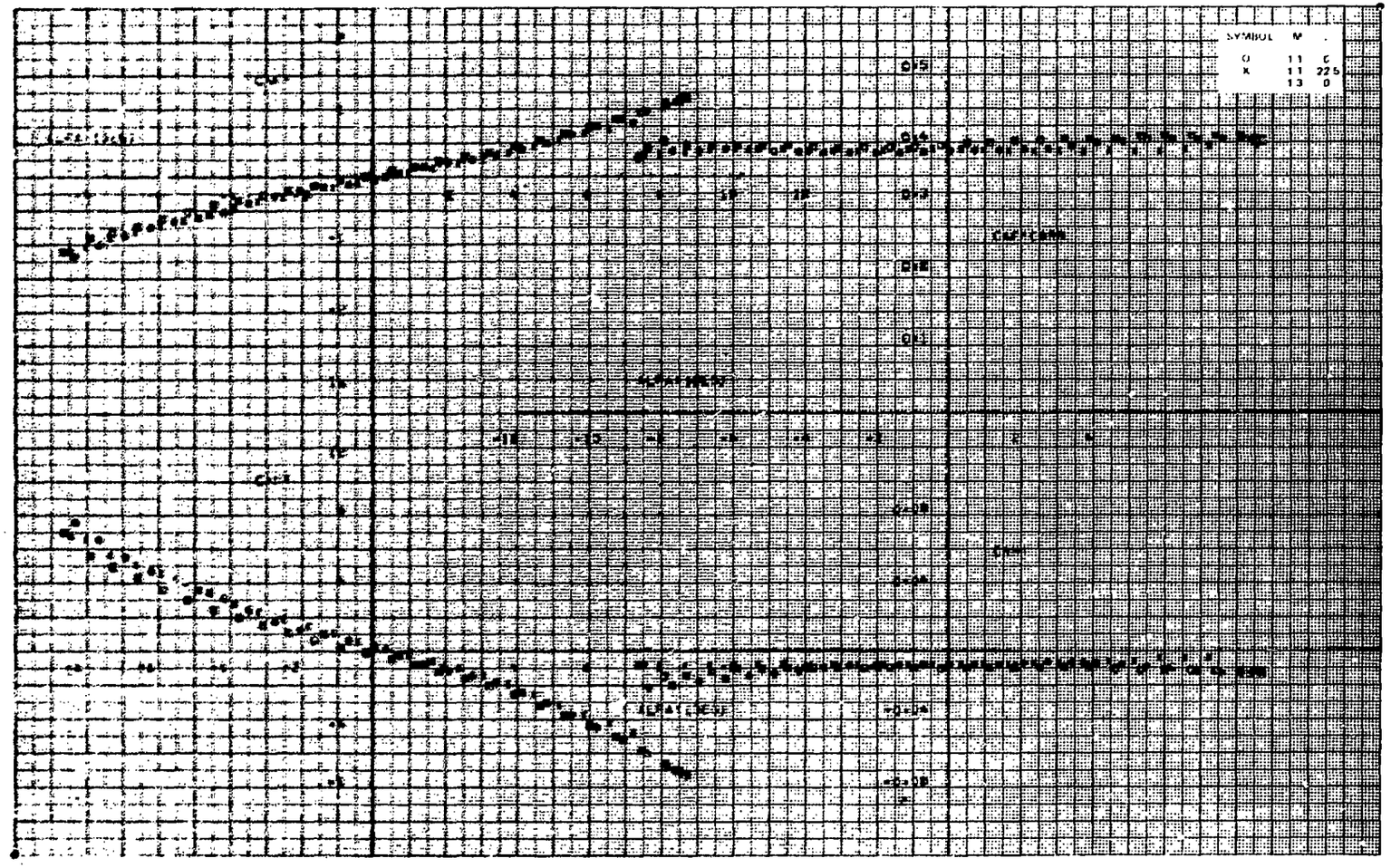


Figure 13. Longitudinal stability coefficients, CR/D = 1.75, α = 0 deg, B/2D = 0.3475, M_∞ = 1.1, 1.3.

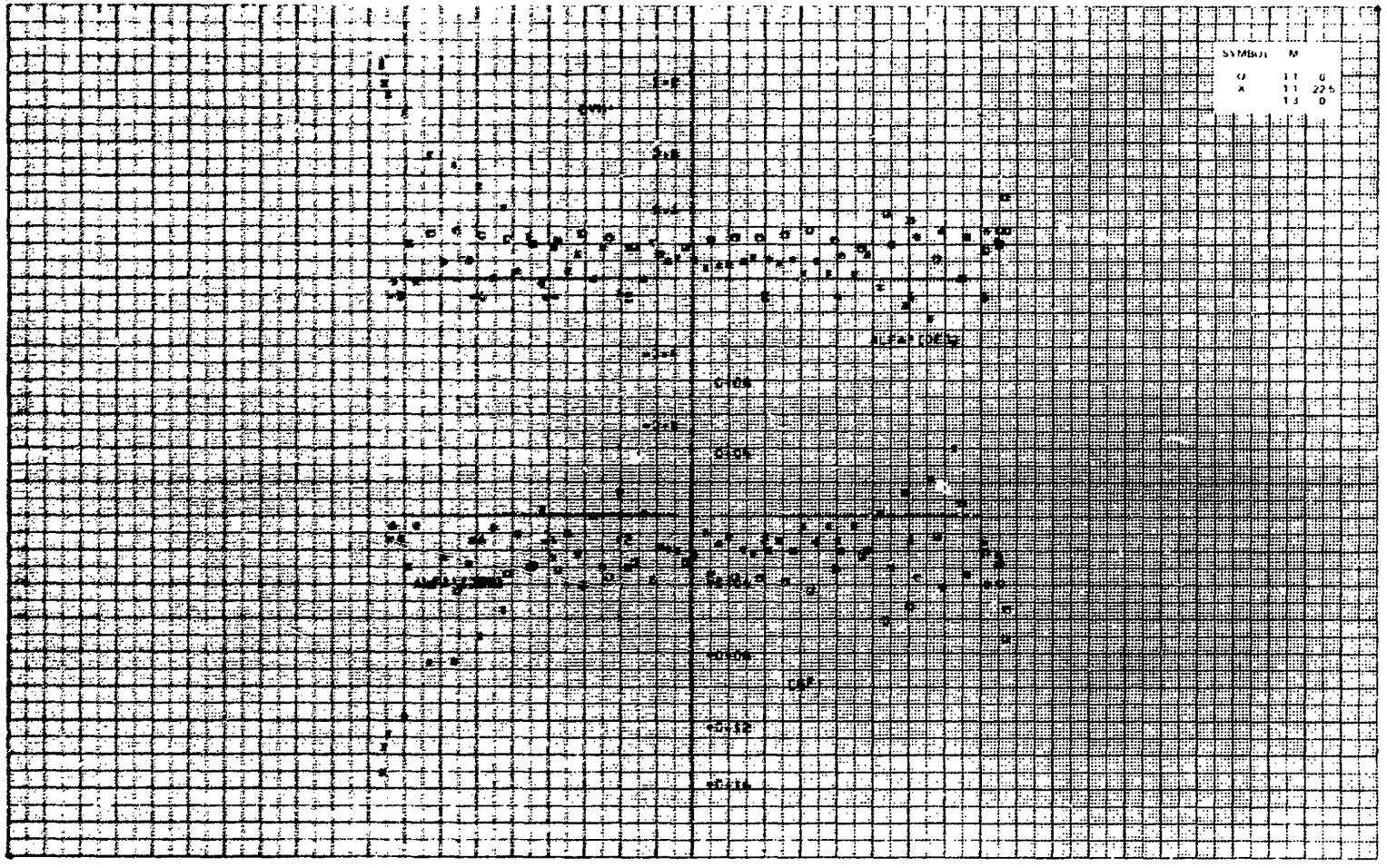


Figure 14c. Continued.

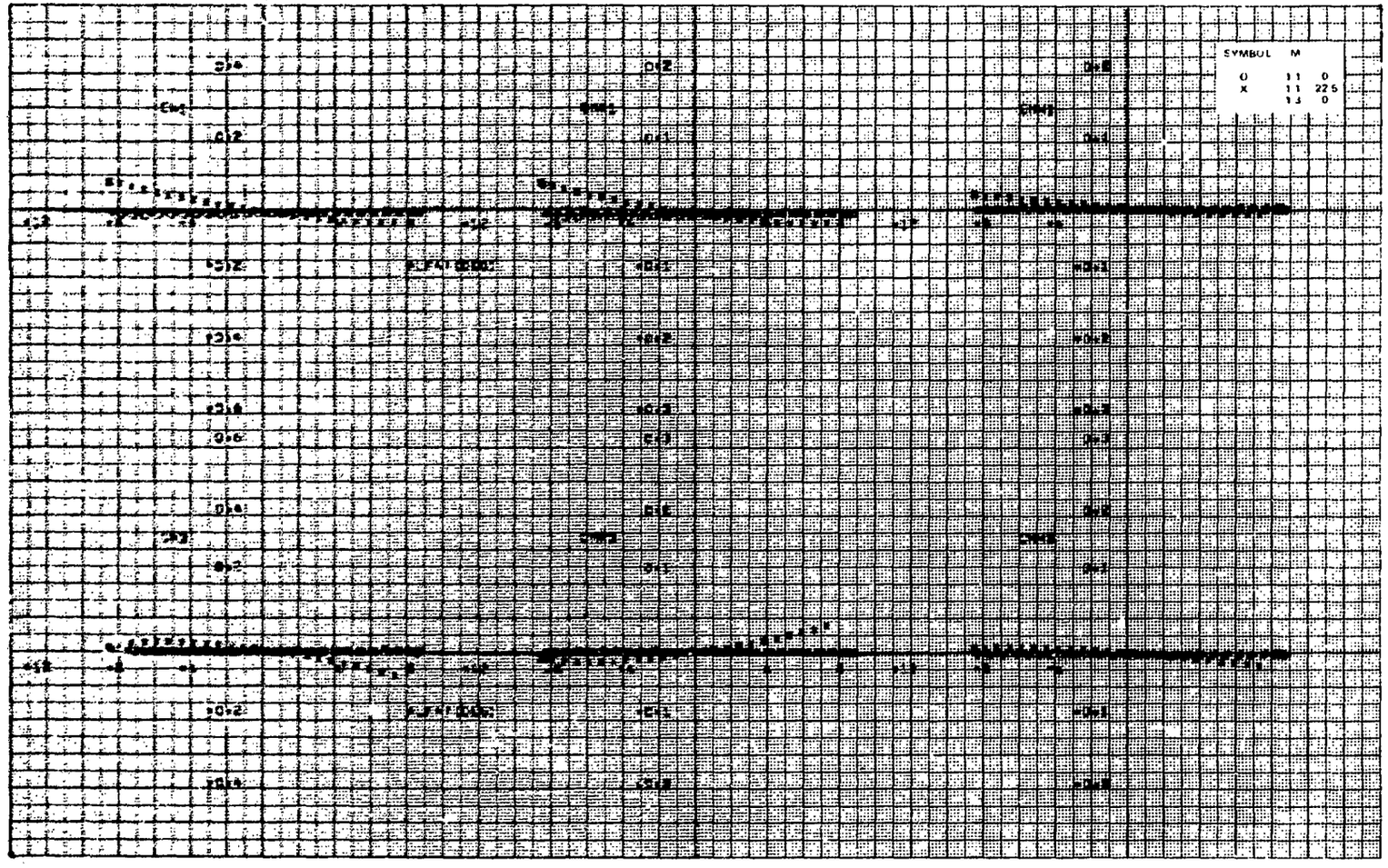


Figure 14c. Continued.

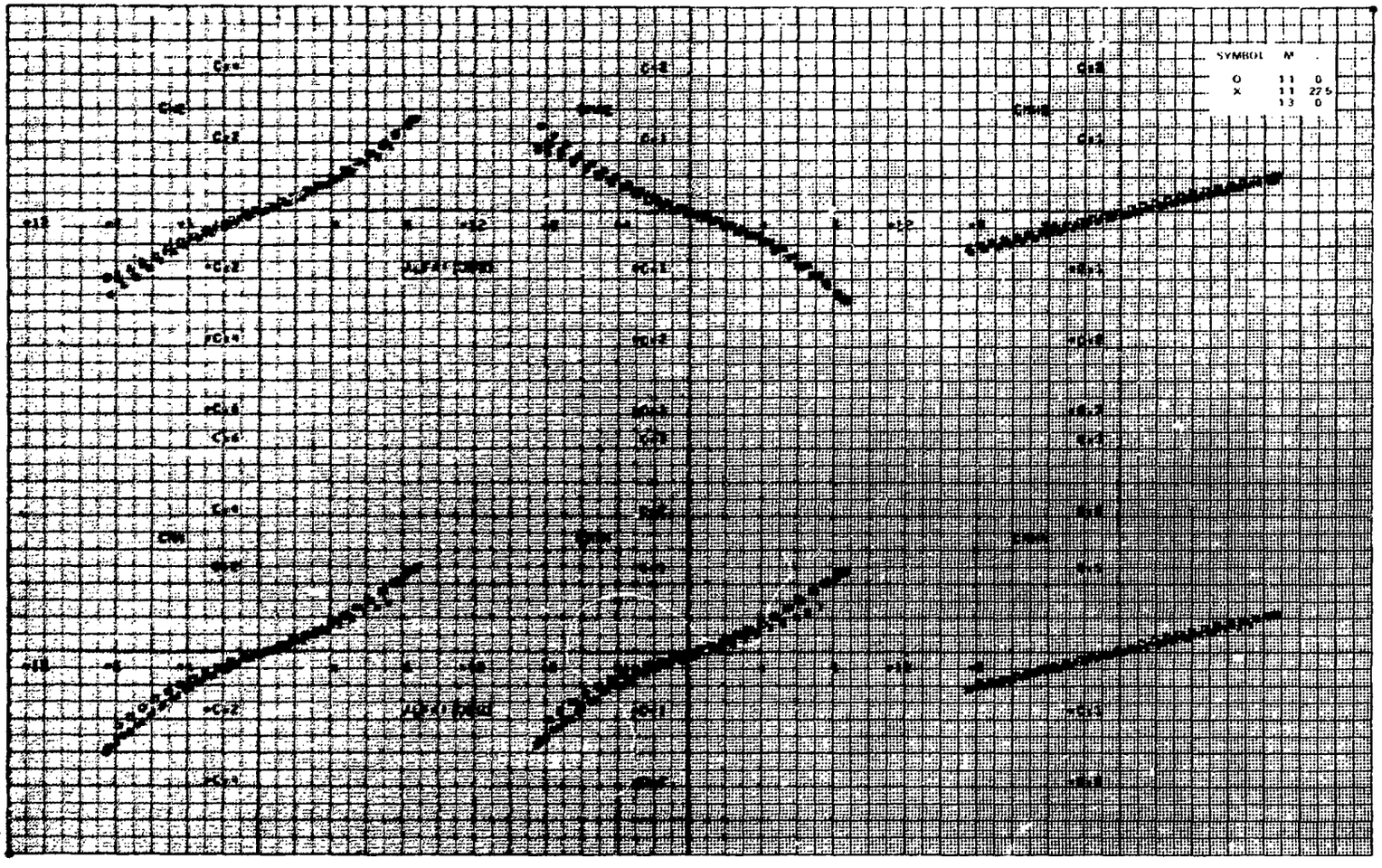


Figure 14c. Concluded.

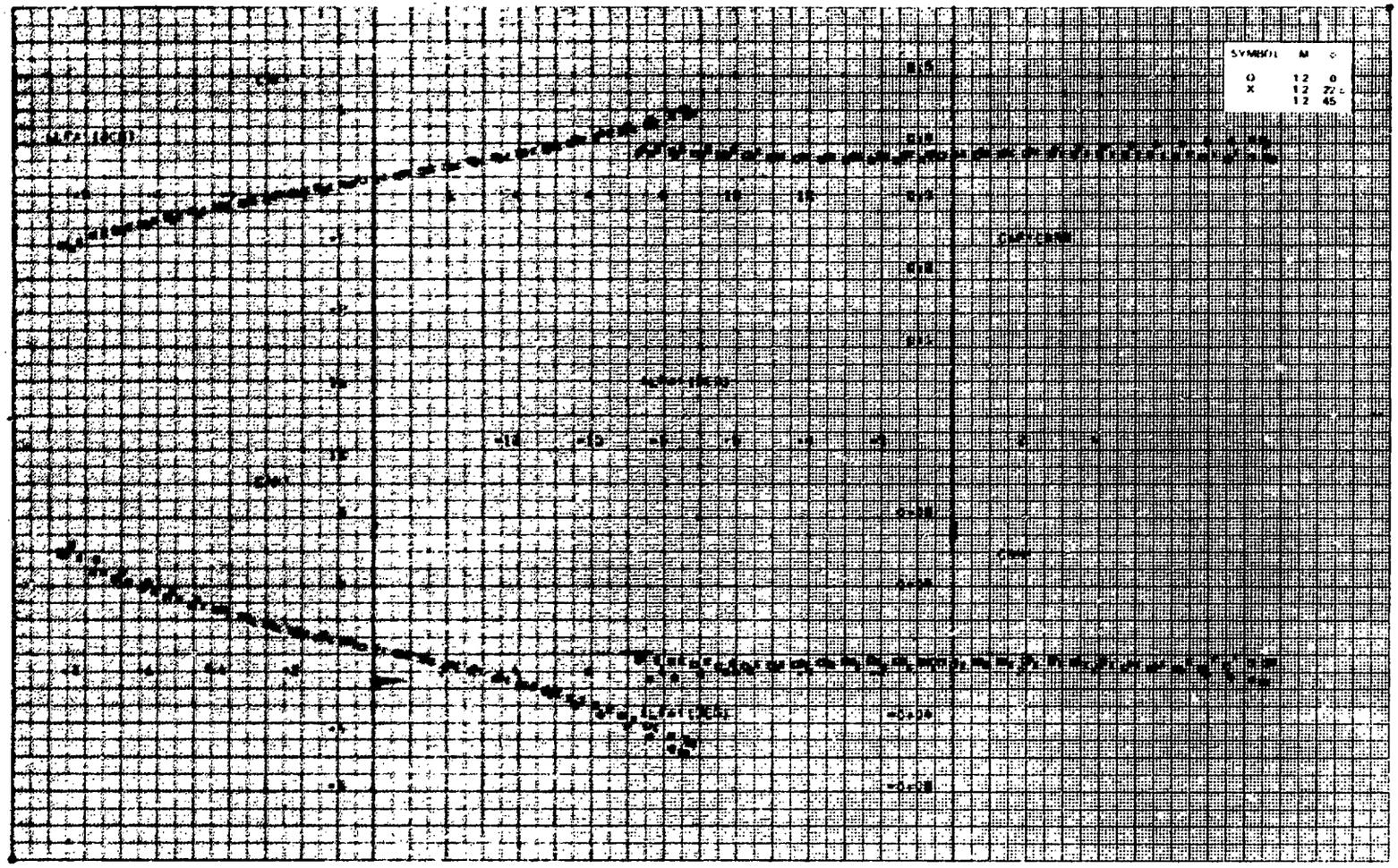


Figure 144. Aerodynamic characteristics coefficients, CR/D = 1.75, γ = 0 deg, B/2D = 0.3475, M_∞ = 1.2.

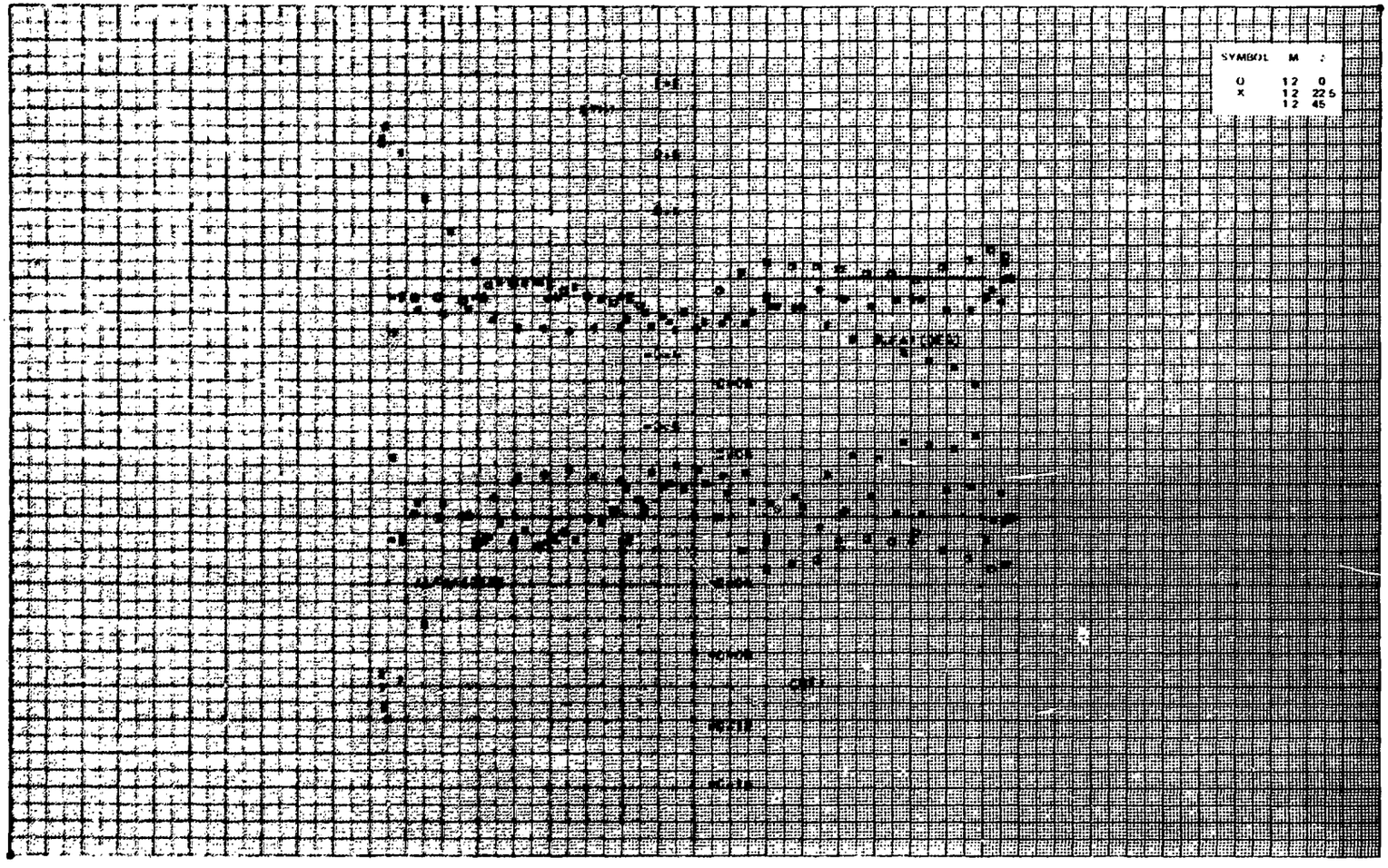


Figure 14d. Continued.

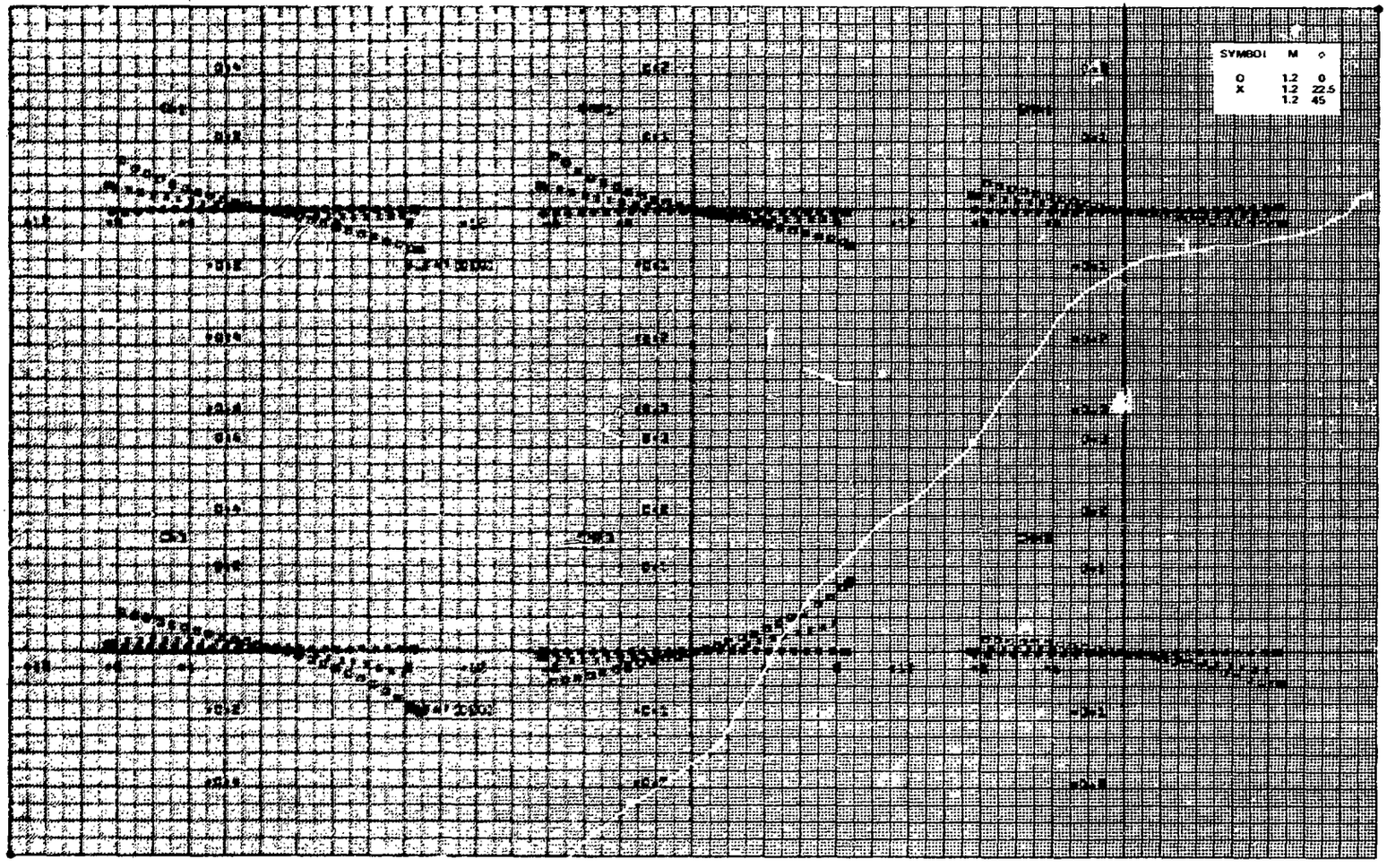


Figure 141. Continued.

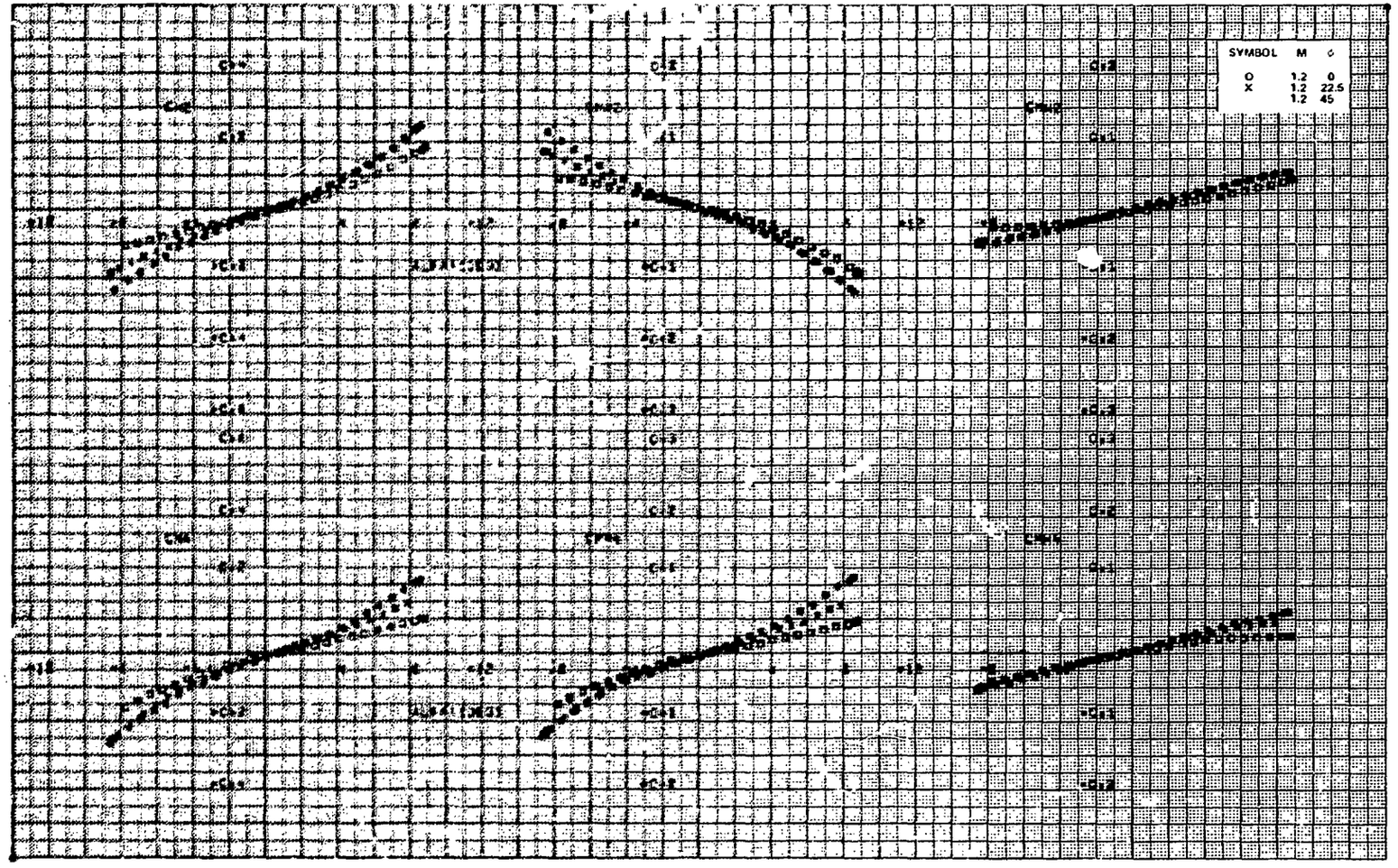


Figure 14d. Concluded.

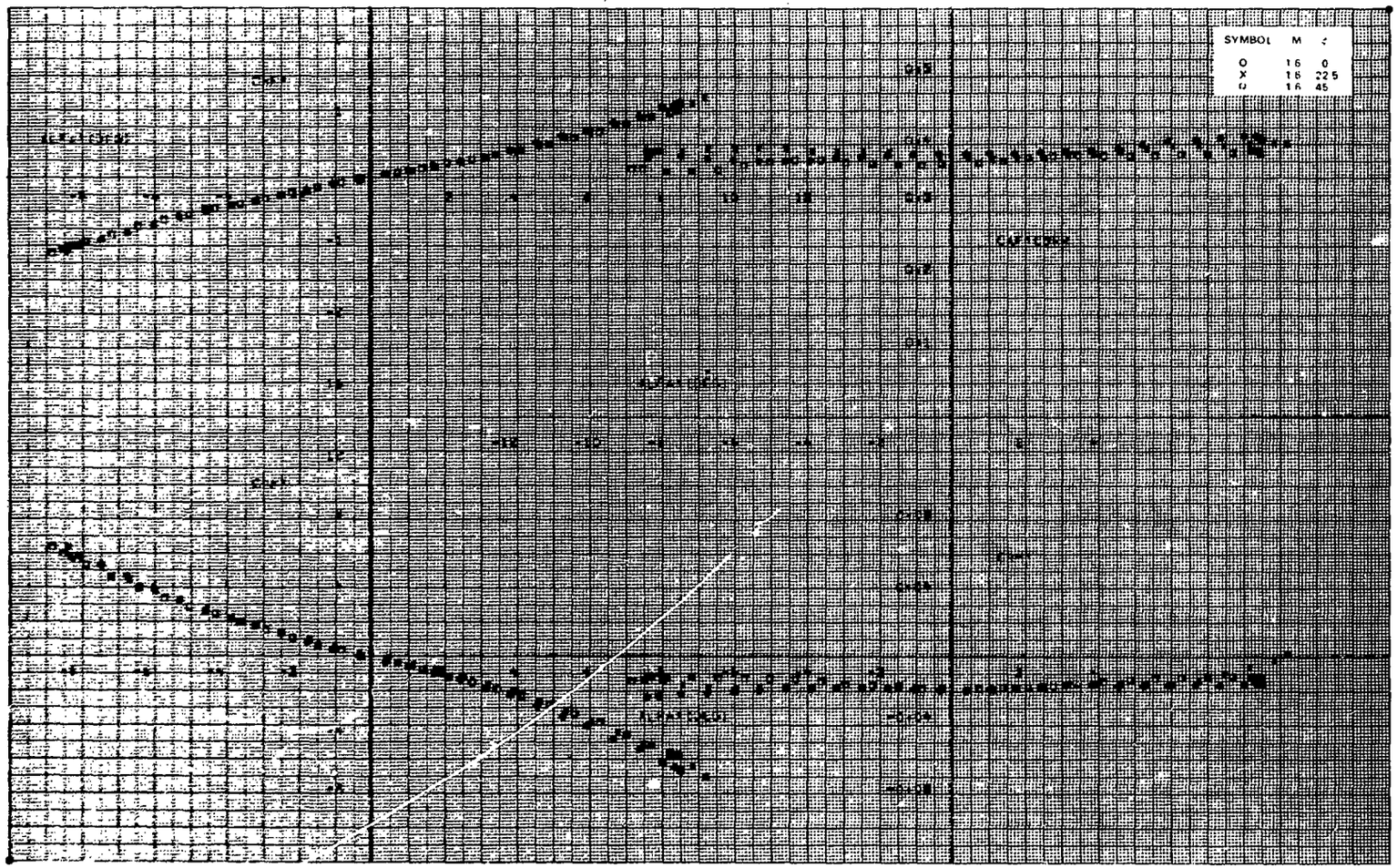


Figure 146. Aerodynamic stability coefficients, CR/D = 1.75, A = 0 deg, B/2D = 0.3475, M_∞ = 1.6.

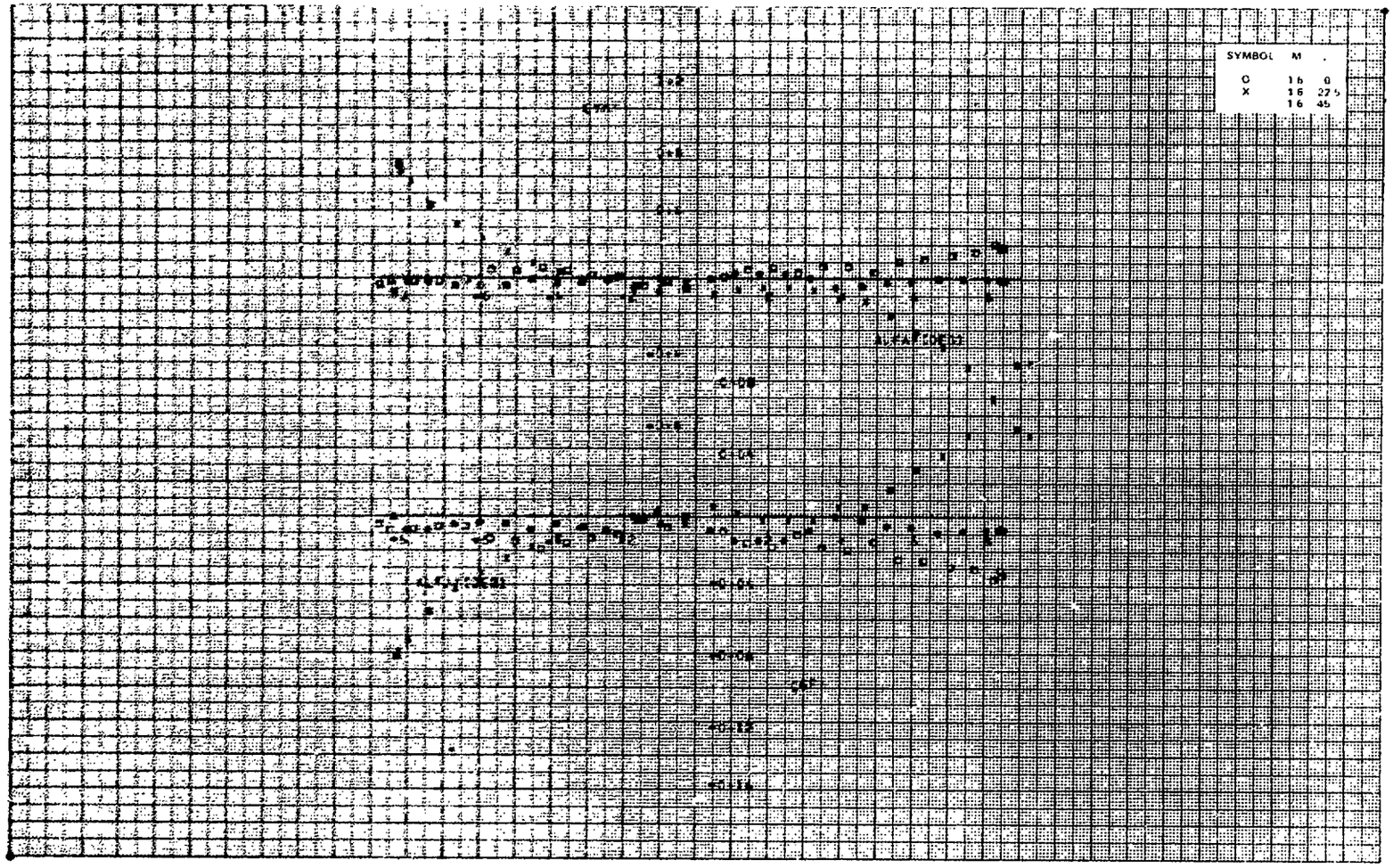


Figure 14e. Continued.

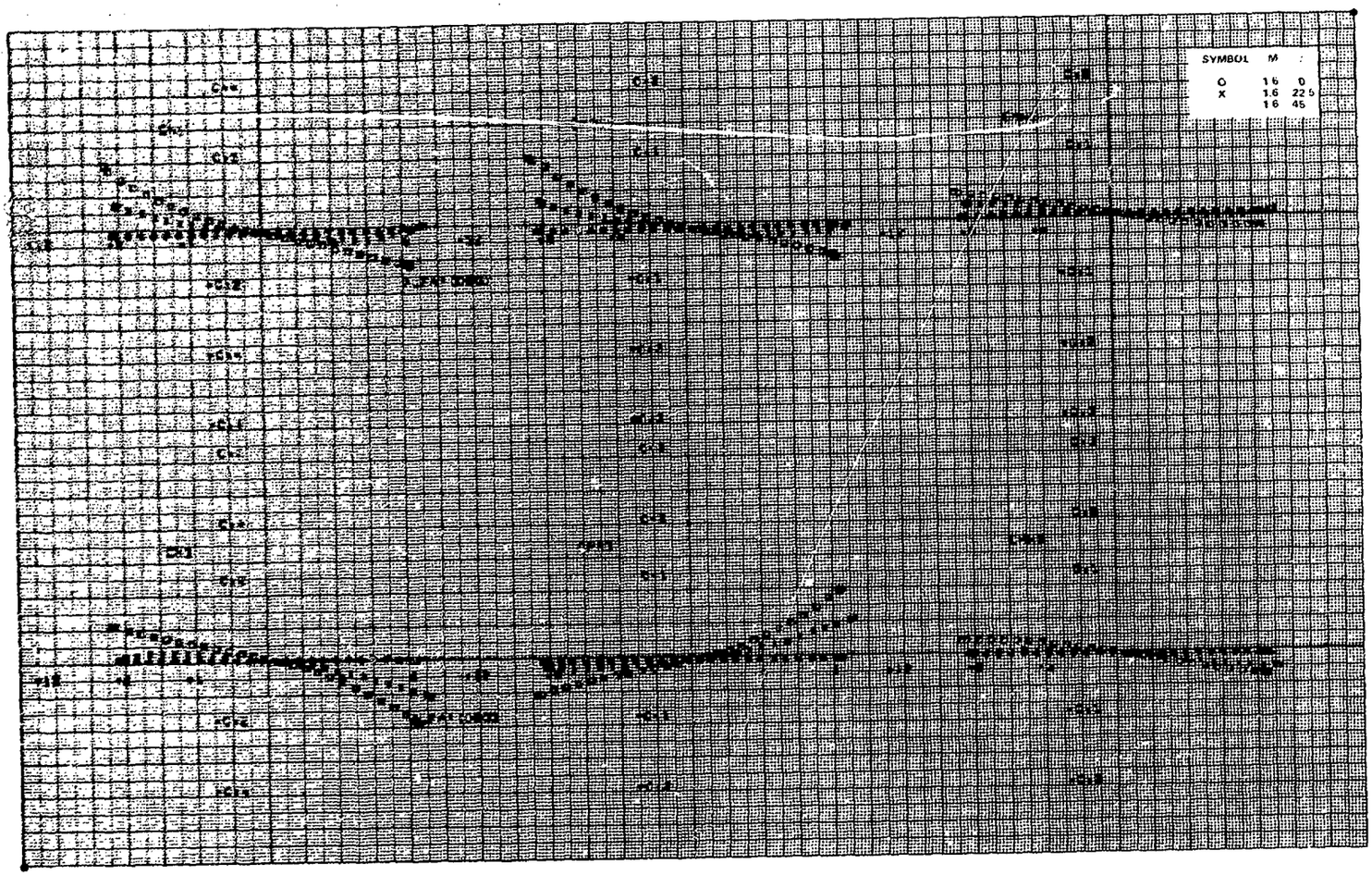


Figure 14e. Continued.

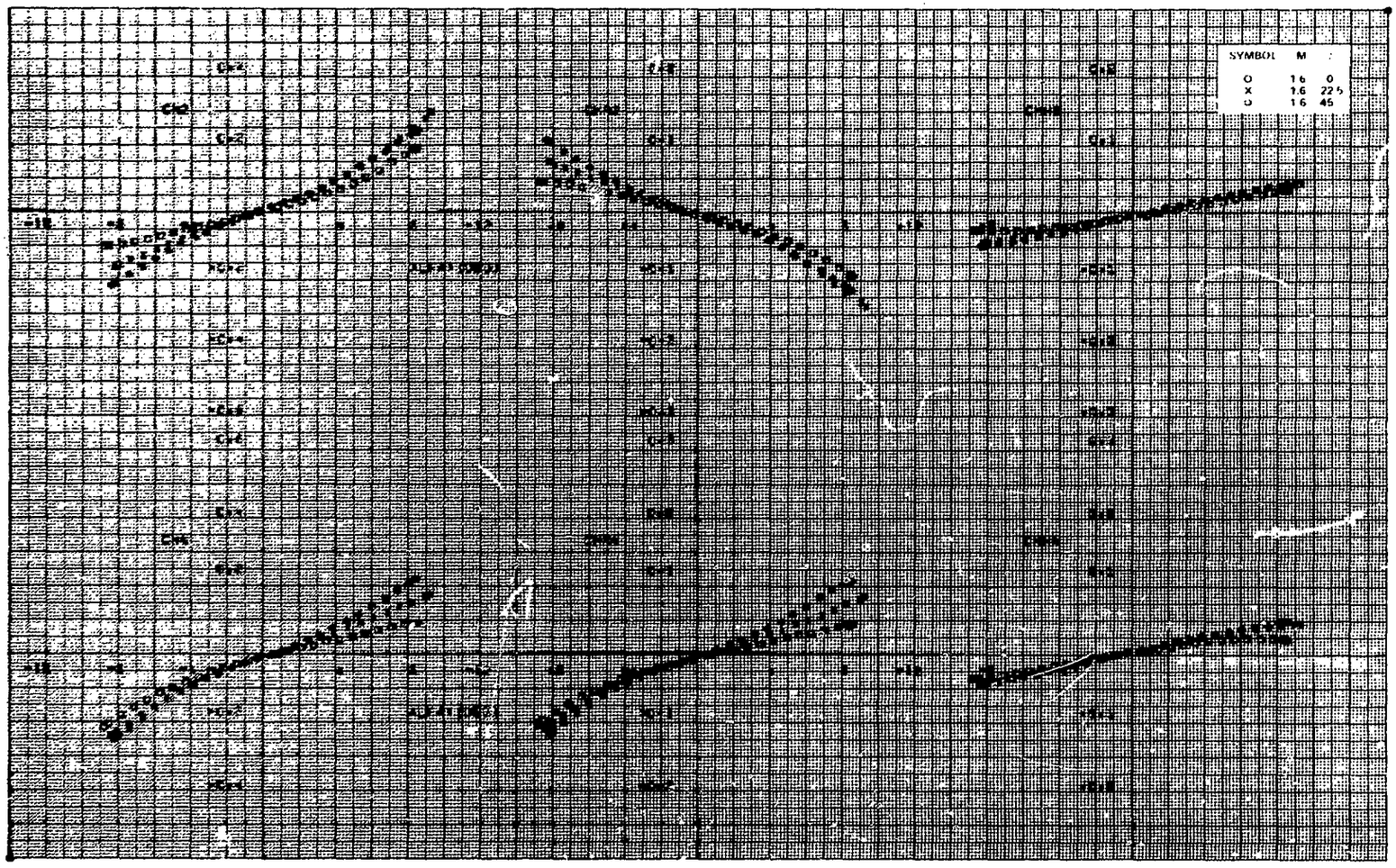


Figure 14e. Concluded.

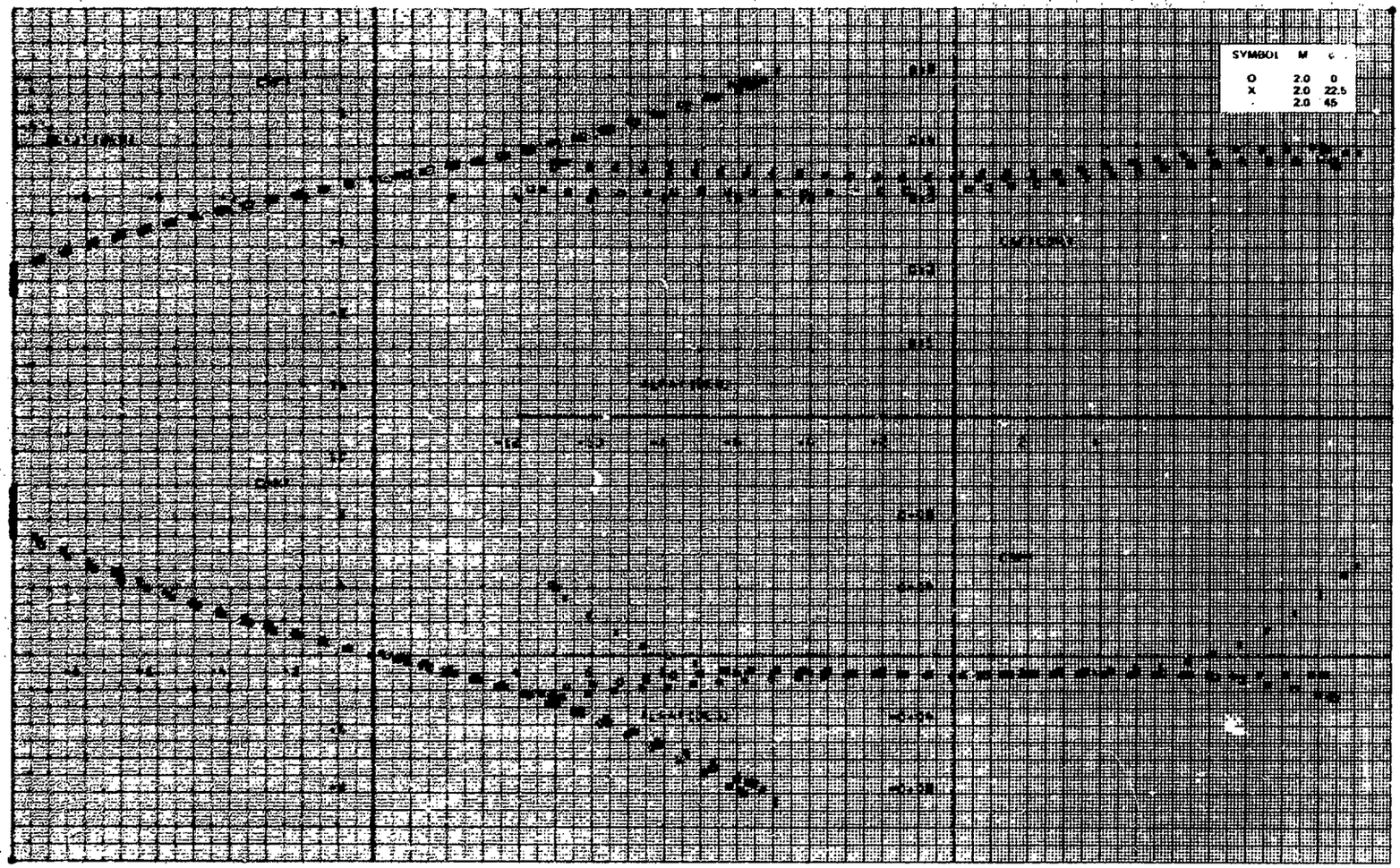


Figure 14f. Aerodynamic stability coefficients, CR/D = 1.75, α = 0 deg, B/2D = 0.3475, M_∞ = 2.0.

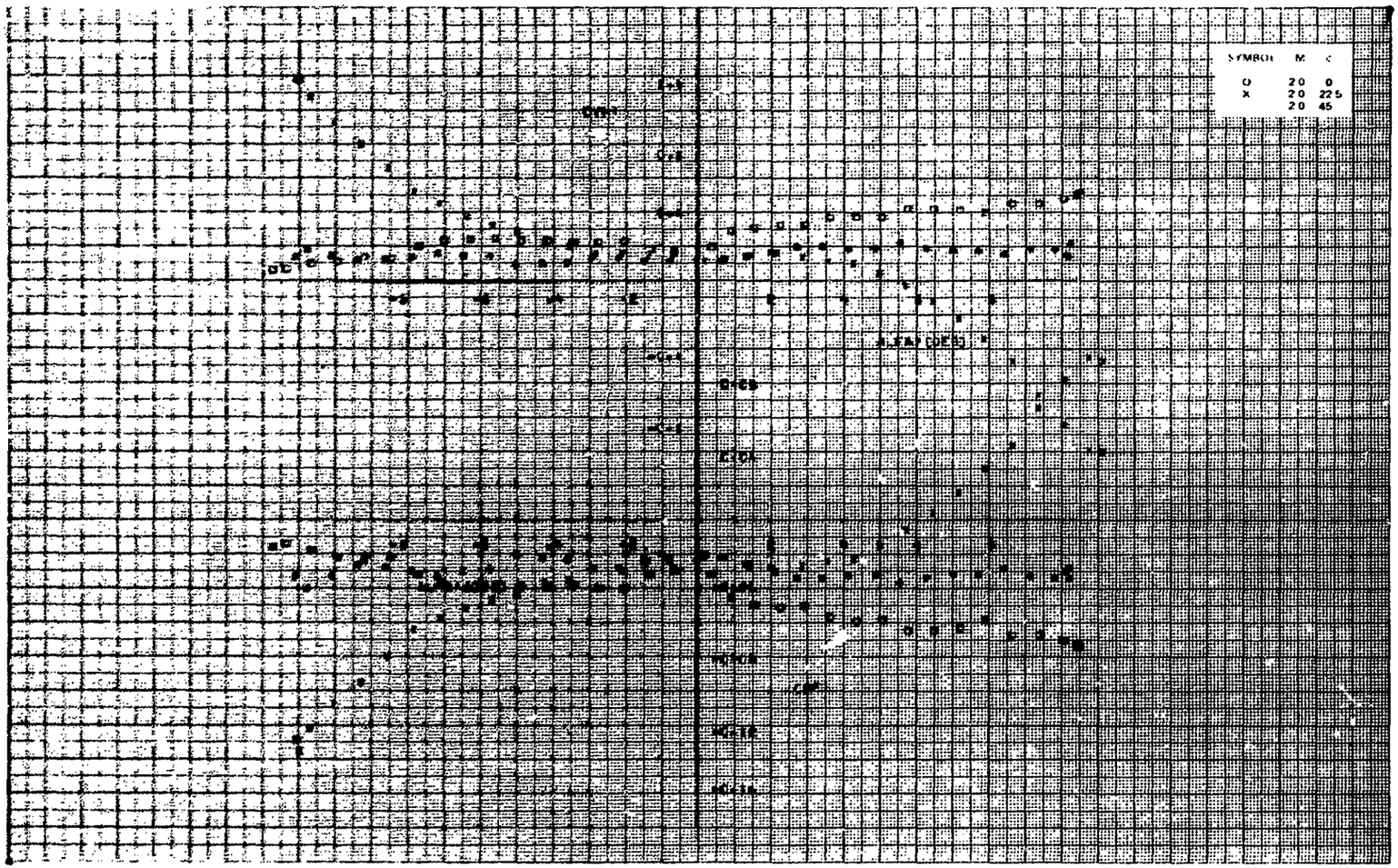


Figure 14f. Continued.

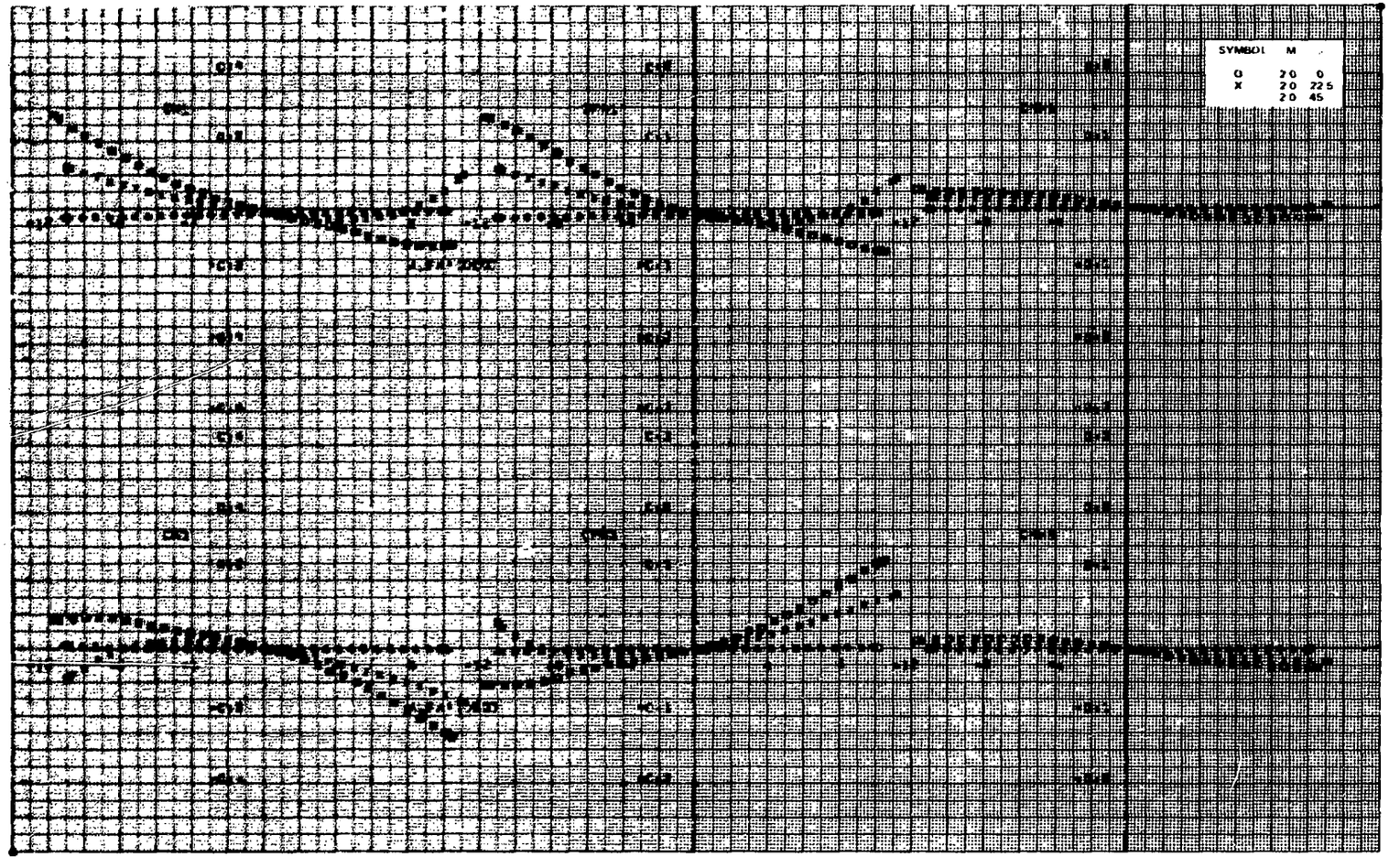


Figure 14f. Continued.

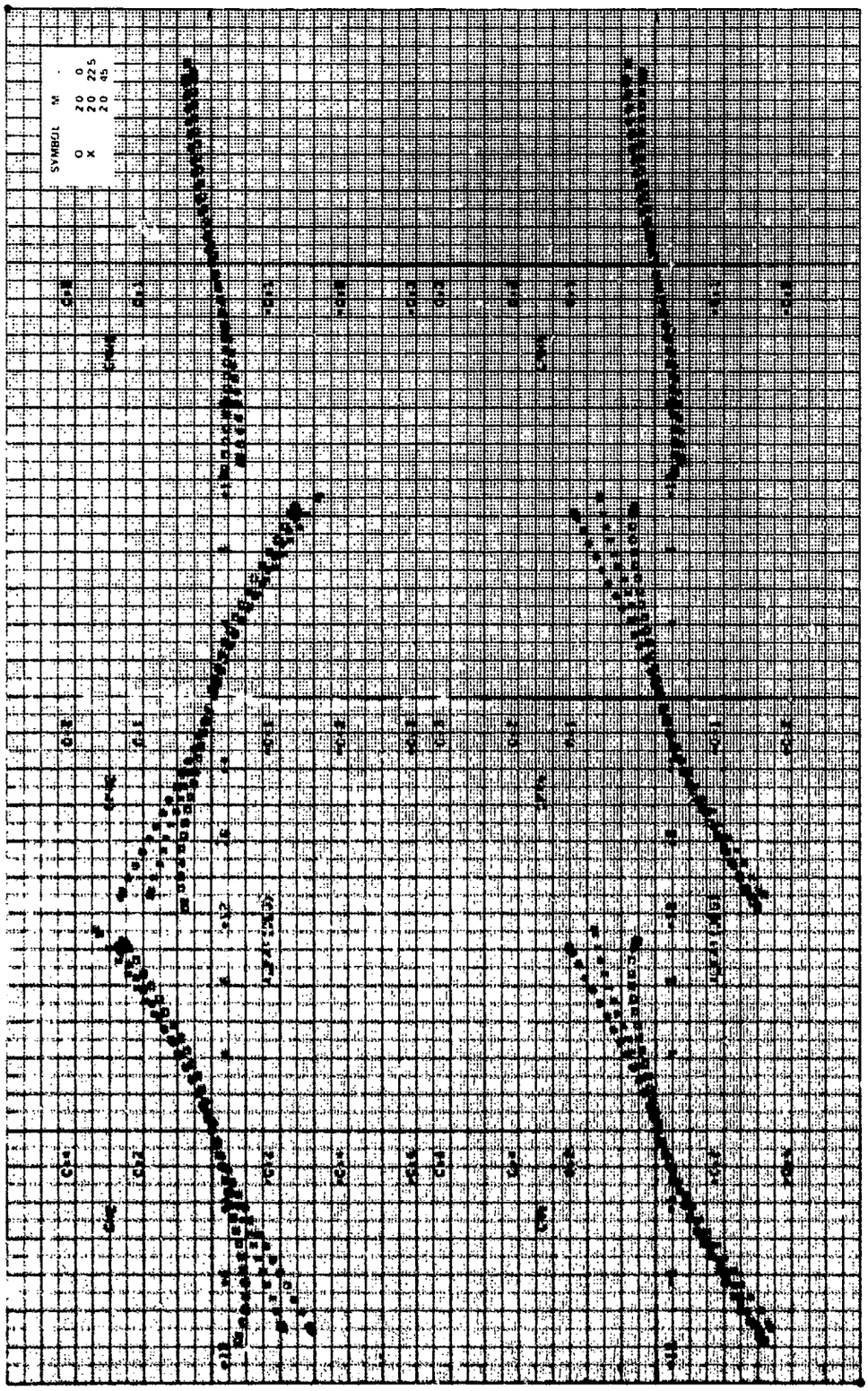


Figure 14f. Concluded.

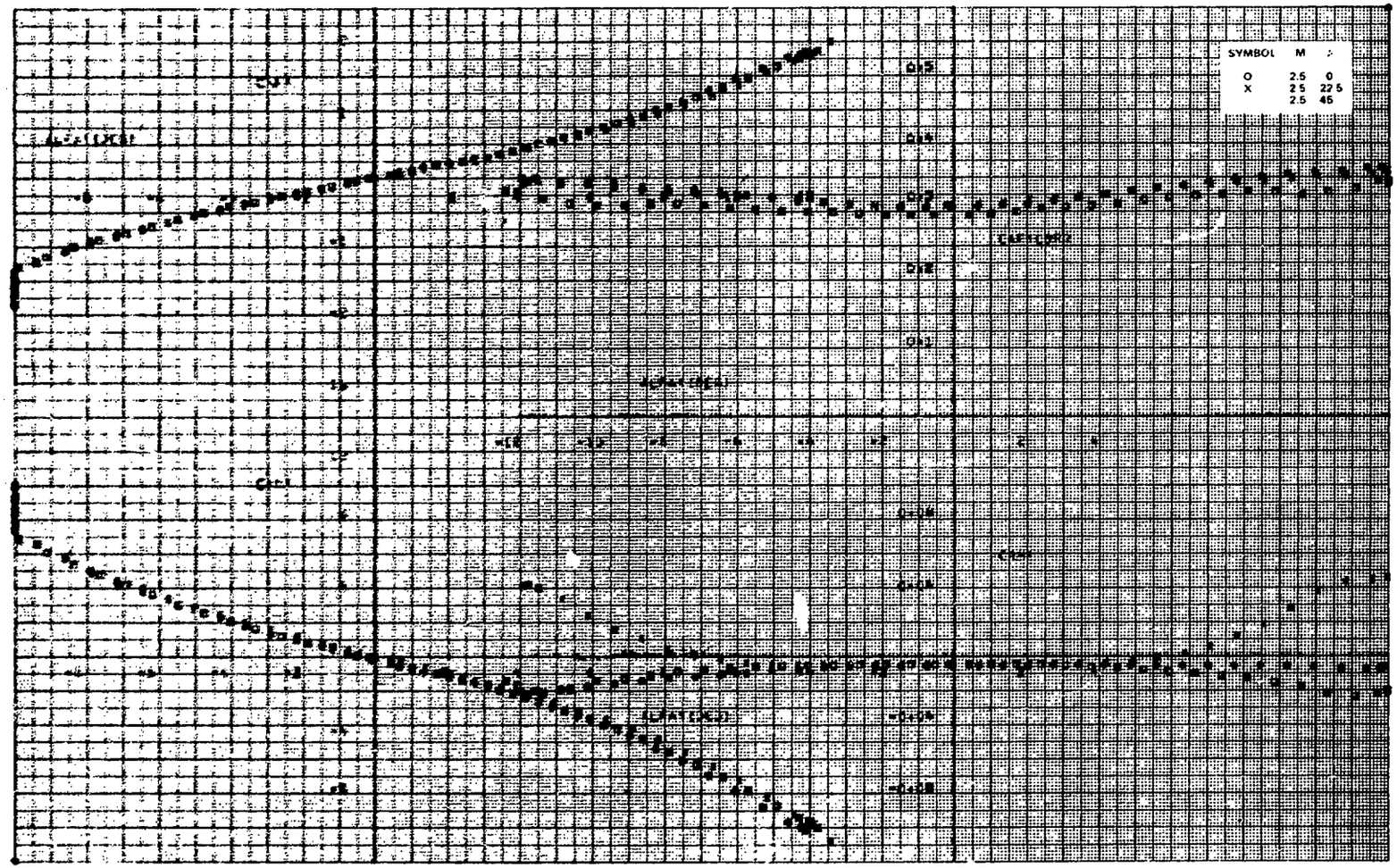


Figure 14. Aerodynamic stability coefficients, CR/D = 1.75, ' = 0 deg, B/2D = 0.3475, M_∞ = 2.5.

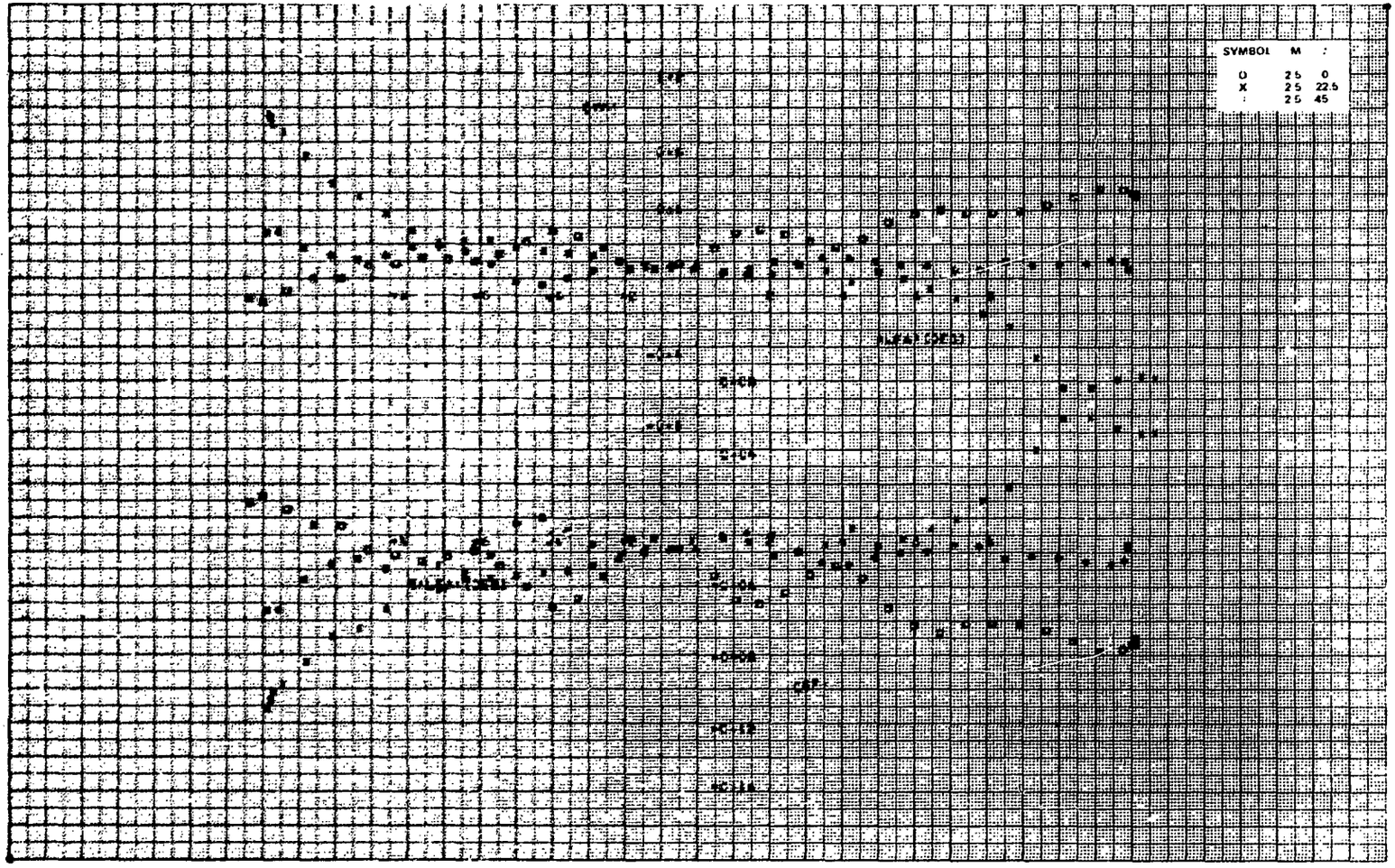


Figure 14g. Continued.

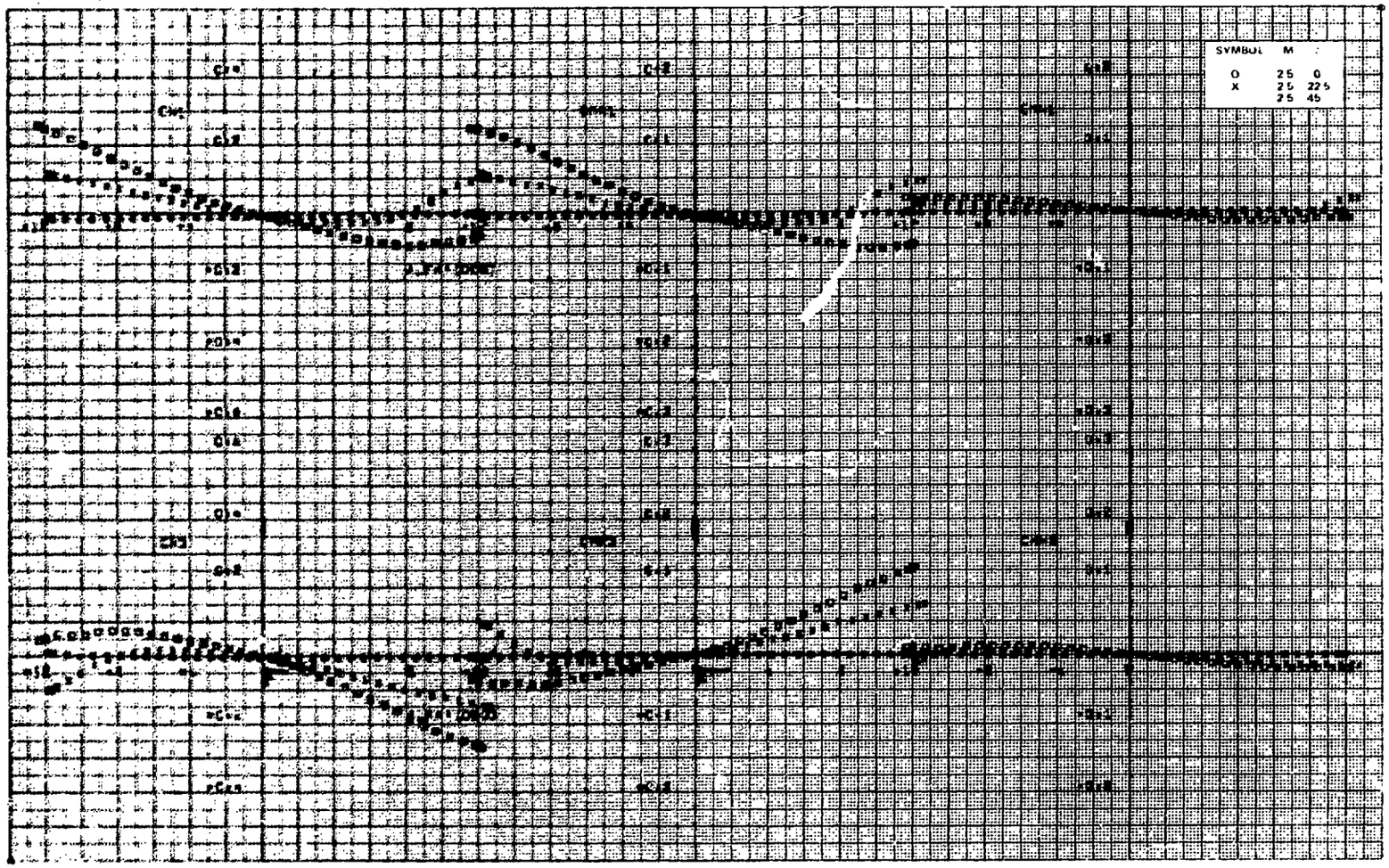


Figure 14g. Continued.

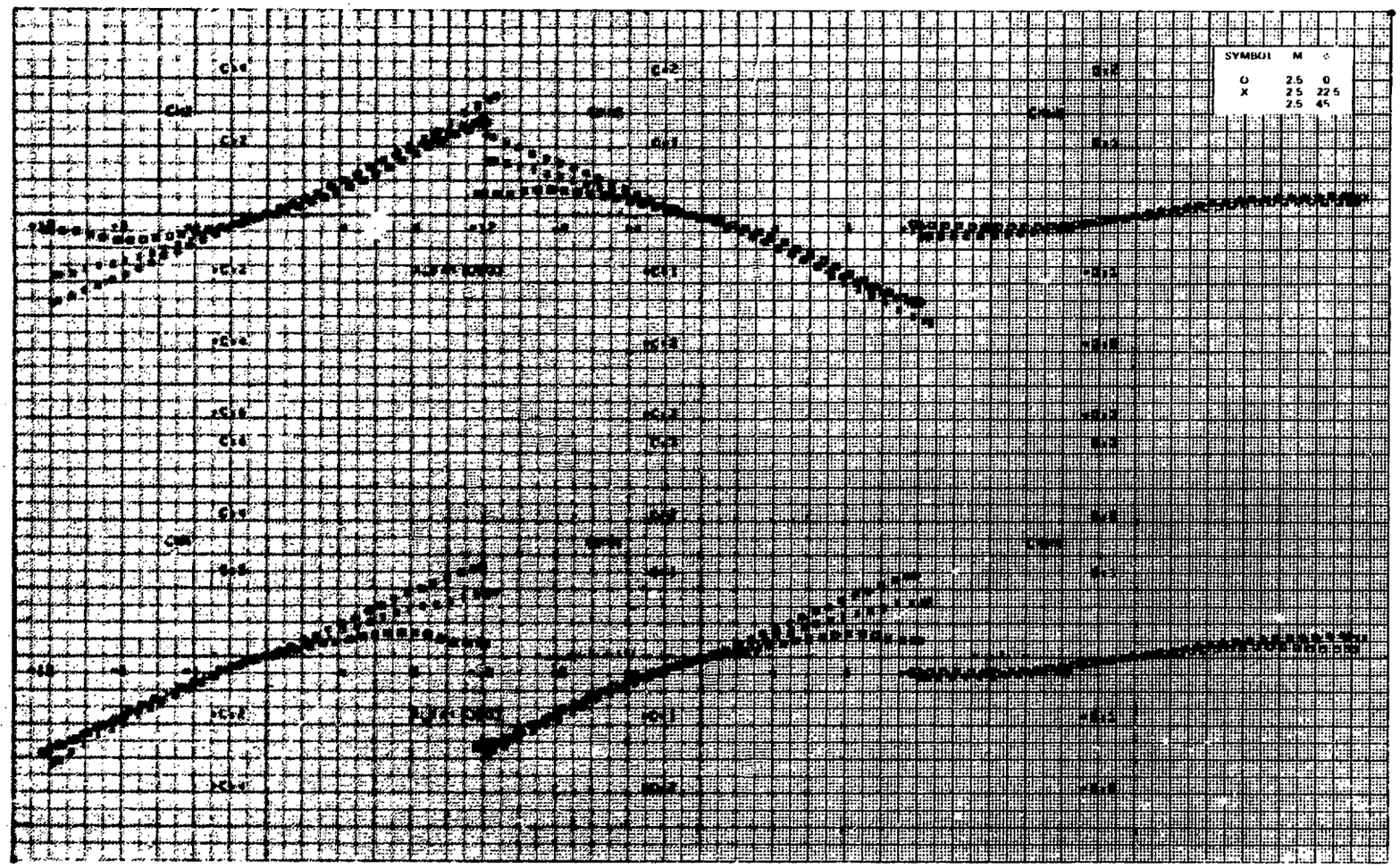


Figure 14g. Concluded.

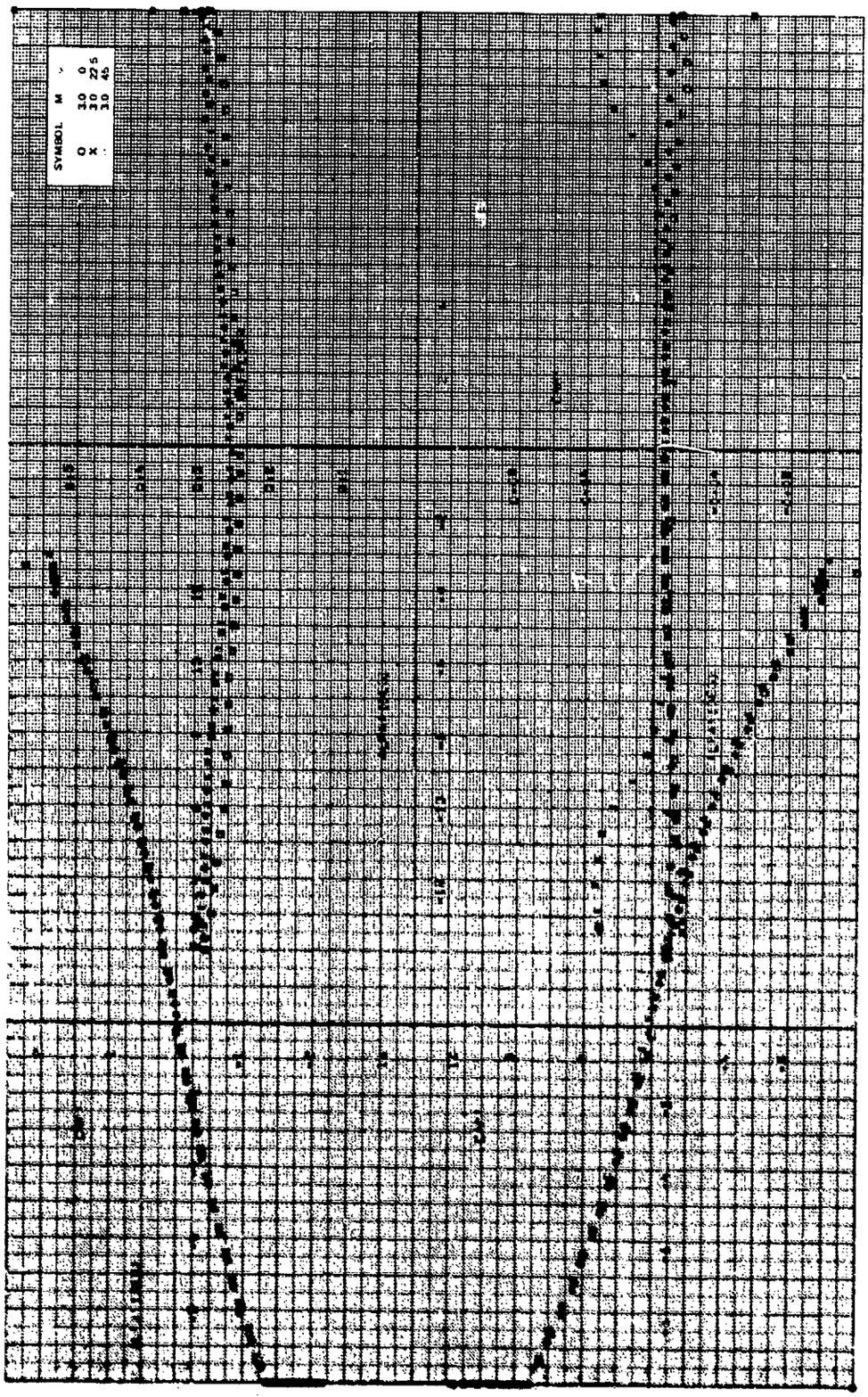


Figure 148. Aerodynamic stability coefficients, CR/B = 1.75, δ = 0 deg, B/2D = 0.3475, M_∞ = 3.0.

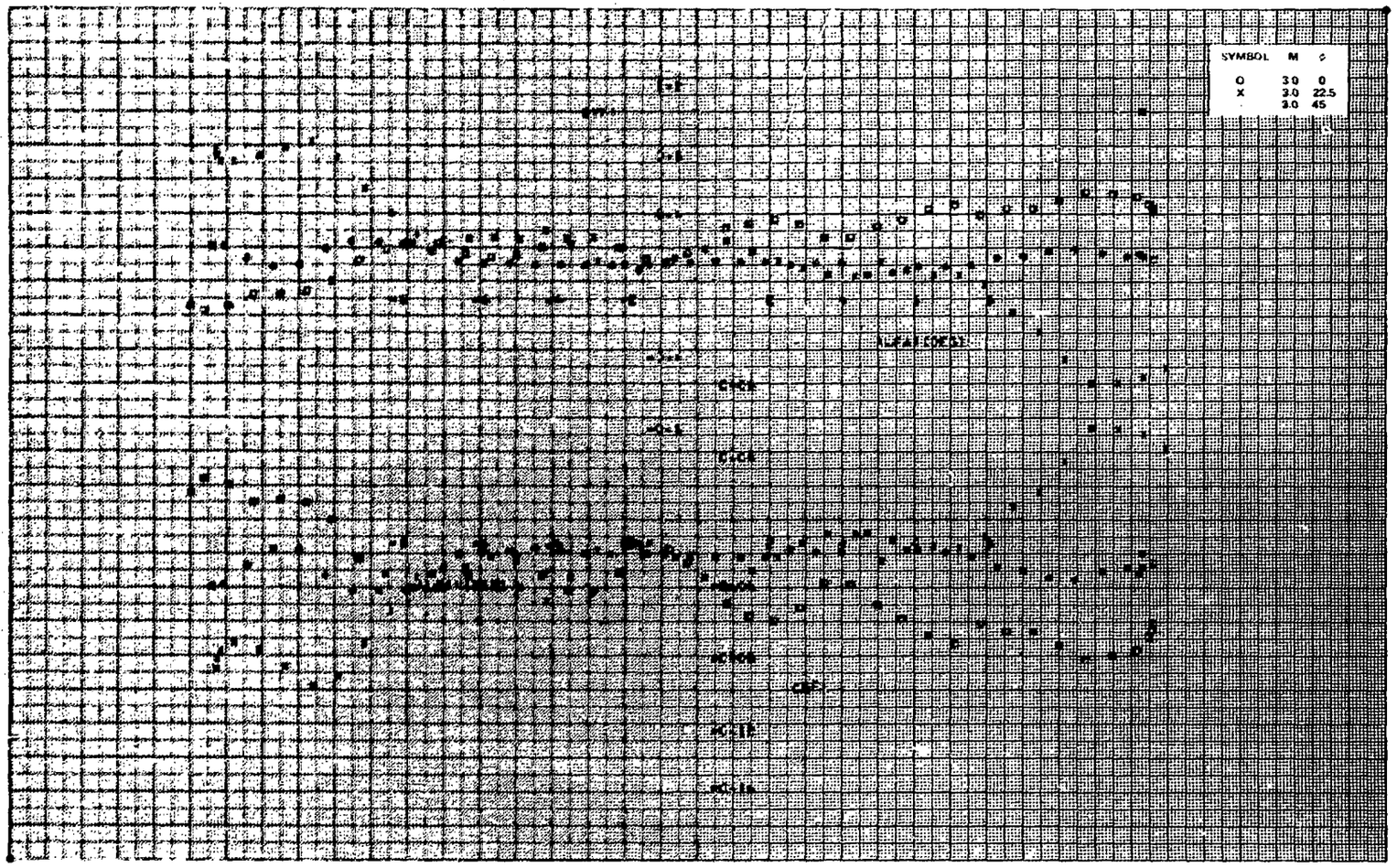


Figure 14h. Continued.

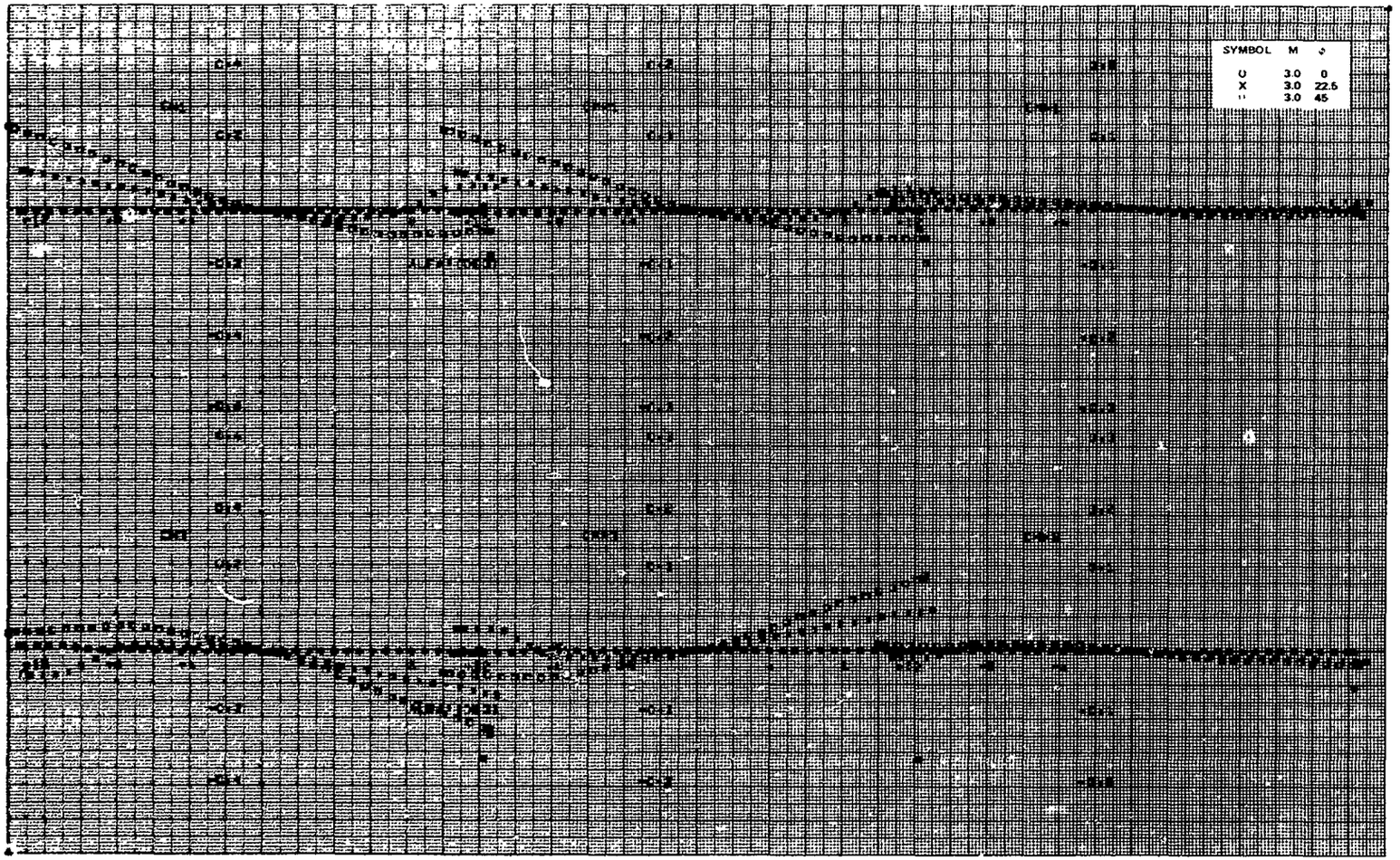


Figure 14h. Continued.

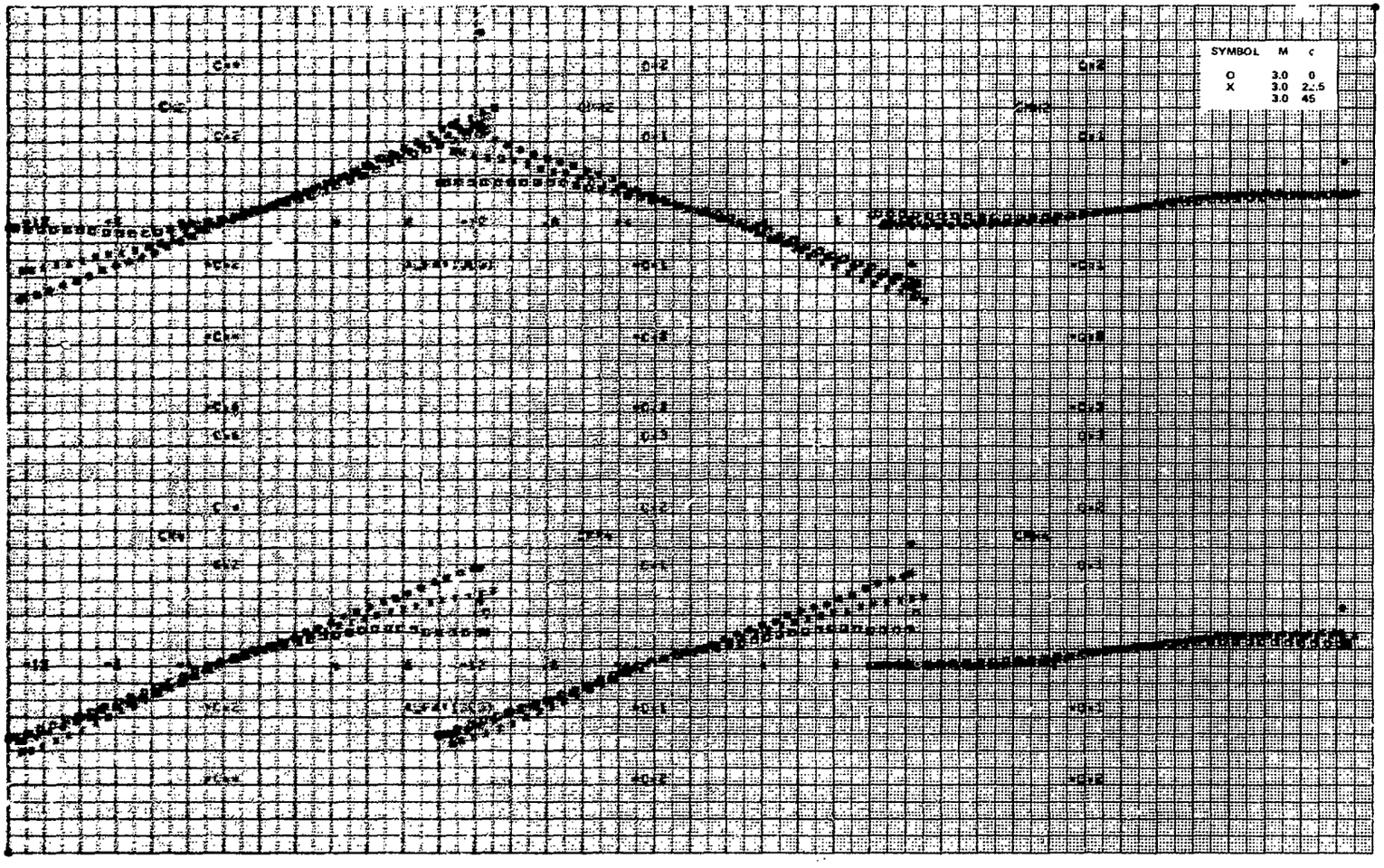


Figure 14h. Concluded.

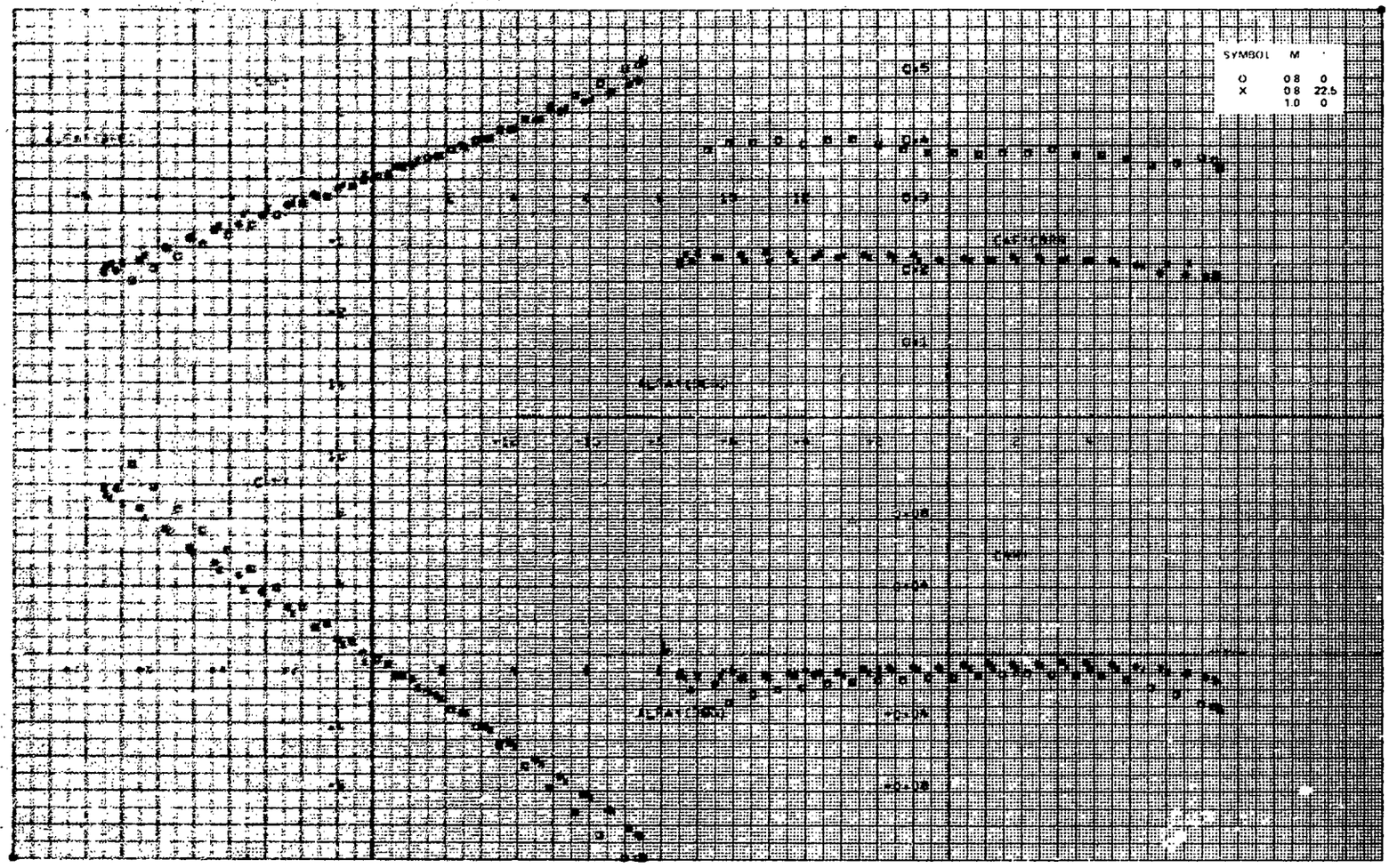


Figure 15a. Aerodynamic stability coefficients, CR/D = 1.75, Λ = 0 deg, M_∞ = 0.8, 1.0.

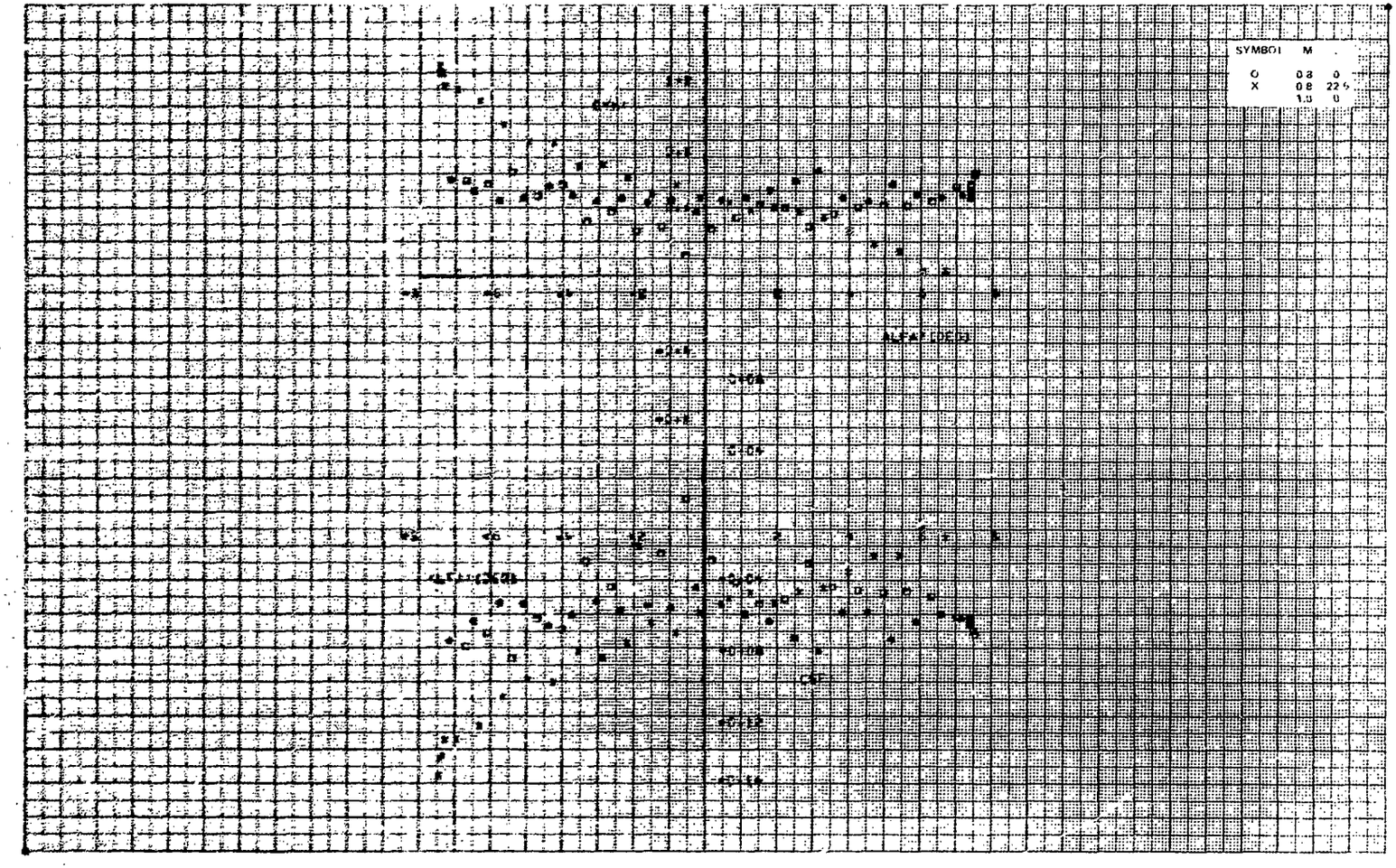


Figure 15a. Continued.

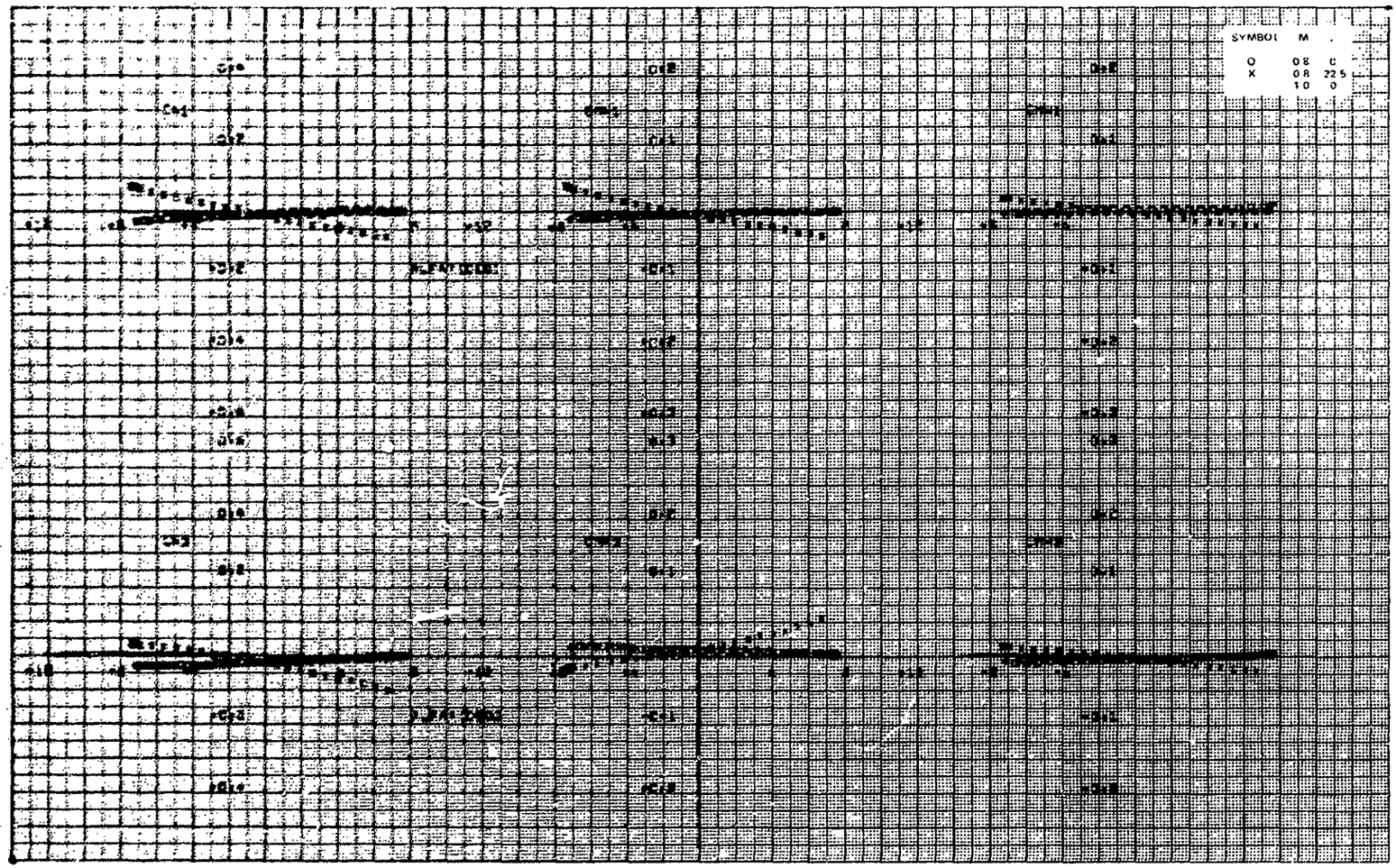


Figure 15a. Continued.

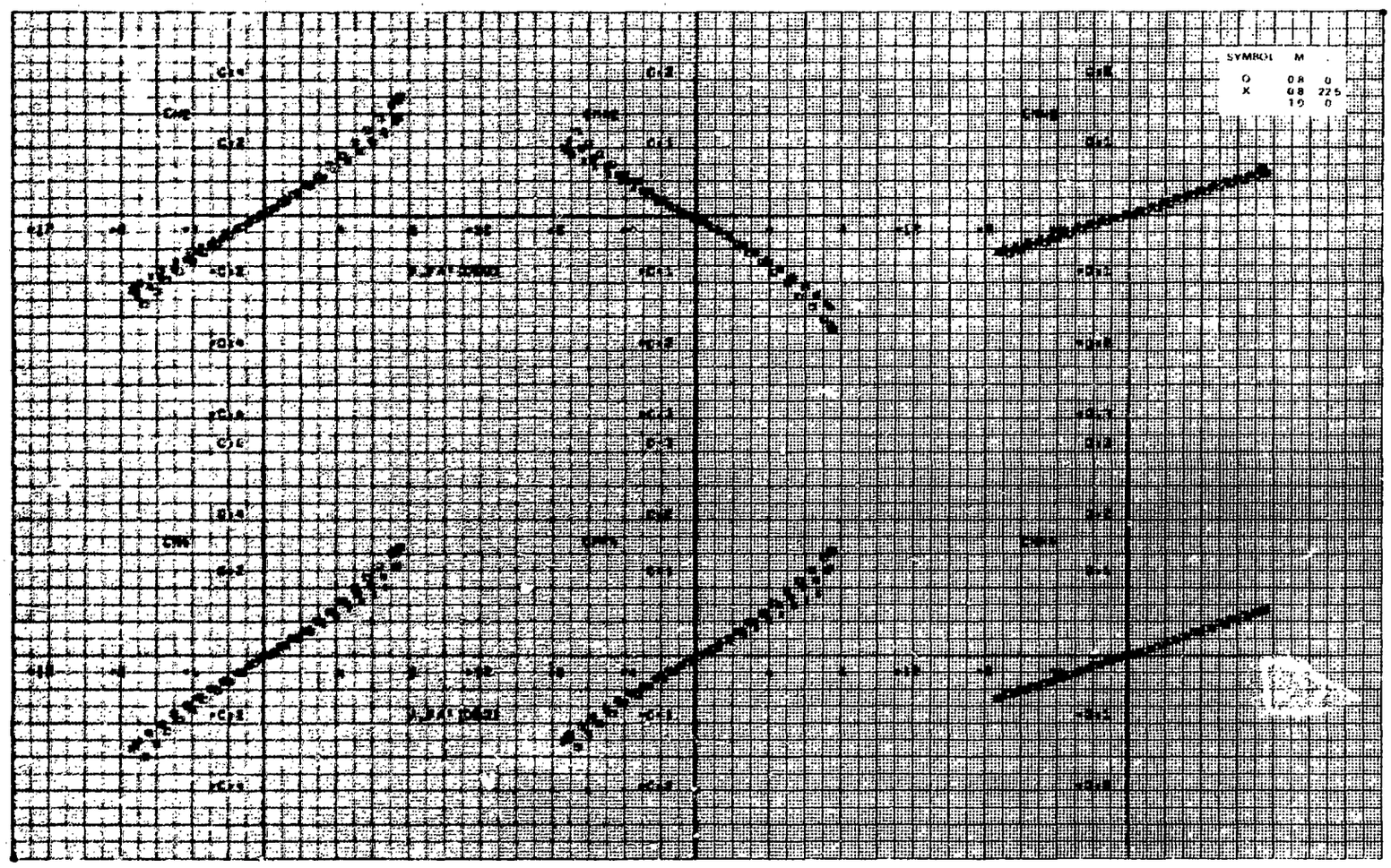


Figure 15a. Concluded.

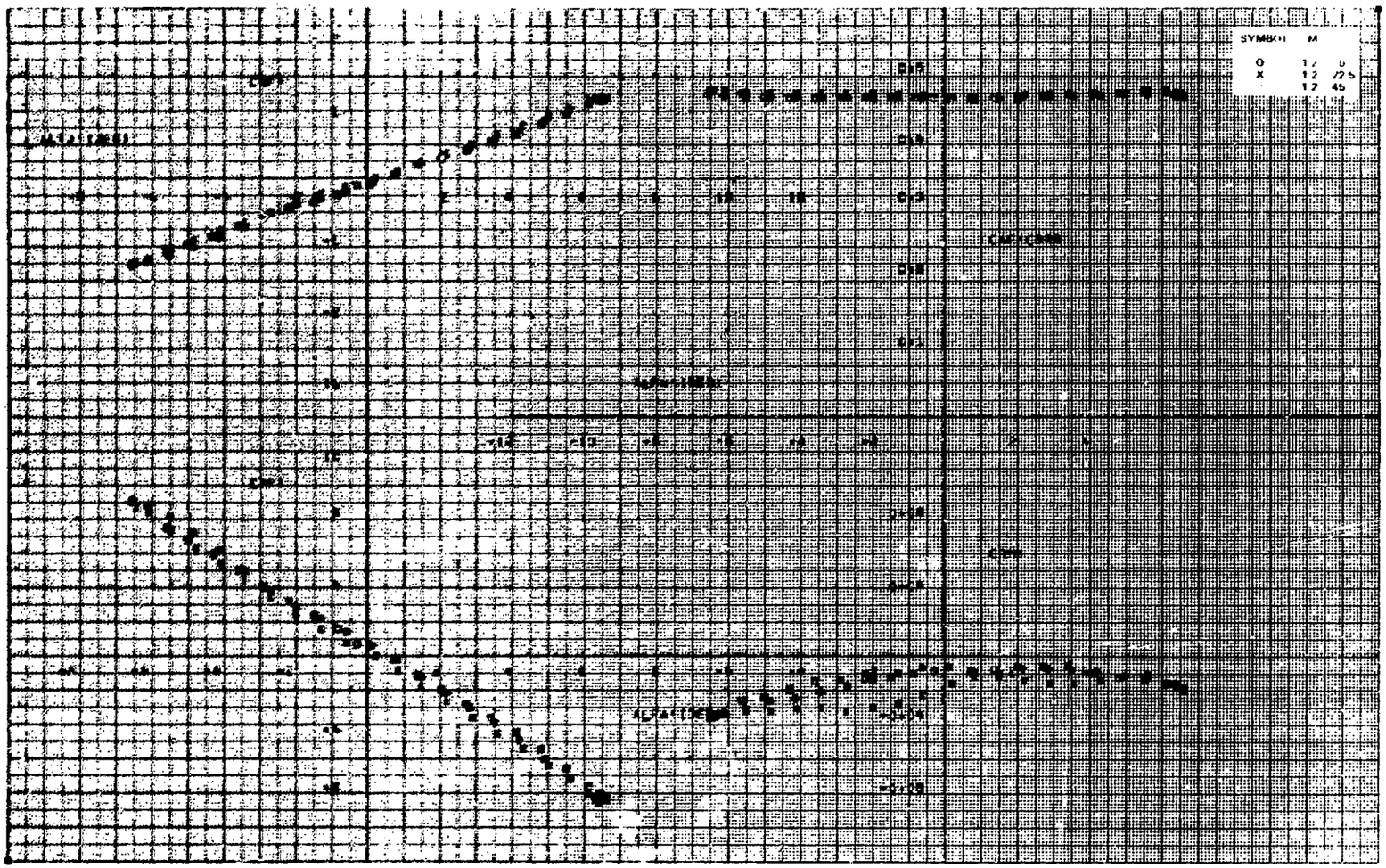


Figure 15b. Aerodynamic stability coefficients, CR/D = 1.75, Λ = 0 deg, M_∞ = 1.2.

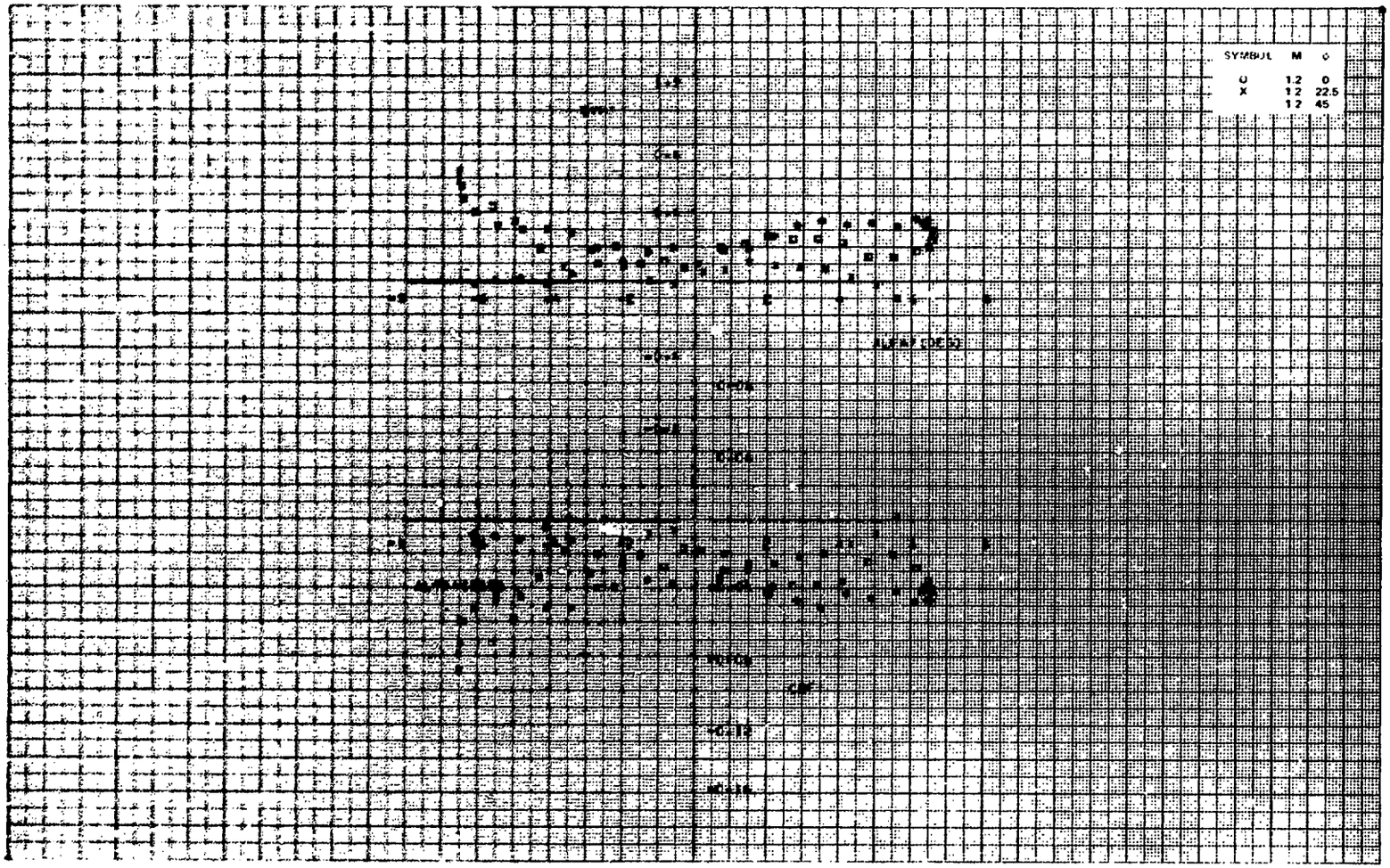


Figure 15b. Continued.

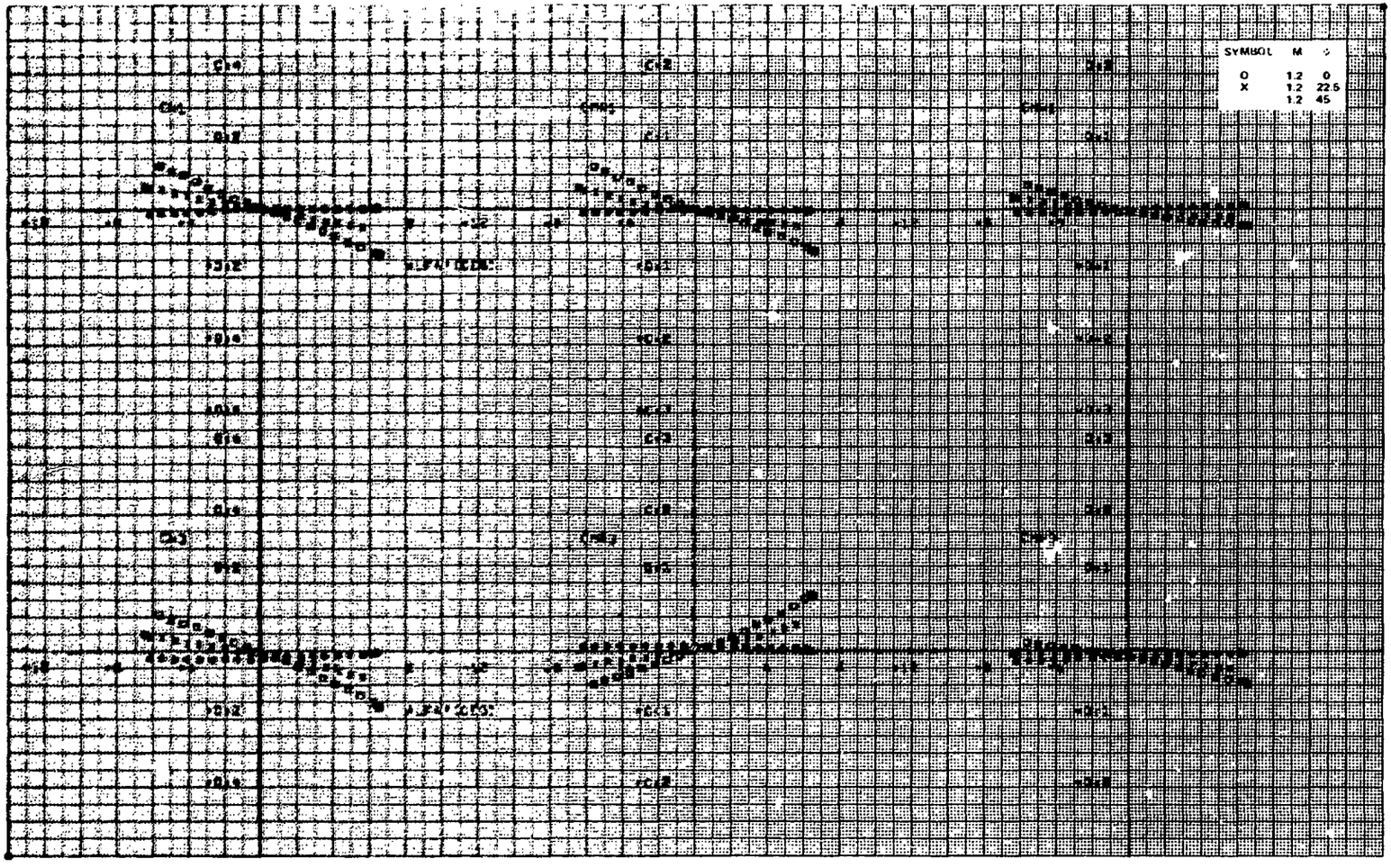


Figure 15b. Continued.

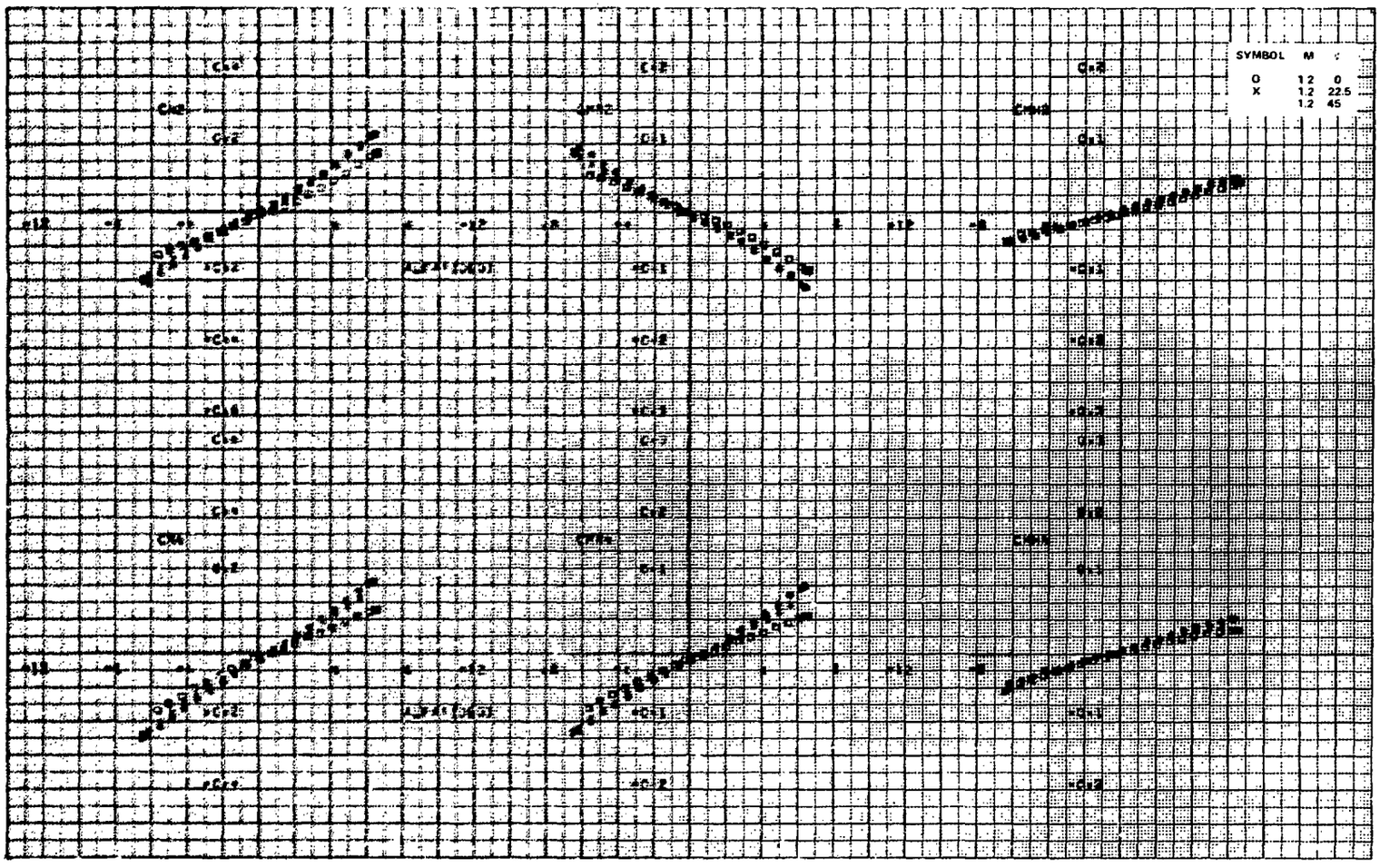


Figure 15b. Concluded.

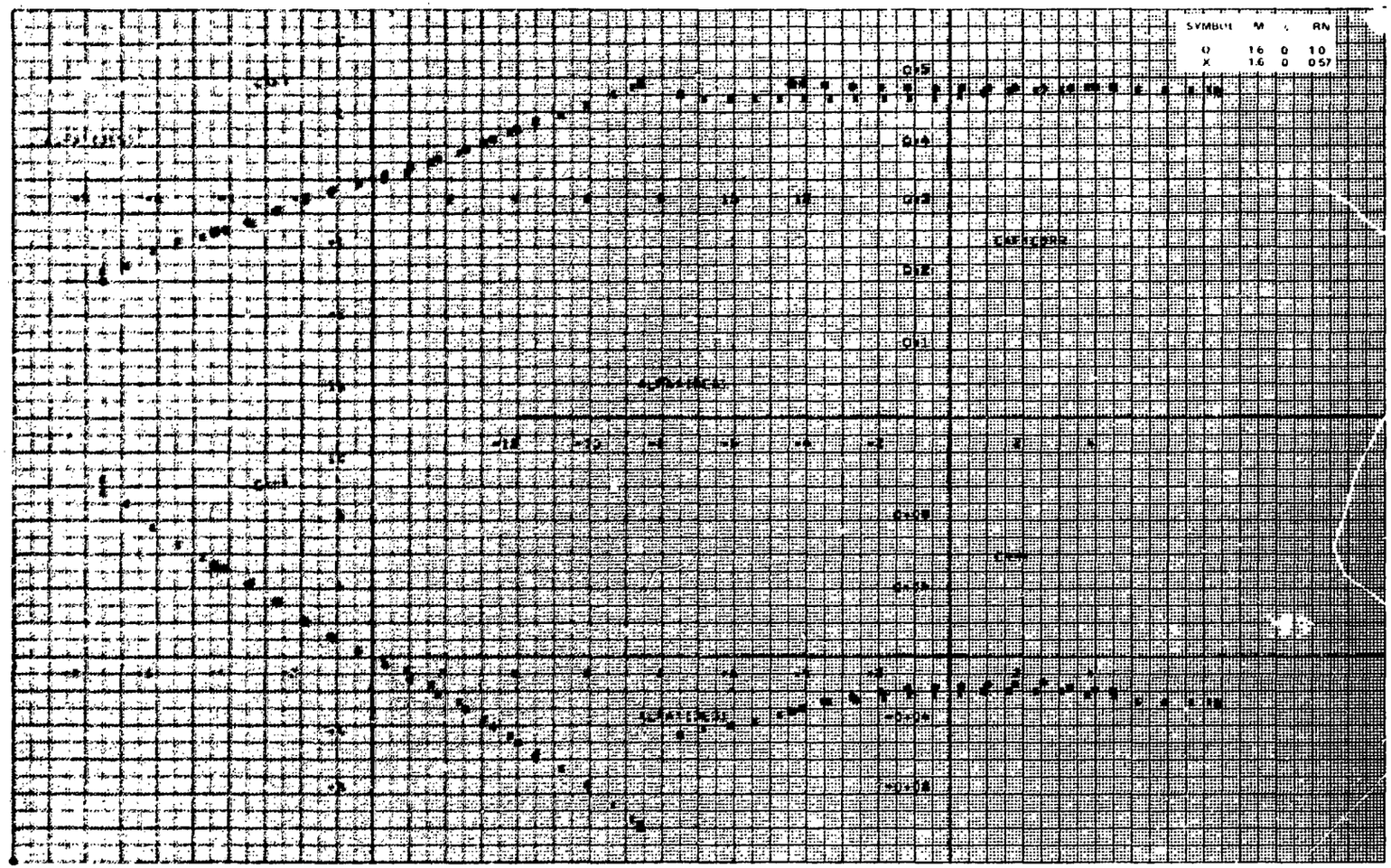


Figure 15c. Aerodynamic stability coefficients, CR/D = 1.75, α = 0 deg, M_∞ = 1.6.

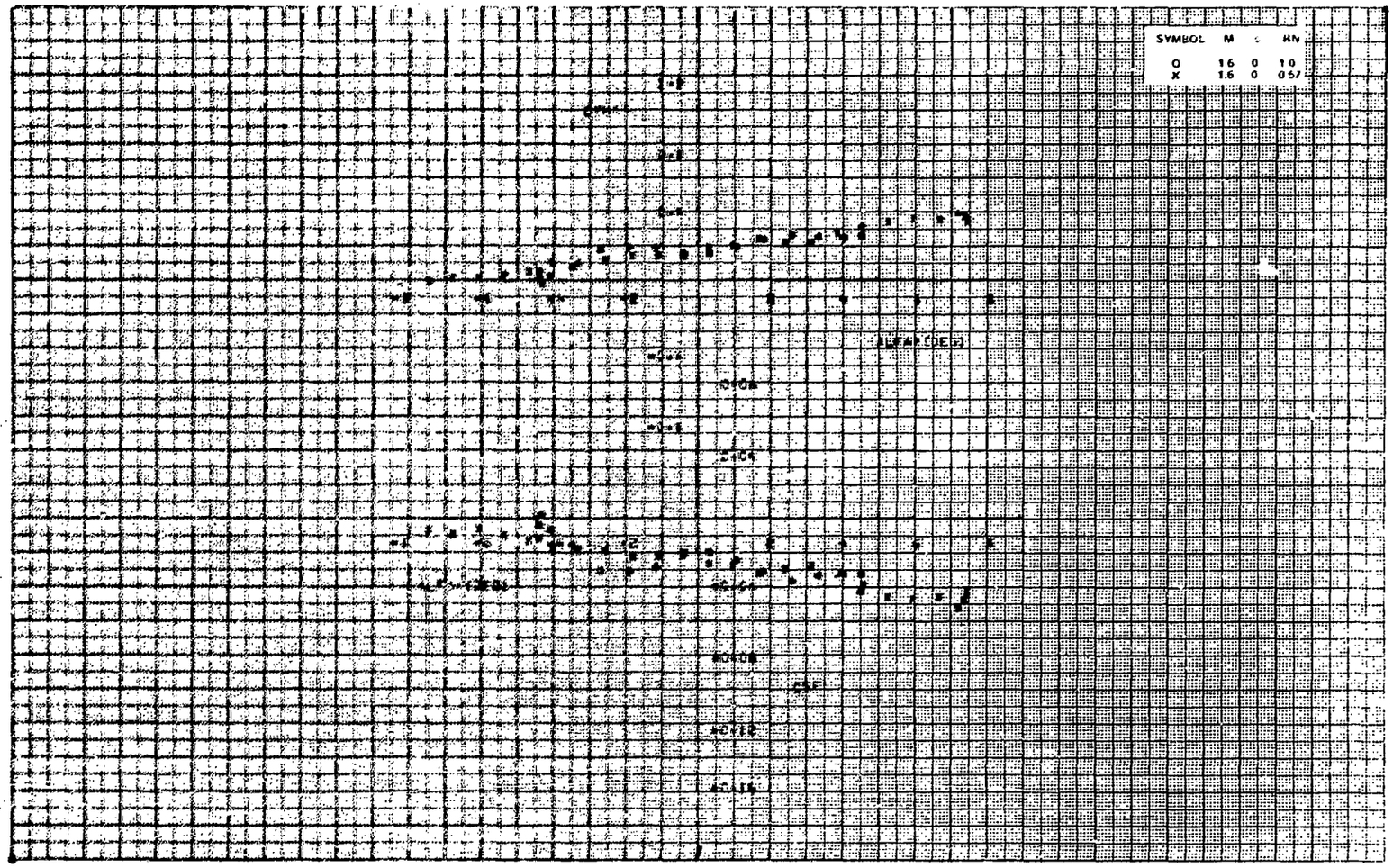


Figure 15c. Continued.

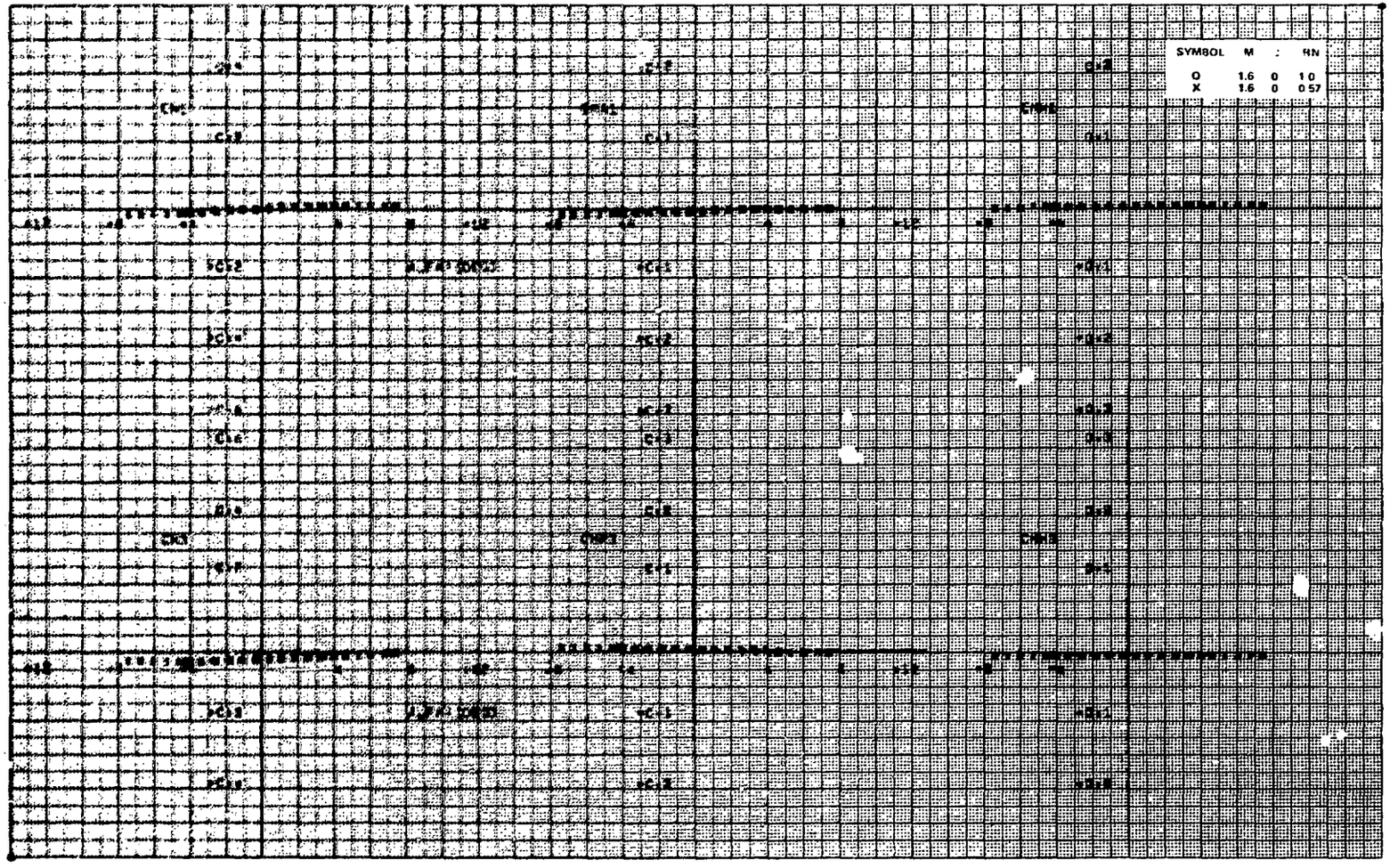


Figure 15c. Continued.

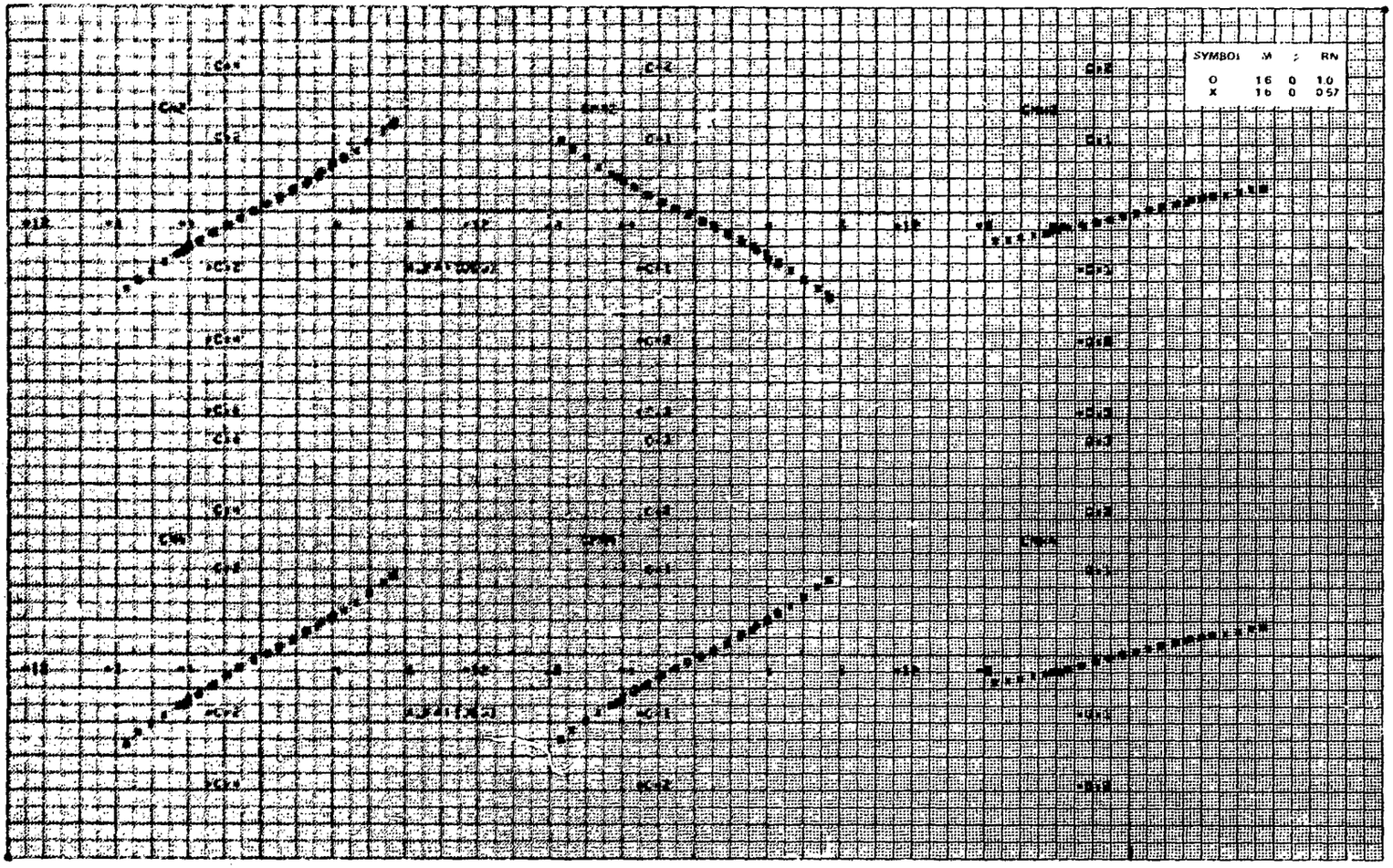


Figure 15c. Concluded.

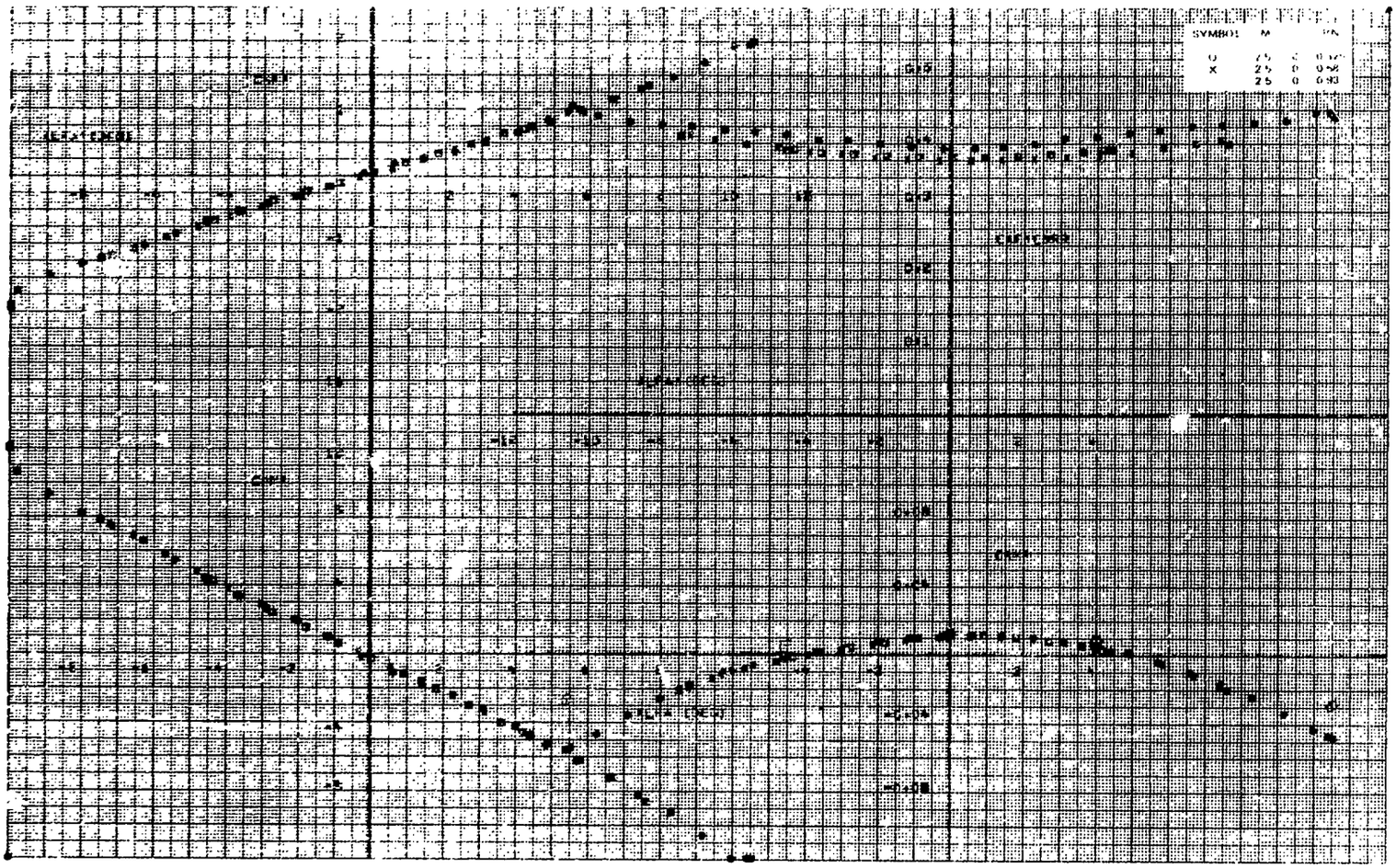


Figure 15d. Aerodynamic stability coefficients, CR/D = 1.75, α = 0 deg, M_∞ = 2.5.

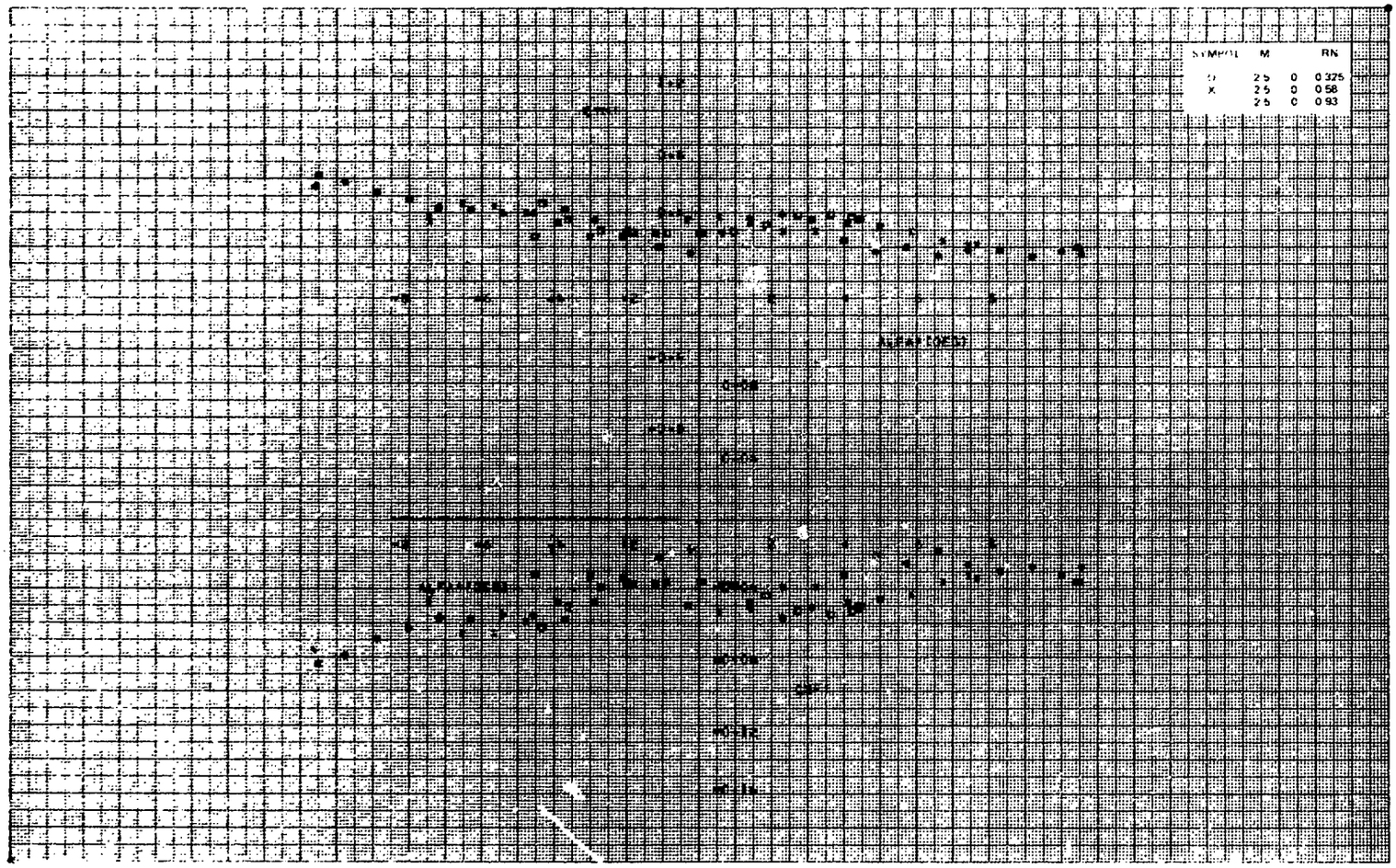


Figure 15d. Continued.

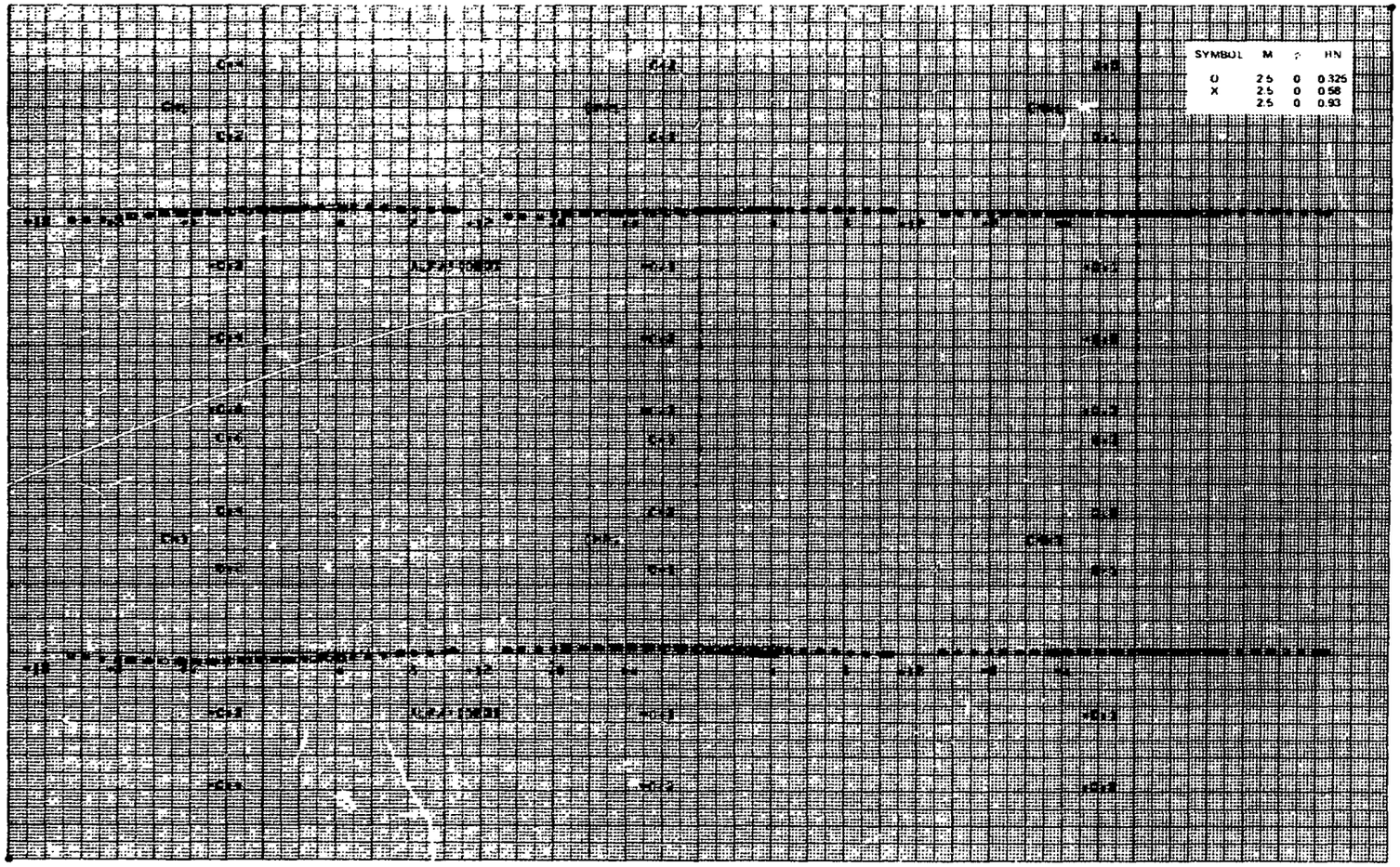


Figure 15d. Continued.

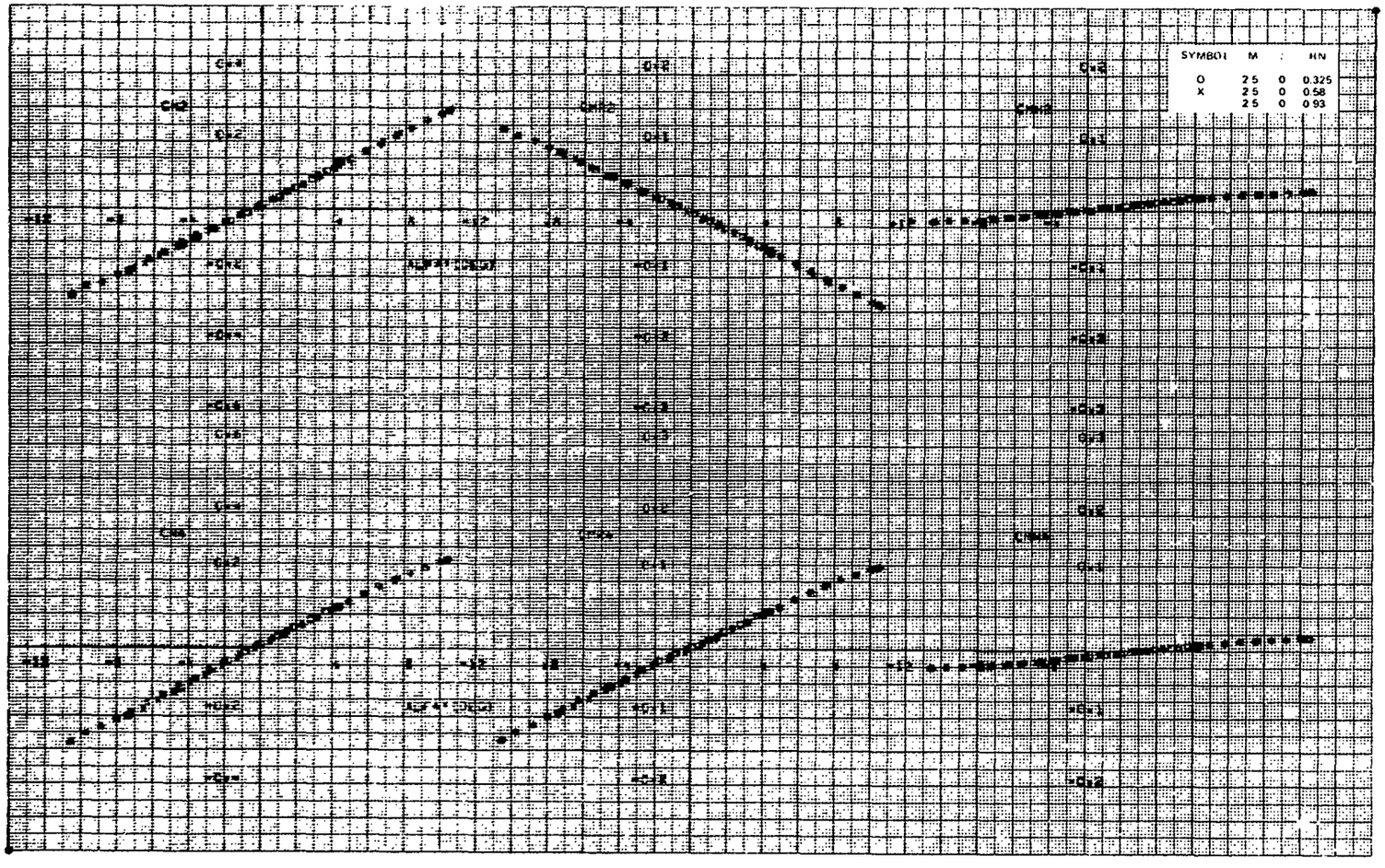


Figure 15d. Concluded.

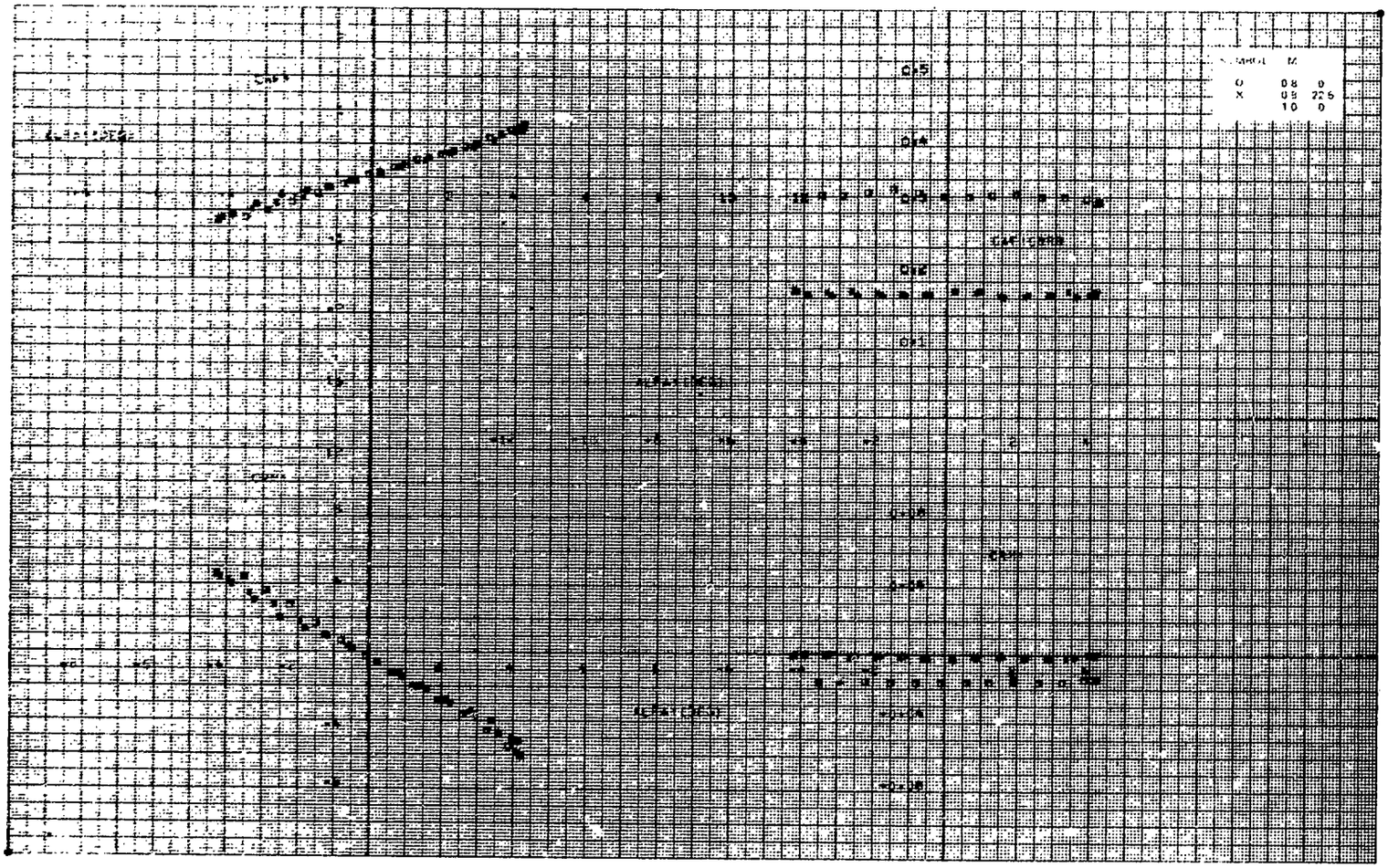


Figure 10a. Aerodynamic stability coefficients, CR/D = 1.0, = 0 deg, M = 0.8, 1.0.

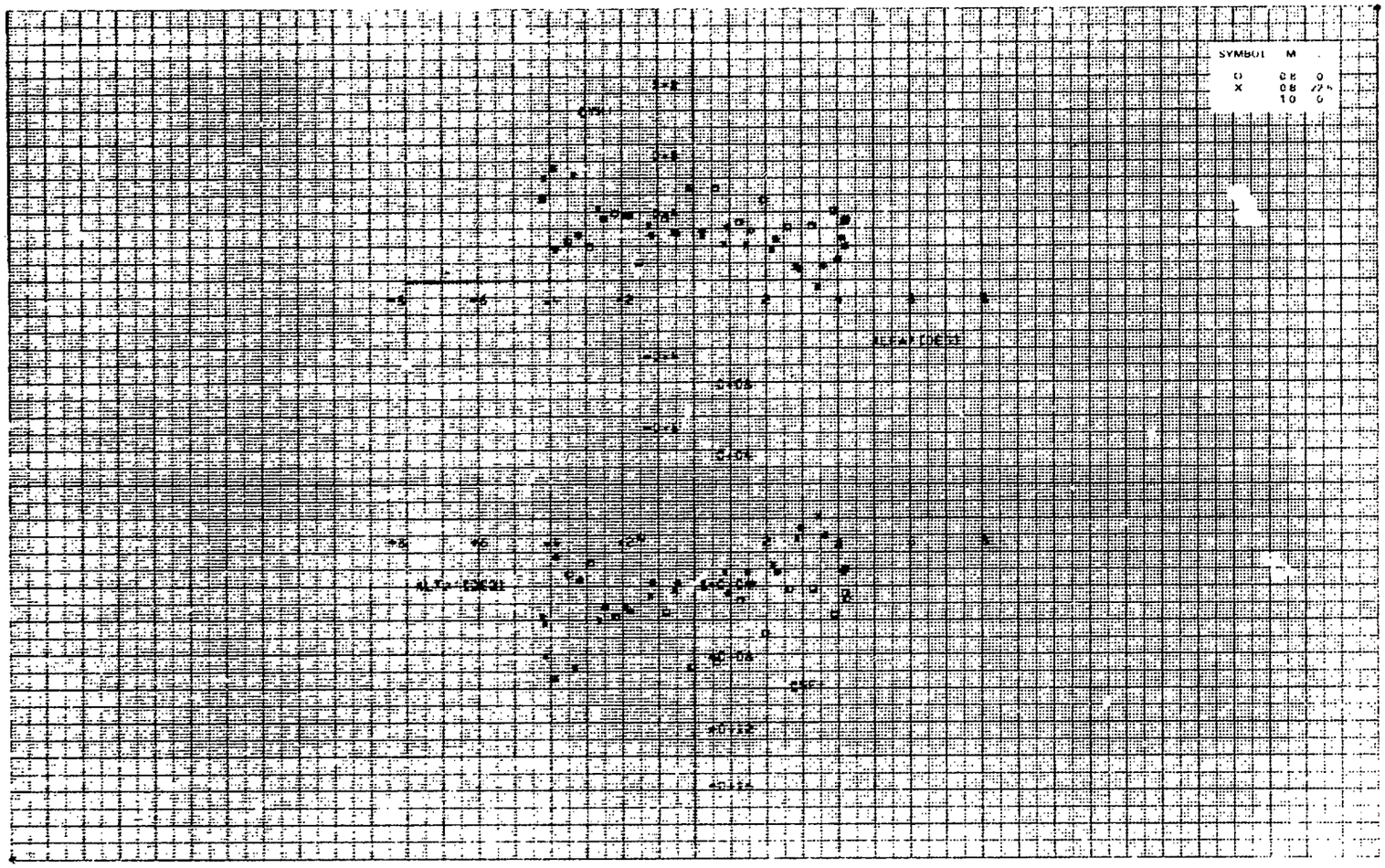


Figure 16a. Continued.

Reproduced from best available copy.

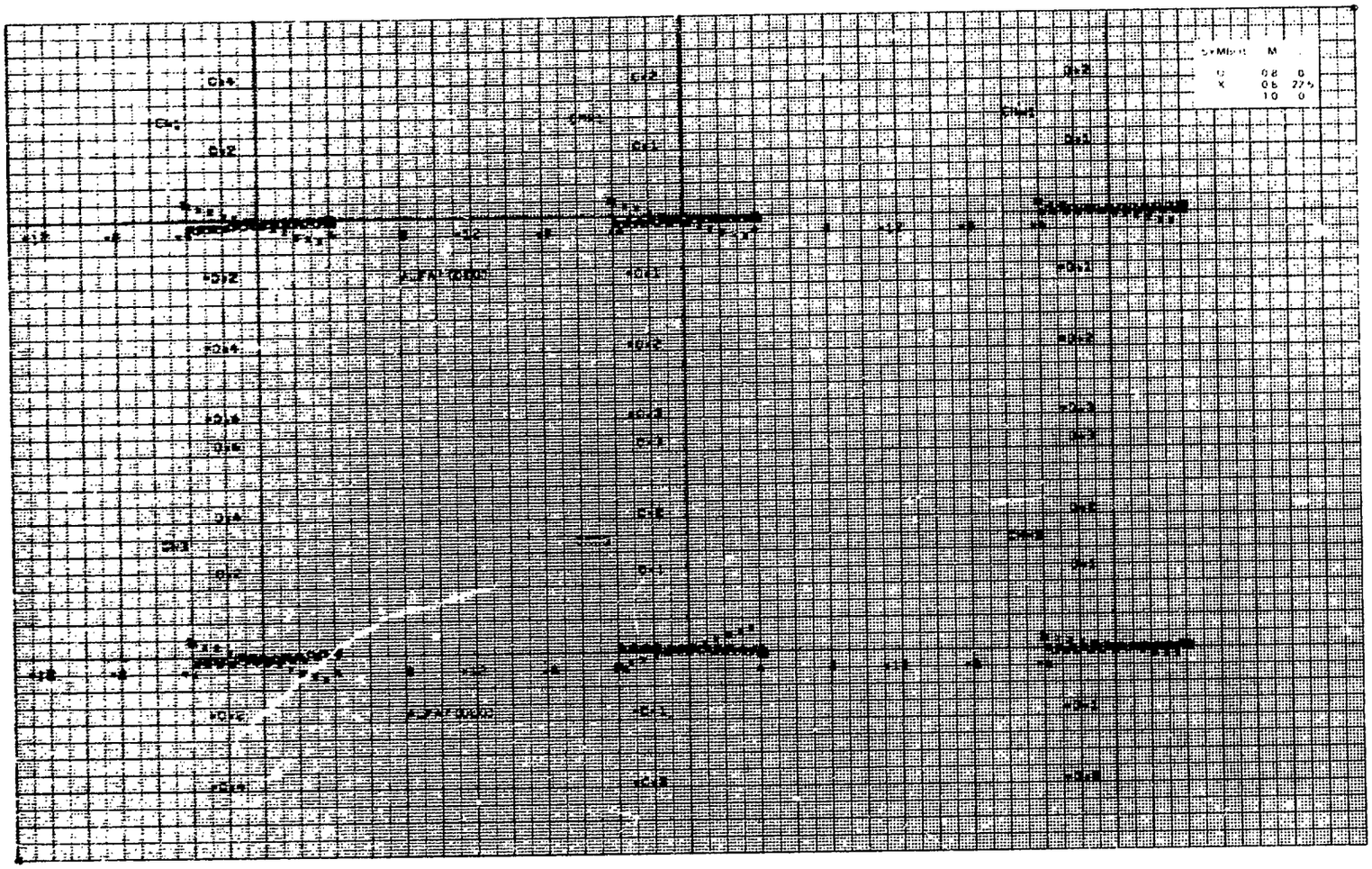


Figure 16a. Continued.

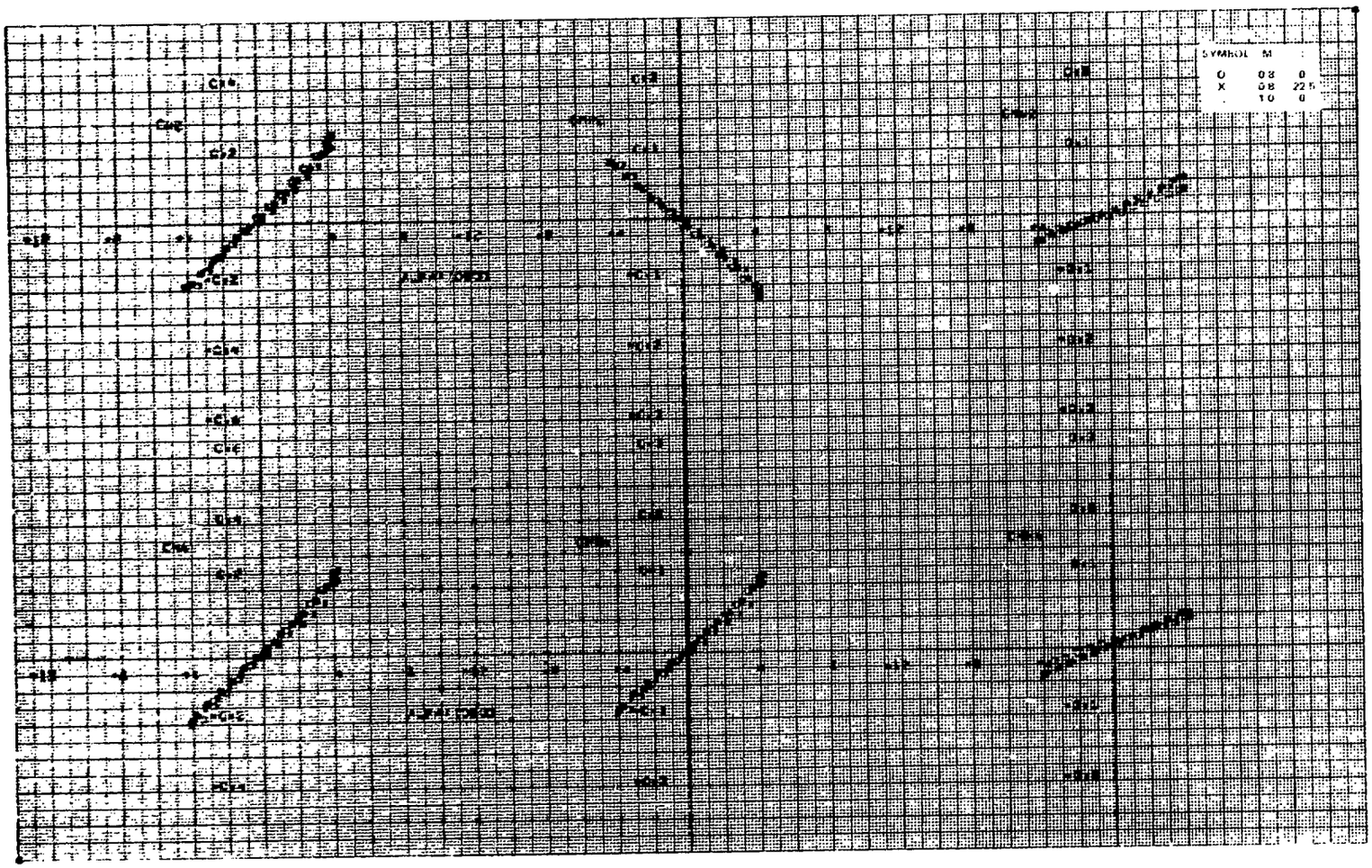


Figure 16a. Concluded.

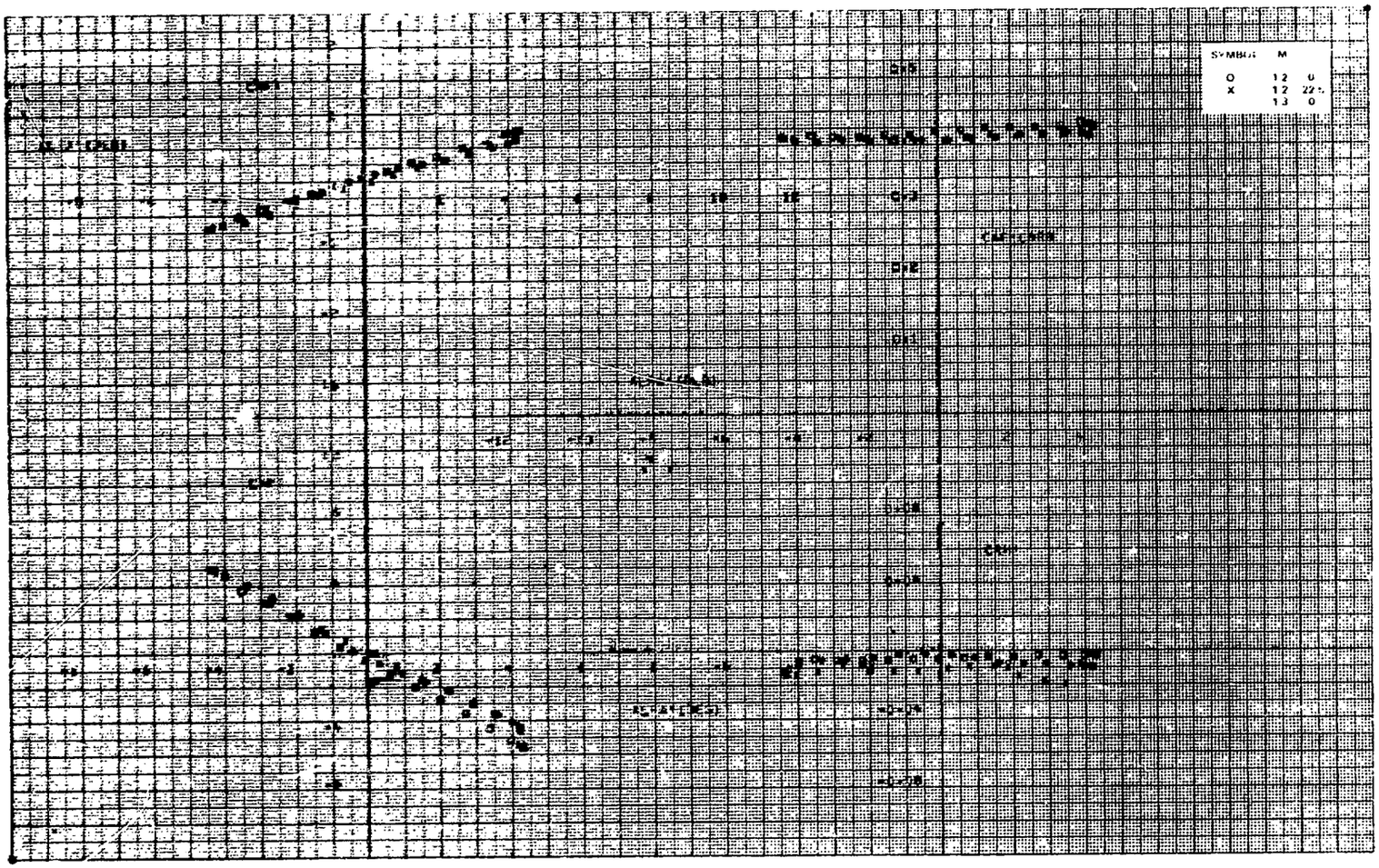


Figure 16b. Aerodynamic stability coefficients, CR/b = 1.0, Λ = 0 deg, M_∞ = 1.2, 1.3.

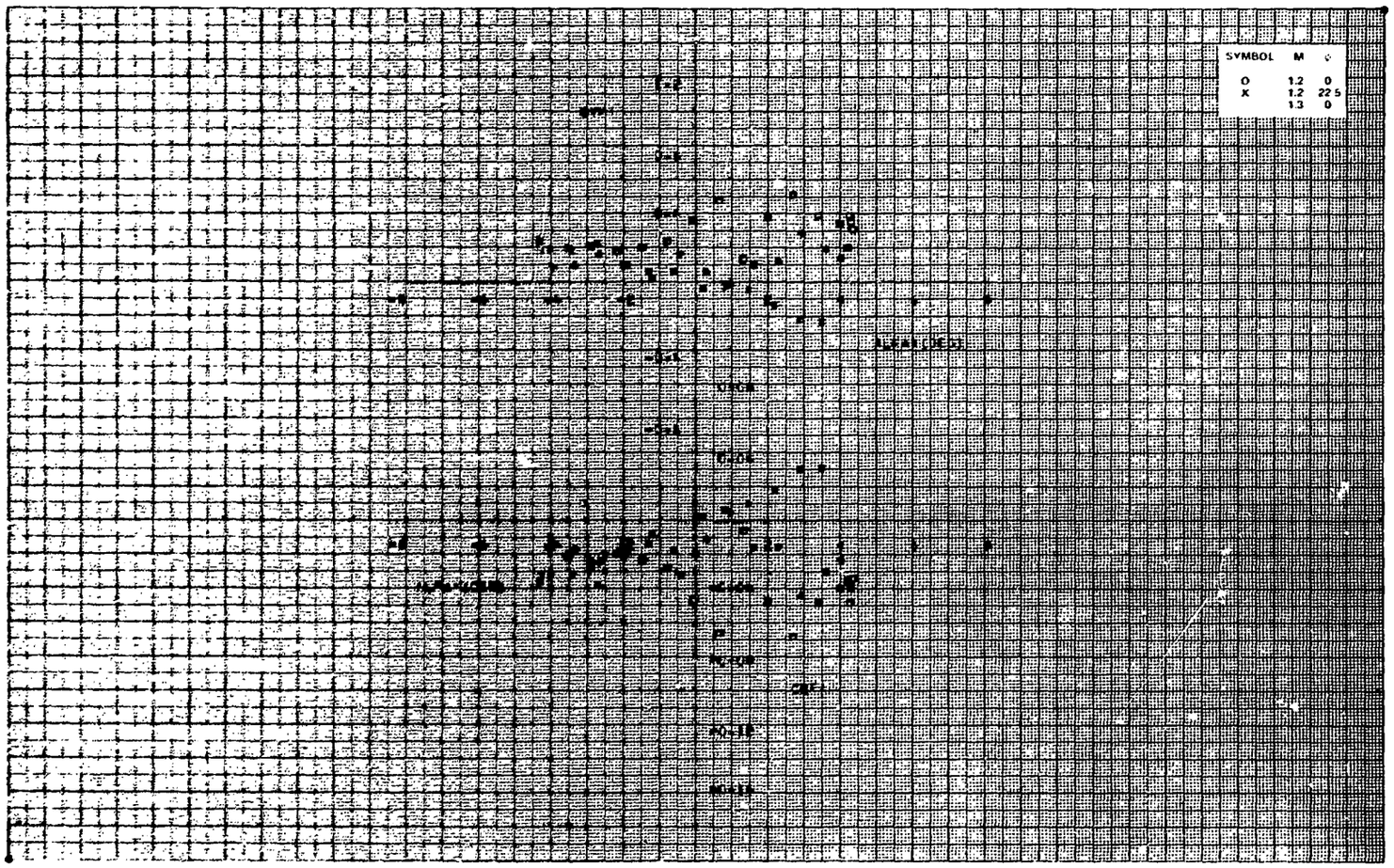


Figure 16b. Continued.

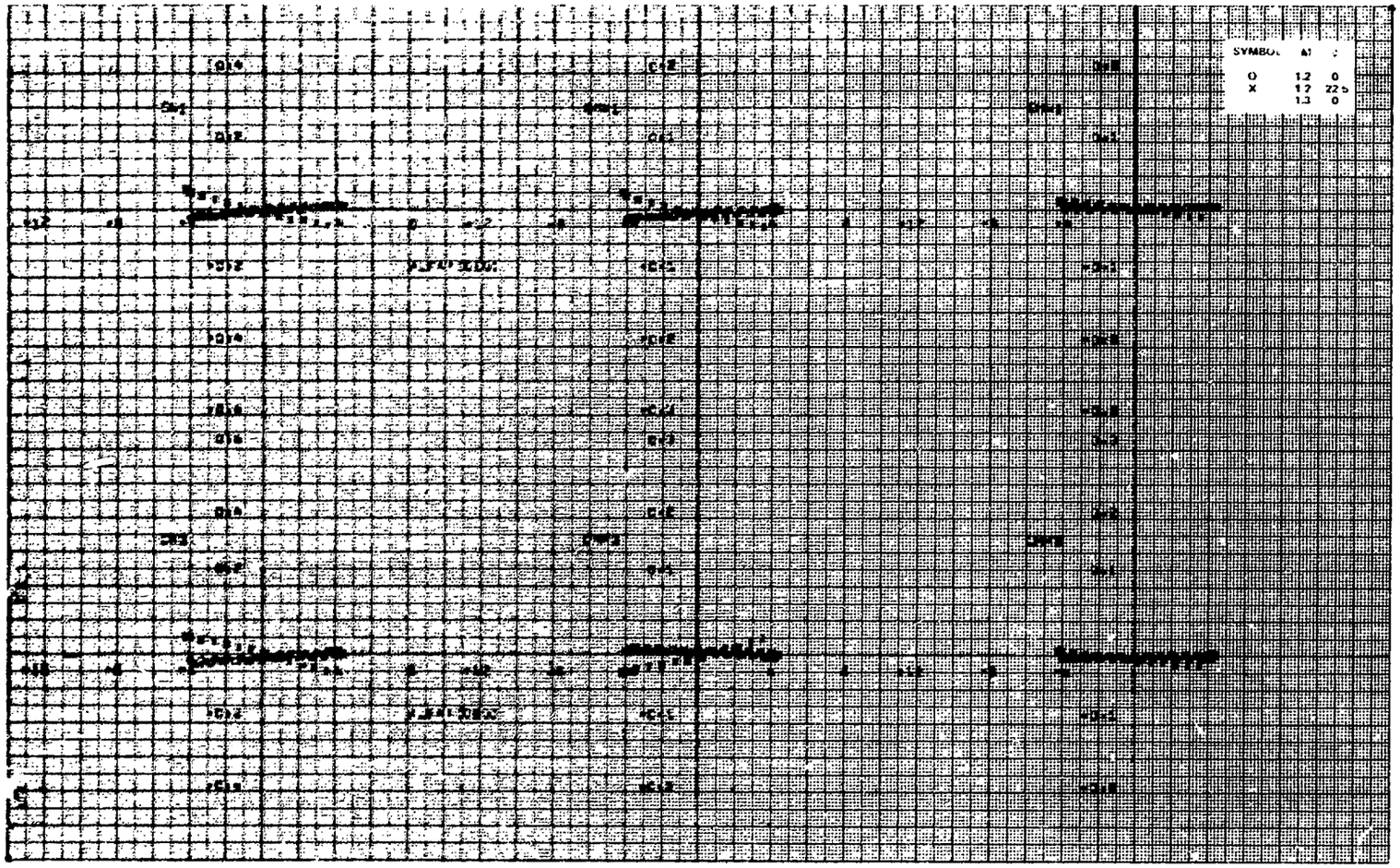


Figure 16b. Continued.

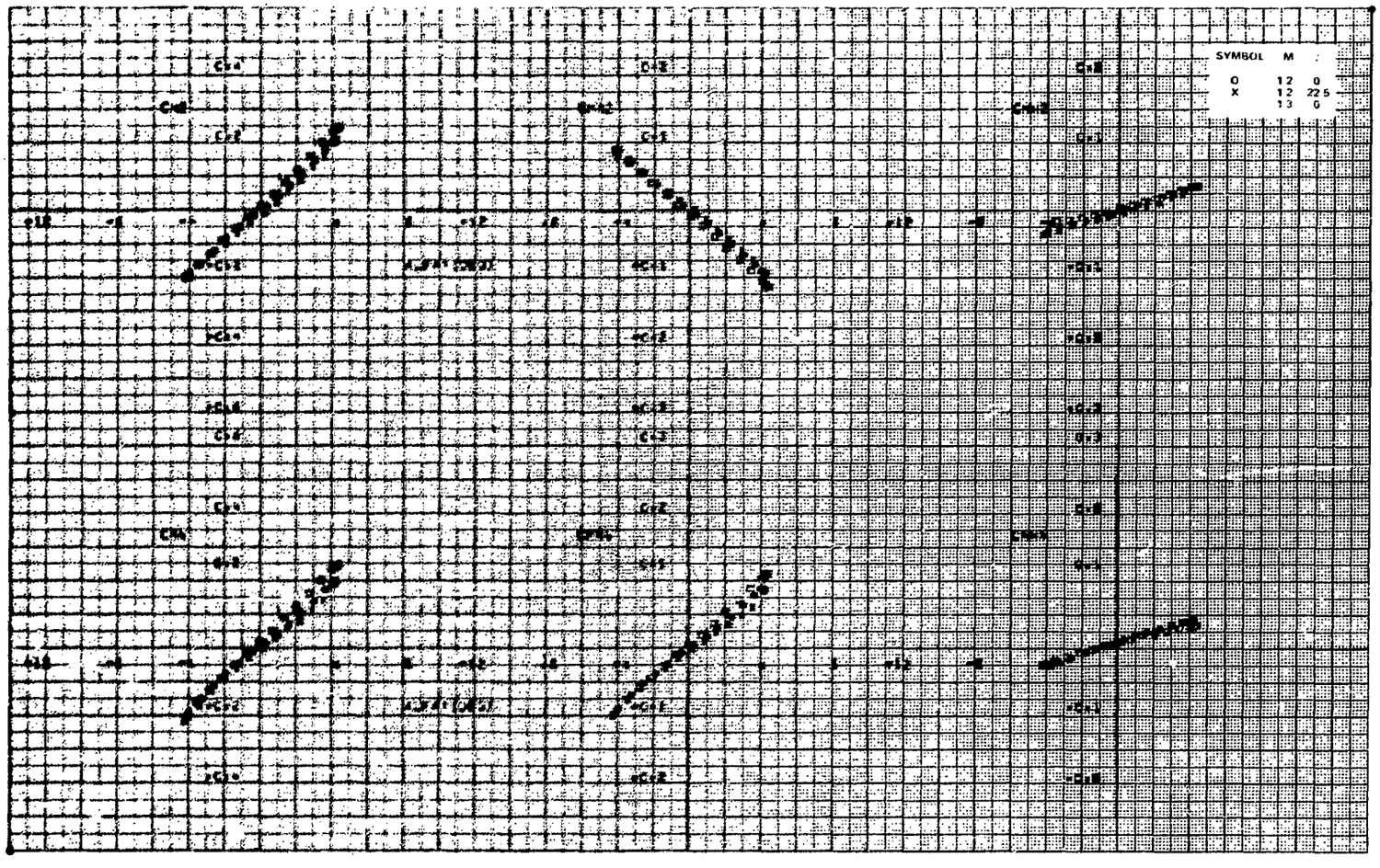
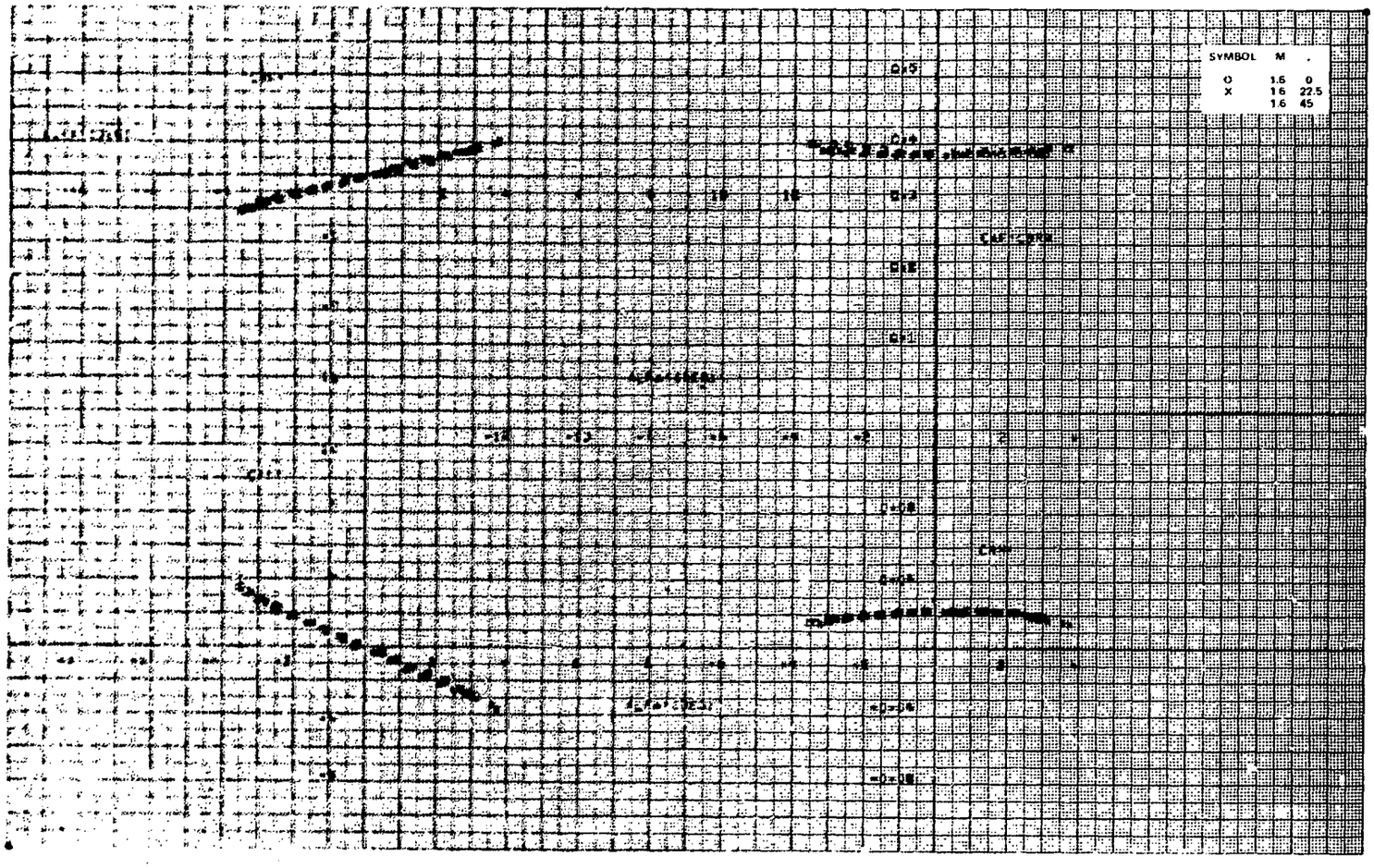


Figure 16b. Concluded.



Aerodynamic stability coefficients, CG/D = 1.0, = 0 deg, M = 1.6.

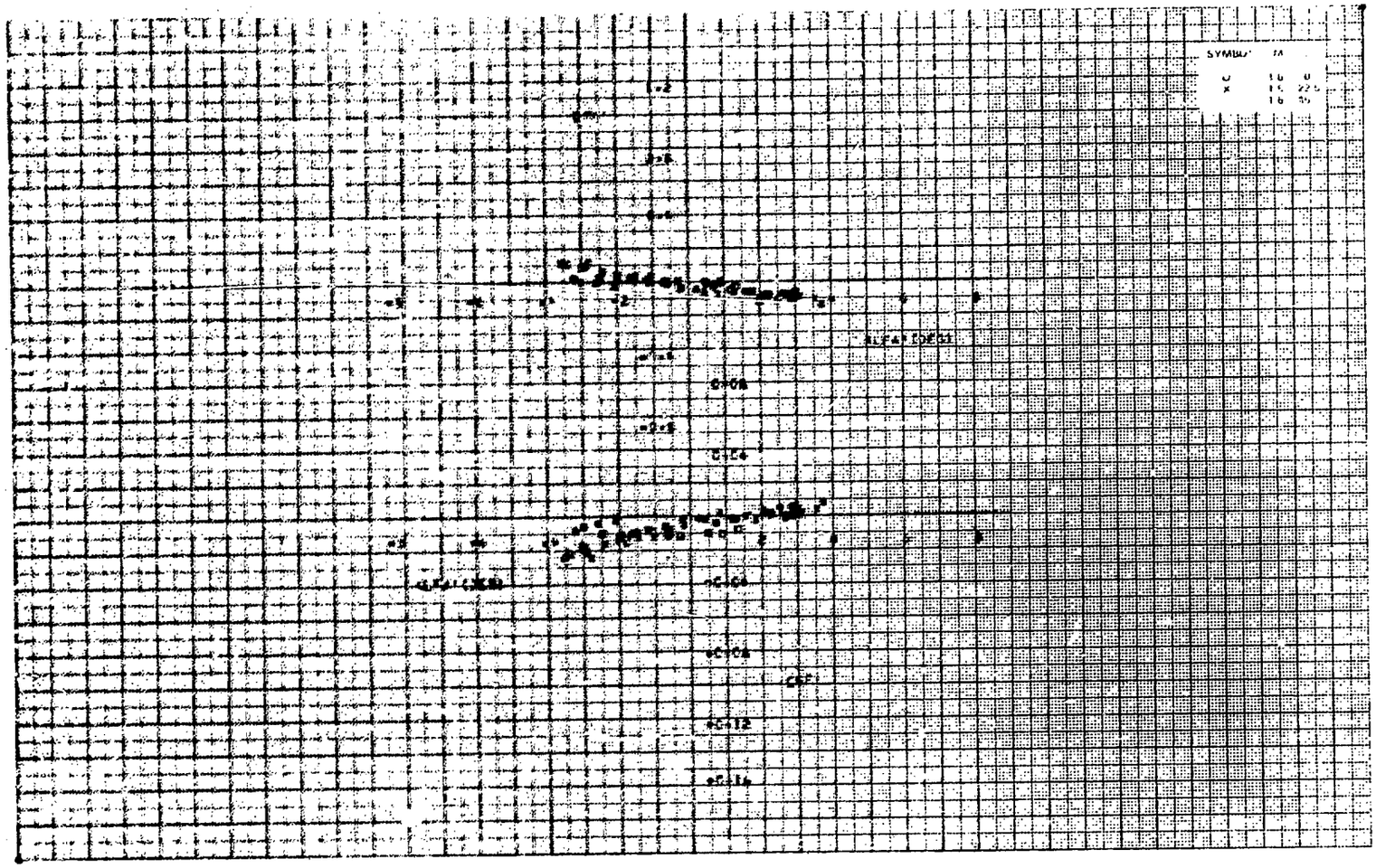


Figure [illegible]. Continued.

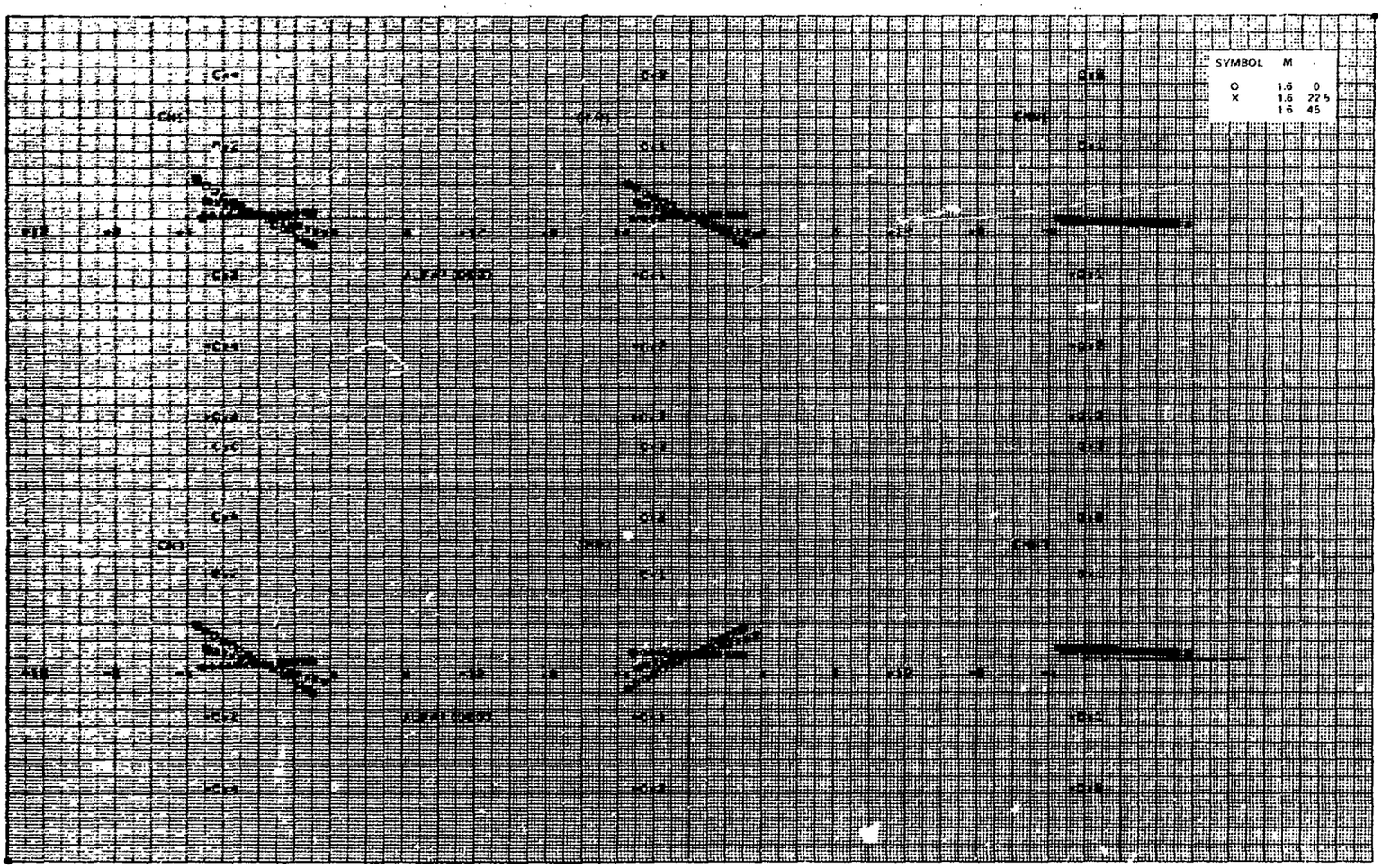


Figure 16c. Continued.

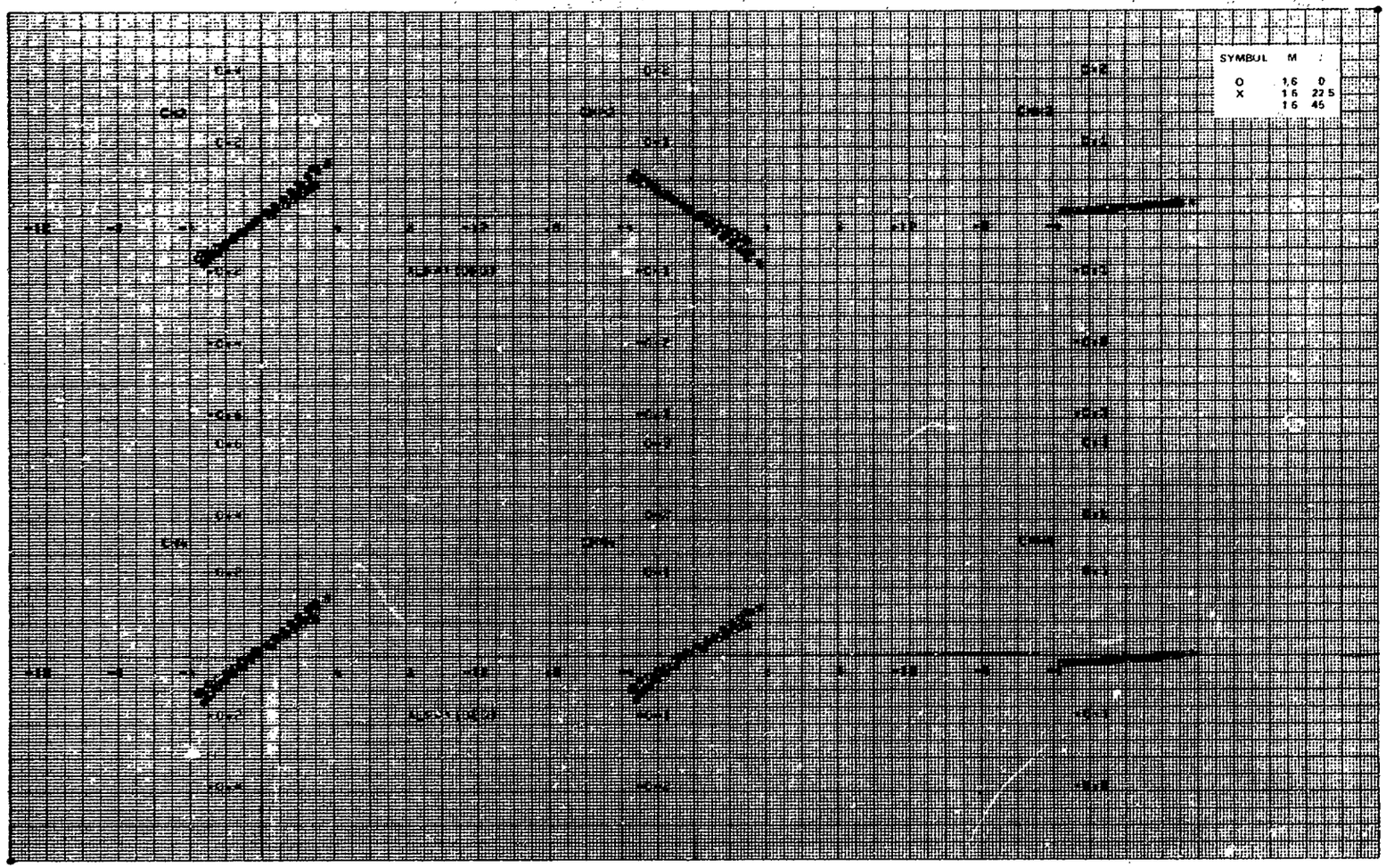


Figure 16c. Concluded.

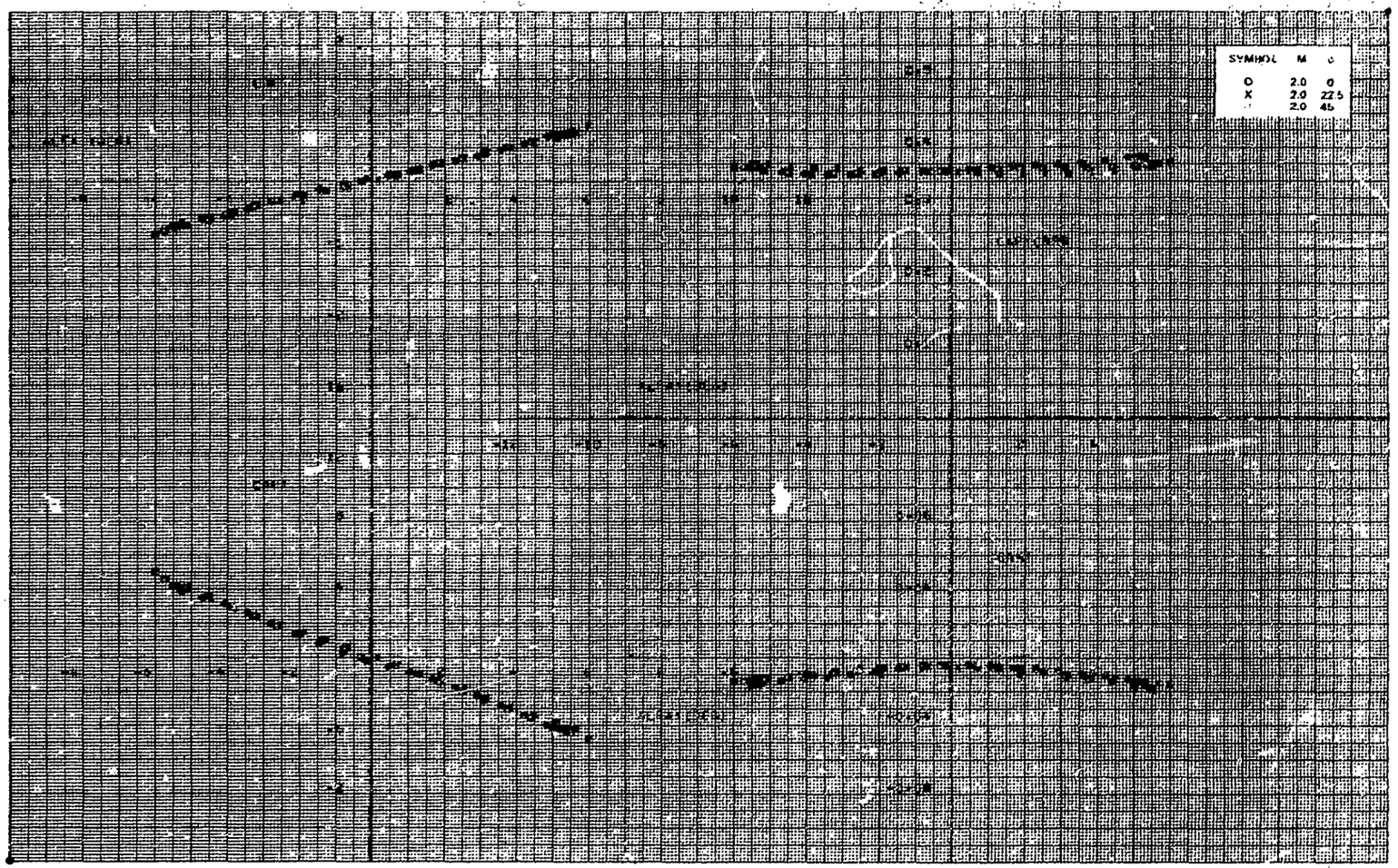


Figure 16d. Aerodynamic stability coefficients, CR/D = 1.0, Λ = 0 deg, M_∞ = 2.0.

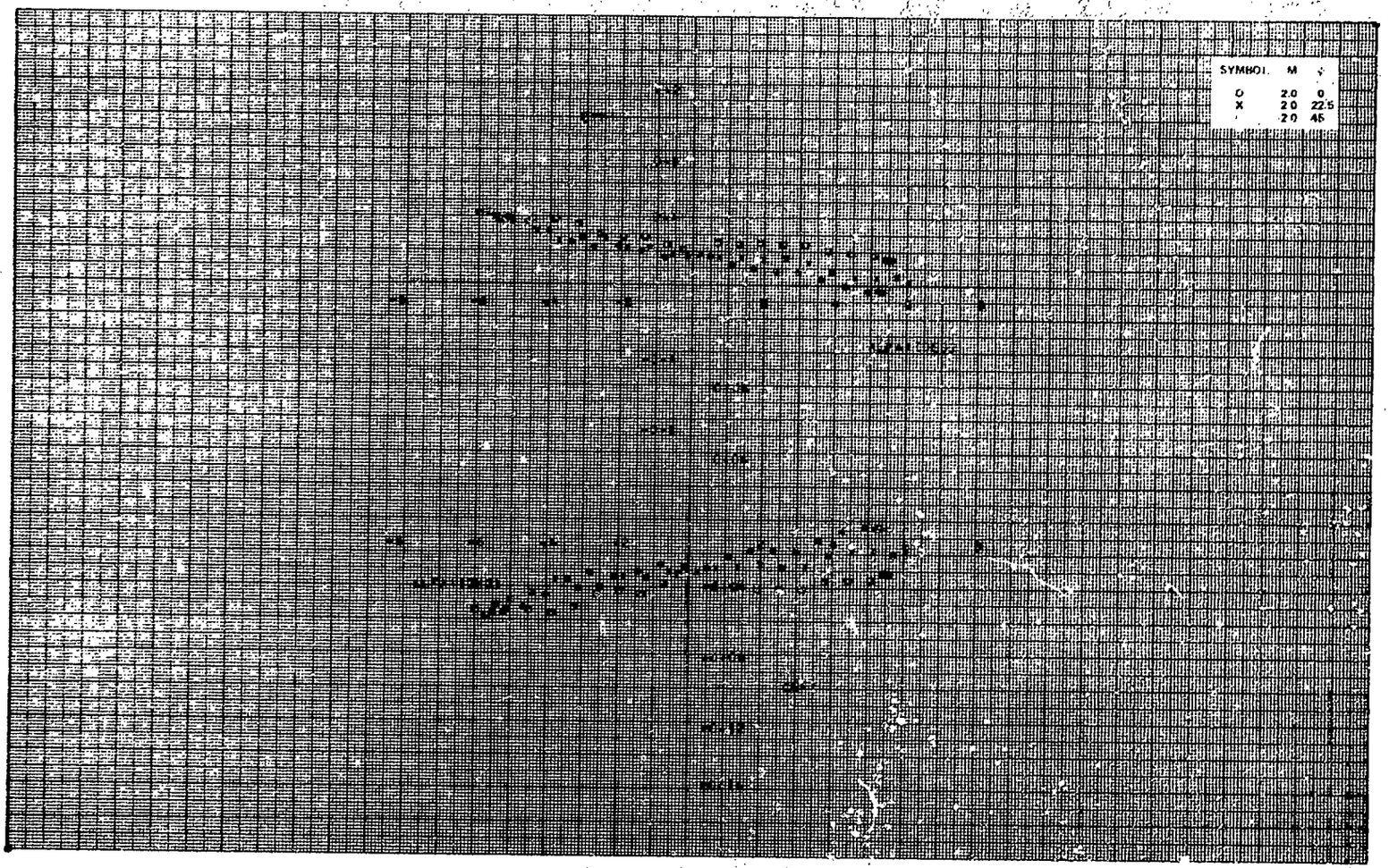


Figure 16d. Continued.

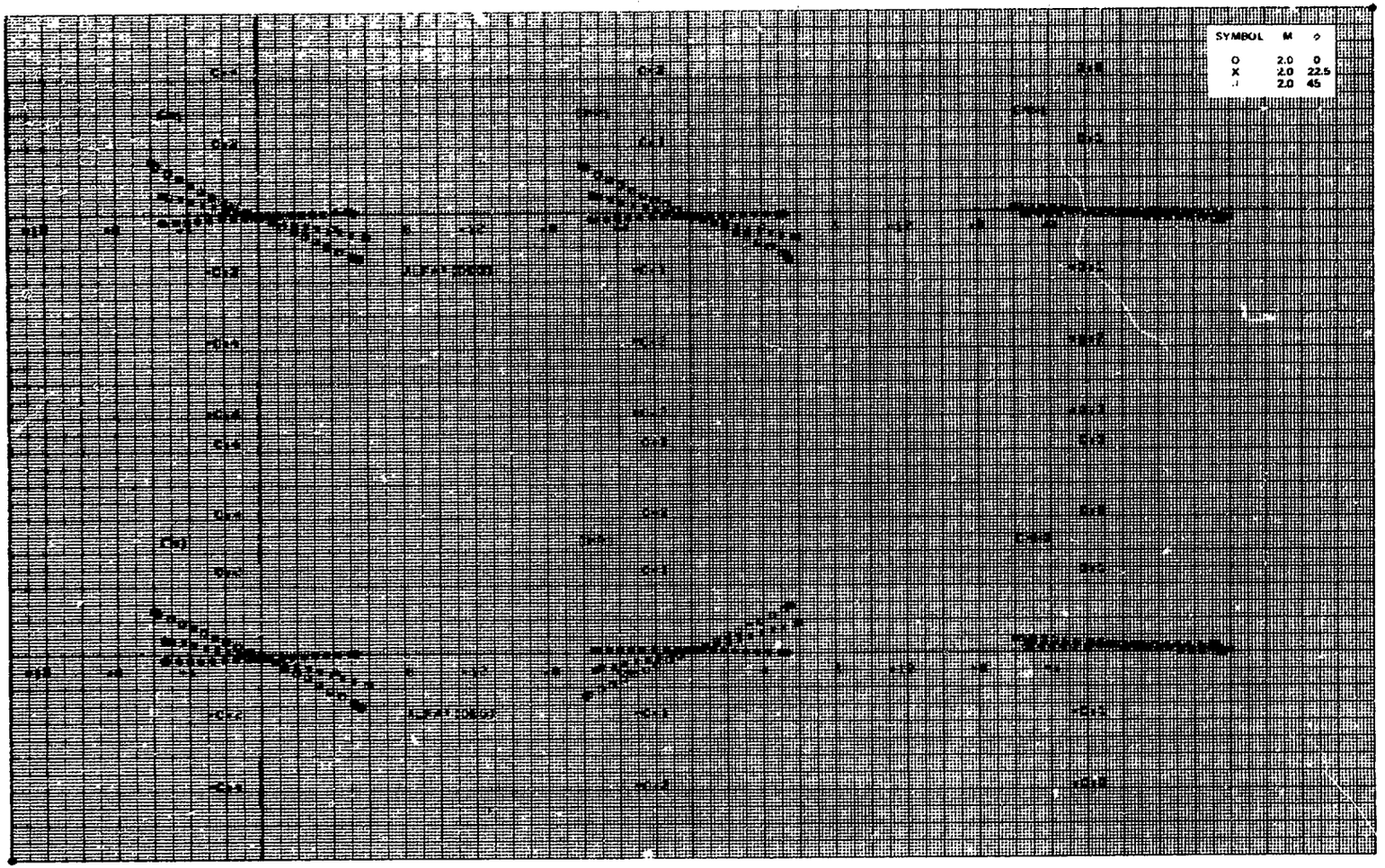


Figure 16d. Continued.

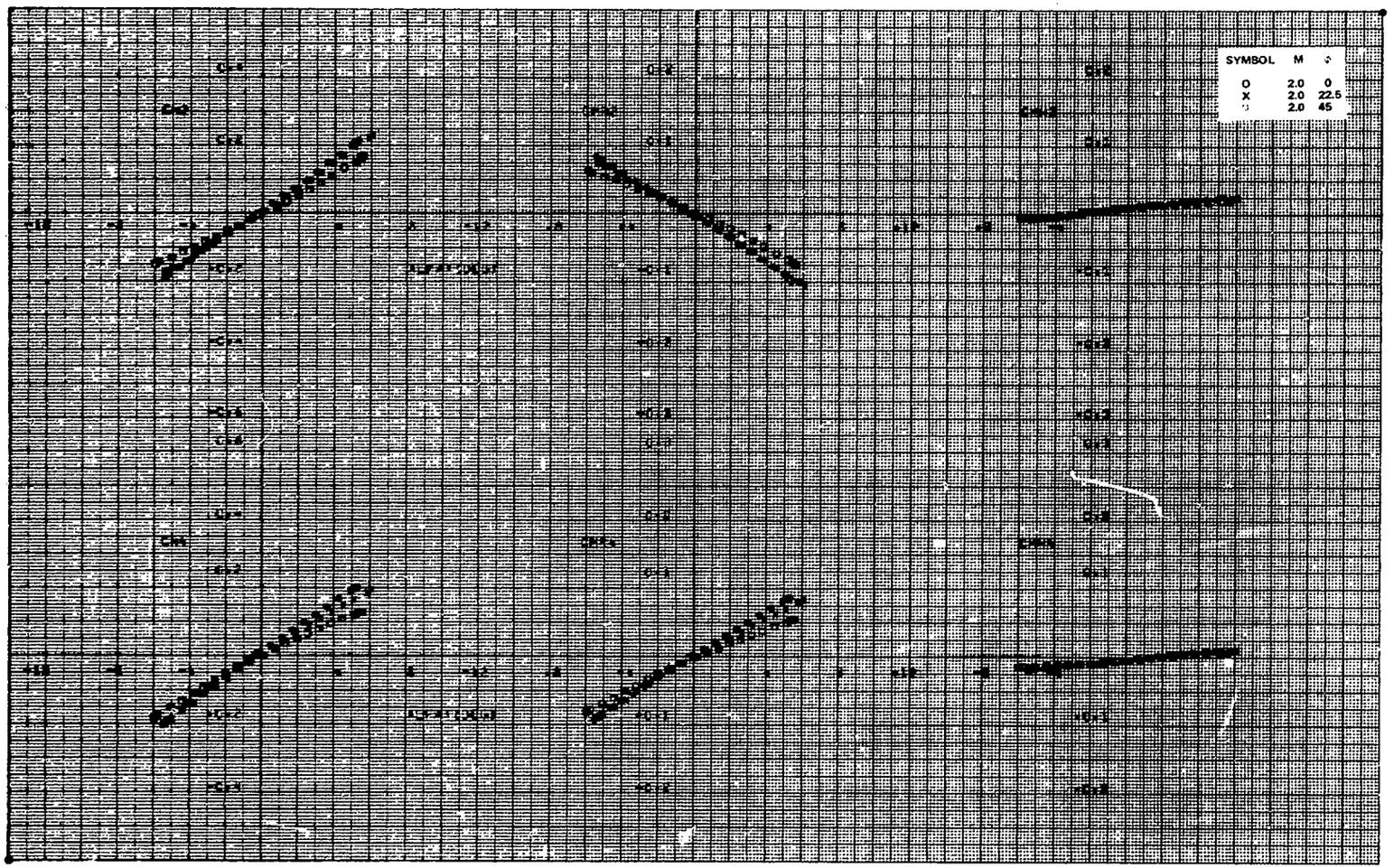


Figure 16d. Concluded.

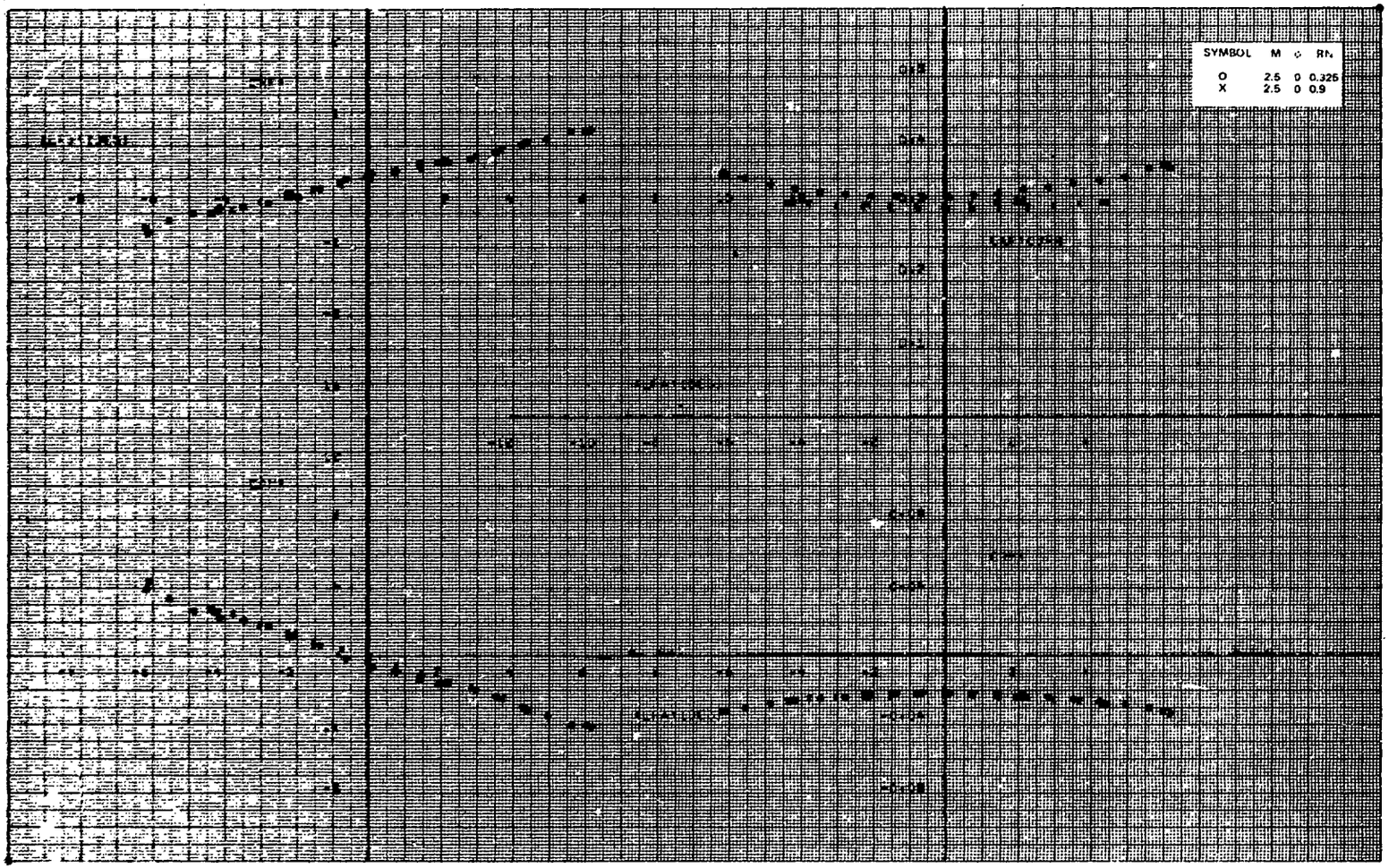


Figure 16e. Aerodynamic stability coefficients, CR/D = 1.0, Λ = 0 deg, M_∞ = 2.5.

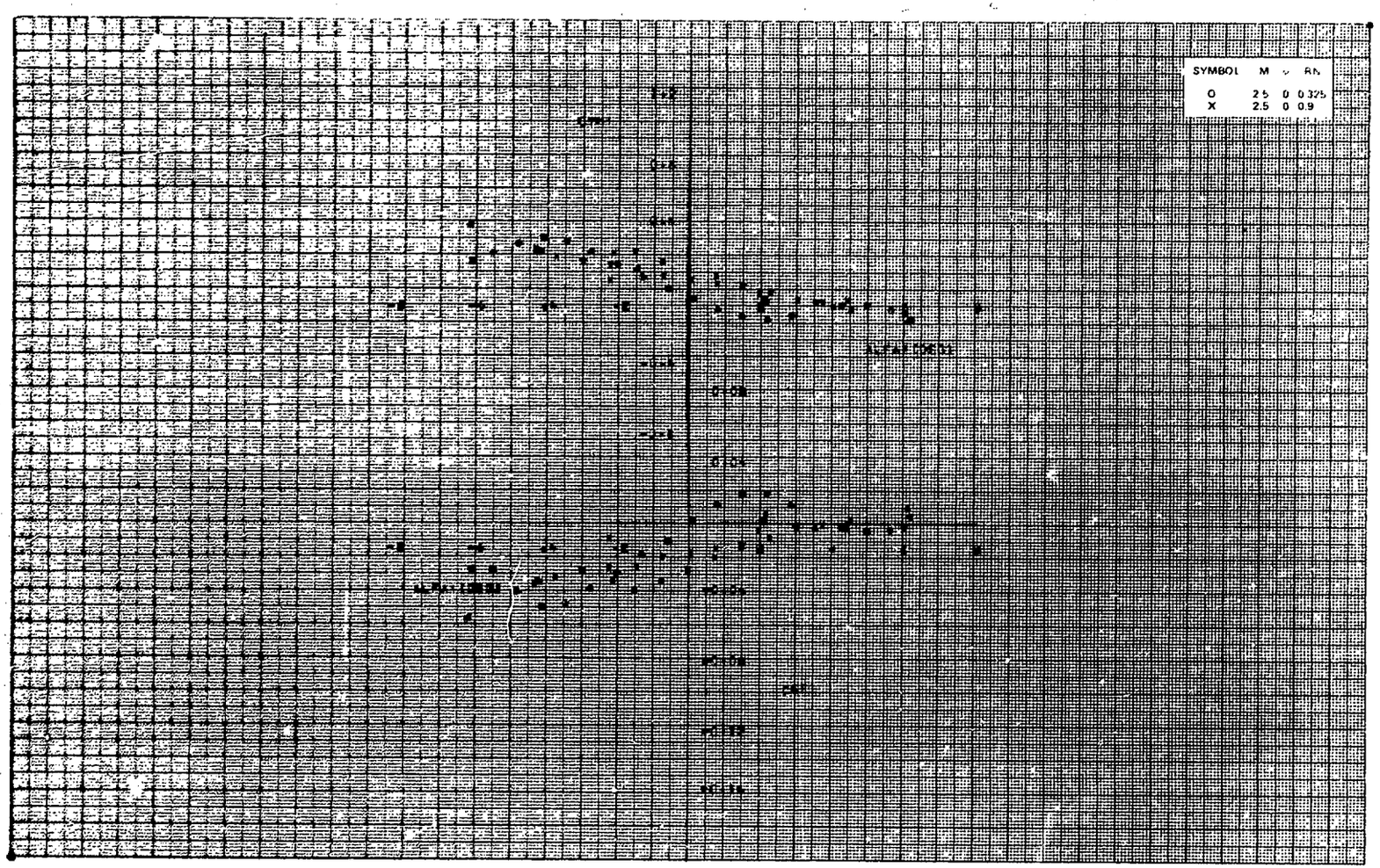


Figure 16e. Continued.

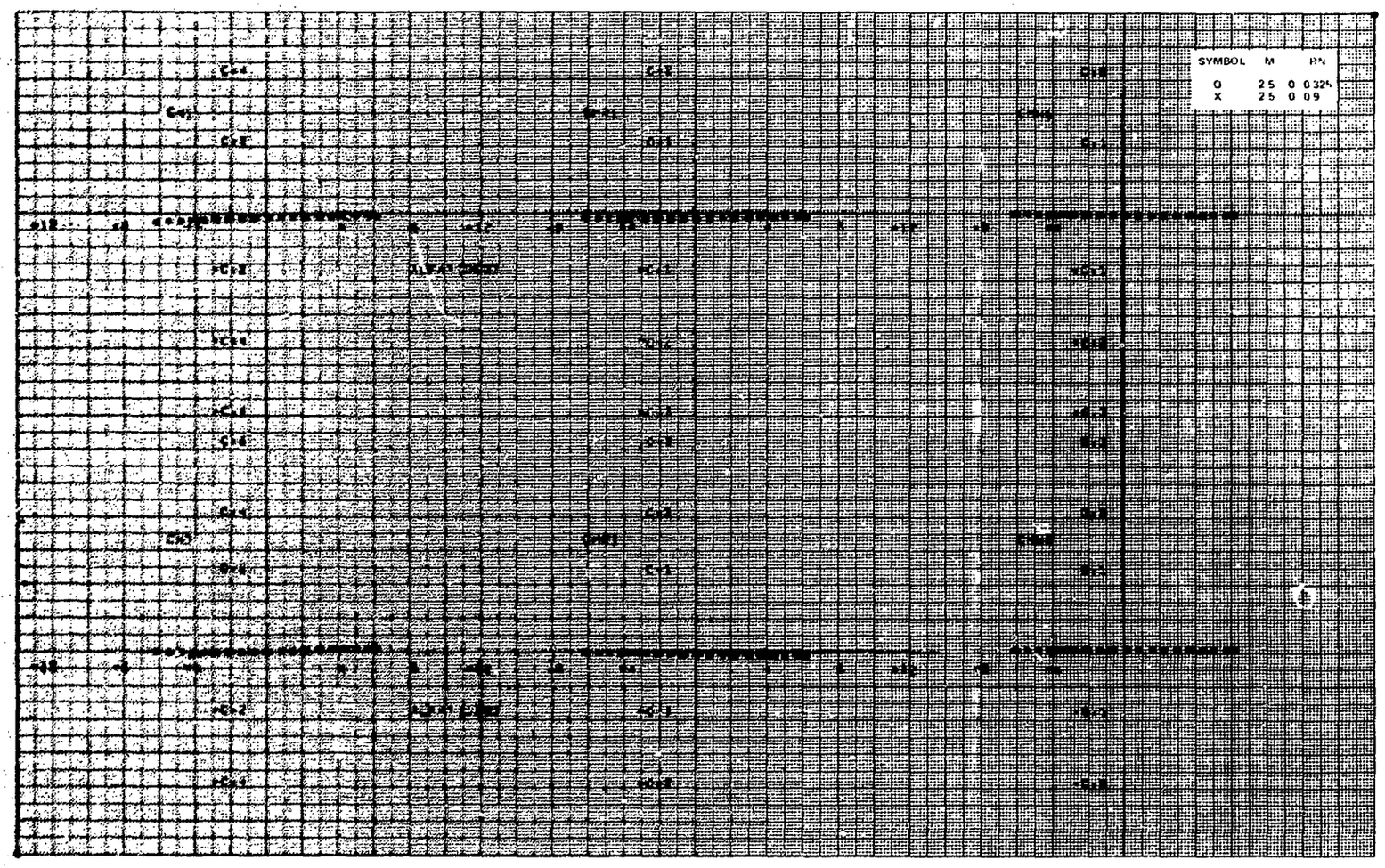


Figure 16e. Continued.

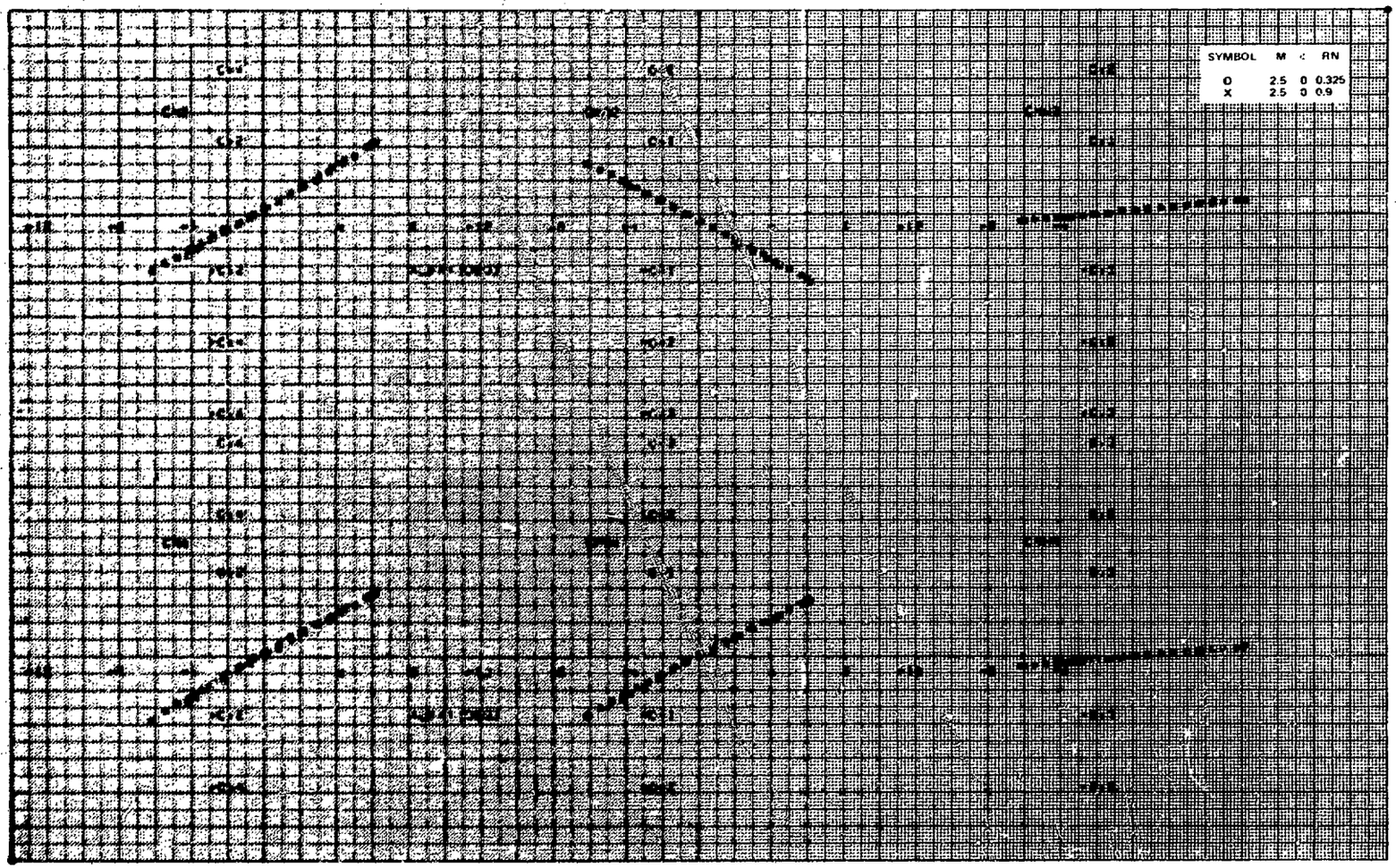


Figure 16e. Concluded.

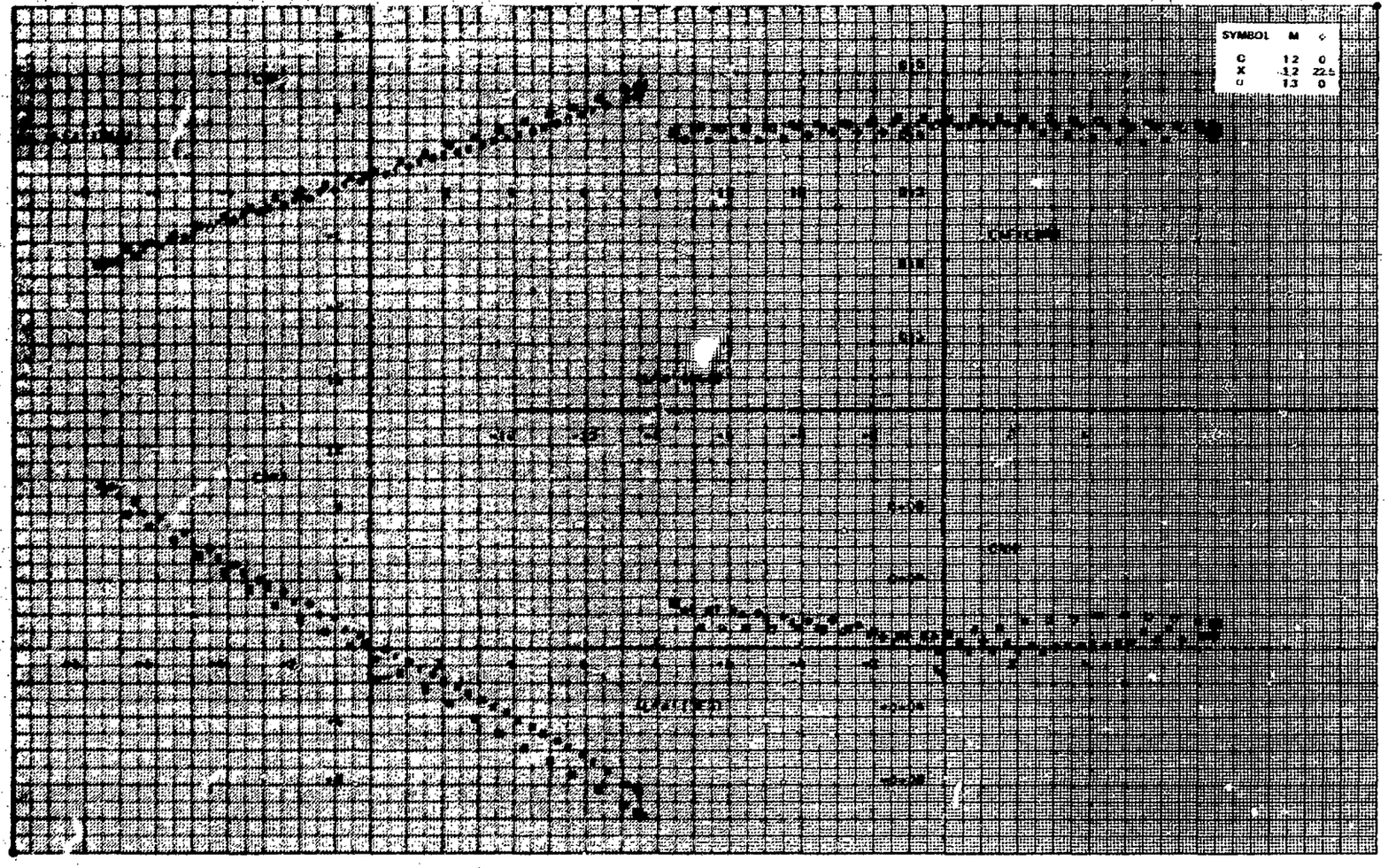


Figure 17a. Aerodynamic stability coefficients, CR/D = 1.0, α = 20.6 deg, M_∞ = 1.2, 1.3.

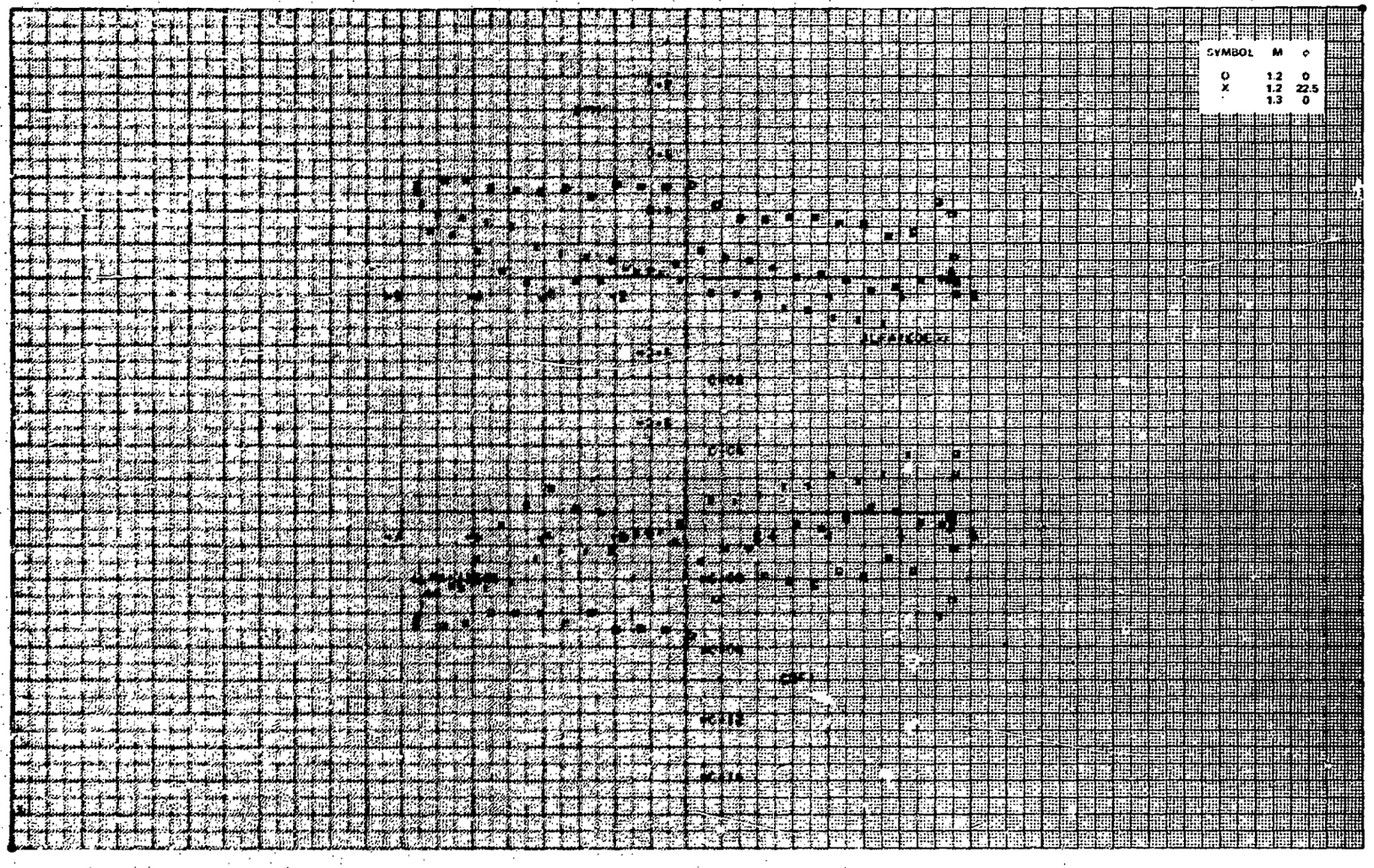


Figure 17a. Continued.

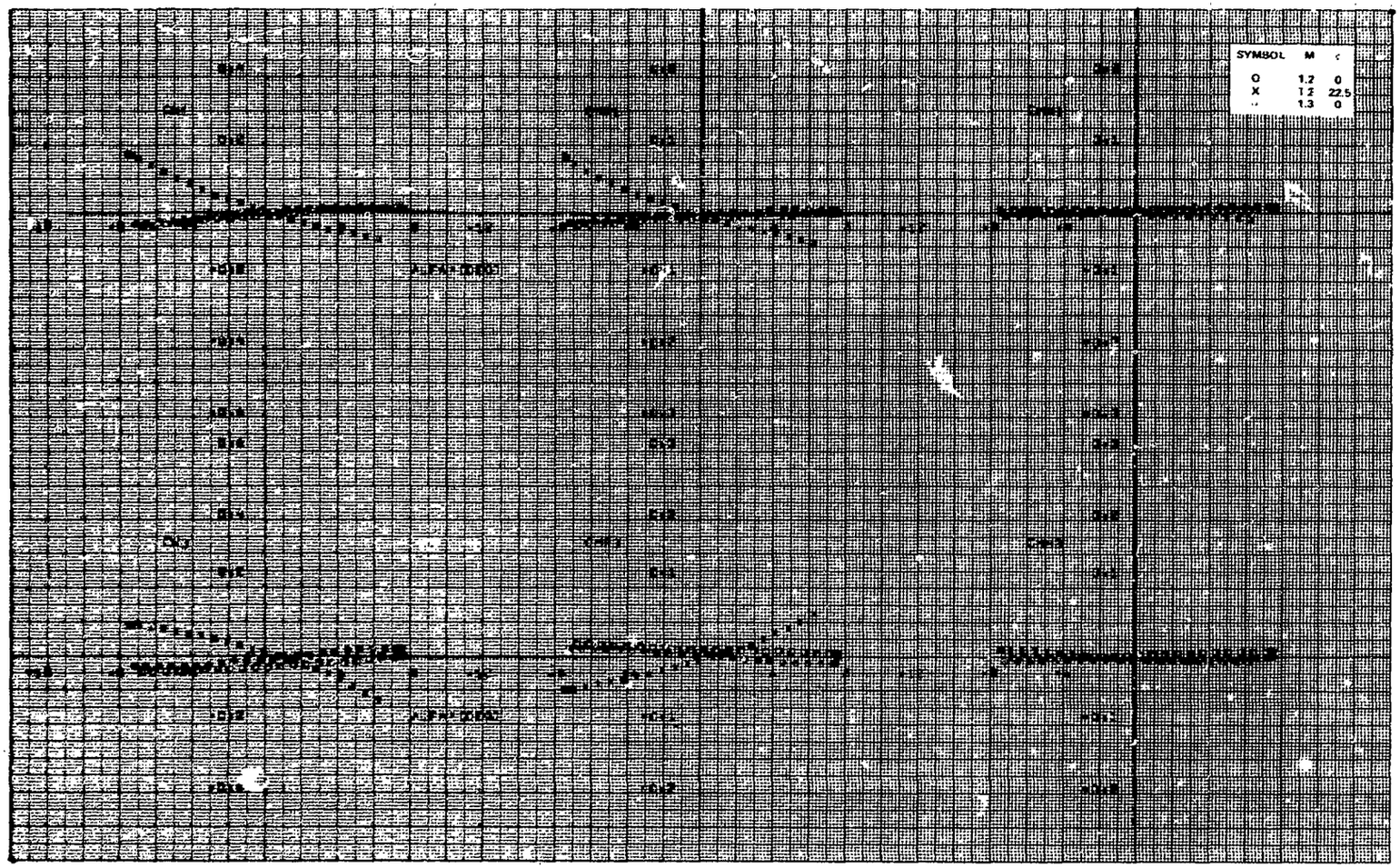


Figure 17a. Continued.

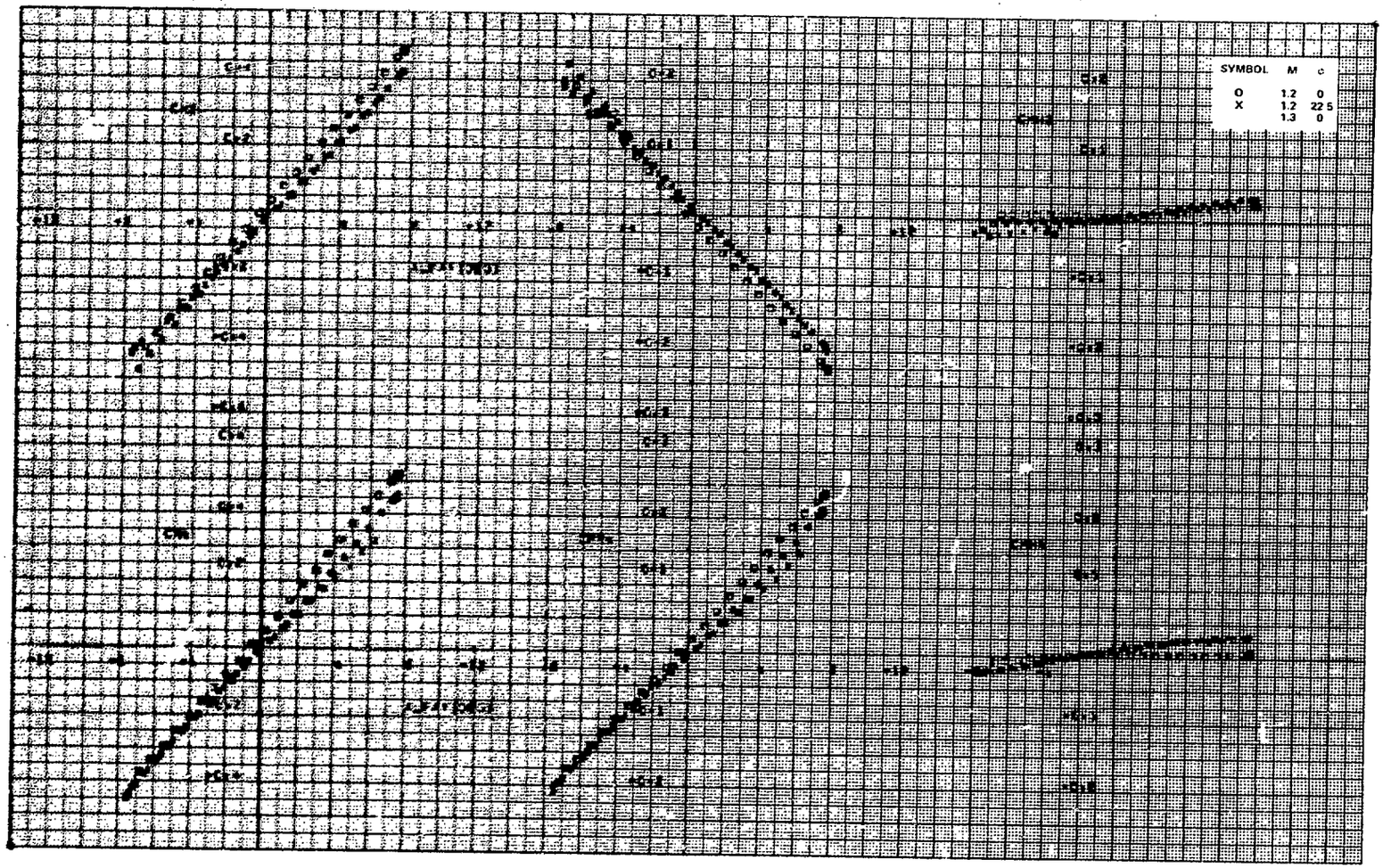


Figure 17a. Concluded.

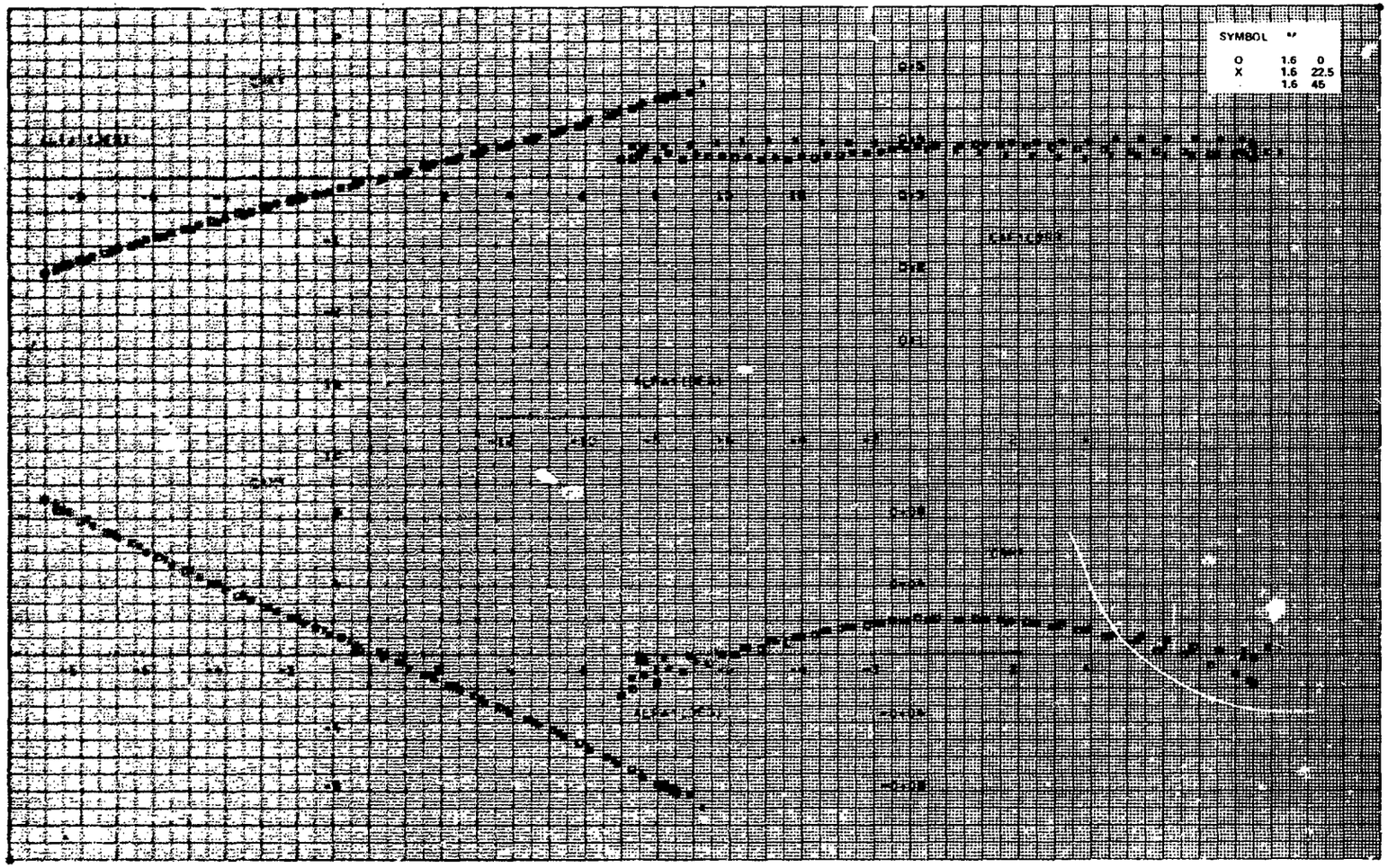


Figure 17b. Aerodynamic stability coefficients, CR/D = 1.0, Λ = 20.6 deg, M_∞ = 1.6.

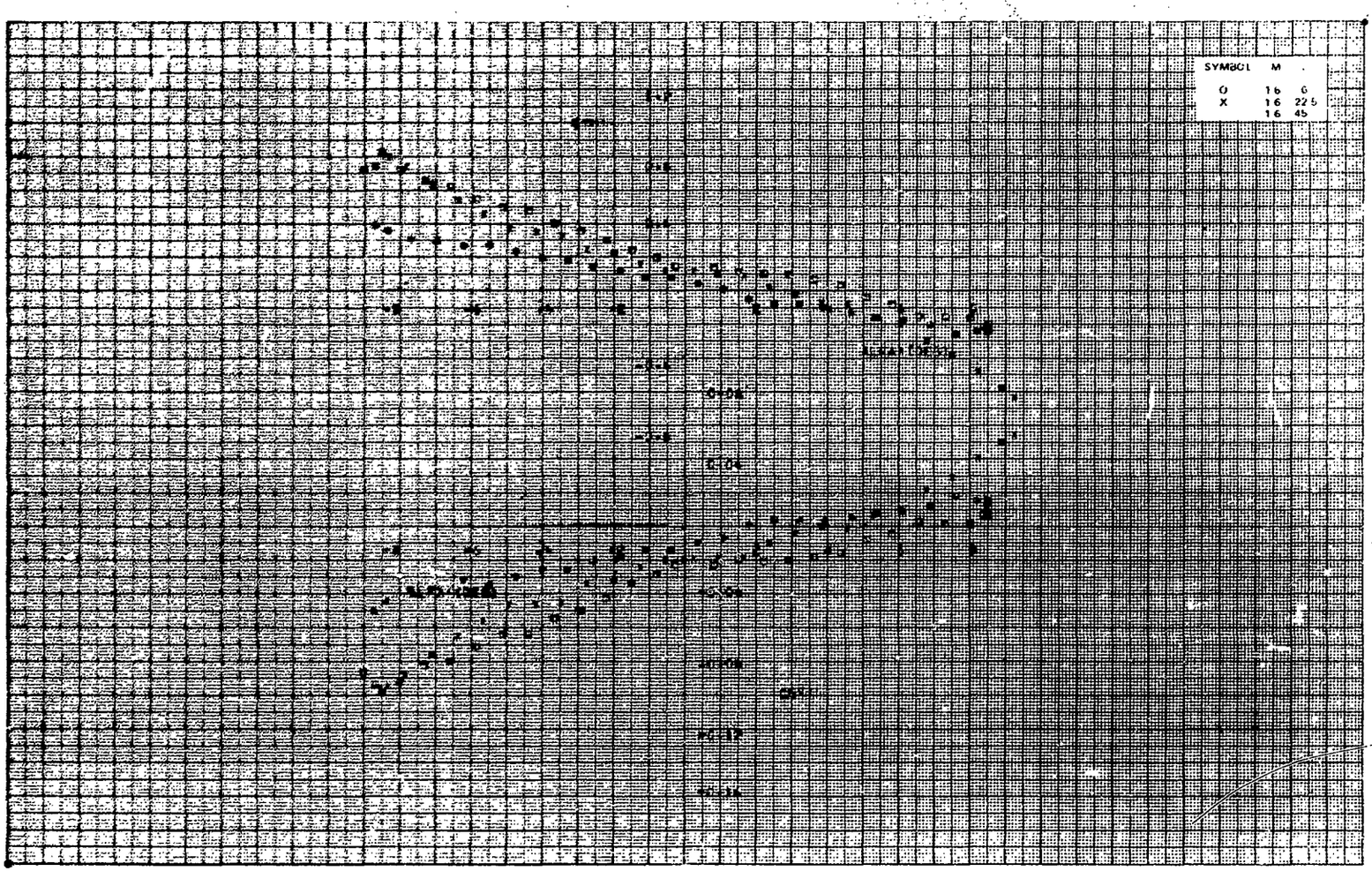


Figure 17b. Continued.

Reproduced from best available copy.

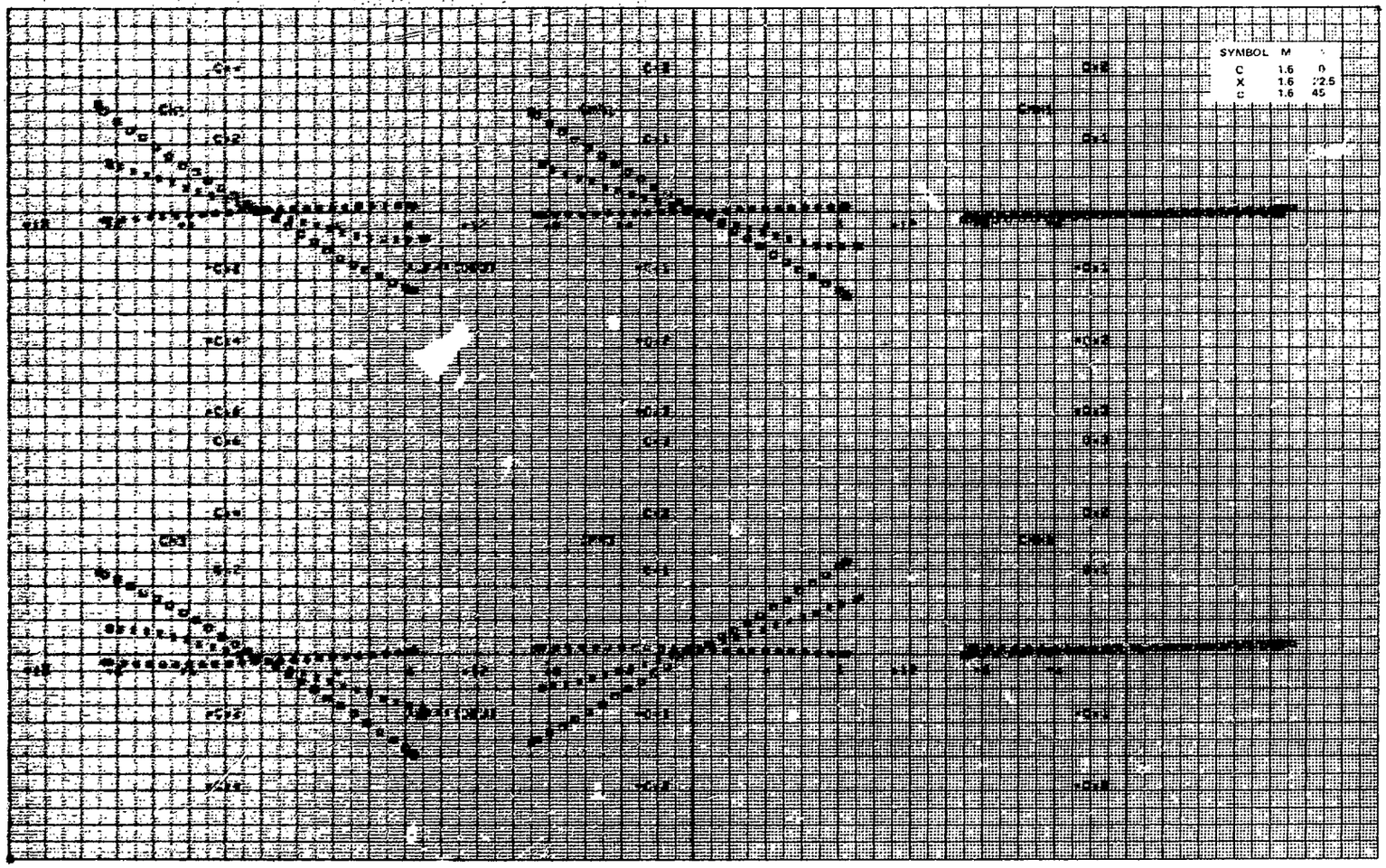


Figure 17b. Continued.

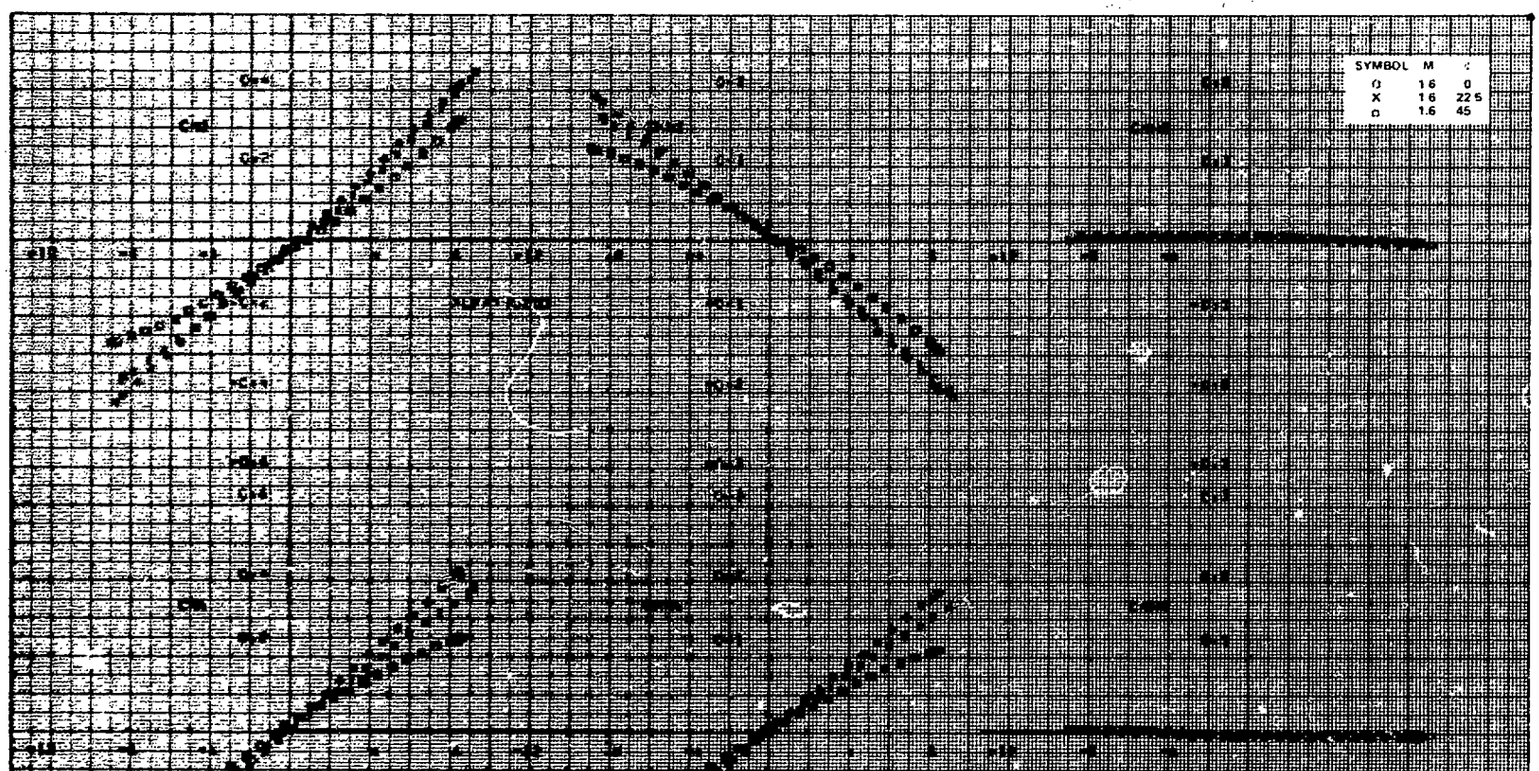


Figure 17b. Concluded.

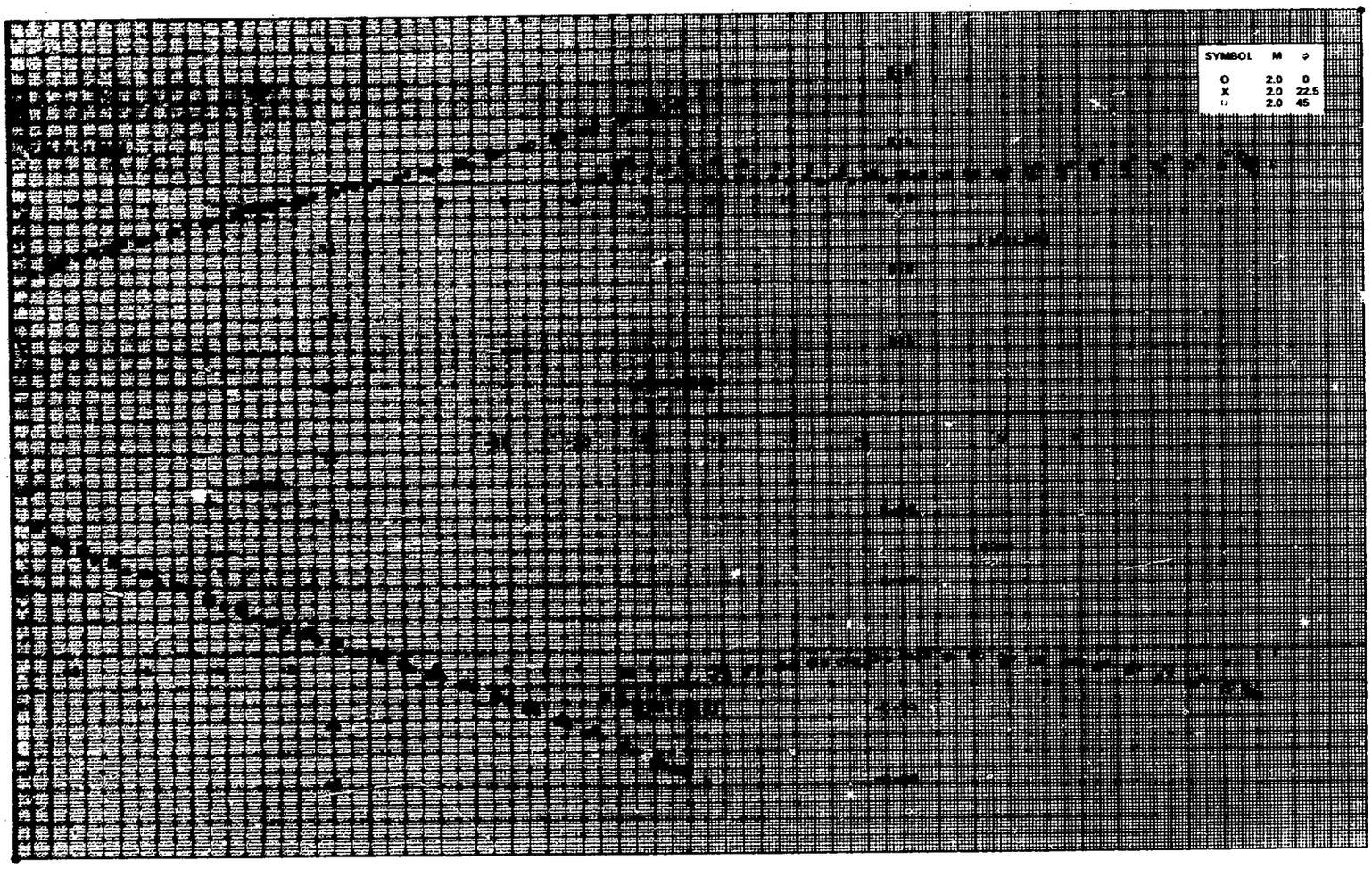


Figure 17c. Aerodynamic stability coefficients, CR/D = 1.0, α = 20.6 deg, M_∞ = 2.0.

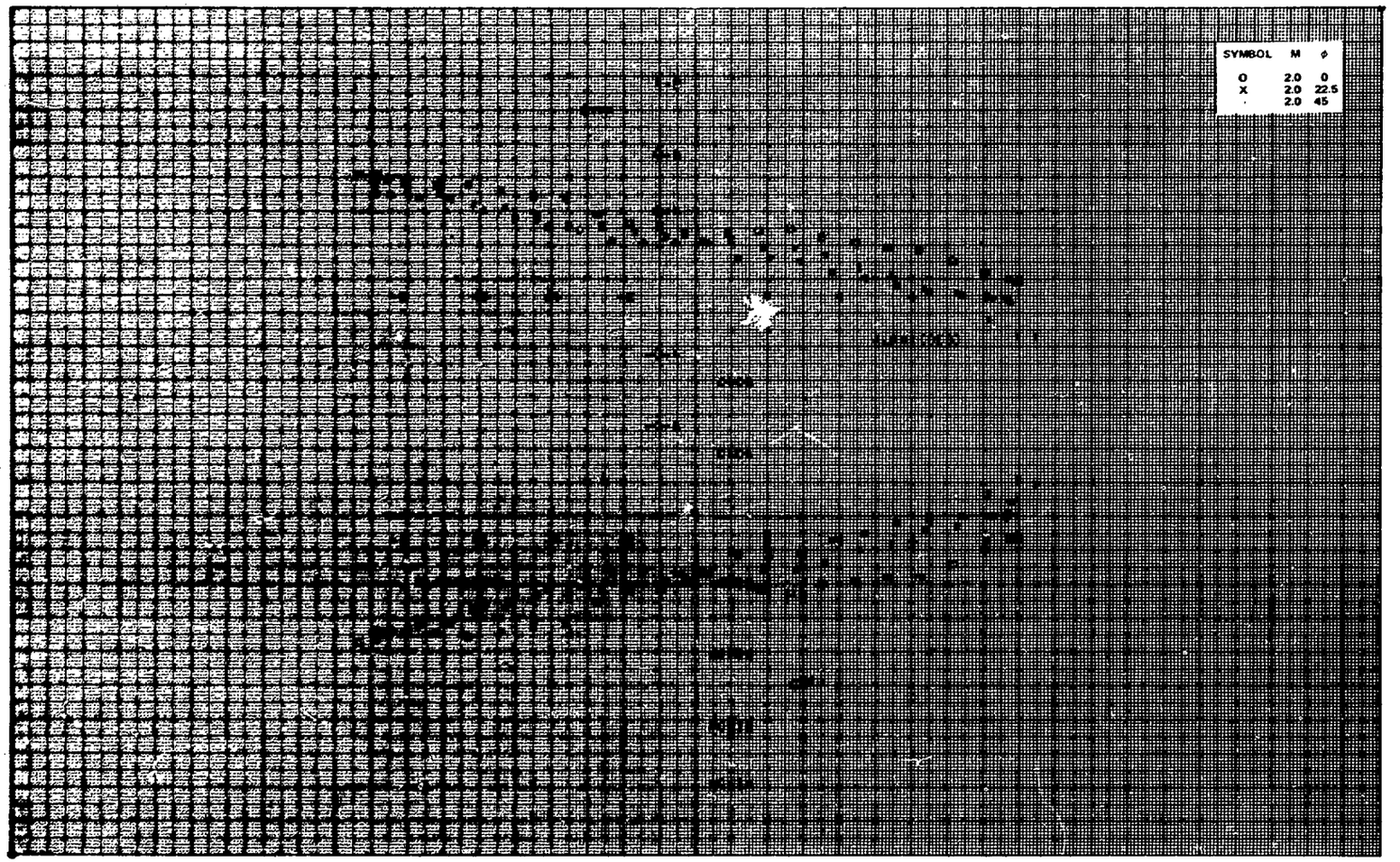


Figure 17c. Continued.

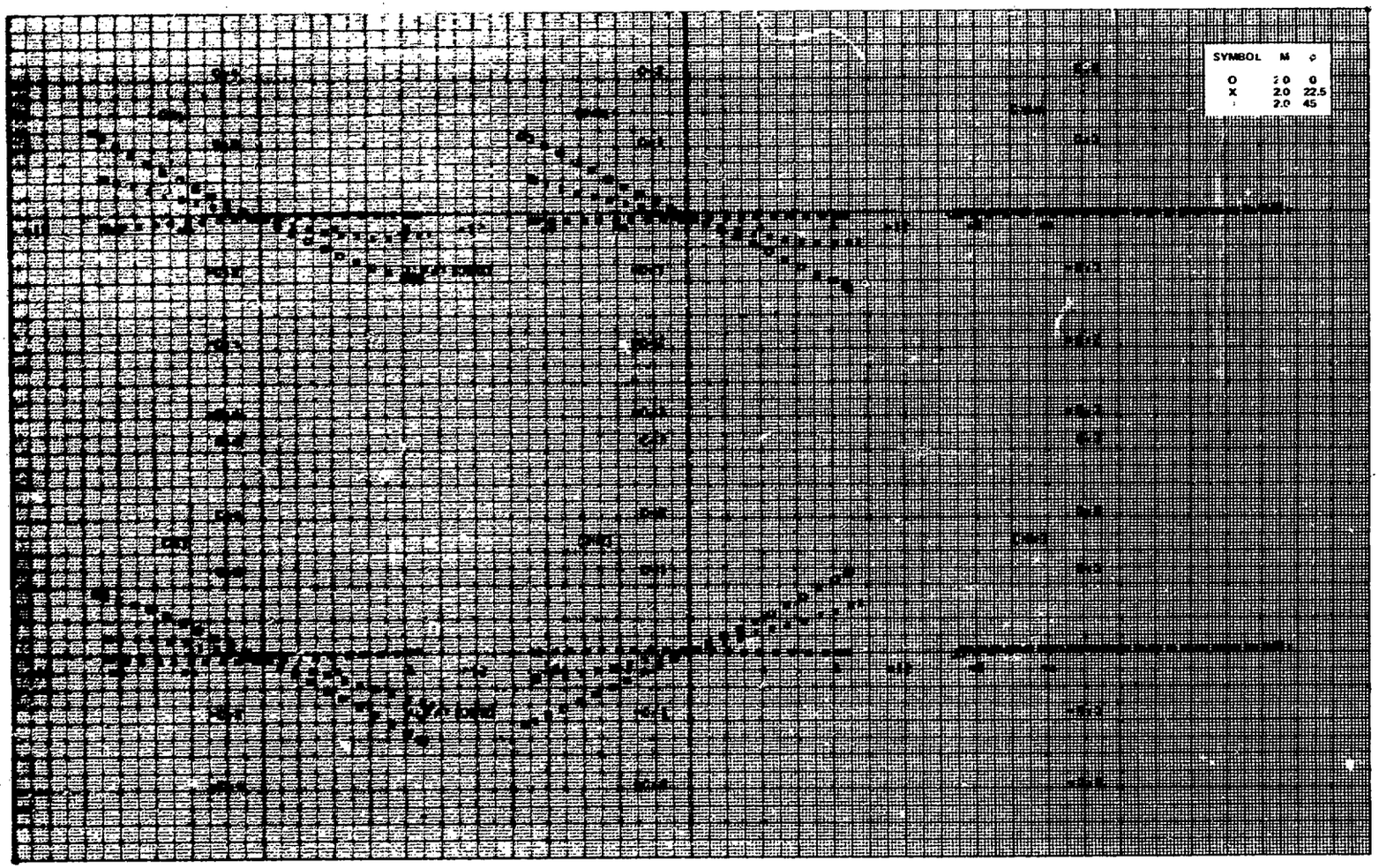


Figure 17c. Continued.

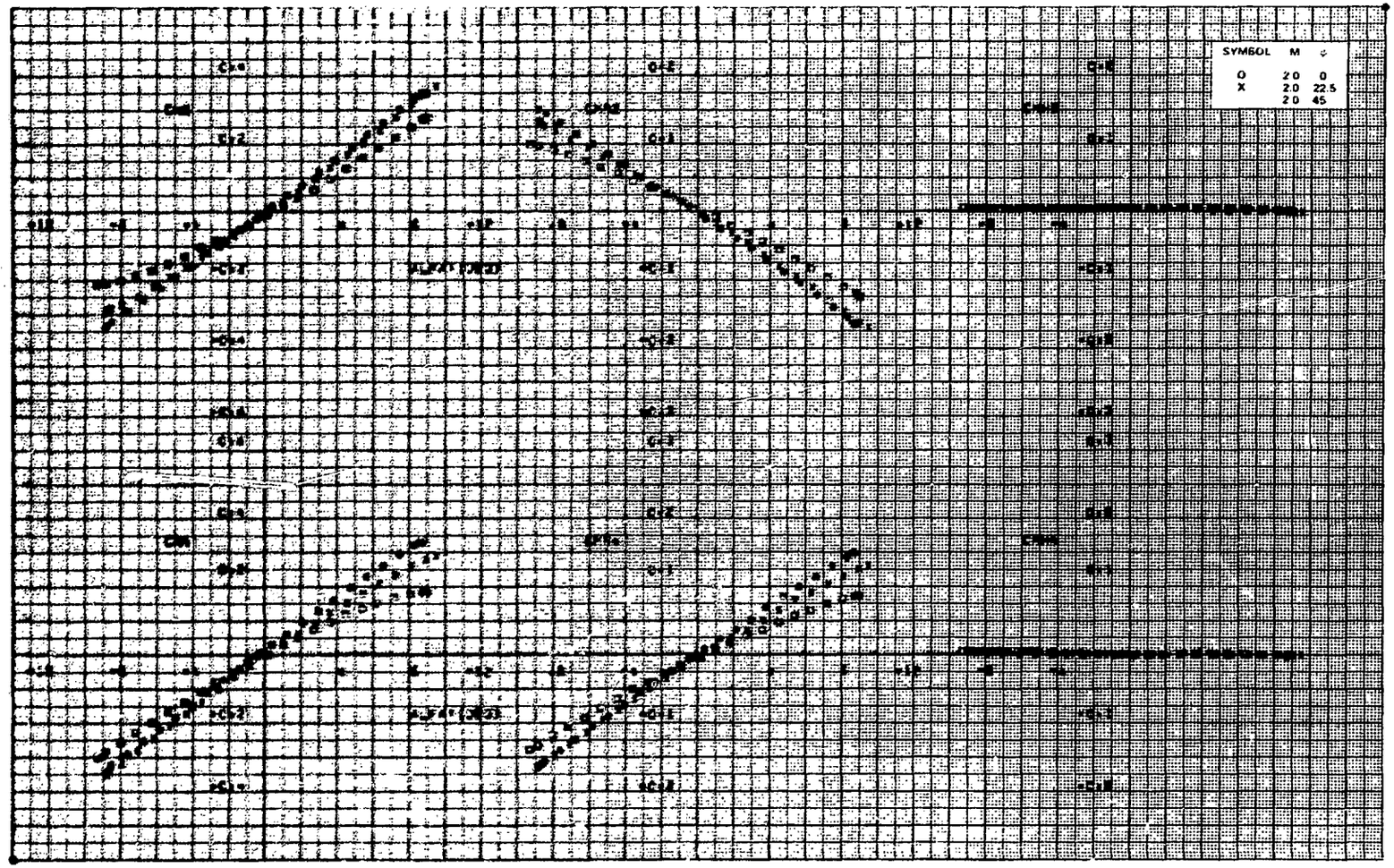


Figure 17c. Concluded.

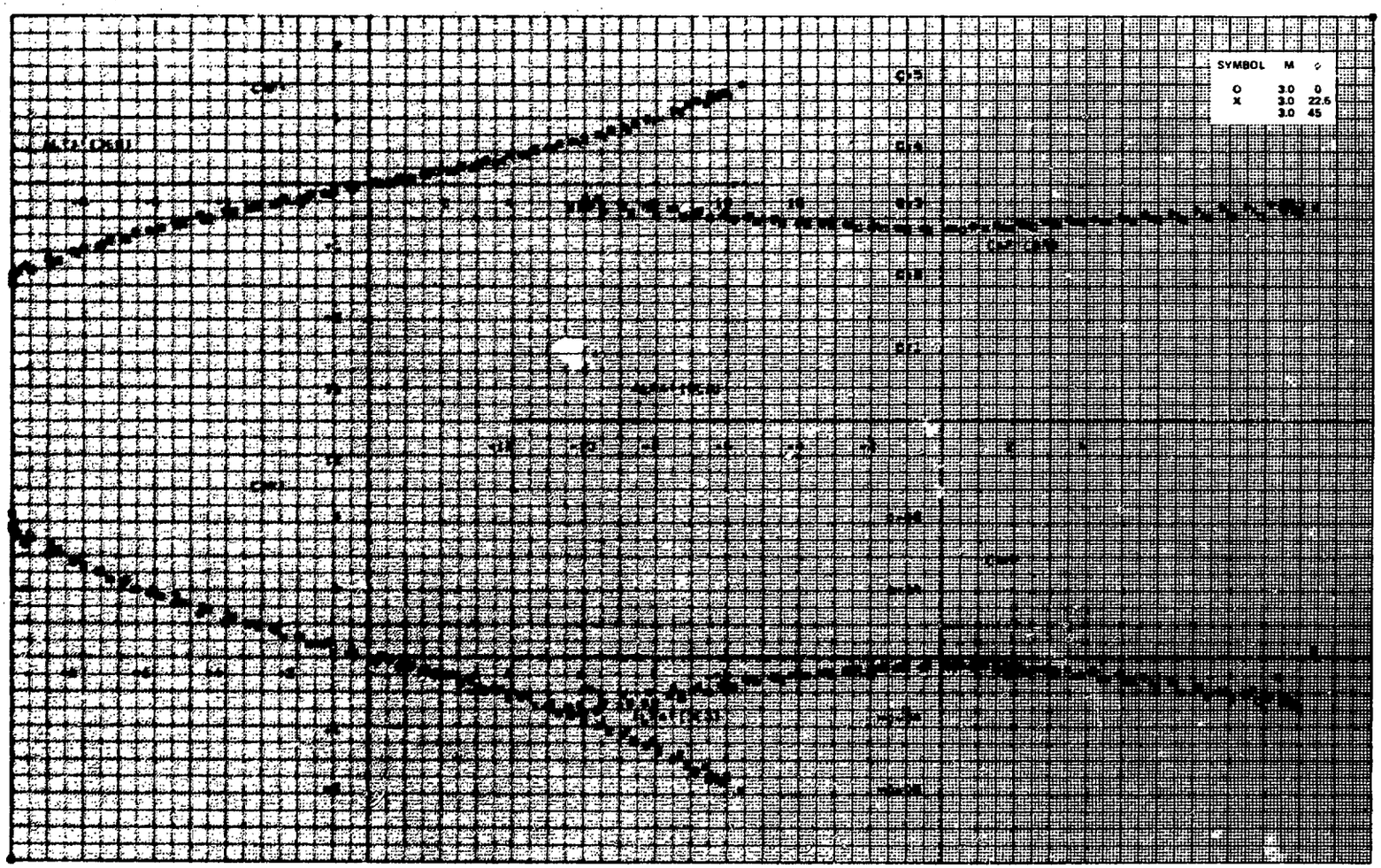


Figure 17d. Aerodynamic stability coefficients, CR/D = 1.0, α = 20.6 deg, M_∞ = 3.0.

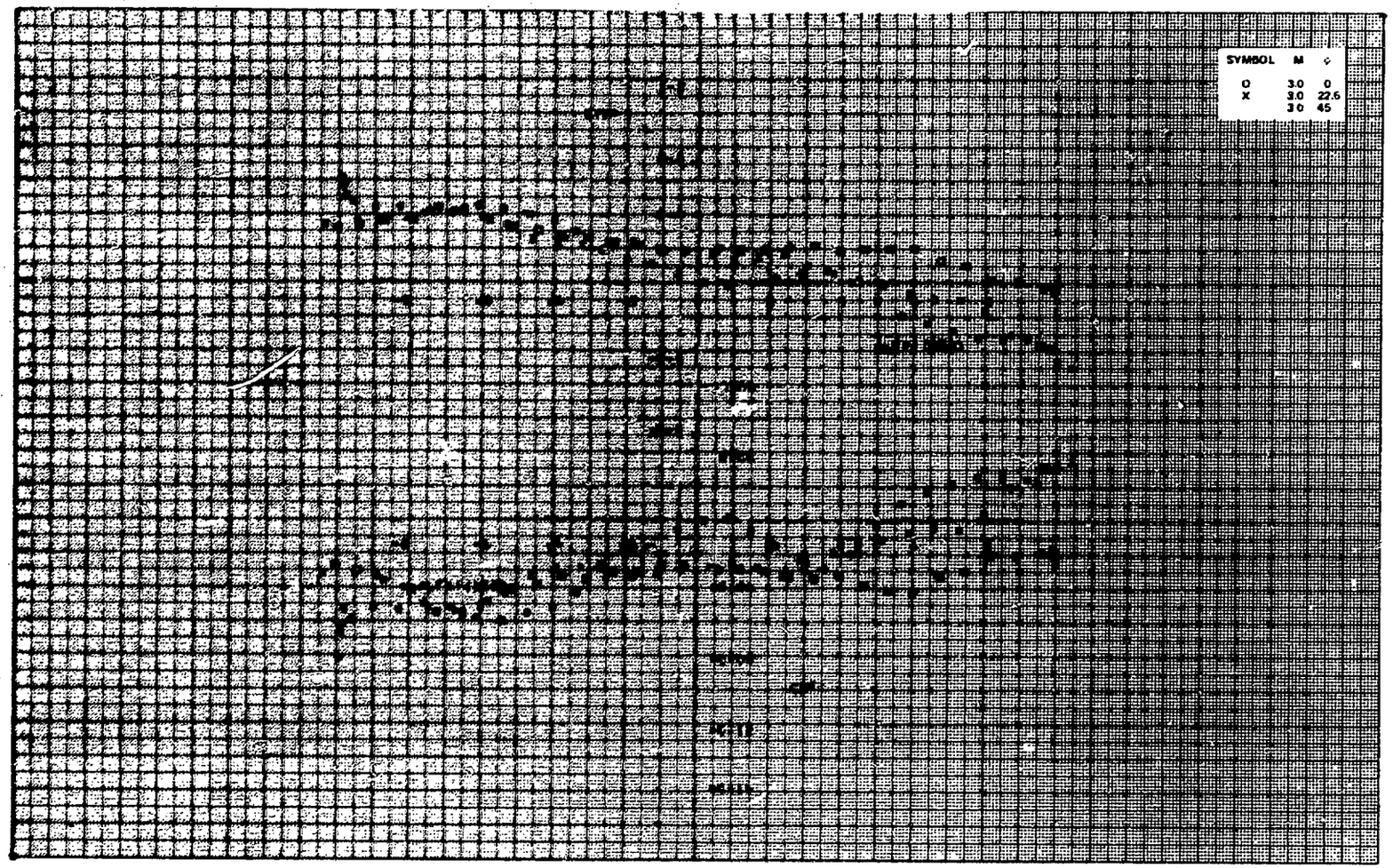


Figure 17d. Continued.

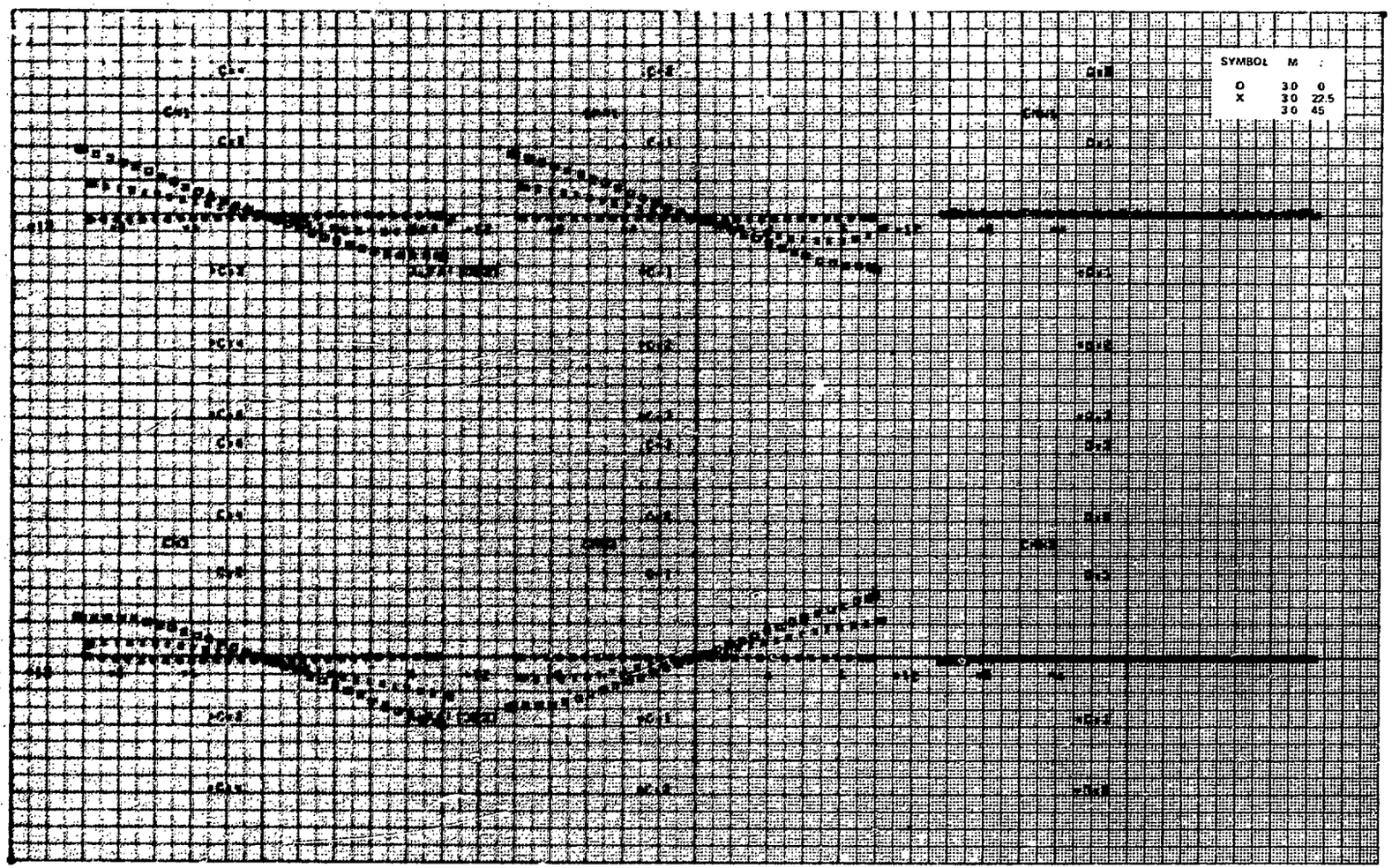


Figure 17d. Continued.

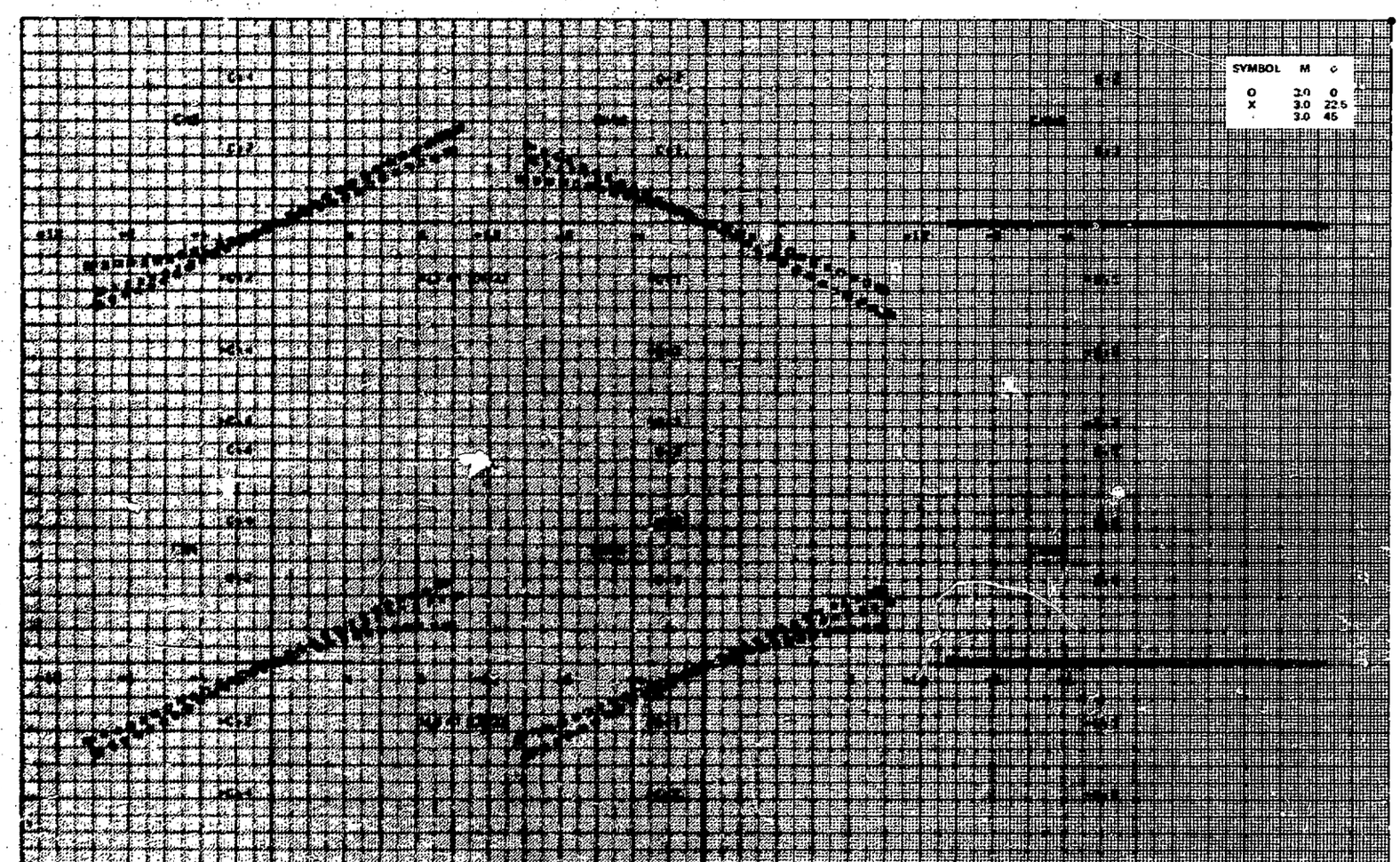


Figure 17d. Concluded.

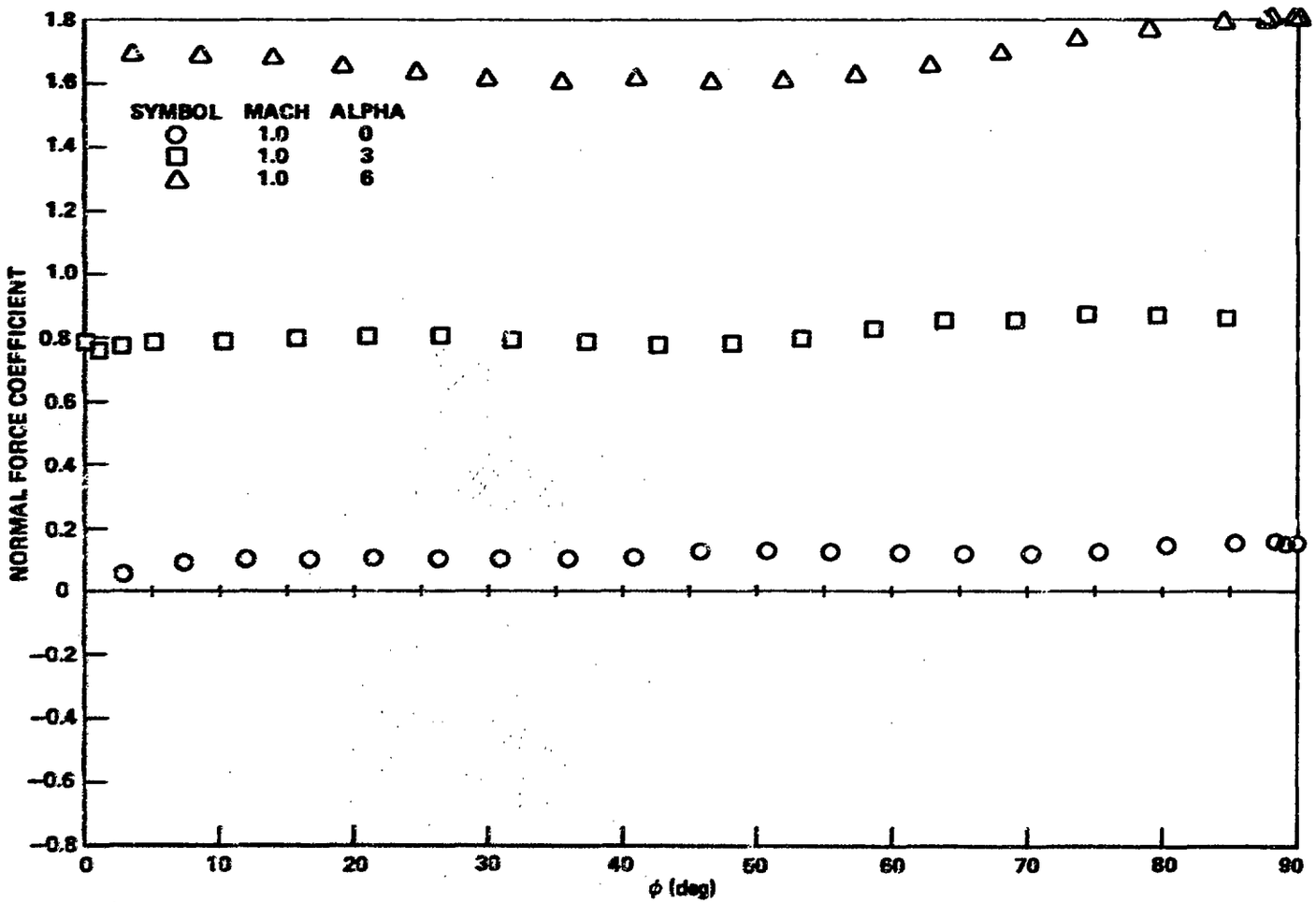


Figure 18a. Effect of roll on stability coefficients, CR/D = 1.75, Λ = 0.0, Mach = 1.0.

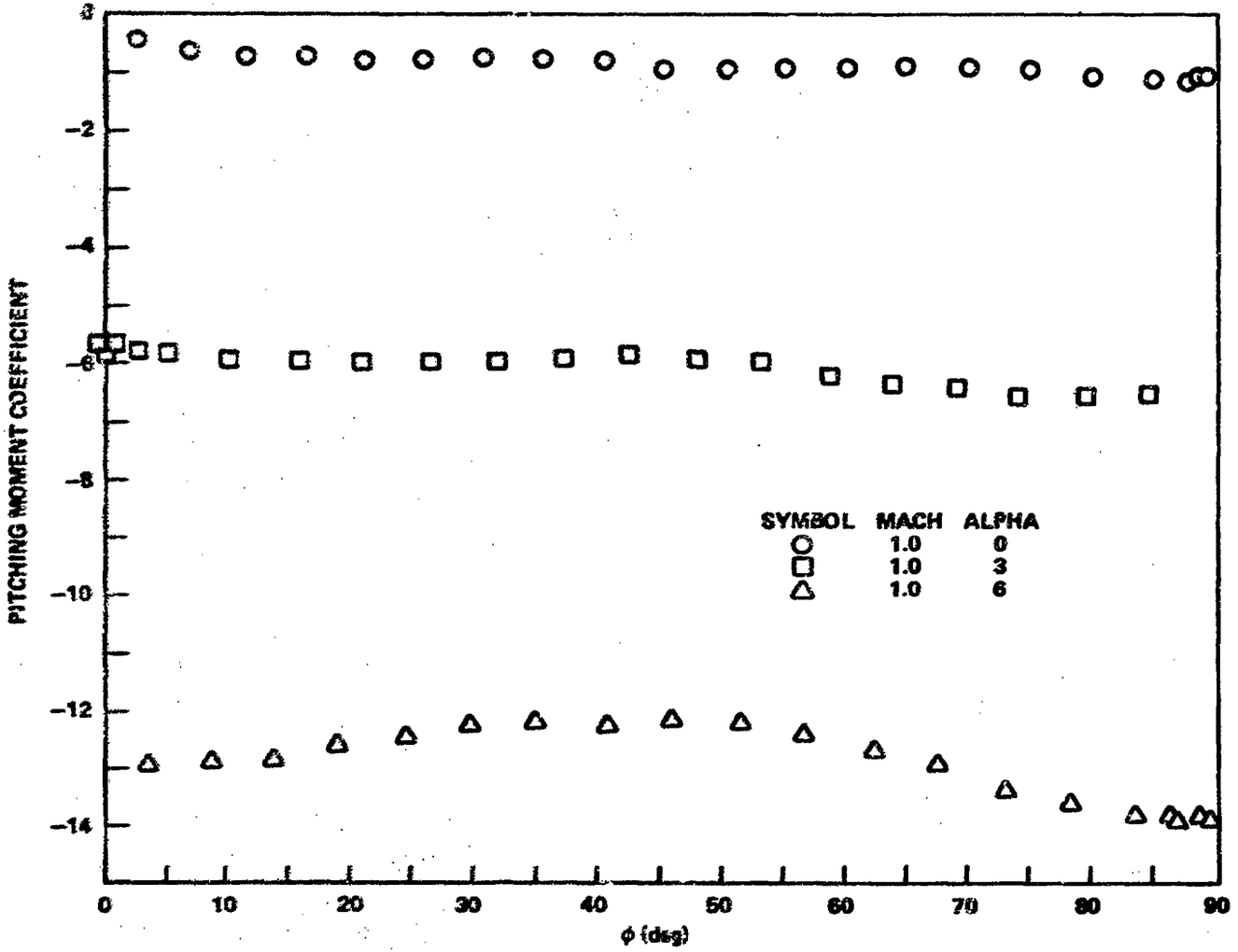


Figure 18a. Continued.

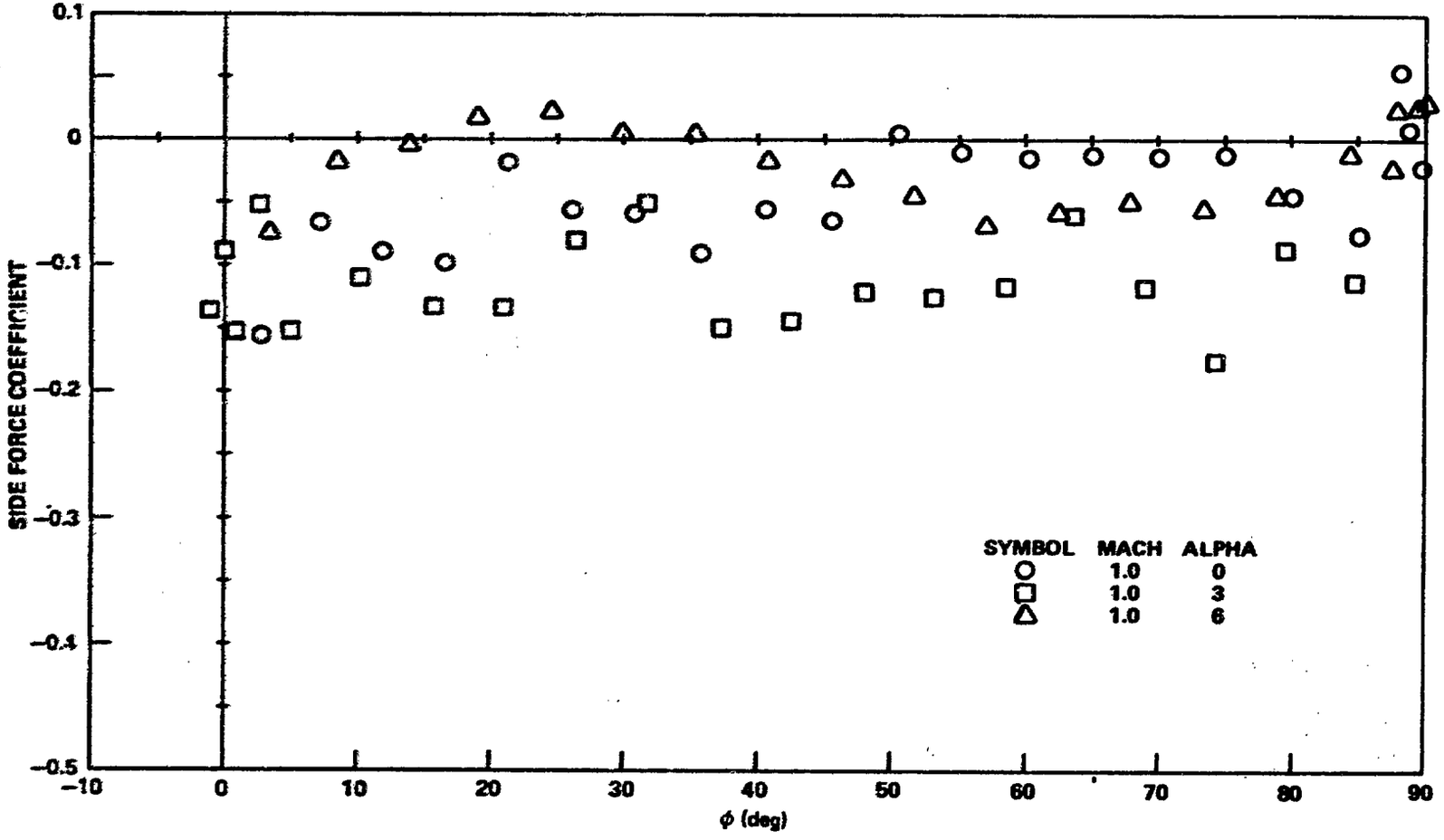


Figure 18a. Continued

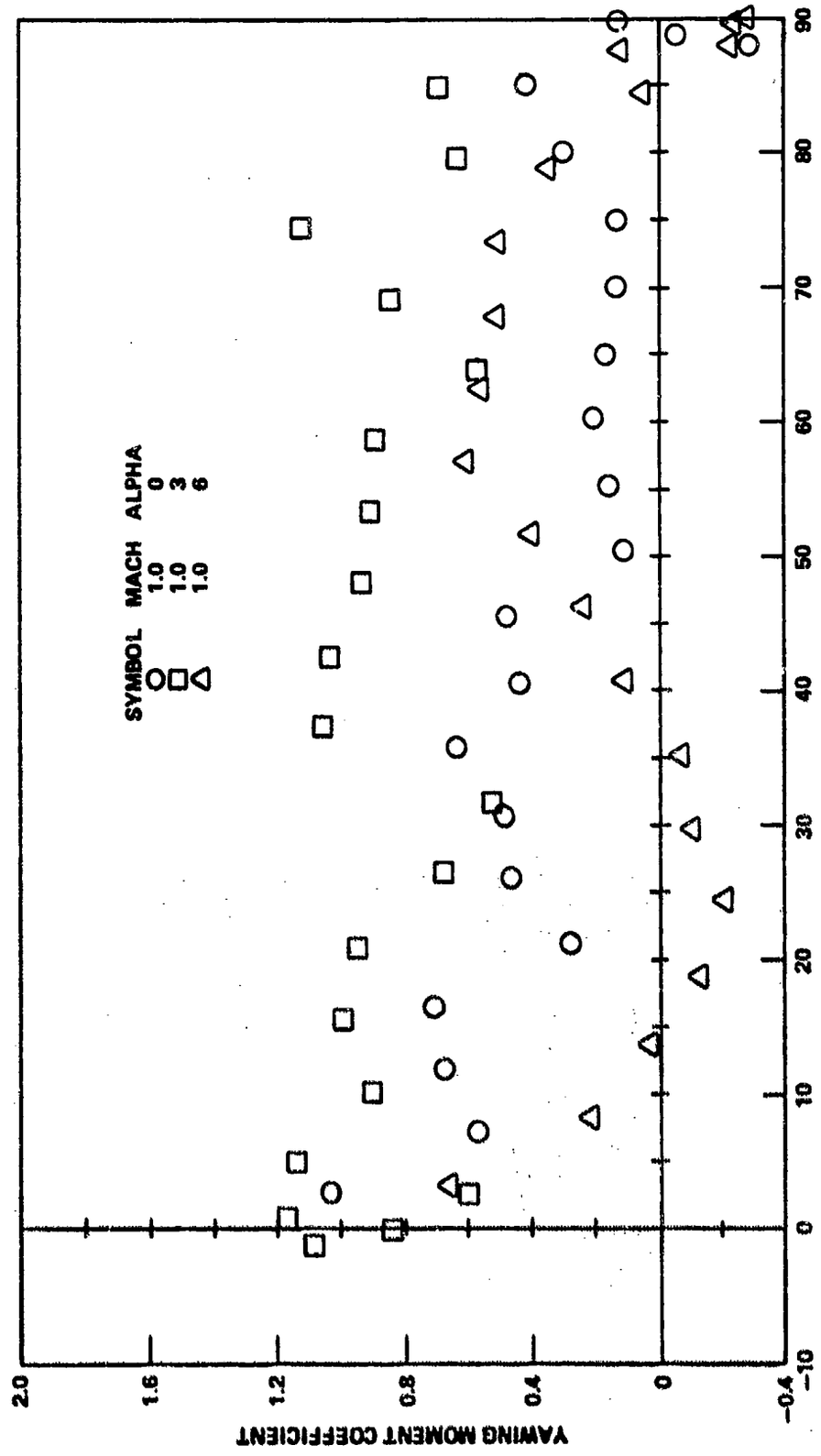


Figure 18a. Continued.

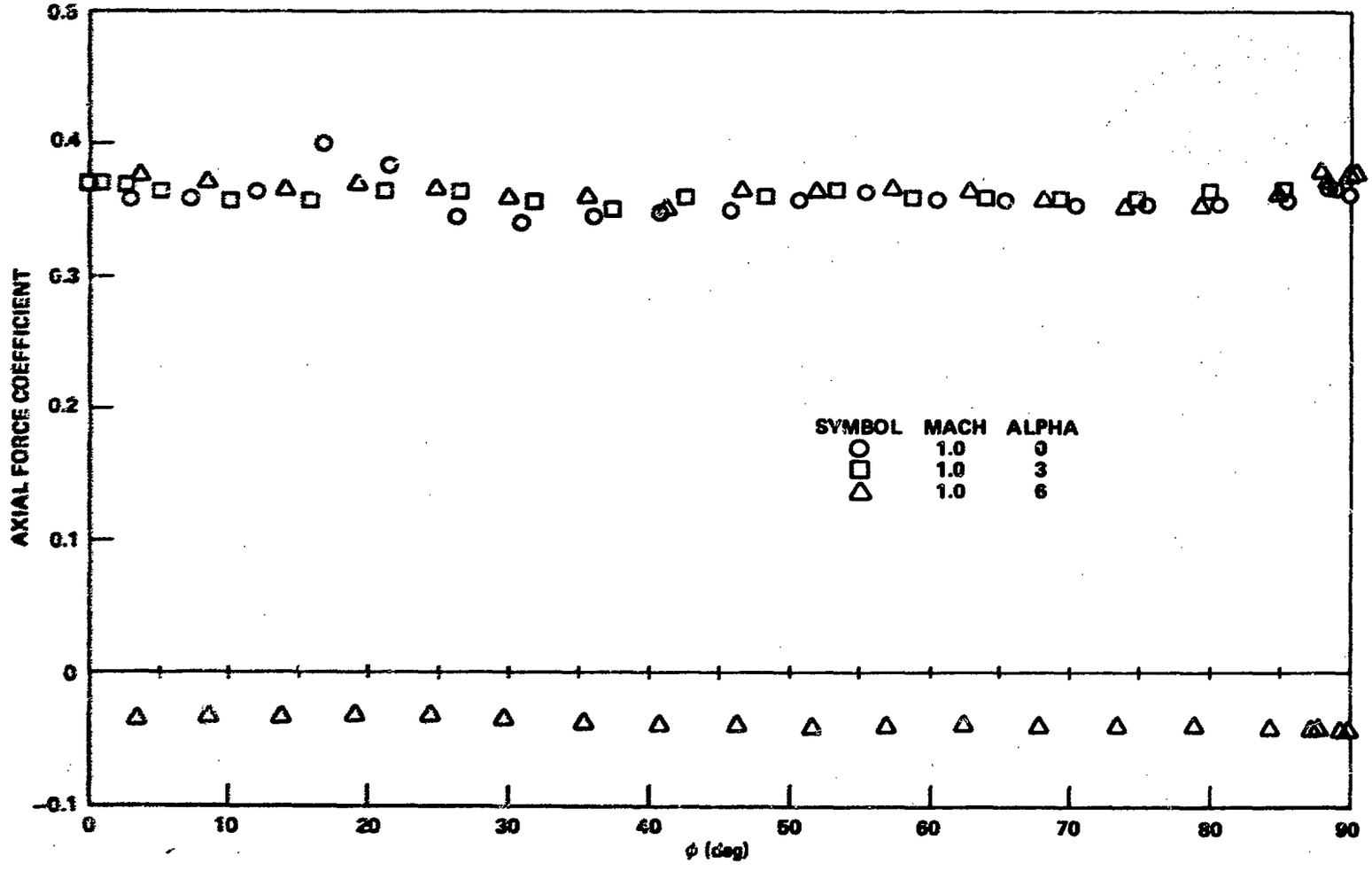


Figure 18a. Continued

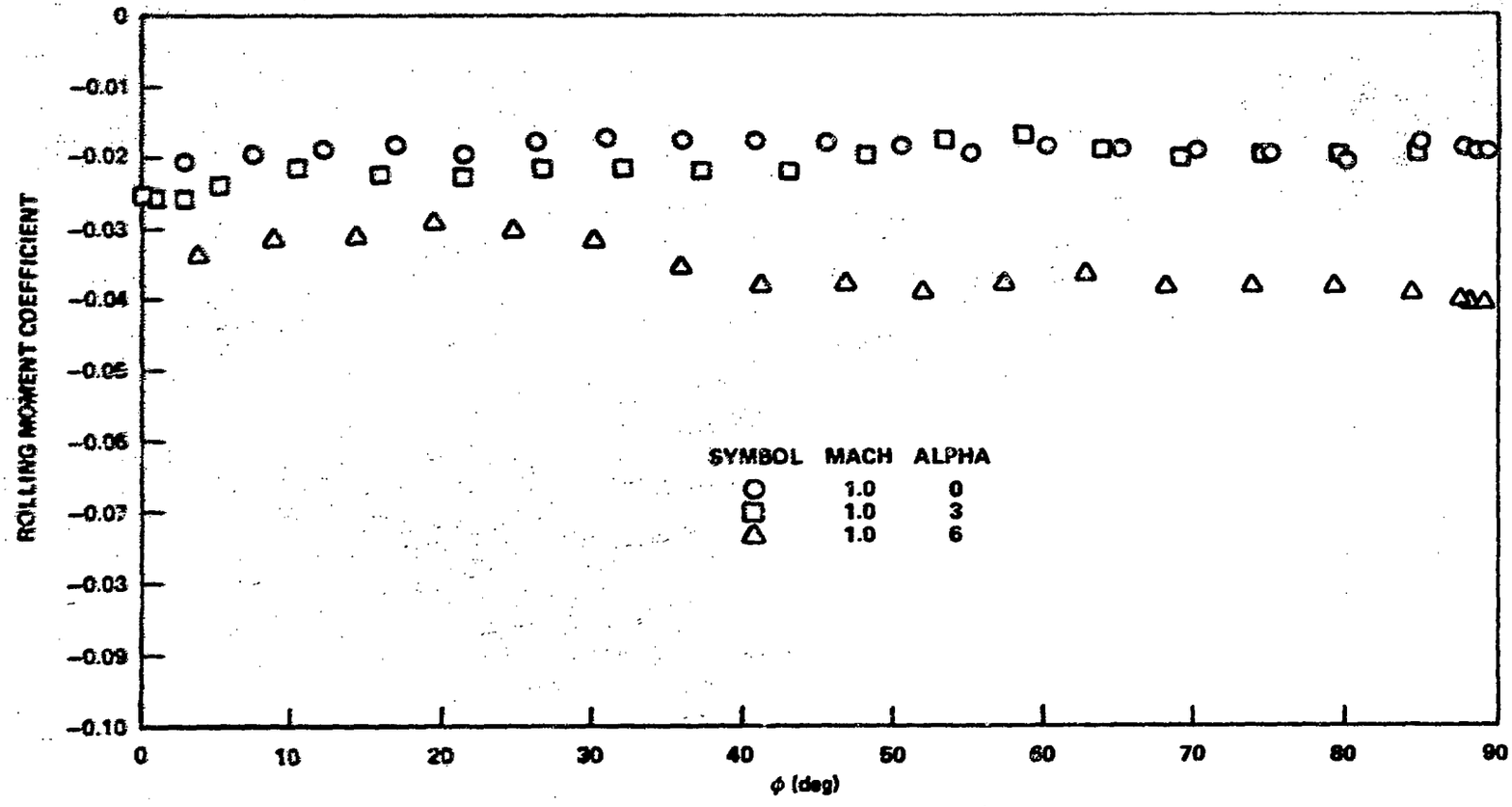


Figure 18a. Concluded.

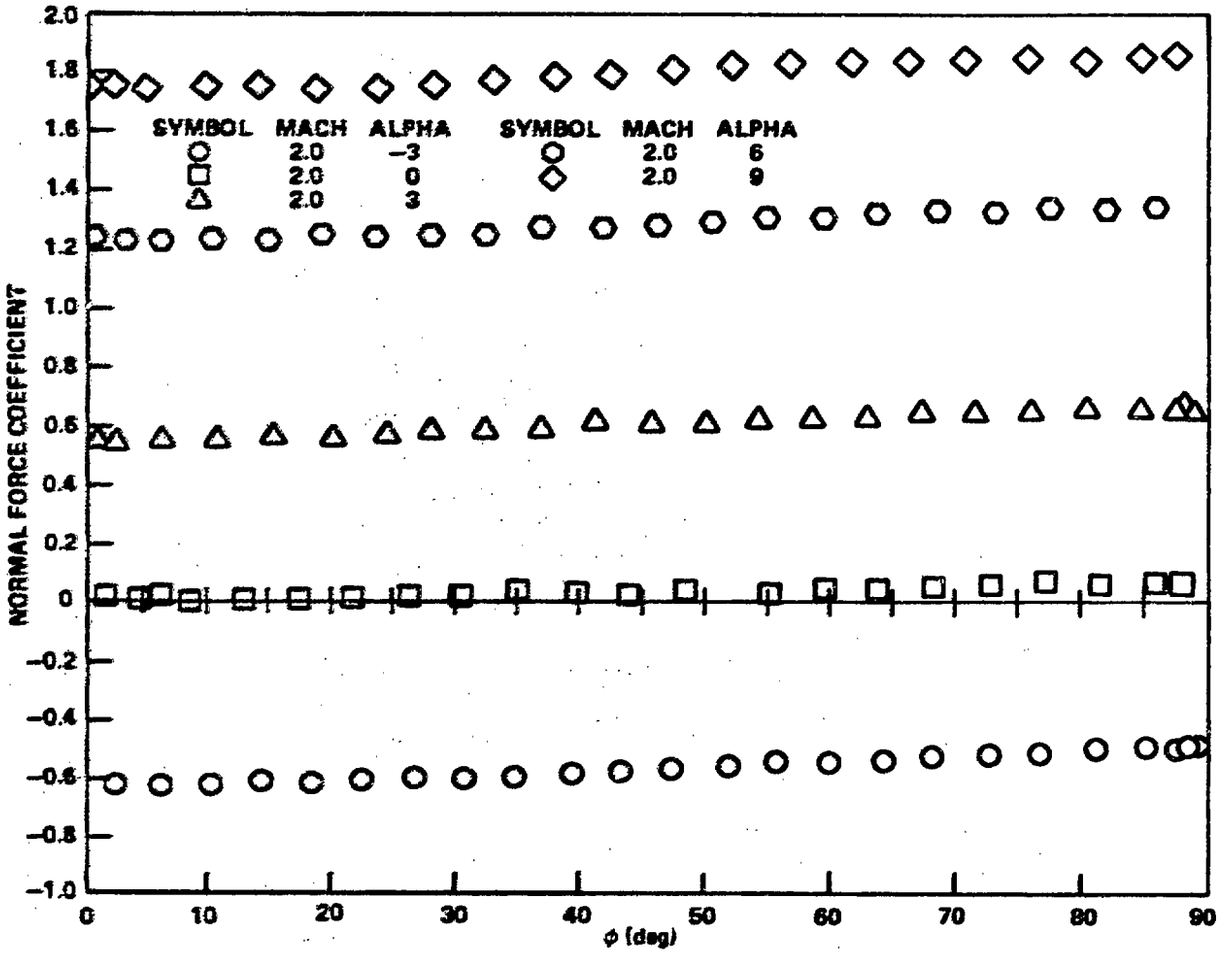


Figure 18b. Effect of roll on stability coefficients, CR/D = 1.75, Λ = 0.0, Mach = 2.0.

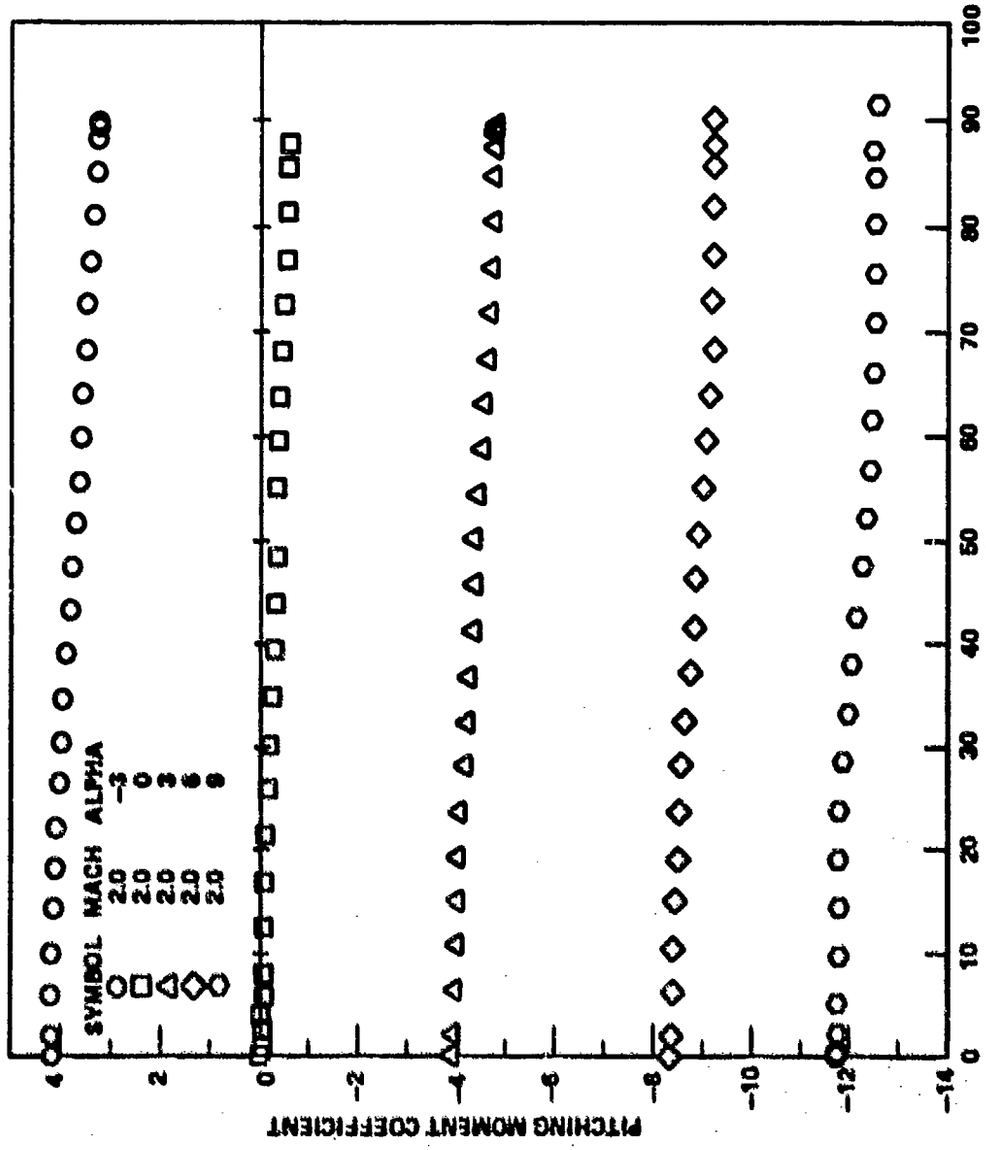


Figure 18b. Continued.

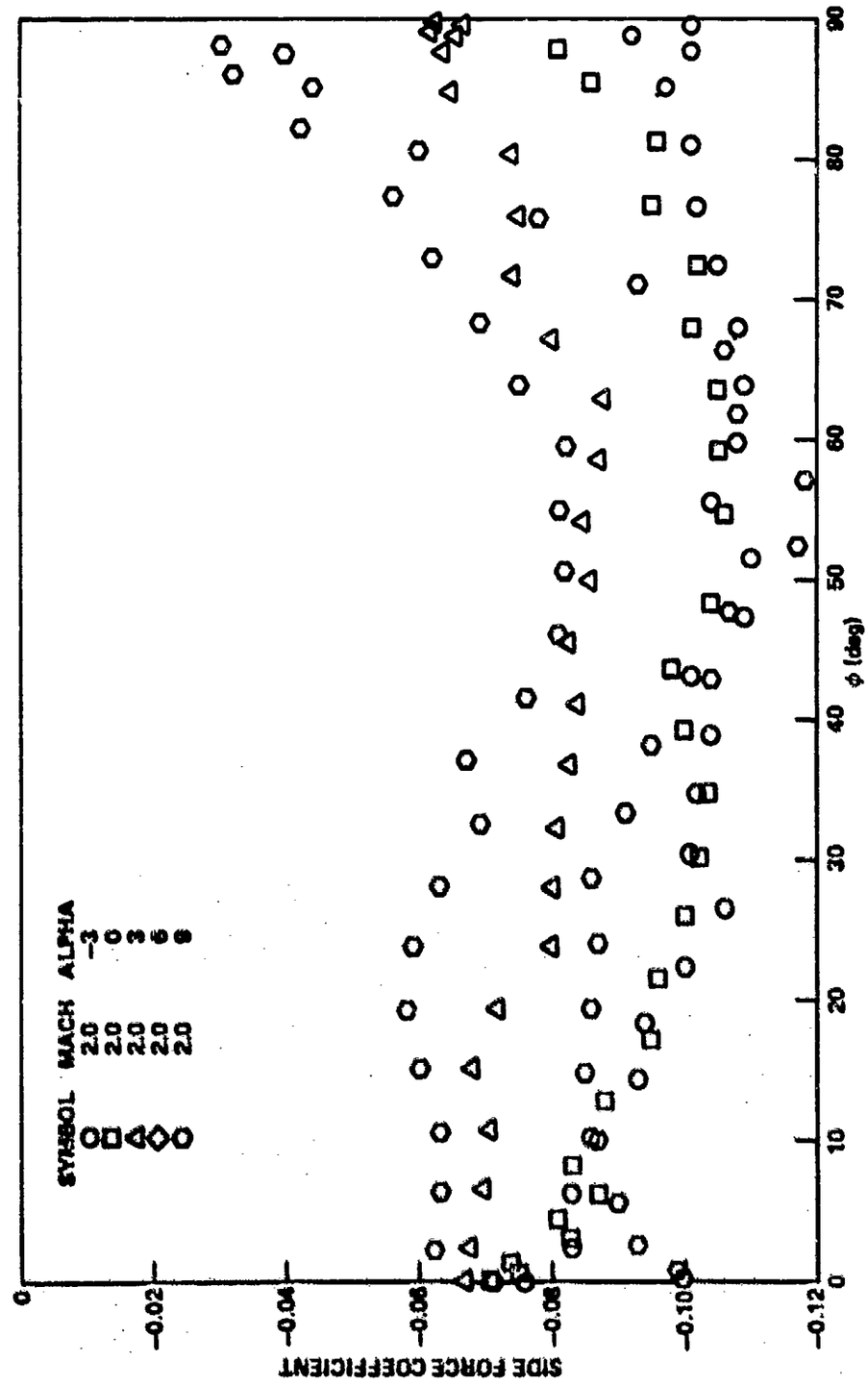


Figure 18b. Continued.

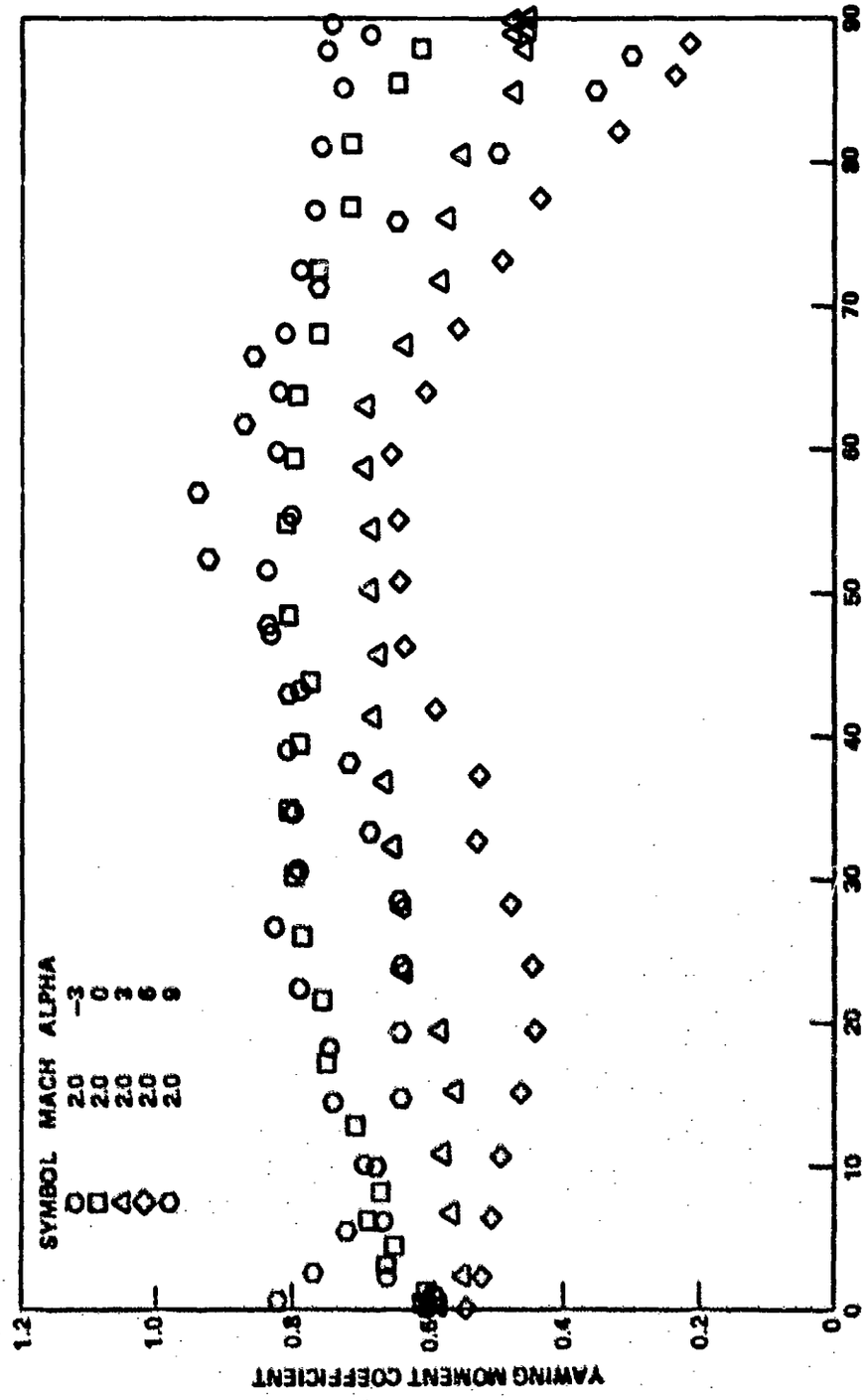


Figure 18b. Continued.

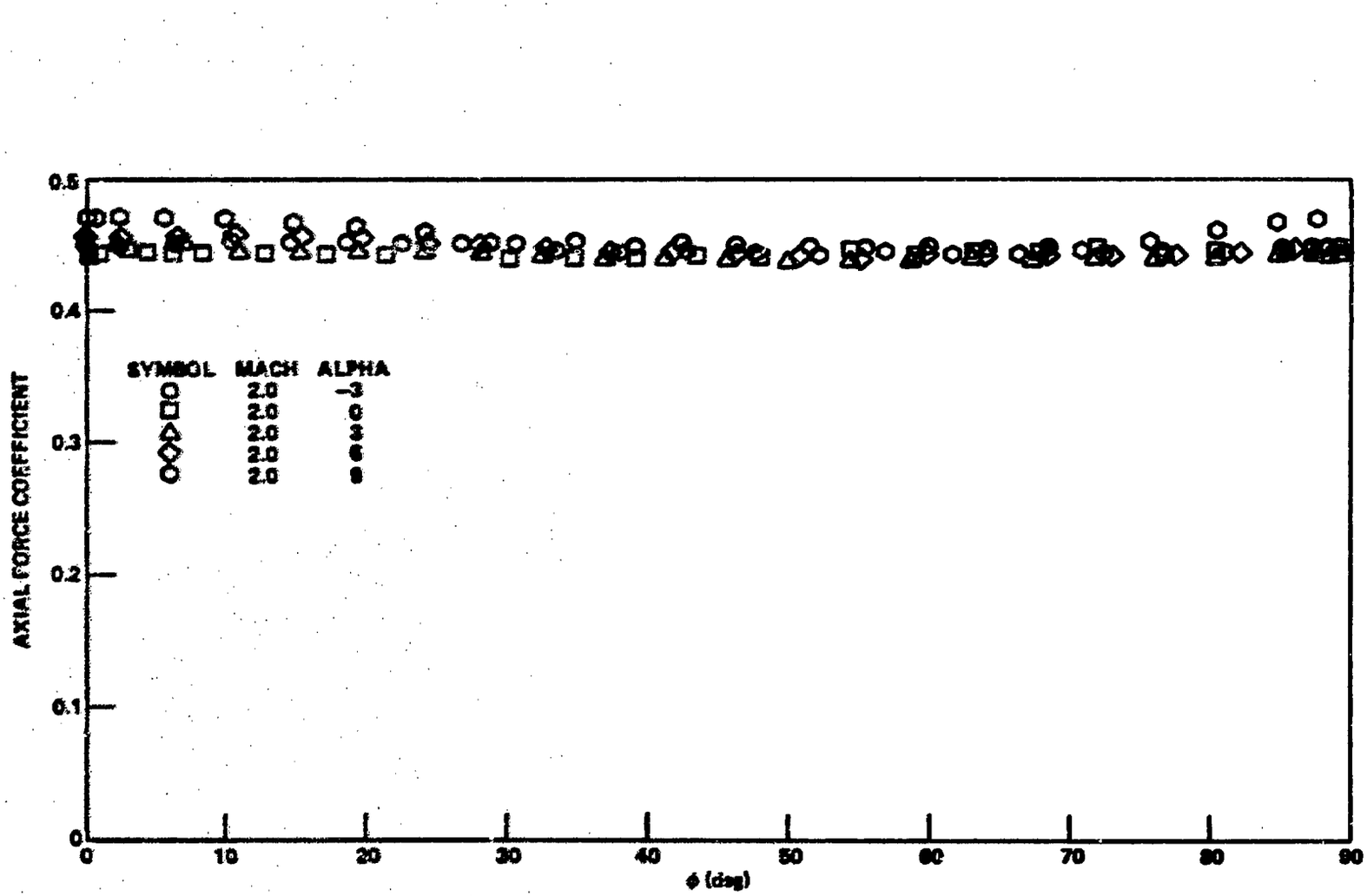


Figure 18b. Continued.

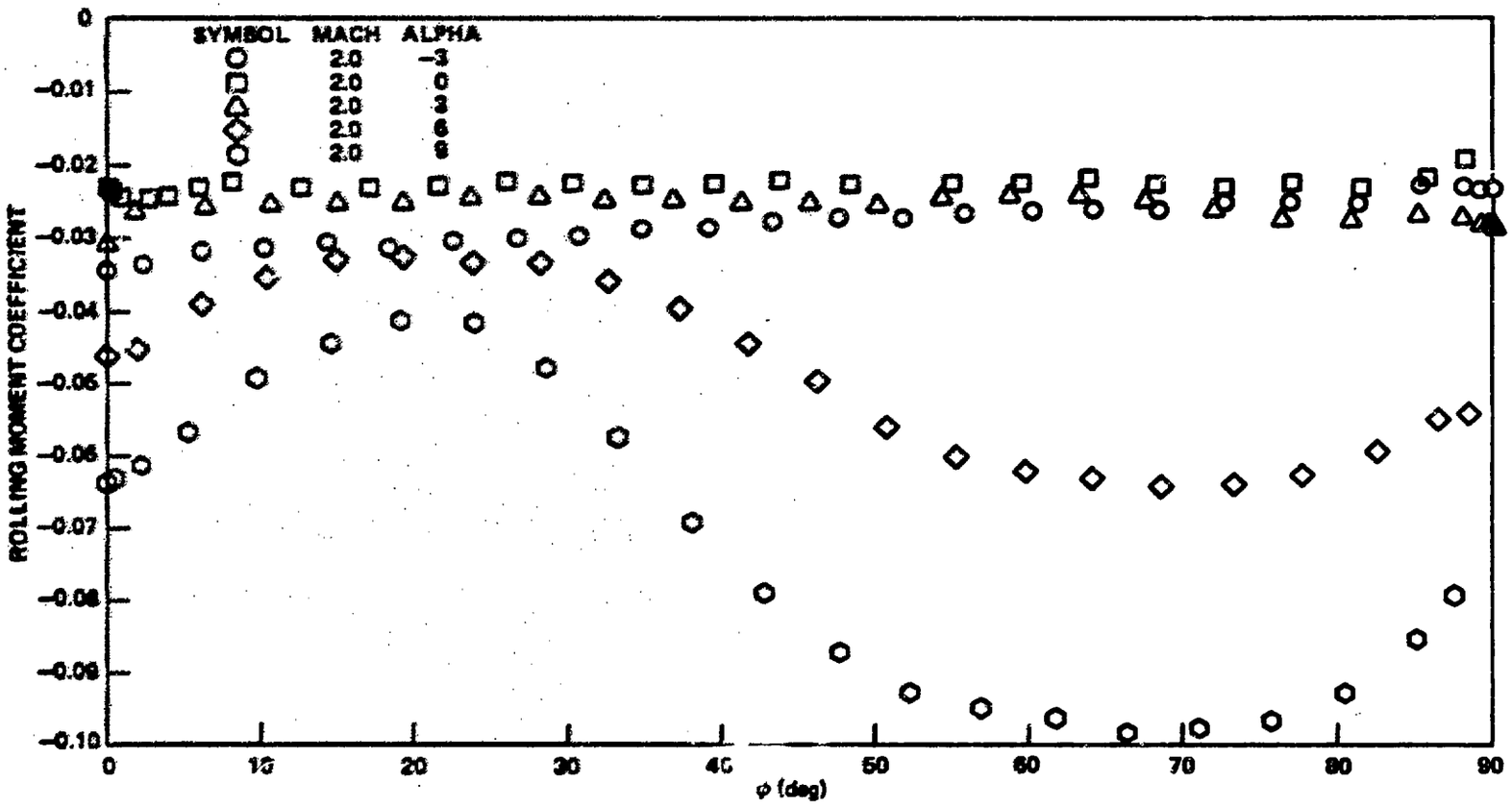


Figure 18b. Concluded.

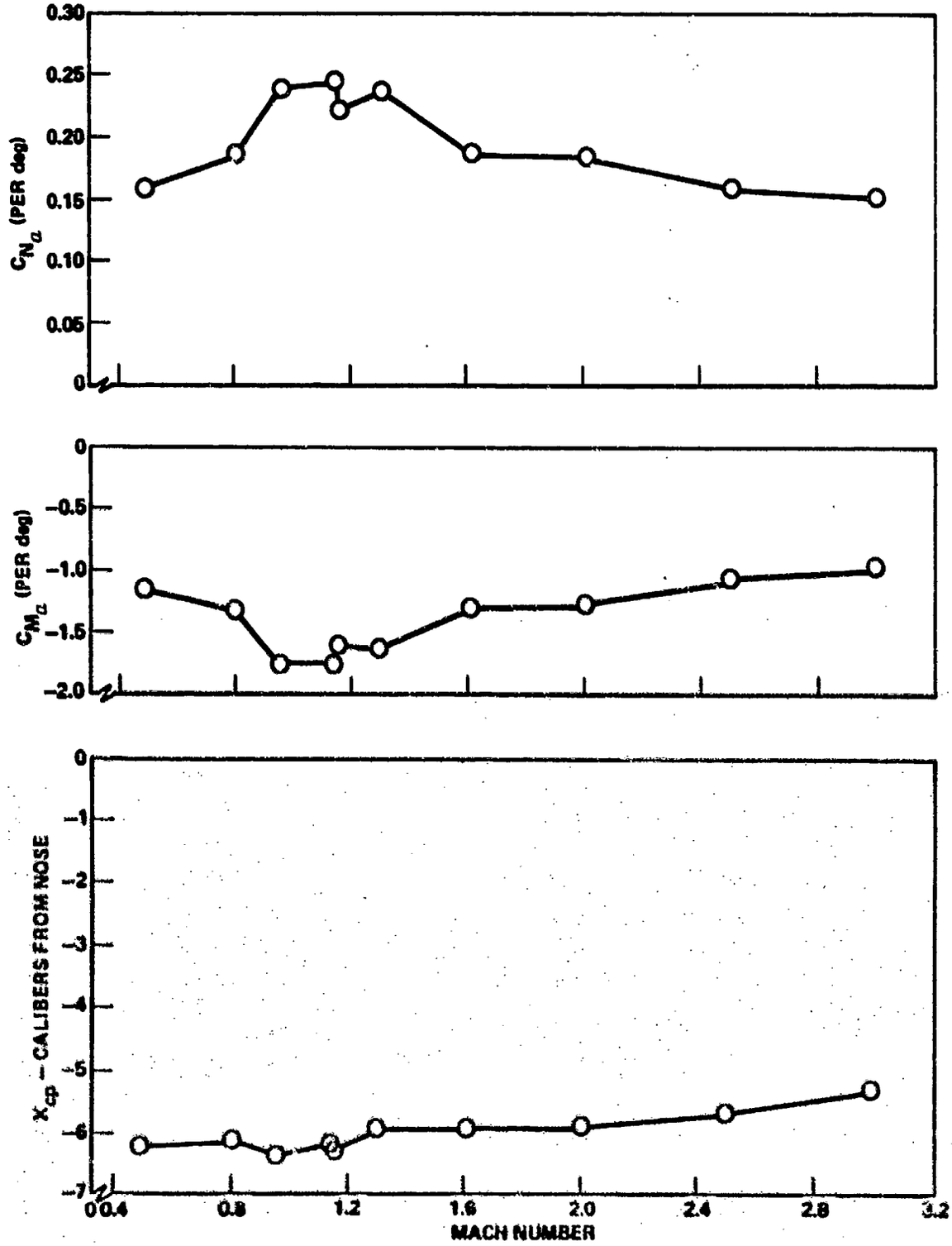


Figure 19. Stability summary - B1F1, ϕ = 0, θ = -10.

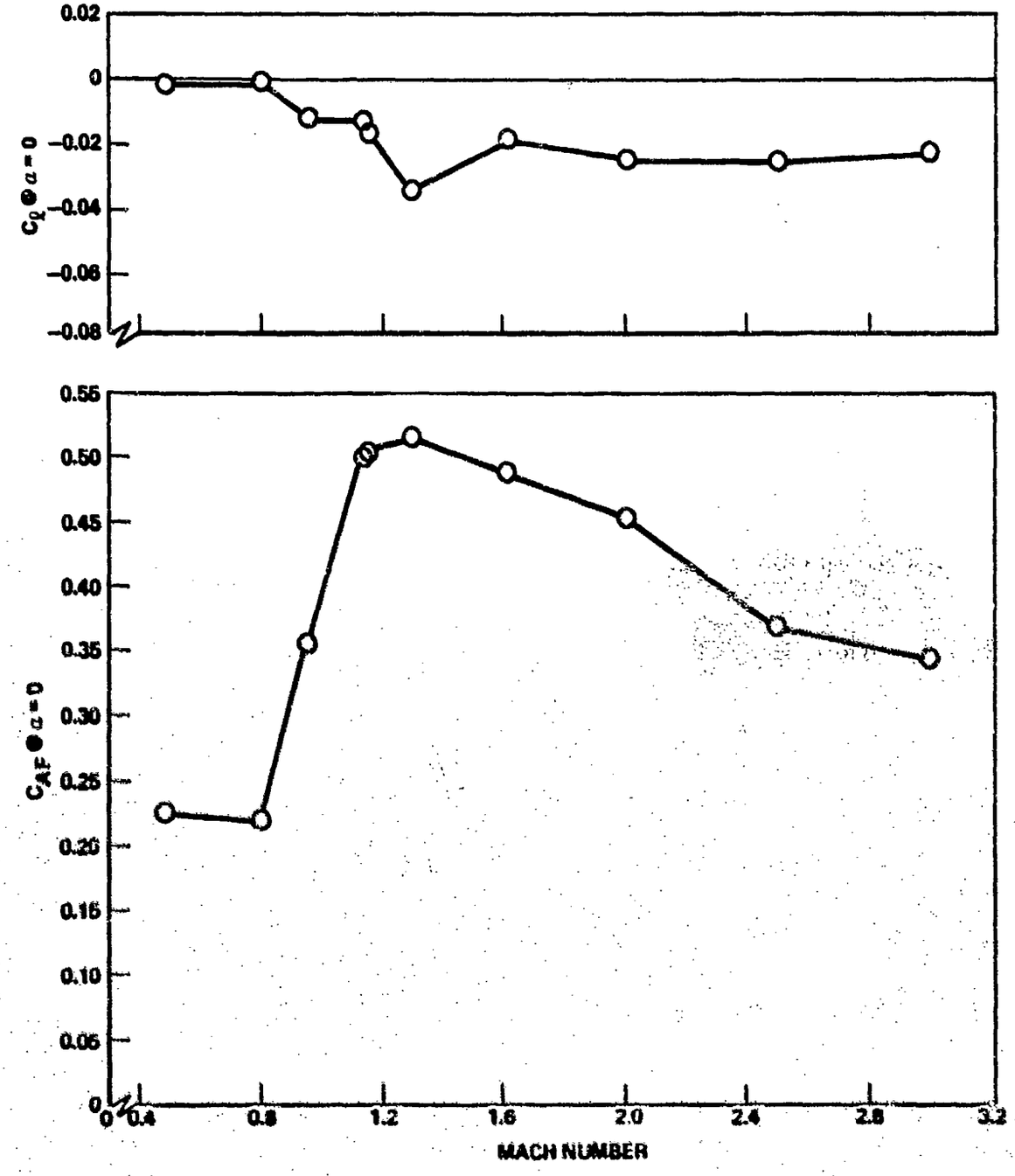


Figure 19. Concluded.

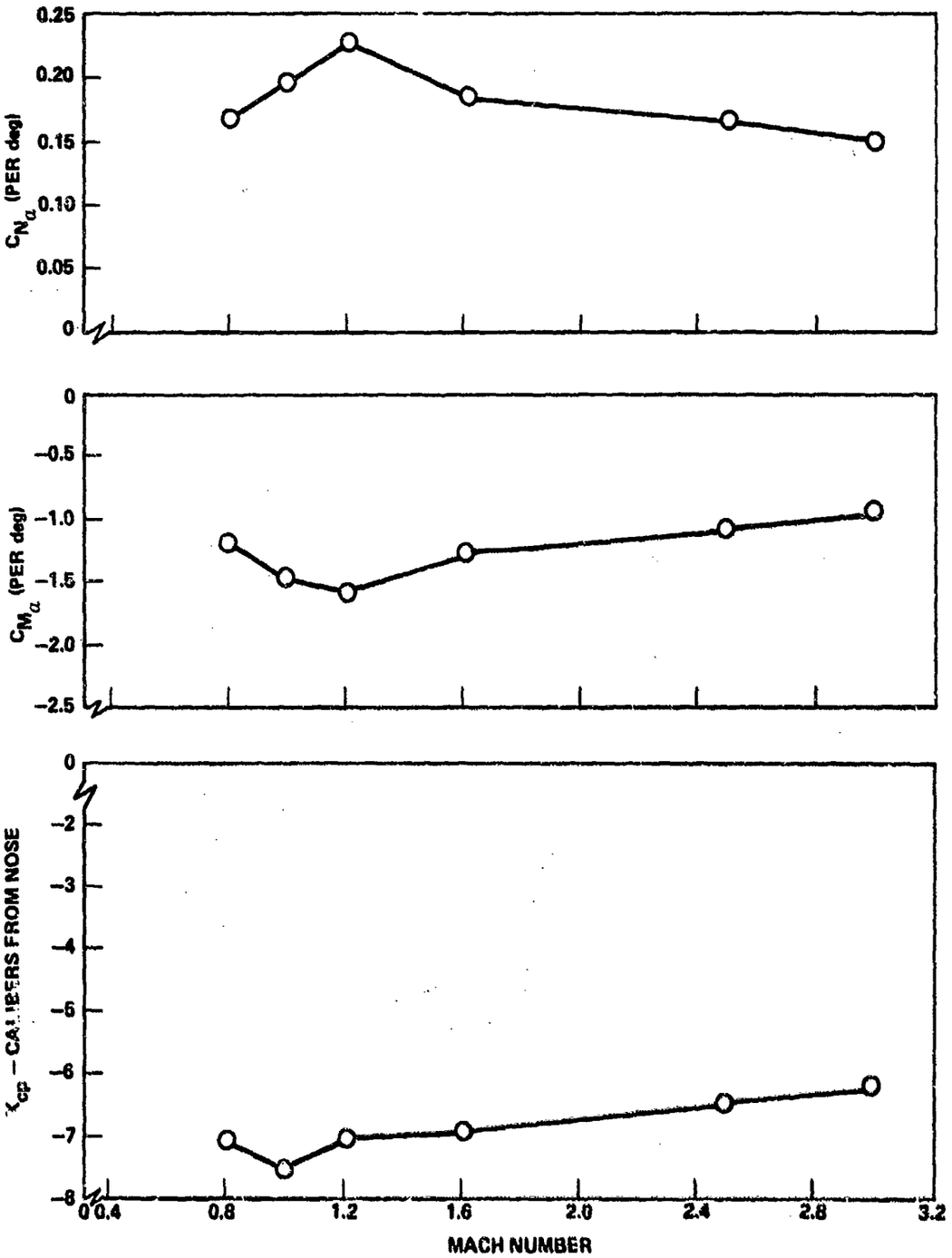


Figure 20. Stability summary - B1F1, $\phi = 0$, $\theta = 0$.

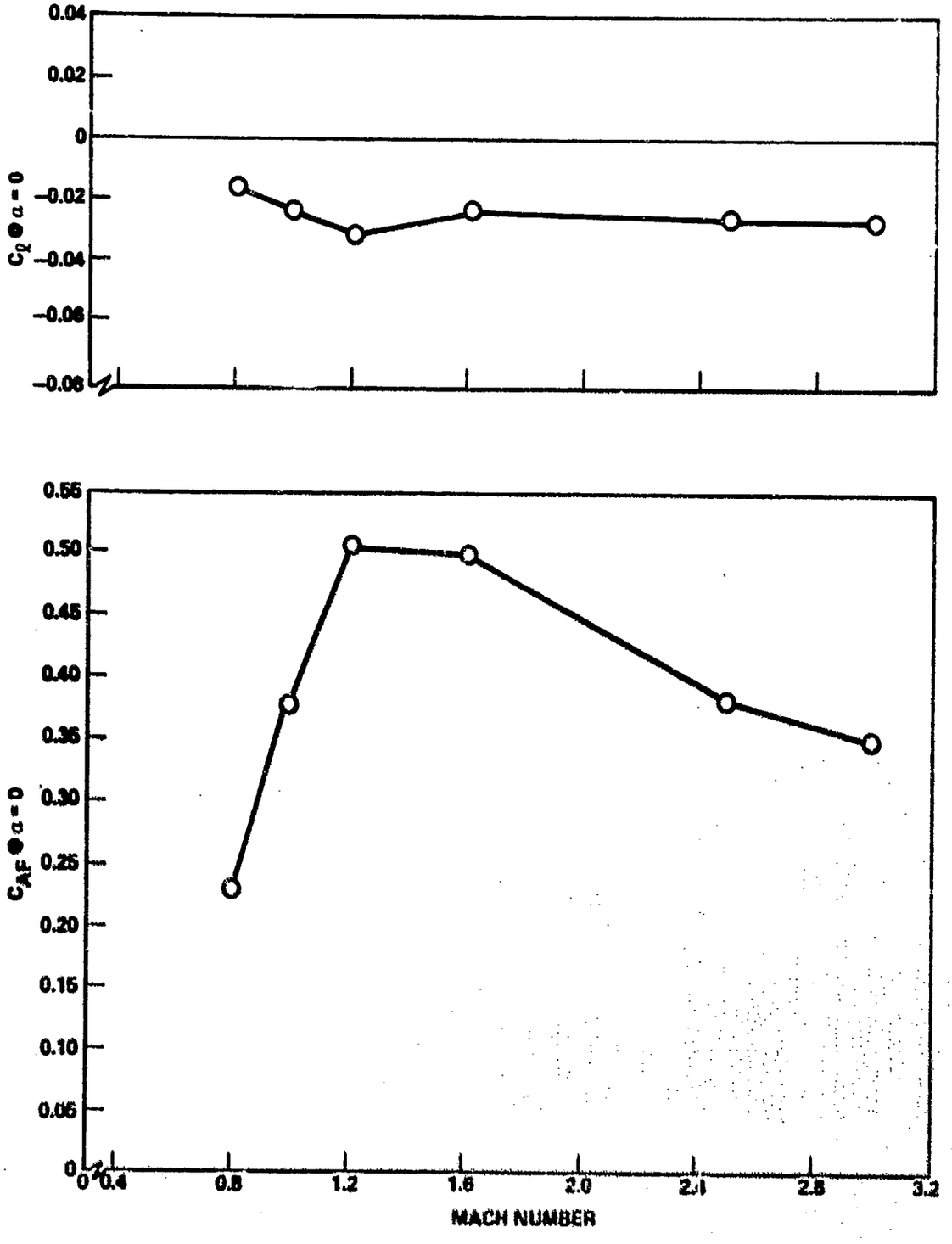


Figure 20. Concluded.

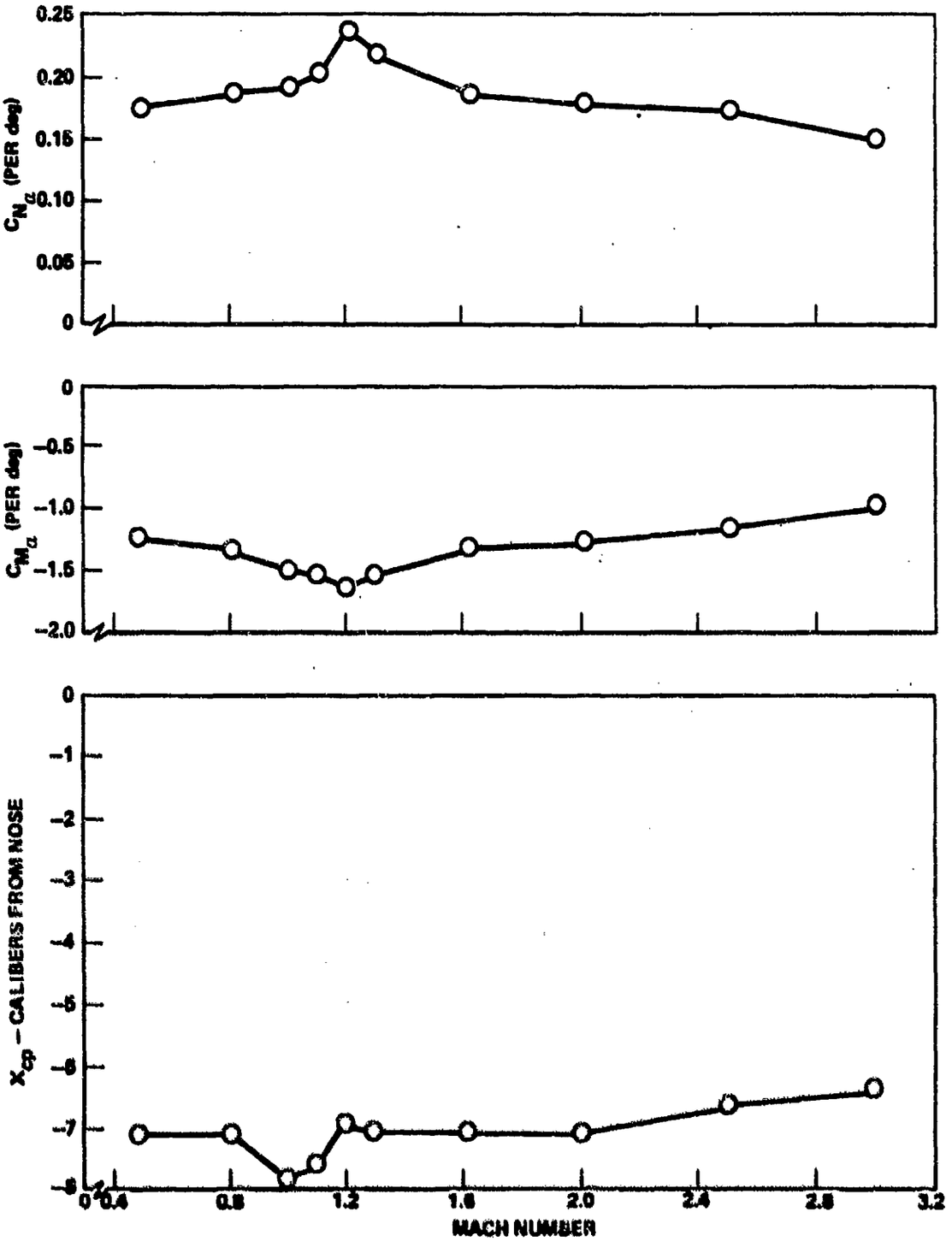


Figure 21. Stability summary - B1F1, $\phi = 0$, $\theta = 10$.

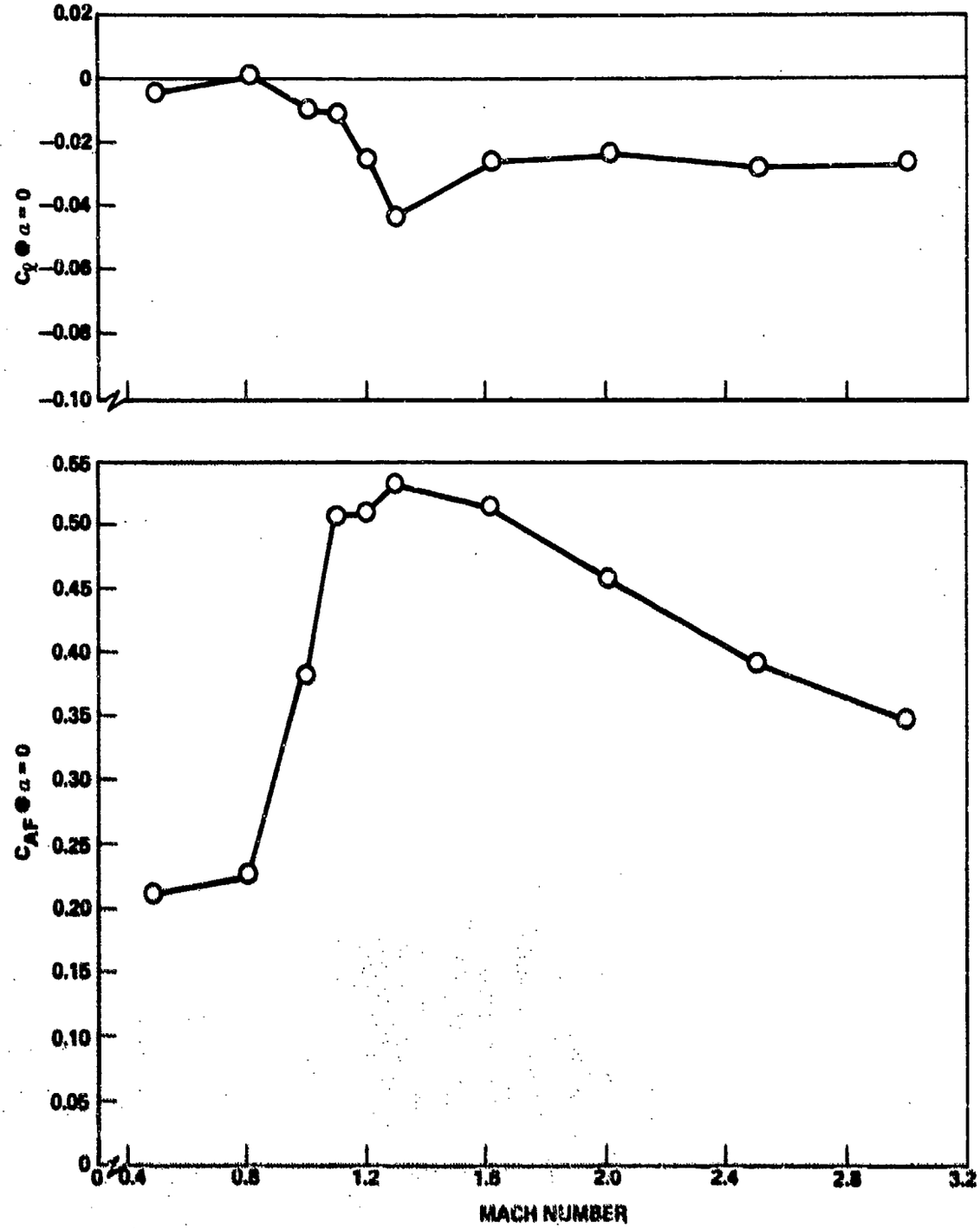


Figure 21. Concluded.

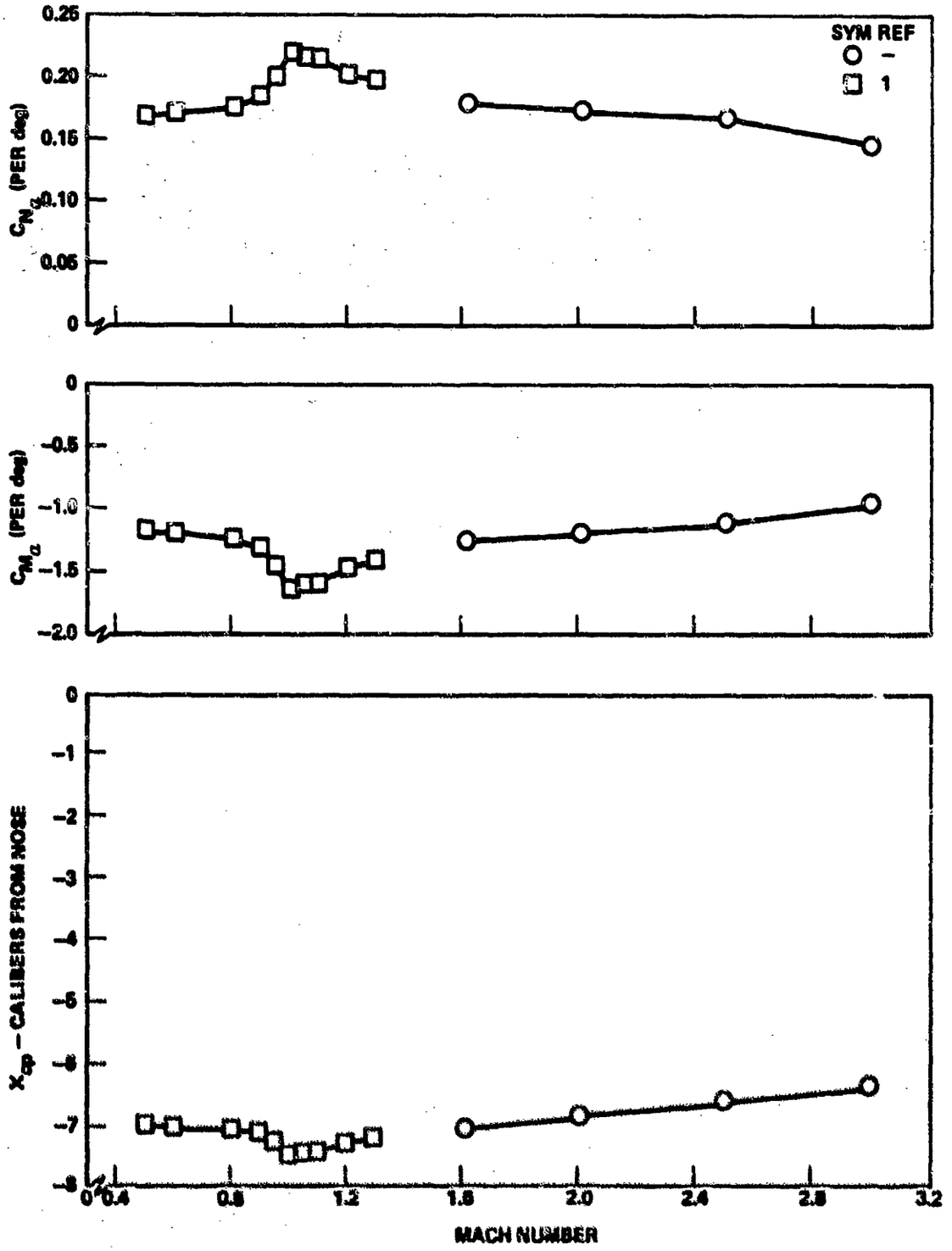


Figure 22. Stability summary - B1F1, $\phi = 0$, $\theta = 22.5$.

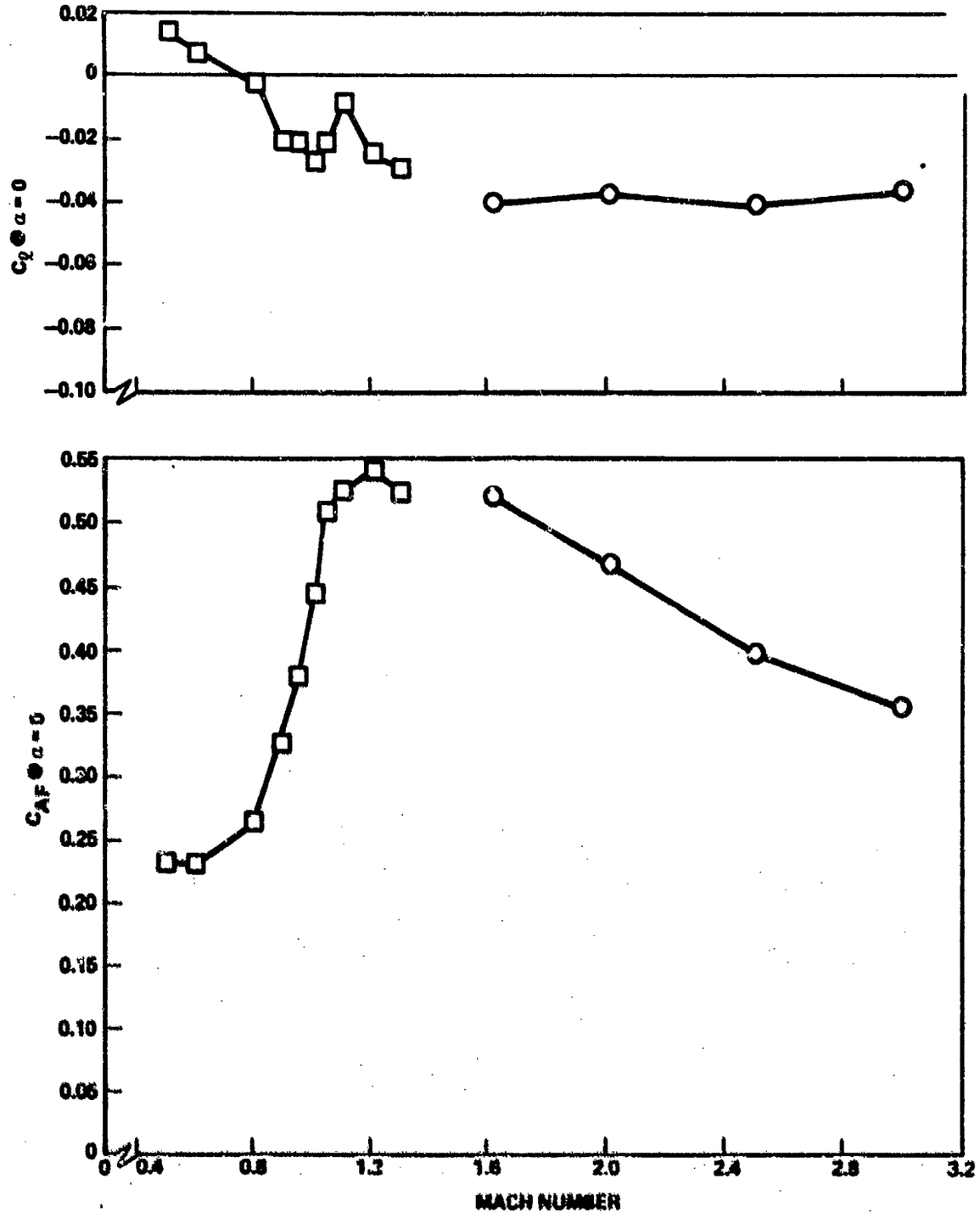


Figure 22. Concluded.

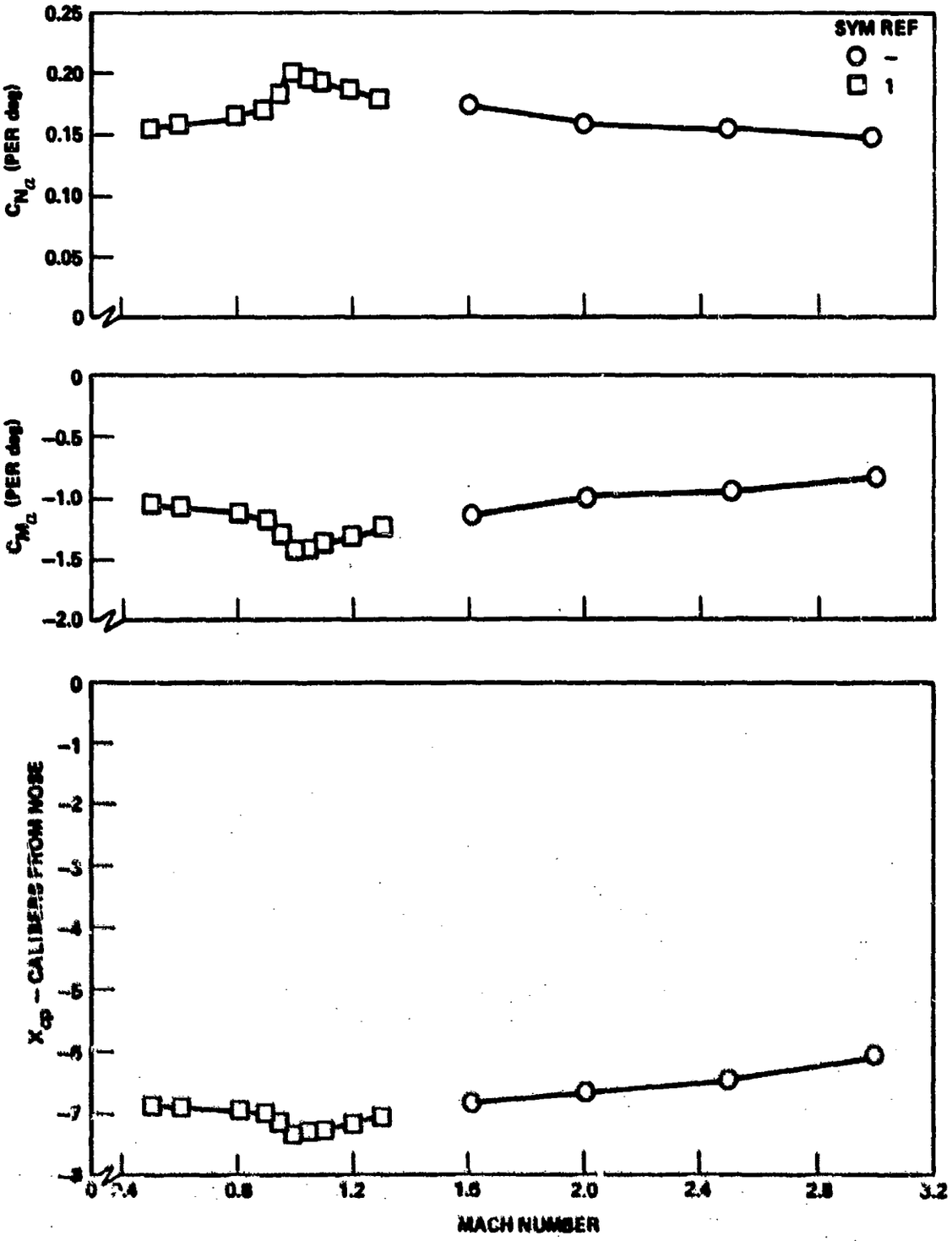


Figure 23. Stability summary - B1F1, $\phi = 0$, $\theta = 45$.

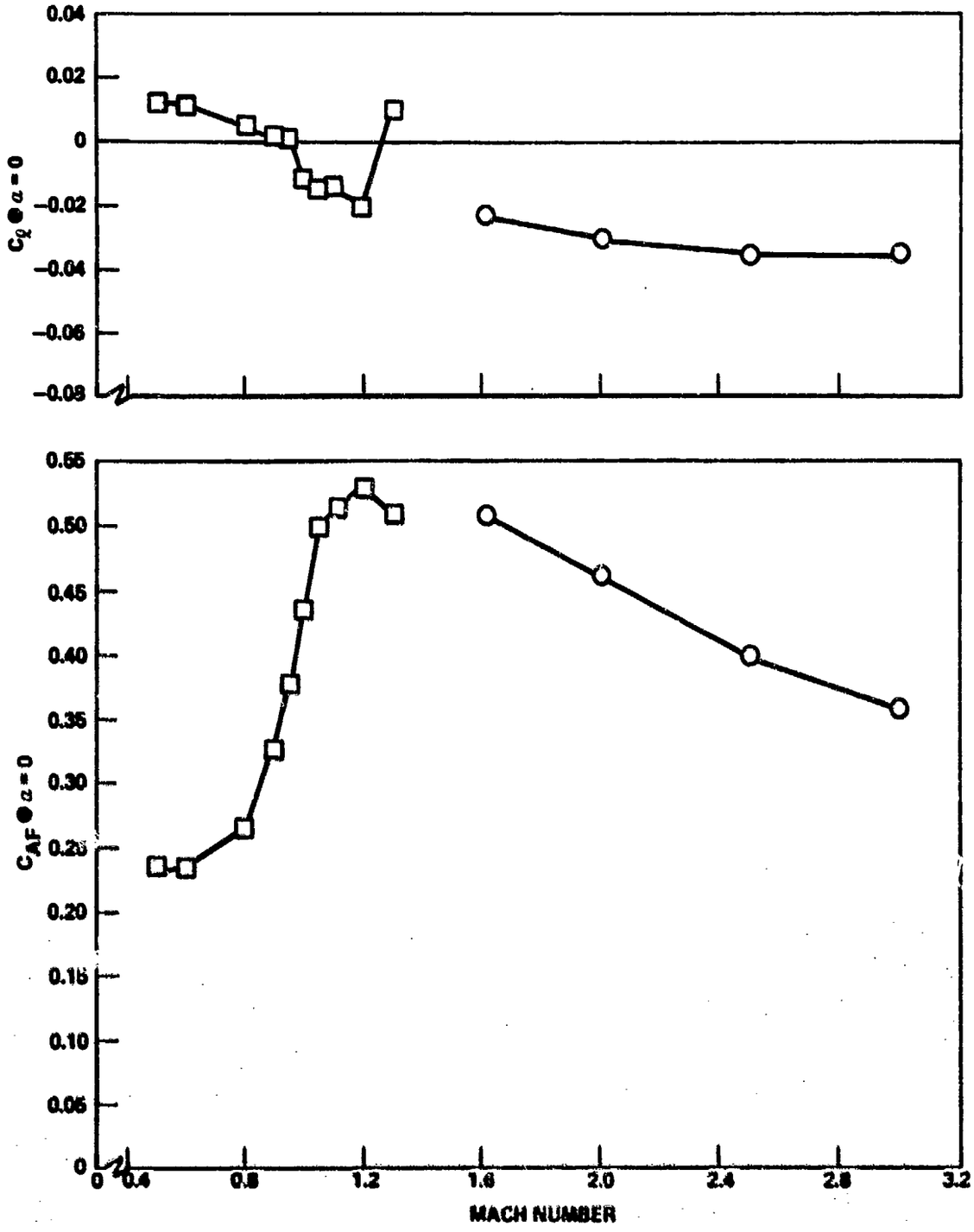


Figure 23. Concluded.

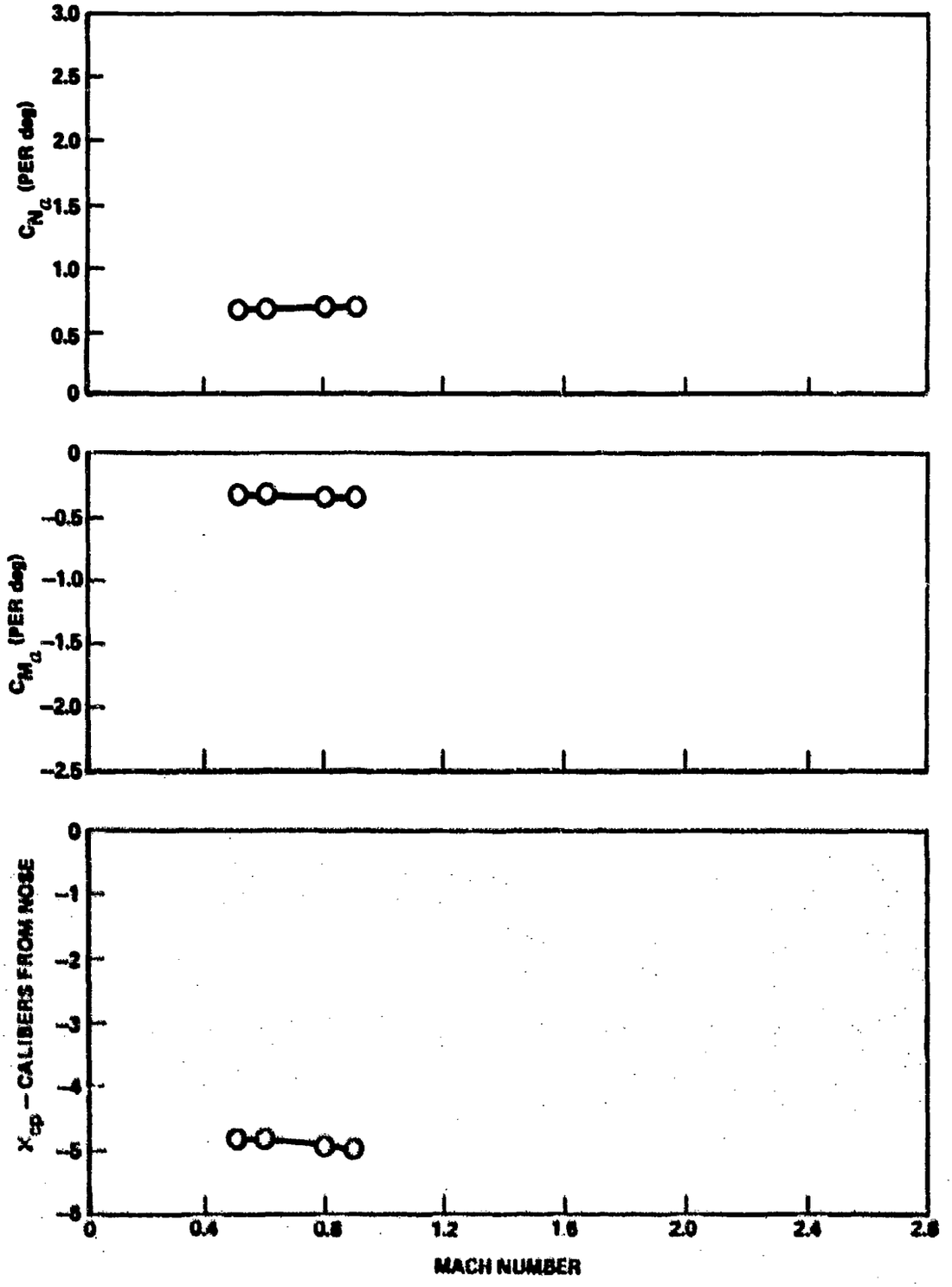


Figure 24. Stability summary - B1F1, $\phi = 0$, $\theta = 112.5$.

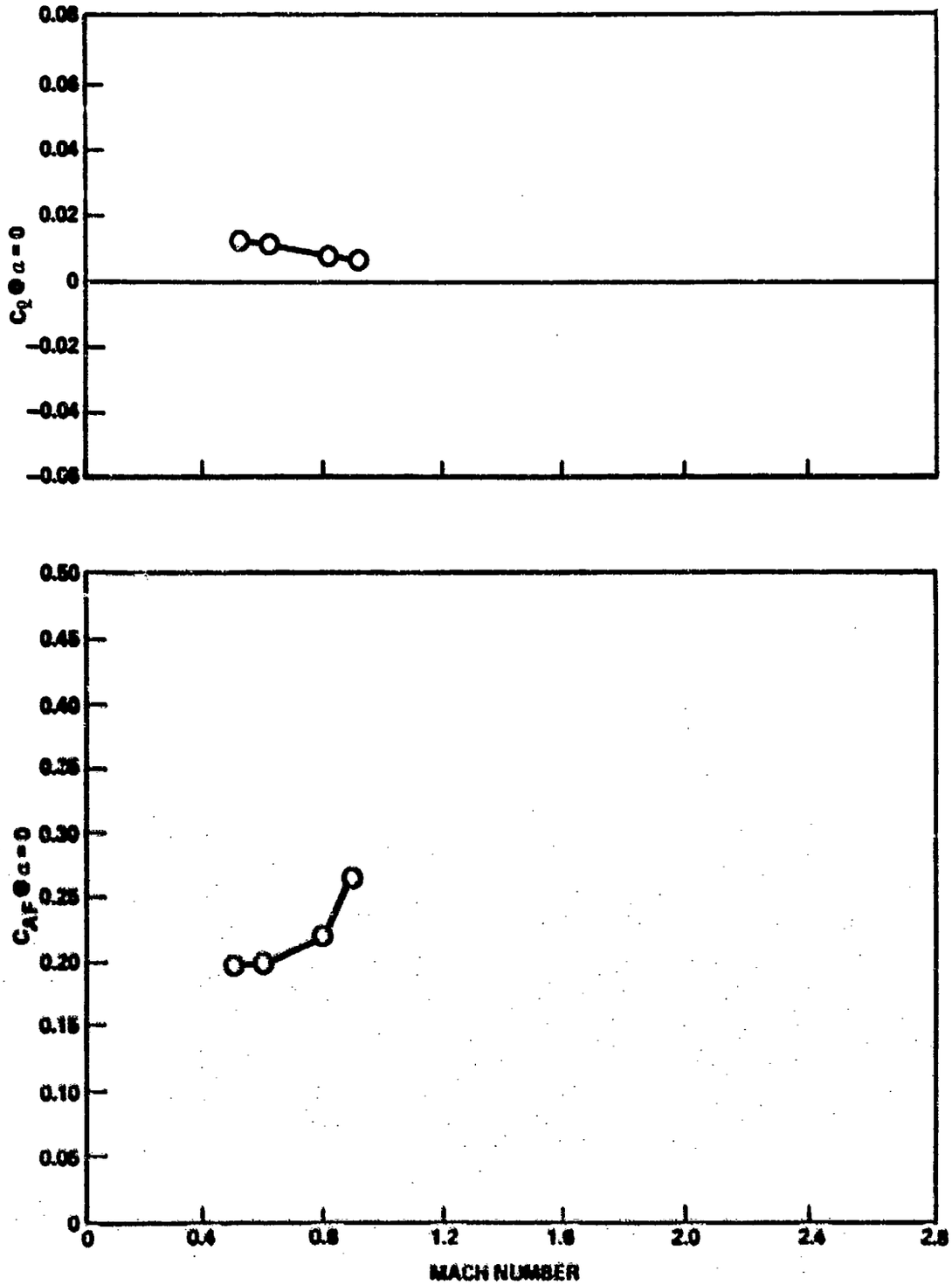


Figure 24. Concluded.

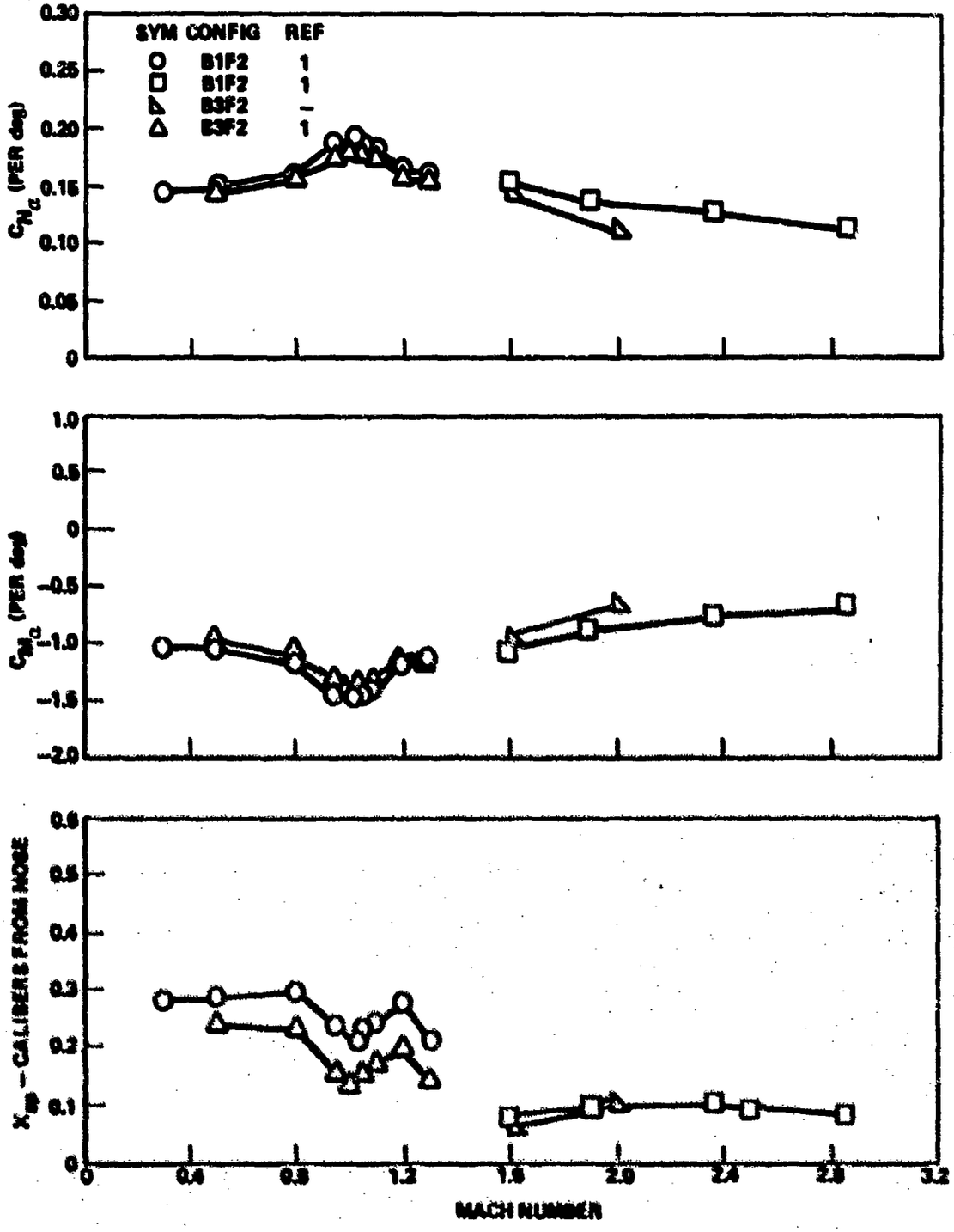


Figure 25. Effect of step down body, $\phi = 0$.

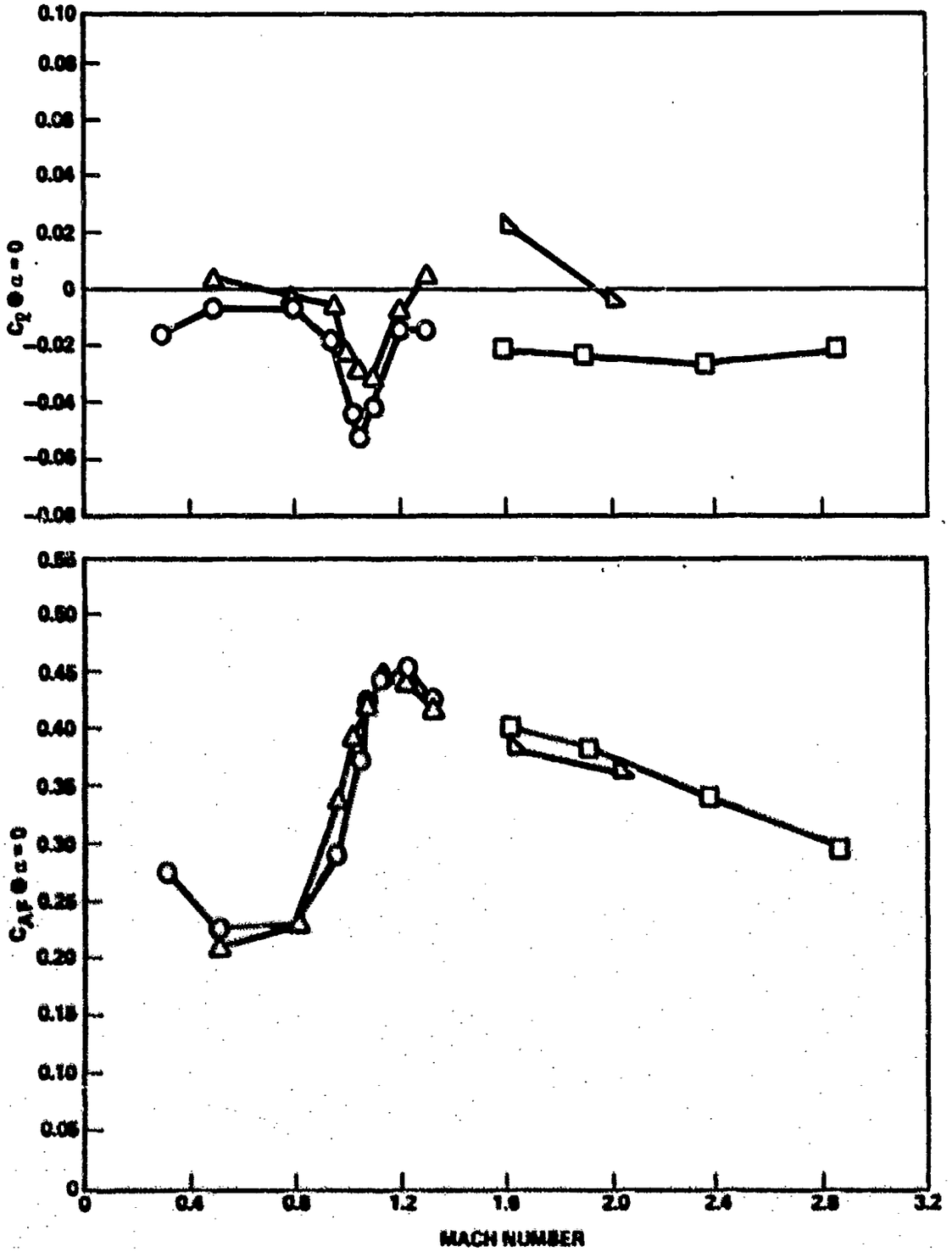


Figure 25. Concluded.

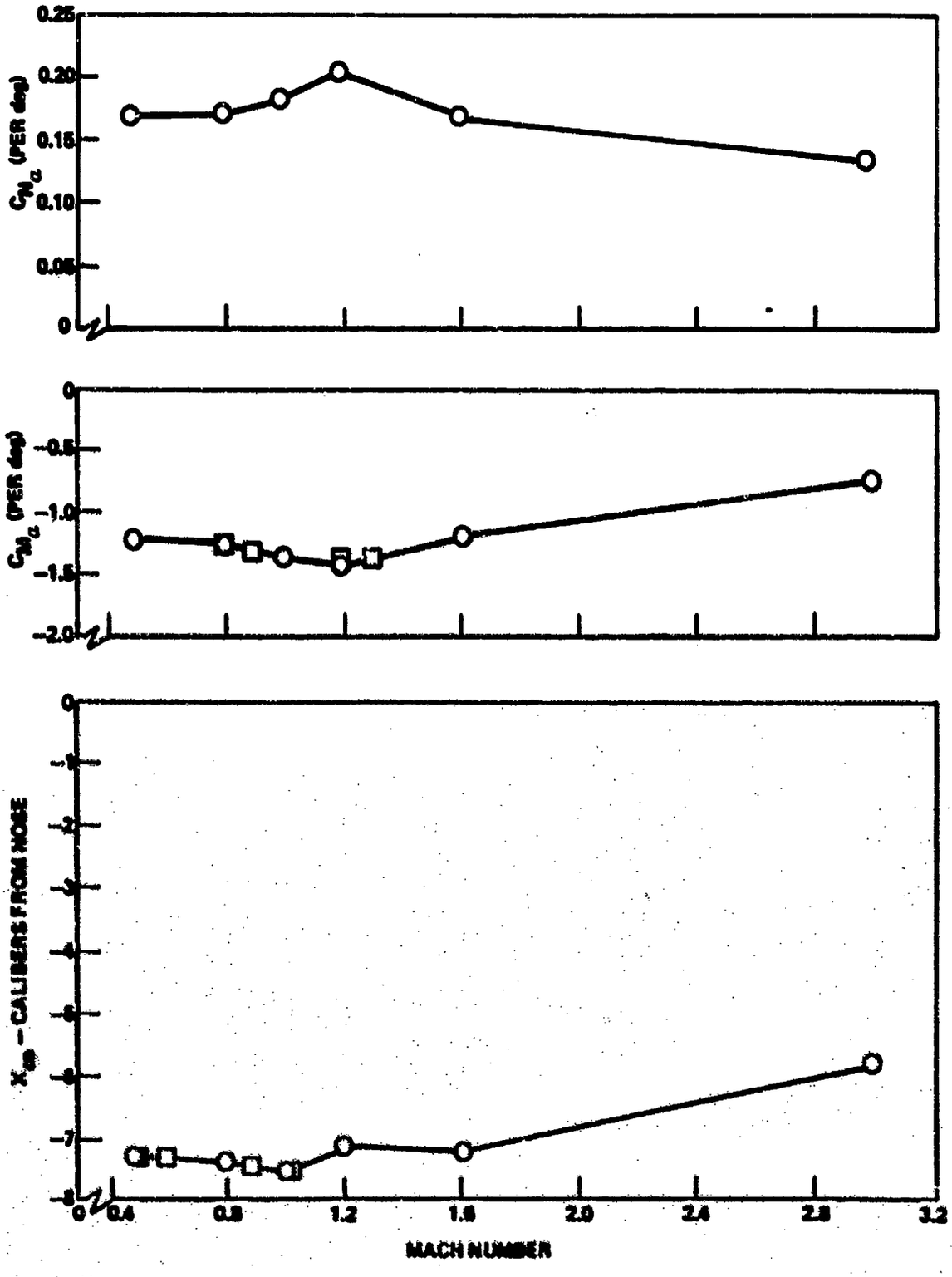


Figure 26. Stability summary - B1F17, $\phi = 0$.

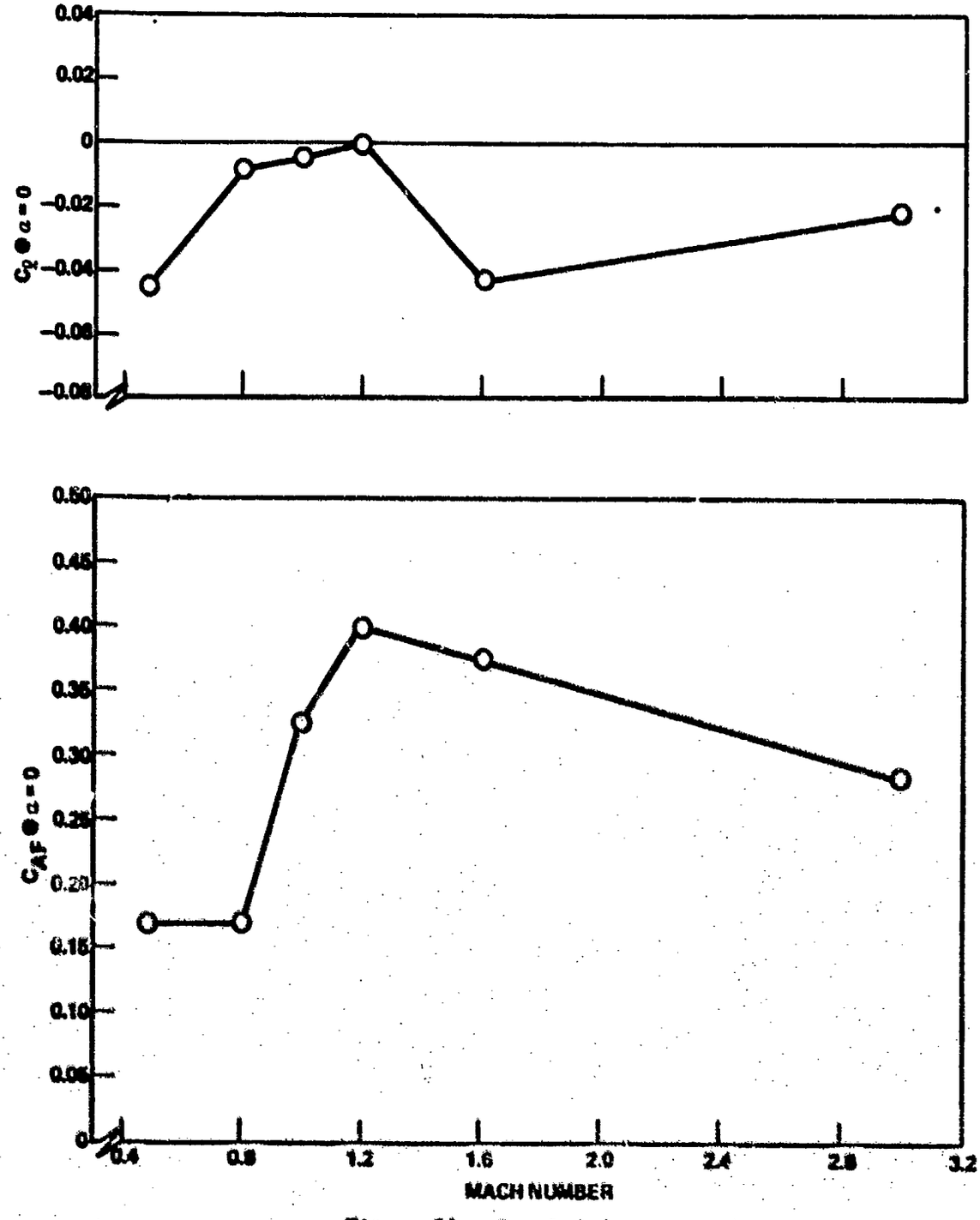


Figure 26. Concluded.

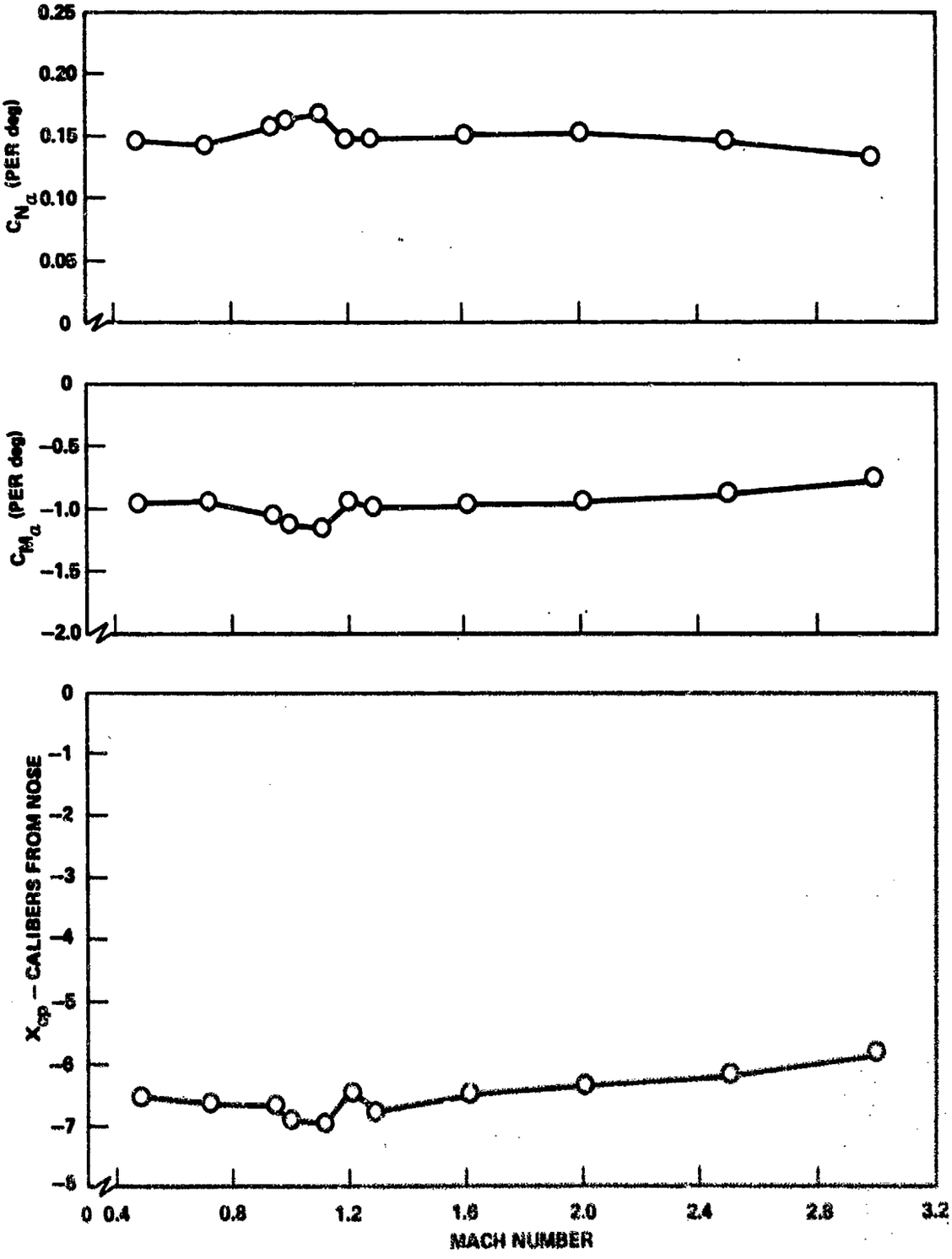


Figure 27. Stability summary, $\Phi = 0$.

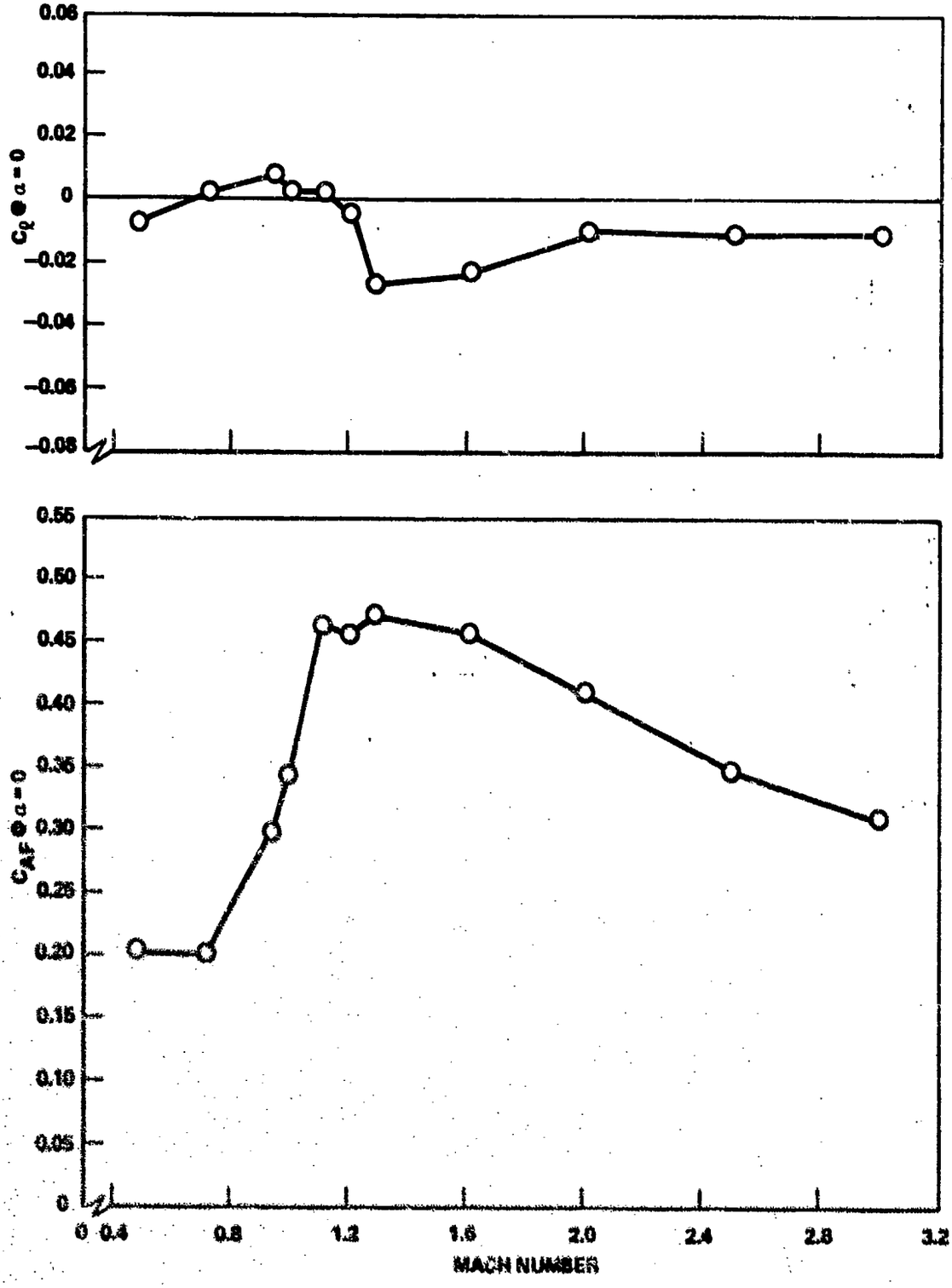


Figure 27. Concluded.

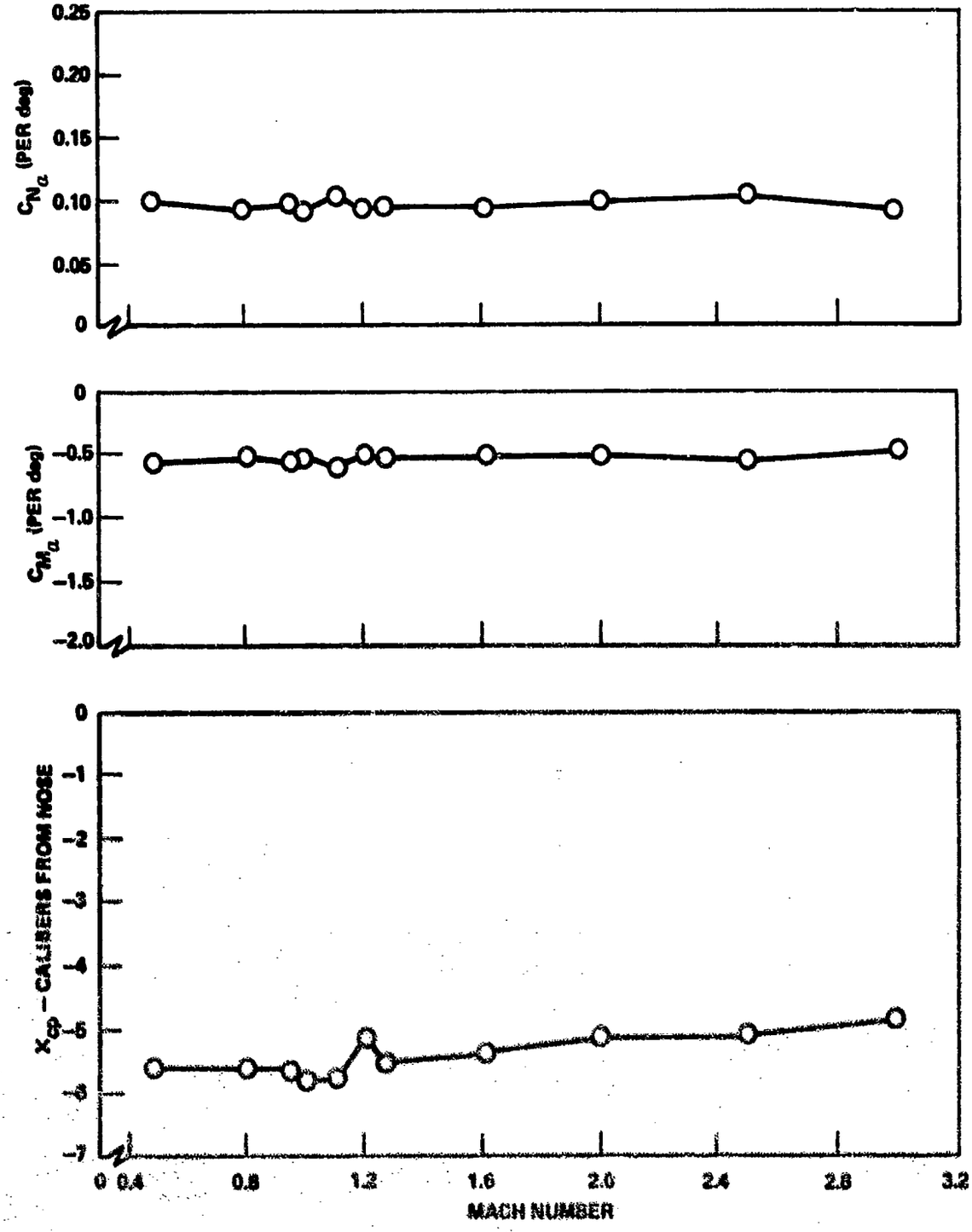


Figure 28. Stability summary - B1F21, $\phi = 0$.

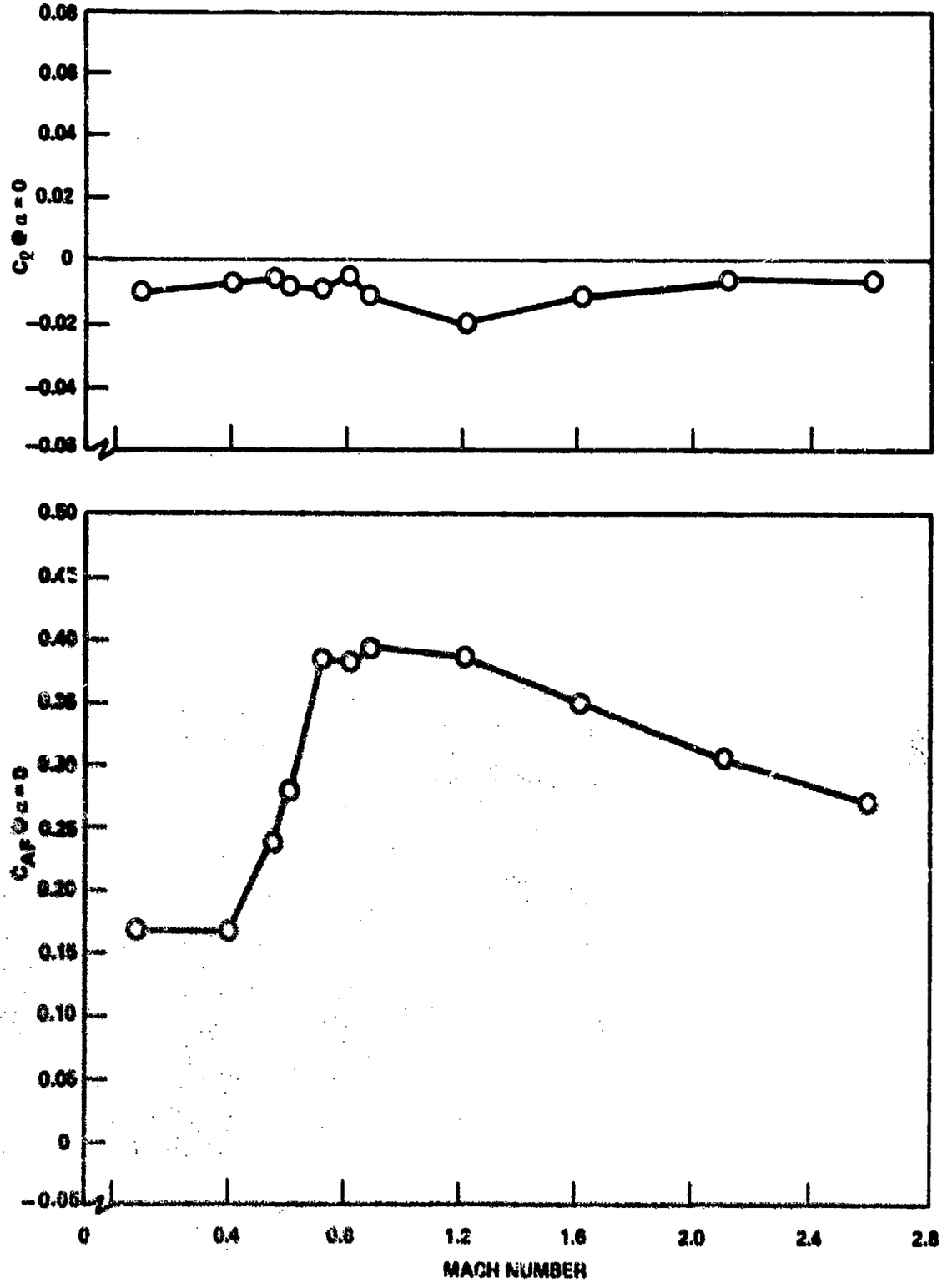


Figure 28. Concluded.

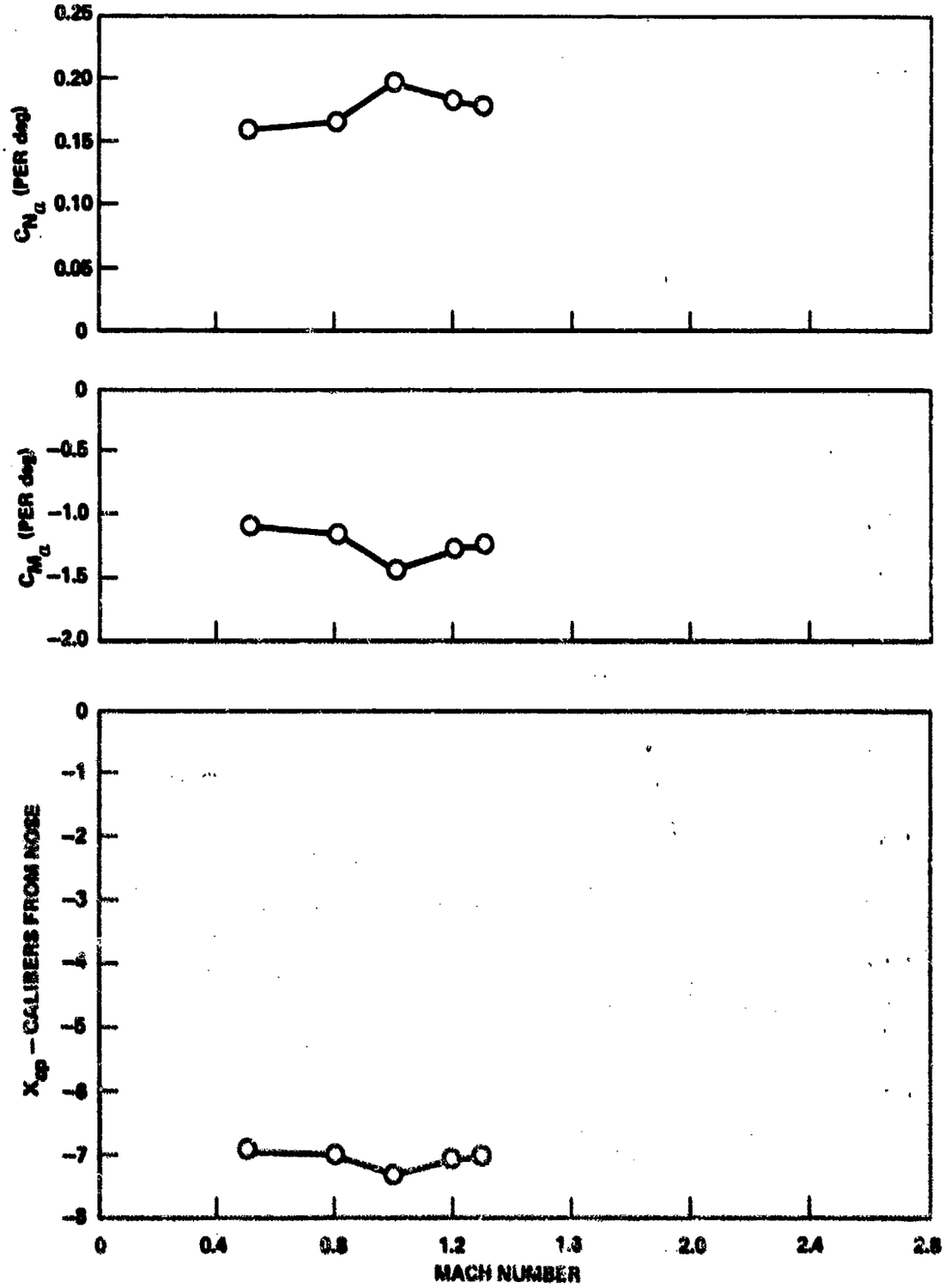


Figure 29. Stability summary - B2F1, $\phi = 0$.

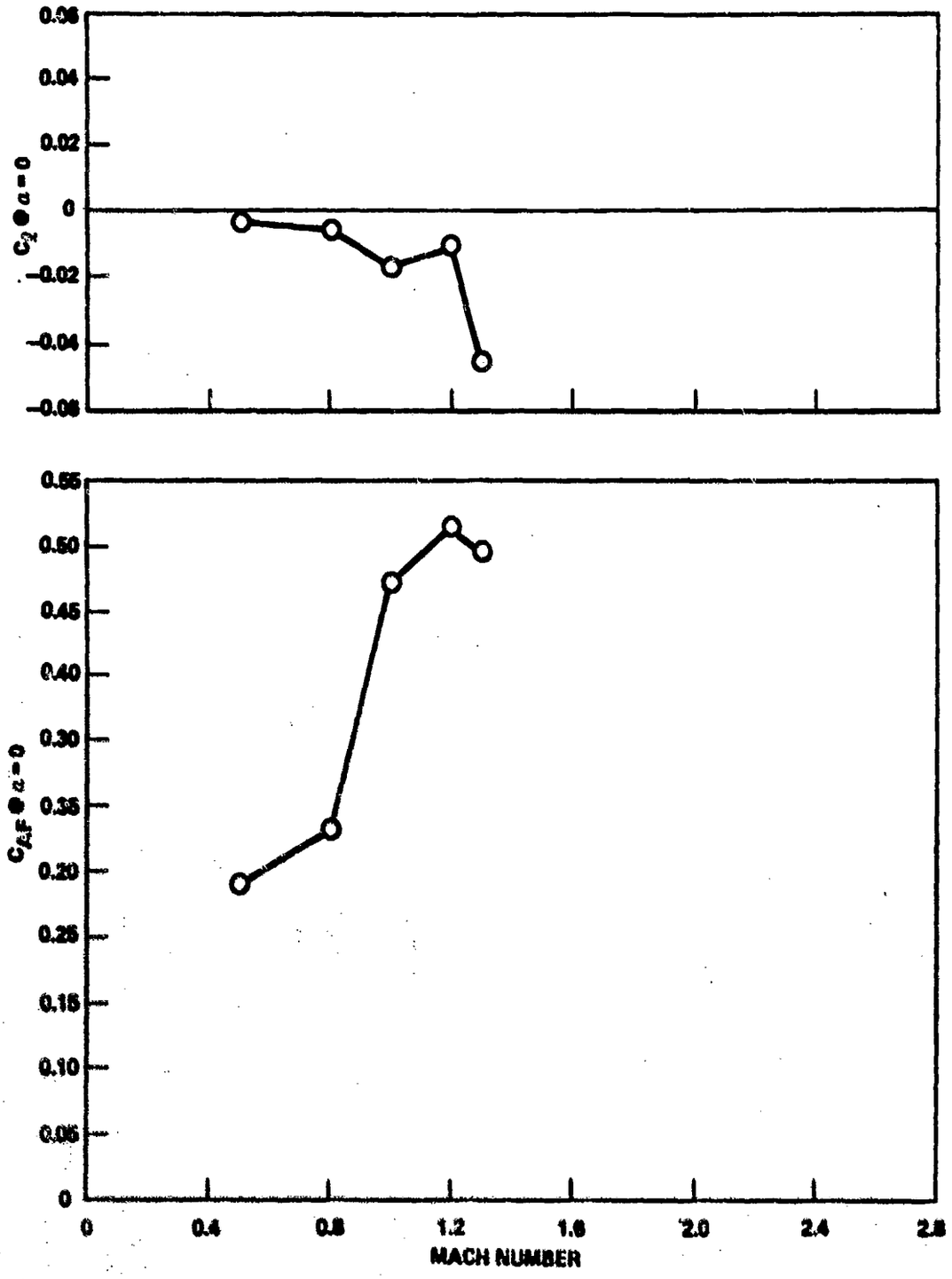


Figure 29. Concluded.

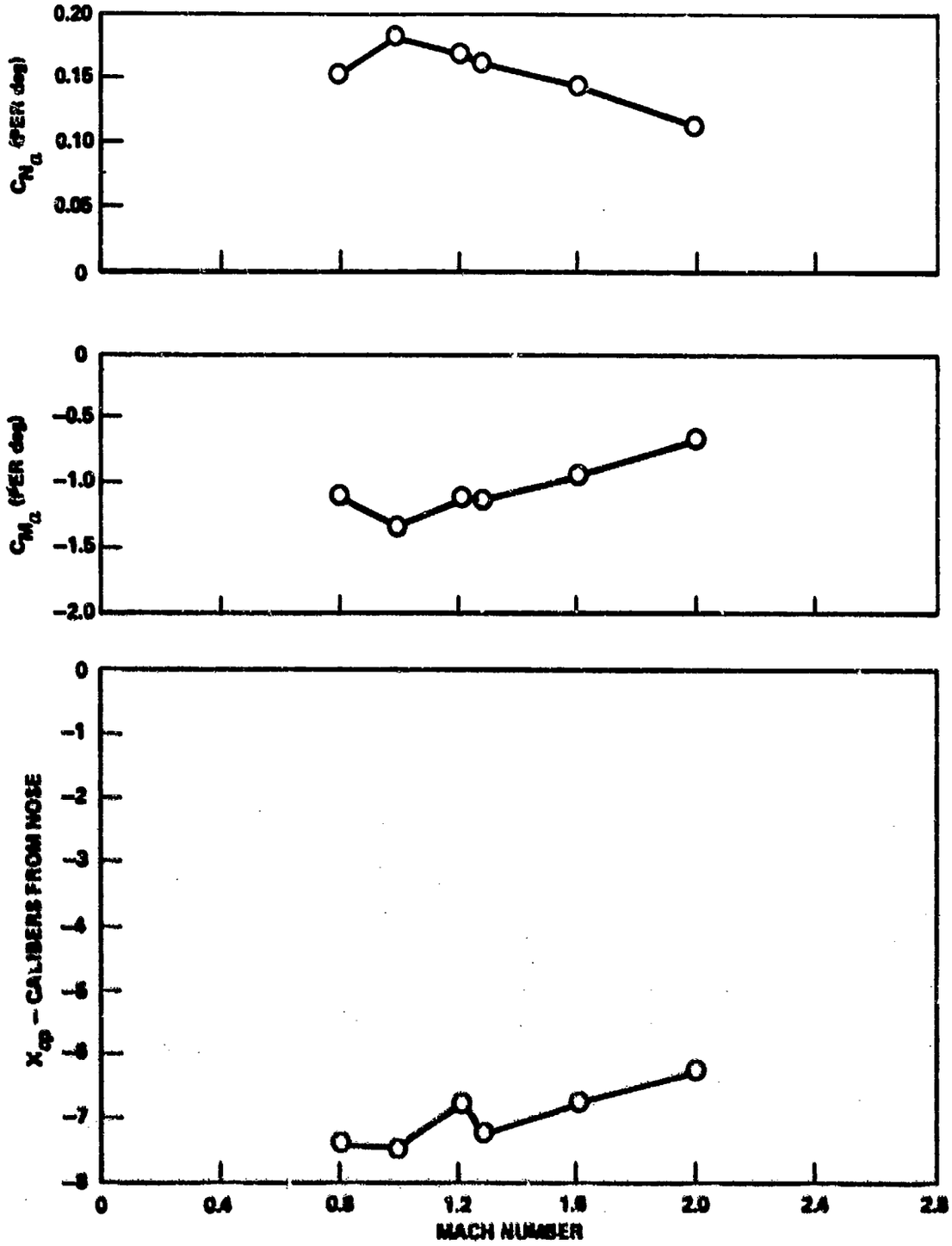


Figure 30. Stability summary - B3F2, $\phi = 0$.

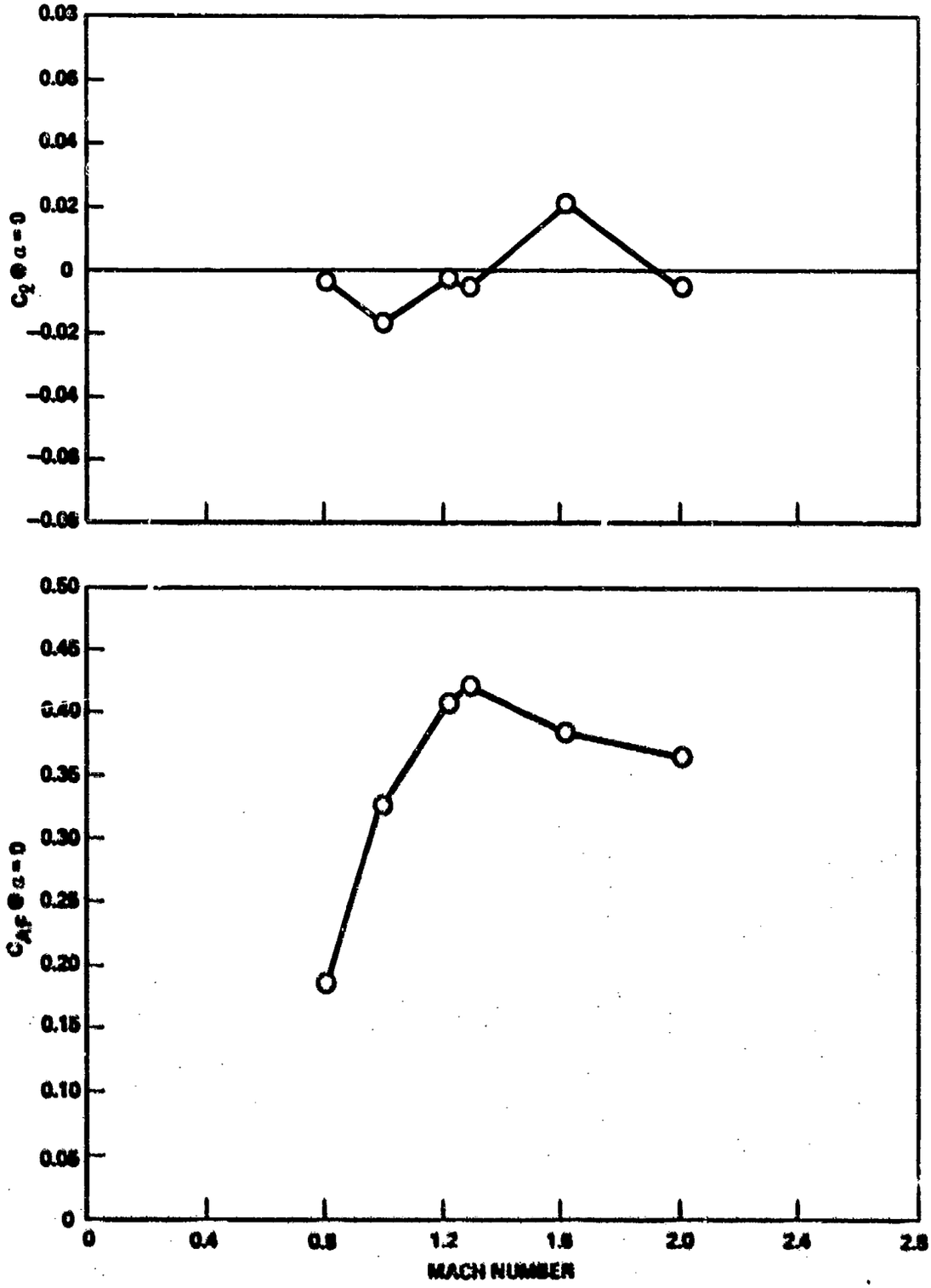


Figure 30. Concluded.

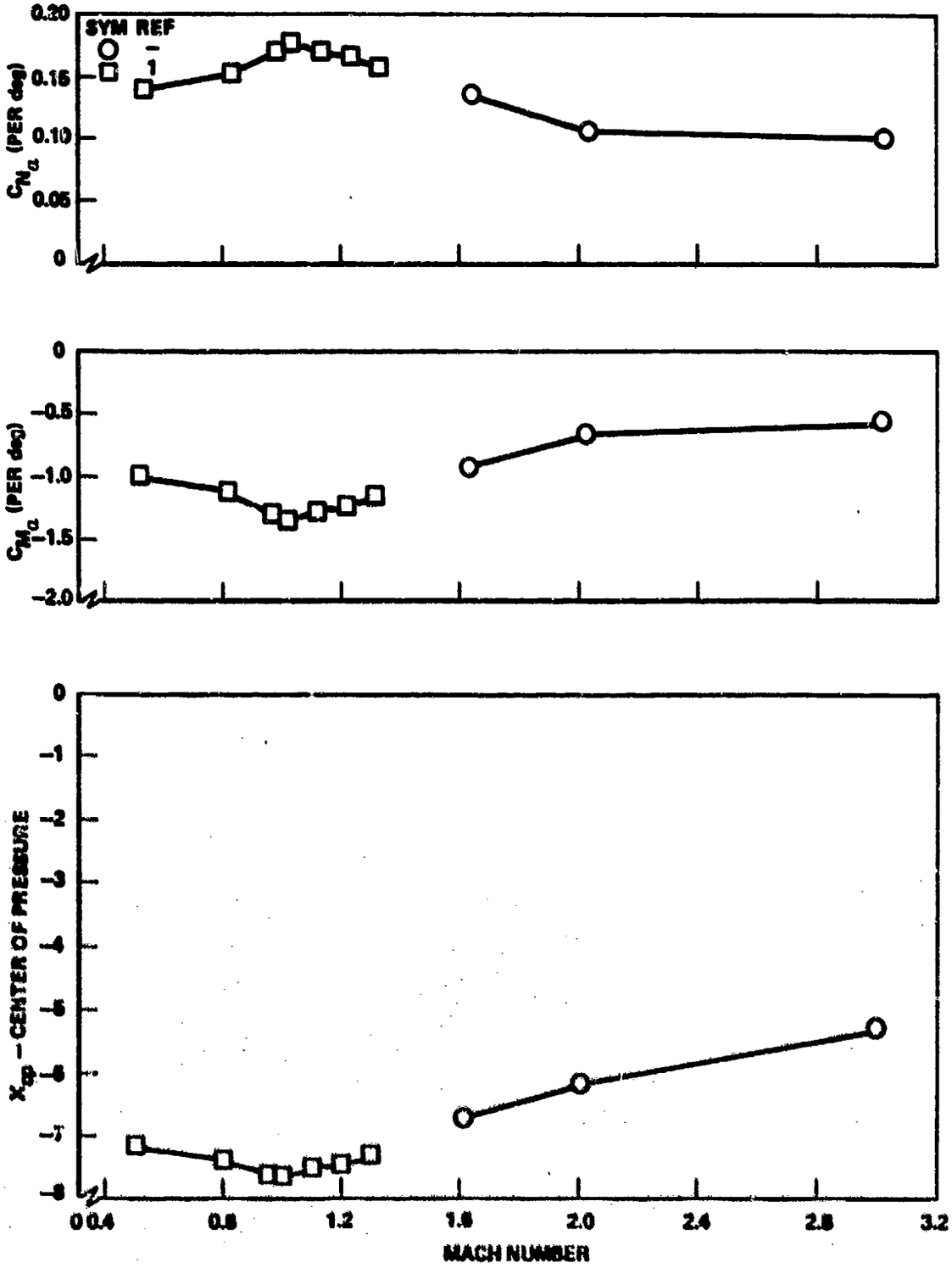


Figure 31. Stability summary - B3F16, $\phi = 0$.

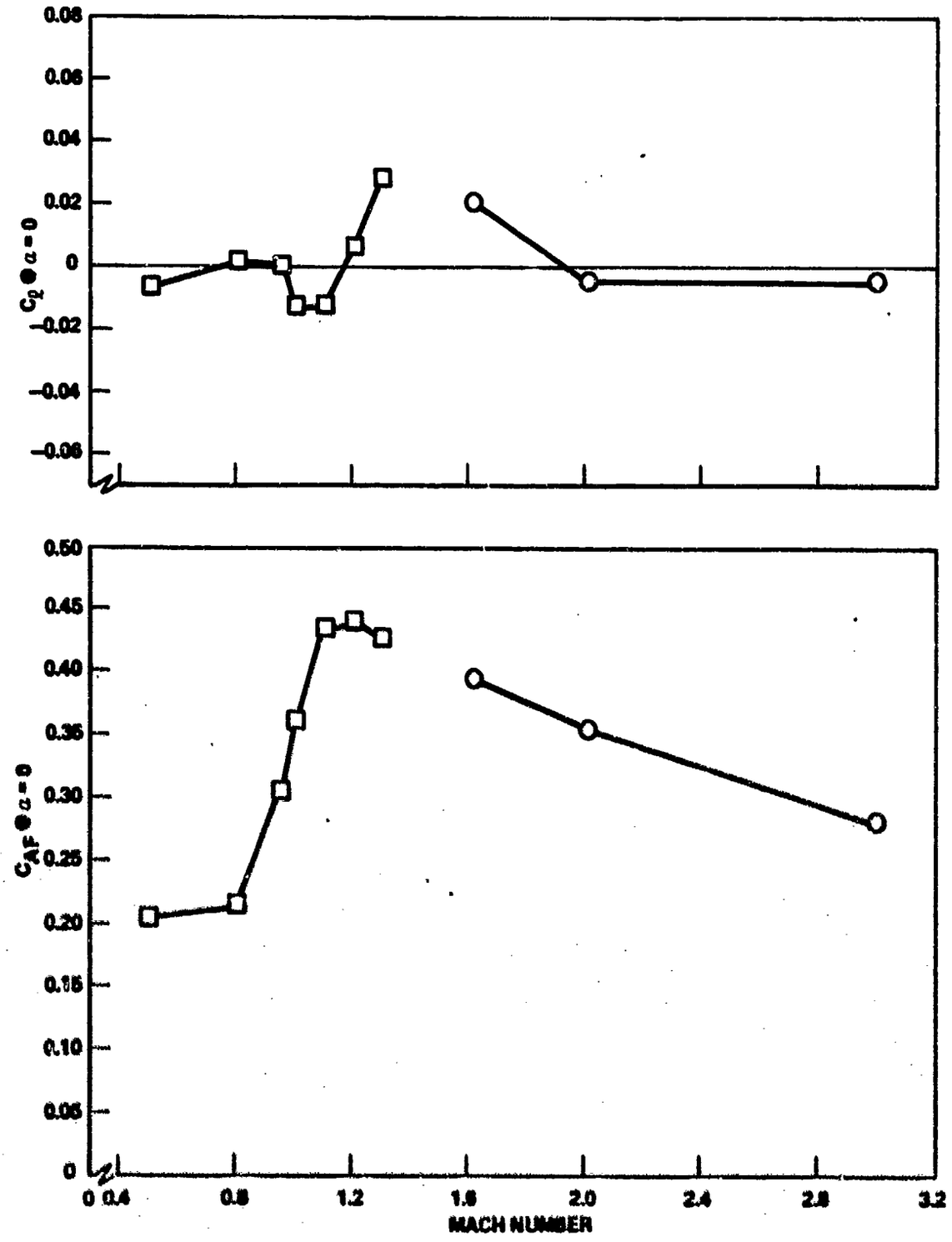


Figure 31. Concluded.

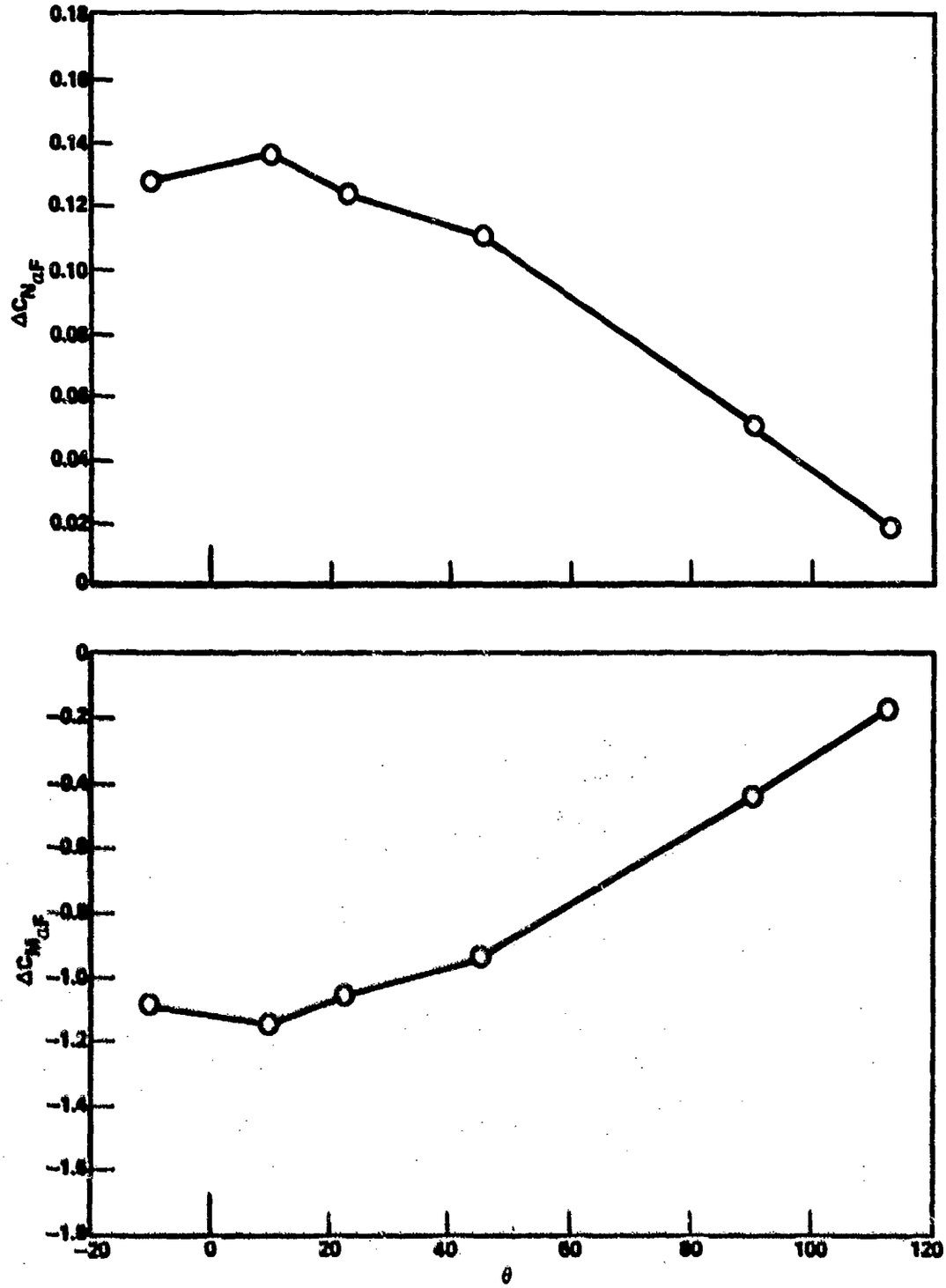


Figure 32. Total fin effectiveness with opening angle, M = 0.5, ϕ = 0.0.

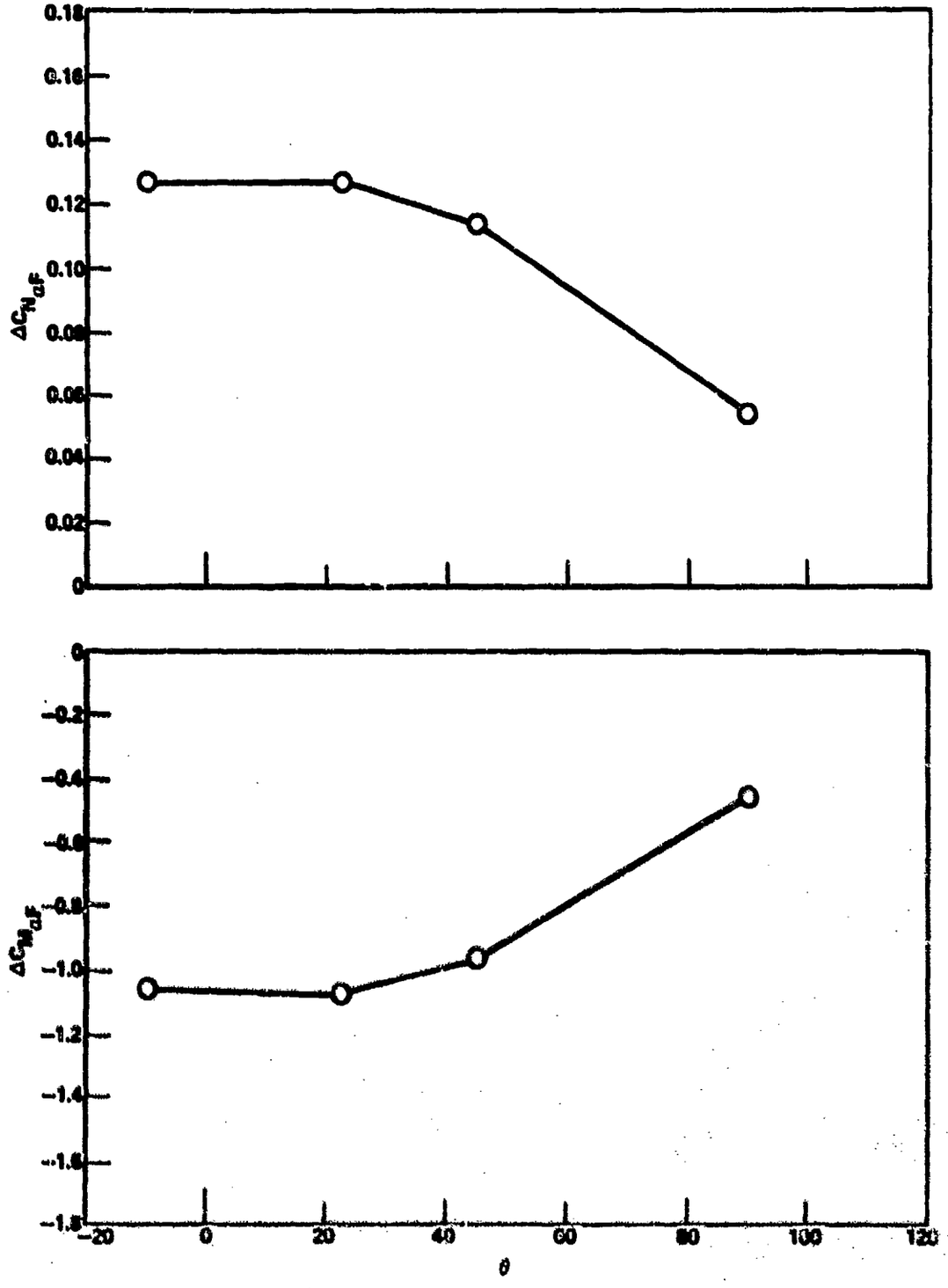


Figure 33. Total fin effectiveness with opening angle, M = 0.6, ϕ = 0.0.

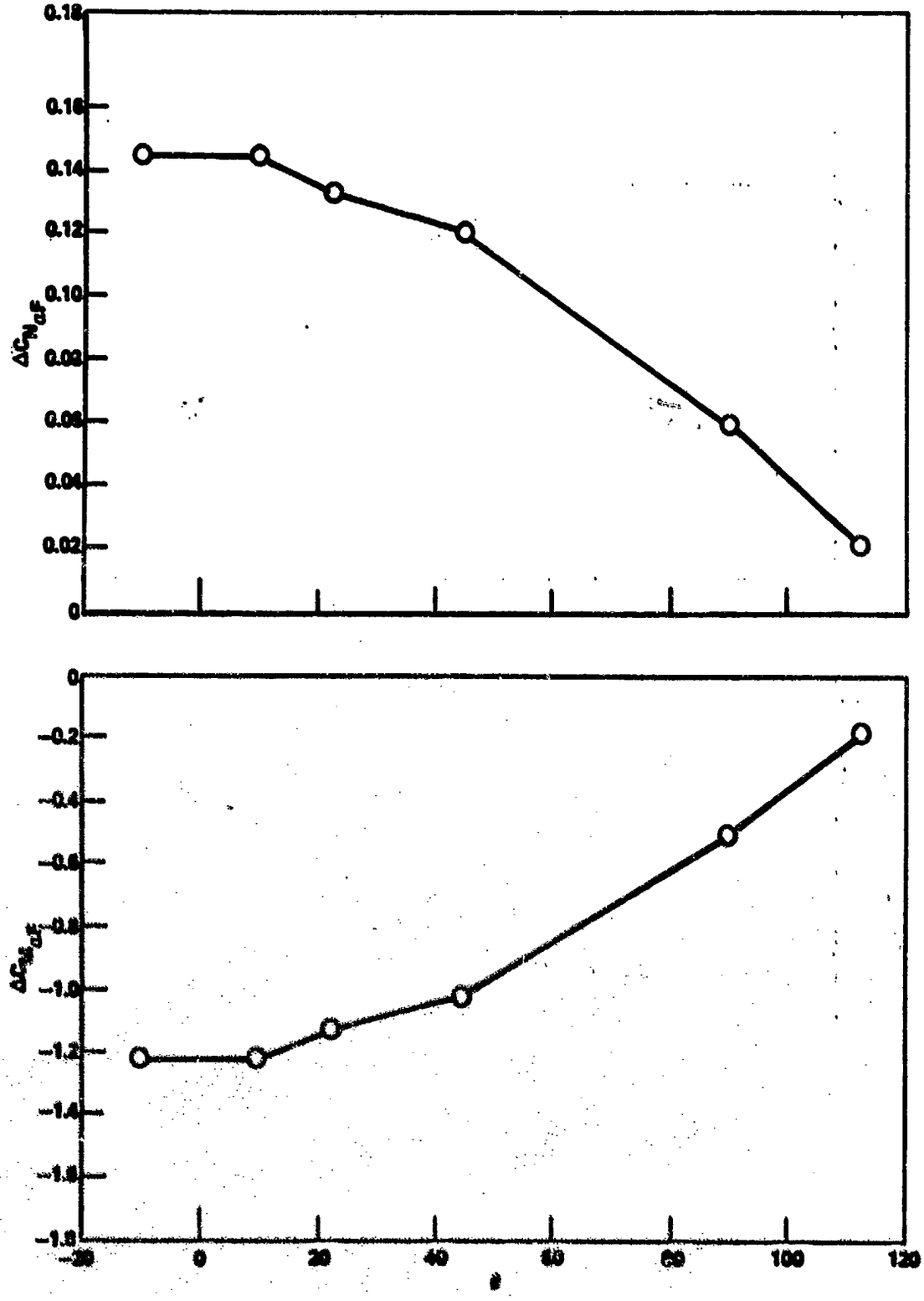


Figure 34. Total fin effectiveness with opening angle, $M = 0.8$, $\phi = 0.0$.

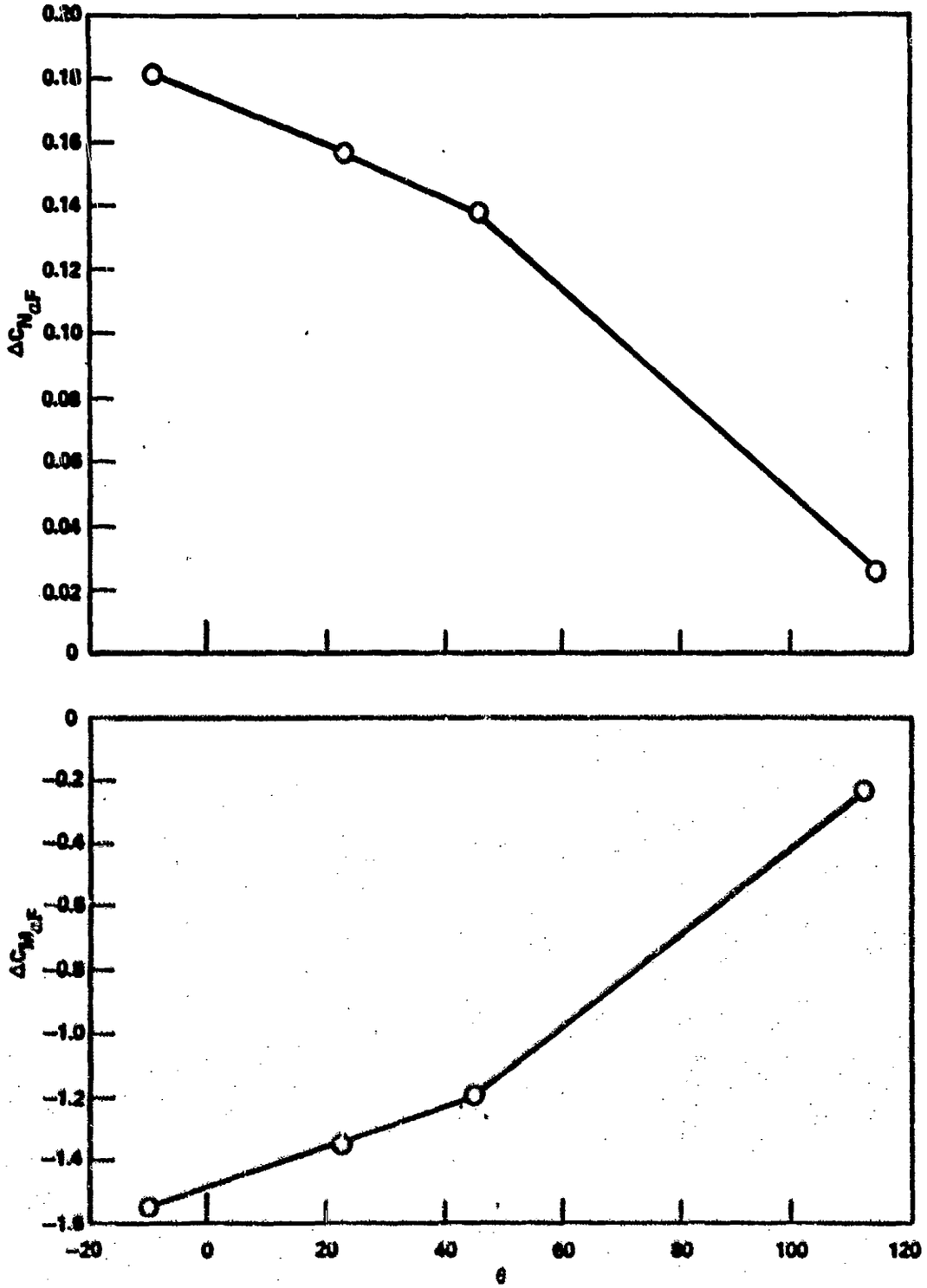


Figure 35. Total fin effectiveness with opening angle, M = 0.95, ϕ = 0.0.

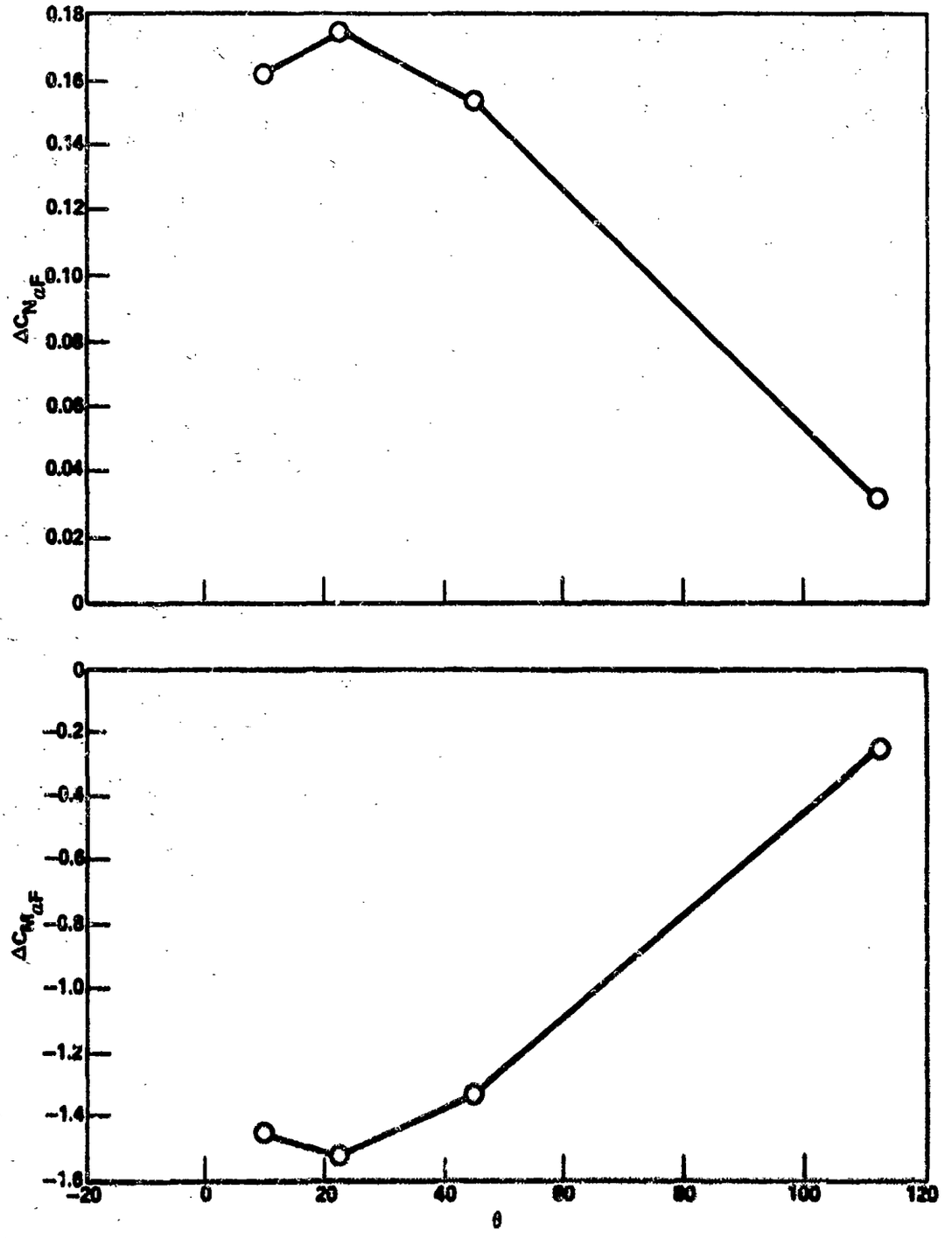


Figure 36. Total fin effectiveness with opening angle, M = 1.0, ϕ = 0.0.

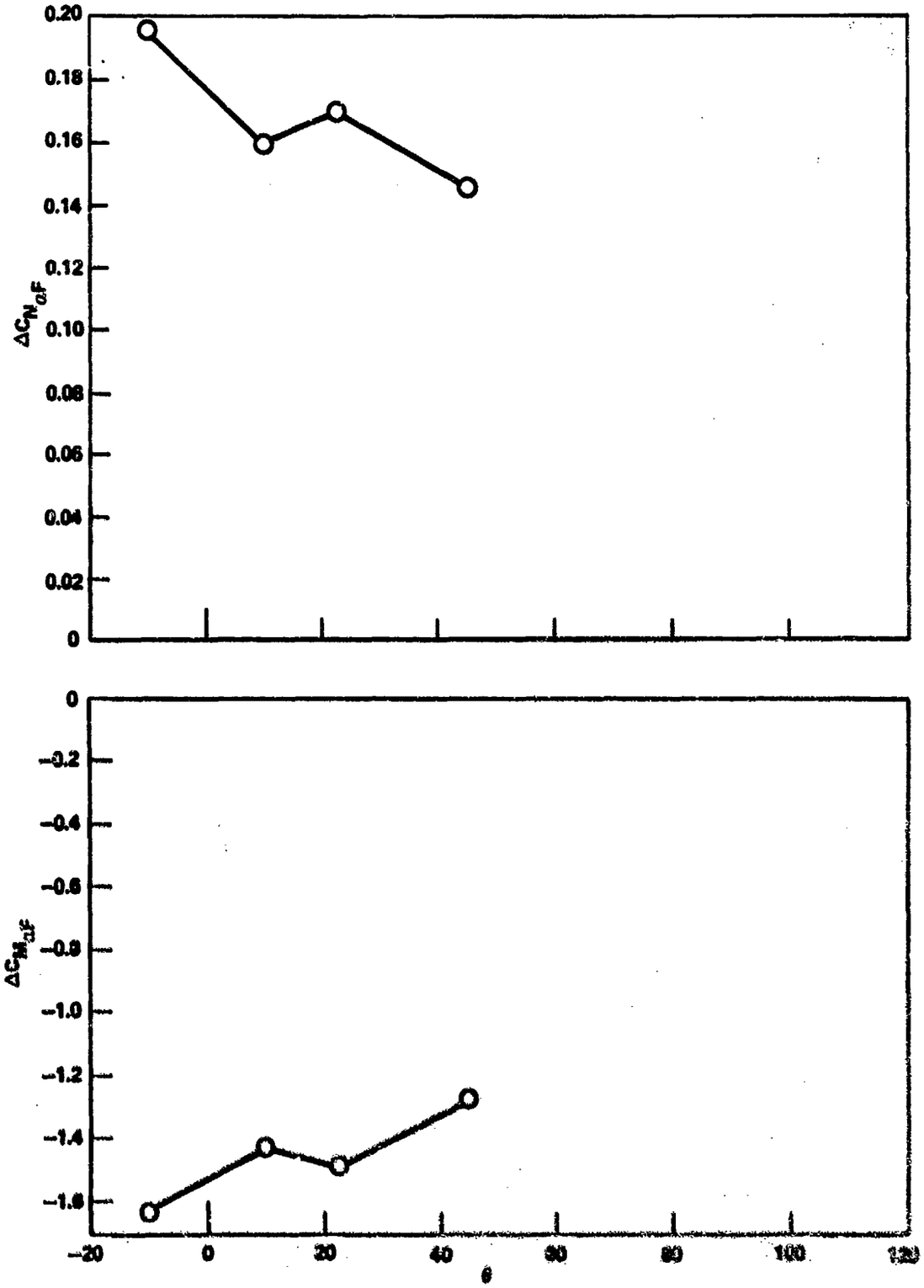


Figure 37. Total fin effectiveness with opening angle, M = 1.1, ϕ = 0.0.

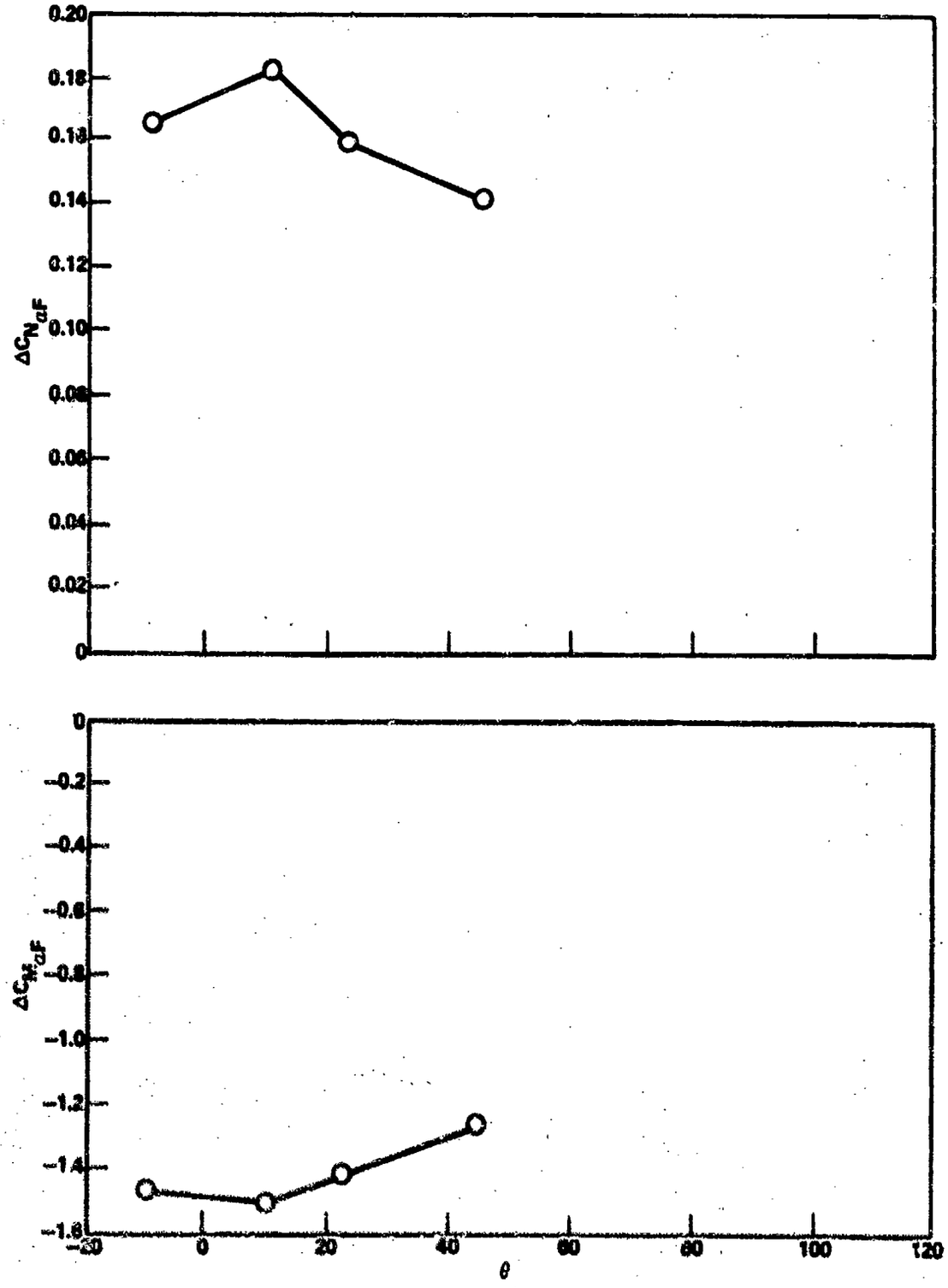


Figure 38. Total fin effectiveness with opening angle, M = 1.2, ϕ = 0.0.

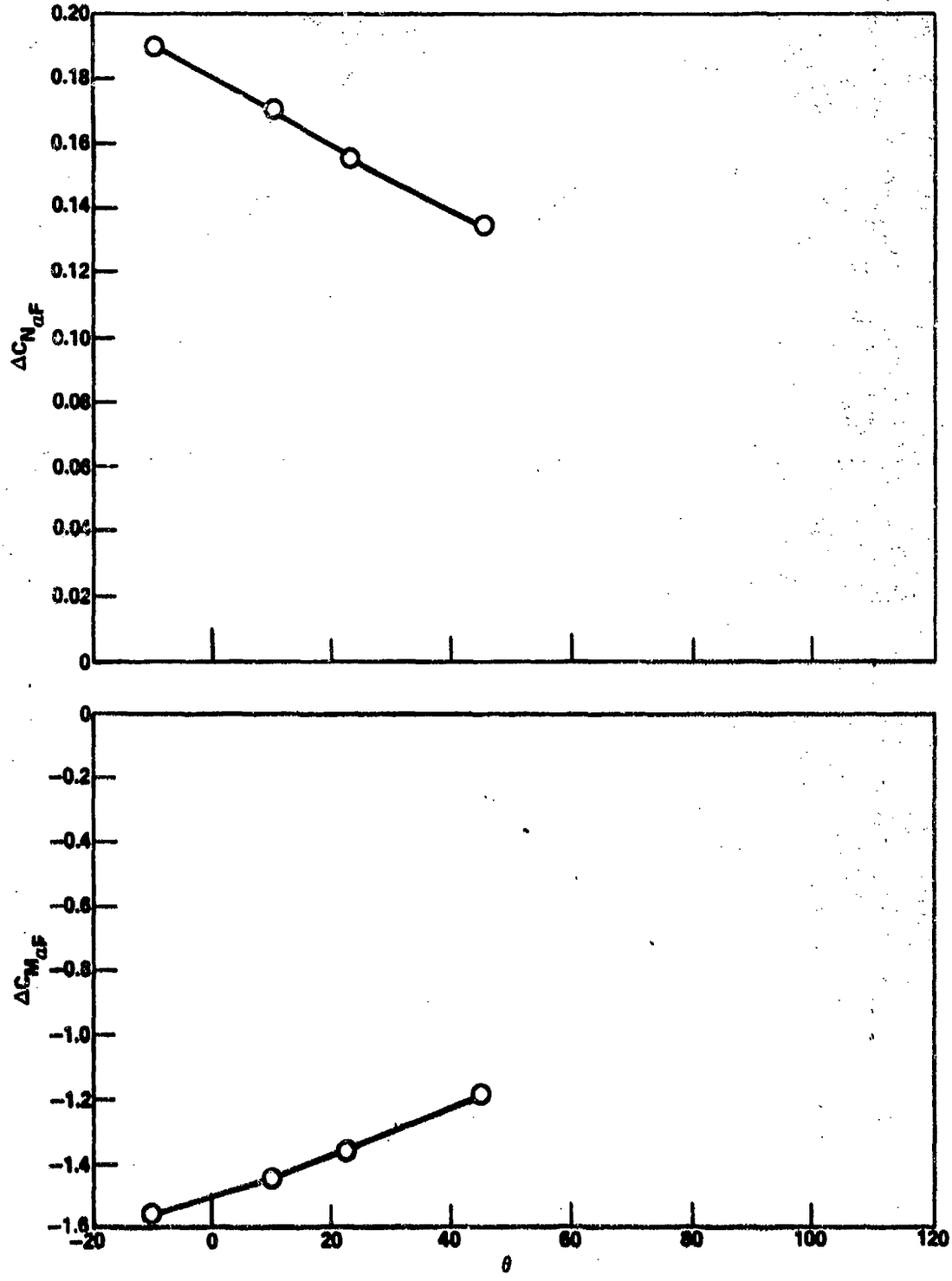


Figure 39. Total fin effectiveness with opening angle, M = 1.3, ϕ = 0.0.

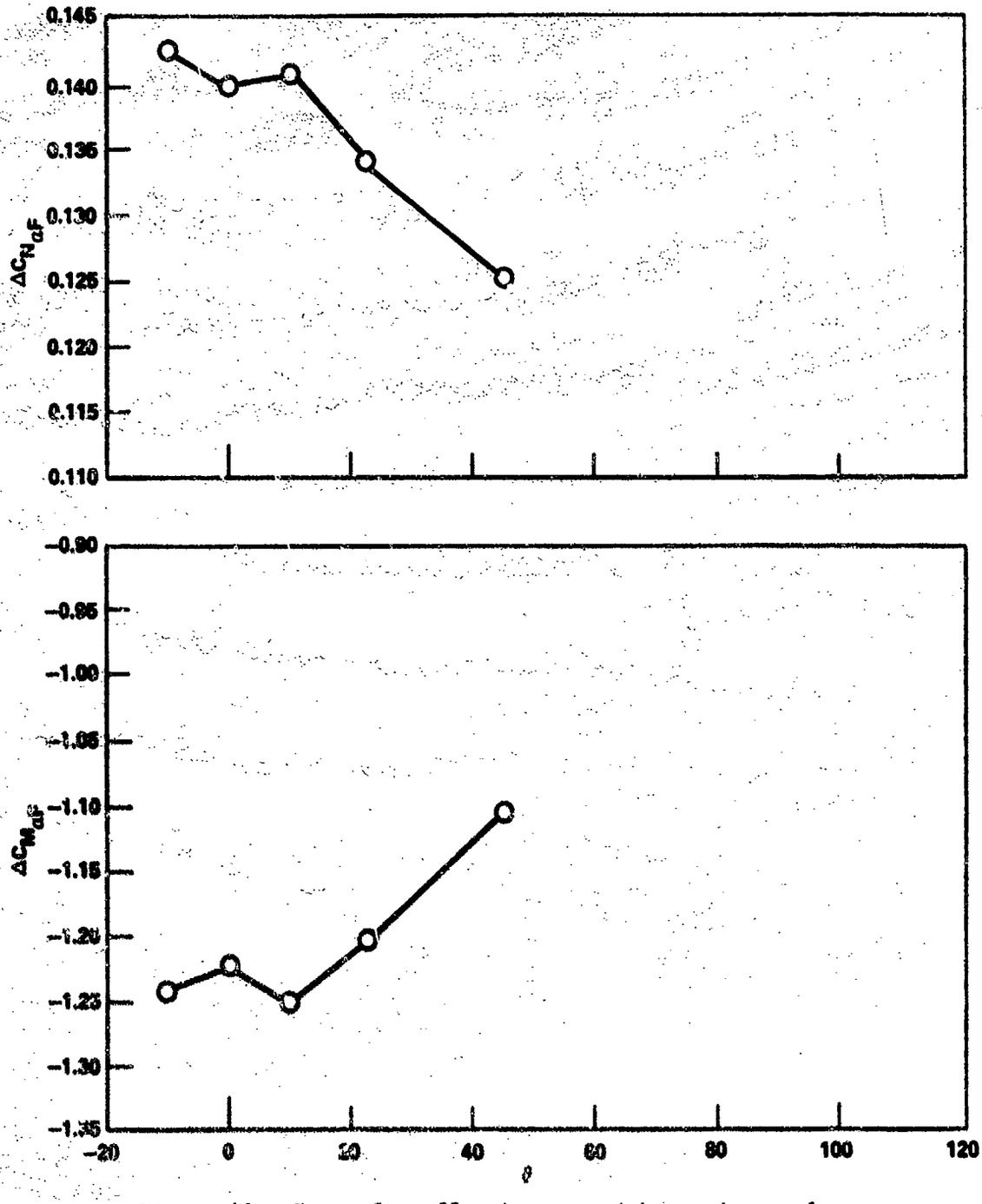


Figure 40. Total fin effectiveness with opening angle, M = 1.6, ϕ = 0.0.

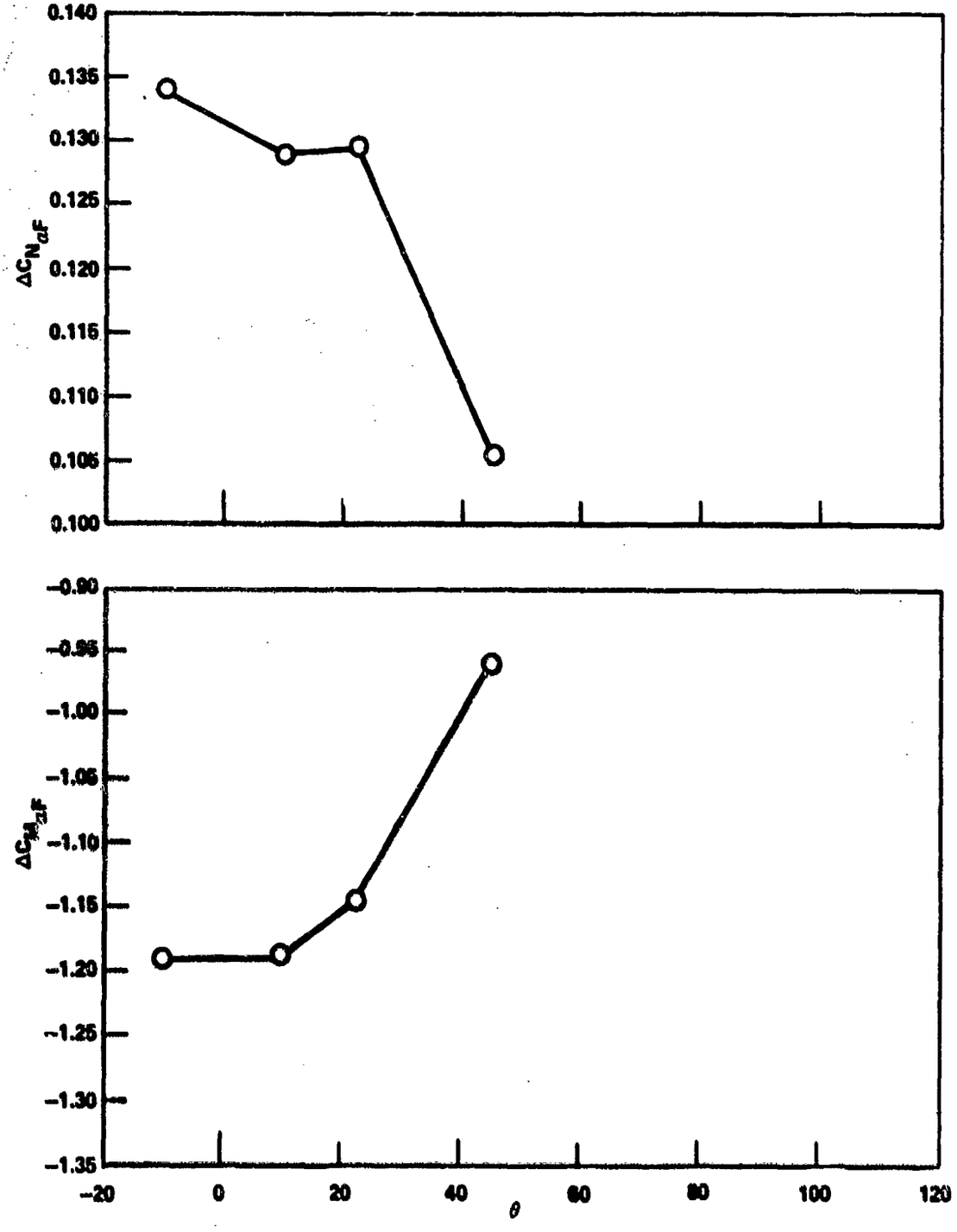


Figure 41. Total fin effectiveness with opening angle, M = 2.0, ϕ = 0.0.

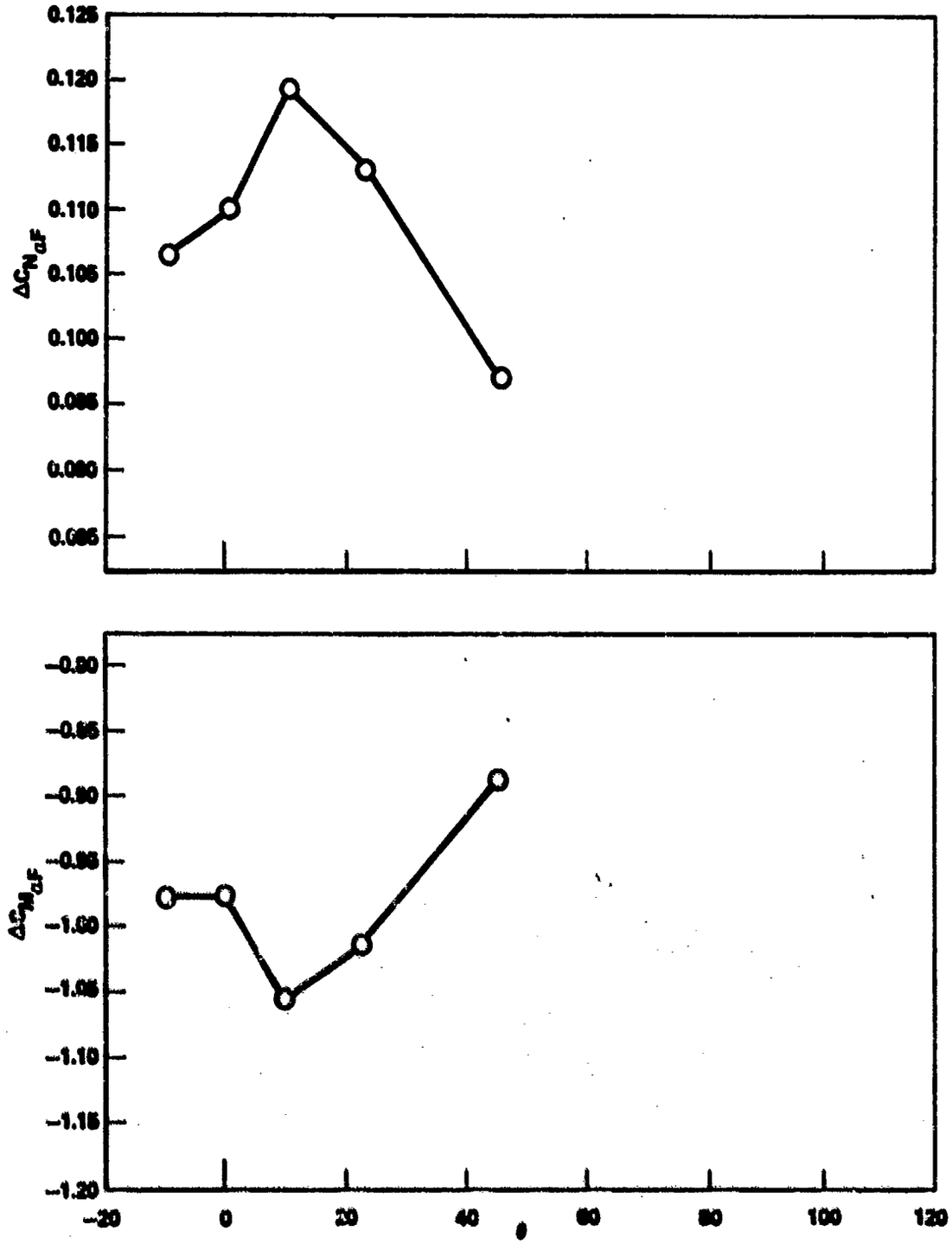


Figure 42. Total fin effectiveness with opening angle, M = 2.5, ϕ = 0.0.

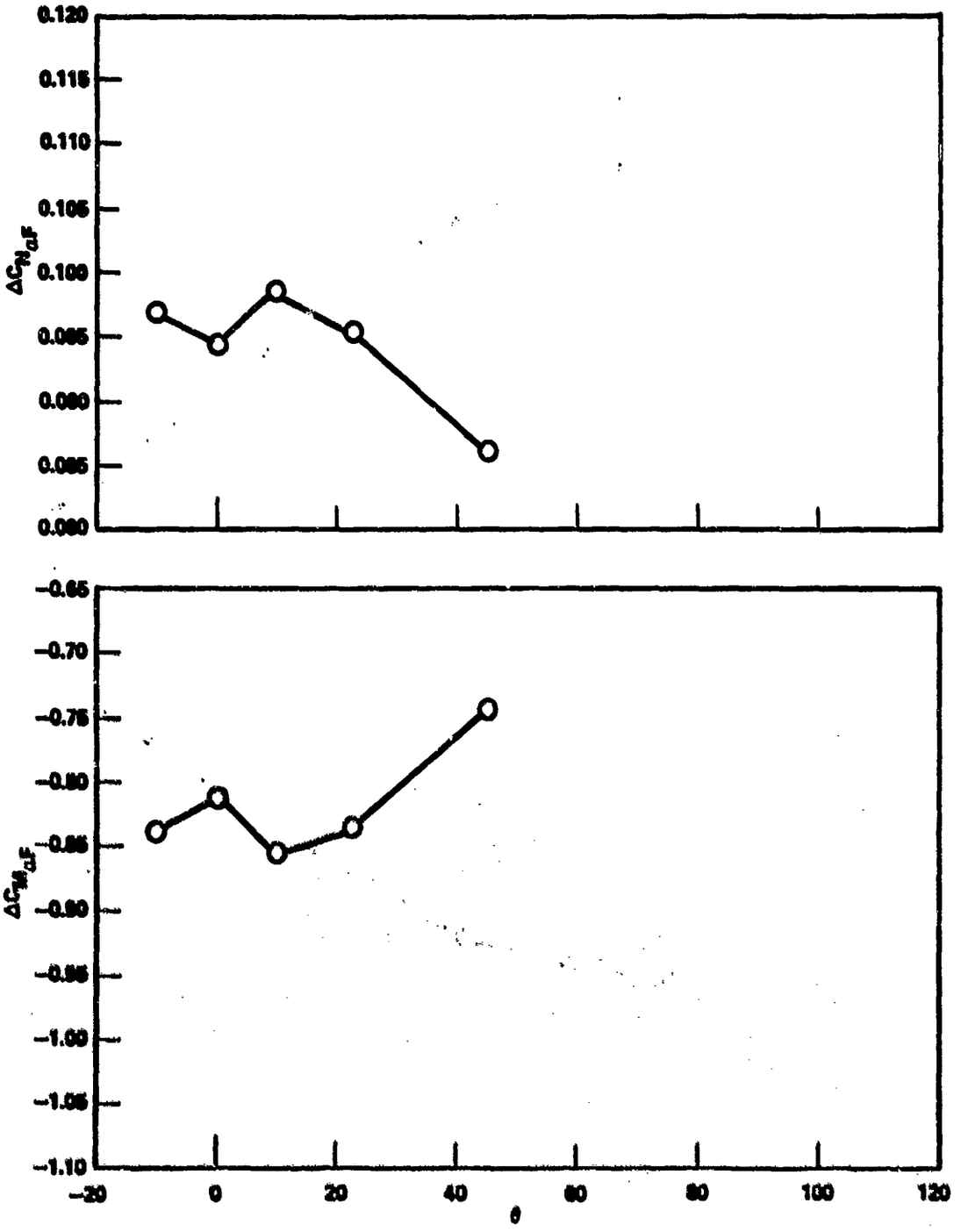


Figure 43. Total fin effectiveness with opening angle, M = 3.0, ϕ = 0.0.

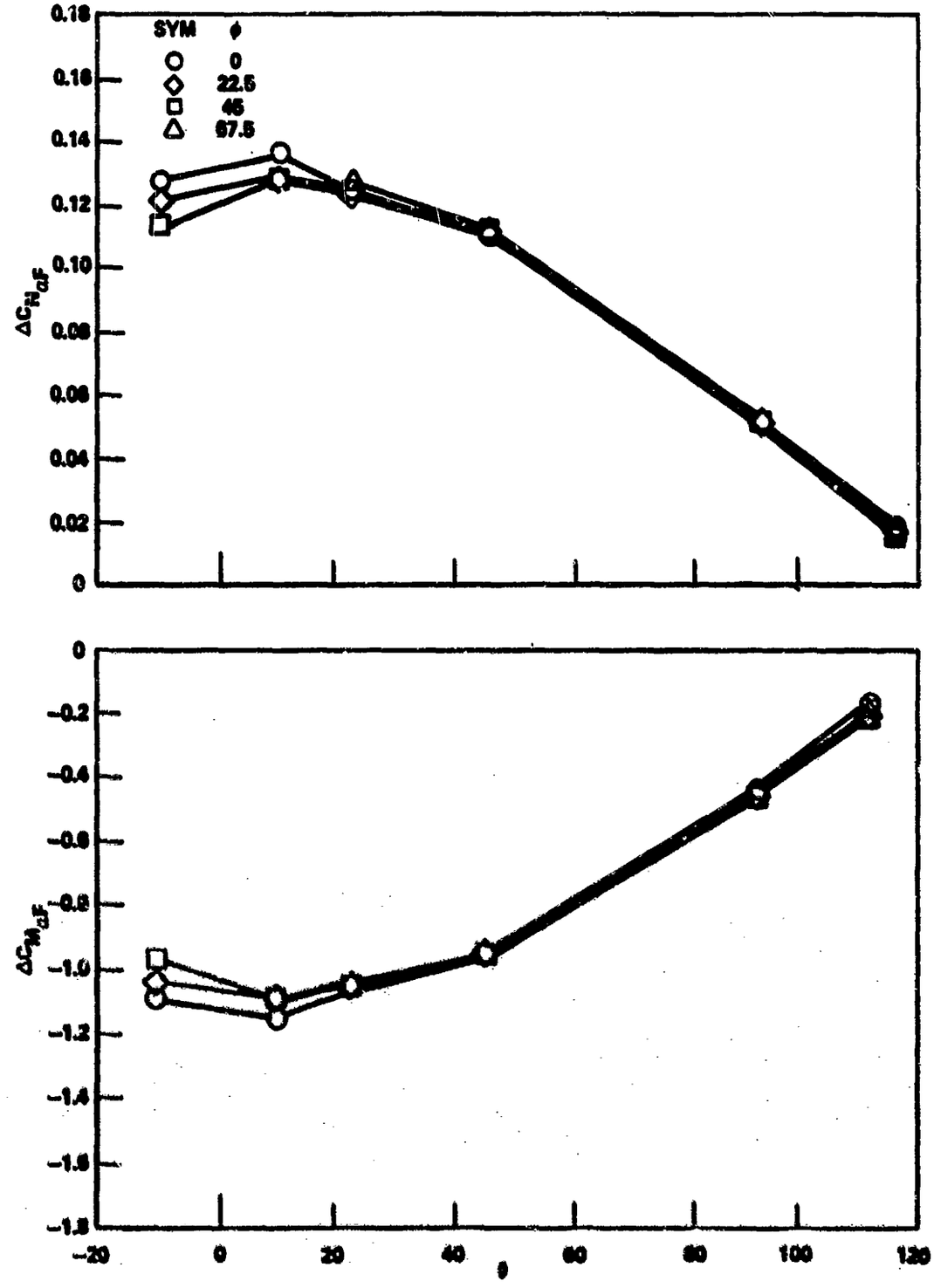


Figure 44. Total fin effectiveness with opening angle, M = 0.5.

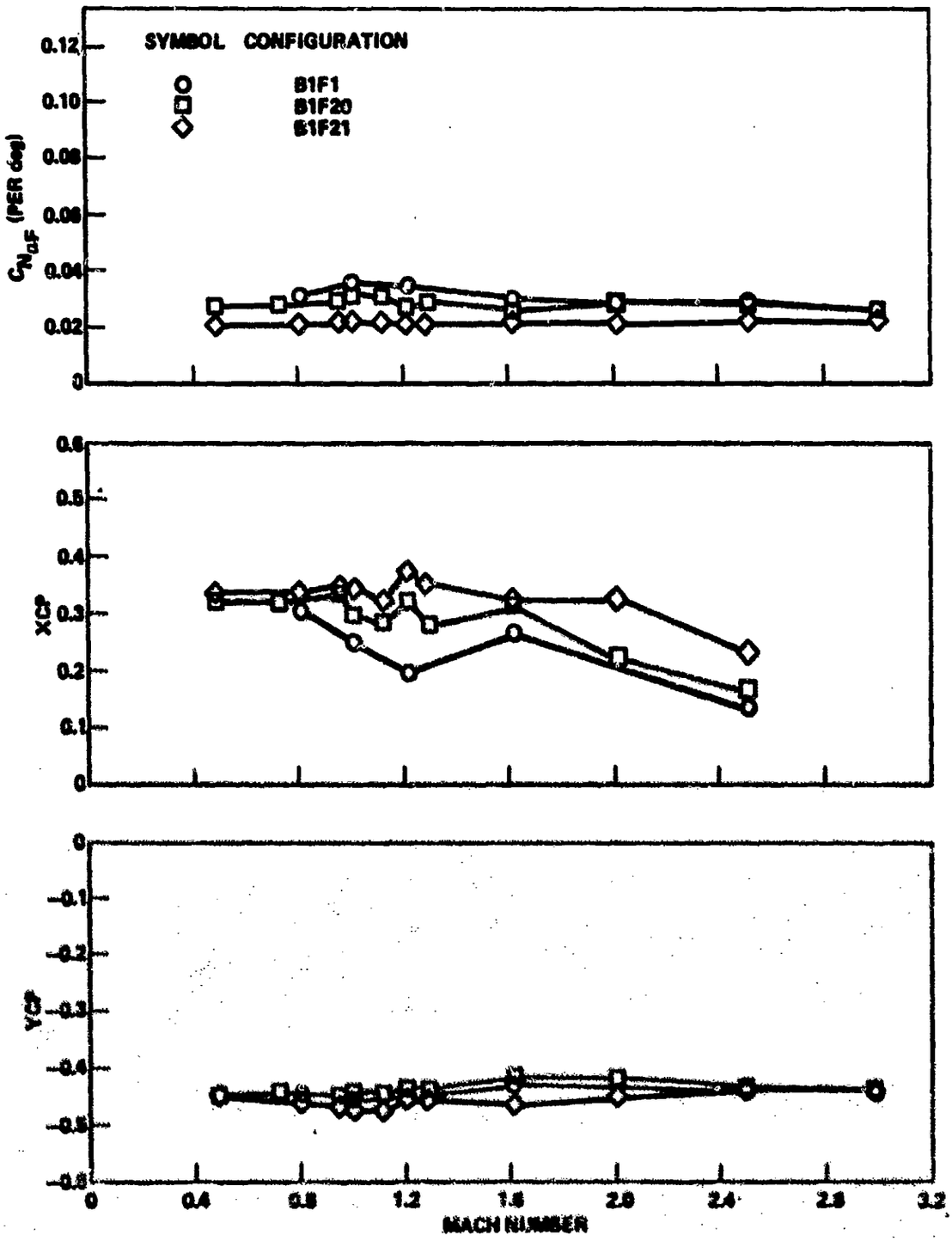


Figure 45. Effect of WAF span on fin panel No. 2, $\phi = 0$.

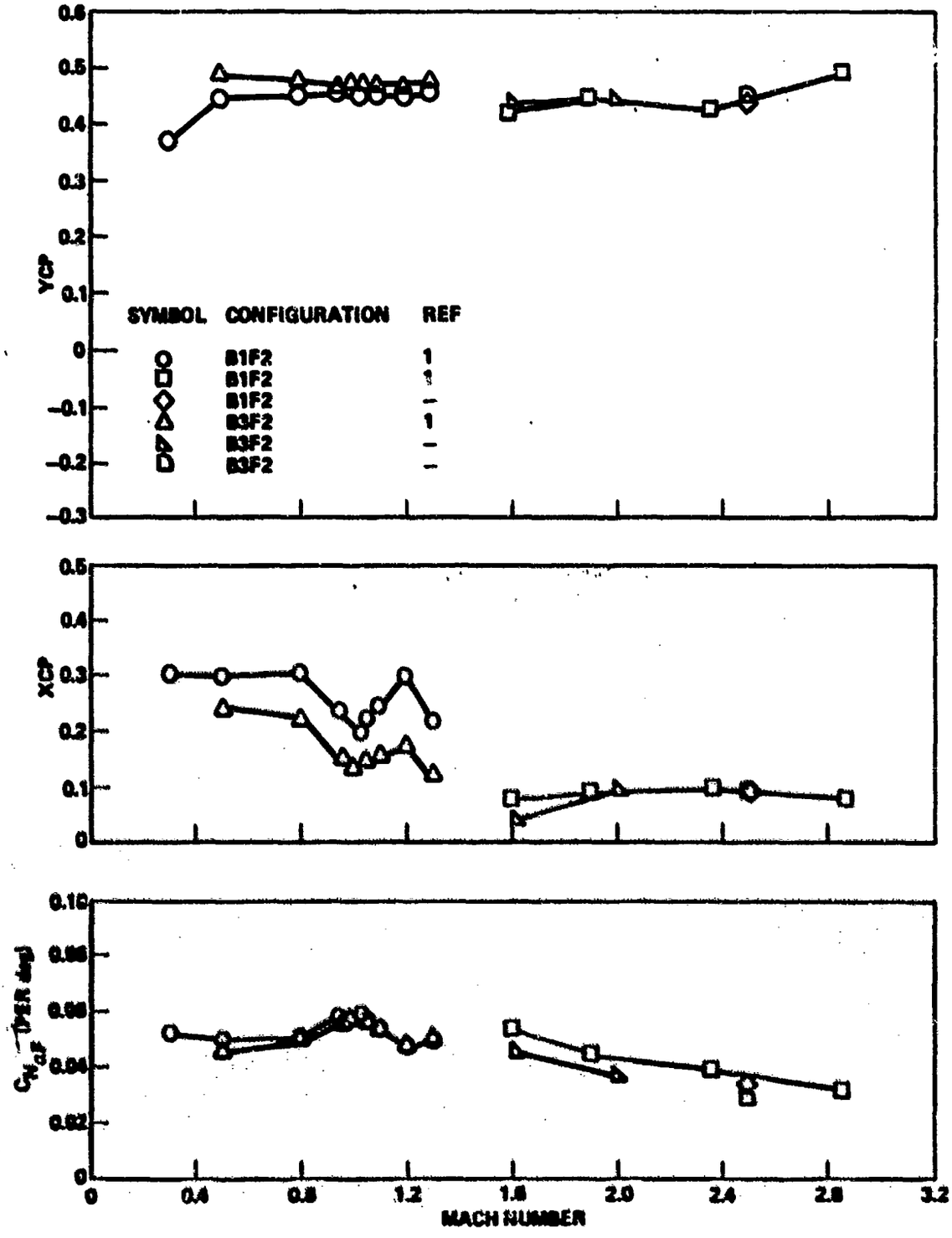


Figure 46. Effect of stepdown body on fin panel No. 4, ϕ = 0.